ISSN 0973-3302

JOURNAL OF ACOUSTICAL SOCIETY OF INDIA

Volume 40 Number 1 January 2013

A Quarterly Publication of the JASI
http://www.acousticsindia.org

JASI

Journal of Acoustical Society of India

The Refereed Journal of the Acoustical Society of India (JASI)

The Journal of Acoustical Society of India is a refereed journal of the Acoustical Society of India **(ASI)**. The **ASI** is a non-profit national society founded in 31st July, 1971. The primary objective of the society is to advance the science of acoustics by creating an organization that is responsive to the needs of scientists and engineers concerned with acoustics problems all around the world.

Manuscripts of articles, technical notes and letter to the editor should be submitted to the Chief Editor. Copies of articles on specific topics listed above should also be submitted to the respective Associate Scientific Editor. Manuscripts are refereed by at least two referees and are reviewed by Publication Committee (all editors) before acceptance. On acceptance, revised articles with the text and figures scanned as separate files on a diskette should be submitted to the Editor by express mail. Manuscripts of articles must be prepared in strict accordance with the author instructions.

All information concerning subscription, new books, journals, conferences, etc. should be submitted to Chief Editor:

Acoustics, Ultrasonics & Vibration Section, CSIR-National Physical Laboratory, Dr. KS Krishnan Road, New Delhi 110 012, Tel: +91.11.4560.8317, Fax: +91.11.4560.9310, e-mail: mahavir@nplindia.org

Annual subscription price including mail postage is Rs. 2000/= for institutions, companies and libraries and Rs. 2000/= for individuals who are not **ASI** members. The Journal of Acoustical Society of India will be sent to **ASI** members free of any extra charge. Requests for specimen copies and claims for missing issues as well as address changes should be sent to the Editorial Office:

Acoustics, Ultrasonics & Vibration Section, CSIR-National Physical Laboratory, Dr. KS Krishnan Road, New Delhi 110 012, Tel: +91.11.4560.8317, Fax: +91.11.4560.9310, e-mail: mahavir@nplindia.org

ISSN 0973-330

Printed at Alpha Printers, BG-2/38C, Paschim Vihar, New Delhi-110063 Tel.: 9811848335. JASI is sent to ASI members free of charge.

JASI

Journal of Acoustical Society of India (JASI)

A quarterly publication of the Acoustical Society of India

Volume 40, Number 1, January 2013

EDITORIAL

ARTICLES

INFORMATION

Ship Noise Reduction Approach

ISociety for Promotion of Nature Tourism and Sports (SPORTS), Indian Register of Shipping (IRS) has performed a literature study focusing on noise from ships in port and the possibilities for noise reduction. As a part of the study it has been established that a ship that is in agreement with the external noise limits imposed by the international maritime organization, IMO, when the ship at berth, potentially can have a significant impact with respect to noise in the surroundings. A calculation example is presented where it is shown that a ship which fulfils the IMO noise limits can have a diesel generator exhaust sound power of 107 dB(A). The IMO noise guiding limits for residential, city areas in the time period 22-07 is 40 dB(A). By applying the most simple noise propagation model it is demonstrated that if the sound power is 107 dB(A) and the noise limit is 40 dB(A), the ship should be berthed more than 600 m away in order not to exceed the noise limit. An excerpt of the unattenuated sound powers of some marine diesel engine exhausts and ventilation fans have been presented and found to be quite significant in light of the environmental noise requirements. I.e. the sound power of the engine exhausts vary between 135 to 142 dB(A) and of the ventilation fans between 81 to 110 dB(A). Noise measurements of secondary noise sources such as reefers, cooling containers, show that the sound power of a single reefer is in the range of 90 dB(A). Each time the number of reefers is doubled the sound power increases by 3 dB. Therefore the noise from reefers can be significant. Standard measures for reducing noise from the major external sources onboard ships have been presented including special noise reducing measures. Some of the presented possible noise reducing measures is listed below:

- Standard silencers on the diesel generator exhaust i.e. reflection type, absorption type and combination type silencers.
- Utilizing the main engine exhaust silencer during port stay for the diesel generator exhaust by rerouting the exhaust.
- On shore power supply
- Standard methods for reducing noise from ventilation systems onboard a ship including adding mineral wool to fan rooms, cylindrical silencers, baffle silencers and noise reducing louvers.

A cost ranking of the different noise reducing measures has been laid out. The cost ranking is based on whether the installation of the noise reducing measure is considered to be cumbersome and time consuming. This is if the installation can be carried out during regular port stay or should be performed on a shipyard. For example installing new silencers in a diesel generator exhaust stack is a major structural change and is performed at a shipyard which is considered to be costly. Whereas, installing mineral wool in a fan 10 room is simple and can be carried out by the ship's crew or a contractor during port stay. A noise reducing measure on this scale is therefore considered less costly.

Mahavir Singh

Journal of Acoustical Society of India : Vol. 40, No. 1, 2013 (pp. 3-19)

Continuous Wave Doppler SODAR for Mid- range Wind Velocity Profiling

Y. Kagawa[1], T. Fukuda[2], T. Yamazaki[2], L. Chai[3]* and M. Singh[4]
[1]Emeritus, Okayama University, Okayama, Japan
[2]Electrical and Electronic Engineering Dept, Nihon University College of Industrial Technology, Narashino, Chiba 275-8575, Japan
[3]Solar Frontier K.K., Japan [4]CSIR National Physical Laboratory. New Delhi, India
**e-mail: chaily123@yahoo.co.jp*

[Received: 12.11.2012; Revised: 28.12.2012; Accepted: 10.01.2013]

ABSTRACT

The SODAR can be a good candidate for the measurement technology of the wind velocity profiling for the wind turbine electric generator, which make measurement possible without expensive tower construction work for wind velocity meters set-up. The Doppler SODAR using continuous wave is proposed and verified by the experiment. Transducers, a transmitter and a receiver both with sharp directivity are used. The wind velocity at the region where the two directivities are crossed can be detected. The profiling or mapping of the objective area can be made by changing the direction of the two directivities. A prototype apparatus is developed for the sound of higher frequency range to scale the system size down for the experimental easiness. The experimental result shows that the wind velocity of the range over 1 m/sec can be measured with the accuracy of few percents even under interfering conditions. Velocity mapping including the wind's directions can be obtained. Spatial measuring range can be extended by lowering the wave frequency to cope with the propagation loss. The use of the continuous wave is simple in circuitry and expected to be robust for noise compared with the pulse type system.

1. INTRODUCTION

In the era of the environmental preservation, the wind turbine electric generation becomes increasingly popular. The wind velocity is the primary concern for selecting the setting-up site. Until now, the wind velocity profiling is made by the wind velocity meters equipped at the selected several places on a tower or a pole put up on the site. The measured data are transmitted to the computer on the ground for a certain period of time. The construction and maintenance of the tower and its removal after the measurement completion are expensive and the data are only available at the vertical spots where the meters are placed. For this reason, there is the need of a means to sense remotely the data more economically without expensive construction work. The Doppler SODAR approach can be a good candidate for mid- range wind velocity profiling as it does not require the construction work but being set up on the ground. The present work is to propose the use of the SODAR with the continuous wave sounding. A simple theory is given and the validity is demonstrated by the model experiment for remote-sensing the flow velocity in quasi-steady state. The requirement of the system for this purpose is that the range is around 100m and the measurable wind velocity with reasonable accuracy

must be 1 from to 10 m/sec. The sound scattering does not come from the moving fluid but from dusts, voids or vortices contained in the moving flow. Therefore, the level of the reflection is as low as 80dB. This is the reason why we discuss the case of a continuous wave sounding. In the experimental demonstration, a simple measuring system is assembled and the experiment is carried out in rather short-range environment with a scaled-down model at the ultrasonic frequency range. As the frequency increases, the transmission loss increases. We believe that the present technique can be applicable to achieve our requirement without much lowering the frequency in real situation. The transmitter and receiver with sharp directivity must be prepared. The wind velocity is measured for the target position at the cross-point of the two directivities. To verify the result, the velocity is compared with the reference value measured by the velocity meter placed at the same position as that of the target. The mechanism of the present approach is also verified by the numerical simulation based on the discrete Huygens • f modeling (Transmission Line Matrix Modeling,TLM) [1], [2].

2. THEORETICAL BACKGROUND

2.1 Sodar

SODAR stands for the abbreviation of Sound Detecting And Ranging. Its operating mechanism is the same as that of RADAR except that the sound wave is used for sensing instead of the electromagnetic wave.

The presence of a target in air can be detected by the signal reflected from the target for the emanated wave. An AC pulsed wave is usually employed for the emanation. The direction of the target is generally determined by the direction to which the wave is transmitted and the distance to the target is determined by the time twice required for the reception of the back-scattered pulse. The "Doppler" SODAR utilizes the Doppler effect to sense the target motion due to the frequency shift of the reflected signal to the emitted signal frequency.

The SODAR and the Doppler SODAR techniques have been used for remote-sensing of the atmospheric fluctuation for the meteorological observation [3], [4]. The sounding is only concerned with the relative atmospheric change high up in the sky. The distance to the target is so long that the AC pulsed sound wave of low frequency must be chosen. The lower frequency means the lower attenuation and the longer wavelength can only accommodate a small number of waves in a single pulse width. This degrades the resolution of the frequency shift of the reflected wave, which determines the accuracy of the target velocity detection[5],[6]. Doppler SODAR mechanism has also been used for the ultrasonic imaging of the cardiac blood circulation for medical diagnosis[7].

The drawback of the AC pulse type mechanism is that the frequency resolution, that is, the velocity measurement accuracy depends on the pulse width in which the number of the waves accommodated is not always enough for reasonable frequency change resolution.

2.2. Doppler Effect -Simple Geometrical Consideration

The system measures the velocity of a moving object by the frequency shift of the wave reflected from the object when it is illuminated. We here explain the effect using a simple model. Referring Fig. 1 (a), as the velocity of a particle moving with velocity v toward the transmitter T at angle q is v cosq (m/sec), the frequency increases to

$$f = \frac{c + \upsilon \cos\theta}{\lambda} = \frac{c + \upsilon \cos\theta}{c} f_T \tag{1.1}$$

where f_T is the frequency of the transmitted wave and c is the propagation velocity of the sound and λ is the wavelength. On the other hand, the frequency f_R of the received signal reflected increases to

$$f_R = \frac{c}{c - \nu \cos\theta} f = \frac{c + \upsilon \cos\theta}{c - \upsilon \cos\theta} f_T \tag{1.2}$$

The Doppler frequency shift is therefore

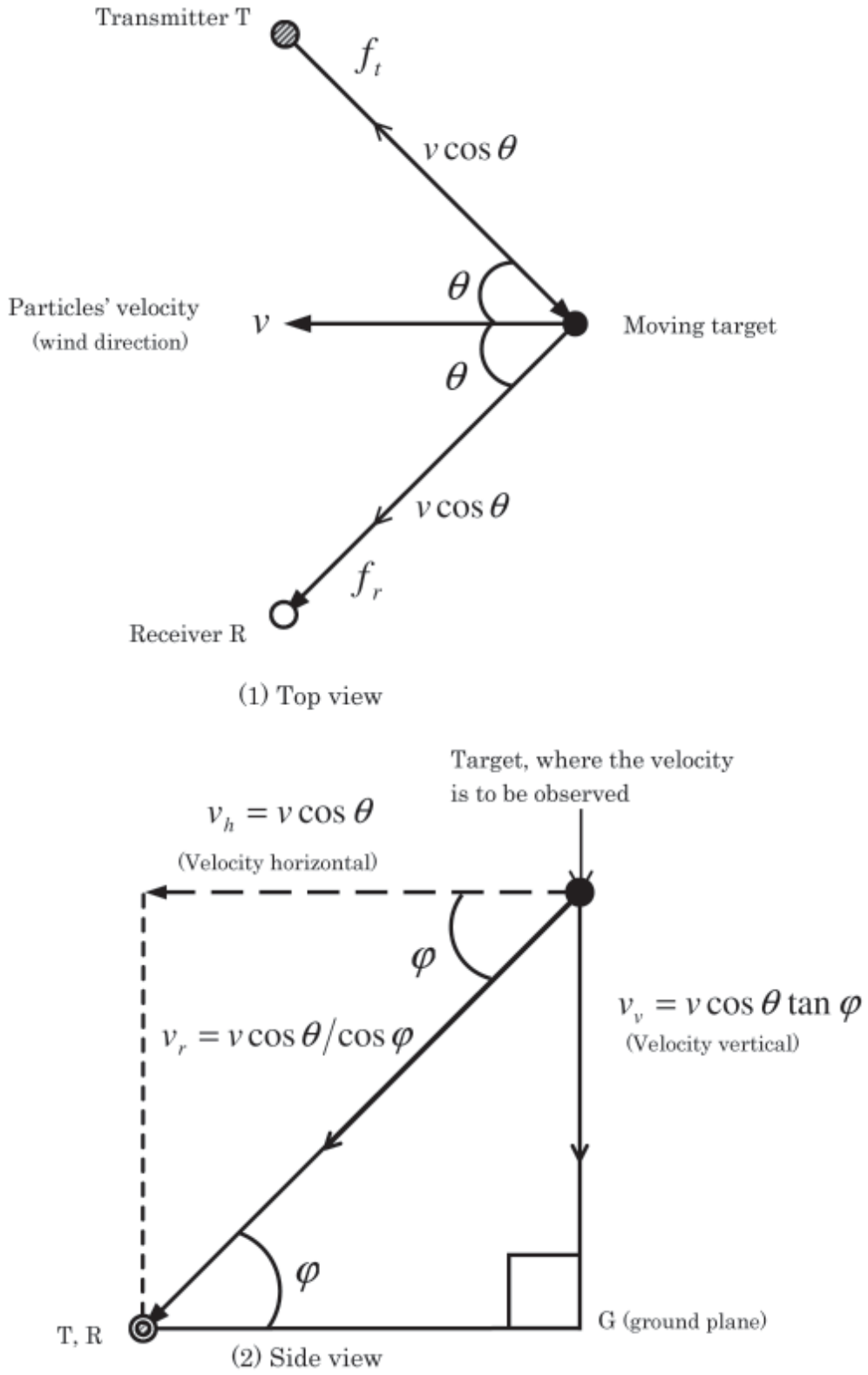

Fig. Reflection model for Doppler effect

$$\Delta f = (f_R - f_T) = \frac{\upsilon(2\cos\theta)}{c} f_T \tag{1.3}$$

for c>>ν.

The velocity of the moving target is given by

$$\nu \frac{\Delta f c}{2(\cos\theta) f_T} \text{ [m/sec]} \tag{1.4}$$

If the target has the elevation as shown is Fig.1(b), the horizontal component of the moving target velocity is

$$\nu_h = \frac{\Delta f c \cos\varphi}{2(\cos\theta) f_T} \text{ [m/sec]} \tag{1.5}$$

The vertical component is given by

$$\nu_v = \nu \cos\theta \tan\varphi \tag{1.6}$$

The actual vertical wind direction can be determined by twice the measurements with two pairs of transducers placed on the ground surface.

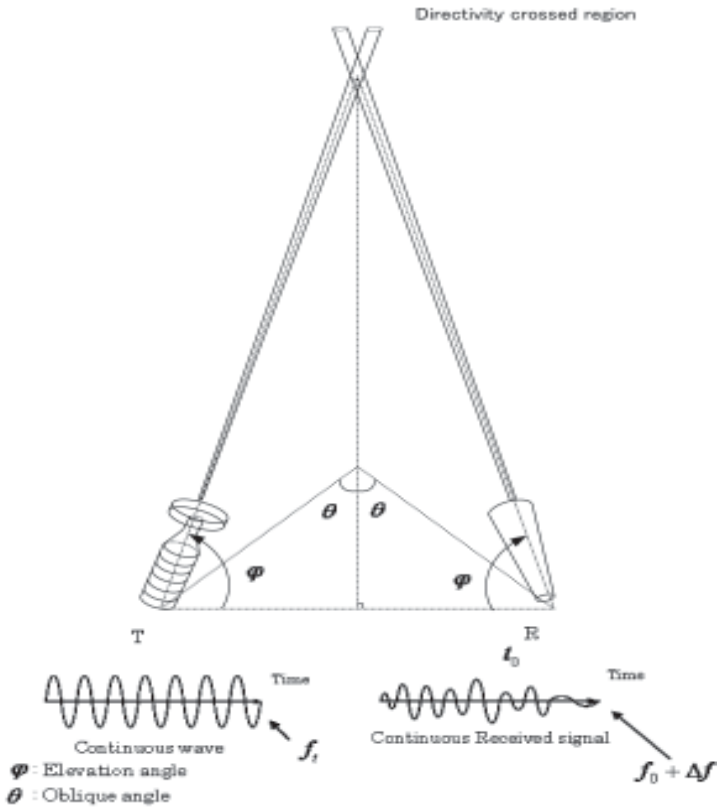

Fig . 2. Transmission and recepition system of a continuous wave Deppler SODAR

3. EXPERIMENTAL SYSTEM FOR VERIFICATION

Figure 2 shows the arrangement of a pair of the transducers, the transmitter and the receiver. The space can be scanned by varying the transducers' directions. The transducers must provide very sharp directivity so that the moving target velocity at the crossed region of the two directivities can be measured as the result of the frequency shift of the received signal.

The sound transmission intensity decays as both distance and frequency increase. The experiment is carried out with a scaled-down model at ultrasonic frequency range. A ultrasonic transmitter as shown in

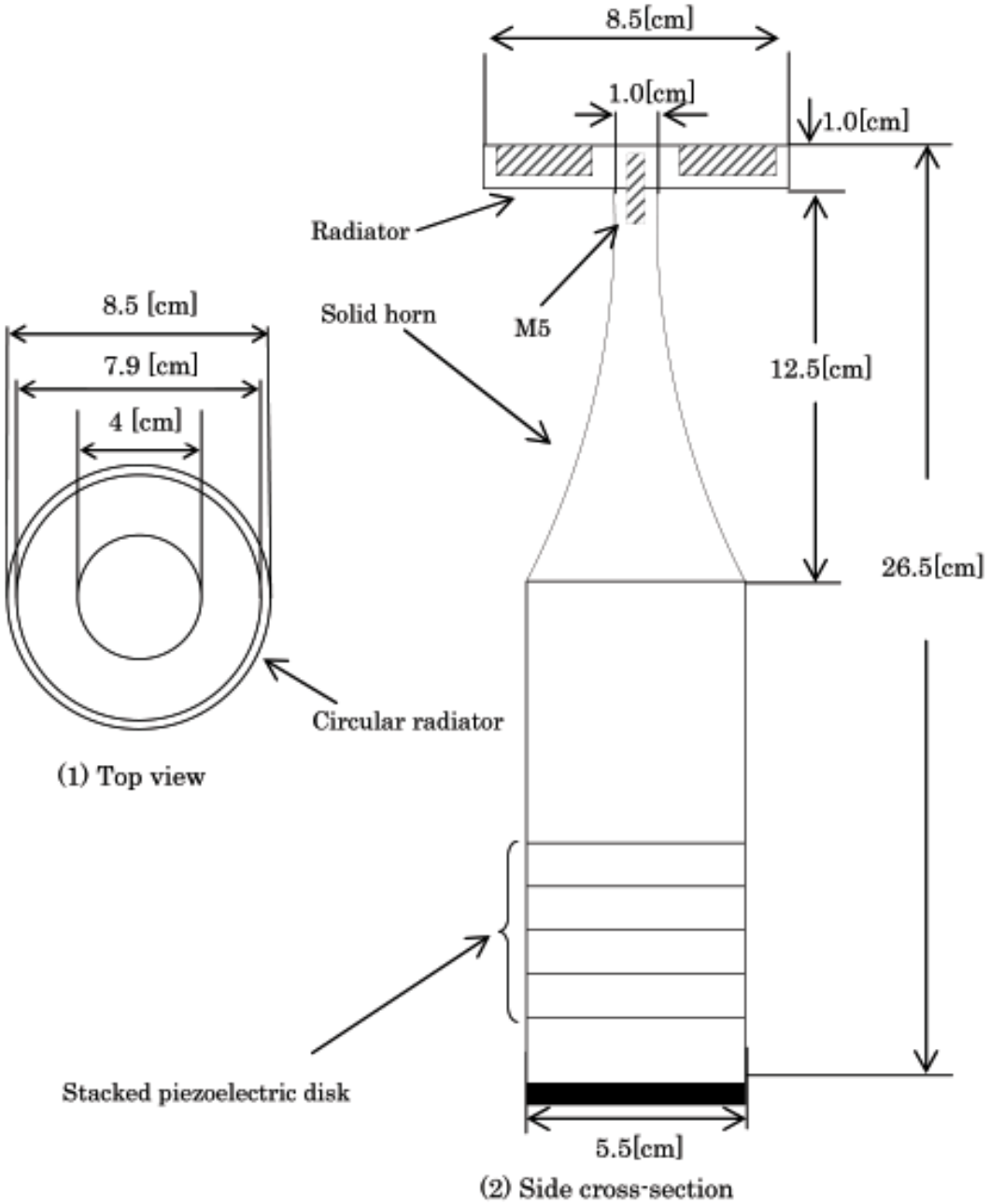

Fig . 3. Ultrasonic transmitter

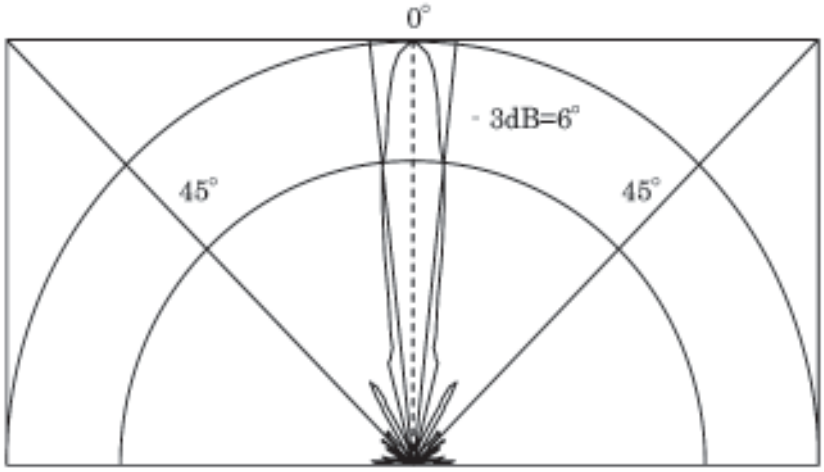

Fig. 4. Transmitter's directivity (sound pressure : 160[dB] at 1/λ distance to 15[W] input f_1: 19.734[Hz]

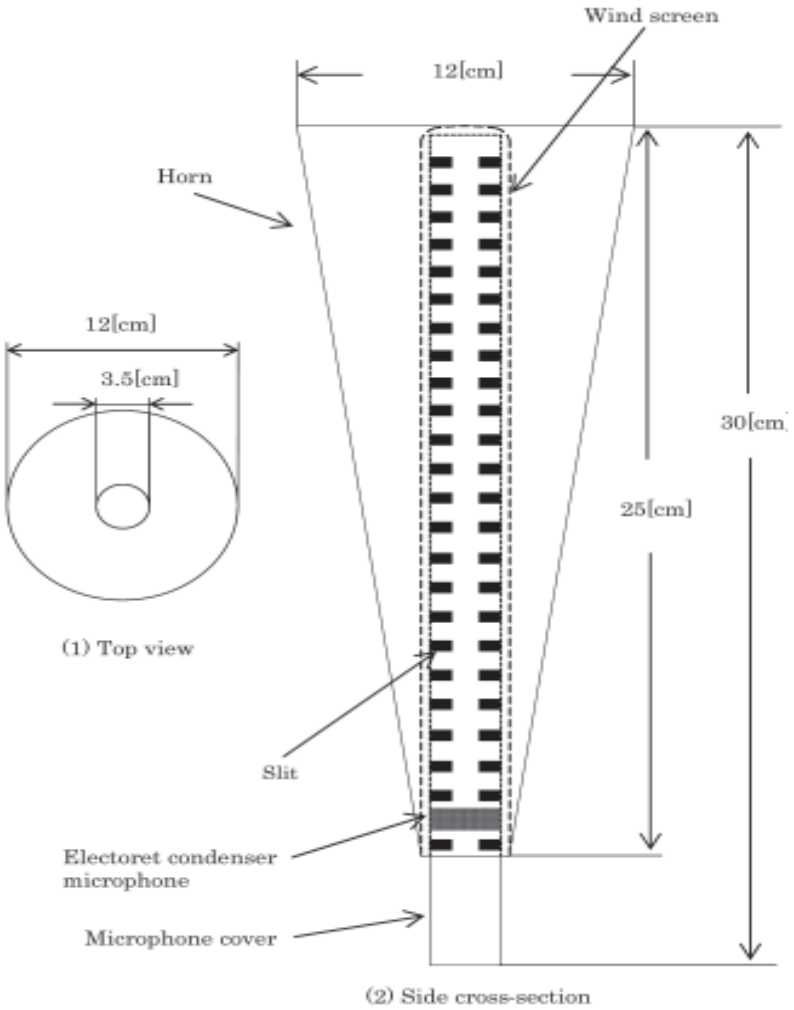

Fig. 5. Ultrasonic receiver

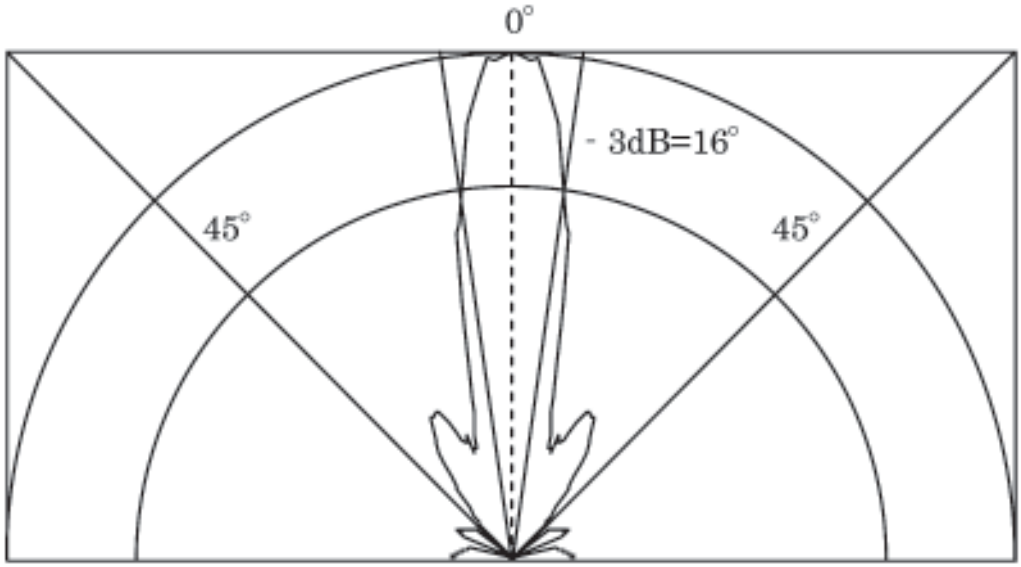

Fig. 6. Receiver fs directivity (Gain :- 33[dB] at 50[cm] for the reference to 0dB=1[V/Pa])

Fig. 3 is used with the solid horn for the displacement amplification to which a disc radiator is connected at its center. The directivity is shown in Fig. 4. The intensive sound pressure is attained with very sharp directivity. The receiver is a bar microphone made of the electrets microphone providing a front end tube with slits. This is originally designed as a directional microphone for audio frequency range. It is placed at the center of a

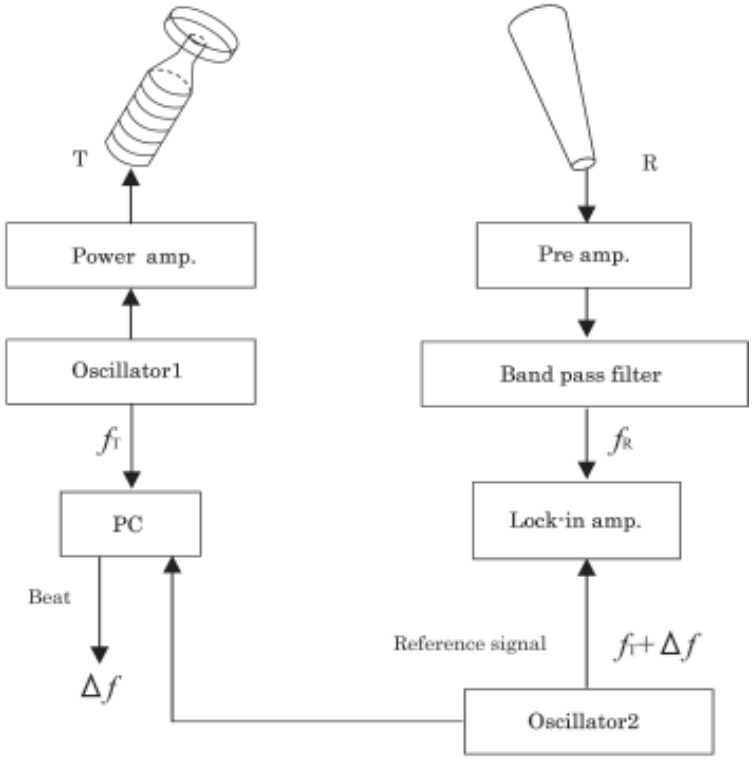

Fig. 7. Block diagram of a proposed Doppler SODAR system

conical horn as shown in Fig. 5. The directivity shown in Fig. 6 is reasonable for our purpose. The receiver can cover the range of the frequency shift, though the frequency characteristic is not given.

The block diagram of the Doppler SODAR system is shown in Fig. 7. As there is no pulse forming and detecting circuitry, the block diagram is very simple. The received signal must be contaminated by the noise so that the lock-in amplifier with the reference signal oscillator 2 is used for frequency identification. This process can be replaced by a mixer circuitry to extract the beat frequency Δf.

The actual experimental set-up is shown in Fig. 8, which includes a blower for the wind source. The wind velocity can be variable by adjusting the electric voltage supplying to the motor. In the target position, a wind velocity meter commercially available (a hot wire-type, V-01-AND2H by Ei Electronics), can be replaced to measure the reference velocity directly on the same spot.

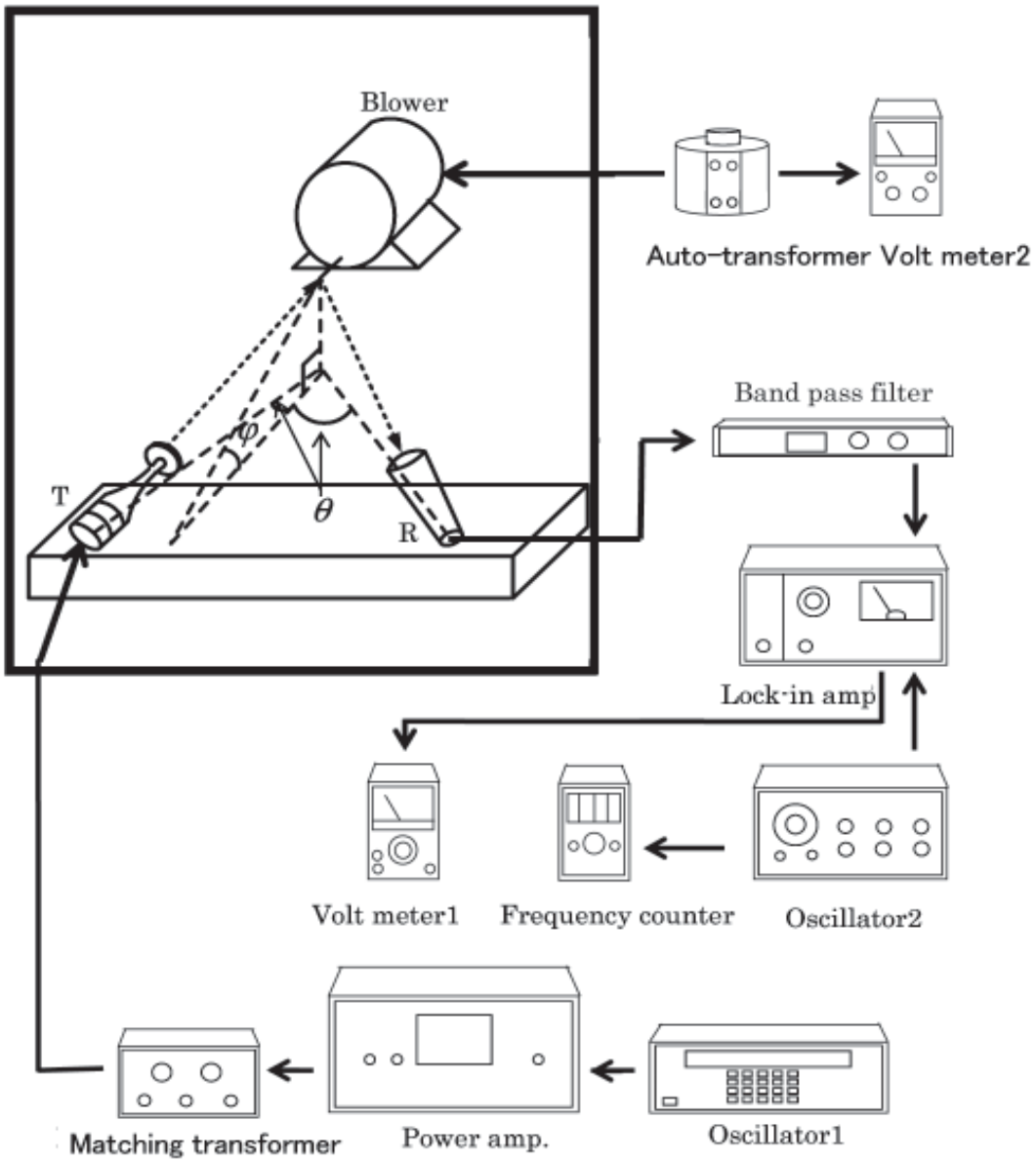

Fig. 8. Experimental set-up

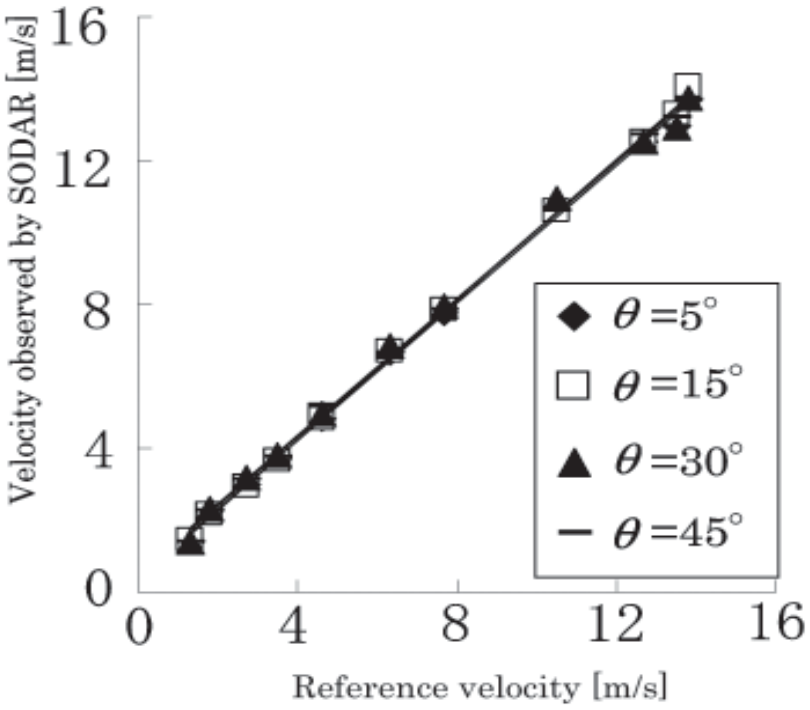

(1) Sound is illuminated against the wind

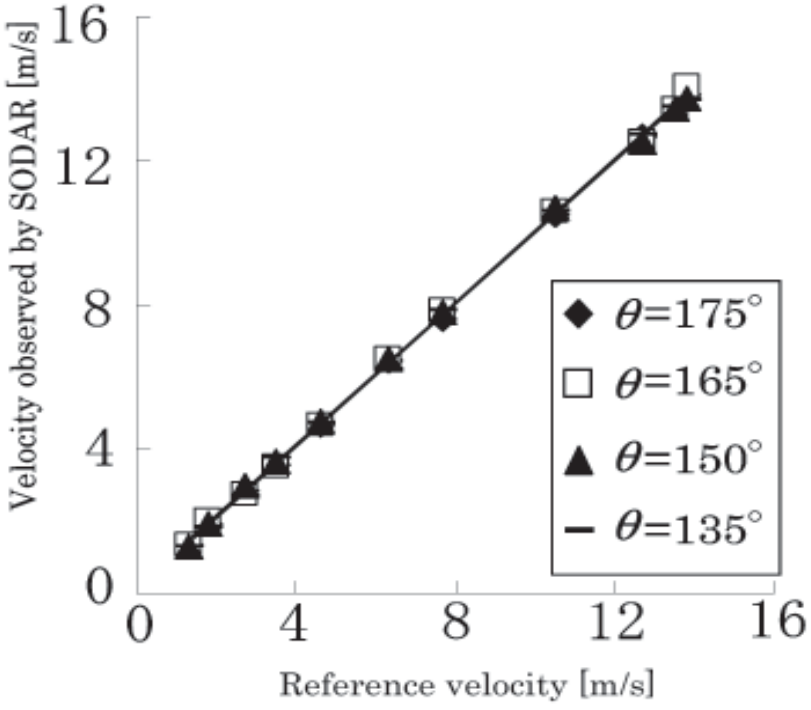

(2) Sound is illuminated for the wind

Fig. 9. Wind velocity for various attacking angle, θ (ϕ = 30°)

A target position is directed to a certain point in front of the blower fs outlet. The wind velocity is calculated from the frequency shift for various attacking angle (θ) with elevation angle (ϕ) fixed.

Figure 9 shows the results, in which the measured velocity is compared with the reference velocity, which are along the line 45•‹inclined regardless the attacking angle. Due to the limitation of the experimental space, the distance from the transducers to the target position is in the range of a few meters. The velocity is measurable over the adjustable range of the blower, say 0.5-15[m/sec].

The measurement is also carried out for various elevation angle (ϕ), with attacking angle (θ) fixed. The results are shown in Figs. 10-1 to 10-4.

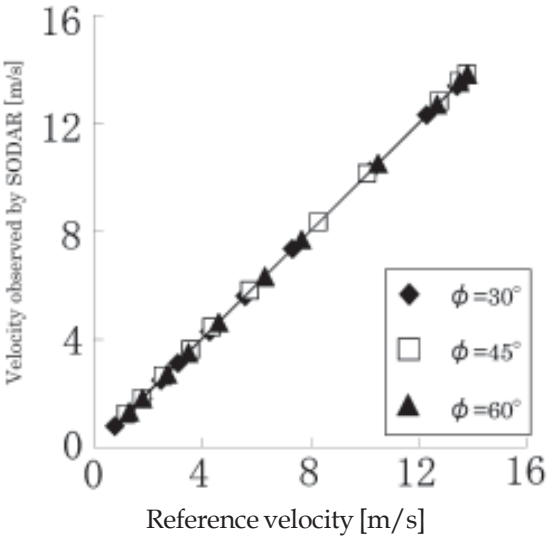

Fig. 10-1. Wind velocity for various elevation angles, (θ = 5°)

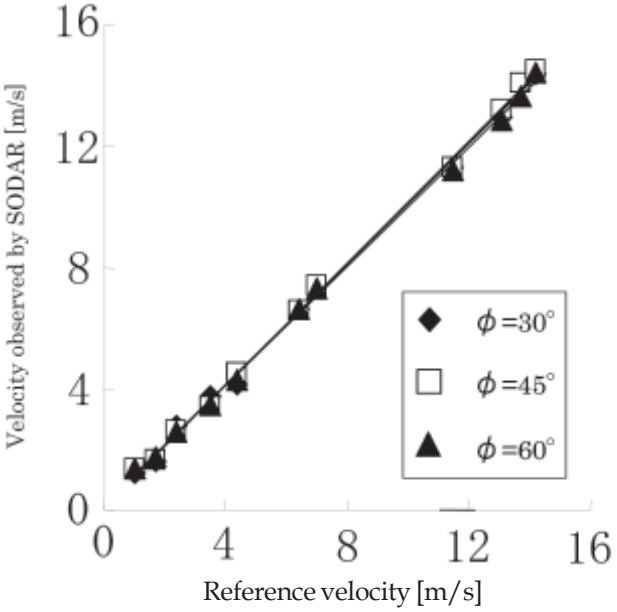

Fig. 10-2. Wind velocity for various elevation angles, (θ = 45°)

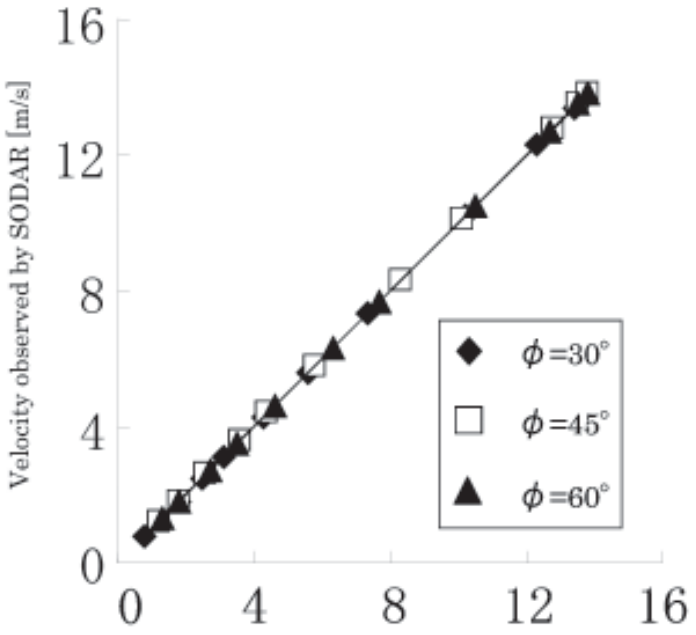

Fig. 10-3 Wind velocity for various elevation angles, (θ = 175°)

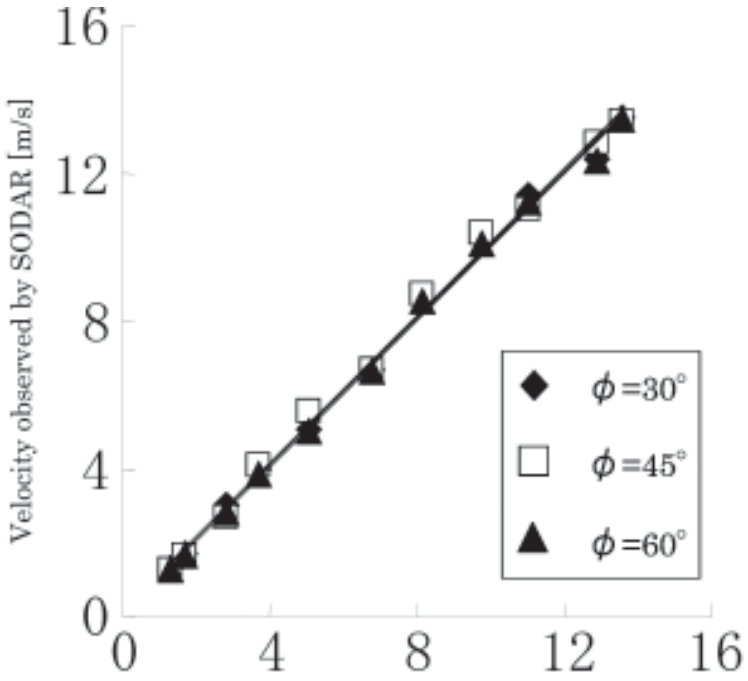

Fig. 10-4 Wind velocity for various elevation angles, (θ = 135°)

The wind field is not uniform but varys over the outlet surface. The velocity distribution on the wave propagation path could effect on the results. To examine this effect, second blower is provided to disturb the sound transmission path. This effect is also examined by the numerical simulation[1].

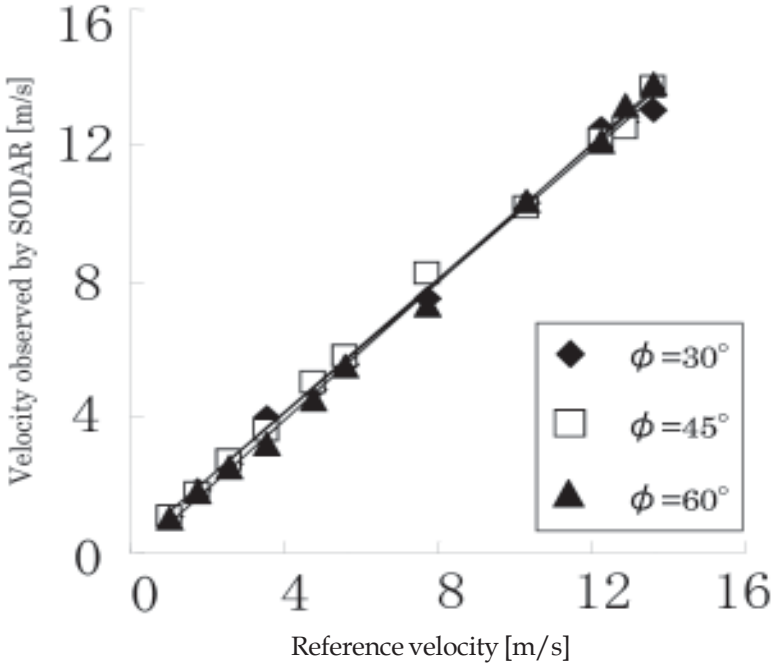

Fig. 11.1 Measured wind velocity for various elevation angle, (blower 1 and blower 2 are placed in the same direction)

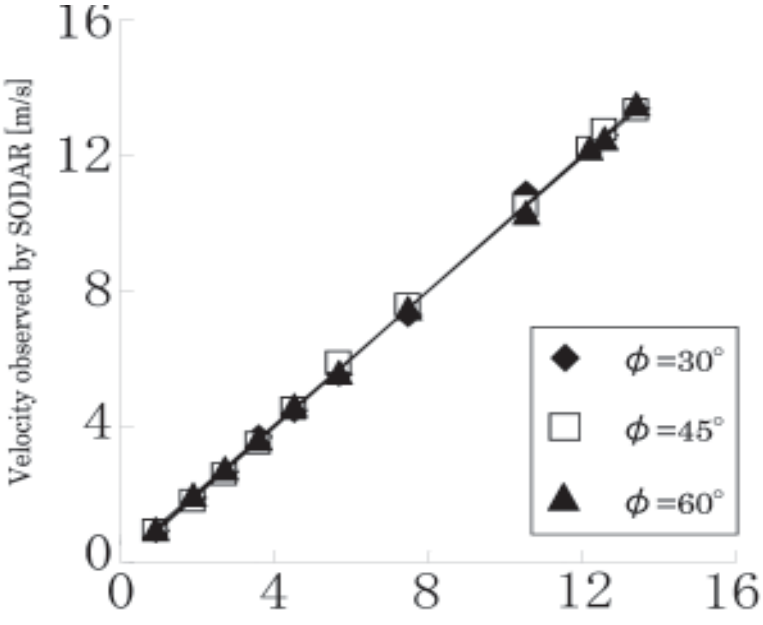

Fig. 11-2 Measured wind velocity for various elevation angle, (blower 1 and blower 2 are placed in the same direction)

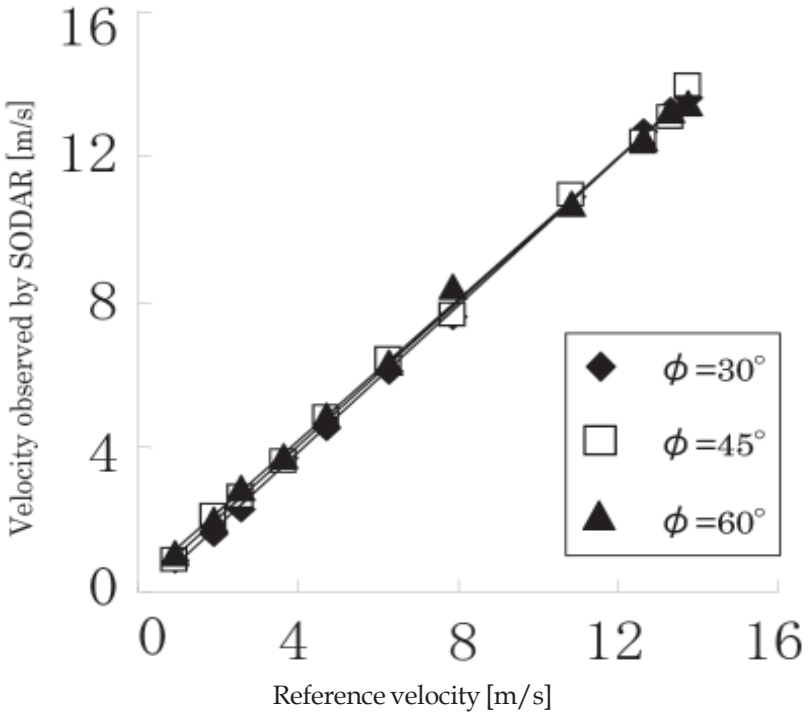

Fig. 11.3 Measured wind velocity for various elevation angle, (blower 1 and blower 2 are placed in the same direction)

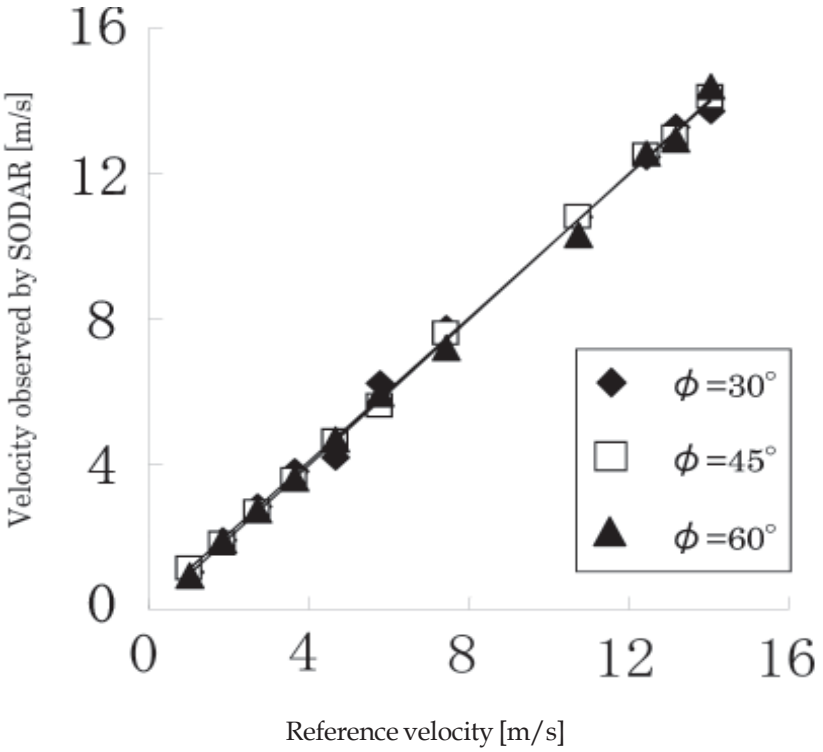

Fig. 11-4 Measured wind velocity for various elevation angle, (blower 1 and blower 2 are placed in the same direction)

The second blower's wind direction can be switched reversely. Figs. 11-1 to 11-4 shows this case. The measured velocity agrees with the reference velocity regardless the elevation angle ϕ and the direction of the disturbing wind, whose velocity is about 4[m/sec] fixed, which could be interpreted as the interference noise.

As shown in Figs. 11-1 and 11-3, some influence is visible near the lower end or for the low wind velocity. This may degrade the measurement accuracy. It is however possible to measure the velocity as low as 1m [m/sec] with the accuracy of less than a few percents.

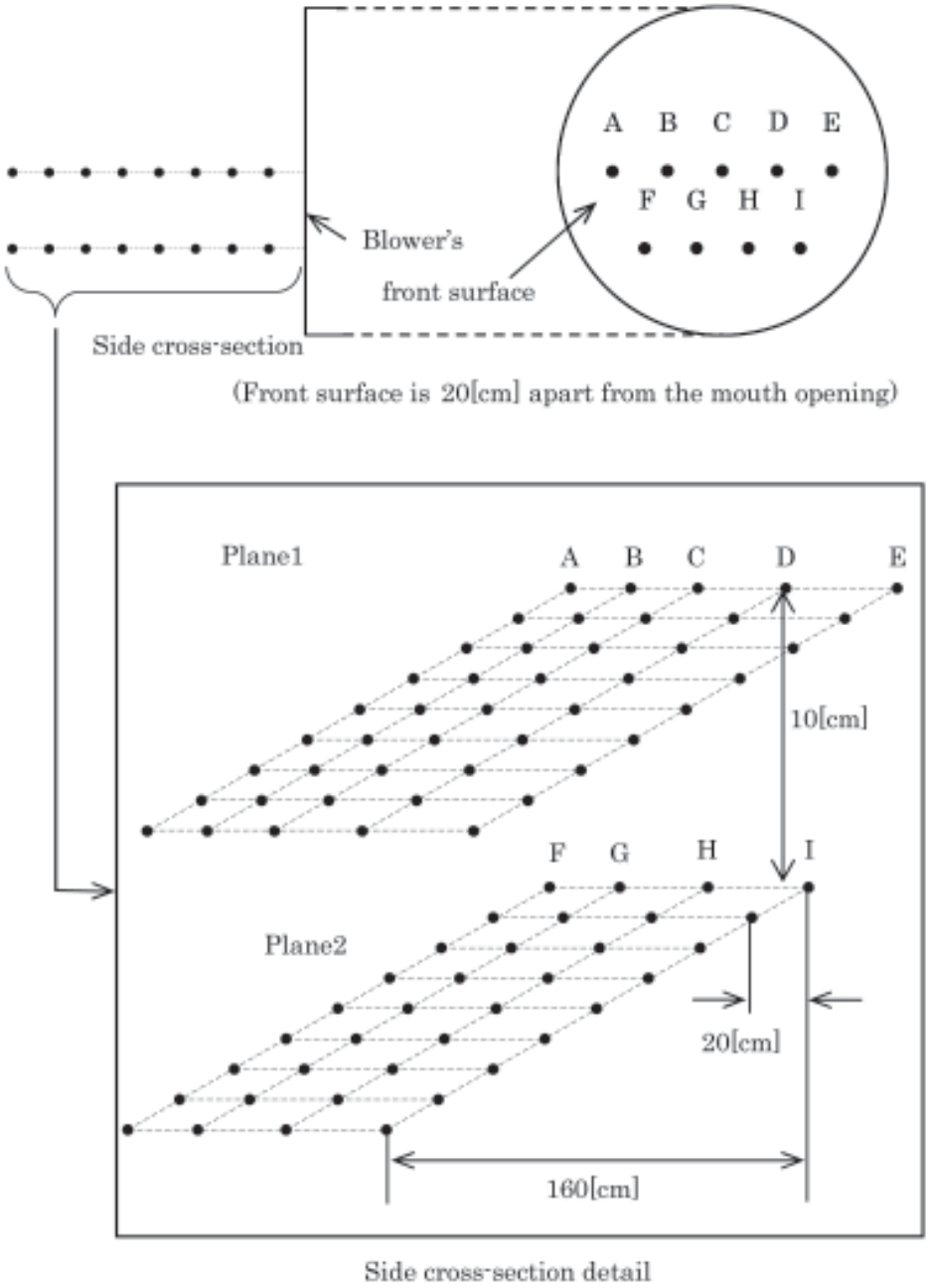

Fig. 12. Observation points

4. WIND VELOCITY PROFILING

Wind velocity distribution is examined over the planes tangential to the blower fs front surface. The detail of the observation points are sketched in Fig. 12.

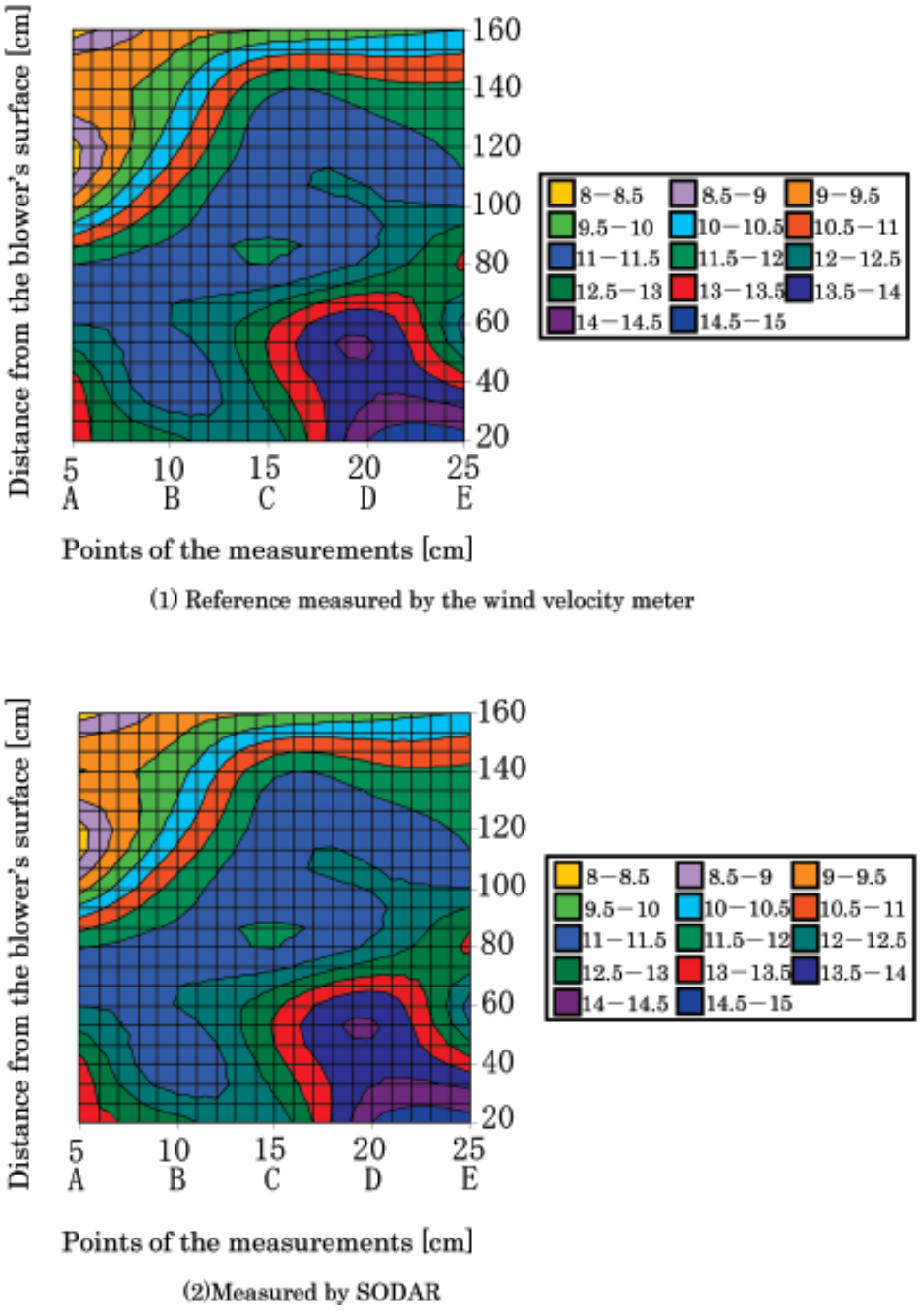

Fig. 13-1 Wind velocity profile

Figure 13 shows the wind velocity distributions, which are visualized based on the values measured at each grid over each plane. The distribution, the velocity measured by the present sensing and the reference value directly measured by the velocity meter at the same spot looks very much the same even for the regions

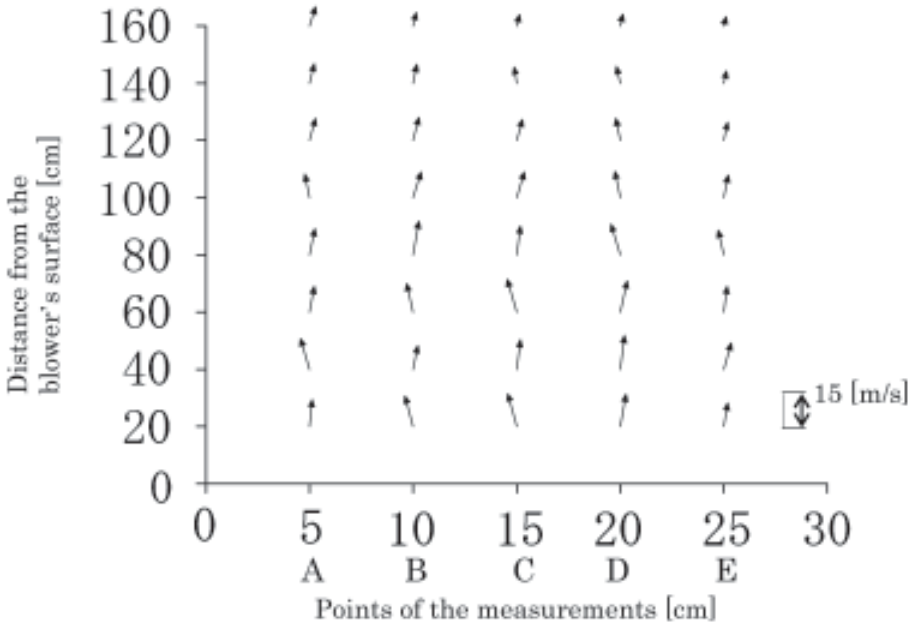

(1)Reference by the wind velocity and wind direction meter

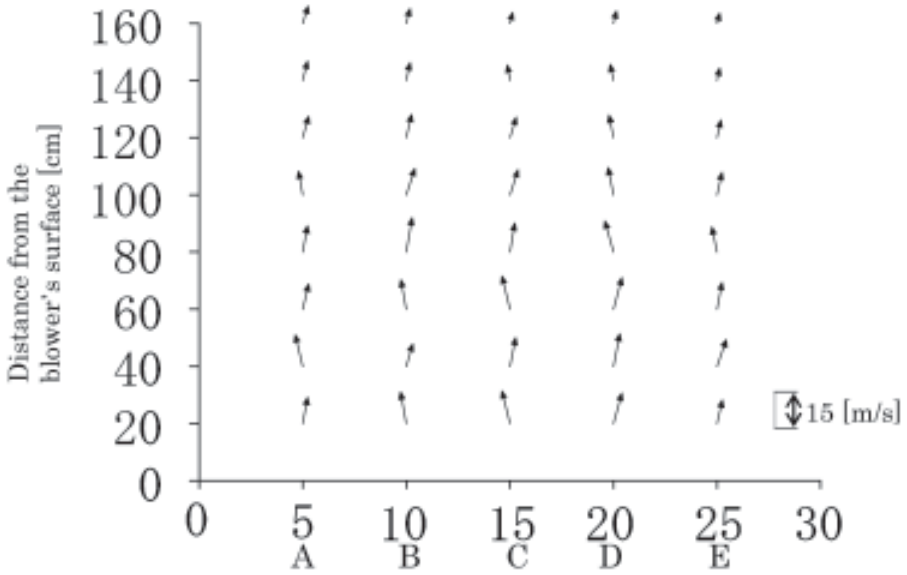

(2) Measured by SODAR

Fig. 14. Wind direction profifle

where the wind velocity is very low. This validates the usefulness of the present measuring approach. The velocity direction can be obtained by the measurements with two pairs of the transducers as discussed in Section II-2. The wind directions are not vertical to the mouth surface as the blower fs wind direction is likely to bend.

Figure 14 shows the results. The wind strength and direction are indicated by the length and direction of the arrow at each point. The arrows remotely sensed and the reference arrows directly measured at the same spots. This again validates the present technique.

5. CONCLUDING REMARKS

The Doppler SODAR using continuous wave emanation is proposed for measuring the wind velocity in mid-range space, aiming at the evaluation of the wind turbine electric generator site selection. The transmitter and the receiver with sharp directivity are carefully selected for the scaled-down model experiment. The wind velocity including its direction can be measured by a system experimentally set-up. The measured velocity distributions at various surfaces are compared with the reference measured value by the velocity meter. The good agreement is established regardless the attacking and elevation angles for shooting the target. This validates the proposed technique and makes profiling the wind distribution possible. The present paper demonstrates our experience with the experiment. The system is yet at the stage of a prototype, but scaling-up to the practical system for 100m range can easily be achievable by choosing a suitable frequency, if necessary.

6. REFERENCES

[1] L. CHAI, T. FUKUDA, K. YAMAZAKI and Y. KAGAWA, 2008. Continuous sound wave Doppler SODAR to short range wind velocity detection, Proc. of 2008 Asia Simulation Conference, Beijing China 10-12.

[2] Y.KAGAWA, T.TUCHYA, T.HARA and T.TSUJI, 2001. Discrete Huygens' modeling simulation of sound wave propagation in velocity varying environments, Journal of Sound and Vibration, **246** (**3**), p 419-439.

[3] S.P. SINGAL and B.S. GERA, 1982. Acoustic remote sensing of the boundary layer, Proc. Indian Acad. Sci. (Engg.Sci.) **5**, Pt.2, p131-157.

[4] R.L. COULTER and M.A. KALLISTRATOVA, 1999. The role of acoustic sounding in a high-technology era, Meteorology and Atmospheric physics, **71**, p 3-13.

[5] R.M. KHANNA and S.K. AGGARWAL, 1994. Doppler SODAR and measurement of atmospheric measurement, IETE Technical Review, **11**, No. 4, p 231-237.

[6] N. Lin, W. Luu, K. Sasaki and Y. Hara, 2003. Investigating wind evaluation by use of a mini Doppler SODAR, Proc. Japan Mechanical Society, **69**(**B**), No. 688, p2598-2605.

[7] T. SHU, 2004. Ultrasonic cardiac diagnosis, Proc. Of Niigata School of Medicine and Welfare Society, **4**, No.1, p103-111.

[8] T. OHTSUKA and K. SEGA, 1991. Intensive ultrasonic sound source for air with a staggered circular disc radiator, *J. Acous. Soc. Japan*, **47**, No. 4, p478-483.

Journal of Acoustical Society of India : Vol. 40, No. 1, 2013 (pp. 20-27)

Using Directivity of Radiated Sound for Noise Control Applications

Gyanishankar Sharma, Abhijit Sarkar* and N. Ganesan
Department of Mechanical Engineering, Indian Institute of Technology Madras
Chennai-600 036 (TN)
**e-mail: asarkar@iitm.ac.in*

[Received: 16.11.2012; Revised: 21.12.2012; Accepted: 07.01.2013]

ABSTRACT

In this paper a directivity based technique to control the noise radiated from vibrating plate in a baffle is presented. A novel concept of local noise control is explored by controlling the directivity pattern for the cases where global noise control is difficult to attain. Finite element simulation is done in commercial software ANSYS to obtain the displacement response. The obtained displacement response is validated by deriving an analytical formula for response using mode summation technique. In the mode summation procedure modes of the unloaded plate is used as a basis for determining the response of the mass loaded plate. This is accomplished by considering the effect of attached point mass as frequency dependent force. The surface velocity is calculated from displacement response which is used in a Rayleigh integral based calculation to arrive at sound pressure at a location and hence the directivity pattern. Control on directivity pattern is achieved by attaching discrete mass at different locations over the plate. Passive technique for noise and vibration control is known to have a poor performance for global control in low and medium frequency region. Hence control on the directivity could be a useful technique for local noise control for low and medium frequency vibration.

1. INTRODUCTION

Noise control from vibro-acoustic sources has been a widely studied topic in the engineering community [1]. Passive and active measures are used to control noise. The passive control methods are broadly classified as (1) source control - wherein efforts are made to directly reduce the source of noise viz. vibration levels, flow ripples, etc. (2) transfer path control – wherein efforts are made to reduce the transmission of the generated noise to the receiver without affecting the source. Reactive mufflers are one of the best examples in this case wherein the sound generated at the source is reflected back. Passive techniques for noise and vibration control works well for high frequency vibration whereas, active techniques spans low and medium frequency vibration. Active control techniques are costly, difficult to implement and works efficiently only for narrow frequency bands.

Noise control as we understand could be of two types i.e. global and local. In global noise control aim is to reduce noise at all the locations over the source. On the contrary in is local noise control the aim is to minimize noise at a specified receiver location. In this work, we attempt to investigate the possibility of controlling directivity as an additional technique for noise control.

In several applications there are instances where the objective of the noise control engineer is to minimize the audible noise at specific locations. For example, in automotive applications the target is to reduce the noise at the driver and passenger ear location. It is acceptable to achieve this target even at the cost of increasing

sound levels at locations away from the passengers. Thus, we attempt to explore the possibility of redistributing the available acoustic energy in different directions such that the noise levels at the specific locations of interest are reduced at the cost of increased noise levels at other locations. Similarly, the concept of directivity control for local noise control could be utilized in aerospace application to direct the radiated sound in upward direction so as to minimize the sound levels in the nearby buildings while takeoff and landing. This concept can have industrial application as well to direct the machinery noise away from direction of workers and to make workplace acceptable.

Chatillon [2] studied the influence of source directivity in noise levels inside an industrial hall through simulation and experiment. Noise level was observed to be changed by 4 dB as the source directivity changes. Zhang [3] observed different horizontal and vertical directivity pattern of railway noise through measurement. Though in the above works aim was not to control the directivity pattern, there are many literature in which the aim is to control directivity for different applications. Juhez et al. [4] developed an acoustic transducer system for long distance echo-ranging application. Directivity controlled piezo-electric transducer for sound reproduction was developed by Be'dard and Berry [5]. Seo and Kim [6] studied directional radiation pattern in structural acoustic coupled system. Three typical directivity patterns i.e. steered, focused and omnidirected are presented.

Voluminous literature is available on the study of the vibration response and acoustic radiation from mass loaded structures [7, 8, 9]. There was no literature found for acoustic directivity control from vibrating structures using passive techniques such as lumped mass addition.

2. DESCRIPTION OF THE SYSTEM

A simply-supported square thin plate is harmonically excited at the center. The structure is placed on an infinite baffle (refer Figure 1(a)). Table 1 shows the parameters for the structural and acoustic medium. The

Table 1. Parameters used for model

Size of plate	1x1x0.01 m^3	Poisson's ratio (í)	0.3
Density of plate (ñ)	7840 kg/m^3	Density of medium ()	1.2 kg/m^3
Young's modulus (E)	210x109 N/m^2	Speed of sound in medium (c)	340 m/sec

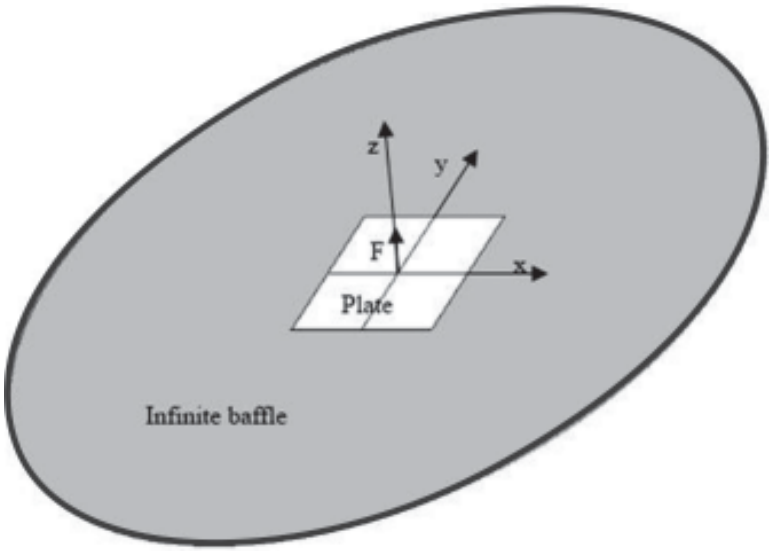

(a)

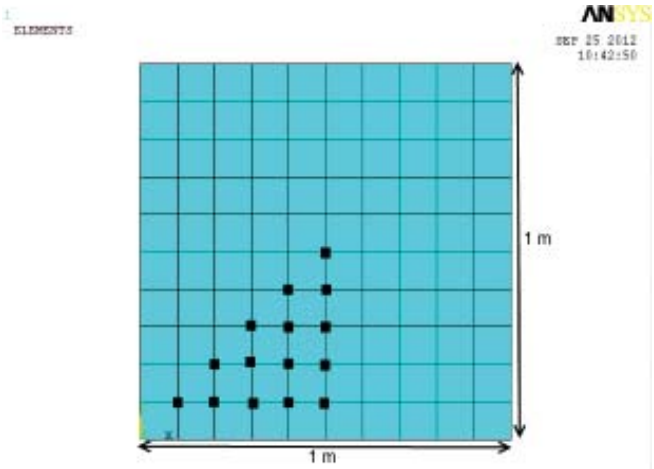

(b)

Fig. 1a. Schematic of a Simply Supported plate on a baffle with harmonic excitation at the center (b) Different locations of mass considered over the plate

applicability of this problem lies in the fact that in high frequency applications many structures of practical importance can be approximated as a rectangular plate to an extent for their sound radiation characteristics. In near field, the sound radiation has alternating maxima and minima, to ensure the decay of near field sound radiation, the analysis is done for ka=3 (where k is acoustic wave number and a is the distance between source and receiver). This allows easy computational implementation based on Rayleigh integral. The objective is to determine the baseline directivity of this vibro-acoustic system. Further, the change in directivity pattern due to lumped mass loading is to be ascertained.

3. METHODOLOGY

To demonstrate the applicability of the proposed concept, we study the directivity patterns of a simply supported plate on a baffle as described above. Accordingly, an APDL script is written to develop the vibration model for Finite element analysis in a commercial software ANSYS. The vibration model can be easily modified for the addition of masses at the desired location. A harmonic analysis is performed with a point load at the center to obtain the displacement response. The displacement response obtained is validated from analytical formula derived using mode summation technique. In mode summation procedure modes of baseline plate is used as basis functions for the response of the mass loaded plate. The response calculation is accomplished by considering the attached point mass as an additional frequency dependent force (owing to inertia forces of the attached mass) on the unloaded structure. Surface velocity can be calculated once the displacement response is known which is then used for a Rayleigh integral based calculation [10] to arrive at the sound pressure at any point of interest. The Rayleigh integral calculation is implemented through a numerical quadrature program developed in MATLAB. Sound pressure is obtained at different locations over the plate and plotted on hemispherical surface to obtain the directivity pattern. The above procedure is repeated for different locations of mass.

3.1 Principle of Directivity Control

Directivity pattern for the radiated acoustic pressure due to structural vibration in the first mode $(\sin\left(\frac{\pi x}{l}\right)\sin\left(\frac{\pi y}{l}\right))$ and second mode $(\sin\left(\frac{2\pi x}{l}\right)\sin\left(\frac{\pi y}{l}\right))$ is shown in the Fig. 2. It can be noted from these results that the dominant radiation is normal to the plate surface for the first mode whereas, the dominant radiation for the second mode is at some angle inclined to the normal of the plate. It is well known that the

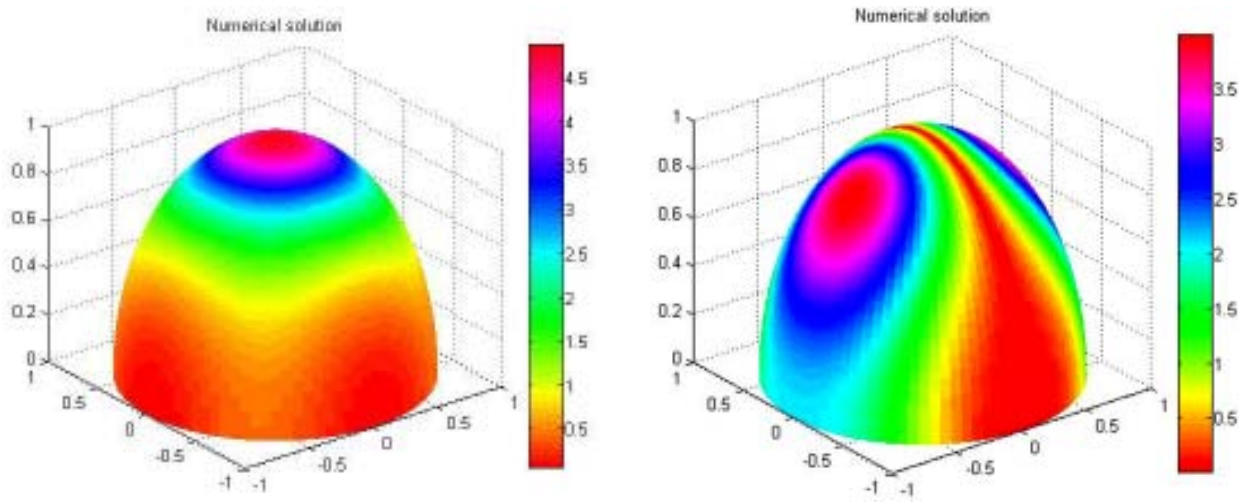

(a) First mode (b) Second mode

Fig. 2. Directivity pattern at 500Hz for (a) first mode (b) second mode of simply supported plate

harmonic forced response of a structure can be obtained as a sum of its modes [12]. Thus, it is inferred that directivity pattern can be altered by altering the modal contribution. This can in turn be achieved by attaching points mass(es) on the structure. Again, the forced response of the mass-loaded structure can be decomposed in terms of the modes of the unloaded or baseline structure. This is because the effect of local mass addition can be effectively modeled as an additional frequency dependent point force on the unloaded or baseline structure. Thus, the contributions of the modes of the baseline structure can be controlled by appropriate placement of the point mass. This forms the principle of directivity control by point mass attachment.

3.2 Natural Frequency Analysis

Analytical formula for natural frequency of baseline plate is available in [11]. Analytical formula for the mass loaded plate is derived using mode summation technique. A finite element simulation is done in ANSYS for validation and a match is obtained as shown in Table 2.

3.3 Structural Response Validation

The response of baseline plate and mass loaded plate to harmonic excitation at the center is obtained by finite element analysis of plate in commercial software (ANSYS) and is validated by developing the analytical formula using mode summation technique. The results obtained from analytical solution is in good agreement with the ANSYS solution (refer Fig. 3). In these results the mode summation was performed using 50 modes of the baseline plate.

Table 2. Natural frequency of baseline mass loaded plate

	Base line plate (Hz)		Mass loaded plate(Hz) (with added mass = 20% of plate mass)	
Mode	Analytical	Ansys	Analytical	Ansys
(1,1)	49.20	49.20	46.58	46.48
(2,1)	123.00	123.00	94.31	91.56
(1,2)	123.00	123.00	122.97	122.97
(2,2)	196.81	196.77	162.37	157.91
(3,1)	246.01	245.98	227.50	224.25
(1,3)	246.01	245.98	245.90	245.90

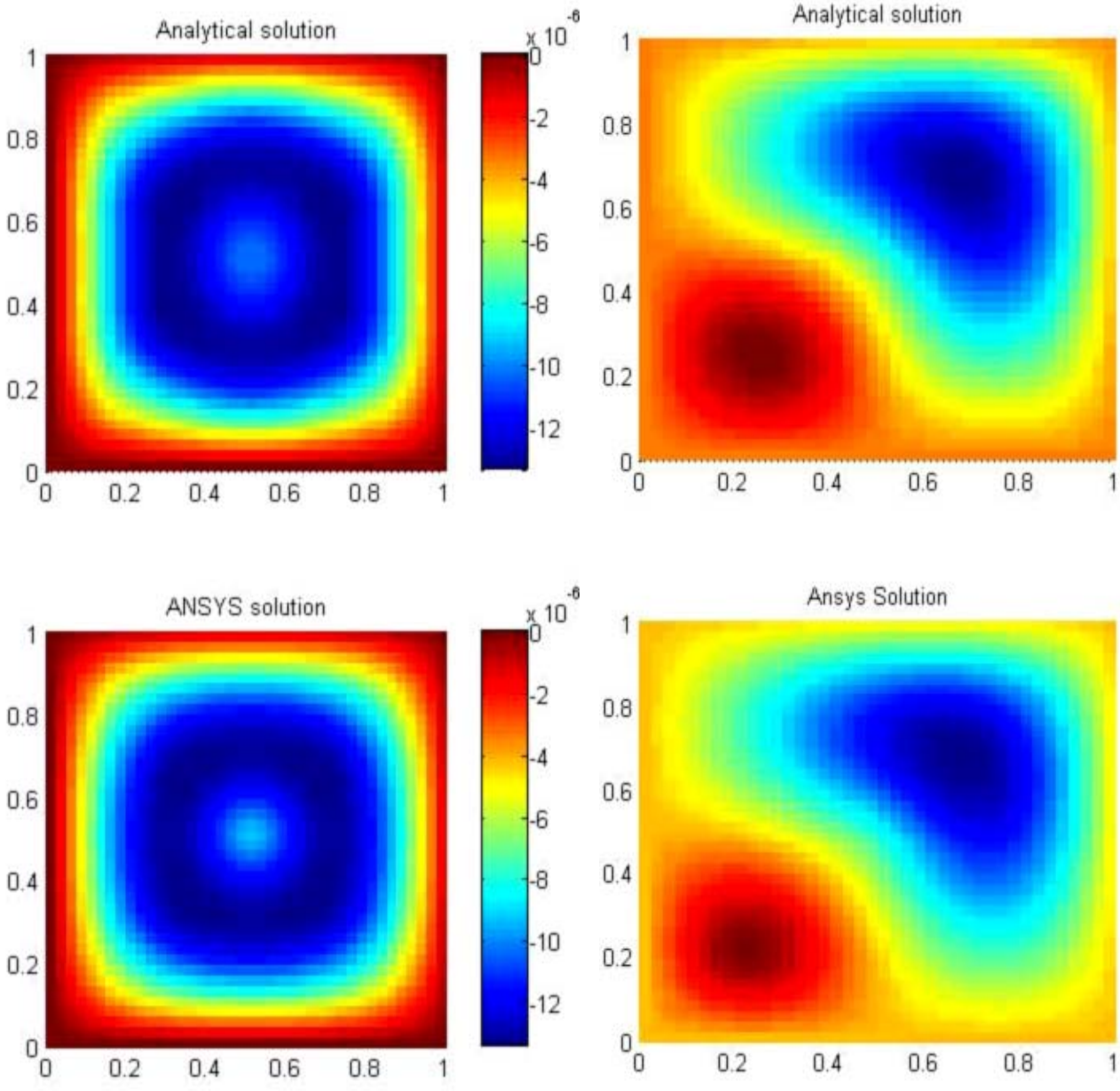

(a) Baseline plate (b) Mass loaded plate

Fig. 3. Response of plate to harmonic excitation at the center from modal summation technique (upper) and ANSYS (lower)

3.4 Directivity Pattern

The various locations of mass over the plate are considered as shown in Figure 1(b) which due to symmetry spans the complete plate. Directivity pattern for all these locations of mass over the plate is analyzed. The top view of hemispherical directivity pattern of baseline plate and mass loaded plate (with added masses = 20 % of plate mass) at 100 Hz excitation frequency and ka=3 is shown in the figures below.

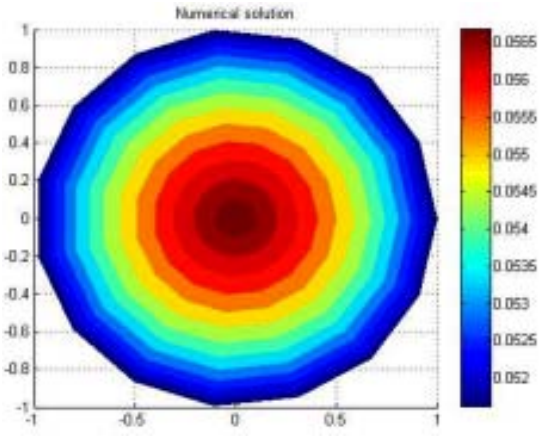

(i) Baseline plate

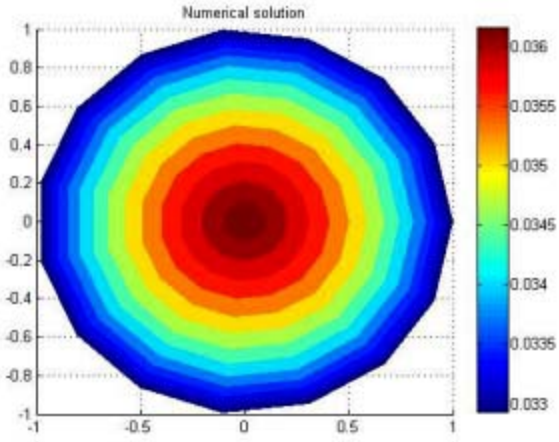

(ii) Mass loading at (0.5, 0.5)

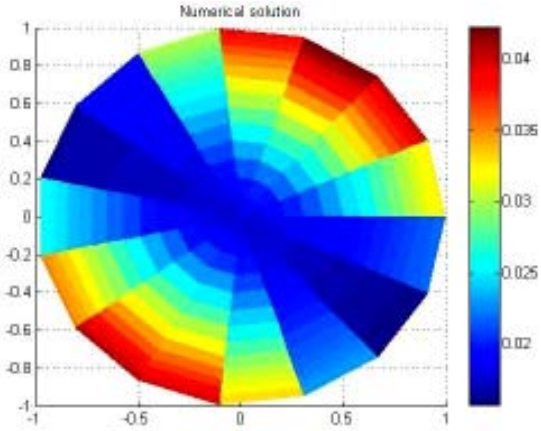

(iii) Mass loading at (0.4, 0.4)

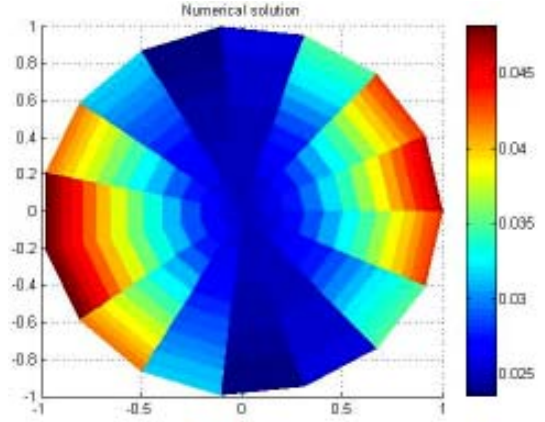

(iv) Mass loading at (0.5, 0.1)

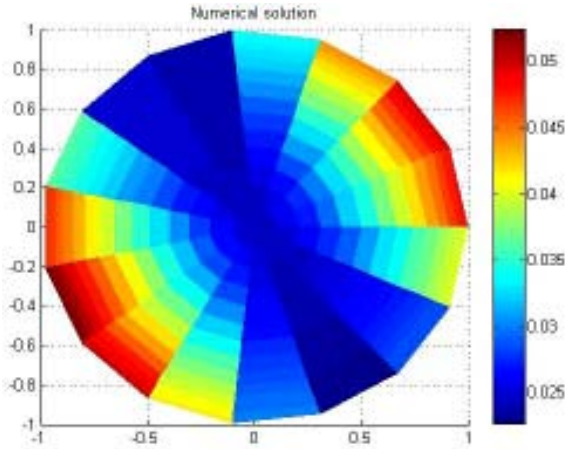

(v) Mass loading at (0.4, 0.1)

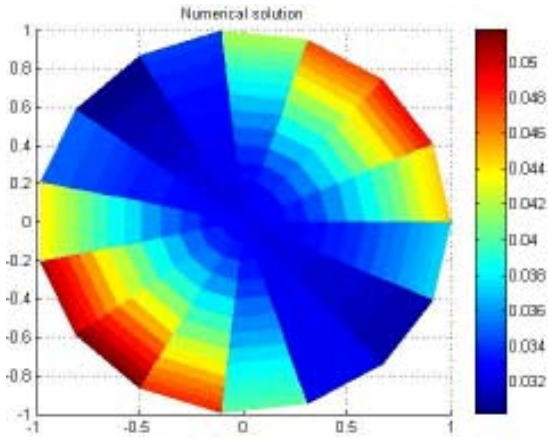

(vi) Mass loading at (0.3, 0.1)

Fig. 4. Directivity pattern from square plate simply supported on all side and harmonic point excitation at the center

4. DISCUSSION

On analyzing the above results of directivity pattern, it is seen that the directivity pattern of baseline plate can be altered by attaching additional mass. The location and magnitude of mass addition plays an important role in controlling the directivity pattern so as to reduce noise at different planes over the plate.

It is seen that when mass location is same as that of forcing the sound pressure is reduced at all the location whereas, directivity pattern is unaltered (refer Figure 4(ii)). This is due to decrease in forcing which results in decrease in vibration.

In the following we present a representative analysis of directivity pattern of baseline plate and mass loaded plate (0.4, 0.4). To give the vibration response of the plate as a single number for quantitative analysis, we calculated the root mean square value of displacement over the plate. This is in consonance with radiation efficiency analysis in acoustics [10]. The RMS value of displacement response of the mass-loaded plate is calculated to be 1.74 times that of the baseline plate. Hence, the vibration is increased due to mass addition. The reason could be explained as we are adding mass on stiffness controlled region. The total sound energy radiated $(\text{using the formula } E = \int_A \frac{p^2}{2\rho_0 c} dA)$ for the baseline plate and mass loaded plate is computed to assign a single quantitative value of sound radiation. It is observed that the total radiated sound energy is decreased by a factor of 3.57 due to mass addition. Thus, the sound pressure averaged (in terms of energy) over all the directions is decreased by a factor of 1.88. In Figure 5, the ratio of sound pressure from baseline plate to sound pressure from mass loaded is plotted on hemispherical surface over all the directions. It is observed from this figure that the sound pressure is decreased at all points. However, the factor by which the sound pressure decreases, varies between 1.4 to 3.2 over different locations (refer Figure 5). Thus, the redistribution of acoustic energy is happening in this case, resulting in higher sound pressure reduction at some locations. The result is interesting as we noted that the vibration increases. However, the observed decrease in acoustic radiation is attributed to phase cancellations between regions of positive and negative vibration response.

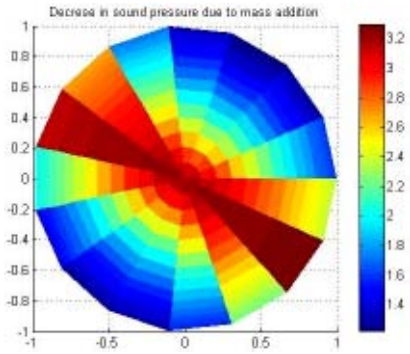

Fig. 5. Ratio of sound pressure from baseline plate to mass loaded (0.4, 0.4) plate plotted over hemispherical surface over the plate

5. CONCLUSION

It is well known that for low and medium frequency vibration passive noise control measures such as point mass attachment etc. are not efficient to control noise in global sense. Thus, directivity of radiated noise can be employed to achieve the noise control locally. In this work, we propose a concept of achieving local noise control in specific directions of interest. This is demonstrated through a model problem of a simply-supported plate in a baffle. For this model problem, the analytical formulation is accomplished and the results are also validated through numerical simulations. The limitation of present analysis is that external point mass addition to the structure may not be acceptable in many applications e.g. external mass attachment may lead to more fuel consumption for aerospace or automobile application. Topology optimization is a possible solution to

above limitation where one can actually remove some mass over the plate to control directivity. The external point mass can also be embedded in flat plate itself by thinking of functionally graded material to create the density difference. As future work similar demonstrations need to be carried on for more complicated structures such as curved shells, built-up strctures, composites, etc. In this work we have demonstrated the concept for a specific model problem i.e. fixed dimension steel plate radiating noise into air. As a future work, the results obtained can be generalized by appropriate non-dimensionalization. A numerical algorithm to find optimal location(s) and magnitude of mass is also planned as future work.

6. REFERENCES

[1] D.A. BIES and C.H. HANSEN, 2003. Engineering Noise Control: Theory and practice, Spon press.
[2] J. CHATILLON, 2007. Influence of source directivity on noise levels in industrial halls: Simulation and experiments, Applied Acoustics, **68** (682).
[3] X. ZHANG, 2010. The directivity of railway noise at different speeds, *Journal of Sound and Vibration,* **329** (5273).
[4] J. A. GALLEGO-JUHEZ, G. RODNGUEZ, J.L. S. EMETENO, P. T. SANZ and J. C. LHZARO, 1993. An acoustic transducer system for long-distance ranging applications in air, Sensors and Actuators A, **37** (397).
[5] M. BE'DARD AND A. BERRY, 2008. Development of a directivity-controlled piezoelectric transducer for sound reproduction, *Journal of Sound and Vibration,* **311** (1271).
[6] H.S. SEO and Y.H. KIM, 2005. Directional radiation pattern in structural-acoustic coupled system, *J. Acoust. Soc. Am.,* **118** (92).
[7] A.E. EKIMOV and A.V. LEBEDEV, 1996. Experimental Study of Local Mass Influence on Sound Radiation From a Thin Limited Cylindrical Shell, Applied Acoustics, **48** (47).
[8] S. LI AND X. LI, 2008. The effects of distributed masses on acoustic radiation behaviour of plates, *Applied Acoustics,* **69** (272).
[9] J.S. WU and S.S. LUO, 1997. Use of analytical numerical combined method in the free vibration analysis of a rectangular plate with any number of point masses and translational springs, *Journal of Sound and Vibration,* **200** (179).

Journal of Acoustical Society of India : Vol. 40, No. 1, 2013 (pp. 28-33)

Wave Theory Approach for Developing the Mathematical Model of the Right Angled Joint

V.H. Patil and D.N. Manik
Department of Mechanical Engineering
Indian Institute of Technology, Bombay-400 076

[Received: 13.11.2012; Revised: 28.11.2012; Accepted: 08.01.2013]

ABSTRACT

In this study, vibrational energy distribution within the audible frequency range is considered between two plates. The two plates are connected to form a welded joint (line connection), riveted and bolted joint (point connection). The mathematical model for the joints is developed using a spring and dashpot model. The wave approach is used to develop the mathematical model of the coupled plate. The bending wave transmission and reflection efficiencies are determined. The limiting value of high stiffness joint is determined, which represents the weld joint like a rigid joint. The bolt and rivet joints are modelled, with spring dashpot in only one direction and in another direction the joint is considered as rigid. After studying the stiffness effect, the mathematical model is updated to include damping at the joint. The damping has smoothening effect on these efficiencies.

1. INTRODUCTION

Joints are an important part of any complex structure. The waves propagating from one component to other pass through these joints. The joint has its own stiffness and damping, which particularly attenuates the incident wave and then transmits the rest to the other connected component. Leung and Pinnington1 applied wave theory to a right angled joint with compliance. They have found the transmission and reflection coefficients for the joints. The stiffness and damping at the joint are the major factors which influence energy transfer between the coupled systems. Cremer2 and others have studied the attenuation of an incident wave through a joint. Ungar3 has given detailed classification of the damping present in a system, which is responsible for the energy loss. Yoshimura and Okushima4 developed a method to identify the quantitative values of the rigidity and damping coefficients at the joint surface by interactive use of theoretical simulation and experiment. Mead5 worked on aircraft structures having riveted and bolted joints.

2. JOINT MODEL

Figure (1) shows the right angle joint model with spring dashpot attached. For the cases of a joint with springs in all three degrees of freedom, wave approach is used to analyse the joint. In the Fig. (1) k_2, k_2 are linear stiffness and k_3 is rotational stiffness. Similarly, c_1, c_2 and c_3 are the viscous dampers. The plate 1 is in x-z plane and plate 2 is in y-z plane. Both the plates are symmetric about the z axis, in z plane. The coordinate system is taken at the mid of the both plates in z plane and at the joint location. The coordinate system represents $x=0$, $y=0$, $z=0$ at the joint.

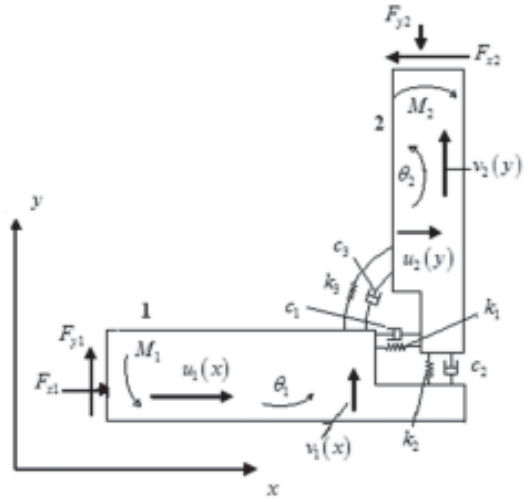

Fig. 1 Linear spring-dashpot model of joint

Consider the incident wave of amplitude A_1 travelling towards the joint in plate 1. Therefore, the wave field in the component 1 is composed of three parts; incident wave, reflected wave and near field wave at the joint. The transverse displacement is given as $v_1(x)$ is given as

$$v_1(x) = A_1\left(e^{-jk_{b1}x} + r_B e^{jk_{b1}x} + r_{B,n} e^{k_{b1}x}\right) \tag{1}$$

In plate 2, the transmitted bending wave and near field wave at the joint gives the transverse displacement $u_2(y)$ as $u_2(y) = A_1\left(t_B e^{-jk_{b2}y} + t_{B,n} e^{-k_{b2}y}\right)$ (2)

where r_B, $r_{B,n}$, t_B and $t_{B,n}$ are the bending wave reflection coefficient, bending wave near field reflection coefficient, bending wave transmission coefficient and bending wave near field transmission coefficient respectively. Here, k_{b1}, k_{b2} are the bending wave numbers for plate 1 and 2 respectively. As the bending wave goes through a corner, longitudinal wave will be induced in both the components as

$$u_1(x) = A_1 r_L e^{jk_{L1}x};\ v_2(y) = A_1 t_L e^{jk_{L2}y} \tag{3}$$

where, r_L, t_L are the longitudinal wave reflection and transmission coefficients respectively. Also k_{L1} and k_{L2} are the wave numbers, generating longitudinal wave in component 1 and 2 respectively.

By equating forces and moments at the joint, boundary conditions developed for the determination of coefficients are

$$\begin{aligned} F_{x1} &= F_{x2} = Z_x(u_1 - u_2); \\ F_{y1} &= F_{y2} = Z_y(v_1 - v_2); \\ M_1 &= M_2 = Z_\theta(\theta_1 - \theta_2). \end{aligned} \tag{4}$$

The transmission coefficients t_B, t_L and reflection coefficients r_B, r_L are determined from the equations (1 to 4).

$$r_B = \frac{[(1-j)(Z_2+\beta_2)-2]}{[(1+j)(Z_2+\beta_2)+2]} - \psi t_B \frac{[(1+j)(Z_1+\beta_1)+2][1+j(Z_2+\beta_2)]}{[1+j(Z_1+\beta_1)][2+(1+j)(Z_2+\beta_2)]} \tag{5}$$

$$t_B = \frac{2[Z_1+\beta_1+Z_2+\beta_2]-2j[1-(Z_1+\beta_1)(Z_2+\beta_2)]}{D} \tag{6}$$

where
$$\begin{aligned} D = {} & X\{-1+j-2(Z_1+\beta_1)-(Z_2+\beta_2)-(1+j)(Z_1+\beta_1)(Z_2+\beta_2)\} \\ & +\psi\{-1+j-(Z_1+\beta_1)-2(Z_2+\beta_2)-(1+j)(Z_1+\beta_1)(Z_2+\beta_2)\} \\ & +\psi Z_3\{-(Z_1+\beta_1)(Z_2+\beta_2)+2j-(1-j)(Z_1+\beta_1)-(1-j)(Z_2+\beta_2)\}. \end{aligned} \tag{7}$$

where

$$\beta_1 = (m_2 C_{B2})/(m_1 C_{L1}); \beta_2 = (m_1 C_{B1})/(m_2 C_{L2}); Z_x = (k_1/j\omega)+c_1; Z_y = (k_2/j\omega)+c_2;$$

$$Z_\theta = (k_3/j\omega)+c_3; Z_1 = m_2 C_{B2}/Z_x; Z_2 = m_1 C_{B1}/Z_y; Z_3 = B_1/(C_{B1} Z_\theta); \psi = \frac{k_{b2}^2 B_2}{k_{b1}^2 B_1}; X = k_{B2}/k_{B1}$$

The efficiencies for the transmitted and reflected bending waves and longitudinal waves are

$$\tau_B = X\psi |t_B|^2; \rho_B = |r_B|^2 \tag{8}$$

2.1 Weld Joint (Rigid Joint)

The weld joint mathematical model is obtained by setting k_1, k_2, k_3 to infinity in Eqs. (5) to (8). Therefore, dimensionless terms Z_1, Z_2, Z_3 become zero.

2.2 Bolt/Rivet Joint (Joint with compliance in only one direction).

Similarly, for the bolt/rivet joint mathematical model is obtained by setting $X = \psi = 1, \beta_1 = \beta_2 = \beta$ and $Z_1 = Z_3 = 0, u_1 = u_2, \theta_1 = \theta_2.$ in Eqs. (5) to (8).

3. RESULTS

Here the two mild steel plates, each of size 300 X 300 X4 mm were considered to form a weld joint, bolt/rivet joint. The critical frequency f_{cr}, for 4 mm thickness plate is 3210 Hz. The transmission and reflection efficiencies are plotted against frequency in Figs. (2) to (3), without considering the damping at the joint.

From Fig. (2), the maximum value of τ_B for low stiffness value to very high stiffness is approximately 0.48. This indicates that a maximum up to 48% of the supplied energy is transmitted by a flexural wave. As the joint stiffness increases, the frequency for attenuation of increases. Reflection efficiency ρ_B plotted against frequency in Fig. (3), almost 50% to 90% of supplied energy is reflected back by the softer joint. A very stiff joint 10 GN/m to N/m, reflect less amount of energy compared to softer joint. The peaks in the reflection efficiency are observed for stiffness value of 1 MN/m and 100 MN/m in the frequency range at the same location where dips are observed in Fig. (2). From Figs. (2) and (3), the efficiency plots for $k_y = \infty$ N/m resemble the efficiency plot in for a rigid joint. Therefore 100 GN/m stiffness is taken as joint stiffness value for the weld joint.

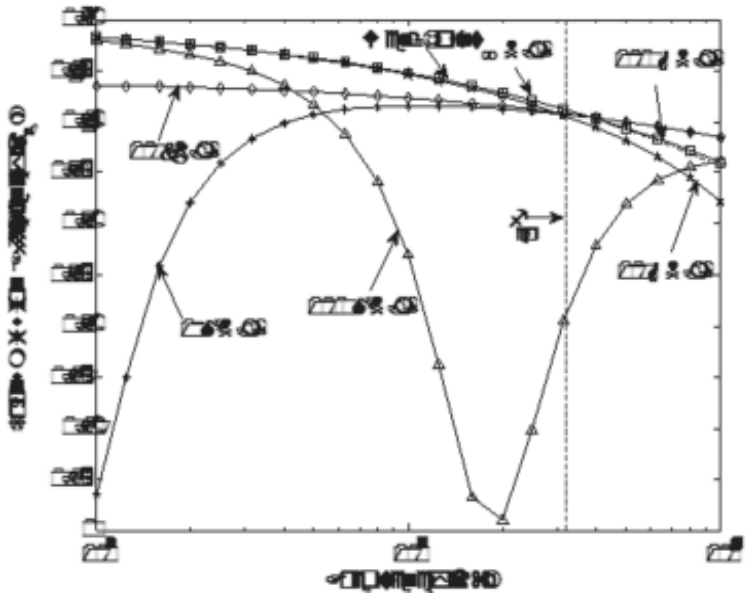

Fig. 2. Bending wave transmission efficiency (τ_B) for various stiffness values

4. EFFECT OF DAMPING

The effect of damping on the τ_B and ρ_B efficiencies of the coupled plates is shown in Figs. (4) and (5).

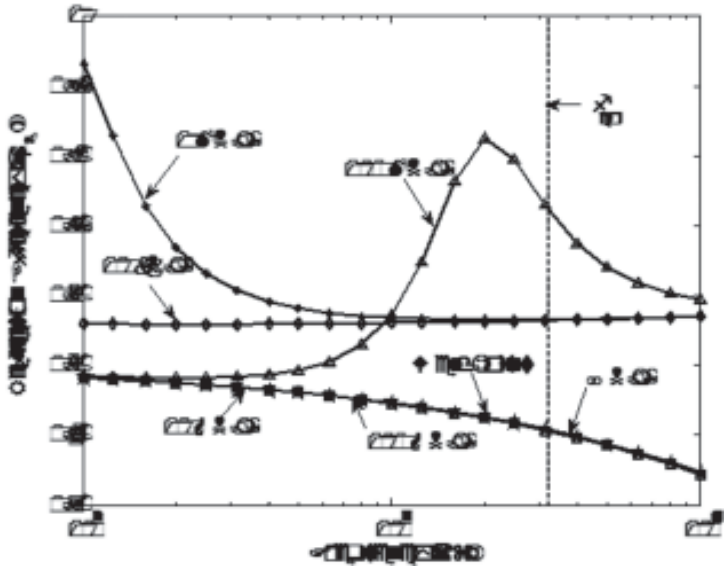

Fig. 3. Bending wave reflection efficiency (τ_B) for various stiffness values.

Here, the assumption of viscous damping is used to represent the joint damping. The curve becomes smooth as damping increases. At very high damping, τ_B never becomes zero as compared to lower damping value of zero and 100 Ns/m. Similarly, the peak in the ρ_B decreases and becomes smooth with the increase in the damping.

5. CONCLUSION

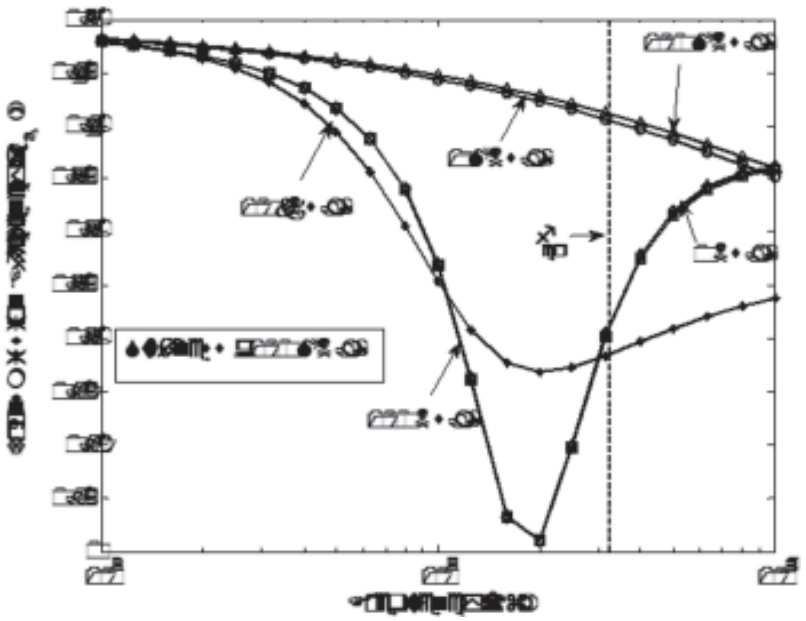

Fig. 4. Effect of variation of damping on bending wave transmission efficiency (τ_B)

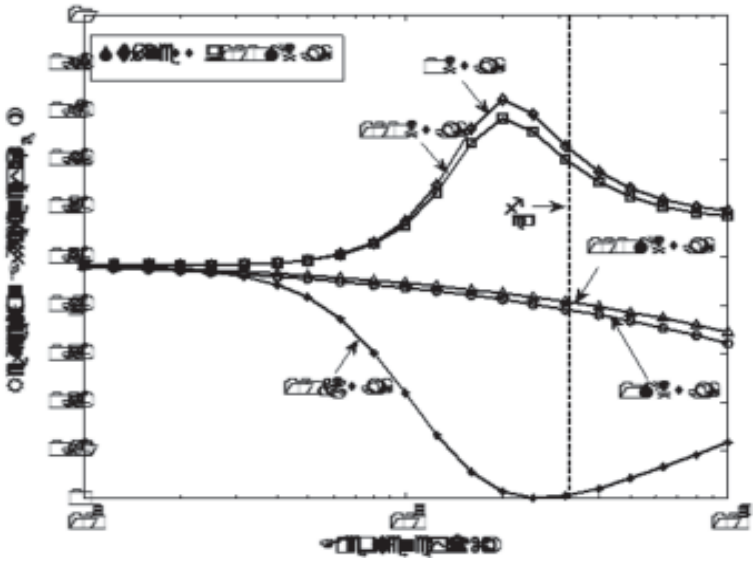

Fig. 5. Effect of variation of damping on bending wave reflection efficiency (ρ_B)

In conclusion, the limiting value of stiffness (100 GN/m) for weld joint is obtained. For riveted and bolted joints, stiffness has more effect on the energy transfer between the coupled systems and the effect of damping is more at low stiffness of the joint. The damping can be controlled by application of lubricating layer between the two faces. The bending wave transmission efficiencies determined can be used to determine the coupling loss factor of the various joint connections.

6. REFERANCES

[1] LEUNG, R. and PINNINGTON, R. Wave propagations through right angled joints with compliance – flexural incident wave, *Journal of Sound and Vibration*, **142** (1), 31-46,(1990).

[2] CREMER, L., HECKL, M. and UNGAR, E.E. *Structure-Borne Sound* , Berlin: Springer-Verlag, (1987).

[3] UNGAR, E.E. The status of engineering knowledge concerning the damping of built- up structures, *Journal of Sound and Vibration,* **26**(1), 141-154, (1973).

[4] YOSHIMURA, M. and OKUSHIMA, K. Measurement of dynamic rigidity and damping property for simplified joint models and simulation by computer, *Annals of CIRP* **25**, 193-198, (1977).

[5] MEAD, D. J. The damping, stiffness a fatigue properties of joints and configuration representative of aircraft structures, *WADC-University of Minnesota Conference Acoustical Fatigue,* 235-261, (1961).

Journal of Acoustical Society of India : Vol. 40, No. 1, 2013 (pp. 34-39)

Noise pollution in Wards of a Hospital in Tiruchirapalli City

V. Bhanumathy, R. Geetha and M. Sangeetha
Department of physics, Seethalakshmi Ramaswami College, Tiruchirapalli

[Received: 18.11.2012; Revised: 28.11.2012; Accepted: 08.01.2013]

ABSTRACT

Environmental noise present in hospitals is a common stressor and is recognized as a serious health hazard for patients, doctors and medical care workers. The aim of the work is to assess the existing noise levels in a 112 bed hospital situated in the heart of Tiruchirapalli city. The plan of the study was to measure the variations of noise in various wards of the hospital and appraise the main sources of noise. Noise levels in 12 places , 6 inside the wards and 6 outside the wards were measured at two and a half hour intervals over a period of 12 hours. The equivalent sound level and peak sound pressure levels were monitored by a digital sound level meter Quest suite professional 2900, during a week in May 2012. The highest mean Leq(A) was 67.7 dB(A) and maximum noise level was 80.6 dB(A) during the measurement time in female ward and the lowest mean Leq(A) 62.1 dB(A) and minimum 55.8dB(A) in the general ward. Maximum noise levels were recordrd in the reception outside the wards of the hospital.The observed noise levels exceeded the recommended CPCB & WHO guidelines for hospitals. It is found that ward structures, location and various activities like conversation of patients, nurses , visitors and traffic resulted in different levels of noise in different wards. The study concludes that noise is a problem in the city hospital where the study was undertaken.

1. INTRODUCTION

Hospitals are extremely noisy, and noise levels in most hospitals far exceed recommended guidelines. Many studies have revealed that extended exposure to noise pollution may cause auditory and non-auditory disorders, such as temporary or permanent hearing loss, sleep disruption(Freedman et al.,), cardiovascular dysfunction, speech interference and mental health distortion(Ising and Kruppa). Conversation among patients, staff and visitors, sounds of doors, carts, phones, beepers, movement of hospital equipment etc., make up the "Sound environment" which is a risk to healthcare. Whether by accident or incident, the accumulation of noise and unwanted distraction add up to a negative healthcare experience. The United States Environmental Protection Agency (USEPA) recommended a guideline value for continuous background noise as 45 dB(A) during the day and 35 dB(A) at night in patients' room. The International Noise Control and the World Health Organizations (WHO) have recommended that noise levels in hospital areas should be 35-40 dB in the day time and 30-40dB(A) in the evening.. In India, noise around hospitals is around 85 dB(A) in major cities(The Hindu Dec 10, 2010). The present study was undertaken to assess noise levels, patterns and sources on wards in a 112 bed room hospital at the heart of Thiruchirapalli city.

2. MATERIALS AND METHODS

The study was conducted after obtaining institutional ethical clearance at the 112 bedded hospital with

a bed occupancy rate of 85% and a daily attendance of about 350 outpatients. The hospital is located in a commercial area at the heart of Tiruchirapalli city housing many shopping complexes with hectic activity from morning 7a.m to evening 9p.m.Many two wheelers and automobiles ply near the hospital and traffic hold up is a frequent event. Impatient drivers honk their horns unmindful of the presence of a big hospital. Sound levels in 12 places inside the hospital were recorded using a Digital Sound Level Meter (Quest suite Professional 2900) in dB (A) units, representing the sound level measured with the A-Weighting network. The instrument incorporates a type-1 microphone and records sound ranging from 50-110 dB(A). Fast mode was used to record the readings. The Sound Level Meter was placed at body level for measurements. The readings were taken throughout the day at five minute interval between successive recordings. Observations were done in one week during the morning 7.30-10.00 a.m., forenoon 10.30-1.00 p.m., afternoon 1.30-4.00 p.m., and evening 4.30-7.00 p.m. The parameter used in the discussion of noise pollution is the equivalent continuous noise level (L_{eq}) expressed in dB(A) which is the mean rate at which energy is received by the human ear during the period monitored. The other variables obtained were the maximum (L_{max}) and minimum (L_{min}) at each place. The data were tabulated using Microsoft excel 2010 and descriptive statistics carried out using the statistical package SPSS for windows, version 14.0.

3. RESULTS AND DISCUSSION

The values of equivalent sound levels (L_{eq}), Standard Deviation (SD), maximum (L_{max}) and minimum (L_{min}) sound levels inside and outside the wards during the measurement periods are shown in Tables 1&2 and L_{eq}

Table 1. Equivalent continuous noise level(L_{eq}), standard deviation(SD), maximum (L_{MAX}) and minimum (L_{MIN}) readings dB(A) inside the wards in the hospital

Time	Ward	Noise levels dB(A)			
		Leq	SD	LMAX	LMIN
7.30-10.00	Male ward	65.46	1.41	80.37	56.80
	Female ward	66.14	1.02	79.91	60.21
	General ward	63.03	1.00	77.24	57.21
	ICU	61.41	1.40	78.10	50.84
	Single room	67.79	2.30	82.29	62.47
	Triage	67.34	1.62	81.23	63.00
10.30-13.00	Male ward	67.30	1.43	81.89	58.49
	Female ward	67.63	1.15	82.14	60.46
	General ward	63.56	2.76	79.67	56.97
	ICU	64.80	2.03	81.70	52.16
	Single room	66.34	0.83	78.99	60.80
	Triage	67.89	2.11	83.41	59.19
13.30-16.00	Male ward	67.07	1.02	82.53	58.87
	Female ward	67.70	1.24	80.56	59.84
	General ward	64.40	3.29	78.26	57.34
	ICU	64.07	1.02	80.60	51.74
	Single room	67.97	1.86	81.36	62.76
	Triage	68.96	1.41	84.03	61.91
16.30-19.00	Male ward	64.03	6.56	79.54	55.46
	Female ward	65.16	6.71	78.69	57.83
	General ward	62.09	3.49	76.41	55.81
	ICU	63.36	3.09	82.44	48.03
	Single room	67.97	2.18	83.36	60.43
	Triage	67.80	1.57	82.29	62.14

Table 2. Equivalent continuous noise level(L_{eq}) , standard deviation(SD), maximum (L_{MAX}) and minimum (L_{MIN}) readings dB(A) outside the wards in the hospital

Time	Sites	Noise levels dB(A)			
		Leq	SD	LMAX	LMIN
7.30-10.00	Lecture hall	71.04	5.45	82.07	62.26
	Pharmacy	65.00	3.19	81.60	55.40
	Corridor	66.81	1.62	81.20	59.11
	Reception	68.27	2.71	83.77	60.70
	Auditorium	62.37	5.39	74.96	56.31
	OP	64.06	5.92	79.50	56.10
10.30-13.00	Lecture hall	66.46	1.52	76.37	63.71
	Pharmacy	70.31	2.05	89.36	58.06
	Corridor	68.54	1.20	83.80	60.54
	Reception	71.87	1.19	90.49	60.66
	Auditorium	67.20	2.66	82.76	59.66
	OP	68.90	1.56	82.54	59.57
13.30-16.00	Lecture hall	68.81	1.62	81.21	63.11
	Pharmacy	72.51	2.35	91.20	60.23
	Corridor	68.03	1.45	82.34	61.16
	Reception	71.24	2.32	87.89	62.41
	Auditorium	67.34	2.54	80.29	61.26
	OP	68.33	1.42	82.47	60.34
16.30-19.00	Lecture hall	63.61	6.36	77.50	59.29
	Pharmacy	72.14	2.13	90.71	60.17
	Corridor	67.66	0.48	82.66	60.66
	Reception	70.84	3.01	87.16	62.47
	Auditorium	66.80	1.50	77.33	61.49
	OP	69.51	3.34	85.29	59.36

pattern over the day are displayed in Fig. 1 & 2. On all monitored wards the average equivalent sound levels (L_{eq}) were 65.73±2.75 dB(A), 67.57± 1.71 dB(A), 68.04±1.80 dB(A) and 66.75±3.37 dB(A) during morning, forenoon, afternoon and evening respectively.

Inside the wards, ICU and general ward were the quietest (63.74 & 64.24 dB(A)), as the general ward had partitions for individual patients and visitors were restricted inside the ICU. Triage being the casuality hall, had more patients and attendantsand tended to be the noisiest (69.82 dB(A)).

The present study reveals that the average equivalent sound levels (L_{eq}) in all places in the chosen hospital exceeded the WHO guidelines. The heavy inflow of about 350 patients and more than 100 students everyday with no restriction on the number of visitors are the contributing factors to such high noise levels. It is astonishing to note that even the lowest recorded noise level was 20 dB(A) more than the recommended WHO level of 40 dB(A). Such high levels could slow down the recovery of patients, sick children and might contribute to undesirable physiological and behavioral effects on the children admitted.

The highest L_{eq}(72.51dB(A)) and maximum (91.20 dB(A)) sound levels were recorded in the pharmacy followed by reception and corridor,outside the patients' wards. Pharmacy was the nosiest place in the entire hospital during the whole day except in the morning 65 dB(A) because of heavy influx of patients, visitors, movement of ambulance and vehicles as this is situated very close to the city road. Noise contribution on the ward corridors came from movement of hospital equipments and conversation of nurses as nursing stations were close to all the corridors of the hospital.

Table 3. Average L_{eq} dB(A) over the day in the hospital

Time	Leq	SD	95% CI lower	95% CI Upper
Morning	65.73	2.75	63.98	64.47
Forenoon	67.57	2.24	66.14	68.99
Afternoon	68.03	2.37	66.53	69.54
Evening	66.02	3.15	64.75	68.75

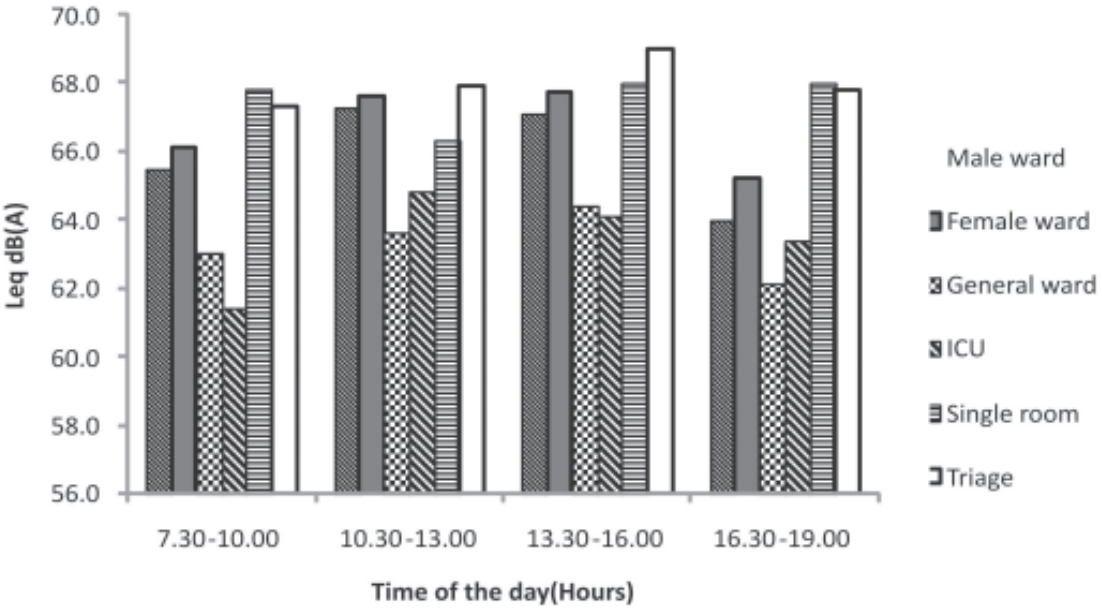

Fig. 1. Noise levels inside the wards

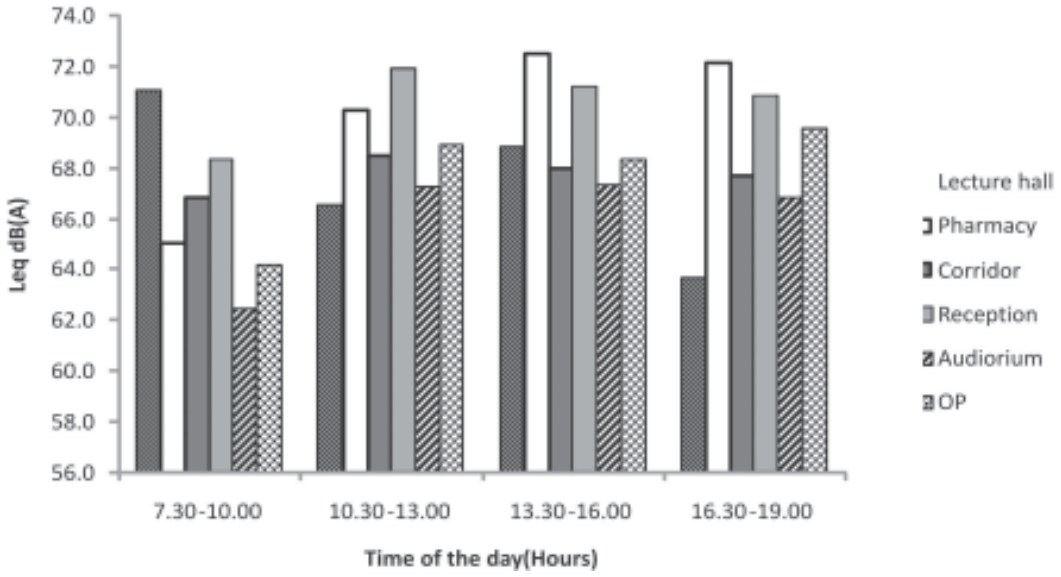

Fig. 2. Noise levels outside the wards

Table 4. The Leq dB(A) values in the hospital at various places and their confidence intervals

Places	Leq	SE	95% CI lower	95% CI Upper
Male ward	68.51	0.32	67.88	69.14
Female ward	66.68	0.15	66.38	67.00
General ward	64.24	0.27	63.71	64.78
ICU	63.74	0.28	63.18	64.30
Single room	64.92	0.12	64.68	65.15
Triage	69.82	0.19	69.44	70.2
Lecture hall	66.95	0.07	66.8	67.1
Pharmacy	71.94	0.24	71.45	72.42
Corridor	69.79	0.15	69.5	70.09
Reception	69.16	0.18	68.81	69.51
Auditorium	64.42	0.13	64.16	64.68
OP	66.63	0.16	66.01	66.65

It can also be observed in Table 3 that morning was the quietest time and the afternoon ,quite noisy. The L_{eq} measurements for each ward and their confidence intervals show that ICU and general ward tended to be the quietest because general ward was separated with partitions for individual patients (Table 4). The mean values of noise in general ward, ICU and single room turned out to be the same ($p>0.05$) and the means were different in all the other wards ($p<0.05$) It can also be observed in Table 4 that morning wass the quietest time and the afternoon ,quite noisy.

The noise levels were similar to the values measured in the post anesthesia care unit of a hospital in Lyon, France(67.1dB(A))(Allaouchiche, 2002), and certainly greater than in countries like Taiwan (52.6 to 64.6dB(A)) (Yar-YuanPai 2007, Juang,2010), Tanzania(45.7 to 62.dB(A)) (Moshi 2010,Philomini 2011) Athens, Greece()(Tsiou c 1998, Tsara v., 2008) and Slovok Republic(35 to 60dB(A))(Sobotova.pdf)

The strategies should focus on the co-ordination and limitation of activities by nurses and visiting patients' relatives and conversation only in a low voice. It should be noted that the physical status of wards, proper site location for hospitals, municipal planning, traffic, equipment selection and maintenance are also necessary for the reduction of hospital noise.

4. CONCLUSION

This study shows that there is noise pollution problem on wards of the chosen hospital in Thiruchirapalli city which can cause interference with the doctor-patient relationship and patient care services. The measured noise levels were found to be higher than WHO acceptable limit on hospital buildings. It is observed in this study that conversations of patients and nurses, movement of hospital equipment, overcrowding of patients' relatives vehicular noise are important contributors to noise levels on wards. Therefore, noise monitoring for an optimal hospital environment and the study of the influence of noise, on the quality care and the performance of staff are further needed.

5. REFERENCES

[1] A. ANNA MOSHI, 2010. *et al.*, Noise Pollution on Wards in Iringa Regional Hospital, Tanzania. *World Applied Sciences Journal* **11** (**5**): 599-603.

[2] B. ALLAOUCHICHE, 2002. *et al*., Noise in the postanaesthesia care unit, *British Journal of Anaesthesia* **88**(**3**) 369-73.

[3] FREEDMAN N.S., KOTZER N. and SCHWAB R.J., 1999. Patient perception of sleep quality and etiology of sleep disruption in the intensive care unit. Am. J. Respir. Crit. Care Med., **159**(**4**), 1155-11622.

[4] Hospitals suffer from serious pollution- The Hindu,Dec 10,2010

[5] ISING, H. and B. KRUPPA, 2004. Health effects caused by Noise: Evidence in the Literature from the past 25 years. Noise Health, **22**: 5-13.
[6] D.F. JUANG; 1C.H. LEE; 1T. YANG; 2M.C. CHANG, 2010. Noise pollution and its effects on medical care workers and patients Environ. Sci. Tech., **7** (**4**), 705-716, Autumn.
[7] KULWA M. PHILIMONI, 2011. *et al*., Noise Pollution on Wards in Bunda District Hospital in Lake Victoria Zone, Tanzania. International Journal Of Environmental Sciences **1**, No 5.
[8] SABOTOVA *et.al*., The acoustical environment and health risk in hospitals http://isee.ehc.ro/past_celadna/session3/11_sobotova.pdf.
[9] TSARA V, NENA E, SERASLI E, VASILEIADIS V, MATAMIS D and CHRISTAKI P., 2008. Noise levels in Greek hospitals. Noise Health **10**:110-2.
[10] TSIOU C, EFTYMIATOS D, 1998. *et al*., Noise sources and levels in the Evgenidion Hospital intensive care unit. Intensive Care Med. Aug; **24** (**8**):845-7.
[11] WHO guidelines for Community Noise, World Health Organisation (WHO), 2010. <http://whqlibdoc.who.int/hq/2010>
[12] YAR-YUAN PAI, 2007. International Journal of Occupation Safety Ergon; Vol 13: 83-90.

Journal of Acoustical Society of India : Vol. 40, No. 1, 2013 (pp.40-45)

Preliminary Study on Automotive Horn Sound Quality

B. Venkatesham[1]*, N. Pradeep[2], Goutham[2] and Jongdae Kim[2]
[1]*Department of Mechanical Engineering, Indian Institute of Technology Hyderabad-502 025*
[2]*Electronics Engineering Department, Hyundai Motor India Engineering Pvt. Ltd, Hyderabad-500 084*
**e-mail: venkatesham@iith.ac.in*

[Received: 15.11.2012; Revised: 24.12.2012; Accepted: 11.01.2013]

ABSTRACT

Sound Quality (SQ) is a parameter that provides product differentiator in a competitive market. Automotive horn sound design is a compromise between the need to generate warning signals and also customized sounds for different manufacturers. Customized sound for a product will provide uniqueness to the manufacturer brand image. The sound quality study of automotive horn is a multi-disciplinary problem. The knowledge of electro-acoustic, musical acoustics and statistics will help the designers for providing optimized sound quality products.

The aim of the current investigation is to develop a methodology for studying automotive horn sound quality. It has been discussed the methodology of recording horn sounds for Jury listening test. It has been prepared Jury listening Questionnaire. The recorded sounds are analyzed to calculate different objective parameters like loudness, sharpness, roughness, fluctuation of strength and tonality. Relative sensory pleasantness index considers as an aurally adequate psycho-acoustic index to explain pleasantness as the global behavior of horn sound. This value has been calculated from objective parameters.

1. INTRODUCTION

Human brain interprets the source of cause and provides instruction to react. It acts like a processor. This study will be a part of Psycho-acoustic study. Psycho-acoustic study is a science to read out human perception and acoustics. Every working product can create a specific sound. This sound may be pleasant or unpleasant based on human perception. Some sounds are generated for warning purposes. The purposes of these sounds are alert people and grab attention of people. These sounds convey some information. For example, alarm sound, ambulance siren sound, Factory siren sound, Police vehicle siren sound, and vehicle horn sound etc. The focus of the current study is vehicle horn sound. Vehicle horn sound is one of the major noise sources in urban noise pollution. People use horn very frequently countries like India. The major reasons for honking might be

The automotive horn sound is more impulsive in nature and creates more annoyance to listeners. Sound

- Traffic indiscipline (i.e., not following lane system)
- Low confidence in driving
- Vehicle Overtaking
- Cross-Junctions
- People walking on the road
- Blind turns & Hair-pin turns
- Hurriedness in people
- Animals crossing road
- Genuine Warning signal
- Habitual

Quality of Horn is necessary for reducing traffic noise annoyance.

Most of the automotive manufacturers are interested to create uniqueness to their Vehicle horn sound and should be more pleasant to listeners with proper warning. This motivates for a current study of Automotive Horn Sound Quality.

Sound Quality (SQ) study includes subjective test or Jury test and objective test. The purpose of subjective test is to collect human perception of sound. Objective test data can be used to calculate Sound Quality (SQ) metrics like loudness, sharpness, fluctuation of strength, Roughness and tonality etc., based on empirical equations. These two tests have independent results. The relation between these results can be established with a proper analysis. Existing literature related to automotive horn sound is in the references [1-4].

Guillaume Lemaitre [1-3] etc., from France studied extensively on the sound quality of car horns. They have discussed about the perceived quality of car horn sounds within a psycho-acoustical frame work. They studied timbre of car horns similar to the timbre of musical sounds. Their second paper provides insights into the design of new sounds suitable for European environment. Hai Ann ThiPhan [4] etc., From Japan conducted cross-cultural experiments between Vietnamese and Japanese to understand the annoyance from road traffic noise with horn sounds.

2. METHOD

The purpose of subjective test is to capture human perception about different sounds. This test can be conducted with actual product sounds in the field. It may not be possible to conduct test all times due to limitation of resources and complex interaction with other sounds. An alternative approach is to develop a procedure in the laboratory.

The main focus of the current study is as follows:

i) Psycho-acoustic analysis of horn sound data to estimate objective parameters,

ii) A subjective test to identify subjective parameters, and

iii) Data analysis to correlate subjective parameters with objective parameters.

It has been developed test setup for recording of horn sound. The recorded sound samples have been used in subjective test and objective test. Instrumentation, Mounting frame fabrication and test recording procedure details has been considered in test setup preparation. The subjective test has been conducted with recorded sound samples.

Objective data calculate SQ metrics and psycho-acoustic indices. Psycho-acoustic indices provide a global description of sound in terms SQ Quantities. The relations used in calculation of objective parameters are empirical in nature. Relative sensory pleasantness index considered as an aurally adequate indices for automotive horn sound.

2.1 Experimental Test Setup

The laboratory test setup development for recording horn sounds has been discussed in this paper. Binaural Head Set (BHS) instrument used to record horn sounds. Figure 1 shows the mounting frame dimensions with Cross-sections. These dimensions are estimated based on Horn sound standard and also the actual mounting position of Horn in a car. Different holes are provided on the horizontal arm of mounting frame to mount the hornin different locations. The mounting location is not changed in the current study.Table 1 shows the summary of horn sound sample recording test conditions.

2.2 Experimental Test Setup

The subjective test consists of three major tasks. First one is a preparation of sound samples for listening with proper instrumentation; the second one is jury evaluation methods and the last one is jury evaluation questionnaire.

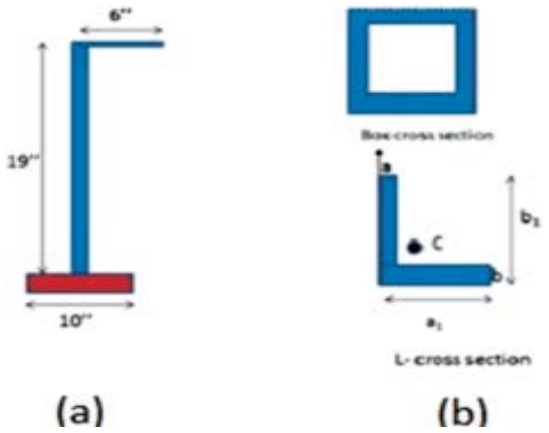

Fig. 1. (a) Dimensions of mounting (b) Cross-sectional details

Table 1. Recording test setup details

	Environment	**Open ground (neglected wind noise effect)**
	Recording duration	15 Sec with continuous Honking
	Data recording details	24 bits, 44100 Hz sampling rate
	Distance	2m from Horn in Front direction
	Number of Horns	5 Manufactures, 10 Disc type, 4 Shell type total: 14
	Tested Horns	14
	Type of Horns	Disc and Shell type
	Number of Trails	2

S.No.	1	2	3	4	5	6	7	8	9	10	11	12	13	14
Notation	M1DH1	M1DH2	M1SH1	M1SH2	M2DH1	M2DH2	M2DH3	M2DH4	M2SH1	M2SH2	M3DH1	M3DH1	M4DH1	M5DH1
Horn Type	Disc	Disc	Shell	Shell	Disc	Disc	Disc	Disc	Shell	Shell	Disc	Disc	Disc	Disc

There are different types of Jury evaluation tests are available in the literature. Detailed explanations of Jury evaluation methods for automotive applications have been provided in reference [5]. Based on the problem objective, three types of tests are selected as part of jury evaluation methods. These are

(i) Relevant Test (RT)

(ii) Semantic Differential Test (SDT)

(iii) Pair Comparison Test (PCT)

The purpose of relevant test is to identify the significant horn model, which people can recognize it as a car horn. These results are strongly depends on subject knowledge and experience. Semantic differential test (SDT) consists bipolar variables with seven verbal Interval scale. Each bi-polar variable may have a linking with another variable. The purpose of Pair Comparison Test is to check the subject response consistency and preferred choice.

2.3 Objective Data Analysis

Major psycho-acoustic metrics are Loudness, specific loudness, roughness, sharpness, and fluctuations of strength defined or calculated based on application. Each metric represents one type of sound behavior but global representation is possible with psycho-acoustic indices. For example, relative sensory pleasantness is a function of loudness, roughness, sharpness and tonality. It is used to describe global behavior of most of the sound quality applications. Even Horn Sound Quality also described with relative sensory pleasantness index. These indices are monaural (i.e., Calculations are conducted for each ear signal without combining signals). It generates two separate values for left and right channels.

Fastl [6] provides the detailed information about psycho-acoustic metrics and psycho-acoustic indices with formulas etc., Developed MATLAB [7] code based on these formulas to calculate objective data parameters for all recorded sound samples.

3. RESULTS AND DISCUSSION

Objective parameter metrics in relative percentage are shown in Box plot format in Figure 13. The Box plot data shows 25% to 75% quartile in a box format. The1.5 time quartile range is shown as whisker length. Beyond whisker length represents outliers. Red mark shows the outlier points. Mean line shown with objective metrics.

Total sound pressure level data have a smaller range variation and highest mean relative percentage. Fluctuation strength and Roughness values are proportional. Data with higher sharpness mean value and lower Roughness mean value can be interpreted as the dominance of higher order harmonics. Two horns tonality is shown as outliers in the Box - plot.

Relative sensory pleasantness index calculated for all horns considering M2DH3 horn as a reference sound sample for calculating pleasantness index. If the pleasantness index value is higher than reference horn sound pleasantness index value, those sound samples are pleasant. Pleasantness index values less than reference sound, then those horn sound samples are unpleasant.

Figure 3 shows the pleasantness index for objective data generated using BHS unit. It can be observed that shell horns, (M1SH1, M2SH1, M1SH2, M2SH2) are more pleasant compared to disc type horns. These results are useful to identify extreme pleasant or unpleasant horn sound samples with respect to reference sound.

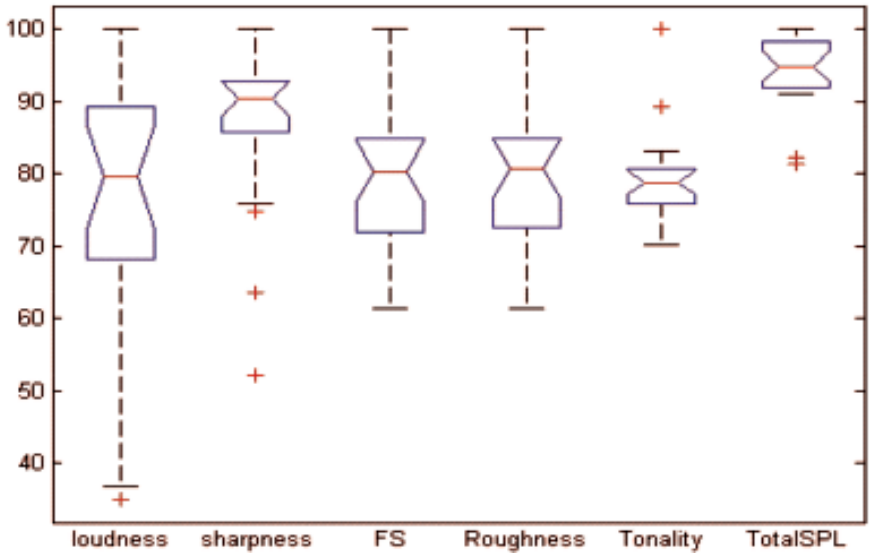

Fig. 2. Objective data analysis results in a box-plot representation

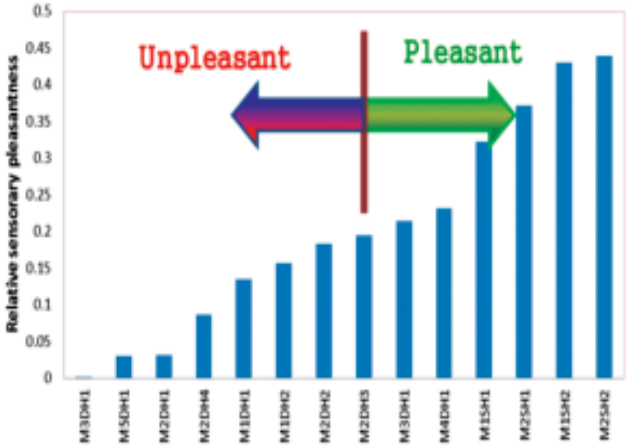

Fig. 3. Comparison of different horn pleasantness index

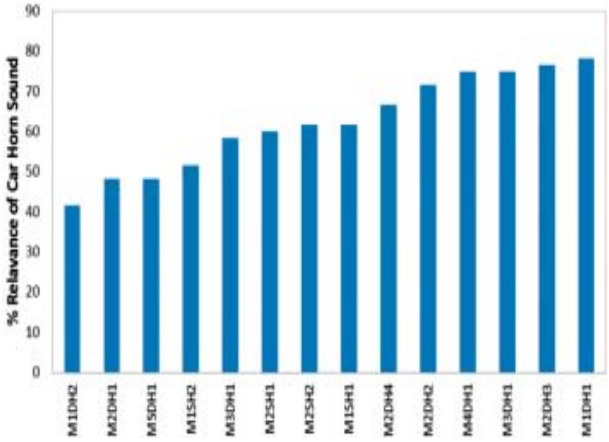

Fig. 4. Relevant percentage of different car horn sounds

The purpose of relevant test data is to identify car horn sound.Number of responses recognized as a car horn sound normalized with the number of responses for each horn and multiplied by 100 to represent as a percentage.Most of the subjects have knowledge associated with the disc horn as a car horn. A cognitive effect plays an important role in relevant test.

Table 2 shows a summary of pleasantness data results of objective and subjective data analysis. It should be observed that identification of pleasantness or unpleasantness for extreme psycho-acoustic parameter metrics is simple but it is difficult for other horn sound samples. The results depend on the instrumentation, cognitive effects, subjective knowledge and experience. There is a lot of research scope to understand all these parameters.Subjective test data of Relevant test and SD test could be used to develop a design chart to relate relevant percentage of car horn recognition to pleasantness.

Table 2. Summary of pleasantness data results in subjective and objective data analysis

	M2DH1	M2DH2	M2DH3	M2DH4	M2SH1	M2SH2	M4DH1	M1DH1	M1DH2	M1SH1	M1SH2	M3DH1	M3DH2	M5DH1
Subjective data	Pleasant	Pleasant	Pleasant	Pleasant	Unpleasant	Pleasant	Pleasant	Pleasant	Pleasant	Pleasant	Pleasant	Unpleasant	Unpleasant	Unpleasant
Objective data	Unpleasant	Unpleasant	Unpleasant	Unpleasant	Pleasant	Pleasant	Pleasant	Unpleasant	Unpleasant	Pleasant	Pleasant	Pleasant	Unpleasant	Unpleasant

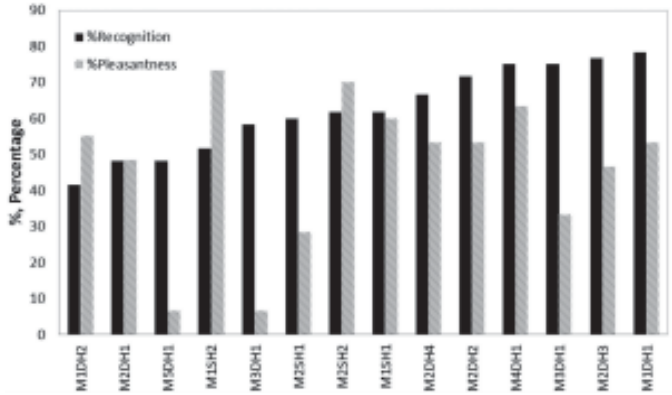

Fig. 5. Design chart based on RT and SDT test

Figure 5 shows results from RT test and SD. A few comments based on subjective test results are:

- The different horn model has different values of percentage recognition and percentage of pleasantness.
- Shell horns have a higher pleasantness index and also some models have a good percentage of recognition as a car horn sound.
- These graphs might be used as a design optimization chart.

The pair comparison test has questions related to forced choice and pair comparison similarity. The forced choice response is in the form of binary input and pair comparison similarity response is in the form of interval scale. In a PC test, a forced choice method used to select a horn sound sample in a given pair. Based on this response, relations are established for different horn sounds. Associative laws are used to develop a relation at different stages. It has been observed that shell horn sound samples are more preferred choice than disc samples.

Based on subjective data analysis, the following observations are made

- Analysis of subjective data shows that disc type horns have recognized as car horn sound. This result might depend on subject knowledge and experience.
- Shell horns are more pleasant and preferred choice based on SD test and PC test results.

4. SUMMARY

Preliminary study of sound quality analysis for automotive horn has been discussed in this paper.The experimental setup for sound recording has been discussed.

Some of the significant points of have been discussed in the current article are

1. A comprehensive subjective test evaluation method has been developed to get the subject response related to automotive Horn. The three models of the Jury evaluation questionnaire provided basic information of subject's perception about horn sound.
2. It has been observed from subjective test data that soft, calm, relax and slow sounds are more pleasant.
3. It has been observed from the current investigation that shell horns are more pleasant.

5. ACKNOWLEDGEMENT

We would like to thank Hyundai Motors Engineering India Pvt. Ltd (HMIE) for financial support to conduct current investigation and Indian Institute of Technology Hyderabad for providing the required resources.

6. REFERENCES

[1] GUILLAUME LEMAITRE, BORIS LETINTURIER and BRUNO GAENGEL, 2008. Model and estimation method for predicting the sound radiated by a horn loudspeaker-With application, *Applied Acoustics,* **69**, 47-59.

[2] G. LEMAITRE, P. SUSINI, S. WINSBERG, B. LETINTURIER and S. MCADAMS, 2007. The sound quality of car horns: a psychoacoustical study of timbre, *ActaAcustica united with Acustica*, **93**, 457-468.

[3] G. LEMAITRE, P. SUSINI, S. WINSBERG, B. LETINTURIER and S. MCADAMS, 2009. "The Sound Quality of Car Horns: Designing New Representative Sounds", *ActaAcustica united with Acustica*, **95**, 356-372.

[4] HAIANHTHIPHAN, TSUYOSHI NISHIMURA, HAI YEN THIPHAN, TAKASHI YANO, TETSUMI SATO and YORITAKA HASHIMOTO, 2008. Annoyance from road traffic noise with horn sounds: A cross cultural experiment between Vietnamese and Japanese, 9th International Congress on Noise as a Public Health Problem (ICBEN, Foxwoods, CT.

[5] NORN OTTO, SCOTT AMMAN, CHRIS EATON and SCOTT LAKE, 2001. "Guidelines for Jury Evaluations of Automotive Sounds", *Sound and Vibration*, pp. 1-13.

[6] HUGO FASTL and EBERHARDZWICKER, Psycho-acoustics Facts and Models, Springer Publications.

[7] MATLAB User Manual.

Journal of Acoustical Society of India : Vol. 40, No. 1, 2013 (pp. 46-50)

Speech Intelligibligy in School Class Rooms -A Case study of Schools in an Indian Town

G. Muthu Shoba Mohan
Mohamed Sathak School of Architecture, Kilakarai

[Received: 13.11.2012; Revised: 29.11.2012; Accepted: 17.01.2013]

1. INTRODUCTION

The chief function of a school classroom is instruction, and instruction comes and likely will continue to come, by word-of-mouth and listening. The school classrooms are established to promote learning, which is by speaking and listening. In elementary school classrooms, most learning involves listening to the teacher and to each other. Therefore, acoustics is one of the most important physical properties that determine how well the school classroom building can serve its primary function. Thus the exclusion of noise and reverberation are indispensable in adapting classroom to the function of oral instruction in elementary school classrooms.

2. SCHOOLS IN INDIAN TOWN

Despite the existence of guidelines for school and classroom noise, and a body of research on the effects of noise on children and teachers in the classroom, there is relatively less information on noise levels outside the classrooms and its influence within the classrooms (Dockrell and Shield 2002). The acoustics of school classrooms in India are also influenced by climatic factors. In a warm-humid climate, where air-conditioning and tightly closed enclosures for the classrooms are not in practice the noise inside classrooms is highly influenced by the external noise as the windows and doors are kept open.

The Speech Intelligibility is influenced by the background-noise, reverberation time and the distance from the source to the listener. In the classrooms of the warm-humid climate regions the possibility of increased background noise in the classrooms due to the intrusion of noise through the open windows and doors along with the noise from fans remains higher than that in the enclosed classrooms. As the background noise is a fundamental parameter for determining the intelligibility in classrooms, the assessment of speech intelligibility in such classrooms becomes necessary. It is necessary to assess how far the typical Indian classrooms satisfy the requirement of better learning environment for school children.

3. SPEECH INTELLIGIBILITY IN CLASSROOMS

Speech Intelligibility (SI), which quantifies the quality of verbal communication, is a major concern regarding the acoustical characteristics of classrooms. SI is the percentage of speech material presented to an average listener which is correctly transmitted from a speaker to a listener . Non-optimal classroom design, acoustical conditions and SI can result in impaired verbal communication between a teacher and a student, with detrimental effects on learning. Both Bradley (2007) and Hodgson (2002) have carried out experimental and theoretical studies to investigate the relationship between background-noise, Reverberation Time and Speech Intelligibility in the classroom.

4. STUDY AREA

The schools evaluated are from an educationally advanced town Nagercoil located in the southern part of India, in the Kanyakumari District, which is one of the 32 districts in the state of Tamilnadu, having 808 schools out of which 522 are primary and middle schools with about 190,000 students . The locations of the schools in relation to noise sources vary; some are adjacent to busy roads, others are set back from the road,

separated from the roadside by playgrounds; many are located away from main roads, on side streets. It was therefore necessary to survey schools subject to a wide range of noise levels.. Hence the study area was classified under three categories as: i)Schools located near public roads (Noisy-sites);ii) Schools located in Housing sites; and iii) Schools located in Quiet sites.

5. METHODOLOGY

A total of 120 classrooms in 25 schools in the three sites were studied. The surveyed schools were attended by children from the 1st to the 8th grades (6-14 years old) of the fundamental educational system, which corresponds to primary and middle schools. Internal and external noise surveys were carried out around the schools to provide information on typical sound levels and sources to which children are exposed while at school. Many of the schools surveyed were exposed to noise from road traffic; the average external noise level was measured outside each school. Detailed internal noise surveys were carried out in the classrooms together with classroom observations to verify the acoustical conditions of the classrooms for the development of teaching learning process. External noise levels were compared with internal levels to determine the influence of external noise on the internal noise environment of the classrooms.

Reverberation time was measured in the classrooms when the classrooms were empty and when they were occupied by the students. The software ClassTalk was used to calculate also the RT in the classrooms. The speech intelligibility parameters like Signal to noise ratio, Speech Intelligibility and Speech Transmission Index (STI) at different locations in the classrooms were computed and discussed. The means to improve the speech intelligibility are also discussed and presented.

6. SOURCES OF NOISE IN THE CLASSROOM

The noise in a classroom is made up of external noise which is transmitted through the building envelope and open windows and doors, plus internally generated noise, as a result of which children in school may be exposed to noise from a wide variety of sources. The predominant external noise source, particularly in urban areas, is likely to be road traffic (Shield and Dockrell 2002) although aircraft noise may also affect many schools, with fewer schools exposed to railway noise.

In addition to external noise transmitted through the building facade, open windows and doors to a classroom, noise inside a classroom may include noise from teaching equipment (computers, projectors and so on), noise from building services (fan) in the classroom and noise transmitted through the walls, floor and ceiling from other parts of the school.

It was found that the dominant source of noise in a school classroom was the noise generated by the pupils themselves as they took part in a range of classroom activities. Class activity noise is the noise created by the occupants of the room whilst working. It is a background noise issue which has not been adequately addressed in classroom acoustics studies.

NATIONAL BUILDING CODE, INDIA (NBC, 2005) NBC 2005 gives recommended values for background-noise levels and reverberation times in teaching spaces for schools. It recommends a value of 40 to 45 dB for background noise, and 35 to 45 dB for libraries and the proposed RT value of 0.75 s for occupied class and a higher value of 1.25 s for the empty classroom. These RT values correspond to an octave band mid frequency of 500 Hz. It is stated that it is preferable to have same limit for other frequencies.

7. MEASURED NOISE LEVELS

7.1 Background Noise level

The background noise (BN) was measured in the three conditions in an occupied classroom in the three zones, namely Noisy-site, Housing and Quiet sites. The average sound levels in the occupied and unoccupied classes for the three zones are shown in Table 1.

Table 1. Average Sound Levels in Class Romms

Schools at	Average sound levels in unoccupied classrooms dBA	Average sound levels in occupied classrooms dBA
Quiet site	46.2	54.7
Housing site	49.7	58.0
Noisy site	52.8	61.2

7.2 External Noise Survey

Measurements made at the curb side of the road helped to characterize the study area as Noisy (located on public roads), partly noisy (located on Housing sites) and Quiet (located in remote areas). The influence of external noise on the existing school planning gives an insight into the acoustic effectiveness of the classrooms. There has not been any particular planning for the schools surveyed and it has been as per the availability of land and other factors that influenced the school planning.

8. MEASUREMENT OF REVERBERATION TIME

The traditional parameter which has been studied in evaluating the effect of room acoustics is Reverberation Time (RT). Reverberation Time is defined as the time (in seconds) it takes for the sound from a source to decrease in level by 60 dB (Sabine 1964) after the source has stopped. Reverberation Time was measured (Table 2) in furnished unoccupied classrooms which had a volume and a seat capacity for the three sites of Noisy, Housing and Quiet.

Table 2. The average values of RT in occupied and unoccupied classrooms are shown below

Distribution of RT at 1kHz in occupied classrooms	
RT values	% of Classrooms
1.25 and above	62.5%
0.8 to 1.25	23.2%
0.6 to 0.8	6.8%
0.6 and below	7.5%

Distribution of RT at 1kHz in unoccupied classrooms	
RT values	% of Classrooms
More than 1.0	5.0%
0.76 to 1.00	21.7%
0.61 to 0.75	16.7%
0.41 to 0.6	46.6%
0.4 and below	10.0%

The stipulated value of RT according to NBC 2005 in unoccupied classrooms should be 1.25s or less at the frequency of 500 Hz and in the occupied classes the permitted value of RT is 0.75s. On comparison with the calculated values from Table, it is seen that only in 36 % of classes, the RT is less than 1.25 s and 0.75 s.

9. SPEECH INTELLIGIBILITY

For good Speech Intelligibility (SI) the learning space should have low noise levels and minimum reverberation (Table. 2).The Speech Intelligibility and the parameters influencing it are to be computed using the software ClassTalk (Murray Hodgsn 1994) and the results are discussed and presented. Speech Intelligibility in percentage at a listener position in a classroom is determined by two main room-acoustical factors: a) Signal-to-Noise Level Difference (SNA), the difference in decibels between the total A-weighted Speech-signal Level (SLA) and the ambient-background-noise level (BGNA), both at the listener's ears (Hodgson 2002), b) Reverberation. The quqlitative ratings ofSpeech intelligibility is given asexcellent etc as stated below.If SI is more than 98% it israted as excellent; 96% to 98 % is very good, 93 to 95 % is good,88% to 92 % 10is fair 80 to 87 % is poor and below 80% is poor.

10. COMPUTATION OF SI AT VARIOUS LOCATIONS IN CLASSROOM

In the classrooms under study, the BN in Noisy, Housing, Quiet zones of classrooms varied from 51.6 to 61.2 dB A, 48.8 to 57.5 dB A and 45.3 to 54.2 dB A respectively. The RT varied from 0.5 to 0.7 s. The background noise has great influence on Speech Intelligibility.

Table 3. SI Values in schools of three sites

Quality of SI	Range of SI	Quiet site	Housing	Noisy site
Excellent	>98%	-	-	-
Very Good	96-98	-	-	-
Good	93-96	8	-	-
Fair	88-93	44	36	16
Poor	80-87	40	28	8
Bad (unacceptable)	<80	8	36	76

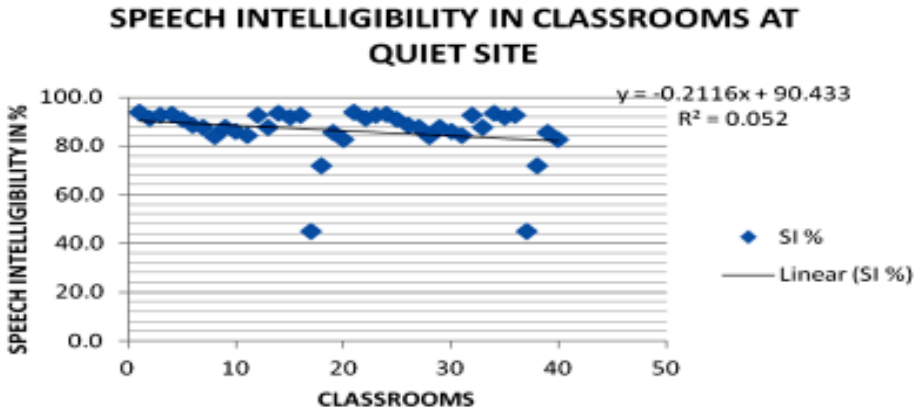

Fig. 1. Speech intelligibility in classrooms at quiet sites

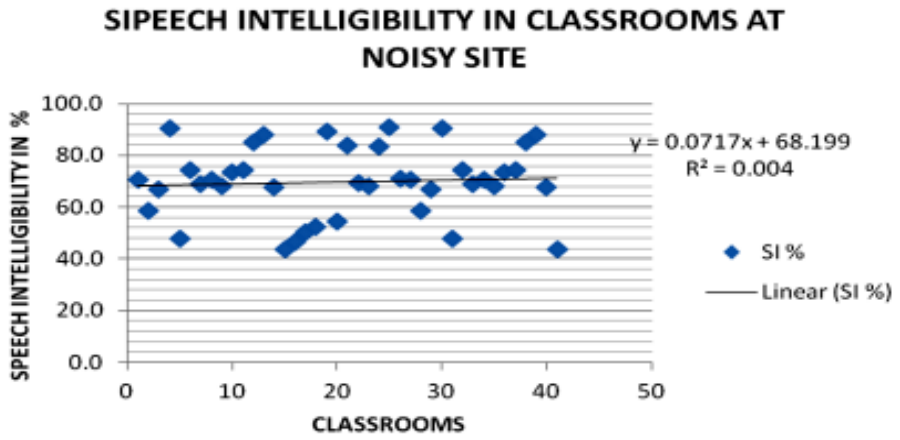

Fig. 2. speech intelligibility in classrooms at noisy- sites summary and conclusions

The Speech Intelligibility in classrooms is the most important factor to attain efficient learning in classrooms, and to fulfil the function of the classroom In classrooms at Noisy-sites the Speech Intelligibility level was less than acceptable in many classrooms and in classrooms of Housing site it was better than Noisy-site but worse compared to Quiet site. The BN and RT stipulated by Indian code NBC 2005 have been found to be higher than the international stipulations. With the BN of occupied silent class of about 9 dB A more than the unoccupied BN as suggested by NBC 2005, the Speech Intelligibility in the rear rows was still less than acceptable. Hence the stipulation of the BN should be for occupied silent class a value as suggested by NBC 2005 45 dBA.

11. REFERENCES

[1] J. BRADLEY 2007 Classroom Acoustics to support student learning: Encyclopedia of language and Literacy development London pp 1-7.

[2] J. DOCKRELL and B. SHIELD 2002 Children's and teacher's perceptions of environmental noise in classrooms. Proceedings. Institute of Acoustics.

[3] M. HODGSON, R. REMPEL and S. KENNEDY, " 1999 Measurement and prediction of typical speech and background noise levels in university classrooms during lectures , *J. Acoust. Soc. Am.* **105**, 226-233.

Hodgson.M " UBC- Classroom acoustical survey ," Can.Acoust.22,3-10,1994

Journal of Acoustical Society of India : Vol. 40, No. 1, 2013 (pp.51-55)

Speech Rhythm in Individuals with Stuttering

M. Santosh, Priyanka Parakh and V. Sahana
All India Institute of Speech and Hearing, Manasagangothri, Mysore-570 006

[Received: 14.12.2012; Revised: 29.12.2012; Accepted: 05.01.2013]

ABSTRACT

The objective of this study was to investigate speech rhythm in persons who stutter. Ten adults who stutter and ten age and gender matched controls participated in the study. Participants in both the groups were native speakers of Kannada. Five sentences were constructed in Kannada and the participants were asked to read out these sentences. Using Praat software, two kinds of rhythm metrics were calculated- pairwise variability indices and interval measures. Pairwise variability indices include normalized Pairwise Variability Index for vocalic intervals (nPVI - V) and raw Pairwise Variability Index for consonantal intervals (rPVI - C). Interval measures include percentage of vocalic intervals, standard deviation of the vocalic and consonantal intervals, and coefficient of variables for vocalic and consonantal intervals. Significant difference ($p < 0.05$) between the two groups was present for all the interval measures except coefficient of variables for vocalic intervals. However, there was no significant difference ($p > 0.05$) between the groups for Pairwise variability measures (nPVI - V and rPVI - C). The durational differences between the successive stressed and unstressed segments are taken into consideration in pairwise variability indices. The findings of the present study indicate that few measures of speech rhythm are deviant in persons who stutter while the others indicate that they follow the same rhythm pattern.

1. INTRODUCTION

Stuttering is a developmental disorder of speech generally characterized by repetitions, prolongations and silent blocks. It is estimated that 1% of the world's population stutters. Stuttering usually starts between 2 and 4 years of age and in 50% of the children, condition persists. Although stuttering is one of the extensively researched topics in the field of speech pathology, till today, its cause remains unknown. Previously, several attempts have been made to understand the underlying mechanisms behind stuttering. Numerous studies have shown timing irregularities in stutterers' fluent speech and report that stutterers have longer voice onset times (VOT), longer voice initiation times (VIT), longer voice termination times (VTT), and longer vowel durations (Agnello, 1975; Agnello, Wingate, and Wendell, 1974 among others) than nonstutterers. However, few other studies (Cullinan and Springer, 1980; McFarlane and Shipley, 1981; Venkatagiri, 1982) did not find any timing abnormalities when compared to nonstutterers. One reason for the differences in the results may be different response modes employed (phonatory gestures, phonation of speech-like sounds, phonation of words, etc.) and differences in the severity of stuttering.

Many other studies have investigated the regularities in the timing of speech and non-speech events. Some studies have found stutterers to be more variable than fluent peers (Boutsen, Brutten, & Watts, 2000), but others have found no differences between groups (Max and Yudman, 2003; Zelaznik, Smith, and Franz, 1994). Most of these studies have investigated the temporal patterning or rhythm at the segmental level. Although stuttering is disorder in the rhythm of speech, to date, surprisingly no study has been attempted quantifying speech

rhythm in sentence level in stuttering individuals. One reason for this could be difficulty with the quantification of speech rhythm.

Over the years, studies in the speech rhythm have mainly focused on classifying languages based on the isochrony principle. Isochrony principle states that languages can be either stress-timed or syllable timed. A third type of rhythm, mora timed was also proposed by Ladefoged (1975).Traditionally languages were classified into different rhythmic classes based on perception. However, with the development of quantification measures like pairwise variability index (PVI), more work is done at the production level. Pairwise variability index (PVI) calculates the pattering of successive vocalic and intervocalic (or consonantal) intervals showing how one linguistic unit differs from its neighbor. Two measures are derived using PVI; normalized pairwise variability index (nPVI) and raw pairwise variability index (rPVI). Both these measures help in computing the variability of successive measurements. Both these measures have been successfully used to classify different languages as stressed-timed, syllable timed or mora-timed. As these durational measures can be used to quantify variability in successive acoustic phonetic intervals, it will be interesting to see if stutterers differ from their fluent peers on these different measures of durational variability. Such evidence will fill remaining gaps in the field's knowledge and help us understanding the mechanisms underlying stuttering. Hence, the aim of this study was to investigate (1) whether stutterers differ from nonstutterers on the measures of speech rhythm

2. METHOD

2.1 Subjects

Ten male adults with stuttering (AWS) in the age range of 17 - 30 (mean age - 21.27 years) years and ten age and gender matched controls (AWNS) (mean age - 20.9 years) participated in the study. Participants in both the groups were native speakers of Kannada. Adults who stuttered reported to have developmental stuttering and no history of other neurological, psychological and communication problems.

2.2 Procedure

Three tasks were recorded from each participant. First was reading standardized 300- word reading passage in Kannada. Second task was conversation between the second author and client. Third task was reading five sentences. First two tasks were used to calculate severity of stuttering and third task for measurement of rhythm. Participants were given set of sentences, and were instructed to silently read and rehearse. Once they were well versed with the material, recording of these sentences was done. They were instructed to read the sentences in their normal loudness and comfortable rate. They were asked to read the same sentences if they made any mistake while reading the sentences. The control participants also read the same set of sentences in the manner described above.

2.3 Analysis

First, the recorded sentences were edited by removing the silences between the words (Grabe & Low, 2002) and also omitting the disfluencies in AWS. Using wideband spectrogram, vocalic and consonantal intervals were measured for all edited sentences. The duration between the onset and the offset of the vowel or cluster of vowels was considered as the vocalic duration. Similarly, the duration between the onset and the offset of the consonant or a cluster of consonants was taken as the consonantal duration. The rules that governed the segmentation of the sounds were based on former studies on rhythm analysis and acoustic analysis (e.g., Peterson & Lehiste, 1967). The boundary between the vocalic and the consonantal interval was indicted by a significant drop in the amplitude and a break in the second formant structure. The identification of consonant boundaries was made easy by the cues obtained from the spectrogram which was associated to the manner of production of that sound. Apart from this standard criterion, a few other factors were considered to obtain consistency in the measurements. As it is difficult to determine the boundaries of approximants reliably, they were taken as a part of vocalic interval (White & Mattys, 2007). Pre- vocalic glides were included in the consonantal duration and the post vocalic glides were included in the vocalic duration (Ramus *et al*., 1999). Aspiration following the stop release was taken in the consonant duration (White & Mattys, 2007). Even though there was significant lengthening noticed in the phrase final position, it was not excluded from the

analysis (White & Mattys, 2007). Further, it was difficult to mark the glottal sound /h/, and hence it was also taken as a part of vocalic interval for uniform analysis.

Subsequent to measuring the vocalic and the consonantal durations, the various measures under the two kinds of rhythm metrics, that is, the interval measures and pairwise variability indices were derived. For calculations of these metrics, the first pair of vocalic and consonantal interval was eliminated to control variations in the speech characteristics related to the abrupt or sudden start of the utterances. The variables calculated under interval measures were percentage of vocalic intervals (Perc V), standard deviation of the vocalic intervals (Delta V), standard deviation of the consonantal intervals (Delta C), variable coefficients of vocalic intervals (VarcoV) and variable coefficients of the consonantal intervals (Varco C). In pairwise variability indices, raw pairwise variability for the consonantal intervals (rPVI-C) and normalized pairwise variability index for the vocalic intervals (nPVI-V) were calculated. The average of each of the rhythm metrics for each participant was calculated and these values were subjected to further statistical analysis. The formulas used to compute different rhythm metrics are provided in appendix.

3. RESULTS

As the goal of this experiment was to obtain the differences in rhythm metrics between persons who stutter and fluent speaking individuals, independent sampled t-test was done to compare the two groups. The mean values of different rhythm metrics were higher for AWS than control speakers except for nPVI. For nPVI, control speakers had slightly higher mean values compared to AWS. Results of independent 't' test showed statistically significant difference ($p < 0.05$) between the groups for all the interval measures except variable coefficient of consonantal intervals (percentage of vocalic intervals, standard deviation of the vocalic and consonantal intervals and variable coefficient of vocalic intervals). However there was no significant difference ($p > 0.05$) between the two groups for the pairwise variability index measures (nPVI - V and rPVI - C).

Table 1. Mean, S.D, 't' values, df values and 'p' values for different rhythm metrics in AWS and control groups

Parameters	Groups	Mean	S.D	't' values	df	p
nPVI	AWS	84.7973	4.41	0.258	18	0.799
	Control	85.9120	12.90			
rPVI	AWS	0.0645	0.083	-1.162	18	0.260
	Control	0.0339	0.003			
PercV	AWS	72.6371	2.56	-2.748	18	0.013*
	Control	69.9350	1.768			
DeltaC	AWS	0.0386	0.086	-2.199	18	0.041*
	Control	0.0321	0.0034			
DeltaV	AWS	0.1667	0.0255	-2.116	18	0.049*
	Control	0.1432	0.024			
Varco V	AWS	49.7421	4.95492	-3.494	18	0.003*
	Control	43.5944	2.532			
Varco C	AWS	87.3082	9.125	0.900	18	0.380
	Control	84.3082	3.146			

AWS- adults who stutter, nPVI- normalized pairwise variability index, rPVI- raw pariwise variability index, PercV- percentage of vocalic intervals, DeltaC - standard deviation of consonant intervals, DeltaV- standard deviation of vocalic intervals, Varco V - variable coefficients of vocalic intervals, Varco C- variable coefficients of consonant intervals. * indicates significance at 0.05 level.

4. DISCUSSION

Here in our study, we investigated the sensitivity of pairwise variability indices and few other additional interval measures in differentiating speech rhythm of AWS and control speakers. Results showed significant difference between two groups only for selected interval measures (PercV, Delta V, Delta C, Varco V). Results highlight that selected rhythm metrics can be objectively used to document the rhythm abnormalities in people who stutter. However, there was no significant difference between the two groups for PVI measures. The durational differences between the successive vocalic and intervocalic segments are considered in pairwise variability index. Pairwise variability index (PVI) calculates the pattering of successive vocalic and intervocalic (or consonantal) intervals showing how one linguistic unit differs from its neighbor (Low, 1998). The values of PVI indices of AWS were similar to control participants. This suggests AWS are indistinguishable from control participants if we measure their rhythm using PVI. The results support similar observations for non-speech sounds (Max & Yudman, 2003) and suggest that individuals who stutter are not deficient with their isochronous rhythm timing if we document using PVI measures.

5. CONCLUSION

This study documents the rhythm abnormalities in persons with stuttering. As there is a mixed literature regarding the notion of stuttering as a disorder of speech rhythm and timing abnormalities, the findings of the present study also is similar, i.e., a few measures indicating that the speech rhythm characteristics are deviant in persons with stuttering while the others indicating that they follow the same rhythm pattern. The results have positive implications for speech language pathologists. Selected activities can be taken up to teach rhythm to patients with aprosodia considering the fact that one knows the type of rhythm in that language.

6. APPENDIX : FORMULAES USED

1. Normalized pair - wise variability index of Vocalic interval (nPVI-V):
   $nPVI\text{-}V = 100*(k=1\Sigma\, m^{-1} \mid (dk - dk+1)/(dk + dk+1)/2 \mid)/(m^{-1})$
2. Raw pair - wise variability index of the Consonantal interval (rPVI-C):
   $rPVI\text{-}C = (k=1\Sigma\, m^{-1} \mid dk - dk+1 \mid)/(m^{-1})$
3. Percentage of Vocalic interval: $\%V = \Sigma V/\Sigma (V + C)$
4. Delta C: ΔC = Standard deviation of C
5. Delta V: ΔV = Standard deviation of V
6. Variable coefficient of consonantal Interval (VarcoC): VarcoC = ΔC/Average C
7. Variable coefficient of Vocalic Interval (VarcoV): VarcoV = ΔV/Average V

Abbreviations index:

m = total number of intervals

d = duration of "kth" interval

V = duration of vocalic interval

C = duration of consonant interval

7. REFERENCES

[1] J. AGNELLO, 1975. Voice onset and voice termination features of stutterers. ***In***: L. M. Webster and L. C. Furst (Eds.), Vocal tract dynamics and dysfluency. New York: Speech and Hearing institute.

[2] J. AGNELLO, M.E. WINGATE and M. WENDELL, 1974. Voice onset and termination times of children and adult stutterers. *Journal of the Acoustical Society of America*, **56**,p. S62.

[3] F.R. BOUTSEN, G.J. BRUTTEN and CR. WATTS, 2000. Timing and intensity variability in the metronomic speech of stuttering and nonstuttering speakers. *Journal of Speech, Language and Hearing Research*, **43**, 513-520.

[4] W.L. CULLINAN and M.T. SPRINGER, 1980. Voice initiation and termination times in stuttering and non stuttering children. *Journal of Speech and Hearing Research*, **23**, 344 - 360.

[5] E. GRABE and E.L. LOW, 2002. Durational variability in speech and the rhythm class hypothesis. In N. Warner, & C. Gussenhoven (Eds.), Papers in laboratory phonology 7 (pp. 515-546). Berlin: Mouton de Gruyter.
[6] P. LADEFOGED, 1975. A course in Phonetics. New York: Harcourt Brace Jovanovich.
[7] L. MAX and E.M. YUDMAN, 2003. Accuracy and variability of isochronous rhythm timing across motor systems in stuttering versus non - stuttering individuals. *Journal of Speech, Language, and Hearing Research*, **46**, 146-163.
[8] S.C. MCFARLANE and K.G. SHIPLEY, 1981. Latency of vocalization onset for stutterers and non - stutterers under conditions of auditory and visual cueing. *Journal of Speech and Hearing Disorders*, **46**, 307 - 312.
[9] G.E. PETERSON and I. LEHISTE, 1960. Duration of syllable nuclei in English. *Journal of the Acoustical Society of America*, **32**, 693-703.
[10] F. RAMUS, M. NESPOR and J. MEHLER, 1999. Correlates of linguistic rhythm in speech signal. *Cognition,* **73**, 265-292.
[11] H.S. VENKATAGIRI, 1982. Reaction time for "s" and "z" in stutterers and non - stutterers: A test of discoordination hypothesis. Journal of Communication Disorders, 15, 55 - 62.
[12] L. WHITE and S.L. MATTYS, 2007. Calibrating rhythm: First language and second language studies. *Journal of Phonetics*, **35**, 501 - 525.
[13] H.N. ZELAZNIK, A. SMITH and E.A. FRANZ, 1997. Differences in bimanual coordination associated with stuttering. *Acta Psychologica*, **96**, 229-243.

Journal of Acoustical Society of India : Vol. 40, No. 1, 2013 (pp.56-60)

Search for Spectral Cues of Emotion in Hindustani Music

Anirban Patranabis[1], Kaushik Banerjee[1], Ranjan Sengupta[1], Nityananda Dey[2] and Dipak Ghosh[1]

[1]C.V. Raman Centre for Physics and Music, Jadavpur University, Kolkata-700 032
[2]ITC Sangeet Research Academy, Tollygunge, Kolkata-700 040

[Received: 16.12.2012; Revised: 30.12.2012; Accepted: 07.01.2013]

ABSTRACT

The foremost element of Hindustani Music (HM) is Rasa - the finest emotional behavior, outcomes from a perfect rendition of any raga that touches the hearts of world music lovers. In this work we attempt to find out the spectral cues of emotion in six ragas. As per literature and research findings, out of these six ragas three are of positive emotion (arousal) and rest three are of negative emotion (valence). Keeping this as standard, our objective is to find out the spectral cues of emotion from the sung signals in these six ragas. Features that communicate emotion are extracted from the music as a function of time. Our study agrees with the fact that emotion is a time varying quantity.

1. INTRODUCTION

Most of us feel that music is closely related to emotion or that music expresses emotions and/or can elicit emotional responses in the listeners. Every known human society is characterized by making music from their very beginnings. One fascinating possibility is that, although different cultures may differ in how they make music and may have developed different instruments and vocal techniques, we may all perceive music in a very similar way. That is, there may be considerable agreement in what emotion we associate with a specific musical performance [1].

In HM, the artist aims at expressing the rasa (emotional flavour) associated with the ragas. There is a well established system of ragas and talas (rhythms) that form its edifice. Ragas can be described a melodic framework with specific tones with a well defined ascending (aroha) and descending (avroha) structure as well as unique phrases (pakkad). Each raga in the HM is conventionally assigned to a corresponding rasa (emotion) and is also known to consistently evoke more than one emotion. As per treatise, nature of raga depends on Vadi-Samvadi and combination of notes (chalan) and that could create more than one Rasa from a single raga. Earlier study indicates that the following parameters are related to the emotional expression of music: pitch or F0 (i.e., the strongest cycle component of a waveform), intensity or loudness, attack or the rapidity of tone onset, tempo or the velocity of music, articulation or the proportion of sound-to-silence, timing or rhythm variation, timbre or high-frequency energy of an instrument/singers formant [1].

In this work we have taken the aalap part of six ragas (eliciting contrasting emotions- joy and sorrow), each of 1min duration, played by an eminent sitar player for analysis. These ragas chosen for analysis are Darbari Kannada, Adana and Mian-ki Malhar and Chayanat, Jayjayanti and Basant. The first three are under the category of pathos or Karuna and the last three expresses the mode of joy/romanticism. It is expected that the associated emotion with these ragas should be within the sound clips and therefore analysis of the sound spectra of each clip might reveal the spectral cues of the associated emotions. Here we did a study to find the spectral cues of emotion from the analysis of the raga clips.

2. EXPERIMENTAL PROCEDURE

For our analysis only the aalap parts were selected from each raga. The digitization of the signal was done at the rate of 44100 samples/sec (16 bits/sample) in mono channel. Signal files, stored as 'wav files', are thus selected for analysis, which constitute the database. Each signal taken is of one minute duration. Pitch was extracted at 10 milliseconds interval using open source software Wavesurfer of KTH, Stockholm. Cool edit software of Syntrellium corporation was used for further signal processing.

3. METHODOLOGY

Since all the six signals are from a single sitar with single artist and so timbre variations are fixed. All the six signals are normalized to 0db and hence intensity or loudness and attack cue are not being considered. Extraction of notes from the pitch profile needs the knowledge of the tonic used by the player. A skilled musician was requested to listen to the signal files one after another to detect the position of tonic Sa in the signal file. The finding of the ratio-intervals is done by first dividing the smoothed pitch values for each song by the pitch value of the 'Sa', tonic of that raga rendering. This gives the frequency ratios for each pitch data. From the ratio data, steady state sequences are created with all consecutive pitch in a sequence, which is terminated when $| x_i+1 - M | > M/30$ where $M = (1/i)\ \Sigma x_i$. If the duration of any sequence were less than that of a certain minimum value (60 milliseconds for this experiment) then the sequence is rejected. Elements of these sequences are considered as suitable candidate data for this analysis [2]. Whenever the ratio is less than 1 it is multiplied by a factor of 2 and when it is greater than 2 it is divided by 2. This effectively folds all pitch data into the middle octave. These are now distributed in 1200 bins of one-cent width each. The peaks of these distributions for each song are purported to be indicative of the sruti positions for that raga rendering (Fig. 1). After getting pitch value of Sa we have calculated the pitch value of other notes from standard sruti model, thus each note is being found out from the along with their duration. Time gap between two successive notes is termed here as silence. Silence to note duration is an important feature for emotion determinant (shown in Table 1).

Musical features can be considered either global or local. Global features are measured over an entire selection of music and are not time-varying. Local features are measured over small sections of time [1]. It is established that the elicited emotion from different segments from the same raga has some specificity, i.e. it might be that different segments from the same raga show different emotions. Also the emotional response from the segments of a raga does not generally correspond to those prescribed in Indian treaties [3]. We took the help of some experienced musicians for identifying the emotional phrases in the music signal along with their time intervals, based on their feelings. These are shown in Table 1. We attempted to match the results of our analysis with this subjective information.

Table 1. Time intervals of emotional phrases in different ragas

Raga	Duration (secs)
Adana	0 - 28.379
Darbari	04.234 - 09.928 and 24.174 - 53.963
Mian-ki-Malhar	04.795 - 48.845
Jayjayanti	07.352 - 12.401, 19.323 - 27.4 and 48 - end
Basant	09.861 - end.
Chayanat	03.737 - 12.537 and 27.805 - 59.349.

Since emotion is a time-varying quantity, in this paper, we tried to analyse the whole signal as well as the small segments in the each signals as marked by the musicians as emotion locations.

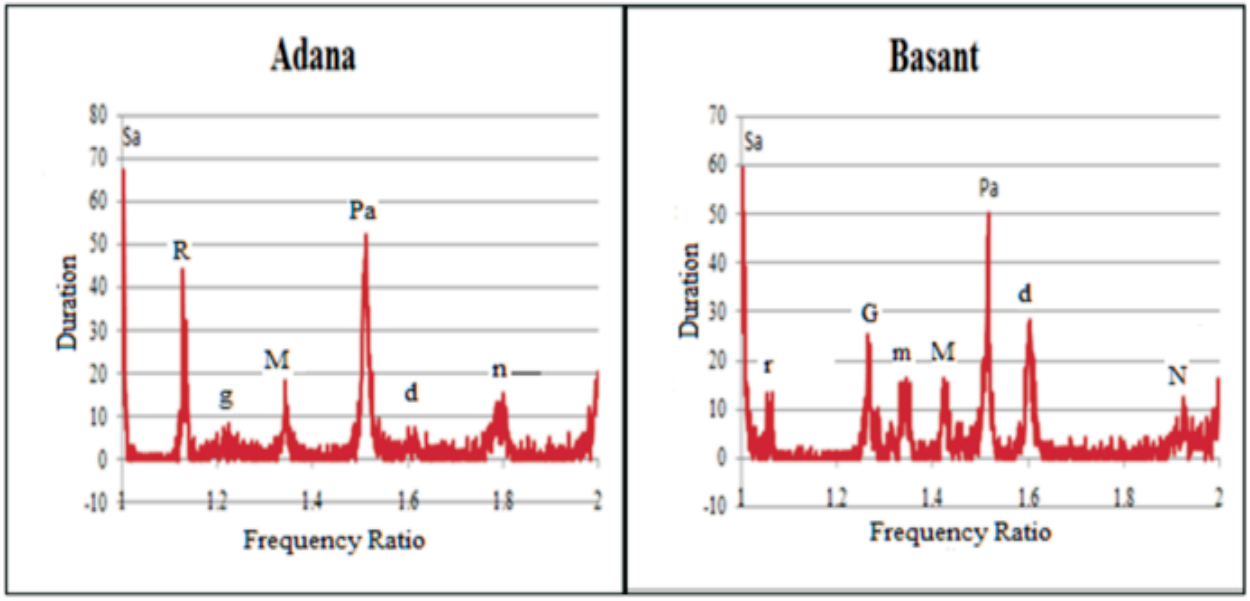

Fig. 1. Two out of six distributions are shown over 1200 bins of 1 cent width

4. RESULTS AND DISCUSSION

After the extraction of pitch data from each signal clips, it is smoothed and the steady state was detected. Fig. 1 shows the frequency distribution of the duration of steady states of raga Adana and raga Basant (1min clip each) spread over 1200 bins of 1-cent interval. The peak shows the ratios, which correspond to different sruti positions utilized in the respective raga. Each peak corresponds to a note utilized in the raga and the height of the peak denotes the number of times the note was hit in the clip. The relationship between the height and the distance between the peaks may give some indication about the nature of the raga and the emotion associated therein. Similar distributions were done from the signals of Adana, Darbari Kannada, Mian-Ki-Malhar, Jay-Jayanti, Basant and Chayanat and the rendered ratios were found out. These distributions showed the preferred notes in the raga used by the artist.

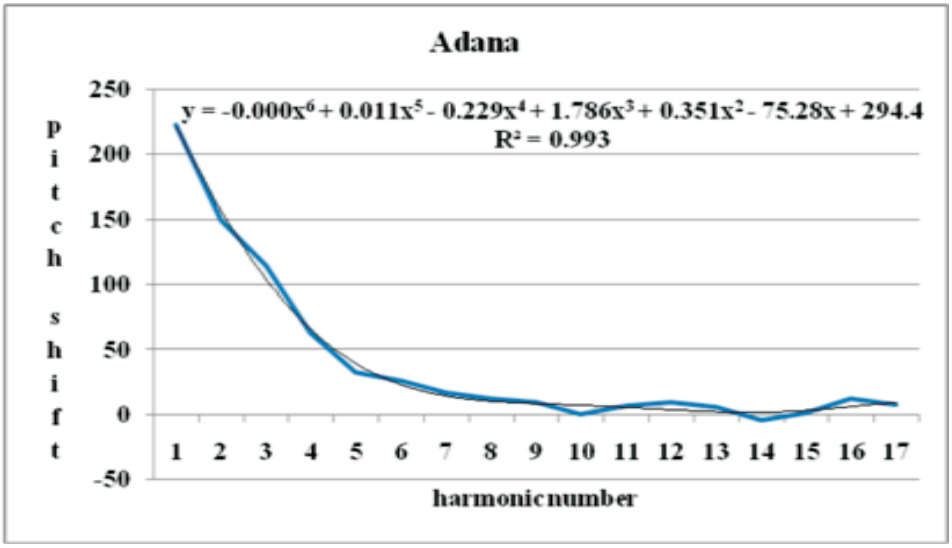

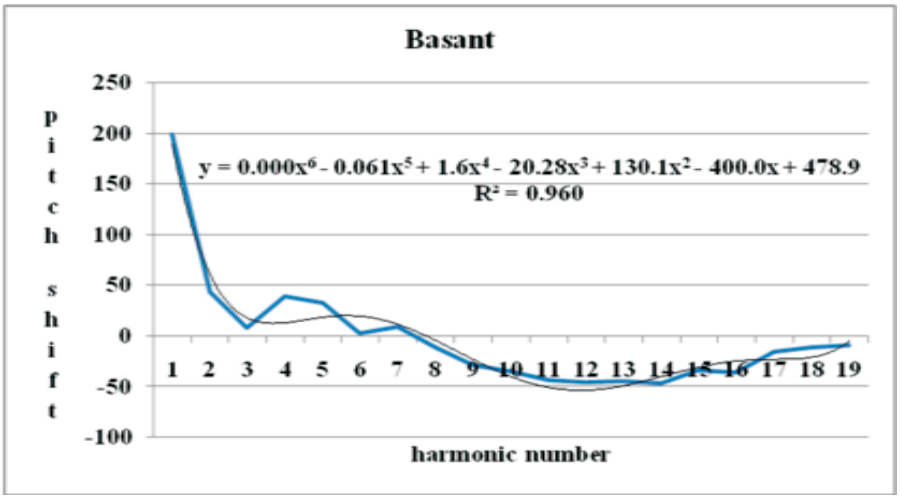

Fig. 2. Two out of six distributions are shown with best fit trend line and R^2 value

The distribution reveals the fact that the partials are more harmonically distributed around the spectral centroid. The figure also shows that pitch shift decreases linearly with the harmonic number for the ragas Adana, Mian ki Malhar and Darbari Kannada which may be an spectral attribute of negative emotion (valence). The ragas Basant, Chayanat and Jayjayanti showed a complex nature of the variation of pitch shift with harmonic number showing an indication of positive (arousal) emotion in the signals. It is also observed that the R^2 value is higher for signals of positive emotions and lower for signals of negetive emotions.

The note sequences in each signal were found out and also their durations were measured [2]. The silence zones in the signals were detected and duration of silence was measured. Silence to note ratio was measured. This is done globally for the entire signal and also over small sections of time interval 10 seconds each. It is understood that this ratio when closer to one reveals a very slow tempo and hence the emotion may be sad/ devotion while this ratio is very less than one reveals a fast tempo and hence the emotion may be joy/happiness [1].

Now comparing Tables 1 and 2 we find the emotion cues and are marked in italics and underlined in table 2. This is an objective evaluation with the help of subjective information. Comparing the above two tables it

Table 2. Ratio of Silence to Note durations local and global

	Local						Global
Time→in sec,	0-10	10-20	20-30	30-40	40-50	50-60	0-60
Adana	0.5337	0.5801	0.5105	0.6497	0.8353	0.8817	0.8817
Darbari	0.4864	0.8106	0.7296	0.6890	0.8512	0.9322	0.9322
Mian-Ki Malhar	0.5493	0.6016	0.6801	0.5232	0.6801	0.6801	0.6801
Jayjayanti	0.7884	0.5709	0.8972	0.6525	0.5709	0.7069	0.8972
Basant	0.8898	1.0593	0.8051	0.9322	0.7627	1.0169	1.0593
Chayanat	0.6288	0.4353	0.4111	0.5079	0.7014	0.5321	0.7014

may be concluded that the silence to note ratio is higher for signals of positive emotions while the ratio is lower for signals of negative emotions. Another interesting conclusion is that a piece of music may be undeniably emotionally powerful, and at the same time be experienced in very different ways by another person who hears it. Different part of a signal reveals different emotions.

with sadness or serenity [5]. Measurement is done for the entire signal (globally) and then over the small

sections of time interval 10 seconds each and is shown in Table 3. Comparing this with the emotion revealing phrases in the signal, as labeled by a musician (Table 1), it may be inferred that the emotion revealing part of Jayjayanti, Basant and Chayanat have higher tempo than the remaining part while Adana, Darbari kannada and Mian ki malhar have lower tempo than the remaining part.

Comparing with Table 3, data matched with the musician's opinion are marked in italics and underlined in

Table 3. Tempo - local and global

	Local						Global
Time → in sec,	0-10	10-20	20-30	30-40	40-50	50-60	0-60
Adana	23	25	22	28	36	38	172
Darbari	12	20	18	17	21	23	111
Mian-Ki-Malhar	21	23	26	20	26	26	142
Jayjayanti	29	21	33	24	21	26	154
Basant	21	25	19	22	18	24	129
Chayanat	26	18	17	21	29	22	133

Table 4. Comparing these two tables it may be concluded that the tempo is higher for signals of positive emotions while tempo is lower for signals of negative emotions. But considering the whole signal at a time, we find very little difference

5. CONCLUSION

1. Emotion in musical signal is time varying and so in order to find the emotional cue in the signal spectra we should concentrate on the smaller segments of signal.
2. Keeping timbre and loudness constant, spectral cues of emotion might lie in the silence to note ratio and other features like pitch/harmonic shift and tempo.
3. Musical signal with positive and negative emotions will have higher and lower tempo respectively.
4. Silence to note ratio is higher for signals of positive emotions while this ratio is lower for signals of negative emotions.
5. Pitch/harmonic shift decreases linearly with the harmonic number for ragas of negative emotion (valence) while a complex nature of the variation of pitch shift with harmonic number indicates positive (arousal) emotion.

6. REFERENCES

[1] MARK DAVID KORHONEN, 2004. "Modeling Continuous Emotional Appraisals of Music Using System Identification", A thesis presented to the University of Waterloo, for the degree of Master of Applied Science in Systems Design Engineering, Waterloo, Ontario, Canada.

[2] A.K. DATTA and R. SENGUPTA *ET AL.*, 2006. "A methodology of note extraction from the song signals", *Proc. Frontiers of Research on Speech and Music*.

[3] ALICJA WIECZORKOWSKA, ASHOKE KUMAR DATTA, RANJAN SENGUPTA, NITYANANDA DEY and BHASWATI MUKHERJEE, 2010. "On Search for Emotion in Hindusthani Vocal music", Adv. in *Music Inform. Retrieval*, SCI **274**, 85-304, Springer-Verlag Berlin Heidelberg.

[4] P.G. HUNTER, E.G. SCHELLENBURG and U. SCHIMMACK, 2008. "Mixed affective responses to music with conflicting cues". *Cognition and Emotion*, **22**, 327-35.

[5] S.O. ALI and Z.F. PEYNIRCIOGLU, 2010. "Intensity of emotions conveyed and elicited by familiar and unfamiliar music" Music Perception: *An Interdisciplinary Journal*, **27**, 177-182.

Journal of Acoustical Society of India : Vol. 40, No. 1, 2013 (pp. 61-65)

Comparing Acoustic Parameters of Conversational and Clear Speech during Reading in Kannada Speaking Individuals with Parkinson's Disease

Lakshmi Venkatesh and Ritu Mary Mathew
Dr. S.R. Chandrasekhar Institute of Speech & Hearing, Bangalore

[Received: 18.12.2012; Revised: 29.12.2012; Accepted: 10.01.2013]

ABSTRACT

The current study compared acoustic parameters of reading samples produced in clear speech and conversational speech conditions by individuals with Parkinson's disease (PD), grouped into three groups of PD (early, middle and late PD) depending on disease progression. A listener judgement task validated that instructions given to persons with PD to speak clearly indeed resulted in differences in speech production with a large proportion of listener's judgments indicating a preference for clear speech condition in comparison to conversational speech condition. Acoustic analysis of reading passages demonstrated significantly increased standard deviation of Fo, standard deviation of intensity as well as greater duration (reduced articulatory rate) in the clear speech condition in comparison to conversational reading. Further differences among the three groups of participants with PD in acoustic parameters reveal trade-off's in the acoustic measures possibly reflecting differences in physiological capacities with the progression of the disease.

1. INTRODUCTION

Hypokinetic dysarthria associated with Parkinson's disease (PD) is considered to be a perceptually distinguishable motor speech disorder associated with basal ganglia control circuit pathology, characterized by a progressive loss of dopamine in the brain. Clinical characterization of hypokinetic dysarthria emphasizes in rank order; monopitch, reduced stress, monoloudness, imprecise consonants, inappropriate silences, short rushes, harsh voice, continuous breathiness, pitch level disturbances, and variable rate [1]. Few studies of speakers with dysarthria have shown that clear speech can have an important effect on intelligibility [2]. Clear speech includes speaking in a deliberate manner, characterized by exaggerated articulation, reduced rate, and increased loudness relative to habitual speech. A recent study examining the acoustic characteristics of clear speech by individuals who have hypokinetic dysarthria due to PD suggested that such an intervention may have the potential to improve intelligibility for some speakers with dysarthria [3]. Acoustic analysis revealed that group of individuals with PD did use some of the clear speech strategies, as indicated by significantly decreased articulation rate, increased mean fundamental frequency (MeanFo) and standard deviation of speaking fundamental frequency (Fo-SD) in clear speech condition in comparison to conversational speech condition during reading and monologue [3]. Studies are necessary to describe production features of clear speech in individuals with dysarthria, so that those production changes that has greatest impact on intelligibility can be emphasized in intervention.

There is increasing evidence that acoustic/perceptual features that characterize the conversational-to-clear speech transformation may vary across languages [4]. There is some research emerging on acoustic and perceptual characterization of properties of clear speech in Indian languages. For example, clear speech in Kannada was characterized by longer vowel durations and decreased speaking rate, higher mean values of pitch, increased amplitude in spectra of consonants and fricative [5]. Research on clear speech and conversational speech in individuals with dysarthria speaking different languages would determine language specific acoustic/perceptual features as well as provide additional support for benefit if any of clear speech over conversational speech. The purpose of this study was to evaluate the differences in clear speech and conversational speech conditions in a reading task among individuals with dysarthria due to PD using acoustic analysis and perceptual judgements.

2. METHOD

A total of 13 speakers with hypokinetic dysarthria due to PD (10 Male & 3 Female; Mean age 61.23 years; mean disease duration; 7.38 years) participated in the study. Participants were grouped into three groups of PD depending on the Hoehn-Yahr Scale of disease progression such that there were four participants each in the early and middle stages and five participants in the late stages of the development of PD. The severity of dysarthria increased with stage. Participants were native Kannada speakers who were able to read and write Kannada. Participants with evident linguistic disturbances were excluded from the study.

Stimuli comprised of a standard reading passage in Kannada. Participants were asked to read in two speaking styles; conversational speech condition and clear speech condition. For the conversational style, the talkers were instructed to read the passage as they would normally speak to someone familiar. For the clear speaking style, the talkers were instructed to read the passage as clearly and precisely as possible as if the experimenter was having trouble hearing them, or in understanding the language or as if there was noise in the background. Both speaking conditions were elicited through the use of instructions, and the participants' speech was audio-recorded as they read the passage.

Acoustic analysis of reading passage was performed by means of a commercially available software (Motor Speech Profile/ Computerized Speech Lab CSL 4300; Kay Elemetrics Corp., USA) which allowed auditory playback of marked segments. The initiation and termination of the reading passage was marked by means of cursors, thereby eliminating the background noise from the sample. Voiced period marks were placed throughout the sample. Acoustic measurements included mean fundamental frequency (meanFo), standard deviation of fundamental frequency (SD-Fo), mean intensity (mean-Int) and standard deviation of intensity (SD-Int), measured across the entire length of the passage. In addition, the total time taken to read the entire passage was also noted. Speech samples comprising of reading passage in both speaking styles produced by participants were given to listeners for comparison to indicate their preference for either of the styles or none in terms of ease of understanding and clarity of speech.

3. RESULTS AND DISCUSSION

3.1 Perceptual Judgments

As seen from Table 1, listeners indicated that clear speech was better in terms of ease of understanding and clarity of speech in comparison to the conversational speech for the task of reading passage. Out of the total 130 responses, 92 listener judgments (70.77%) showed a preference for clear speech. A small number of listener judgments 13 (10%) indicated preference for conversational speech condition over clear speech. 24 (18.46%) judgments reported no preference or suggested that both conditions were perceived similar in terms of ease of understanding and clarity. 67.5% (27) and 62.5 % (25) of the listener judgements were for clear speech condition in the early and middle PD groups respectively.

An increased number of preferences for clear speech (80%) observed in the speech of participants with severe dysarthria associated with the late stage of PD in comparison to early and middle stages of PD suggested that clear speech instructions resulted in changes in speech production among these participants which were detected by listeners to contribute to ease of understanding and clarity in light of increased severity of speech deficits.

Table 1. Percentage and number of listener preferences as clear/conversation or same

Reading Passage		Listener Preference		
		Clear	**Conversation**	**None (same)**
Early	% (Total -40)	67.5 (27)	10 (4)	22.5 (9)
Middle	% (Total -40)	62.5 (25)	10 (4)	25 (10)
Late	% (Total -50)	80 (40)	10 (5)	10 (5)
Overall	% (Total -40)	70.77 (92)	10 (13)	18.46 (24)

3.2 Acoustic Parameters

Wilcoxon signed rank test used to compare the acoustic measures on clear and conversation condition across the 13 participants revealed a significant difference in total duration of reading passage between clear (Mdn = 30.62 sec) and conversation speech condition (Mdn = 25.06 sec; z = 3.181, p = 0.001). A significant difference was seen for SD-Fo of the reading passage between clear (Mdn = 26.59) and conversation speech condition (Mdn = 22.17; z =3.181, p = 0.001), as well as for SD-Intensity of reading passage between clear (Mdn = 7.89) and conversation speech condition (Mdn = 7.27; z = 2.901, p = 0.004). The measures of meanFo and mean-intensity did not differ between reading of passage in the clear condition and conversation condition.

When prompted to use clear speech, participants in the current study consistently took longer duration to read the passage in comparison to conversational speech condition. Interestingly, this was observed across all participants in the study. These results are similar to those reported earlier in terms of a decrease in the articulation rate [3]. The increase in duration for the clear samples may possibly be due to slower speaking rate. Previous research has found that non-impaired speakers produce slower articulation rates when asked to speak clearly [6, 7]. A slower rate of speech has been reported in clear speech due to the wide range of acoustic/articulatory adjustments, inclusive of increased stress and rhythm, hyper articulation of phonemic segments, vowel lengthening, and insertion of long duration and more number of pauses to increase the intelligibility [7, 8].

No significant differences were observed in mean Fo and mean-intensity values between the clear and conversation conditions across speakers. The mean Fo data in the current study are an average of male and female participants' Fo data. Interestingly, the findings of meanFo in conversational reading (159 Hz) are consistent with values reported in an earlier study [4] for conversational reading among participants with PD (157Hz). However, participants in the current study did not increase their mean Fo in the clear condition as seen in the study by Goberman and Elmer [4]. Earlier research on unimpaired speakers has also found higher speaking Fo in clear speech condition compared to conversational speech associated with increased laryngeal tension in clear speech production [7]. Participants in the current study ranged widely in the degree of progression of PD and resulting speech impairment. The lack of differences may have resulted from the variations in the participants. The results of the current study are consistent with several previous findings that speakers with PD already demonstrate a higher speaking Fo that is significantly higher than that of controls [9] and not all participants may be able to raise their further raise their Fo to produce clear speech.

Although there were no difference in the mean values of Fo and intensity, the standard deviation of Fo and standard deviation of intensity were significantly higher in the clear condition in comparison to the

conversation condition. Increased SD-Fo in clear speech is consistent with earlier studies of comparison of clear and conversational speech among speakers with PD [4] as well as those in non-impaired speakers [7]. Compared to controls, PD speakers have been shown to have decreased speaking variability in Fo as well intensity [9] which has been attributed to loss of prosody resulting in perceptions of monopitch and monotonous speech. The results of the current study suggest that all speakers with PD were possibly attempting to increase the range of Fo and intensity across the entire reading passage in order to compensate for the loss of prosody in clear speech condition.

The ratio of clear to conversational speech samples, for all acoustic measures were taken to examine the extent of difference in the acoustic measures in both conditions across the participants (Table 2). All groups demonstrated a ratio higher than one for the duration measure reflecting the increased time or slower articulation time for clear speech in comparison to conversation speech. However, in comparison to middle and late groups of PD, the early PD group showed a greater ratio (Mdn =1.44) probably indicating that they relied on the strategy of slowing down speech rate when directed to speak clearly.

Table 2. Ratio of acoustic measures of clear versus conversational reading

Groups		Total Duration	Mean F0 Ratio	F0- SD Ratio	Mean Intensity	Intensity- SD Ratio
Early PD	Median	**1.444**	0.980	1.073	1.032	1.072
	Mean (SD)	1.441 (0.01)	0.973 (0.01)	1.077 (0.01)	1.036 (0.03)	1.092 (0.082)
Middle PD	Median	1.082	**1.159**	**1.260**	1.003	1.122
Late PD	Median	**1.151**	0.961	**1.157**	**0.987**	1.090
	Mean (SD)	1.171 (0.04)	0.972 (0.04)	1.188 (0.104)	0.945 (0.09)	1.114 (0.158)

Note: Measure differentiating each group with other groups is marked in bold

Examination of the meanFo ratio values by group shows that all participants in the early group showed reduced Fo in the clear condition (meanFo ratio less than 1). Participants in the late group showed inconsistent patterns. However, all participants in the middle stage showed increased meanFo in the clear condition in comparison to conversational reading (meanFo ration greater than 1). No such unique differences among groups were seen for the measures of Fo-SD and intensity-SD. All participants demonstrated an increase in variability in Fo and intensity in the clear condition. This change occurred to the same extent in participants of the three groups. Examination of mean intensity ratios revealed a distinct pattern in the productions by the later group of speakers with PD such that the intensity reduced in the clear speech condition in comparison to the conversation speech condition (mean intensity ratio less than 1). The participants in the late group appears to have achieved the difference between the two conditions with reductions in rate of speech (although not to the extent done by the early group) and increased Fo-SD which was accompanied with decrease in mean intensity. Such differences in the acoustic measures across the three groups of speakers with PD point to possible differences in strategies utilized by the speakers to achieve the perceived changes in the clear speech condition. These changes may well be defined by the physiological capacities and possible trade-off's among the speech systems with the progression of the disease. Detailed analysis of unique contribution of acoustic measures to perceived changes is required to further analyze the differences among the groups. Findings of the current study both perceptual and acoustic measures suggest that clear speech production may hold promise as a simple approach to improving speech production in individuals with PD.

4. REFERENCES

[1] J.R. DUFFY, 2005. *Motor speech disorders. Substrates, Differential diagnosis and Management.* Mosby.

[2] D.R. BEUKELMAN, S. FAGER, C.ULLMAN, E. HANSON and J.A. LOGEMANN, 2002.Impact of speech supplementation and clear speech and the intelligibility and speaking rate of speakers with traumatic brain injury. *Journal of Medical Speech Language Pathology,* **10** (**4**), 237.

[3] A.M. GOBERMAN and L.W.ELMER, 2004. Acoustic analysis of clear versus conversational speech in individuals with Parkinson disease. *Journal of Communication Disorders,* **38**, 215.

[4] R. SMILJANIC, and A.R.BRADLOW, 2005. Production and perception of clear speech in Croatian and English. *Journal of Acoustical Society of America,* **118**, 1677-1688.

[5] P. KUMAR, 2008. *Comparing Acoustic Parameters of Conversational and Clear Speech in Kannada.* Unpublished Master Dissertation, Mangalore University, Mangalore, India.

[6] A.R.BRADLOW, N.KRAUS and E.HAYES, 2003. Speaking clearly for children with learning disabilities: Sentence perception in noise. *Journal of Speech Language, and Hearing Research,* **46**, 80-97.

[7] M.A.PICHENY, N. I.DURLACH, and L.D.BRAIDA, 1986. Speaking clearly for the hard of hearing II: Acoustics of clear and conversational speech. *Journal of Speech and Hearing Research,* **29**, 434-446.

[8] R.M. UCHANSKI, S. S.CHOI, L. D.BRAIDA, C.REED, and N. I. DURLACH, 1996. Speaking clearly for the hard of hearing. IV: Further studies of the role of speaking rate. *Journal of Speech and Hearing Research*, **39**, 494–509.

[9] E.J. METTER, and W.R. HANSON, 1986. Clinical and acoustical variability in hypokinetic dysarthria. Journal of Communication Disorder, **19**, 347.

Acoustical Society of India
(Regn. No. 65-1971)

Executive Council (2010 - 2014)

President	:	**Dr V Rajendran** [KSRCT, Tiruchengode; veerajendran@gmail.com; +91-99 94 13 03 03]
Vice President	:	**NS Naidu** [NSTL, Vizag; nsnaidu04@yahoo.com; +91-94 90 75 05 82]
General Secretary	:	**PVS Ganesh Kumar** [NSTL, Vizag; gkpakki@rediffmail.com; +91-98 66 40 08 94]
Jt. Secretary	:	**Dr K Trinadh** [NSTL, Vizag; hello_trinath@yahoo.co.in; +91-97 04 71 95 00]
Treasurer	:	**Prof AV Sharma** [AU, Vizag; sarmavakella@yahoo.co.in; +91-94 90 43 17 26]
Chief Editor	:	**Dr Mahavir Singh** [CSIR-NPL, New Delhi; mahavir@nplindia.org; +91-98 71 69 33 46]
Council Members	:	**Dr SV Ranga Nayakulu** [VITAE, Hyderabad; nayakulu@rediffmail.com; +91-98 66 53 26 13]
		Dr I Johnson [SJ College, Trichy; jnaadarsh@hotmail.com; +91-94 42 90 48 20]
		Dr Rajiv K Upadhayay [Govt PG College, Rishikesh; rku8@rediffmail.com; +91-94 12 97 28 90]
		Dr S Shekhar [Oxford College, Trichy; acousticssekar@yahoo.co.in; +91-99 94 92 00 30]
		Dr V Bhujanga Rao [Past President; NSTL, Vizag; vepcrew1@rediffmail.com; +91-98 66 44 10 74]
Co-opted Members	:	**Rajshekhar Uchil** [Josts, Bangalore; ruchil@josts.in; +91-98 80 17 08 95]
		Dr NK Narayanan [CIT, Kozhikode; csirc@rediffmail.com; +91-94 46 95 58 30]

INFORMATION FOR AUTHORS

ARTICLES

The Journal of Acoustical Society of India (JASI) is a refereed publication published quarterly by the Acoustical Society of India (ASI). JASI includes refereed articles, technical notes, letters-to-the-editor, book review and announcements of general interest to readers.

Articles may be theoretical or experimental in nature. But those which combine theoretical and experimental approaches to solve acoustics problems are particularly welcome. Technical notes, letters-to-the-editor and announcements may also be submitted. Articles must not have been published previously in other engineering or scientific journals. Articles in the following are particularly encouraged: applied acoustics, acoustical materials, active noise & vibration control, bioacoustics, communication acoustics including speech, computational acoustics, electro-acoustics and audio engineering, environmental acoustics, musical acoustics, non-linear acoustics, noise, physical acoustics, physiological and psychological acoustics, quieter technologies, room and building acoustics, structural acoustics and vibration, ultrasonics, underwater acoustics.

Authors whose articles are accepted for publication must transfer copyright of their articles to the ASI. This transfer involves publication only and does not in any way alter the author's traditional right regarding his/her articles.

PREPARATION OF MANUSCRIPTS

All manuscripts are refereed by at least two referees and are reviewed by the Publication Committee (all editors) before acceptance. Manuscripts of articles and technical notes should be submitted for review electronically to the Chief Editor by e-mail or by express mail on a disc. JASI maintains a high standard in the reviewing process and only accept papers of high quality. On acceptance, revised articles of all authors should be submitted to the Chief Editor by e-mail or by express mail.

Text of the manuscript should be double-spaced on A4 size paper, subdivided by main headings-typed in upper and lower case flush centre, with one line of space above and below and sub-headings within a section-typed in upper and lower case understood, flush left, followed by a period. Sub-sub headings should be italic. Articles should be written so that readers in different fields of acoustics can understand them easily. Manuscripts are only published if not normally exceeding twenty double-spaced text pages. If figures and illustrations are included then normally they should be restricted to no more than twelve-fifteen.

The first page of manuscripts should include on separate lines, the title of article, the names, of authors, affiliations and mailing addresses of authors in upper and lowers case. Do not include the author's title, position or degrees. Give an adequate post office address including pin or other postal code and the name of the city. An abstract of not more than 200 words should be included with each article. References should be numbered consecutively throughout the article with the number appearing as a superscript at the end of the sentence unless such placement causes ambiguity. The references should be grouped together, double spaced at the end of the article on a separate page. Footnotes are discouraged. Abbreviations and special terms must be defined if used.

EQUATIONS

Mathematical expressions should be typewritten as completely as possible. Equation should be numbered consecutively throughout the body of the article at the right hand margin in parentheses. Use letters and numbers for any equations in an appendix: Appendix A: (A1, (A2), etc. Equation numbers in the running text should be enclosed in parentheses, i.e., Eq. (1), Eqs. (1a) and (2a). Figures should be referred to as Fig. 1, Fig. 2, etc. Reference to table is in full: Table 1, Table 2, etc. Metric units should be used: the preferred from of metric unit is the System International (SI).

REFERENCES

The order and style of information differs slightly between periodical and book references and between published and unpublished references, depending on the available publication entries. A few examples are shown below.

Periodicals:

[1] S.R. Pride and M.W. Haartsen, 1996. Electroseismic wave properties, *J. Acoust. Soc. Am.*, **100** (3), 1301-1315.

[2] S.-H. Kim and I. Lee, 1996. Aeroelastic analysis of a flexible airfoil with free play non-linearity, *J. Sound Vib.*, **193** (4), 823-846.

Books:

[1] E.S. Skudzryk, 1968. *Simple and Comlex Vibratory Systems*, the Pennsylvania State University Press, London.

[2] E.H. Dowell, 1975. *Aeroelasticity of plates and shells*, Nordhoff, Leyden.

Others:

[1] J.N. Yang and A. Akbarpour, 1987. Technical Report NCEER-87-0007, Instantaneous Optimal Control Law For Tall Buildings Under Seismic Excitations.

SUMISSIONS

All materials from authors should be submitted in electronic form to the JASI Chief Editor: Dr Mahavir Singh, Acoustics, Ultrasonics & Vibration Section, CSIR-National Physical Laboratory, Dr. K. S. Krishnan Road, New Delhi-110 012 (email: mahavir@nplindia.org Tel: +91-11-4560.8317, Fax: +91-11-4560.9310). For the item to be published in a given issue of a journal, the manuscript must reach the Chief Editor at least twelve week before the publication date.

SUMISSION OF ACCEPTED MANUSCRIPT

On acceptance, revised articles should be submitted in electronic form to the JASI Chief Editor (mahavir@nplindia.org).

ISSN 0973-3302

JOURNAL OF ACOUSTICAL SOCIETY OF INDIA

Volume 40 Number 1 January 2013

A Quarterly Publication of the JASI
http://www.acousticsindia.org

JASI

Journal of Acoustical Society of India

The Refereed Journal of the Acoustical Society of India (JASI)

The Journal of Acoustical Society of India is a refereed journal of the Acoustical Society of India **(ASI)**. The **ASI** is a non-profit national society founded in 31st July, 1971. The primary objective of the society is to advance the science of acoustics by creating an organization that is responsive to the needs of scientists and engineers concerned with acoustics problems all around the world.

Manuscripts of articles, technical notes and letter to the editor should be submitted to the Chief Editor. Copies of articles on specific topics listed above should also be submitted to the respective Associate Scientific Editor. Manuscripts are refereed by at least two referees and are reviewed by Publication Committee (all editors) before acceptance. On acceptance, revised articles with the text and figures scanned as separate files on a diskette should be submitted to the Editor by express mail. Manuscripts of articles must be prepared in strict accordance with the author instructions.

All information concerning subscription, new books, journals, conferences, etc. should be submitted to Chief Editor:

Acoustics, Ultrasonics & Vibration Section, CSIR-National Physical Laboratory, Dr. KS Krishnan Road, New Delhi 110 012, Tel: +91.11.4560.8317, Fax: +91.11.4560.9310, e-mail: mahavir@nplindia.org

Annual subscription price including mail postage is Rs. 2000/= for institutions, companies and libraries and Rs. 2000/= for individuals who are not **ASI** members. The Journal of Acoustical Society of India will be sent to **ASI** members free of any extra charge. Requests for specimen copies and claims for missing issues as well as address changes should be sent to the Editorial Office:

Acoustics, Ultrasonics & Vibration Section, CSIR-National Physical Laboratory, Dr. KS Krishnan Road, New Delhi 110 012, Tel: +91.11.4560.8317, Fax: +91.11.4560.9310, e-mail: mahavir@nplindia.org

ISSN 0973-330

Printed at Alpha Printers, BG-2/38C, Paschim Vihar, New Delhi-110063 Tel.: 9811848335. JASI is sent to ASI members free of charge.

JASI

Journal of Acoustical Society of India (JASI)

A quarterly publication of the Acoustical Society of India

Volume 40, Number 2, April 2013

EDITORIAL

ARTICLES

INFORMATION

Basic Factors of Noise Control

ISound is a pervasive phenomenon and such factors as the high density of new residential construction and the use of high powered equipment in modern lightweight construction systems are leading to higher noise levels in our homes, our work spaces and generally everywhere in our cities. In fact, surveys done in the United States report that the noise level of major cities is rising at the rate of approximately one decibel per year. We can no longer ignore the trend.

While the general field of noise control is quite broad, the Insight program was limited to noise control in buildings; however, the principles of noise control are the same regardless of the environment being considered.

Inadequate noise control has often made a restaurant meal an unpleasant experience. High noise levels in the workplace are distracting and irritating, possibly resulting in higher absenteeism and loss of productivity. Inadequate acoustical privacy is common in office buildings. Conference rooms, despite the fact that their primary purpose is speech communication, are often excessively reverberant and noisy, making it difficult to understand speech from people only a short distance away. Most schools, churches, gymnasiums and swimming pools, as they now exist, could benefit from an acoustical tune-up, improving the quality of their indoor environment and their revenue-earning potential.

A recent survey in Vancouver found about 40% of the tenants in several multi-family dwelling projects dissatisfied with the degree of acoustical privacy in their homes. This was the major problem as far as the tenants were concerned, and it is a major complaint in many of our new apartment and condominium projects.

Elsewhere, in a large hotel in India, the acoustical engineers were overruled by the project designers; in order to save some Rs. 3.7 Crores they provided bedrooms with single glazing and operable sashes for ventilation. When the hotel came into service, most of the rooms had so much traffic noise penetrating, that they were unusable for sleeping. To rectify the situation, the hotel had to install double glazing and air conditioning at a cost of Rs. 9.6 Crores, not including the loss of revenue and general disturbance during the repair work.

Such errors are inexcusable, given that the knowledge exists to design and build quality acoustical environments.

The essence of this Insight program is a discussion of the principles of noise control in buildings. The fundamentals of sound are explained in the first paper, followed by the criteria and methods to control noise within rooms, in the second paper. The third paper examines the issue of noise reduction across walls, floors, windows and doors, and the last paper deals with acoustics of buildings, with an emphasis on machine and plumbing noises and the annoying problem of flanking noise.

Mahavir Singh

Journal of Acoustical Society of India : Vol. 40, No. 2, 2013 (pp.69-76)

Methods for Estimating the Accurate Values of Sound Absorption Measurements

Mahavir Singh* and Dharam Pal Singh
Acoustics, Ultrasonics & Vibration (AUV) Section,
Apex Level Standards & Industrial Metrology Division,
CSIR-National Physical Laboratory, Dr. K. S. Krishnan Road, New Delhi -110 012
**e-mail: mahavir.acoustics@gmail.com*

[Received: 21.01.2013; Revised: 02.04.2013; Accepted: 10.04.2013]

ABSTRACT

In order to check that the reverberation chamber measurement of absorption coefficient was consistent, a short run of repeatability measurements were carried out as per standard procedure. The standard ISO/IEC 17025:2005 on the competence of testing and calibration laboratories requires that these laboratories shall apply procedures for estimating the accurate values of their measurement results. One of the possibilities is to evaluate the accurate values, taking into account all components that contribute significant value to the final result. In case of the sound absorption coefficient value, carried out according to the standard EN ISO 354:2003, the overall value is first of all influenced by the reverberation times T_1, T_2 and the power attenuation coefficients m_1 and m_2, calculated according to the ISO 9613-1 standard and representing the climatic conditions in the reverberation room. In spite of very little difference between the values m_1 and m_2 representing the change of climatic conditions usually, it is the case in laboratory, exponential form of the coefficient's function causes that the accurate value of measurement results increase with frequency very fast. Particularly for the high frequencies, the accurate values of measurements are so important that the evaluation of the sound absorption coefficient is practically not possible.

1. INTRODUCTION

However there is at present no wholly accepted calculations of repeatability and standard error in reverberation chamber absorption coefficient and the data quoted in the literature varies widely. Figure 1 shows a typical RT spectrum for the empty room, along with the IS 8225 minimum curve for the particular room volume of 257 m^3 and surface area of 244 m^2.

Because of lack of uncertainty evaluation based on inter-laboratory validation approach, it has to be carried out by the laboratory itself. Using the general methods specified in GUM[1], first of all we need to establish a relationship between the mesurand Y and other quantities X_1, X_2,...X_n (input values) through a function f, called the measurement equation

$$Y = f(X_1, X_2, \ldots\ldots\ldots\ldots X_n) \quad (1)$$

Such equation must express not only the physical relation from which we can obtain the value of mesurand Y but also it should be accompanied by a quantitative statement of its uncertainty which arises from the uncertainties of the input values of directly measured quantities x_1, x_2 ...x_n being the estimates of X_1, X_2, ...X_n.

In general, uncertainty components (each of them - represented by estimated standard deviation, termed standard uncertainty and noted u(xi) or, shortly, ui) are categorized according to the method used to evaluate

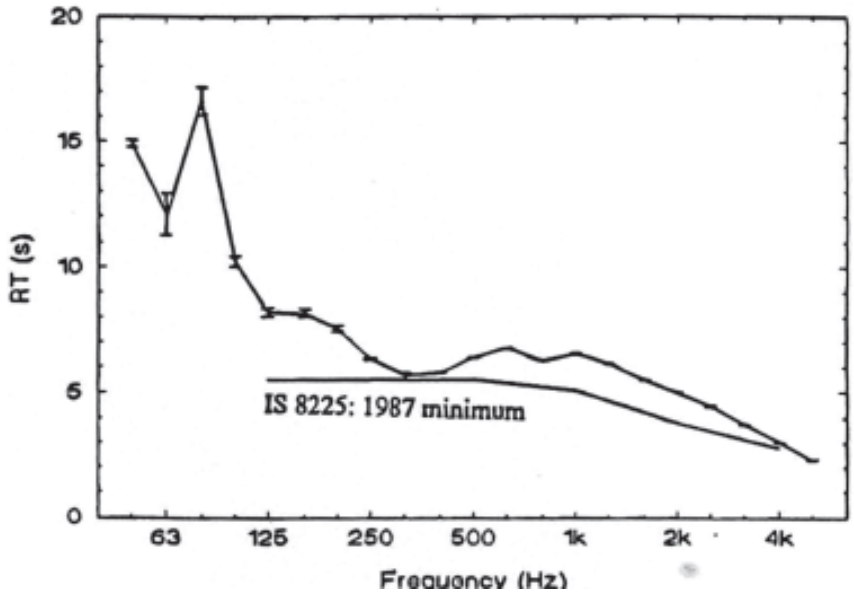

Fig. 1. Average reverberation time in empty chamber plotted with IS 8225-1987 minimum curve. The error bars represent ± one standard error

them. There are two methods of evaluating standard uncertainty:

- Type A is based on any valid statistical method, for example the standard deviation of the mean of a series of independent observations s(xi); in such case the standard uncertainty u(xi) = s(xi),
- Type B takes advantage of an outside source (for example, data provided in calibration) and/or of an assumed distribution.

The standard deviation of the estimated measurement result y, called combined standard uncertainty $u_c(y)$, is obtained by combining the individual standard uncertainties u(xi) using the usual statistic method of combining standard deviations "root - sum - squares" according to the formula:

$$u_c^2(y) = \sum_i^n = 1 \left(\frac{\partial f}{\partial x_i} \right)^2 u^2(x_i) \tag{2}$$

and calculating the positive root square of the result.

Equation (2) is called the law of propagation of uncertainty and the partial derivatives $\delta_f/\delta x_i$ is referred to sensitivity coefficients. The products of module $\delta/\delta x_i$ and $u(x_i)$ are usually presented in a table, as "uncertainty budget". This practice is very useful to identify the dominant terms that contribute significant uncertainty to the result.

The measure of uncertainty, that defines an interval in which the value of the quantity subject to measurement (the mesurand Y) can be confidently asserted to lie, is named expanded uncertainty U (it means that one can confidently believe that the value of Y, estimated by y, lies within the limits $y - U \leq Y \leq y + U$).

The expanded uncertainty is obtained by multiplying a combined standard uncertainty by a coverage factor k depending on the desired level of confidence and the type of statistical distribution.

$$U(Y) = ku_c(y) \tag{3}$$

2. UNCERTAINTY ELEMENTS

2.1 Repeatability of Measured Absorption Coefficient

In order to check that the reverberation chamber measurement of absorption coefficient was consistent, a short run of repeatability measurements was made, as recommended by IS 8225. A sample of 12.5 mm thick gypsum board panel (test sample area of 12.8 m^2) was measured six times in the same configuration, being removed from the chamber and replaced for each measurement. The repeatability "r" of the system was the found from

$$r = t\sqrt{2}.\sigma_{n-1} \quad (4)$$

where *t* is student's factor for 95% probability and five degrees of freedom and σ_{n-1} is the standard deviation of the six measurements. The six absorption coefficients are plotted in Fig. 2 along with r and a typical standard error curve from one of the measurements. The average α value of repeatability (r_{95}) is 0.11 in terms of reverberation chamber absorption coefficient and 0.02 in terms of absolute error. The average ?? value of typical standard error is 0.02 in terms of absolute error as shown in Fig. 2.

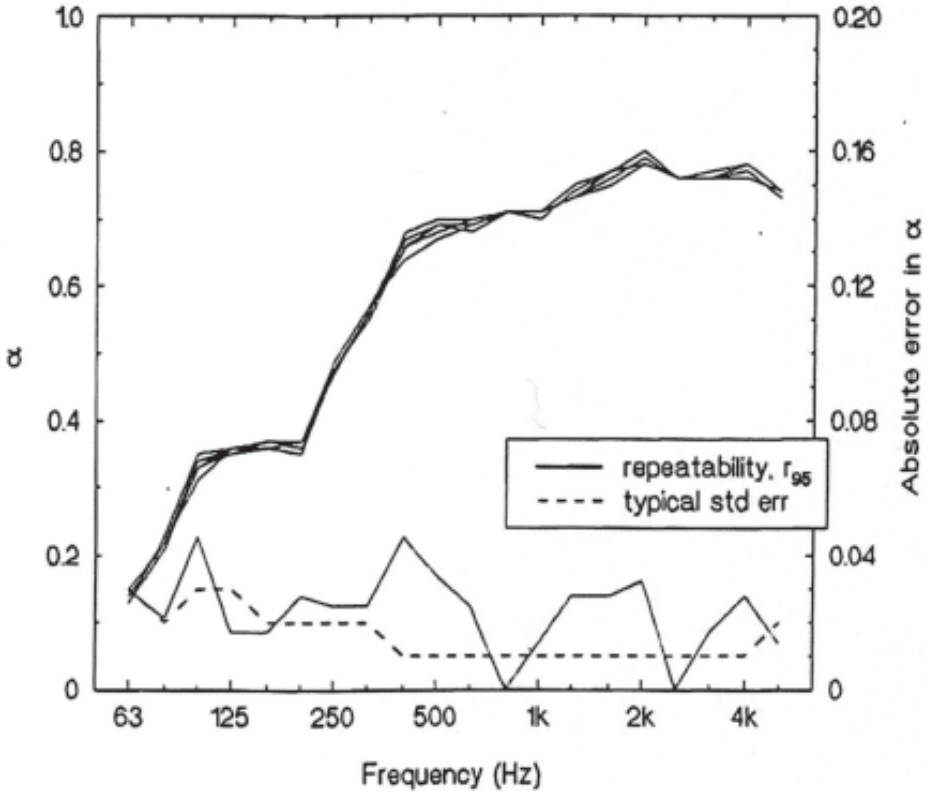

Fig. 2. Repeatability 95% of six gypsum tiles absorption measurements and typical standard error of one

2.2 Reverberation Time

The reverberation time is measured in n points for each frequency band. The mean value T_f calculated from *n* measurements is taken as the estimated measurement result. In this case, the standard uncertainty of T_f is equal to the experimental standard deviation s (T_f) of the mean of a series of independent observations $T_{f,\ i=1,\ldots,n}$.

$$u(T_f) = s(T_f) = \frac{s(T_{f,i})}{\sqrt{n}}, S \quad (5)$$

Student's - t distribution with *n* freedom degrees is assumed.

2.3 Area of Sample

Assuming the rectangular distribution of estimated measurement result, with the boundary of ± 0.005 m^2, the standard uncertainty of sample's area amounts to

$$u(S) = \frac{0.005m^2}{\sqrt{3}} = 0.0029m^2 \tag{6}$$

2.4 Volume of Room

Assuming the rectangular distribution of estimated measurement result, with the boundary of resolution ± 0.5 m^3, the standard uncertainty of room volume amounts to

$$u(S) = \frac{0.5m^3}{\sqrt{3}} = 0.2887m^3 \tag{7}$$

2.5 Environment Factors

The measurement equations for the environmental factors like temperature, atmospheric pressure and relative humidity assume the form:

$$e = e_0 + \delta e_1 + \delta e_2 + \delta e_3 + \delta e_4 \tag{8}$$

where,

e_0 the reading value of the environmental factor in a room,

δe_1 the dispersion of sensor indications,

δe_2 the resolution of sensor indications,

δe_3 the error of sensor indications,

δe_4 the uncertainty of indication error.

The standard uncertainty of dispersion δe_1 is calculated on the basis of the estimated standard deviation of *m* series of *n* measurements.

$$u(\partial e_1) = \frac{S_i(e_1)}{n} \tag{9}$$

where,

$S_i(e_1)$ the experimental standard deviation of ith series equal to

$$Si(e1) = \sqrt{\frac{\sum_{i=1}^{m} S_1(e_{1,i})}{m}} \tag{10}$$

The standard uncertainty of resolution δe_2 is evaluated with the assumption of rectangular distribution with the boundary of resolution supposed, respectively, as b = ± 0.05 °C, ± 0.05 kPa or ± 0.05%.

$$u(\delta e_2) = \frac{b}{\sqrt{3}} \tag{11}$$

Contribution in uncertainty of δe_3 and δe_4 are calculated from the expanded uncertainty U evaluated for normal distribution with confidence level 95% and stated in the calibration certificate of the device.

$$u(\delta e_3) = \frac{U(\delta e_3)}{k_{N,95\%}} = \frac{U(\delta e_3)}{2} \tag{12}$$

$$u(\delta e_4) = \frac{U(\delta e_4)}{k_{N,95\%}} = \frac{U(\delta e_4)}{2} \tag{13}$$

The equation of propagation law of uncertainty has the form:

$$u^2(e) = u^2(\delta e_1) + u^2(\delta e_2) + u^2(\delta e_3) + u^2(\delta e_3) \tag{14}$$

3. UNCERTAINTY OF THE SOUND ABSORPTION COEFFICIENT MEASUREMENT

The sound absorption coefficient ?s of a plane absorber or a specified array of test objects is calculated using the formula

$$\alpha_s = \frac{A_T}{S} \tag{15}$$

where,

A_T the equivalent sound absorption area of the test specimen, m^2

S the area covered by the test specimen, m^2

The equivalent sound absorption area of the test specimen A_T, according to ISO 354:203 [3] is given as follows,

$$A_T = A_2 = A_1 = 55.3V\left[\frac{1}{C_2T_2} - \frac{1}{C_1T_2}\right] - 4V(m_2 - m_1) \tag{16}$$

where,

V the volume of the empty reverberation room, m3

T_1 the reverberation time of the empty reverberation room,

T_2 the reverberation time of the reverberation room after the test specimen has been introduced, s

c_1, c_2 the propagation speed of sound in air at the temperature t_1 and t_2 (respectively), m/s

m_1, m_2 the power attenuation coefficients, calculated according to ISO 9613-1[4] using the climatic conditions that have been present in the empty reverberation room and after the test specimen has been introduced, m^{-1}

The value of m is calculated from the attenuation coefficient α dependent on temperature t, atmospheric pressure p_a and relative humidity h_r, according to the formula

$$m = \frac{\alpha}{10Ig(e)} \tag{17}$$

The detailed analyze of the uncertainty budget leads to a conclusion that the standard uncertainty of sound absorption depends very strongly on the sensitivity coefficients of humidity, particularly at the high frequencies (see Table 1).

Table 1. Sound absorption with its uncertainties and sensitivity coefficients

				Sensitivity coefficients of environment factors					
f, Hz	**αS**	**u_c (α_S)**	**U (α_S)**	**$\delta\alpha_S/\delta pa_1$**	**$\delta\alpha_S/\delta pa$**	**$\delta\alpha_S/\delta hr_1$**	**$\delta\alpha_S/\delta hr_2$**	**$\delta\alpha_S/\delta t_1$**	**$\delta\alpha_S/\delta t_2$**
100	0.14	0.009	0.018	0.00000	0.00000	-0.00023	0.00018	0.00062	0.00085
125	0.31	0.014	0.029	0.00000	0.00000	-0.00035	0.00027	0.00061	0.00116
160	0.54	0.017	0.035	0.00000	0.00000	-0.00056	0.00045	0.00072	0.00181
200	0.64	0.020	0.041	0.00000	0.00000	-0.00082	0.00070	0.00072	0.00227
250	0.82	0.023	0.048	0.00000	0.00000	-0.00120	0.00109	0.00059	0.00301
315	0.92	0.025	0.052	0.00000	0.00000	-0.00177	0.00174	0.00020	0.00382
400	0.94	0.027	0.056	0.00000	0.00000	-0.00267	0.00280	-0.00064	0.00468
500	1.02	0.020	0.041	0.00000	0.00000	-0.00398	0.00437	-0.00182	0.00571
630	0.99	0.019	0.040	0.00001	-0.00001	-0.00617	0.00694	-0.00312	0.00680
800	1.00	0.024	0.049	0.00001	-0.00001	-0.00994	0.01119	-0.00448	0.00811
1000	0.96	0.019	0.039	0.00001	-0.00002	-0.01568	0.01748	-0.00568	0.00929
1250	0.98	0.026	0.053	0.00002	-0.00002	-0.02478	0.02729	-0.00692	0.01062
1600	0.98	0.023	0.047	0.00002	-0.00003	-0.04105	0.04464	-0.00852	0.01224
2000	0.96	0.030	0.060	0.00003	-0.00004	-0.06455	0.06960	-0.01033	0.01418
2500	0.99	0.045	0.093	0.00004	-0,00005	-0.10116	0.10837	-0.01285	0.01702
3150	1.03	0.068	0.139	0.00005	-0.00007	-0.16047	0.17109	-0.01665	0.02146
4000	1.01	0.106	0.217	0.00007	-0.00011	-0.25730	0.27334	-0.02279	0.02829
5000	1.02	0.163	0.332	0.00009	-0.00015	-0.39768	0.42128	-0.03153	0.03816
6300	0.98	0.253	0.516	0.00011	-0.00020	-0.61920	0.65403	-0.04515	0.05338
8000	0.95	0.394	0.804	0.00011	-0.00023	-0.96576	1.01642	-0.06626	0.07662

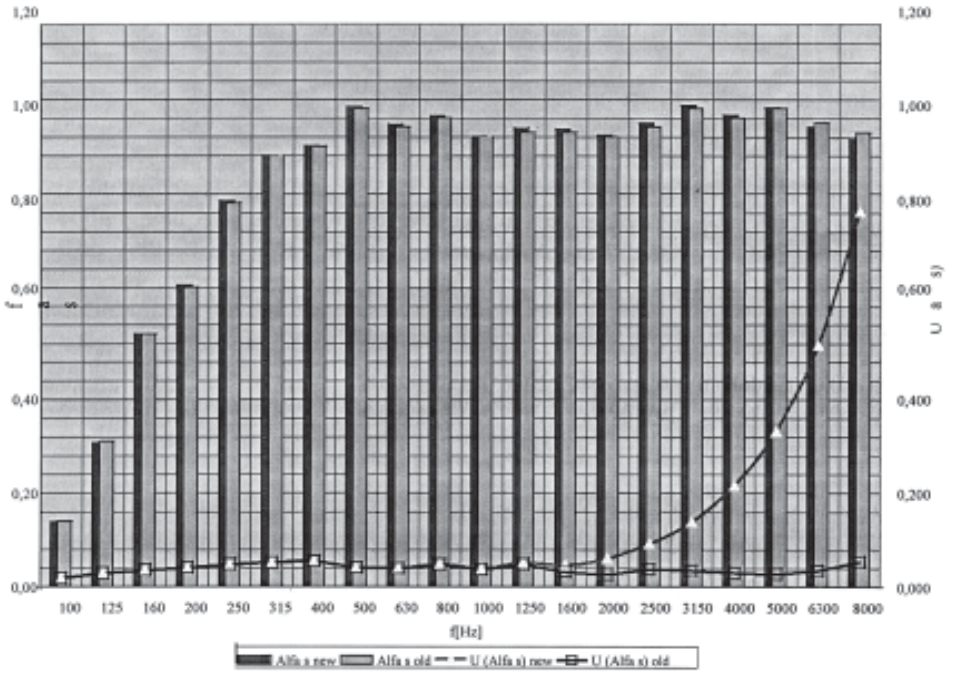

Fig. 3. Comparison the calculation results of the sound absorption coefficient expanded uncertainty carried out according to both version of ISO 9613-1 standard

Table 2. Set of calculation results of sound absorption coefficient á$_s$ and its uncertainties conducted according to both versions of standard ISO 354 [3- 4, 6]

f, Hz	Acc. to ISO 354:2003 [3]			Acc. to ISO 354:1985 [2]			m_2-m_1	Differenc e α $_S$
	α $_S$	u_c (α $_S$)	U (α $_S$)	α $_S$	u_c (α $_S$)	U (α $_S$)		
100	0.14	0.009	0.018	0.14	0.009	0.018	0.000	-0.001
125	0.31	0.014	0.029	0.31	0.014	0.029	0.000	-0.004
160	0.54	0.017	0.035	0.54	0.017	0.035	0.000	0.000
200	0.64	0.020	0.041	0.64	0.020	0.041	0.000	0.005
250	0.82	0.023	0.048	0.82	0.023	0.048	0.000	0.004
315	0.92	0.025	0.052	0.92	0.025	0.052	0.000	0.000
400	0.94	0.027	0.056	0.94	0.027	0.056	0.000	0.001
500	1.02	0.020	0.041	1.02	0.020	0.041	0.000	0.004
630	0.99	0.019	0.040	0.98	0.019	0.039	0.000	0.006
800	1.00	0.024	0.049	1.00	0.024	0.048	0.000	0.005
1000	0.96	0.019	0.039	0.96	0.018	0.037	0.000	0.000
1250	0.98	0.026	0.053	0.97	0.024	0.048	0.000	0.008
1600	0.98	0.023	0.047	0.97	0.015	0.031	0.000	0.005
2000	0.96	0.030	0.060	0.96	0.013	0.026	0.000	0.003
2500	0.99	0.045	0.093	0.98	0.018	0.038	0.000	0.008
3150	1.03	0.068	0.139	1.02	0.017	0.035	0.000	0.007
4000	1.01	0.106	0.217	1.00	0.014	0.029	0.000	0.006
5000	1.02	0.163	0.332	1.02	0.013	0.027	0.000	0.001
6300	0.98	0.253	0.516	0.99	0,017	0.035	0.000	-0.010
8000	0.95	0.394	0.804	0.97	0.026	0.054	0.000	-0.016

In the previous version of standard ISO 354:1985 [2] a possible change of climatic conditions was not taken into consideration ($m_1 = m_2 = 0$). Table 2 presents the calculation results of the sound absorption coefficient α_s and its standard and expanded uncertainties carried out with respect to environment factors and without them. It can be observed that in spite of very little difference between the values m^1 and m^2 (representing the change of climatic conditions), the values of α_s calculated according to [3] in the frequency bands $f \geq 3150$ Hz are considerably greater. Also, the uncertainties of measurement results increase with frequency very fast. Particularly for the high frequencies, the values of uncertainties are so important that the evaluation of ?s is practically not possible.

4. CONCLUSION

The standard error curve was computed from the variance of the measured RTs according to [3]. The evaluation of the uncertainty is very important because it testifies to the quality of measurements. Observing the uncertainty budget for each band of frequency allows finding the deciding factors. In case of sound absorption measurements, it could be very difficult to obtain accurate results due to the important uncertainty at high frequencies bands. The function circumscribing the power attenuation coefficient m calculated according to ISO 9613-1, thanks to the non-linear shape, influences the uncertainty of measurement results in spite of very small changes in environmental conditions in laboratory.

5. REFERENCES

[1] Guide to the Expression of Uncertainty in Measurement. International Organization for Standardization, Geneva, First Edition, 1993. Corrected and reprinted 1995.

[2] IS 8225-1987, Measurement of Sound Absorption in a Reverberation Room, Bureau of Indian Standard, New Delhi.

[3] MAHAVIR SINGH, OMKAR SHARMA and V. MOHANAN, 2004. Repeatability and standard error in reverberation chamber absorption coefficient, ICA2004 (Fr2.B1.4), pp. 3393-3396.
[4] EN ISO 354:1985, Acoustics - Measurement of sound absorption in a reverberation room.
[5] EN ISO 354:2003, Acoustics - Measurement of sound absorption in a reverberation room.
[6] ISO 9613-1:1993, Acoustics - Attenuation of sound during propagation outdoors - Part 1: Calculation of the absorption of sound by the atmosphere.

Journal of Acoustical Society of India : Vol. 40, No. 2, 2013 (pp. 77-90)

Free Field Acoustic Radiation of Composite Plates with Surface Bonded PFC Using RME Technique

Partha Bhattacharya[1] and Atanu Sahu[2]*

[1]Department of Civil Engineering, Jadavpur University, Kolkata 700 032 (W.B.), India
German Aerospace Center (DLR), 38108 Braunschweig, Germany
[2] Institute of Composite Structures & Adaptive Systems, German Aerospace Center (DLR), Lilienthalplatz7, 38108 Braunschweig, Germany
**e-mail: sahuatanu@daad-alumni.de*

[Received: 16.11.2012; Revised: 24.01.2013; Accepted: 27.02.2013]

ABSTRACT

In the present work an attempt is made to develop a mathematical model based on Helmoltz Integral equation and Finite Element methodology to estimate radiated sound from a vibrating baffled composite plate in to the free field. Radiation Mode Expansion (RME) technique is implemented to estimate the radiated sound. Subsequently, it is attempted to reduce the radiated sound by introducing surface bonded IDE-PFC actuators. The model is developed in a MATLAB environment and results are obtained for various locations of IDE-PFC patch actuators.

1. INTRODUCTION

Sound attenuation is usually achieved by means of energy absorbing materials placed on the surface of the radiating structure. This technique works quite well for sounds at medium and high frequencies but is very inefficient at low frequencies because the thickness of the absorbing material necessarily increases with decreasing frequency. It has been reported by Kaczmarska and Augustynska [1] that the addition of sound proofing material used for the sound insulation ability of 'soundproof' cabins averages typically 30-50 dB for frequencies above 500 Hz, but only 0-19 dB for frequencies below 500 Hz. Active noise control is an alternative to this 'passive' strategy where destructive interference is used to reduce the sound pressure field.

A more advanced form of this technique is based on altering the vibrations of a noisy structure such that it radiates very little sound. This alteration is achieved by introducing discrete force actuators. Active Structural Acoustic Control or simply ASAC is one such 'active' strategy and in the present work the focus is on developing an ASAC strategy for vibrating laminated composite plate radiating sound into the free field.

A vibrating structure that is surrounded by an acoustic medium causes pressure perturbations in the medium, which are experienced as sound. An arbitrarily shaped vibrating structure consists of infinite number of natural mode shapes associated with its natural frequencies. If the vibration mode shape pattern of a simply supported plate structure resting on an infinite baffle is studied, it can be seen that the fundamental mode shape exhibit a dome shaped pattern, whereas the second mode is represented by a sine wave in the major axis and a sine along minor axis. The fluid immediately next to the plate reacts differently for each mode shape. The fundamental mode displaces the fluid outward virtually in phase over the entire surface. On the other hand for the second mode the fluid sloshes back and forth between each oscillating trough of the sine wave. The vibration of the plate in its first mode transports the fluid in front of the plate farther away,

whereas, the net fluid motion due to the second mode remains transverse and never propagates far from the planar surface [Bevan [2]]. However the structural mode shapes do not radiate independently. In fact, the strong dependence on inter-modal coupling between structural modes affects the radiated sound power such that reducing dominant structural modes may have little affect on the radiated power.

Apart from identifying structural mode shapes, researchers developed the concept of surface velocity filters or acoustic radiation filters. Acoustic radiation filters describe the radiated power in terms of discrete surface velocities and the surface radiation resistance as shown by Cunefare [3]. This concept can be termed as modal approach for characterizing acoustic radiation from vibrating structures. It must be noted that the term 'modal' here refers to acoustic radiation modes and are independent of structural vibration modes or should not be confused with acoustic cavity modes. Borgiotti and Jones [4] first introduced a modal representation using Singular Value Decomposition (SVD) to represent radiation efficiencies and singular velocity patterns. Baumann, Saunders and Robertshaw [5] implemented feedback control by using radiation filters in frequency weighted cost functions to minimize the most efficient radiation modes. Elliot and Johnson [6] implemented feed forward control of beams and plates using radiation filters. Gibbs *et al.* [7] developed a Radiation Modal Expansion (RME) technique, exploiting the acoustic radiation bounding properties, thereby reducing computation effort for real time digital signal processing applications. Bhattacharya *et al.* [8] in their work had shown that the bounding properties of the acoustic radiation modes are very much dependent on the size and geometry of the vibrating structure.

In the present work an attempt is made first to estimate the radiated sound power from a baffled plate subjected to mechanical excitations and thereafter introducing surface bonded Piezo Fiber Composite patches with Inter-digitated Electrode (IDE-PFC) to observe the changes in the radiated energy behaviour of the same plate. The mathematical model is presented in the next section.

2. MATHEMATICAL BASIS

2.1 Acoustic Model

Acoustic wave propagation through a homogeneous elastic fluid such as air is described by the well-known wave equation. In the case of harmonic time dependence, this equation reduces to Helmholtz differential equation, which is as follows,

$$\nabla^2 p(r) + k^2 p(r) = -i\omega\rho_0 q(r) \tag{1}$$

where *p(r)* is the complex acoustic pressure amplitude at location 'r' and q(r) is the external sound source. The Helmholtz differential equation can be rewritten in an integral form called the Helmholtz integral equation. In the present work the analysis is restricted to a flat plate like structure. The schematic of the structure is given in Fig. 1. When it is assumed that the structure is placed in a baffle, the Helmholtz integral equation reduces to Rayleigh second integral [9] given by,

$$p(r) = \frac{i\omega\rho_0}{2\pi}\int_S v_n(r_s)\frac{e^{-ik|r-r_s|}}{|r-r_s|}dS \tag{2}$$

The Rayleigh integral is solved with a primitive numerical scheme. The plate is divided into 'N' rectangular elements of equal size, which are small compared to the acoustic wavelength. It is assumed that the normal velocity is constant across each element. That makes each element behave like an elemental radiator or piston that moves with constant harmonic velocity. For this discretization, the Rayleigh integral can also be written as $p_f = Z_f v_n$ (3)

where $\boldsymbol{p}_f$ is the vector with pressures in a set of field points, v_n is the vector with normal surface velocities of the elemental radiators, and Z_f is a frequency dependent transfer matrix, whose elements are given by,

$$(Z_f)_{ij} = \frac{i\omega\rho_0 S_e}{2\pi}\frac{e^{-ikr_{ij}}}{r_{ij}} \tag{4}$$

where, S_e is the surface area of the elemental radiator and r_{ij} denotes the radial distance between the radiating point and the measuring point.

For the same discretization, the expression for the sound power reduces to the summation:

$$W = \frac{S_e}{2}\mathrm{Re}(v_n^H p) \tag{5}$$

where, p is the vector with surface pressures, evaluated at the same points on the surface as v_n.

With the substitution of $p = Zv_n$, the sound power 'W' can be obtained in terms of discrete number of velocity measurements as, $W = v_n^H R v_n$ (6)

In this equation R = (Se/2)Re(Z) is the so called radiation resistance matrix.

This matrix R can be written as,

$$R = \frac{\omega^2\rho_0 S_e^2}{4\pi c_0}\begin{bmatrix} 1 & \frac{\sin(kr_{21})}{kr_{21}} & \cdots & \frac{\sin(kr_{1N})}{kr_{1N}} \\ \frac{\sin(kr_{12})}{kr_{12}} & 1 & & \vdots \\ \vdots & & \ddots & \vdots \\ \frac{\sin(kr_{N1})}{kr_{N1}} & \cdots & \cdots & 1 \end{bmatrix} \tag{7}$$

As is seen in Eq. (7), the matrix R is a function of frequency and for online control, it becomes computationally expensive to estimate 'R' at various frequencies. RME technique as described by Gibbs *et al*.[5] in their paper helps one to circumvent this problem and the same is implemented in this paper as well.

2.2 IDE - PFC Model

In case of IDE-PFC patches (actuator), the electric field along the length of the patch between two consecutive electrode fingers is assumed to be linearly distributed with alternate electrodes being suitably grounded. It is assumed that there is a perfect bond between the piezo layer and the elastic substrate (no-slip condition).

In the present development only d33 actuation induced by the interdigitated electrode is considered and hence only E_3 field (along axis 3) is taken in the modeling. Therefore, the electric field can be expressed in the form, $\{E\} = \begin{Bmatrix} 0 \\ 0 \\ E_3 \end{Bmatrix}$ (8)

Following the formulation for PFC with IDE as given by Azzouz *et al.* [9] , the electric field is related to the electric potential as,

$$\{E\} = \begin{Bmatrix} E_{31} \\ - \\ E_{3np} \end{Bmatrix} = -\begin{bmatrix} \frac{1}{h_1} & - & 0 \\ - & - & - \\ 0 & - & \frac{1}{h_{np}} \end{bmatrix} \begin{Bmatrix} \phi_1 \\ - \\ \phi_{np} \end{Bmatrix} \tag{9}$$

In general h_1, h_2,,…, hnp are the spacing of interdigitated electrode for 1, 2,…, np piezoelectric layer, though in the present case only one piezoelectric actuator layer is considered.

The PFCs are composite materials comprising of uniaxially aligned active piezoceramic fibers and a matrix phase and therefore the effective fibrous volume comes into play. So, the right hand side of Eq. (9) is to be suitably multiplied with fiber volume fraction.

The electro-mechanical coupling relationship is developed by assuming a uniform voltage distributed over the entire piezo-element and therefore following Eq. (9) the electric field within the IDE-PFC actuator patch is,

$$\{E^a\} = -\frac{1}{h_{ide}}[B_\phi]\{\phi^a\} \tag{10}$$

where,$[B_\phi]$ is a unit matrix and hide is the spacing of IDE.

3. SOLUTION METHODOLOGY

The flat plate like structure considered for the present study is first discretized using four-node isoparametric finite element whereby each element is considered as an elemental radiator (piston). For the m x n discretized structure, the radiation resistance matrix is then developed. As shown by Cunefare [1], the radiation modes and the corresponding radiation efficiencies are then obtained by carrying out a Singular Value Decomposition (SVD) on the matrix R. On carrying out the SVD, the efficiency of the radiation modes are arranged in the decreasing order of importance and one obtains the corresponding eigen vector representing the radiation mode shapes. Because the radiation matrix, R depends upon the frequency, the singular value decomposition must be performed at all the frequency steps. As a result the radiation efficiency and the radiation mode shape also is a function of frequency. The radiation efficiency plots as well as the radiation mode shapes are stored.

In the next phase of the work, a free vibration analysis is carried out on the same structure and the structural mode shapes along with the corresponding frequencies are obtained. Thereafter, a response analysis is performed on the structure following Eq. (11).

$$[M]\{\ddot{x}\} + [K]\{x\} = \{F_m\} + \{F_{el}\} \tag{11}$$

where, $\{F_m\}$ is the mechanical load vector and $\{F_{el}\}$ is the electrical load vector generated by the surface bonded IDE – PFC patches and subjected to electrical voltage. On carrying out the response analysis one can obtain the surface velocities with and without the control voltages and finally one can obtain the radiated sound power from the vibrating plate from Eq. (6).

4. RESULTS & DISCUSSION

As has been already mentioned, the present work is an attempt to estimate the radiating sound power from a vibrating laminated composite plate structure in the free field with and without using surface bonded IDE-PFC actuators in presence of the mechanical loading. In order to achieve the objective, a rectangular plate with surface bonded IDE-PFC patches (Fig. 3) is considered as the test structure. The material and geometric properties of the host structure and the actuator are given as follows;

Properties of the Host Structure:-
Length, L = 1.5m; Width, b = 1.24m; Thickness = 8 layers @ 0.00025m;
Lay-up sequence: $(0/90/45/-45)_s$
Material used: Carbon fibre reinforced laminated composite

E_{11} = 143.92 GPa, $E_{22} = E_{33}$ = 8.82 GPa, ν_{12} = 0.29, $\nu_{23} = \nu_{31}$ = 0.4,
$G_{12} = G_{23} = G_{31}$ = 4.45 GPa, Density, ñ = 1542 kg/m^3.
Properties of the IDE-PFC Actuator:-
Length of actuator patch, L_a = 0.2 m
Width of actuator patch, b_a = 0.165 m
Thickness of actuator patch, t_p = 0.001 m
Spacing of interdigitated electrode, h_s = 0.0005 m
Young's Modulus, E_a = 70 GPa, Poisson's Ratio, ν = 0.3,
Piezoelectric stress/charge constant, e_{33} = 34.52 C/m^2,
Dielectric constant, k = 0.1153X10^{-7} F/m, Fiber volume fraction, V_f = 0.2

The developed finite element code written in the MATLAB platform is first validated for the piezo actuation obtained from the surface bonded IDE-PFC patch and the results are shown in Table 1.

From the above table it can be said that the developed code works well for the piezo actuation employing IDE-PFC patches.

Table 1. In-plane force generated from IDE-PFC actuator patch for an applied voltage of 50 volts

Present Finite Element (X10^2 N/m)	Theoretical Solution (X10^2 N/m)(Ref. [8])
3.452	3.452

In the next step the radiation resistance matrix, R, is evaluated for the baffled plate structure and SVD is carried out for the same over the frequency range of interest. In this particular example, SVD has been carried out over a frequency range of 0-225 Hz. Typical radiation mode shapes for the vibrating plate at 10 Hz and 225 Hz are shown in Fig. 2. The radiation efficiency curves are then obtained with the radiation mode shapes evaluated at 225 Hz as the cut off frequency and the radiated power is evaluated. It is very important to note that the radiation behavior of flat plate like structure is dependent only on its geometry and is independent of the boundary condition and material properties.

The plate which is then fixed all along its edges is then subjected to a transverse pressure of 140 N/m^2. The acoustic power radiated for the first 6 modes are then calculated based on Eq. (6) and are shown in the Fig. 3.

Subsequently, an electrical voltage of 50 Volts is applied on the surface bonded IDE-PFC patches along with the mechanical load as already mentioned. A study is then carried out by positioning the piezo patches at various locations on the plate (Fig. 4 (I-V)) and the effect of which on the radiated sound power are observed.

Case I

For the first case, two actuator patches are placed on the plate and the direction of piezoelectric polarization is shown using the arrowhead (Fig. 4 (I)). An electrical voltage of 50 Volts is applied on the patches.

The radiated sound power for the first six radiation modes is obtained and is presented in Fig. 5. It is interesting to note that the energy radiated in the 2nd and the 3rd radiation mode (anti symmetric modes) shows a significant increase whereas the symmetric modes show a reduction in the radiated energy level. Another important issue in the present scenario is that although the overall radiated energy is less for the

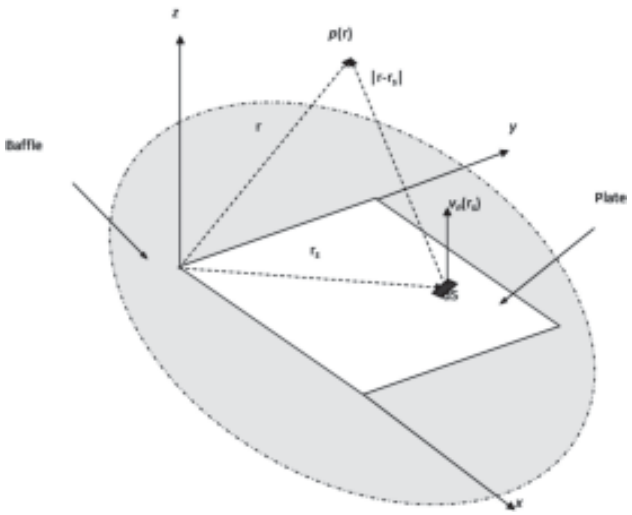

Fig. 1. Geometric Interpretation of Rayleigh Integral

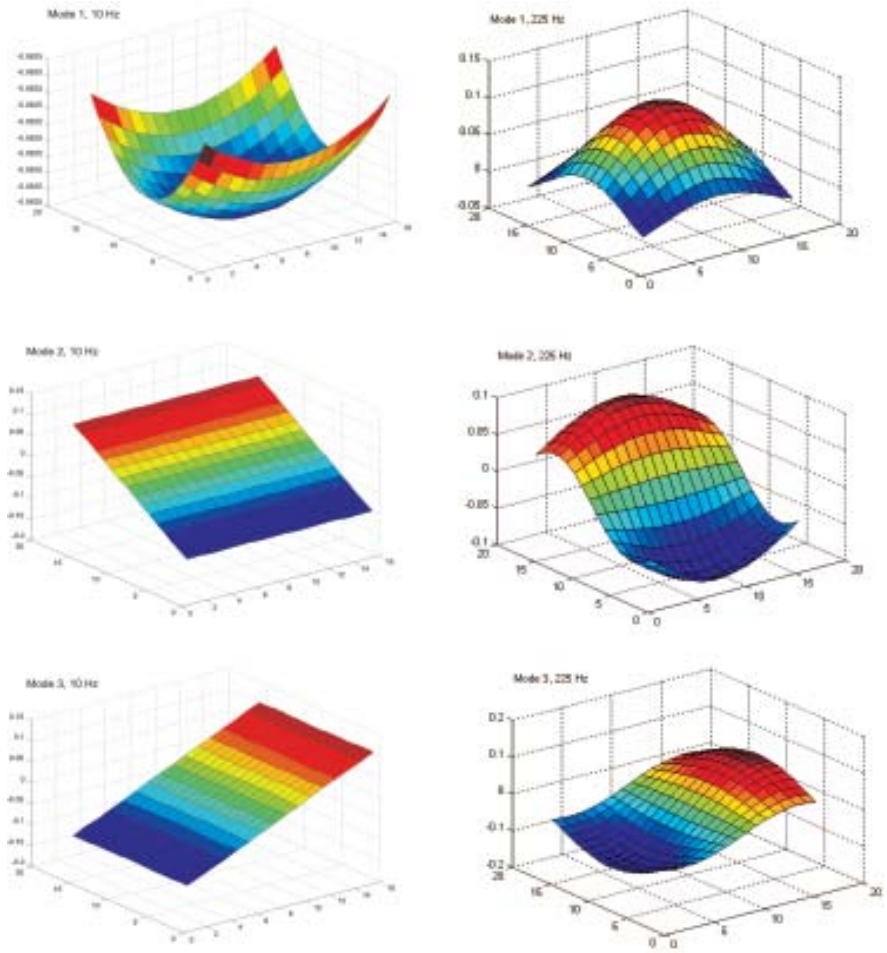

Fig. 2. Radiation mode shapes for the laminated composite plate at 10 Hz and 225 Hz

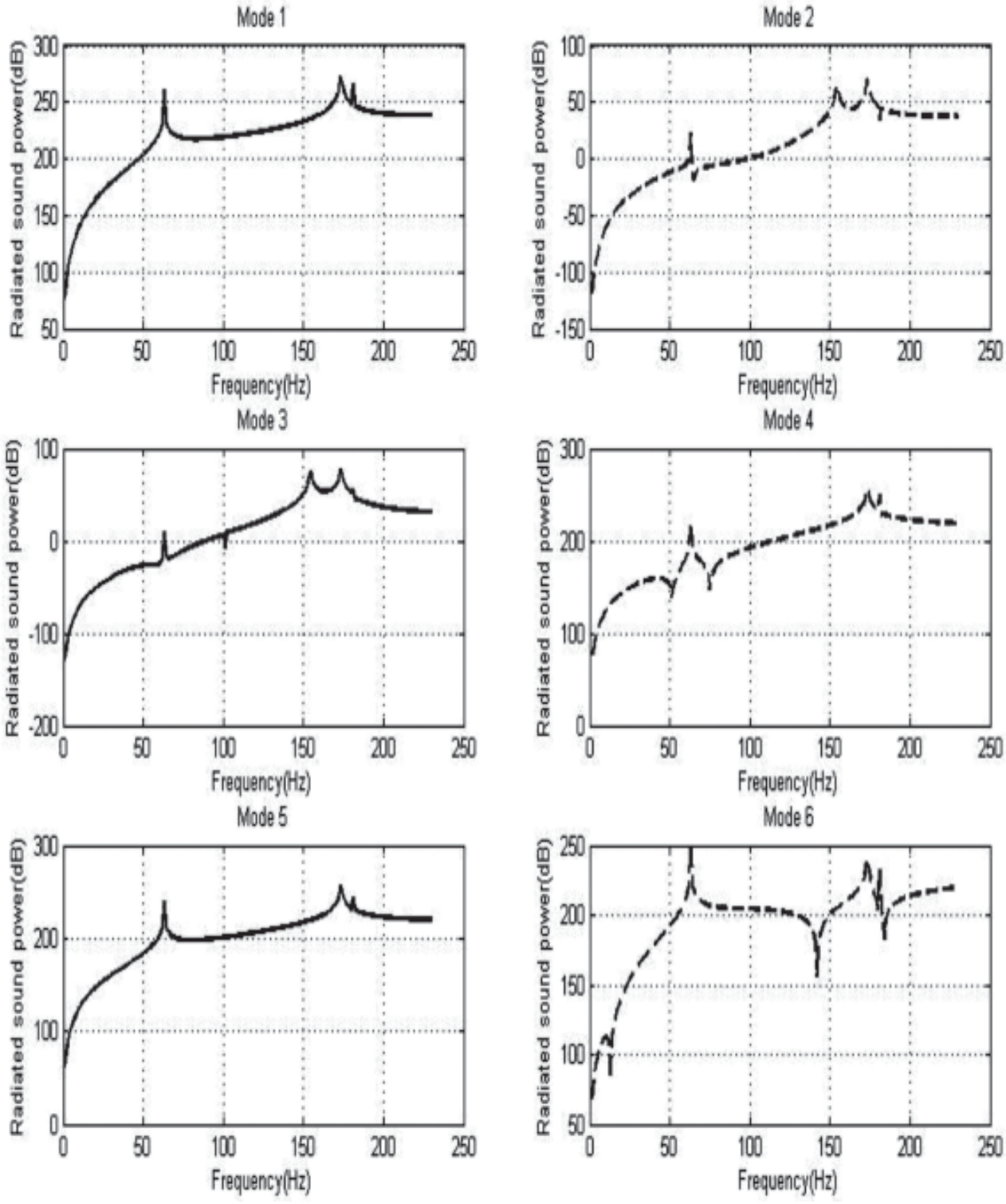

Fig. 3. Radiated acoustic power (dB) from the baffled plate without piezo actuation

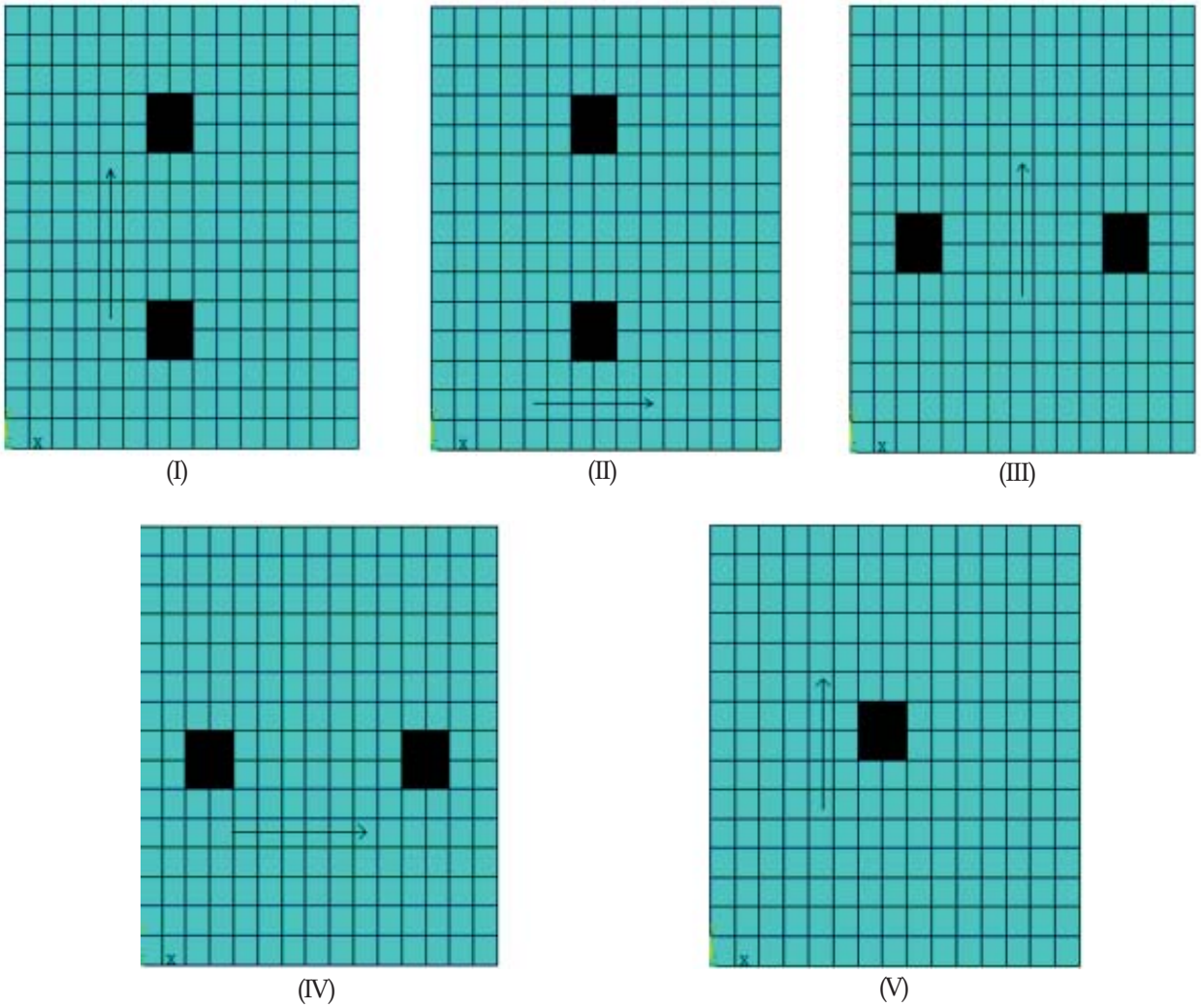

Fig. 4. Finite Element Mesh showing positions of the piezo patches (shaded area) along with the direction of polarity (shown with arrow)

symmetric modes, in case of first and the fifth modes certain structural frequencies appear to contribute significantly in the energy plot.

Case II

In the second case the position of the piezo patches are kept the same but the polarization direction is altered as shown in Fig. 4 (II). Similar radiated energy plots for the first six radiation modes are obtained and are presented in Fig. 6. It is observed that the radiated energy does not differ very much in comparison to Case I except that in mode 1. Another important point that needs a special mention is that for mode 1, 3 and 5 some of the structural modes that contributes to the radiated energy in Case I get nullified.

Case III

In this case, the two piezoelectric patches are placed along the width direction as shown in Fig. 4 (III). The polarization direction is shown with the arrowhead. Radiated acoustic energy from various acoustic modes from the vibrating plate in dB is calculated for this particular case and is presented in Fig. 7. It is observed in this particular case that for first and the 5th radiation mode, the radiated energy at around 150 Hz shows a

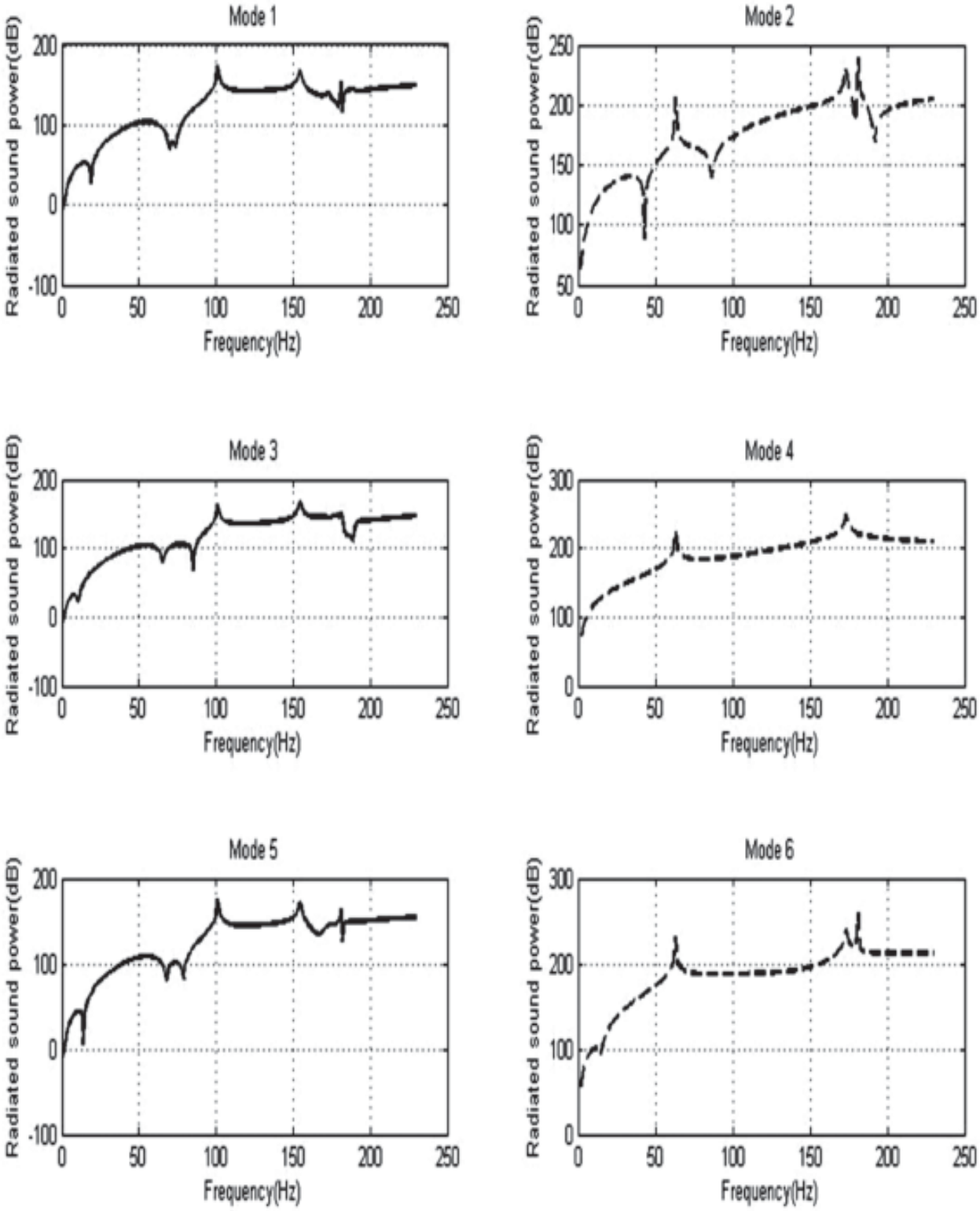

Fig. 5. Radiated sound power (dB) (with piezo actuation) from the plate in the free field for piezo polarity along Y-axis (Case I)

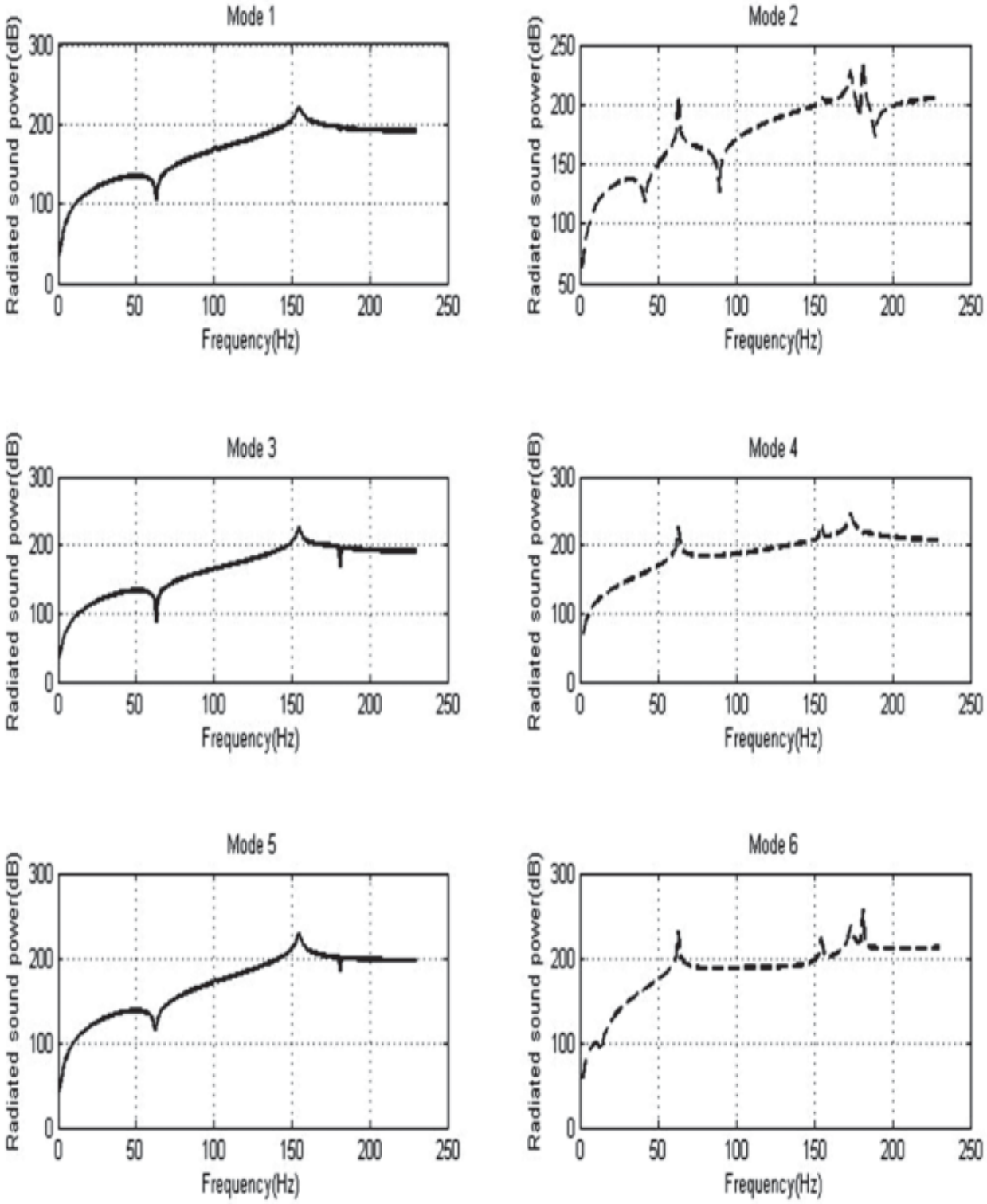

Fig. 6. Radiated sound power (with piezo actuation) from the plate in the free field for piezo polarity along X-axis (Case II)

sharp increase when compared to that seen in Case 1 and Case II. For all other modes the trend is very similar to that observed in Case 1 and II.

Case IV

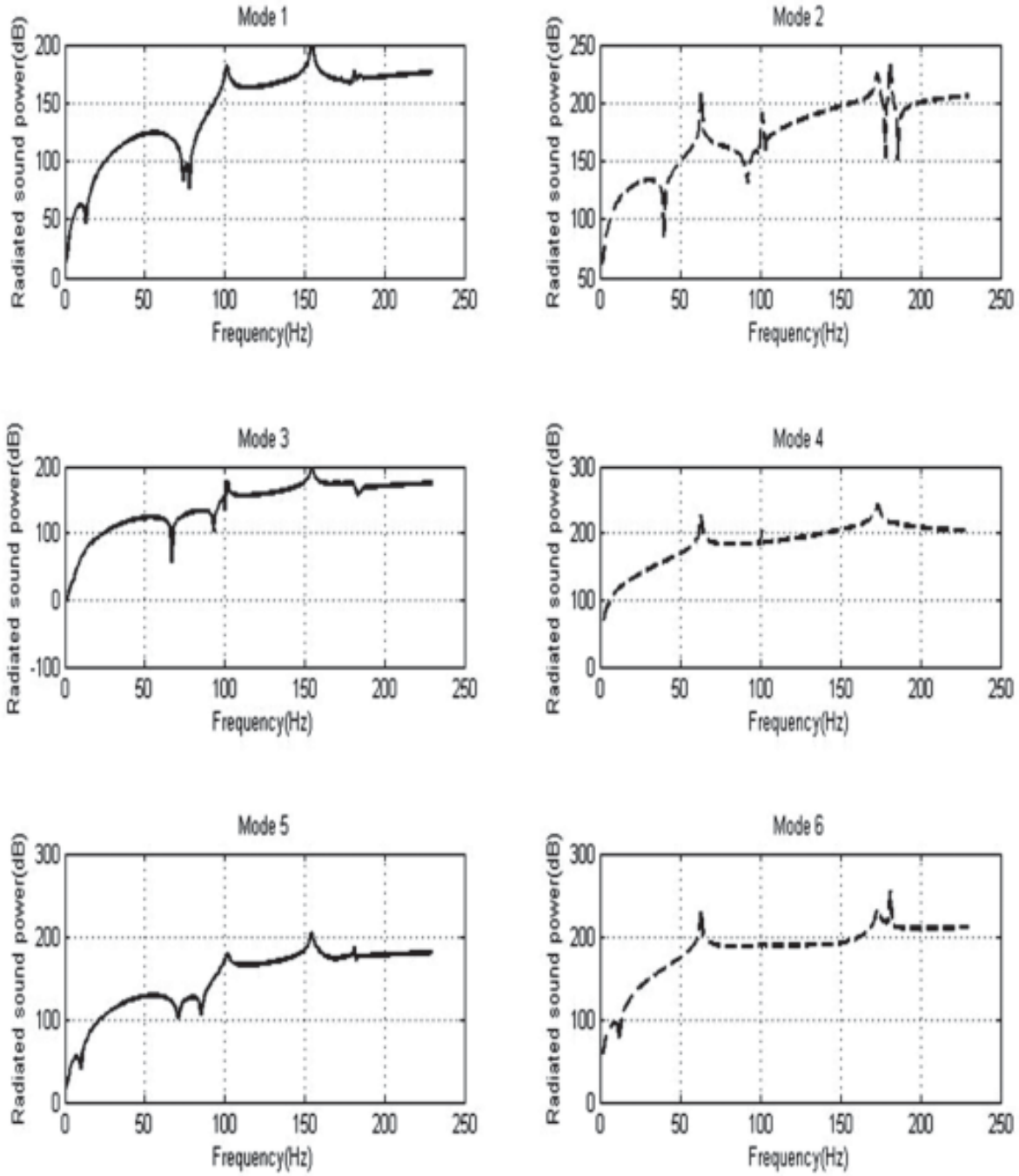

Fig. 7. Radiated sound power (with piezo actuation) from the plate in the free field for piezo polarity along Y-axis (Case III)

The position of the piezoelectric patches in this example is kept the same as that for case III. The polarity direction is altered and is shown in Fig. 4 (IV). The results showing the radiated energy in dB in this particular case are plotted in Fig. 8. From the results it is observed that they are very similar to those obtained in Case II.

Case V

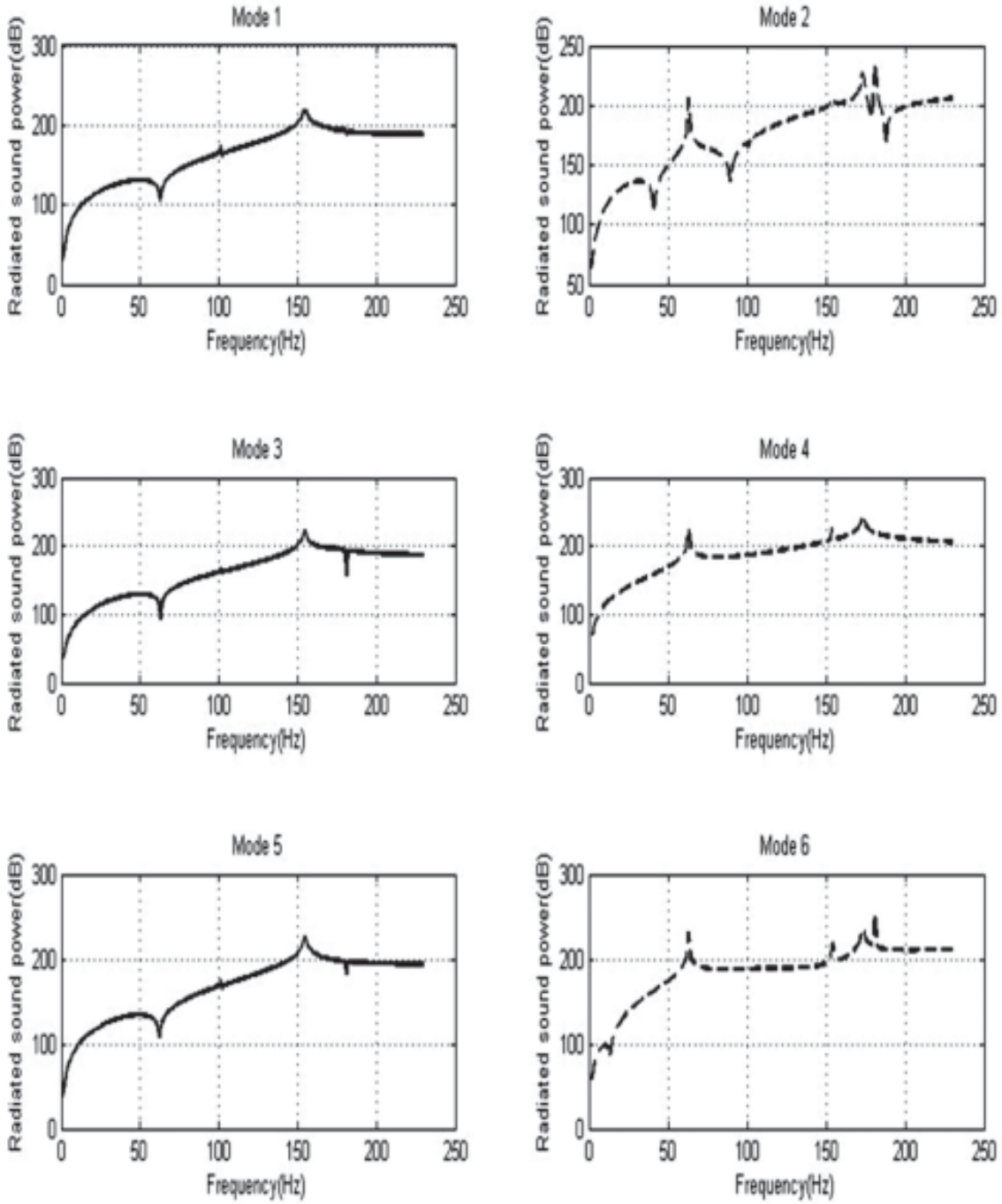

Fig. 8. Radiated sound power (with piezo actuation) from the plate in the free field for piezo polarity along X-axis (Case IV)

In this case, actuator patches are placed at the middle of the plate and the radiated sound power are plotted for first 6 modes and are presented in Fig. 9.

5. CONCLUSIONS

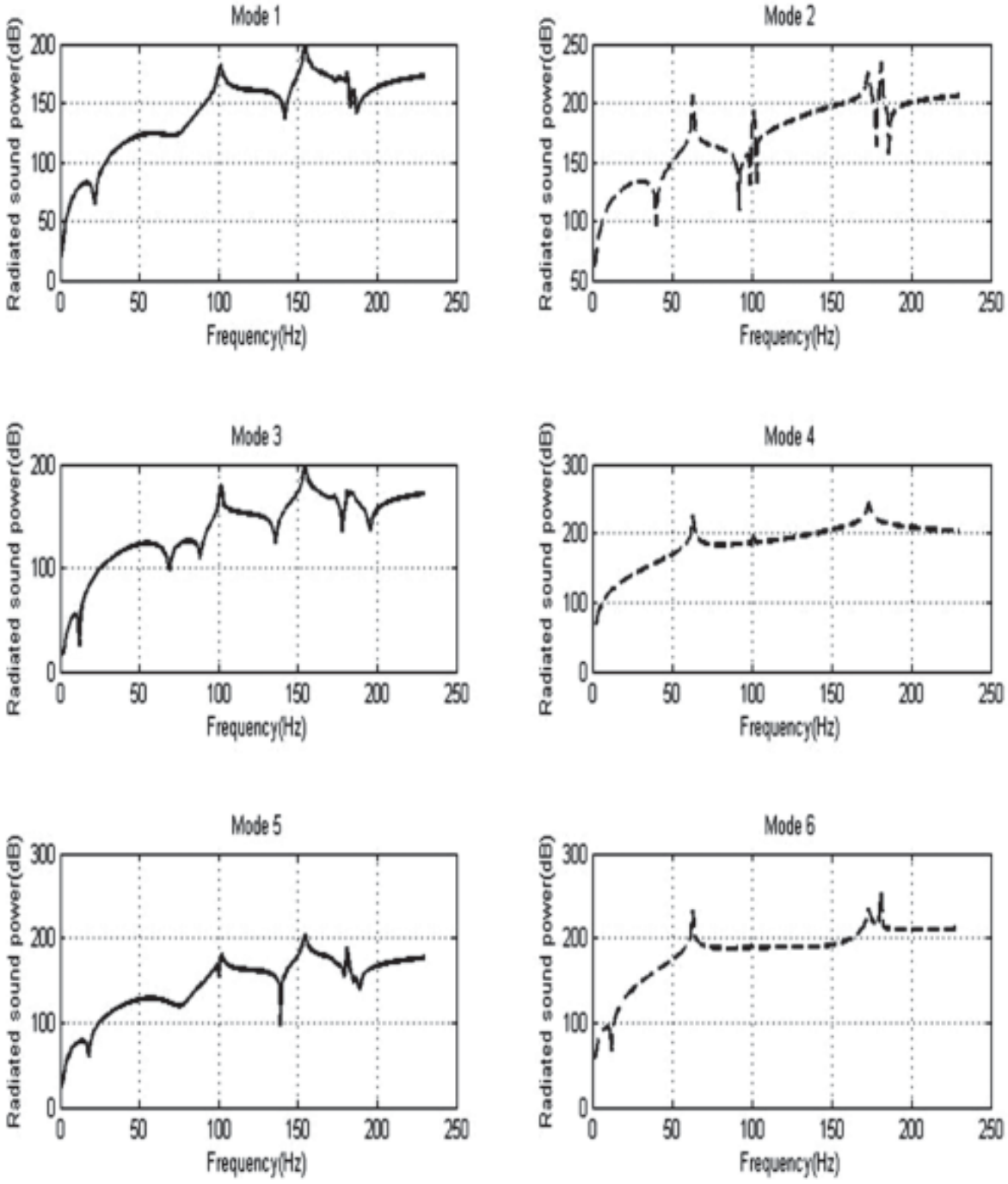

Fig. 9. Radiated sound power (with piezo actuation) from the plate in the free field for centrally placed piezo with polarity along Y-axis (Case V)

In the present work, Rayleigh's integral approach to the solution of the Helmholtz's Equation is carried out and Radiation Modal Expansion method is implemented to calculate the radiation efficiency and the radiation mode shapes of the vibrating composite plate structure. Thereafter, a finite element model based on Lagrange's equation for the laminated plate bonded with IDE-PFC patch actuator is developed. Radiation energy for the vibrating structure with and without the piezo patches are the evaluated for various piezo location and piezo polarity.

It is generally observed that with the introduction of the piezo patches, the radiated energy associated with the first, fifth and the sixth radiation mode, which are pumping modes and are symmetric in nature, show a reasonable reduction. On the contrary, in the second and the third radiation mode, the bare plate which hardly contributes to any radiation energy starts pumping a significant energy into the free field once the piezoelectric patches are actuated.

The position and the polarity of the piezo patches also affect the radiated energy from the baffled plate by influencing the structural modes. From the obtained results it can be concluded that the positioning of the piezo patches on the vibrating plate has got a significant role in the overall sound radiation. In the future it is planned to do an optimization study to properly identify the piezo position and also the polarity direction such that the radiated sound power can be minimized effectively.

6. ACKNOWLEDGEMENT

The authors wish to acknowledge the Department of Science and Technology (DST), India for providing the necessary support under the DST-PURSE scheme.

7. REFERENCES

[1] A. KACZMARSKA and D. AUGUSTYNSKA, 1992. Study of sound insulation of control cabins in industry in the low frequency range *J. Low Frequency Noise Vib.*, 11, 42–46.

[2] J.S. BEVAN, 2001. Technical Report NASA/CR-2001-211265, Piezoceramic Actuator Placement for Acoustic Control of Panels,.

[3] K.A. CUNEFARE, 1991. The minimum multimodal radiation efficiency of baffled finite beams, *J. Acoust. Soc. Am.*, **90**, 2521–2529.

[4] G.V. BORGIOTTI and K.E. JONES, 1994. Frequency independence property of radiation spatial filters, *J. Acoust. Soc. Am.*, 96, 3516–3524.

[5] W.T. BAUMANN, W.R. SAUNDERS and H.H. ROBERTSHAW, 1991. Active Suppression of Acoustic Radiation from Impulsively Excited Structures, *J. Acoust. Soc. Am.*, **90**(6), 3202-3208.

[6] S.J. ELLIOTT and M.E. JOHNSON, 1993. Radiation modes and the active control of sound power, *J. Acoust. Soc. Am.*, 94, 2194–2204.

[7] G.P. GIBBS, R.L. CLARK, D.E. COX and J.S. VIPPERMAN, 2000. Radiation modal expansion: Application to active structural acoustic control, *J. Acoust. Soc. Am.*, **107**, 332 – 339.

[8] P. BHATTACHARYA, M. ROSE and O. HEINTZE, 2009. 9th International Conference on Vibrations Problems, IIT Kharagpur, India, 19-22 January, Active structural acoustic control of laminated Plates using RME technique.

[9] F.J. FAHY, 2001. Foundations of Engineering Acoustics, Academic Press.

[10] A.A. BENT, 1997. PhD Thesis, MIT, Active Fiber composites for Structural Actuation.

[11] M.S. AZZOUZ, C. MEI, J.S. BEVAN and J.J. RO, 2001. Finite Element Modeling of MFC/AFC actuators and performance of MFC, *J. of Intel. Mat. Sys. and Struct.*, **12**, 601-612.

Journal of Acoustical Society of India : Vol. 40, No. 2, 2013 (pp. 91-107)

Shape Reconstruction of Underwater Objects from Acoustic Returns

T. Ratna Mani, Raj Kumar* and O. Vijay Kumar
Naval Physical and Oceanographic Laboratory (NPOL)
Email: ratna_mani51@yahoo.com
**Defence Institute of Advanced Technology (DIAT), Pune*

[Received: 15.12.2012; Revised: 21.03.2013; Accepted: 12.04.2013]

ABSTRACT

Ramp response technique is reported in literature for extraction of profiles ofunderwater objects. This paper presents the application of time frequency analysistoolsWigner Distributions (WD's), in extraction of profiles of underwater objects from reflections (echo) and exploitation of the profile extracted in generation of 2-D image of the object. This method is developed for extraction of profiles, mainly from short/medium transmitted pulses, that are of interest in practical applications. This method has been verified for various pulse parameters of the incident wave, like pulse frequency, pulse length as well as different size and shape of the scattering body.The profiles thus obtained are used in reconstruction of object shape.Inverse Radon function is employed for filtered back propagation i in 2-D shape reconstruction. The results for different underwater objects shapes are presented here, employing simulated backscatter (echoes).

1. INTRODUCTION

Inverse scattering techniques retrieve the shape and size information of an underwater object from available measurement or observation data, such as far-field backscattered frequency spectrum at certain aspects. Most of the data is observed /captured in time domain and exploited for differentapplications.Computer-aided tomography,or reconstructive tomography refers to the cross-sectional imaging of an object from either transmission or reflection data by illuminating the object from many different view directions or aspect angles.

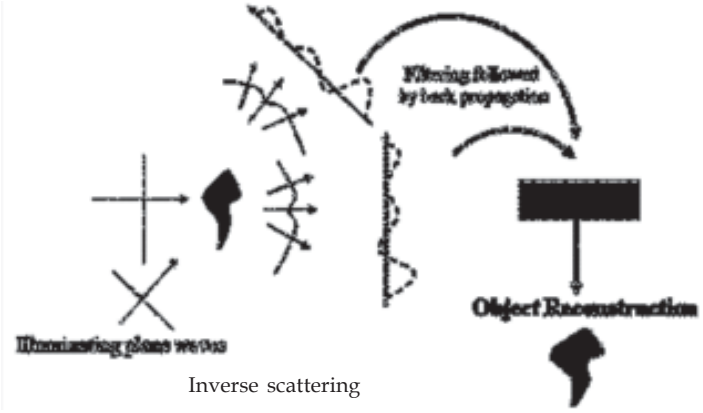

Fig. 1. Inverse scattering

In ocean tomography, underwater objects are imaged by reflection tomography. Reconstructive acoustic tomography reconstructs an image of the objectfrom projections recorded at all aspect angles.The transformation of object functionto image is done by single dimension projection views of the object. The sonartransducer is moved from point to point around the entire circumference of acircle so as to view the object from all possible aspect angles, thus compilinga complete set of projections over 3600 of aspect angle viewing. The imagerepresents a 2-D map of the 3-D acoustic reflectivity function when projectedon the imaging plane.Similar to X-ray absorption tomography the tomographic imagingsonar, the poor resolution is overcome by viewing the object at many aspect angles θ, enabling the reconstruction of a high-resolution image ofthe object .In bi-static sonar ,the image can be obtained by fewer no of projections. This is based on obtaining the object profiles in few multiple angles and thenapplying limiting surface technique iteratively to obtain the 3D image. In both the cases the profile functions /object functions have to be obtained for reconstruction of the image. In General, the profile function is obtained based on impulse/ wideband input. However, in practice the sonar transducers are narrowband and the sound propagating in underwater media also has certain response. In addition the requirement of operations also imposes certain minimum duration for the transmission pulse. The velocity of sound in this media 1500 meters/second (approximately) also has certain effects on the received data. Hence to obtain the images pulse, compression has to be carried out, or profile function has to e obtained by processing the received data.

The forward scattering is found for given incidentacoustic waves and the physical properties ofthe object by simulation or observation data. For generation of back scatter from the object, exact analytic solutions [1, 2] can be derived and used for objects of simplegeometries, such as sphere, infinite cylinder,and spheroid, while approximate methods areoften used for objects of more general shapes.The most popular method for inverse scattering for underwater objects is the ramp response technique. This is basedon twice integrating the impulse responseobtained from the underwater object. X.M.Zhang *et al*. [2] developed a numerical method to obtain the ramp response for underwater objects in acoustic field, that requires limited data infrequency domain.The concept of impulse response technique isfirst introduced by E.M. Kennaugh [8] and applied to electromagnetic scattering problems,based on the physical optics approximation.The impulse response of an object was interpretedas the second derivative of the profile function.The profile function is defined as the crosssectional area along the direction of the incidentwave. Consequently, by integrating the impulseresponse twice, it was found that the rampresponse of the object is proportional to itsprofile function [4]. The ramp response techniquehas been utilized in electromagneticscattering for profile reconstruction [1]. Thistechnique has also been applied in acousticwave filed for solving inverse problems, likeunderwater acoustical imaging and non-destructiveevaluation methods.The methods based on impulse responsetechniques have limited practical applications asthe wide band returns from the underwaterbody are highly influenced by the media. Thepractical signals have limited bandwidth,generally very narrowband due to the limitationsof the projectors/sensors. In addition, the pulsewidths used is based on certain criteria andvaries from short pulse to medium pulse. Theramp response technique cannot be applied forthis type of signals. However, as the profilefunction is the cross sectional area along thedirection of propagation, the reflected wave canbe interpreted as sum of discretised wavesreturning from the scattering body, and can beconsidered as time series data, with timevarying frequency content. Time series datahave been traditionally analysed in either thetime or the frequency domains.For signals with time-varying frequencycontent, the combined time-frequency (TF)representations, based on the Cohen class of (generalized) Wigner Distributions (WD's) offer a powerful analysis tool. Using them, it ispossible to: 1) trace the time-evolution of theresonance features usually present in a standardSonar Cross Section (SCS), or in a Radar Cross Section (RCS) and 2) extract target information that may be difficult to even notice in anordinary SCS or RCS In the underwaterapplications. The time frequency techniques aregenerally used to get time and frequencylocalisation of the signal. This information isvaluable in frequency estimation of signals, anddetection and classification of targets.Application of time frequency analysis forscattering/inverse scattering is not much reportedin literature. Time-frequency analysis can becarried out, on the reflected signal, for theprofile function extraction. The instantaneousamplitude correspond to the cross section of thescattering body , that is The profile function is the timeseries of amplitude at discrete time intervals,can be obtained from summing the energy fromall frequency bins corresponding to each time step. This technique is applied to

extract profilefunction of two-dimensional objects. The results were verified from the ramp response technique for single cycle signal. The results also obtained are very close to the object shape simulated. The scatter was simulated by numerical method (Kirchhoff's integration). This technique is verified on different pulse lengths and pulse parameters like CW, LFM couple of time frequency methods i.e., STFT and Winger Ville were used as time frequency analysis. The results were comparable for short pulses. But for pulses of longer duration, Winger Ville performs better. The advantage of this method is that it can be applied on any type of signals and with any pulse length. The signals can narrow-band or broad-band based on the requirement. By appropriately choosing the pulse parameters and processing parameters this technique can be used on any pulse of practically used in underwater applications.

Further,the object shape is reconstructed from the profiles obtained from multiple angels. This reconstruction is done by inverse radon function with profiles as input. For comparison the radon transform in 2D is obtained and the shape is reconstructed with inverse radon function. However radon transform the incident wave is considered as an impulse /wideband signal .The reconstructed object shape from pulsed signal is comparable with that of theoretical reconstructed image (by radon and Inverse Radon)Simulated projection data corresponding to an idealized object are often used in the development and evaluation of reconstruction algorithms.

2-D objects of shapes given in Figure 1b have been selected for simulation and the echo from the object was simulated by numerical method. The simulated time series is used for profile extraction. Profile function is obtained via Wigner-Ville Distribution. With these generated profiles2-D image is reconstructed.

2. ACOUSTIC REFLECTION TOMOGRAPHY

In mono-static sonar application the source and receiver are collocated so that after insonification by the acoustic source, the object scatters some of the energy backwards to the receiver [12]. The transducer-object geometry is depicted in Fig. 2 where$x$and y represent a Cartesian coordinate system with an origin O located atthecentre of the scene to be imaged by the sonar. The scene includes theobject of interest. The sonar measurement system reflectively projects thethree-dimensional reflectivity function$\tilde{n}(x, y, z)$ of the objects on the twodimensionalimaging plane (or x $y$plane) shown in Fig.2. the z direction is perpendicular to the xyplane. The direction of propagation of the sonartransmission is at an angle$\hat{e}_j$to the x -axis and $f(x, y)$ denotes the 2-D distributionof the amplitude of the signal backscattered from the object. Theobject function $f(x, y)$ that is reconstructed in acoustic reflection tomographyis the two-dimensional spatial distribution of the projected reflectivity function, that is, $f(x,y) = \int \tilde{n}(x, y, z)\, dz$.

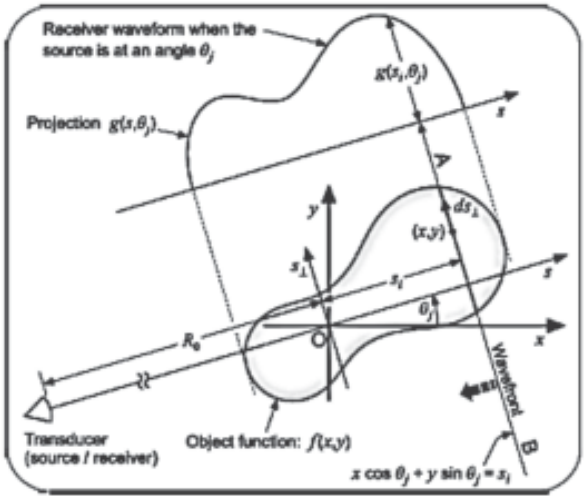

Fig. 2. D view of the transducer-object geometry & the projection signal for insonification angle θj.

In Fig. 2, the sonar transducer and the object are widely separated sothat a planar wave front projected on the imaging (or xyplane) plane canbe represented by the straight line AB, which is defined mathematically bythe equation $x\cos\grave{e}_j + y\ \sin\grave{e}_j = s_i$. Here s_i is the perpendicular distance ofthe line from the origin O. The two-way propagation time for the wave frontAB is given by $t_i = t_0 + 2(s_i/c)$, where c is the speed of sound propagationin the underwater medium. The distance of the origin from the transduceris $R_0 = (ct_0)/2$. As the signals backscattered from all of the points alonga wave front are in phase, the total signal received at time t_i is found byadding the backscattered signals f(x,y)for values of x and y along the line $x\cos\grave{e}_j + y\ \sin\grave{e}_j = s_i$. This can be represented mathematically as

$$g(s_i.\theta_j) = \int f(x,y)\, ds_1 \qquad (1)$$

where $\int f(..)\, ds_1$ denotes integration along the line $x\cos\grave{e}_j + y\ \sin\grave{e}_j = s_i$The integral in Equation (1) is referred to as a wave front integral. The set of wave front integrals $g(s_i.\grave{e}_j)$ where $-\infty < s_i < \infty$, forms the function $g(s_i.\grave{e}_j)$ that defines the projection of f(x,y)for the angle j . Reconstructive acoustic tomography reconstructs an image of the object from projections recorded at all aspect angles. The object function f(x,y)is reconstructed from the inverse of the integral equation given by

$$g(s_i.\theta_j) = \int f(x,y)\, ds_1$$

$$= \int f(s_i\cos\theta_j - s_1\sin\theta_j,\ s_i\sin\theta_j - s_1\cos\theta_j)\, ds_1$$

Here, the coordinate pair (si, s1) represents the rotation of the coordinatepair $f(x, y)$ through an angle, that is $x = s_i\cos\theta_j - s_1\sin\theta_j \quad y = s_i\sin\theta_j + s_1\cos\theta_j$

The 2-D function $g(s_i.\grave{e}_j)$ represents the Radon transform of $f(x, y)$.Using the inverse Radon transform or other suitable reconstruction algorithm, an image of the object that is represented by the two-dimensional distribution $f(x, y)$can be recovered from the projections recorded at all aspect angles j , where $0 < j < 2\eth$. The inversion is given by,

$f(x,y) = R^{-1}g(si.q_j)$

WhereR^{-1} {.}denotes the inverse Radon transform operator.

However in underwater applications the velocity of the sound is nearly 1500mt/sec. Due to this slow speed the returns from different range cells do overlap for signals of finite pulse width. Hence with the limited bandwidth of the transmitted pulse the wave front integral is different from that of impulse transmission. The backscattered signal may be considered as sum of wave front integrals with different phases.The phase difference of wave fronts corresponds to time difference corresponding to different range cells .Hence the profile function has to be obtained by pulse compression corresponding to each range cell.

3. PROFILE FUNCTION

Ramp Response Technique:When an incident pulse pt represented by a delta function in time (t) encounters an object in a homogeneous, isotropic Medium, the phenomenon of wave diffraction or scattering occurs. The incident pulse is scattered in all directions. The waveform scattered in a direction opposite to the direction of incidence is called the backscattered impulse response. The ramp response is defined as a time-domain backscattered signal at a distant observation point in response to an incident ramp signal. The ramp signal is a function defined to be the second integral of the incident impulse function. In practice, the projector-hydrophone system is inverseused for the ramp response measurement. The projector generates an acoustic pulse and sends it out, while the hydrophone is used to receive the backscattered impulse response. Consequently, the backscattered impulse response is integrated twice with respect to time to yield ramp response. As we only need the backscattered signals, the projector and hydrophone should be set together:

$$P_R(t) = \int t \left(\int P_I(t)dt'\right) dt$$

where, c represents the sound velocity in the water and A (ct/2)is the area of cross section of the object

perpendicular to the line of sight. The function A (ct/2) is called a profile function, which is shown in Figure 3. Here t denotes the propagation time of the acoustic wave. Zero propagation time is defined as when the wave crosses the centroid (geometric centre) of the object. For the acoustically rigid bodies, Eq. (6) shows the linear relationship between the profile function and the ramp response of the object in the medium. By computing the ramp response of an object, the profile function can be obtained

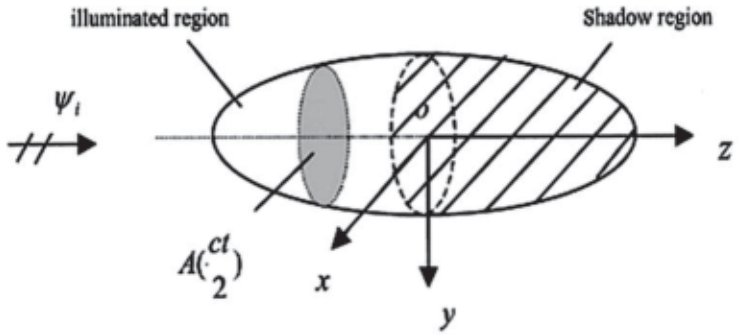

Fig. 3. An incident acoustic wave illuminates an object and profile function

4. TIME-FREQUENCY ANALYSISAND SHAPE EXTRACTION

On the other hand, it can be proven that theramp response $P_R(t)$ and the normalized complex backscattering amplitude $\Gamma(\omega)$ are Fourier transform pairs in the acoustic far field[10]
It is shown as below:

$$PR(t) = \frac{1}{2\pi}\int_{-\infty}^{+\infty} \Gamma(\omega)_{e^{-i\omega t}}\, d\omega$$

Here the normalized complex backscattering amplitude G is defined as:

$$\Gamma(\omega) = \frac{S(\omega) + S^*(-\omega)}{(-j\omega)^2}$$

where, S (ω) is the backscattered frequency spectrum in the acoustic far field. The symbol ''*'' denotes complex conjugate. Eqn. (7) isused to calculate the ramp response of the object. It should be noted that the normalized complex backscattering amplitude Γ is specified completely by scattering information of the object, and describes the frequency dependence of the scattering mechanisms, an inherent property of the object. The ramp response $P_R$describes the shape, size, and orientation information of the object. Moreover, Eq. (8) can be further simplified as follows:

$$P_{R(t)} = \frac{1}{2\pi}\int_{-\infty}^{+\infty} \Gamma(\omega) e^{-i\omega t} d\omega \left[\frac{1}{2\pi}\int_{-\infty}^{+\infty} \frac{s(\omega)}{(-\omega)^2} e^{-i\omega t} d\omega + \left(\int_{-\infty}^{+\infty} \frac{s(\omega)}{(-\omega)^2} e^{-i\omega t} d\omega\right)^*\right]$$

$$= \frac{1}{\pi}\int_{-\infty}^{+\infty} \frac{1}{(-\omega)^2}[S_r(\omega)\cos(\omega t) + S_i(\omega)\sin(\omega t) d\omega \qquad (9)$$

where$S_r(\omega)$ and $S_i(\omega)$ are the real and imaginary parts of $S(\omega)$, respectively. In the acoustic far field, the relationship between the scattering field potential Øs and the backscattered frequency spectrum S (ù) could be obtained as:

$$\lim_{r\to\infty} S(\omega)\frac{e^{jkr}}{r} \tag{10}$$

Now, 1) to obtain the profile function (ramp response) for the band limited signal, the integral in the equation may be restricted to the signal bandwidth. 2) The integral, corresponding frequency components is obtained at discreet time instances. This method of profile function extraction is suitable for practical applications of band-limited signals. However this requires back scattered signal to be represented/converted to time frequency representation. Profile function can be obtained by forming the integral of amplitude of all the frequency components for the corresponding time instances. However this may have some smearing/ broadening effect on the profile function due to band limiting of the signal and can be compensated in image reconstruction. Two Time-Frequency methods for this application that have been used and compared are STFT and Wigner -Ville distributions. The Fourier Transform decomposes a signal into its constituent frequency components. Looking at the Fourier spectrum we can identify the frequencies. However, we cannot identify their temporal localization. Time Frequency Distributions (TFDs) map a one-dimensional signal into a two-dimensional function of time and frequency, and describe how the spectral content of the signal changes with time. From a strict mathematical point of view, we want to have a joint distribution, which will give us the fraction of the total energy of the signal at time t and frequency ?; i.e., we look for the function P(t, ?). The aim of time-frequency analysis is to come up with appropriate candidates for P(t, ?).TFD are appropriate tools for non-stationary signal analysis, synthesis, and processing. Different types of time frequency distribution have been developed for that purpose. Two early forms of time-frequency analyses are: the Short-Time Fourier Transform (STFT), used to generate the spectrogram (SP) [Koenig, Dunn and Lacy, 1946; Allen, and Rabiner, 1977], and the Wigner-Ville distribution (WVD) [ClaasenandMecklenbrauker, 1980]. Studies of the well known linear TFD Short-Time Fourier Transform (STFT) have been published by Nawad and Quatieri, [1988], and Allen [1977] among others. The time-frequency distribution ideally describes how the energy is distributed, and allows us to estimate the fraction of the total energy of the signal at time t and at frequency ?. The above statement states that the energy should be positive. In order to achieve fine simultaneous time-frequency resolution in a non-stationary time series, we must deal with the uncertainty principle [Williams, Brown and Hero, 1991]. The uncertainty principle restricts us from achieving arbitrarily fine resolution simultaneously in both the time and the frequency domain. The condition to satisfy in the uncertainty principle is given by the inequality $\Delta\omega\Delta t \geq 1/2$, wherethe selection of Δt (time resolution) and $\Delta\omega$ (frequency resolution) parameters is not arbitrary. A trade-off between them should be considered in order to reach the desired "good" resolution. Next, an overview and a brief description of the advantages/limitations of the Spectrogram (SP), the Wigner-Ville (WVD), are presented.

4.1 Short-Time Fourier Transform (STFT)

In order to introduce time-dependency in the Fourier transform, a simple and intuitive solution consists in pre-windowing the signal x(u) around a particular time t, calculating its Fourier transform, and doing that for each time instant t. The resulting transform, called the short-time Fourier transform (STFT, or short-time spectrum), is

$$F_2(t,\nu,h) = \int_{-\infty}^{+\infty} x(u)h^*(u-t)e^{-j2\pi\nu u}\,du \tag{11}$$

where h(t) is a short time analysis windowlocalized around t = 0 and v = 0.The STFT $F_x(t,v,h)$can be considered as the result of passing the signal x(u) through a bandpassfilter whose frequency response isH (î" v), and is therefore deduced from a mother filter H(î) by a translation of v. So the STFT is similar to a bank of band-pass filters with constant bandwidth. The spectrogram is better able to resolve temporal evolution of frequency content, buthas a trade-off in time resolution versus frequency resolution in accordance with the uncertainty principle. To overcome this restriction, several classes of Time-Frequency representations have been proposed, including wavelet methods and quadratic time-frequency distributions such as the Wigner-Ville distribution.

4.2. Wigner-Ville Distribution

For a signal, s(t), with analytic associate x(t),the A time-frequency energy distribution, which is particularly interesting, is The Wigner-Ville distribution (WVD) defined as:

$$W_2(t,\nu) = \int_{-\infty}^{+\infty} x(t+\tau/2)x^*(t-\tau/2)e^{-j2\pi\nu t}d\tau \quad (12)$$

Or equivalently as:

$$W_2(t,\nu) = \int_{-\infty}^{+\infty} x(\nu+\xi/2)x^*(\nu-\xi/2)e^{-j2\pi\xi t}d\xi \quad (13)$$

The Wigner-Ville distribution Ws(t, w) of a time series signal s(t) defined as:

$$W_s(t,\nu) = \int_{-\infty}^{+\infty} s(t+\tau/2)s^*(t+\tau/2)e^{-j\omega t}d\tau \quad (14)$$

The time series function s(t) in Eqn. (9) can be either real or complex. The only type of complex signal considered in this paper is the analytic signal, which is defined as (s(t) + iH[s(t)]) where H denotes the Hilbert transform [e.g., Cohen, 1994]. The analytic signal has the same spectrum (or, to be precise, the spectrum multiplied by two) as that of the original real signal at positive frequencies but keeps the spectrum at negative frequencies zero. A significant characteristic of WVD, which essentially correlates the signal with a time and frequency-translated version of itself, is that it does not contain a windowing function as those in the Fourier and wavelet frameworks. This unique feature frees WVD from the smearing effect due to the windowing function, and, as a result, the WVD provides the representation that has the highest possible resolution in the time-frequency plane. For example, if a wave packet is non-zero only for t • (t1, t2), it can be shown that the corresponding W_s have to be 0 for t outside this exact time interval. There is, however, a well-known disadvantage of using WVD. When there are multiple components in a signal, the WVD can become difficult to interpret with its cross terms. A two-dimensional (2-D) low-pass filter can suppress the cross-term interference in the time frequency plane. Both these time frequency methods were applied obtain time frequency distributions of the signal. The resolution properties in frequency and time domains , for the three methods is illustrated in Figure 3. The Wigner-Ville Distribution is best for both time and frequency resolutions. Integrating across the amplitude of the frequency band on each time instance the profile function is obtained.

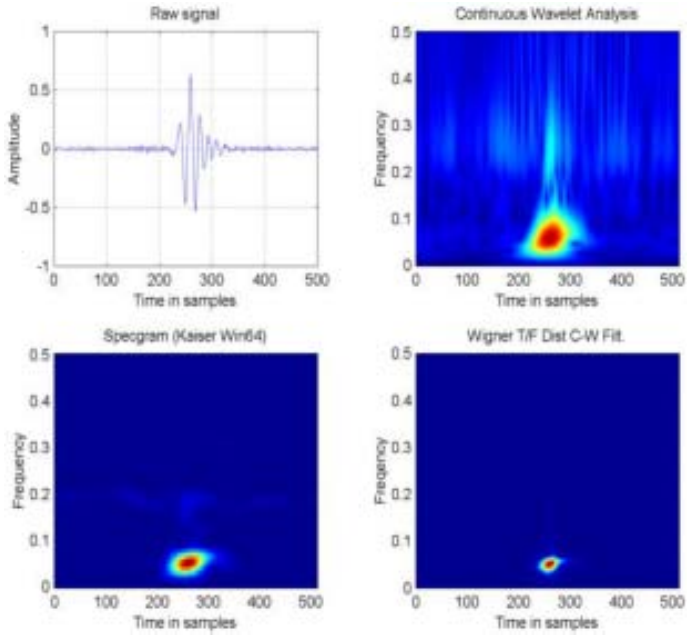

Fig. 3. Signal and Time And Frequency Analysis forDifferent Techniques

5. PULSE COMPRESSION ANDRECONSTRUCTION OF THE OBJECT SHAPE(2-D)

The back scatter is simulated for different objects, as time series for different view angles, for the same pulse width and pulse frequency. The time series mapped to time frequency domain by Wigner-Ville distribution (WVD) for each view angle.

$$W_2(t,w) = \int_{-\infty}^{+\infty} s(t+\tau/2)s^*(t-\tau/2)e^{-j\omega t}d\tau$$

From the two dimensional time -frequency mapping, profile function corresponding to time is obtained by, integrating the amplitude of each frequency component over the frequency band, for each time instance.This leads to pulse compression. The pulse is compressed by a factor *CF*, where CF=PW/t for PW is pulse width and *t* is sample time.

The profile function is $P_{R(t)}$ is

$$P_{R(t)} = \frac{1}{2\pi}\int_{-\omega}^{+\omega} \Gamma(\omega)e^{-i\omega t}d\omega$$

$$\Gamma(\omega) = \frac{S(\omega)+S^*(-\omega)}{(-j\omega)^2}$$

The profile functions are obtained by for all aspect angles for reconstruction of image. The set of profile forms the radon transform of the object in terms of reflection tomography .Therefore set of profilesat all aspect angles *j* , where 0<*j* > 2are obtained. This set can be transformed by any back projection operator. The inverse Radon transform is employed in image reconstruction. An image of the object that is represented by the two-dimensional distribution *f*(*x*,*y*),has been recovered from the projections recorded at all aspect angles *j*.The theoretical radon transform is also computed for comparison with that obtained via time frequency tools ,for pulsed wave form .

6. RESULTS AND DISCUSSION

The 2D view of underwater object is employed in simulation of back scatter illustrated along with results for each object.

The forward scatter of object hasbeen simulated by numerical method [9] for single cycle, multiple cycles and for different frequencies. The refection coefficient is assumed to be uniform and equal to unity. The profile function was obtained by using ramp response technique via time frequency analysis [2]. The shape/contour obtained of results obtained using profile function [2] is very close to the object shape/contour simulated by numerical method. Several shapes were used in simulations for different pulse parameters, size of the objects, as well as different sizes of the spatial grid and sampling frequencies. The parameters used in simulation are i.e., frequency; 25 KHz, transmitter angle è1 = 95and receiver angle è2 = 95. The other parameters as taken like size of the body 10 × 1 meters and sound velocity = 1500 meters/sec. Rectangular body is defined as the basic shape and another rectangle/triangle is either added or subtracted to obtain the shape. The forward scatter of object has been simulated by numerical method for different cycles and for different frequencies. The parameters like placement of the alteration (P.S), width of theshape for modification (w), and alteration type (a+ or a–) are described along with the result.The results in general conforms that for Pulsed signal the profile function can be obtained by time frequency tools , by pulse compression . If the pulse is close to impulse equivalent then profile obtained by ramp response is better .However result from WVD is also sufficiently close to object shape and efficiently used in object recognition /classification.

6.1 Profile Function via Time Frequency Analysis

Figures 5 to 7 indicates the time seriesgenerated and profile function extracted formono static case. Figure 4a, depicts time series from simulation for P.S = 200, w = 10, type = a– and No. of cycles = 3. Figure 4b and 4c

denotes the corresponding profile functions extracted from time series generated in Figure 3a. By ramp response technique (4b), and Wigner Vile technique (4c). The parameters used in simulation are i.e., frequency; 25 KHz, transmitter angle $è_1 = 95^0$and receiver angle $è_2 = 95^0$. The other parameters as taken like No. of cycles = 3; No. of finite elements; 500 × 50, Element type as rectangular, size of the bodyas 10 × 1 meters and sound velocity = 1500 meters/sec. In Figure 4a exhibits the time series from simulation for P.S = 1000, w = 20 type = a– and at P.S = 3000, w = 20 type = a– and No. of cycles = 20. The No. of finite elements is set as 4000 x500.

In Fig. 5a exhibits the time series from simulation for P.S = 1000, w =20 type = a- and at P.S = 3000, w =20 type = a- and No. Of cycles = 20.for a bi-static reception, with incidence at 95 and receiver at 40.The No. of finite elements is set as 4000 x500. The profile function extracted from Fig. 5a by ramp response technique (6b), by STFT technique (6c), and Wigner vile technique (5d) is shown in Figs. 5b, 5c, and 5d.

In Fig. 6a exhibits the time series from simulation for P.S = 1000, w =20 type = a- and at P.S = 3000, w =20 type = a- and No. Of cycles = 80.for a bi-static reception, with incidence at 90 and receiver at 80. The No. of finite elements is set as 4000 x500. The profile function extracted from Fig. 6a by ramp response technique (6b), by STFT technique (6c), and Wigner vile technique (6d) is shown in Figs. 6b, 6c, and 6d.

From results, it is clear that the computational technique can be used on any shape of the object. However, the profile extraction function most suited on impulse incidence may not suitable for wide pulses, and for all practical applications the pulse does have finite pulse width. From the above results, it is also observed that shorter pulse gives the better definition than wide pulse.For practical applications the ramp response method may not suitable for profile extraction .Methods based on time- frequency distribution /analysis presented here for extraction of profile function are more suitable for most practical applications. Out of the methods presented the Wigner Ville is better than the other methods, due to its inherent auto correlation property. This method is also better suited for noise added signals i.e. in practical environment. Profile functions from many angles are used on reconstruction of the object image. The set of profile functions are transformed to image by Inverse-Radon transform.

6.2 Image Reconstruction

The results for reconstruction of simulated objects by two methods are depicted below. Three object shapes are simulated .The object function/profile functions are obtained for different angles via pulse compression via WVD. 2D images are reconstructed by applying the Inverse-radon function. The ideal profile functions were also obtained by Radon transform. The image from this also is reconstructed by ideal I-radon transform.

The results obtained for shape reconstruction for both the cases for different are presented from figure 7 to figure 9.The '..' in Figure(..x) Indicates the figure number. In the results ,Figure(..) is 2D shape of the objects employed in simulation of backscatter. The transmission pulse used in simulation is 20 cycles. The profile functions obtained for all angles is plotted in figure (..a). The theoretical radon transform for the image is depicted in figure(..b) . The reconstructed image of the object via inverse radon is in figure (..c).The radon transform obtained forpulse via WVD is presented in figure (..d).The reconstructed image of the object by the pulse compressed time series by applying WVD processing technique and further back propagated and reconstructed image is in depicted in figure (..e).In case of third object is frame with uniform reflection coefficient.

The shape reconstructed is fairly close to the original shape through WVD is better than obtained by theoretical radon. This may be due to filtering process involved in pulse compression .i.e integration of the frequency components of the WVD output. Post processing the image obtained shall improve the quality of the image. The last object simulated is a structure that is, the general acoustic reflecting surface of a mine type of object. The results here are quite comparable to that of ideal impulse imaging.

7. CONCLUSION

The shape reconstructed is fairly close to the original shape. This is can be efficiently used in object recognition and classification. The method proposed i.e. Application of WVD in profile function extraction therefore can beeffectively used in obtaining the shapereconstruction of underwater objects. .Forall practical

Fig. 5 object shape

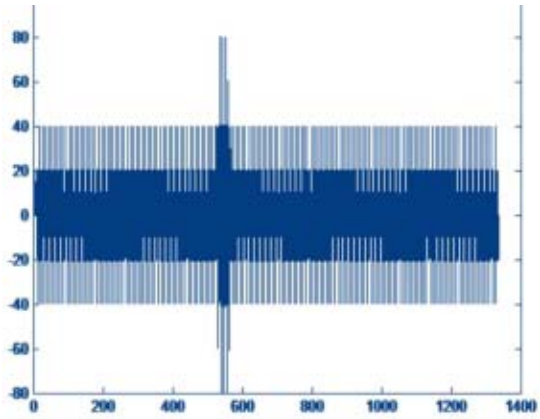

Fig. 5 (a) Time series obtained from simulation

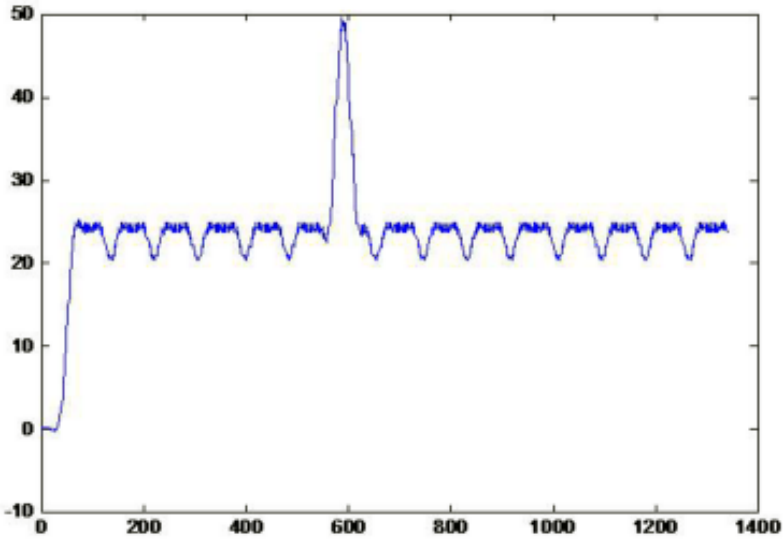

Fig. 5b. profile functions extracted from time series of Fig. 5a. by ramp response technique

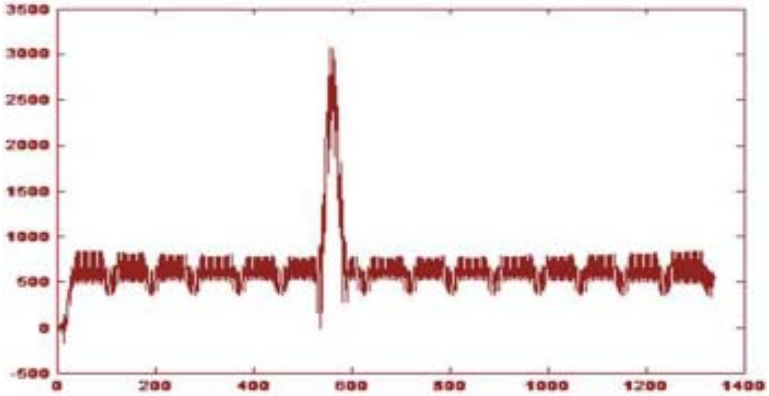

Fig. 5c. profile functions extracted from time series in Fig. 6a TFD (WVD) technique

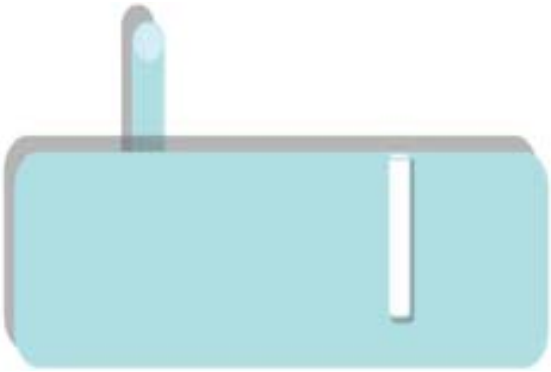

Fig. 6. object shape

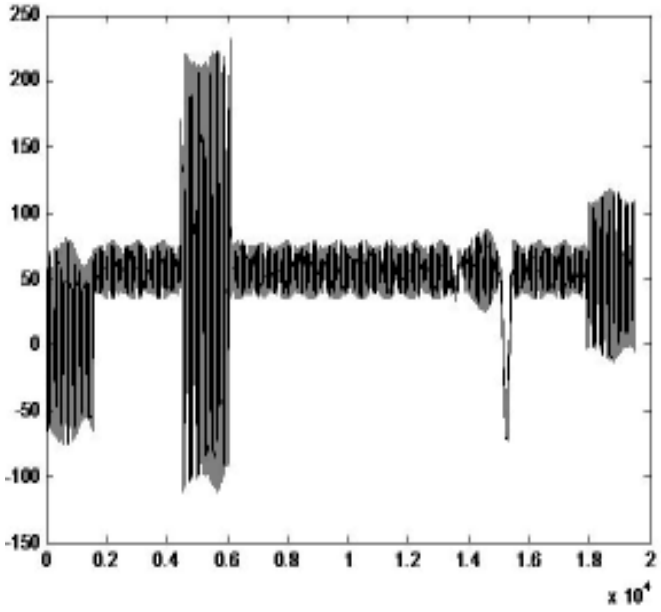

Fig. 6(a). Back scttered Time series obtained from simulation for pulse length of 20 cycles

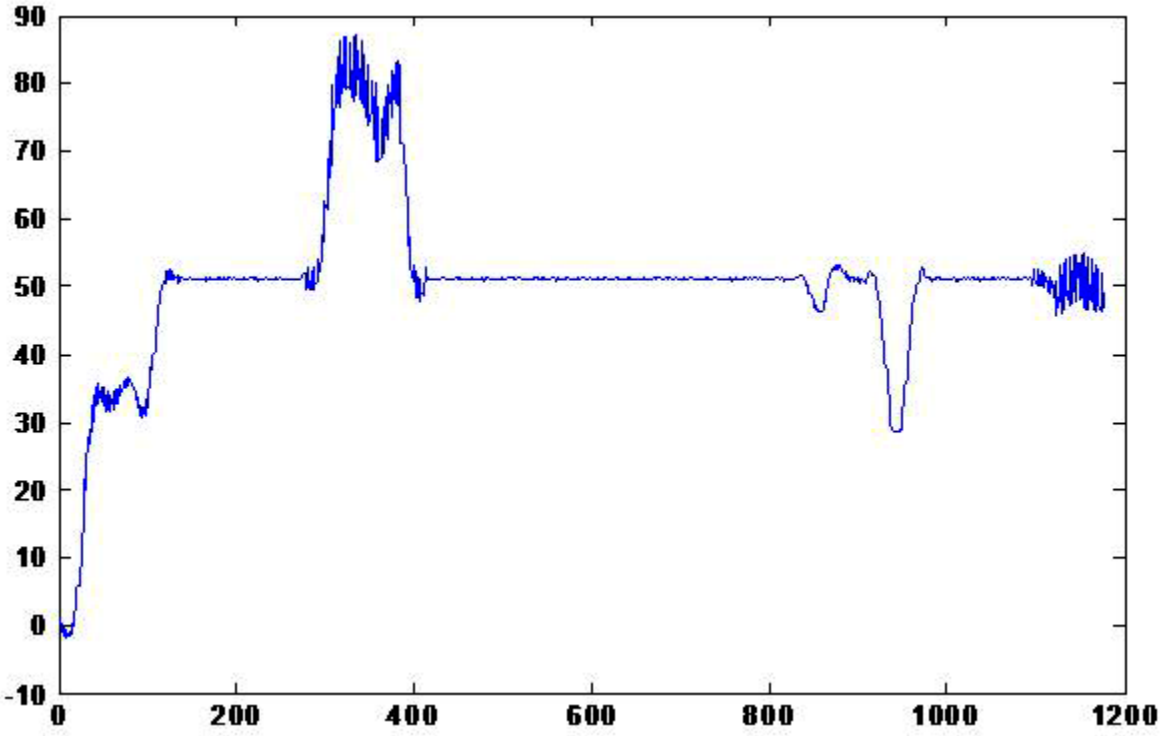

Fig. 6b. profile functions extracted from time series in Fig. 6a. by ramp response technique

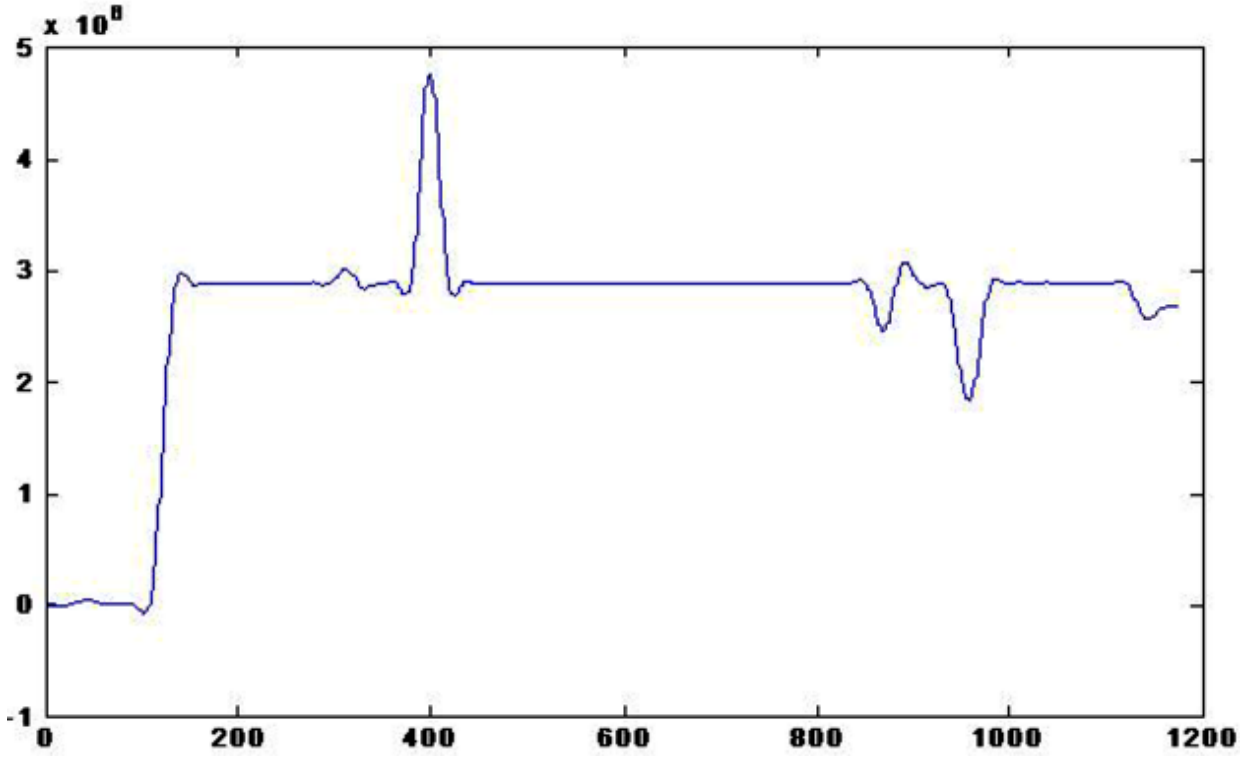

Fig. 6c. Profile functions extracted from time series in Fig. 6a. TFD (WVD) technique

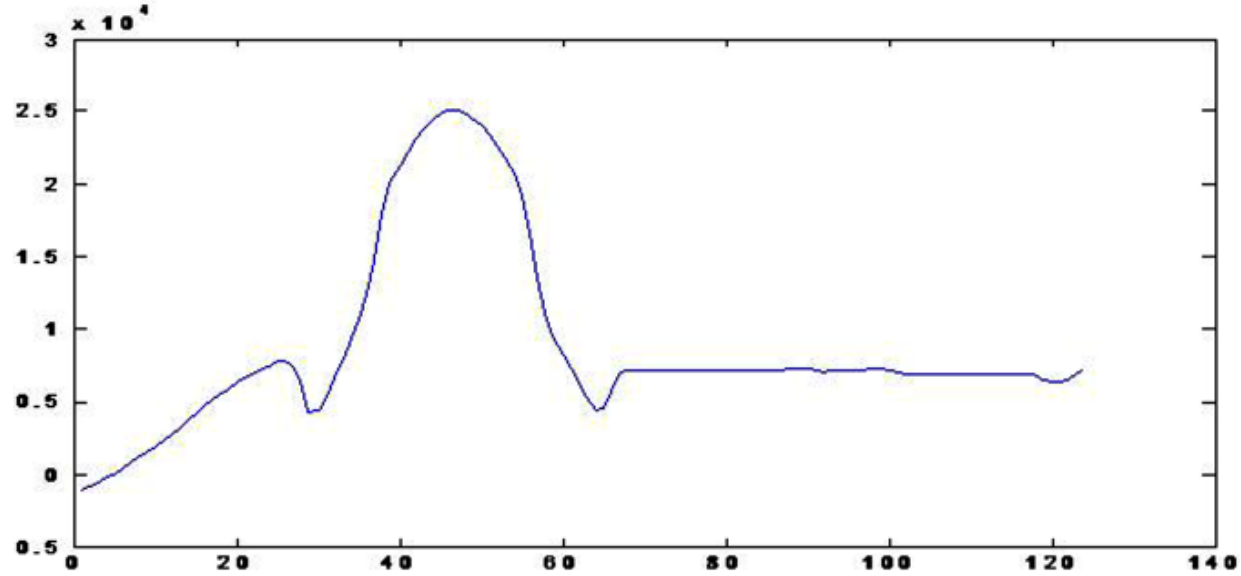

Fig. 6d. Profile functions extracted from time series in Fig. 6a. by STFT technique

Fig. 7. Object shape

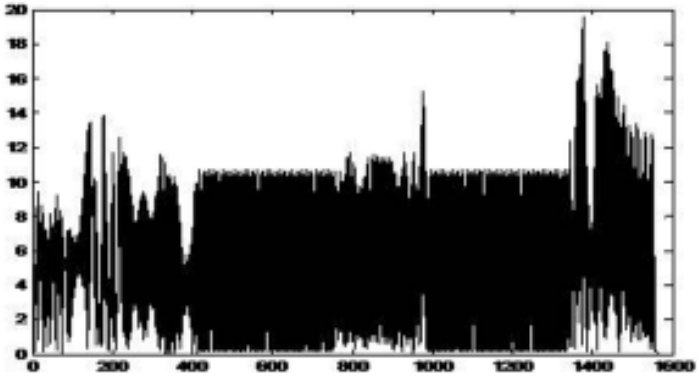

Fig. 7 (a). Back scttered Time series -pulse length of 80 cycles

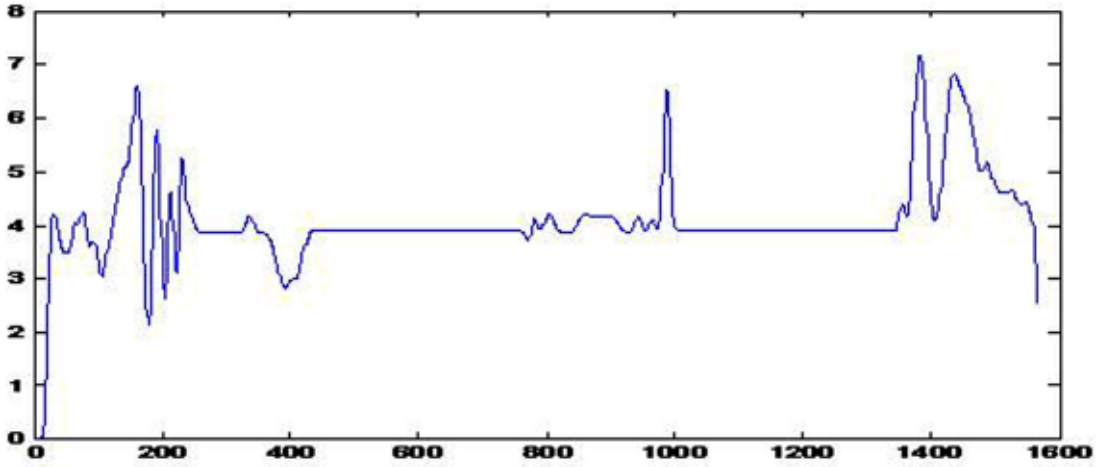

Fig. 7b. Profile functions extracted from time series in Fig. 7a by ram p response technique

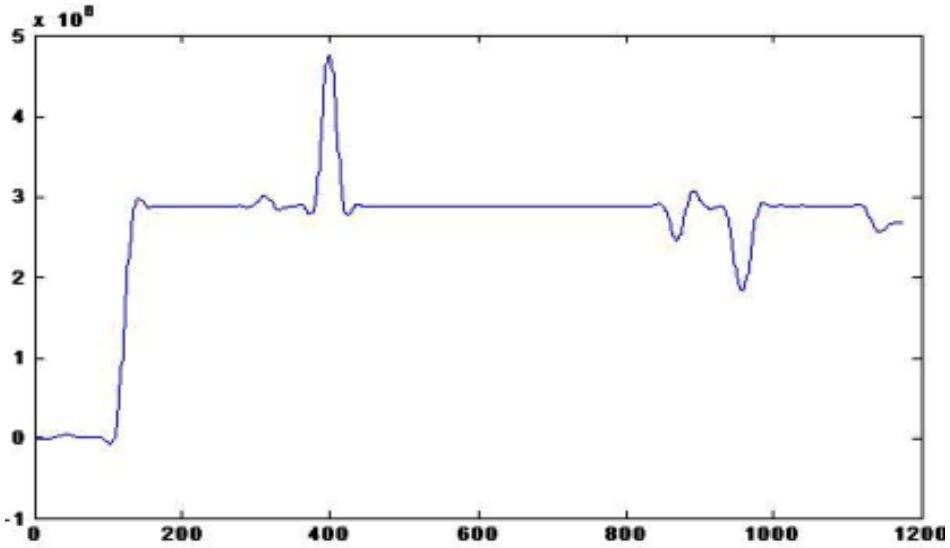

Fig. 6c. Profile functions extracted from time series in fig. 6a. TFD (WVD) technique

Fig. 7. Object shape

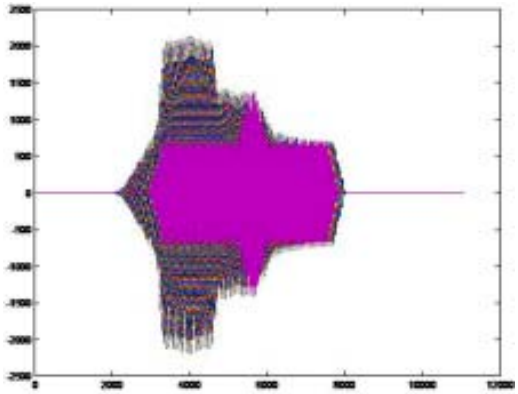

Fig. 7a. Time series for Object shape of fig. 10 for all aspect angels

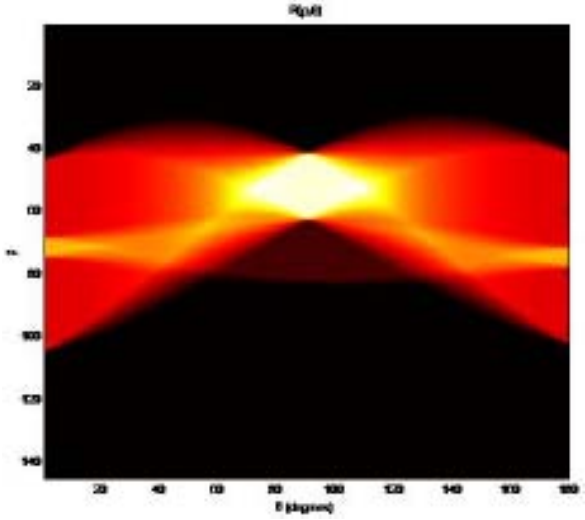

Fig. 7b. Radon transform for Object shape of Fig. 7. by Radon function

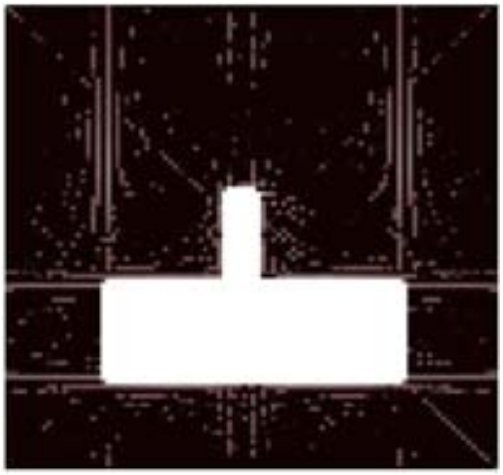

Fig. 7c. Shapereconstructed, by applying Inverse Radon function on Fig. 7b

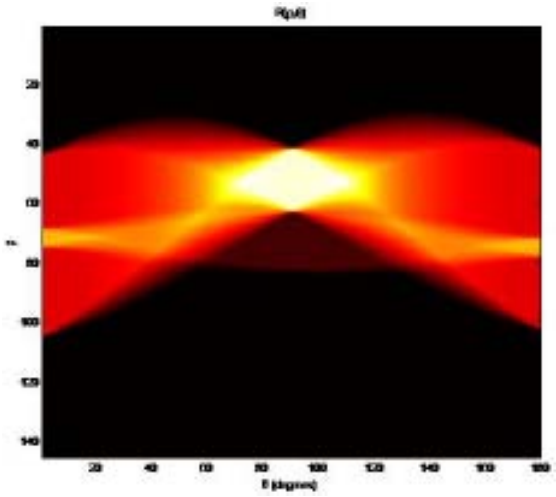

Fig. 7d. Radon transform for object shapeof Fig. 7. by WVD for time series of Fig. 7a

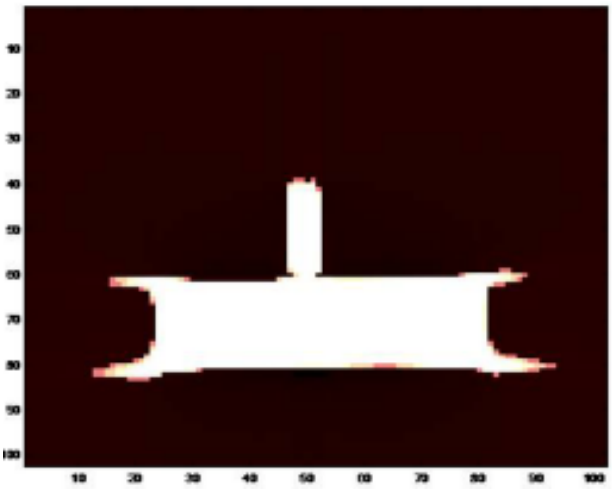

Fig. 7e.Shapereconstructed, by applying Inverse Radon function on of Fig 10d

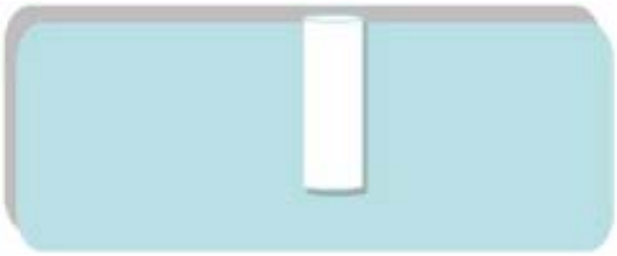

Fig. 8. Object shape

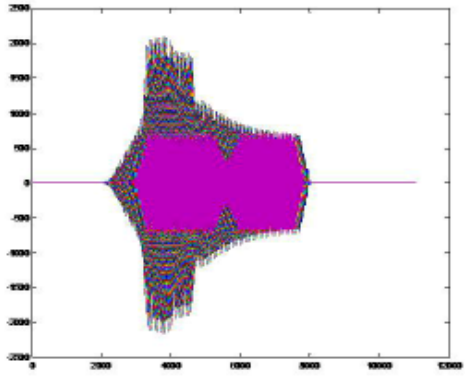

Fig. 8a. Time series for object shape of Fig 8. for all aspect angels

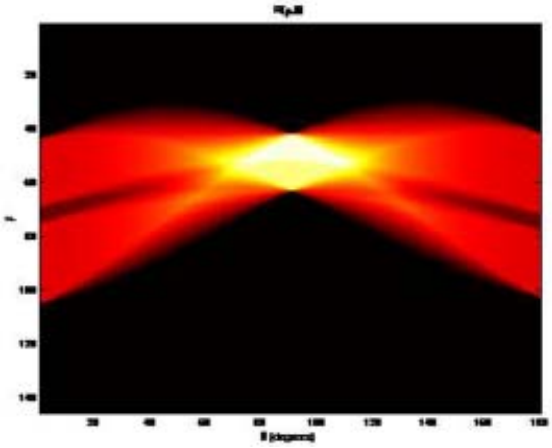

Fig. 8b. Radon transform for object shape of Fig 8. by radon function

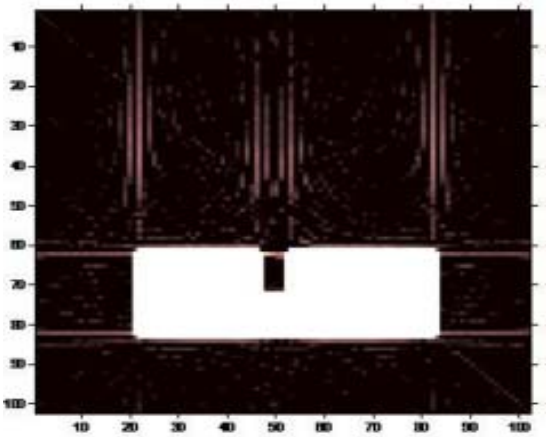

Fig. 8c. Shapereconstructed, by applying Inverse Radon function on Fig. 8b

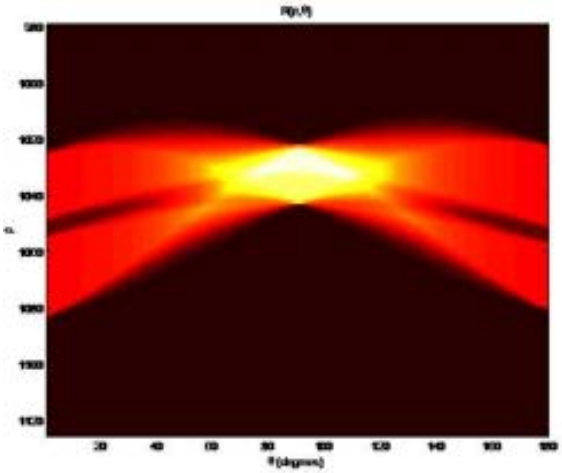

Fig. 8d. Radon transform forObject shape of Fig. 8. by WVD for time series of Fig. 8a

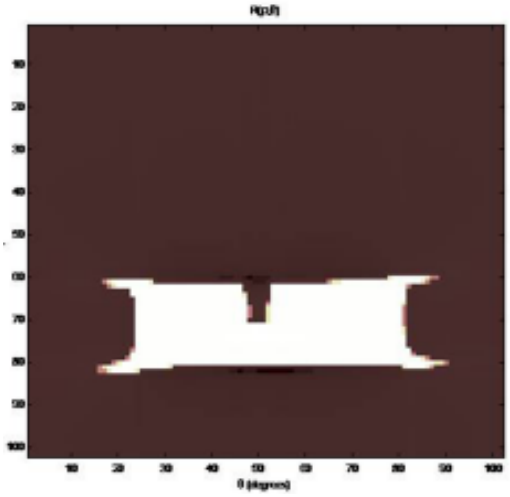

Fig. 8e. Shapereconstructed, by applying Inverse Radon function on Fig 8d

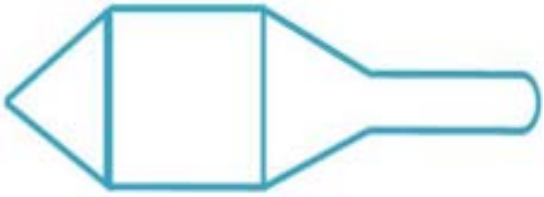

Fig. 9. Object shape

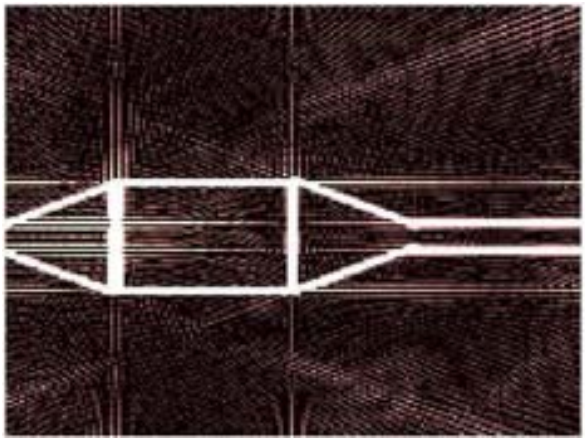

Fig. 9c. Shapereconstructed, by applying Inverse Radon function for ideal radon transform

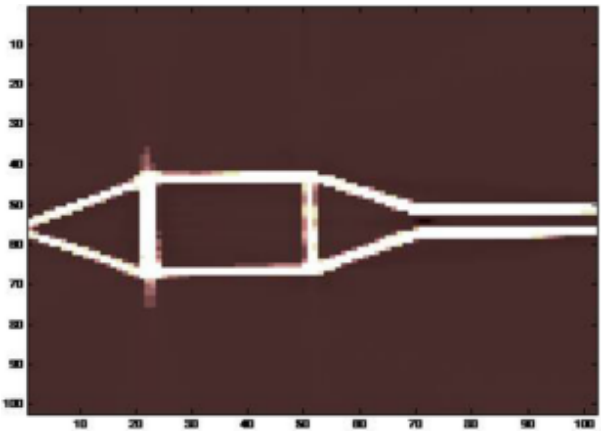

Fig. 8e.Shapereconstructed, by applying Inverse Radon function by obtaining the radon transform by WVD

applicationstime- frequency distribution /analysis based technique may be applied for extraction of profile function. The Inverse -Radon is applied for back propagation in obtaining the image. However any other back propagation techniques that can be more computational efficient can be used in image/shape reconstruction. The results obtained very close to the object shape and can be used in recognition and classification of underwater objects.

8. ACKNOWLEDGMENT

The authors gratefully acknowledge the support of Director, NPOL. The authors also acknowledge the support of Vice Chancellor, DIAT (DU), Pune for the support and encouragement.

7. REFERENCES

[1] J.D. YOUNG, "Radar imaging from ramp response signature" 1976, IEEE Trans. Antennas and Propagation AP-24 276.

[2] X.M. ZHANG, W. LI and G. R. LIU, 2002 "A new technique in ramp response for acoustic imaging of underwater objects", Applied Acoustics **63**.
[3] WELLI ,G.R. LIU, size X. M. Zhang" 2004 Size identification of underwater objects from back scattering signals of arbitrary looking angles", Journal of Computational Acoustics, Vol. **12**, No. 3.
[4] WEL LI ,G.R. LIU, V.K. VARADAN, " 2004 Acoustical imaging of underwater objects using the bi -static ramp response signals", Smart materials and structure, Vol-**13**.
[5] P.C. WATERMAN, "New formulation of acoustic scattering", Journal. Acoustic. Soc. Am. 45 (1969)
[6] B. BOASHASH, 2003 "Time Frequency Signal Analysis and Processing: A Comprehensive Reference," ELSEVIER.
[7] CARLOS I HUERTA-LOPEZ, YONGJUNE SHIN, EDWARD J POWERS and JOSE M ROESSET " 2000 Time-Frequency Analysis Of Earthquake Records", 12WCEE.
[9] E.M. KENNAUGH and D.L. MOFFATT," 1965 Transient and impulse response approximations", Proceedings, IEEE.
[10] T. RATNA MANI, RAJ KUMAR and O.VIJAY KUMAR," 2013 Numerical Computational Technique for Scattering from Underwater Objects", Defence Science Journal, Vol. **63**, No. 1, January.
[11] T. RATNA MANI, RAJ KUMAR and O.VIJAYKUMAR ," 2011 Application of Time Frequency Analysis Methods in Inverse Scattering ",Proceedings of SYMPOL.
[12] BRIAN G. FERGUSON and RON J. WYBER, 2005 Application of acoustic reflection tomography to sonar imaging, J. Acoust. Soc. Am. **117** (**5**), May.

Journal of Acoustical Society of India : Vol. 40, No. 2, 2013 (pp. 108-115)

Noise Control of a Hand Drill Using Hybrid Muffler

R. Praveena, Gyanadutta Swain and B. Venkatesham*
Indian Institute of Technology Hyderabad, Yeddumailaram-502 205 (A.P.)
**e-mail: venkatesham@iith.ac.in*

[Received: 05.04.2013; Revised: 25.04.2013; Accepted: 29.04.2013]

ABSTRACT

Extensive use of flexible hand tools in workshops and domestic applications are common. These tools are designed for multipurpose and low cost. This requirement makes designer to choose a compact and integrated system. So, it involves lot of challenges to design a quieter product. This paper emphasises in reducing the noise levels of a hand drill. The performance and noise characteristics of instrument are tested experimentally, followed by some analytical calculations on various subassemblies of the product to find out the dominant noise source. Experimental results show that fan is the major noise source and this characteristic is being observed at high frequency region. After conducting parametric studies a suitable hybrid muffler of short length is mounted on the instrument to reduce the noise levels to a considerable value. The concept of noise reduction is verified with the prototype of a muffler by measuring its insertion loss.

1. INTRODUCTION

Acoustic noise problems exist in wide variety of applications.Sound pressure levels depend on the part of the total mechanical or electrical energy transformed into acoustical energy. All noise control regulation acts emphasize in developing a quieter product. In the noise management data sheets for electric drills, by department of commerce, government of western Australia it is mentioned that the quietest form of hand drill is the cordless variety that produces about 78 dB (A) and a normal hand drill produces about 90 dB (A) to 94 dB (A) and hammer hand drills produce in excess of 100 dB (A) [1].The Internal components of hand drill such as fan, gear arrangement, motor and bearing act as various sources for noise which produce high sound pressure levels that can cause noise induced hearing loss if a person is exposed to it for a longer time duration.

2. DESCRIPTION OF HAND DRILL

A hand drill consists of an electric motor that rotates a replaceable drill bit to make holes in wood, plastic, or metal. Various components such as motor, bearing and fan are mounted on a single rotating shaft. A gear arrangement connects the output shaft with the input shaft for speed reduction. Chuck is mounted on the output shaft where drill bit is mounted. Figure 1 shows different components of a typical hand drill.

3. METHODOLOGY FOR QUIETER DESIGN

Methodology that must be followed to determine the best solution for quieter product involves the following steps 1) Identification of potential noise sources, 2) Analysis of noise sources and noise generation mechanism, 3) Source Ranking, 4) Noise propagation and 5) Develop noise control measures for themajor sources based on noise propagation mechanism.

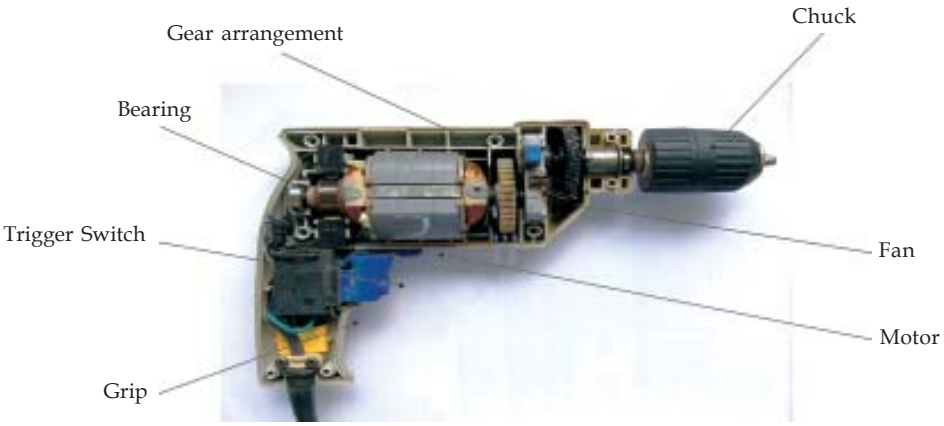

Fig. 1. Various components of a Hand drill

3.1 Potential Noise Sources

The first step is to list all the potential noise generating sources and then classify into two broad categories as a)Air borne noise: fan, windage b) Structure borne noise: gears, bearings, electro-magnetic forces and commutator.

3.2 Analysis of Various Noise Sources

Fan: Fan is made of plastic material and isintegrated with the input shaft on which the motor is mounted. The number of fan blades are 34. Rotating speed of the fanmeasured using thetachometer is 24500 rpm.

Blade passing frequency of fan is calculated as

$$f_b = \frac{\text{Number of Blades x Rotatingspeed}}{60} = \frac{34 \text{ x } 24500}{60} \text{ Hz}$$

Gear: A helical gear arrangement is provided in the instrument. Gear meshing frequency is calculated from the measured speed and number of teeth of the gear.Number of teeth on driver and driven are 6 and 47, respectively.Speed of driven gear is 2950 5% rpm. The driver speed ranges from 21952-24263 rpm. Gear meshing frequency $f_g = \frac{\text{Number of teeth X RPM}}{60}$ = 2195.2Hz-2426.3Hz

Motor: The drive unit is a 2 pole DC motor with a rated voltage of 220 V and working speed of 24500 rpm.

Bearing: It is a ball bearing designated as 626ZZ.It is a double chrome steel shielded ball bearing having seven number of balls with a runout speed of 34000 rpm. Bearing can withstand a dynamic load upto 2.34 kN.

3.3 Experimental Analysis

Noise generated due to drilling operations is not considered in this study. The focus is only on the noise generated from the instrument. The generated noise is measured using class A sound level meter. Measurements are taken at 1 meter distance at various angles. Both A weighting and C weighting at faster and slower time scale has been measured and the difference of measurements had been taken to check for any low frequency sources. Figure 2 shows the A weighted sound pressure measurement values at various angles with respect to hand drill orientation. A-weighted Soundpressure levels of each individual source components are also estimated for source ranking.

Fig. 2. Directivity of a hand drill

Figure 3 shows the frequency spectrum and Table 1 gives the various sound pressure parameters at 00. It is observed from the spectrum that the dominant sound pressure levels are at high frequencies and also it is broad band. Sound source is steady based on measured parameter value.So, this infers that fan acts as the primary noise source.

3.4 Source Ranking

To achieve effective noise control solution source ranking [2] is done to find out the dominant noise source. Fig. 4 shows the source ranking.It is observed that the dominant noise source is air-born and also a steady source.Contribution ofstructure-bornnoise is not significant in the current model.Multiple fan noise control solutions are available in the literature [2]. Noisereduction at source is ideal.However providing a solution at the source is not possible due to logistic constraints.So it has been decided to use a path control solution. One of the best solutions to control flow noise is by means of a muffler [3]. An extensive literature is provided for designing a muffler [4].

Table 1. Various sound pressure parameters at 0°

LAF_{max}	LAS_{max}	LAF_{min}	LAS_{min}	LA_{eq}
81.64	81.13	78.23	79.3	80.78

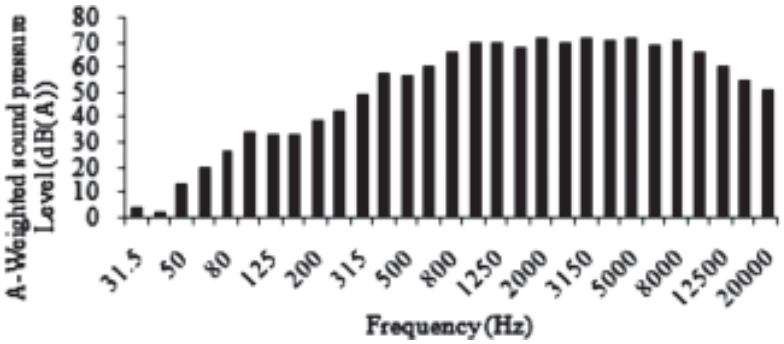

Fig. 3. One-third octave sound pressure spectrum of a hand drill

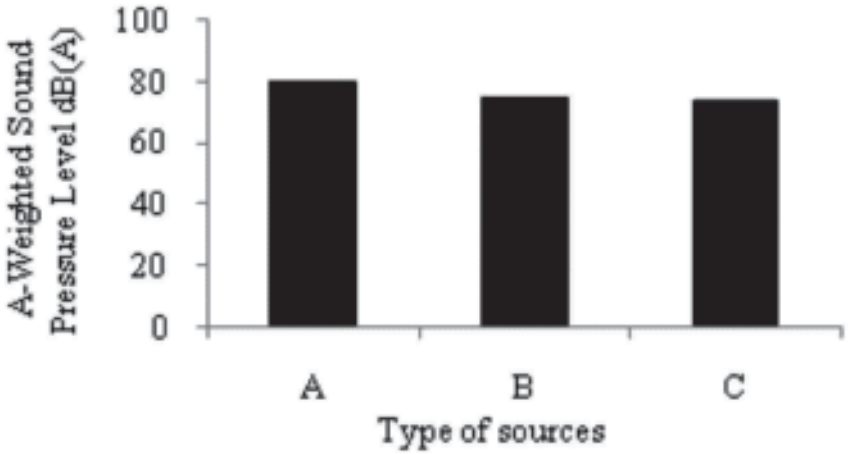

Fig. 4. Source Ranking, A-Fan, B -Gear train, C- Motor and Bearing

A hybrid muffler has been proposed as a solution. It has both reactive and dissipative solutions. Constraints like weight of the muffler, space limitations, back pressure and cost have been considered while designing a muffler. Figure 5a and 5bshows the schematic diagram and also isometric view of a muffler model with all dimensions in mm.Proposed hybrid muffler consists of a side inlet and end outlet with absorptive lining. Extensive parametric studies are conducted before developing the prototype. Computational model of proposed model is developed using commercial software LMS virtual lab [5].Air gap in this model is not symmetric with respect to centre.

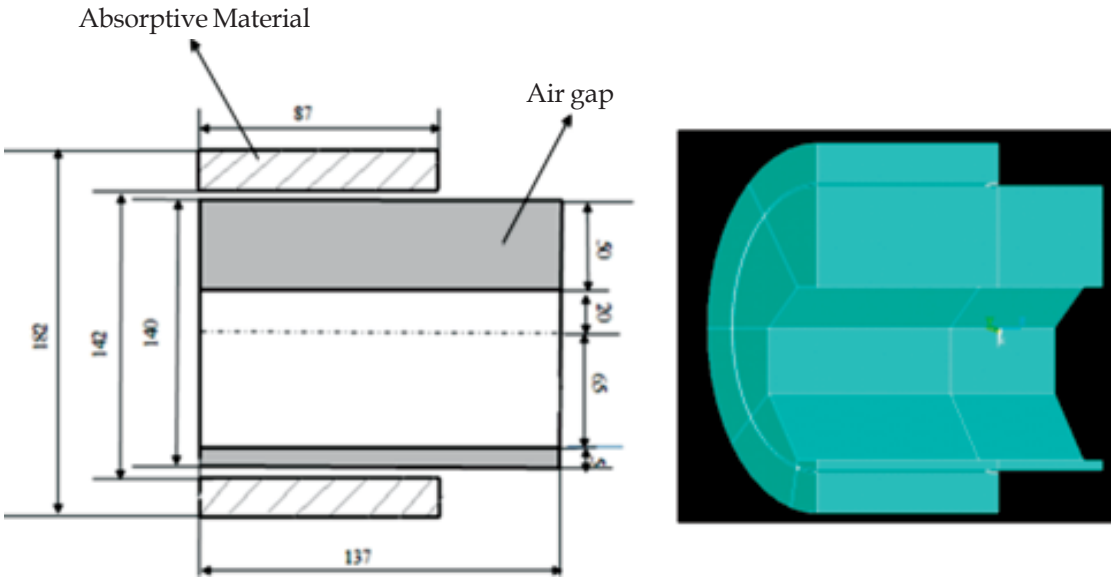

Fig. 5a. Schematic Fig. 5b. Isometric diagram of muffler view of muffler model

4. NUMERICAL MODEL

Completed muffler volume is meshed with 8 noded brick elements (SOLID 185).Air properties are applied to elements associated with air gap. Similarly complex velocity and density are applied to materials associated with absorptive material. Perforation is modelled as transfer relation admittance. A unit velocity as input excitation and anechoic termination (z=ρc) as outlet condition has been modelled. Dimensions of muffler are given in Figure 5a; other dimensions used in parametric studies are given below. Thickness of the perforated

sheet: 0.001m, Centre to centre distance between holes: 0.0075m are kept constant. Specific Flow resistance: 0, 10000, 20000 rayls /meter, Mach number: 0, 0.1, 0.2., Porosity: 5%, 10%, 20%, Hole diameter: 0.002, 0.003, 0.004 meter. The underlined values are taken as default values.

5. RESULTS AND DISCUSSION

Figure 6 shows the effect of specific flow resistance on transmission loss. It is inferred that as the flow resistance increases peaks shift towards lower frequencies. The resistance to the sound propagation in the absorptive material increases as the flow resistivity increases, so the peaks shift towards low frequencies. Similar behaviour is observed in reference [6].When SFR=0, mufflerbehaviour is not exactly same as concentric tube resonator (CTR) which is due to asymmetry in air gap.It is observed from computational results that as the Mach number increases peaks shift towards lower frequencies. Significant change in high frequencies is observed.The maximum achievable transmission loss iscontrolled by Mach number.As flow velocity increases flow noise contributes as self-generated noise. Fig. 7 shows the variation of porosity. As the porosity increases the peaks are shiftedtowardshigher frequency [6].It can be observed thathigh frequency region can be improved byselecting a higherporosity value. Fig. 8 shows a comparison of concentrictube resonator model with side inletand endoutlet model.The presence of uneven air gap in the modelandshort lengthleads to amismatch inthe peak frequency valuescalculated by analytical method. So, existing simple analytical models have their own limitation for this application.

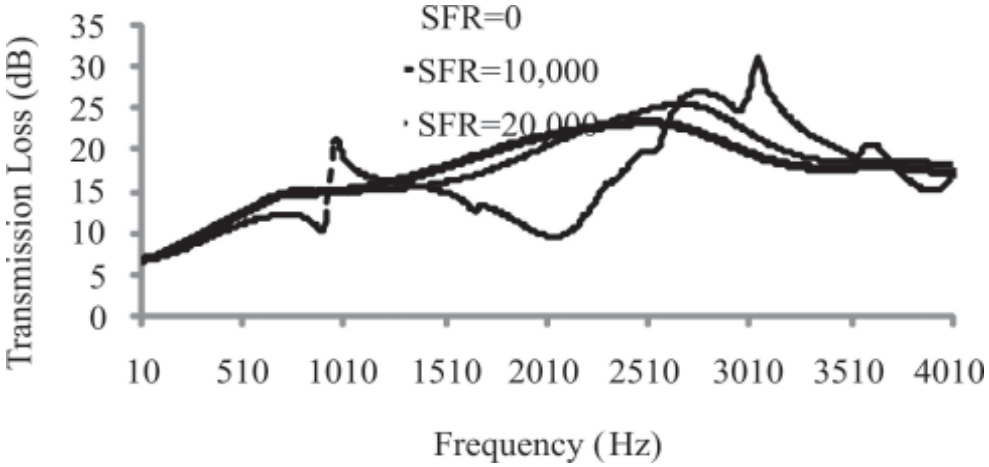

Fig. 6. Effect of specific flow resistance on transmission loss

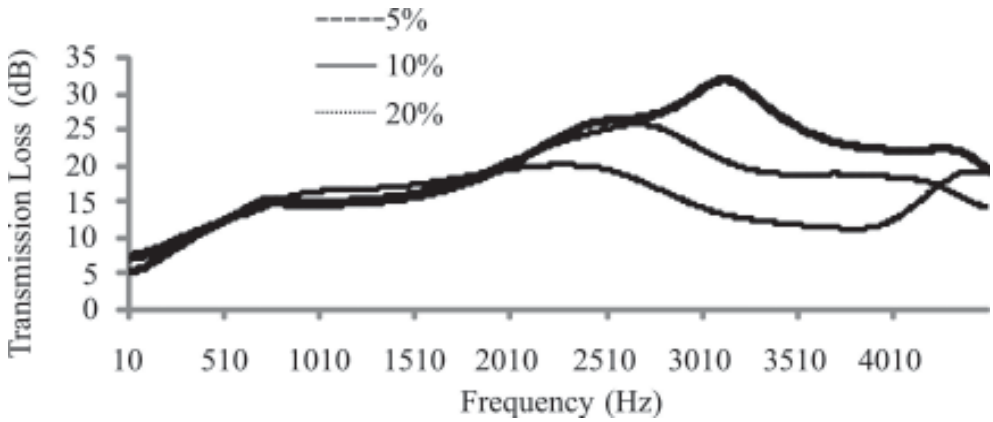

Fig. 7. Effect of porosity on transmission loss

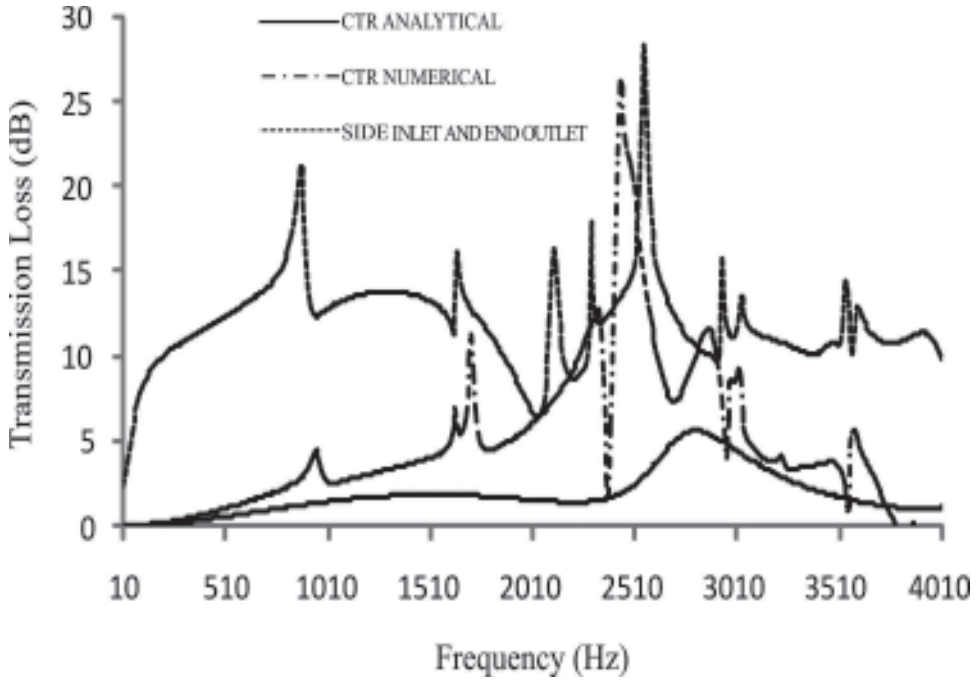

Fig. 8. Comparison of side inlet and end outlet with CTR model

Based on these parametric studies a prototype is made. Parametric studies suggest developing a muffler with high SFR absorptive material, higher porosity in perforated sheet are best for higher frequency noise control and also effective over a broader frequency range. The insertion loss of the muffler is measured.Figure 9 shows the muffler prototype that is mounted on hand drill. Specifications are outer diameter 0.18m, inner diameter: 0.14 m porosity: 0.35, hole diameter: 0.005m, centre to centre distance between holes: 0.0075.

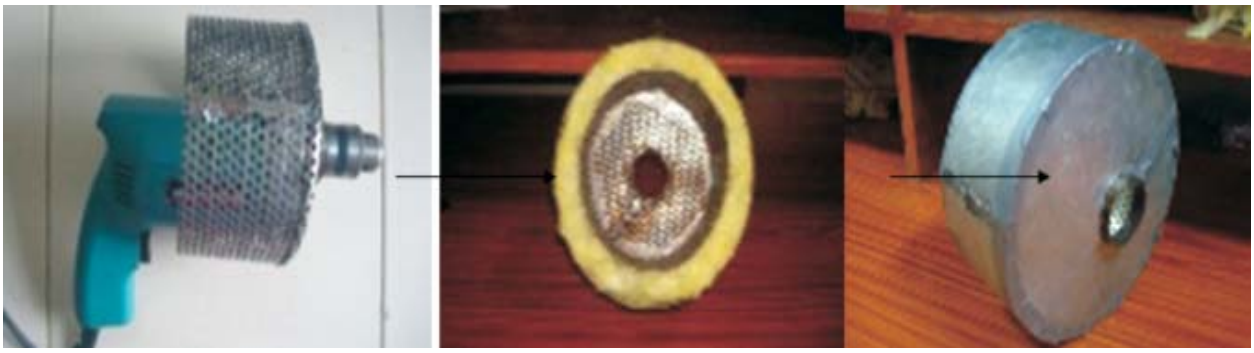

(a) (b) (c)

Fig. 9. Hybrid muffler in different orientation

Figure 10 shows a comparison of sound pressure with and without muffler. Table 2 shows a comparison of sound pressure levels at various angles with respect to hand drill orientation as shown in Fig. 1. Fig. 11 shows the insertion lossspectrum. Itshows that the muffler is effective at higher frequencies.There are certain limitations in the current study.The length of the muffler is much smallercompared to thediameter dueto which the effective length for sound attenuation is reduced.Since the cross sectiondimensions of the muffler are much larger than the wavelength, the incident sound fieldcontains avery large number of higher order modes [7].

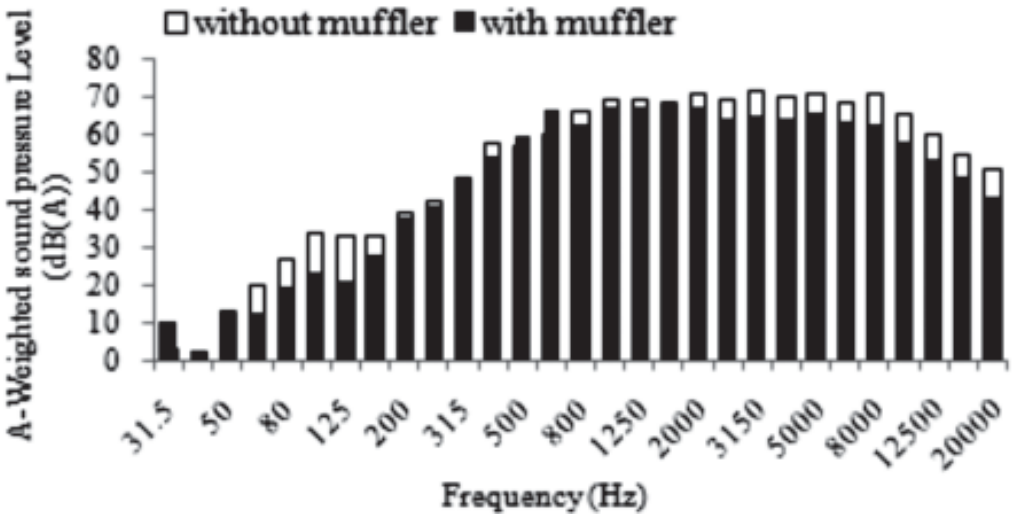

Fig. 10: A-weighted SPL with and without muffler

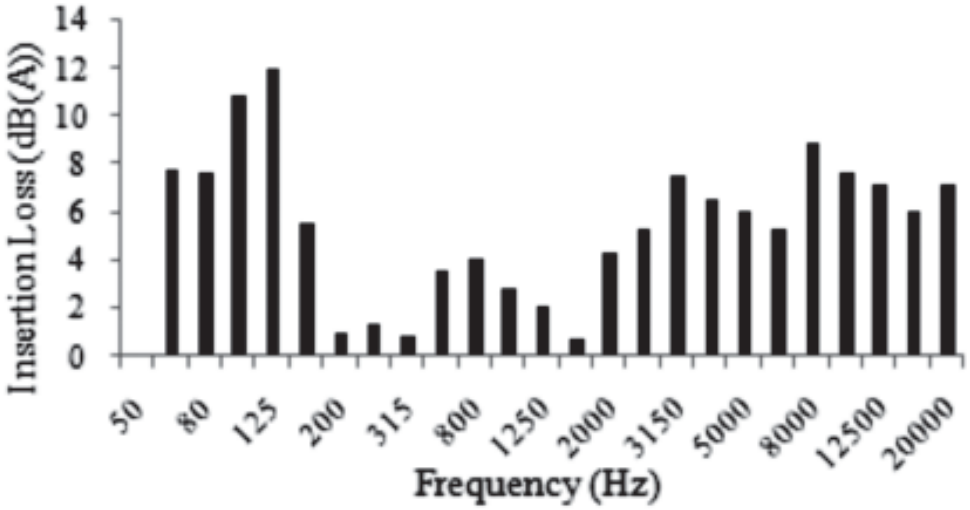

Fig. 11. Insertion Loss spectrum of prototype muffler

This might result in an entrance loss [7] which needs to be characterized.The muffler has been modelled with an uneven air gap, so the amount of air flow is different along the circumference of thehand drill. Due to this there are challengesin validating with the analytical model

Table 2. A-weighted sound pressure level with and without muffler in different orientations

6. SUMMARY

Noise sources in the hand drill machine have been identified based on acoustical and vibration measurement and fan has been identifiedas the major noise source.This is done based on the concept of source ranking.A passive noise control technique has been proposedin the form of a hybrid muffler to control fan noise. A prototype has been prepared based on extensive parametric study using numerical models.An attempt has been made to reduce the sound from the hand drillby using muffler concept. This concept helped to get insertion loss of 4-5 dB (A).This paper described the complete noise control approach by integrating analytical,computational and experimental methods.Similar approach can be extended to other industrial products.This model can be further improved with an even air gap mufflerby optimising themufflerdimensions with considerable back pressure and thereby achieving more reduction in noise levels.

7. REFERENCES

[1] Noise management data sheets http://www.commerce.wa.gov.au/worksafe/content/safety_topics/noise/Further_information/Electrical_drills.html

[2] DAVID A. BIES and COLIN H. HANSEN, 2009. Engineering Noise Control Theory and practice,Taylor & Francis.

[3] H.S. KIM, J.S. HONG, D.G. SOHN and J.E. OH, Development of an Active Muffler System for Reducing Exhaust Noise and Flow Restriction in a Heavy Vehicle, Department of Mechanical Engineering, Institute of Noise Control Engineering,Auburn University.

[4] M.L. MUNJAL, 1987. Acoustics of Ducts and Mufflers, John Wiley.

[5] LMS Virtual lab Rev -10, User's manual.

[6] M.L. MUNJAL and B. VENKATESHAM, 2000. Analysis and design of an annular air gap lined duct for hot exhaust systems, *Proceedings of the IUTAM Symposium on Designing for Quietness*, Kluwer Publications, Holland.

[7] IstvanL.Ver, Leo L. Beranek. Noise and vibration control engineering principles and applications 2006, John Wiley & Sons.

Journal of Acoustical Society of India : Vol. 40, No. 2, 2013 (pp.116-120)

Genetic Algorithm Based Neural Network for Classification of Rolling Element Bearing Condition

G.S. Vijay[1]*, Srinivasa P. Pai[2] and N.S. Sriram[3]
[1]*Department of Mechanical and Manufacturing Engineering, MIT, Manipal (Karnataka)*
[2]*Department of Mechanical Engineering, NMAMIT, Nitte (Karnataka)*
[3]*Department of Mechanical Engineering, VVIET, Mysore (Karnataka)*
**e-mail: vgs.mpl@gmail.com*

[Received: 15.12.2012; Revised: 19.01.2013; Accepted: 22.02.2013]

ABSTRACT

In this paper, the performance of Multi Layer Perceptron Neural Network (MLPNN) based on features selected using Fisher's Criterion (FC) and Genetic Algorithm (GA) has been compared for rolling element bearing condition classification. Vibration signals have been acquired from four conditions (normal bearing, bearing with defect on inner race, bearing with defect on outer race and bearing with defect on ball element) of a deep groove ball bearing (6205) from a customized bearing test rig under different conditions of load and speed. Several statistical features in time domain and frequency domain were extracted from denoised vibration signal. GA was also used to optimize the learning rate, momentum factor and number of neurons in the hidden layer. MLPNN based on GA has been found to perform better than that based on features selected using FC, thereby helping in effective classification of rolling element bearing condition.

1. INTRODUCTION

Rolling element bearings (REBs) are widely used in industrial and domestic applications. In industrial applications, these bearings are considered as critical mechanical components and a defect in such a bearing, if not detected in time can cause malfunction and may lead to catastrophic failure of the machinery [1]. Different methods are available for detection and diagnosis of bearing defects. They can be broadly classified as vibration and acoustic measurements, temperature and wear debris analysis. One of the commonly used techniques for bearing fault detection is vibration measurement [1, 2]. The vibration signals measured can be analysed in time domain, frequency domain or time-frequency domain. Vibration signals collected from rolling element bearings have lot of noise because of varying compliance and presence of defects [1]. The REB vibration signals due to defects alone are weak, compared to the harmonics of the resonant frequency of the system (noise). There is a need to remove or reduce this noise and extract dominant features in order to perform fault diagnostics. Conventional noise reduction or signal pre-processing techniques like Adaptive Noise Cancellation (ANC) and High Frequency Resonance Technique (HFRT) or envelope technique need information about resonant frequencies of the rolling element bearing system [2]. Also the bearing vibration signals are not really cyclostationary (they are rather pseudo cyclostationary) [3, 4]. Wavelet based denoising is increasingly being used in condition monitoring applications, in order to increase the data's reliability and improve accuracy of signal analysis and to increase the signal-to-noise ratio (SNR) [4]. Wavelet transform due to its sparsity, locality and multi-resolution nature has emerged as an effective tool for denoising. The Artificial Neural Network (ANN) has been widely used in fault diagnostics [2]. Different architectures have been studied in bearing fault diagnostics. Multi Layer Perceptron Neural Network (MLPNN) with back propagation is one of

the widely used ANN type [6-9]. While designing an ANN architecture, the focus is always on developing a compact network structure, with minimum number of nodes in the input layer and hidden layer and achieve an overall good generalization ability (in terms of high accuracy on test data). Thus there is a need to reduce the dimensionality of the features extracted from the bearing vibration signals, in order to select the most sensitive features, so that there is dimensionality reduction of the ANN inputs and lead to a compact network. There are several dimensionality reduction techniques (DRT) like Principal component analysis (PCA), Linear Discriminant Analysis (LDA), Fisher's Criterion (FC), Singular Value Decomposition, Genetic Algorithm (GA), etc. Efforts are also needed to optimize the design of MLPNN architecture in terms of learning rate, momentum factor, number of neurons in the hidden layer etc. GA can be effectively used for optimizing these parameters and also select the most sensitive features [11].

In this context, this paper presents results of comparison of MLPNN trained and tested using features selected from denoised vibration signals from REBs from four conditions namely normal, defect on inner race, outer race and ball. The features selected using FC and GA has been compared. GA has also been used to optimize MLPNN architecture.

2. EXPERIMENTAL FRAMEWORK

Experiments were conducted on a customized test rig as shown in Fig.1. The test bearing has been mounted on the left side of the horizontal shaft. A 6205 deep groove ball bearing was tested under four conditions namely - normal (N), defect on inner race (IR), defect on the outer race (OR) and defect on the ball (B). Experiments were conducted for a radial load of 0 and 1.7 kN and a shaft speed of 622 rpm. Vibration signals (acceleration) were acquired through the Y accelerometer at a sampling rate of 48000 samples/s for a time period of 5.08 s, and were processed by the data acquisition system (DAQ) hardware and stored in the computer for further analysis. For each experiment, a data vector of size 250000 was generated, which was divided into bins of 5000 samples, such that it would encompass the probable occurrence of defect characteristics in one cycle.

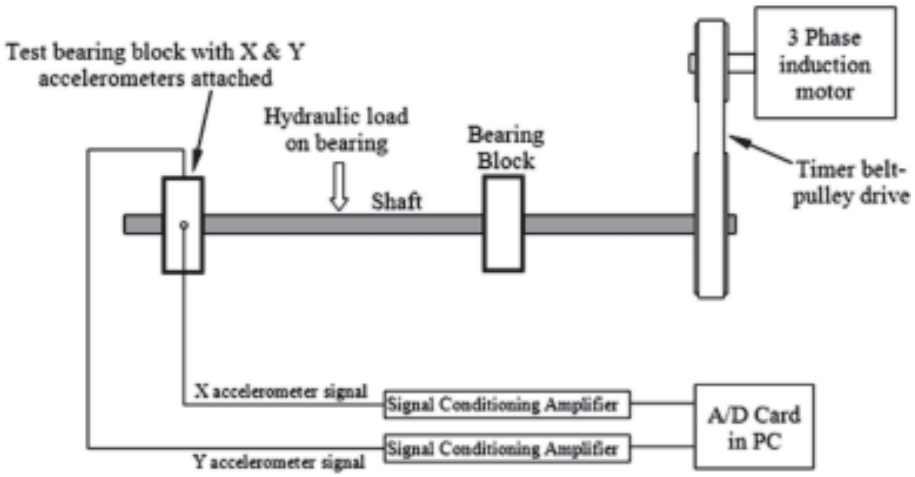

Fig. 1. Bearing test rig used in the work

3. BEARING CONDITION MONITORING SCHEME

3.1 Denoising Scheme

In this work, 'K-hybrid thresholding rule' (K-HTR), proposed by Hong and Liang [5] has been used. The raw bearing vibration signals obtained from the test rig has been decomposed to four levels using Discrete Wavelet Transform (DWT). Daubechies 8 is used as the mother wavelet. The K-HTR scheme is able to retain the impulsive nature of the REB vibration signals in the denoised signal, thereby increasing its kurtosis value. The details of K-HTR scheme and its associated equations are available in [5].

3.2 Feature Extraction

The denoised vibration signals with a vector size of 250000 1 were divided into 50 non-overlapping bins each with 5000 data. From each bin, 30 features have been extracted, 17 time domain features and 13 frequency domain features, details of which are available in [10]. This formed a single pattern. For four conditions of bearing, two loads and one speed condition, a total of 400 patterns were extracted. The feature set matrix consisted of 30 features 400 patterns. Each feature was normalized, so as to get values between 0 and 1. The patterns were thoroughly mixed, out of which 75 % were used in the training data set and the remaining 25 % in the test data set.

3.3 Dimensinality Reduction

Fisher's Criterion (FC) has been used for dimensionality reduction. The Fisher discriminant distance $J_k^{P,Q}$ between the two bearing conditions P and Q for the kth feature set can be computed using Eq. (1) [12].

$$J_k^{P,Q} = \frac{\left| Mean(t_k^P) - Mean(t_k^Q) \right|^2}{\left[Std(t_k^P) \right]^2 + \left[Std(t_k^Q) \right]^2} \tag{1}$$

where, t^P_k and t^Q_k are the kth feature set for the bearing conditions P and Q respectively. For four bearing conditions, the Fisher Discriminant Power (FDP) is calculated as the sum of the pair wise distances [12] as given in Eq. (2).

$$F_k = J_k^{N,IR} + J_k^{N,OR} + J_k^{N,B} + J_k^{IR,OR} + J_k^{IR,B} + J_k^{OR,B} \tag{2}$$

A distance based threshold method (threshold θ method) given in Eq. (3) is used for selecting the sensitive features.

$$\theta \approx \sum_{k=1}^{s} F_k^* \Big/ \sum_{k=1}^{f} F_k \tag{3}$$

where, 'f' is the total number of features extracted (30 in this work) and 's' is the number of selected features such that, the sum of 's' largest FDPs divided by the sum of all the FDPs is approximately equal to θ.

GA is a popular global optimization tool that can optimize the solution to a given problem by using the concepts of evolutionary computing. GA can been used to simultaneously select sensitive features [11] and optimize ANN simulation parameters, *viz*., number of neurons in hidden layer, learning rate and momentum rate.

3.4 Multilayer Perceptron

Multilayer Perceptron (MLP) is a widely used ANN architecture which can be applied to a wide variety of engineering problems. It consists of an input layer, where the number of neurons is equal to the number of features selected (5 in this work), a hidden layer, whose number of neurons are fixed by trial and error and using GA for optimizing the same and an output layer with four neurons, representing four conditions of the bearing, which has been represented using a binary scheme. The activation functions of the hidden and output layer were sigmoid. The different schemes discussed above, along with MLPNN were implemented using customized MATLAB programs. The MLPNN was trained using back-propagation algorithm. The learning rate and momentum rate were set by trial and error and also optimized using GA.

4. RESULTS AND DISCUSSION

FC selected 5 features out of a set of 30 based on the threshold . Table 1 shows the performance of the MLPNN to which the features selected by FC were given as input. It is clear that for 25 neurons, with learning rate of 0.03 and momentum rate of 0.0019 the performance of the MLPNN was the best with a training error of 0.0035, an

Table 1. MLP performance with features selected using FC as inputs

Neurons	Training error	Training accuracy (%)	Test accuracy (%)	Learning rate	Momentum rate
15	0.0049	93.33	89	0.030	0.0019
20	0.0051	92.67	89	0.030	0.0019
25	0.0035	96.33	92	0.030	0.0019
30	0.0062	90.67	88	0.030	0.0019
35	0.0078	87.33	85	0.030	0.0019

accuracy of 96.33% on the training data.

GA in this paper is not only used to select the most sensitive features, but also to optimize MLPNN training parameters *viz*., (i) number of neurons in the hidden layer (ii) Learning rate, and (iii) Momentum rate. The GA program creates a population consisting of eight real valued genomes (chromosomes). Length of each genome is 8. Fitness values of 8 genomes are computed. Parents for crossover are selected based on Normalised Geometrical Rank selection method. Crossover offsprings are produced with a probability of 0.6 using multi-point crossover. Some of the crossover offsprings are mutated with a probability of 0.2. Fitness of each offspring produced by crossover and mutation is computed. The average of the classification accuracies for training and test itself is the fitness value of a genome. Genomes are arranged in the descending order of their fitness values (Good genomes first and worst genomes last). The GA is set to run for a maximum of 150 generations or until

Table 2. Comparison of MLP performance for features selected by the GA and the FC

	MLP performance for features selected by	
Parameters	**GA**	**FC**
Features selected	14, 15, 17, 24 & 28	1, 5, 17, 20 & 21
Best Fitness Value (%)	95.83	94.17
Training accuracy (%)	96.67	96.33
Test accuracy (%)	95.00	92.00
MSE reached	0.0046	0.0035
Number of neurons	17	25
Learning Rate	0.0175	0.0300
Momentum Rate	0.0030	0.0019
Number of generations	150	----

the maximum fitness value attained is 99%. The MLPNN is set to run for a maximum of 2000 epochs or a minimum training error (MSE) of $1\ 10^{-4}$.

Table 2 compares the performance of the MLPNN with the GA and FC selected features as input. It is clear that the performance of the MLPNN in both the cases is similar in terms of the accuracies on the training data and the test data. However, the GA-based MLPNN performs slightly better than the FC-based MLPNN in terms of the dimension of the hidden layer, *viz*., 17 for GA-based MLPNN and 25 in case of FC-based MLPNN. Further, the number of neurons in the hidden layer, learning rate and momentum rates used by the GA-based MLPNN are the values optimized by the GA, whereas in the FC based MLPNN, these values have been fixed by trial and error, i.e., the values which gave best performance of the MLPNN have been selected.

5. CONCLUSION

In this paper, the MLPNN has been used for classification of REB based on features selected using FC and using GA. GA has also been used to optimize the MLPNN architecture in terms of number of neurons in the hidden layer and simulation parameters *viz*., learning and momentum rate. GA-based selection of the input features takes much longer time as it depends on the performance of the MLPNN for computing the fitness value, whereas the FC-based selection of input features is faster as it is independent of the performance of the MLPNN. MLPNN based on GA gave a comparable performance with that using features selected using FC. Hence MLPNN using GA can be effectively used to classify REB condition.

6. REFERENCES

[1] N. TANDON and A. CHOUDHURY, 1999. A review of vibration and acoustic measurement methods for the detection of defects in rolling element bearings, *Tribology International*, **32**, 469-480.

[2] M.S. PATIL, JOSE MATHEW and P.K. KUMAR RAJENDRA, 2008. Bearing signature analysis as a medium for fault detection: A review, *Journal of Tribology*, **130**, 014001.1 - 014001.7.

[3] ROBERT B. RANDALL and JEROME ANTONI, 2011. Rolling element bearing diagnostics-A tutorial, *Mechanical Systems and Signal Processing*, **25**, 485-520.

[4] Z. K. PENG and F. L. CHU, 2004. Application of the wavelet transform in machine condition monitoring and fault diagnostics: a review with bibliography, *Mechanical Systems and Signal Processing*, **18**, 199-221.

[5] HOONBIN HONG and MING LIANG, 2007. K-Hybrid: A Kurtosis-Based Hybrid Thresholding Method for Mechanical Signal Denoising, Journal of Vibration and Acoustics, *Transactions of the ASME* , **129**, 458-470.

[6] C. CASTEJON, O. LARA and J.C. GARCIA-PRADA, 2010. Automated diagnosis of rolling bearings using MRA and Neural Networks, *Mechanical Systems and Signal Processing*, 24, 289-299.

[7] CHUN-CHIEH WANG, YUAN KANG, PING-CHEN SHEN, YEON-PUN CHANG and YU-LIANG CHUNG, 2010. Applications of fault diagnosis in rotating machinery by using time series analysis with Neural Network, *Expert Systems with Applications,* **37**, 1696-1702.

[8] P.K. KANKAR, C. SATISH SHARMA and S.P. HARSHA, 2011. Fault diagnosis of ball bearings using machine learning methods, *Expert Systems with Applications*, **38**, 1876-1886.

[9] JAFAR ZAREI, 2012. Induction motors bearing fault detection using pattern recognition techniques, Expert Systems with Applications, **39**, 68-73.

[10] G.S. VIJAY, P. SRINIVASA Pai and N. S. SRIRAM, 2011. "Bearing diagnostics - A Radial Basis Function Neural Network approach", *Proceedings of the 24th International Congress on Condition Monitoring and Diagnostics Engineering Managemen*t, *Advances in Industrial Asset Integrity Management* (COMADEM 2011), Stavanger, Norway, ISBN 0-9541307-2-3, 843-854.

[11] B. SAMANTA, K.R. AL-BALUSHI and S.A. Al-ARAIMI, 2006. Artificial Neural Networks and Genetic Algorithm for bearing fault detection, *Soft Computing*, **1**0, 264-271.

[12] G.Y. GARY and Kuo-CHUNG LIN, 2000. Wavelet packet feature extraction for vibration monitoring, IEEE Transactions on industrial electronics, **47** (**3**), 650-667.

Journal of Acoustical Society of India : Vol. 40, No. 2, 2013 (pp. 121-130)

Localization of Low Flying Aircraft Based on Its Acoustic Signature

A. Saravanakumar*, S. Arunkumar and K. Senthilkumar
Division of Avionics, Department of Aerospace Engineering, Madras Institute of Technology Campus, Anna University. Chennai-600 044 (Tamil Nadu)
**e-mail: Saravanakumar_a@yahoo.com*

[Received: 21.02.2013; Revised: 25.03.2013; Accepted: 27.04.2013]

ABSTRACT

An aircraft generates an acoustic impulse that propagates outwards from the source. The position of the source and hence the trajectory can be estimated by measuring the relative time of arrival of the impulse at a number of spatially distributed sensors. The time difference for the acoustic wave front to arrive at two spatially separated sensors is estimated by cross correlating the digitized outputs of the sensors. The time delay estimate is used to calculate the source bearing and the position of the source is found using triangulation technique using the bearings from two widely separated receiving nodes. The flight parameter of the aircraft is obtained by Cepstrum method using acoustic Multipath delays. The signal emitted by an UAV arrives at a stationary sensor located above a flat ground via a direct path and a ground-reflected path. The difference in the times of arrival of the direct path and ground-reflected path signal components is known as the Multipath delay. A model is developed to predict the variation with time and Cepstrum method is formulated to estimate the motion parameters like speed and altitude of the aircraft.

1. INTRODUCTION

Acoustic techniques have been widely used in variety of fields. An aircraft which is an acoustic source produces sound that can be received by placing sensors on the ground that captures the sound waves propagated through the air. Acoustic sensors are used widely because of their passiveness, affordability, robustness, and compatibility. Ground sensors are often deployed in remote areas for surveillance and early warning purposes [1]. Due to the high levels of acoustic energy radiated by the propulsion systems of aircraft and by the engines of vehicles, it is possible to detect these sources using passive acoustic sensors mounted close to the ground. Here described a technique that utilizes the Lloyd's mirror effect [2] of the radiated sound to estimate the speed, altitude of a low-flying aircraft by using only a single sensor. The localization of acoustic source is usually done with sensor array in which the output of each sensor is a scalar corresponding to the acoustic pressure. For linear trajectory, we consider a different approach for solving this problem using Acoustic Vector Sensor whose output is a vector corresponding to the acoustic pressure and acoustic particle velocity. The main advantage of these vector sensors over traditional scalar sensors is that they make use of more available acoustic information, hence they should outperform sensor array in accuracy of localization [6]. An array of sensors has been used to find the non linear trajectory as it will be a convenient way to find the trajectory of an aircraft.

2. EXPERIMENTAL PROCEDURE

2.1 Multipath Propagation

In a Multipath propagation environment, two or more attenuated and delayed replicas of the same radiated

signal are received at a sensor. Based on the model of the Lloyd's mirror effect, a method has been formulated to estimate the flight parameters of the source. In that method, the time-frequency distribution of the sensor output is treated as an image. This image is preprocessed to enhance the fringe pattern and then the flight parameters are extracted from the resultant image by optimizing a cost function. The temporal variation of the multipath delay (time difference between the arrival of the ground-reflected path signal and the direct path signal), and then minimize the sum of the squared deviations of the noisy multipath delay estimates from their predicted values over a sufficiently long period of time. The multipath delay is estimated by finding the Cepstrum of the sensor output over a short time interval [3, 5]. The performances of the proposed flight parameter estimation methods are evaluated using real data recorded from the sensor.

2.2 Time-delay Model

Consider an airborne acoustic source (aircraft) moving in a straight line at constant subsonic speed v and constant altitude ht over a hard ground. An acoustic sensor is located at a height hr above the ground [5]. The source is at the closest point of approach (CPA) to the sensor at time τ_c, with the ground range at the CPA being d_c. However the aircraft which we considered flies at varying velocity and at different altitudes. But for study purpose we consider that it is flying at constant velocity, constant altitude and follow a straight line.

The source emits a broadband random acoustic signal, which arrives at the sensor via a direct path and a ground-reflected path. A model for the temporal variation of the multipath delay is derived below using a quasi-stationary approach.[4,8] To calculate the multipath delay at a given time t, the source is assumed to be fixed at the position at an earlier time $\tau(< t)$ which accounts for the sound propagation delay from the source to the sensor. For this model the height of the sensor from the ground surface is about 1 meter. The source-sensor geometry used for the calculation of multipath delay time is depicted below[5].

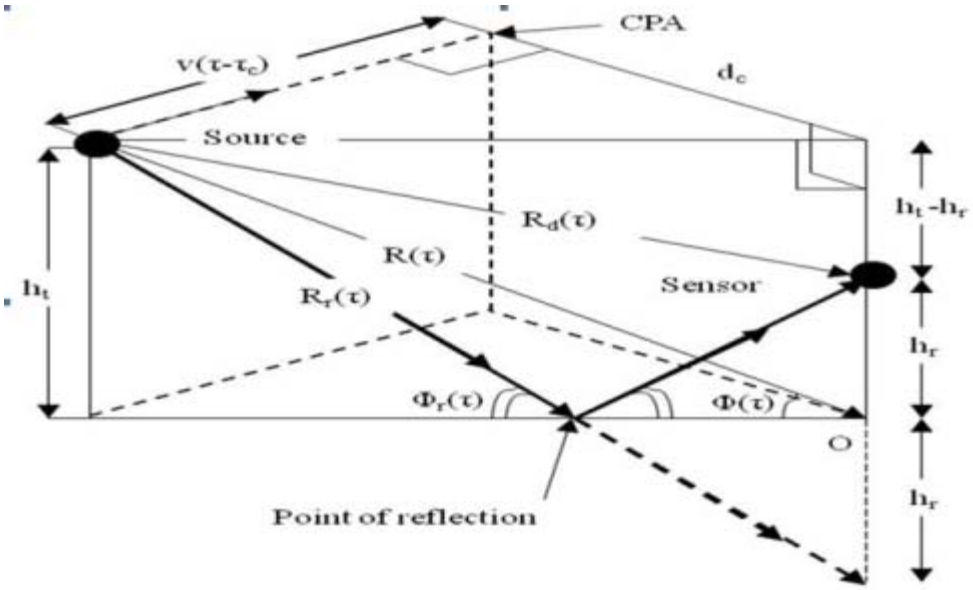

Fig. 1. Source-sensor geometry

The delay time for the desired model is obtained as

$$D(t) \cong \frac{2(c_r^2 - v_r^2)/c_r^2}{\sqrt{v^2(c_r^2 + v_r^2) + c_r^2 v_t^2(\tau - \tau_c)^2 - v_r v_t(\tau - \tau_c)}} \quad (1)$$

where, the values of v_r, v_t, γ, c_r given by

$$v_r = v / h_r \tag{1a}$$

$$v_t = v / h_t \tag{1b}$$

$$\gamma = \sqrt{(1 + (d_c / h_t)^2} \tag{1c}$$

$$c_r = c / h_r \tag{1d}$$

Note that D(t) is a function of $\{v_r, v_t, \tau_c, \gamma\}$ or equivalently the flight parameters $\{v, h_t, \tau_c, d_c\}$. The main flight parameters such as $\{v_r, v_t, \tau_c, \gamma\}$ or equivalently $\{v, h_t, t_c, \gamma\}$ estimated using a non-linear least square method [5]. That is by minimizing the sum of squared deviations of delay estimates from their predicted values. Defining the parameter vector as

$$z = [v_r, v_t, \tau_c, \gamma]^T \tag{2}$$

The estimate of z which is $\hat{z} = [\hat{v}_r, \hat{v}_\tau, \hat{\tau}_c, \hat{\gamma}]^T$ is obtained by minimizing the cost function

$$P(z) = \sum_{k=1}^{K} [\hat{D}(t_k - D(t_k, z))]^2 \tag{3}$$

where,

$\hat{D}(t_k)$ is the multipath delay time at t_k and $D(t_k, z)$ is the corresponding predicted value using(1) the model for $1 \le k \le K$. Given the sensor height h_r, the speed, altitude and CPA ground range of the source is estimated as

$$\hat{v} = h_r \hat{v}_r$$

$$\hat{h}_t = \hat{v} / \hat{v}_t \tag{4}$$

$$\hat{d}_c = | \hat{h}_t \sqrt{(\hat{\gamma}^2 - 1)} | \tag{5}$$

(6)

The multipath delay at time t_k is estimated using Cepstrum method.

2.3 Model for Linear Trajectory

The relationship between the target trajectory and the single sensor can be simply described by two parameters. One is the slant range from the sensor to the CPA (closest point to approach), denoted as r. The other is x_0, which represents the initial position coordinate to a new axis that is built along the trajectory line and makes the CPA as its origin.

2.4 Triangulation Method for Non-linear Trajectory

By knowing the sensor separation distances and the speed of sound propagation in the medium, a three-element linear array can be used to estimate the range and bearing of the source by measuring the time delay between the center sensor and each of the other two sensors [7].

The Fig. 3 shows the principle of triangulation using two nodes. The source and the two nodes, labeled 1

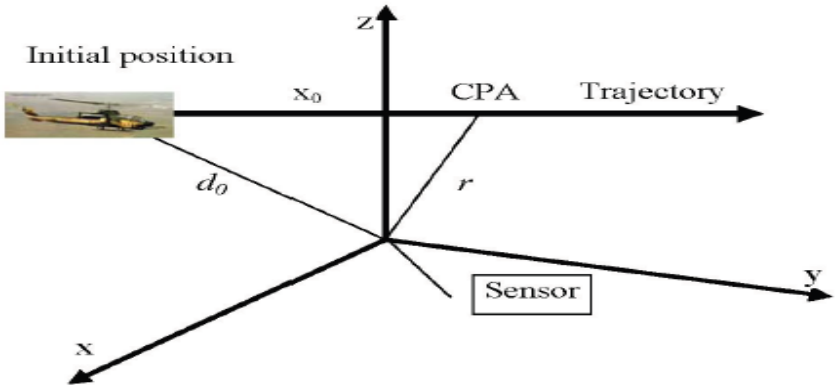

Fig. 2. Parameter model for a single sensor

and 2, are located on the x - y plane at coordinates (x_s,y_s), (x_1,y_1), and (x_2,y_2), respectively, with the y axis pointing towards the north. The bearing lines from the two nodes intersect to determine a unique source location. Assuming line-of-sight propagation, the source position is given by (7)

$$x_s = (y_s - y_1)\tan\theta_1 + x_1, \quad (8)$$

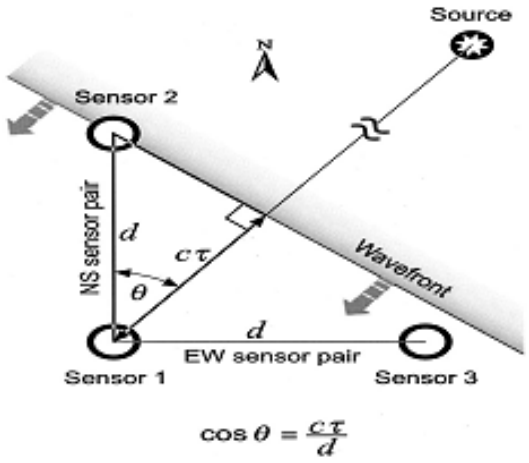

Fig. 3. Triangulation method for finding the position

$$y_s = (x_2 - x_1 + y_1 \tan\theta_1 - y_2\tan\theta_2)/(\tan\theta_1 - \tan\theta_2).$$

The source bearing can be estimated using either pair of sensors or both. An estimate of the source bearing with respect to the NS sensor pair axis is given by (9)

$$\theta_{NS} = \cos^{-1}(c\tau_{12}/d)$$

where c is the speed of sound propagation in air and ?12 is the time delay between sensors 1 and 2 and same wise calculated for EW pair. Since both pairs are orthogonal, it could also be found as

$$\theta_{NS}=\tan^{-1}(\tau_{13}/\tau_{12}). \quad (10)$$

2.5. Cepstrum

Consider a signal which has an echo i.e., delayed components of the signal. When Fourier spectral density (spectrum is taken), the spectrum of signal with echo has the form of envelope that modulates a periodic function of frequency i.e., the spectrum of echo. By taking log of spectrum, the product is converted to sum of two components, one of the original signal and the other an additive periodic component whose fundamental frequency is the echo (delay).In conventional analysis, such periodic components show up as lines or sharp peaks when the original wave form contained an echo. This new spectral representation domain was not frequency domain nor is it time domain, so it is termed as quefrency domain. The cepstrum of the data block is obtained by applying a FFT to the logarithm of its power spectrum.

2.6 Data analysis to Estimate Multipath Time Delay

The data from sensor are processed in overlapping blocks, each containing 40000 samples, with 50% overlap between two consecutive data blocks. Each data block is divided into three 50% overlapping sections and their periodograms are calculated using FFT (Fast Fourier Transform). The three periodograms are then averaged to give the power spectrum of the data block. The cepstrum of the data block is obtained by applying a FFT to the logarithm of its power spectrum. Each peak in the cepstrum corresponds to a rahmonic and the position of the first rahmonic (peak) along the quefrency axis gives the multipath delay estimate. The delay time estimated and the predicted delay time gives the error delay value which is minimized using a cost function.

2.7 Calculation of Direction

Filtering has been done on the pressure signal which is multiplied with velocity vectors to obtain the intensity vectors in each axis. By assuming a cylindrical coordinate (r, θ, ϕ) with Acoustic Vector Sensor as origin

$$\theta = \cos^{-1} I_Z / \sqrt{(I_X{}^2 + I_Y{}^2 + I_Z{}^2)}$$
$$\phi = \cos^{-1} I_Z / \sqrt{(I_X{}^2 + I_Y{}^2)} \quad (12)$$

where I_X, I_Y, I_Z are the intensity vectors along X, Y, Z axis respectively. To find the initial direction average of ten samples in each direction has taken and applied the above formula. For getting the direction of CPA time taken from initial position to CPA has calculated using aircraft velocity (v) and distance from CPA to initial position (x_0) both of them obtained through iteration of aircraft parameters.

3. RESULTS AND DISCUSSION

The total duration of the flight is about 690 seconds. The data has pressure component and three velocity components but the main interest is on pressure component which is sampled at a frequency of 20 kHz and the number of samples is around 1 crore and 37 lakh. The duration of flight is truncated for about 200 seconds such that this period of duration gives the exact flight period.

Total duration of flight = 689.04695 seconds

Sampled frequency = 20000 kHz

Total number of samples = 13780939

Truncated duration = 200 seconds

Number of samples = 4000000

A. Initial estimation of the parameters

The initial estimate of is obtained using the following procedure.

1) Finding the time $\hat{t}_0^0$ at which $\hat{D}^{-1}(t) \equiv 1/\hat{D}(t)$ is the minimum.

2) Computing

3) Calculating $\hat{v}_r^0 = -c_r \frac{\hat{D}_+^{-1} + \hat{D}_-^{-1}}{\hat{D}_+^{-1} - \hat{D}_-^{-1}}$ *and* $\hat{v}_\tau^0 = -\left(\frac{4}{c_r}\right)\frac{\hat{D}_+^{-1}\,\hat{D}_-^{-1}}{\hat{D}_+^{-1} - \hat{D}_-^{-1}}$

where $\hat{D}_-^{-1}$ and $\hat{D}_+^{-1}$ are the respective gradients of two straight lines that provide best fit to the first few and last few data points of .

4) Calculating $\hat{t}_c^0 = \hat{t}_0^0 - \frac{\hat{\gamma}^0 v_r}{c_r v_t}$

3.1. Calculated Parameters for Finding the Trajectory

From the recorded pressure signal the following parameters are calculated

Initial Position from CPA = 14m

Closest Point of Approach = 8.2m

Source frequency = 1692.7 Hz

Time to reach CPA from initial position t_{CPA} = 5.6 seconds

Initial range to aircraft, d_0 = 16.1892m

Initial position

In Cylindrical coordinate

$(d_0, \theta, \phi) = (16.1892\text{m}, 123.1547^0, 32.6635^0)$

In Cartesian coordinate

(x_1, y_1, z_1) = (11.4020m 7.3134m -8.8656m)

Closest point of approach

In Cylindrical coordinate

(r, θ, ϕ) = (8.1807m, 129.38570, 44.96250)

In Cartesian coordinate

(x_2, y_2, z_2) = (5.7617m 3.6956m -4.4800m)

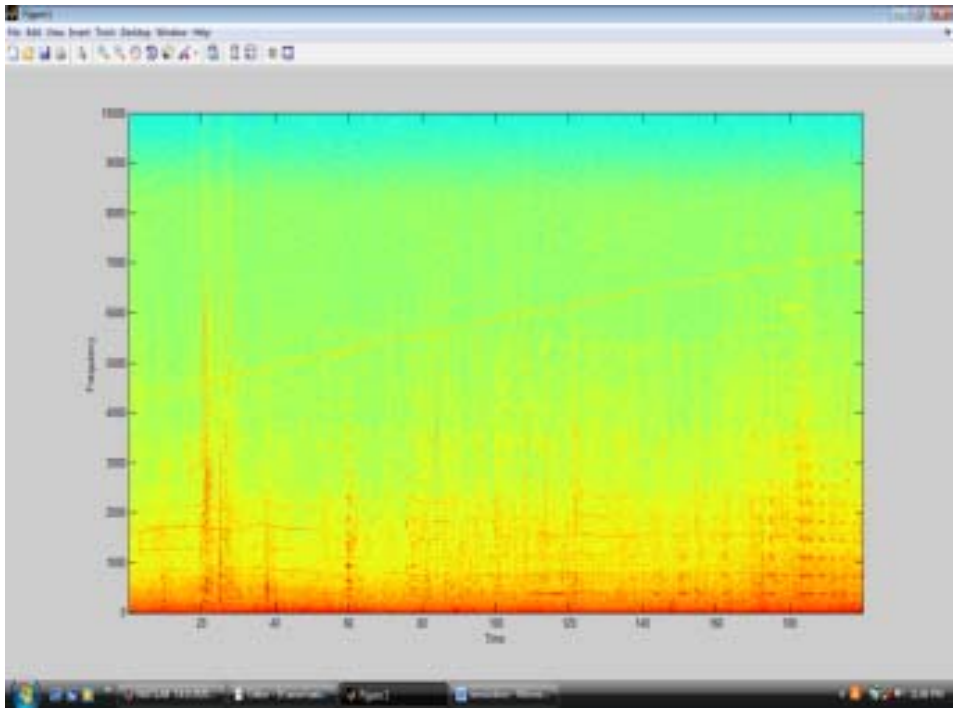

Fig. 4. Spectrogram of a flight transit

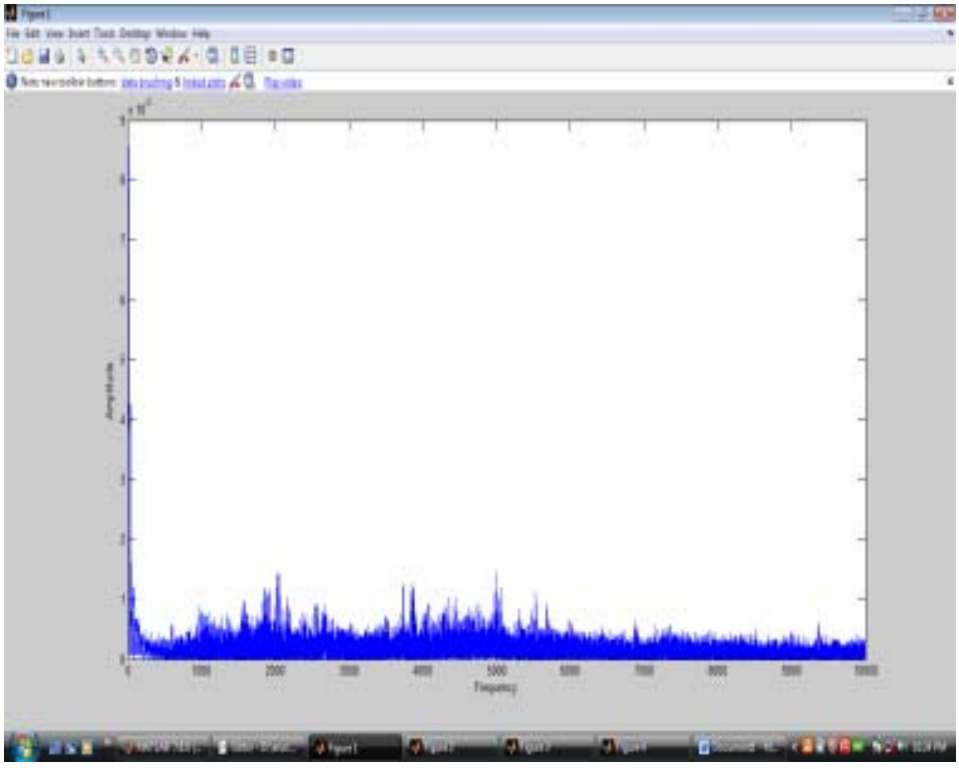

Fig. 5. Fast Fourier transform of a block

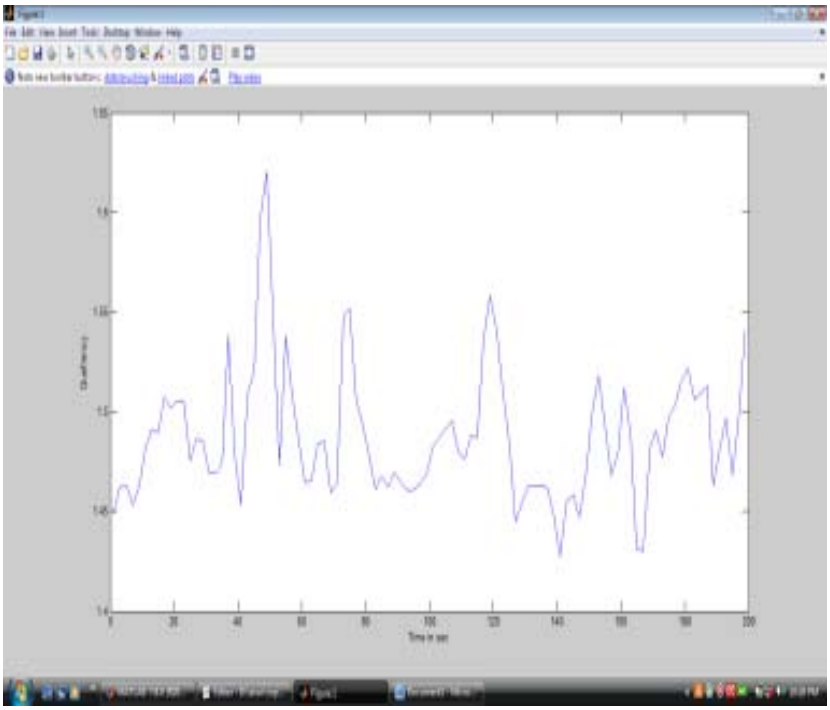

Fig. 6. Multipath delay vs time

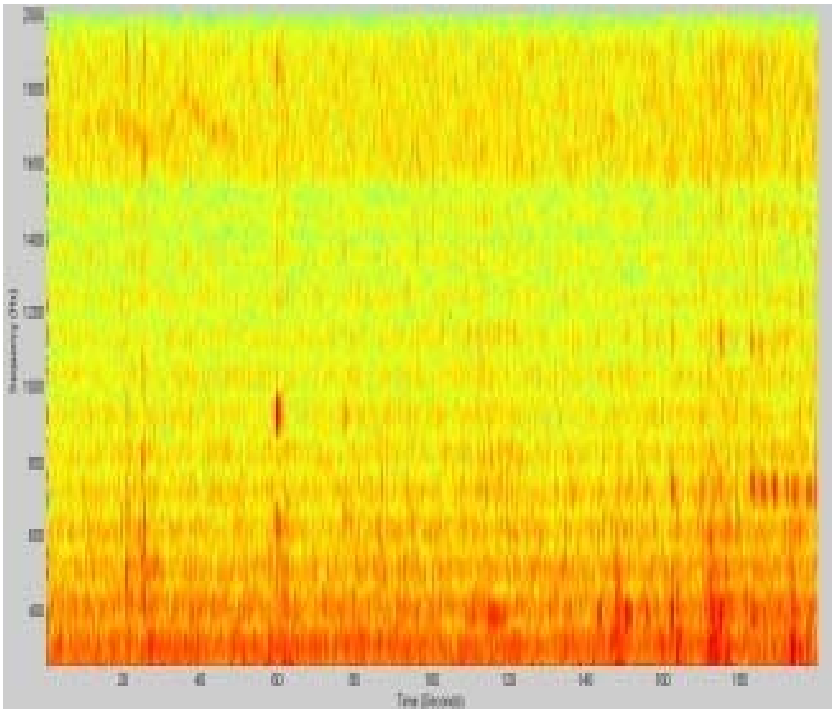

Fig. 7. Spectrogram of Intensity vector in X direction

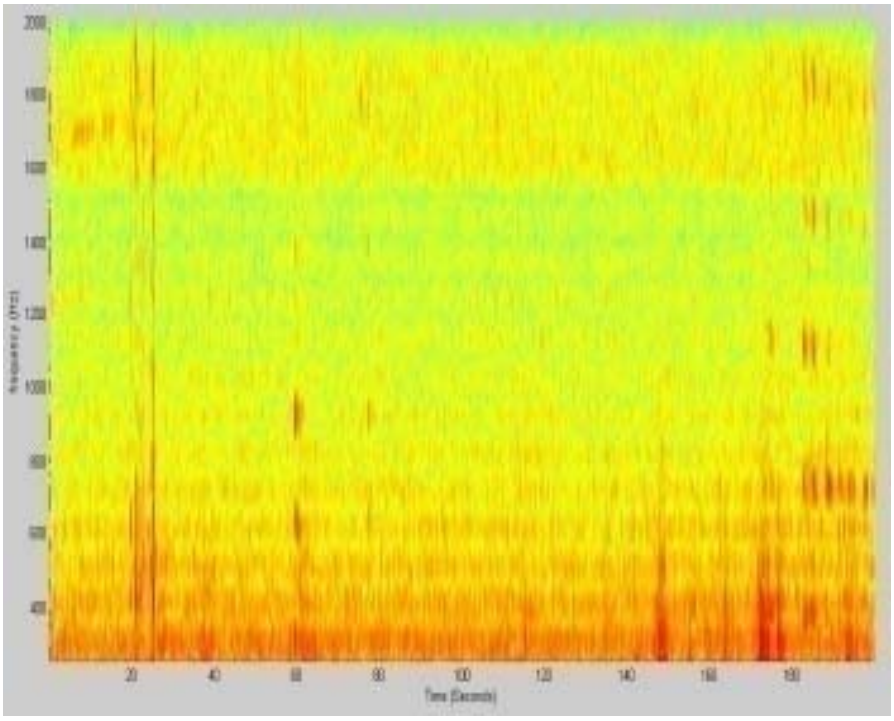

Fig. 8. Spectrogram of Intensity vector in Y direction

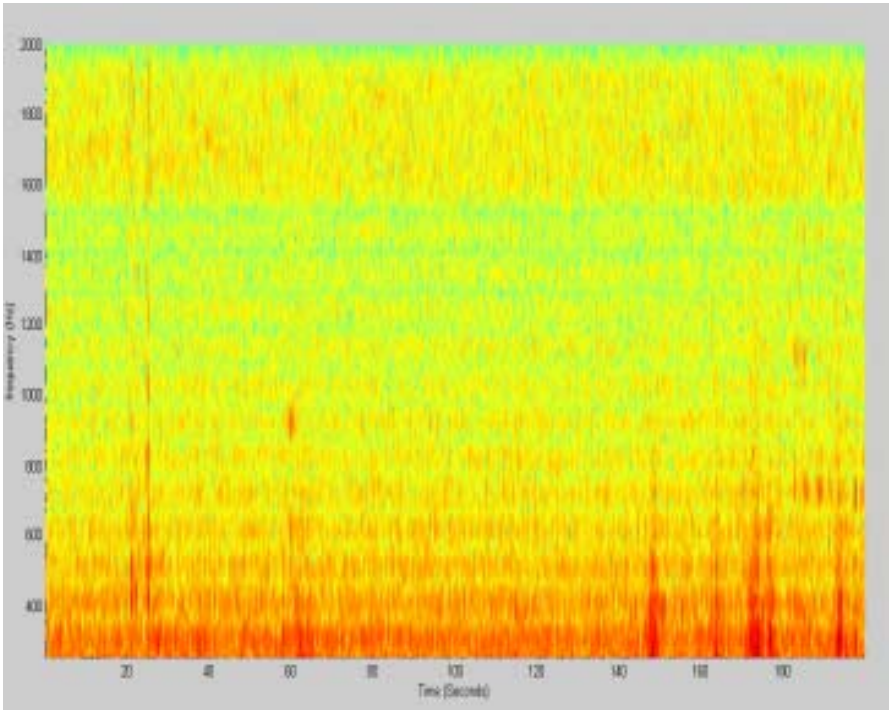

Fig. 9. Spectrogram of intensity vector in Z direction

The multipath delay is calculated for different values of time. The maximum multipath delay is found to be 1.1 ms which occurs at 22nd second. This delay value is used to calculate the delay inverse from which the initial estimation of the parameters is found. The estimated values of velocity and Altitude using Cepstrum are 35 m/s and 15 m respectively.

Based on the Cartesian coordinates obtained for initial position and CPA, trajectory has been plotted.

4. CONCLUSION AND FUTURE WORKS

In this work, flight parameters such as velocity, altitude and straight line trajectory of an aircraft are estimated using a single Acoustic Vector Sensor on the assumption that aircraft following a straight line trajectory. This method exploits the both the scalar as well as vector properties of sound signal for trajectory estimation. Cepstrum algorithm is used to calculate the four flight parameters with the pressure signal obtained. from a single AVS. The pressure signal along with velocity vectors are filtered and multiplied to get the intensity vectors. By making use of intensity vectors direction has been found out. Non linear trajectory of the source is found by triangulation method and it is in progress.

5. REFERENCES

[1] H.E. DEBREE, JELMER WIND, ERIC DRUYVESTEYN and HENK TE KULVE, 2010, "Multipurpose Acoustic Vector Sensors for Battlefield Acoustics - A passive sensor to detect multi events that can be used on multiple platforms", NATO Symposium DAMA, Norway.

[2] K.W.LO, S.W. PERRY and B.G. FERGUSON, 2002, "Aircraft flight parameter estimation using acoustical Lloyd's mirror effect", *IEEE Transactions on Aerospace & Electronics Systems* , **38** (**1**).

[3] DAI HONGYAN ZOU and HONGXING, 2007, "Aircraft motion parameter estimation via Multipath time-delay using a single ground based passive acoustic sensor". *Journal of electronics*.

[4] TAOWANG and QUNWAN, 2007. "Motive Parameters Estimation Using Narrow-band Passive Acoustical Measurements". *IEEE Transactions of Aerospace and Electronic Systems.*

[5] KAM W.LO, BRIAN G.FERGUSON, YUJINGA and LAIN MAGUER, 2003. "Aircraft Flight parameter Estimation using Acoustic Multipath delay". *IEEE Transactions of Aerospace and Electronic Systems*, **39** (**1**).

[6] S. SADASIVAN, HE DEBREE and TOM BASTEN, 2009. "Acoustic Vector Sensor based Intensity Measurements for Passive Localization of Small Aircraft", *Journal of Acoustical Society of India,* **36**(**1**) 8-13.

[7] BRIAN G. FERGUSON, LIONEL G. CRISWICK and KAM W LO, 2002. "Locating far-field Impulsive sound sources in air by triangulation", Acoustical Society of America.

[8] KAM W. LO and B.G. FERGUSON, 2000. "Broadband Passive Acoustic Technique for Target Motion Parameter Estimation", *IEEE Transactions of Aerospace and Electronic Systems*.

Journal of Acoustical Society of India : Vol. 40, No. 2, 2013 (pp. 131-136)

Absorption Studies of Aniline and Esters

K. Sathi Reddy, D. Shanmukhi Jyothi* and D. Linga Reddy
Department of Physics, College of Natural Science, Arba Minch University, Ethopia
Dept of Physics, Sardar Patel College, Secunderabad-500 025, (AP)
Dept of Physics, UCS, Osmania University, Hyderabad -500 007, (AP)
**e-mail: jyothi6physics@gmail.com*

[Received: 16.01.2013; Revised: 17.03.2013; Accepted: 26.04.2013]

ABSTRACT

Ultrasonic velocity(v), density(ρ),viscosity(η) for binary mixtures of Aniline with Methyl Acetate, Ethyl Acetate, Amyl Acetate have been measured at room temperature of 300.15K over entire volume component percentage range. The ultrasonic velocity (v) is measured with Pulse Echo Overlap technique at a frequency of 2MHz. The density (ρ) measurements have been carried out by 10ml specific gravity bottle. The viscosity (η) measurements have been carried out by using Canon-Fenske Viscometer with an accuracy of ±0.3% . Attenuation Coefficient (α) is measured using a Cathode Ray Oscilloscope for a transmitted pulse and n^{th} echo. Relaxation times (τ), Absorptivity (A) are computed using measured data of ultrasonic velocity (v), density (ρ), viscosity (η).

1. INTRODUCTION

Ultrasonic is a useful tool to know the nature of molecular interaction in pure, binary and ternary liquids. But no sufficient data is available in the binary mixture of Aniline in Methyl Acetate, Ethyl Acetate, Amyl Acetate. Ultrasonic method found extensive application [1-2] in characterizing the various aspects of the physico-chemical behavior of liquid mixtures such as molecular interaction and association. Molecular association and complex formation in liquid mixtures through ultrasonic velocity measurements have been studied by Reddy and Naidu [3]. Ultrasonic velocity of a liquid is related to binding forces between atoms and molecules. The sound velocity in liquid mixtures is known to be a quantity which depends on concentration in a variety of manners according to the nature of each component liquid. Accurate measurements of ultrasonic velocity deliver the information about the physical and chemical behavior of solutions and liquid mixtures.

In a material scattering and absorption are produced by various dynamical interactions which typically arise from enharmonic force between the atoms, the presence of free charge carriers, cycling to localized spin states and the presence of impurities [4]. When acoustic waves are propagated through a liquid, dissipation of acoustic energy that is associated with changes in the molecular structure of the medium results from the finite time, which is required for these changes to take place. Ultrasonic velocity has been a subject of active interest during the recent years [5-7]. Nomoto and co researchers made successful attempt to evaluate the sound velocity in binary mixtures. In the present communication we focus on the ultrasonic behavior of liquid mixtures at 300.15K temperature with Aniline as the base and few esters Methyl Acetate, Ethyl Acetate and Amyl Acetate as mixtures.

2. EXPERIMENTAL

The samples are taken for the present study are of Analar reagent grade and procured from Sd.Fine Chemicals Limited,Bombay,India. The liquids are thoroughly distilled to remove the dissolved impurities

using standard chemical procedures like steam distillation. Liquids practically are immiscible with water, volatile in steam and possessing a high boiling point.

By taking two liquids in separate burettes, and with Job's variation method of continuous variation has been used to prepare the mixtures of required proportions.

The ultrasonic velocity measurements are made with the help of microprocessor based ultrasonic Pulse Echo Overlap technique (model UX4400M) with built in time Velocity and thickness measuring feature with a frequency of 2MHz. supplied by Roop Telesonic Ultrasonic Ltd,Bombay,India. The internal circuit of (ULTRASONIX4400M) is designed with full solid state version. Further outstanding stability of operation is ensured by dynamic use of integrated circuit and PCB mounted gold switches. It has special memory features which enable one to enter testing procedures like angle and type of transducer for permanent storage and direct digital read out of Ultrasonic velocity up to an accuracy of ±1m/s.

The Pulse Echo Overlap (PEO) method is very versatile and highly accurate technique for measuring the velocity of the ultrasonic waves in materials of liquids and solids structures. A highly absolute accuracy is obtained from this system, since the method is capable of accurately measuring from any cycle of one echo to the corresponding cycle of the next echo. The PEO method is able to handle diffraction (beam spreading) and phase correction properly, so that absolute accuracy of the PEO method may exceed the accuracy of most of the other methods. However, precision of some other methods is better than PEO method. The PEO method may operate either with transducer bonded to the specimen or directly with RF bursts. On the negative side, because of transducer effects, the leading cycles of successive echoes are attenuated and trailing cycles are burst up, so that great care has to be taken to obtain proper cycle for cycle match.In view of the above advantages and accuracy of the system the PEO technique has been adopted for measuring velocity and attenuation.

The densities of all the mixtures have been determined with 10ml. specific gravity bottle and mass (m) of a given volume of the liquid is determined by using a single pan opto- electrical balance. The results of the densities are accurate to ±0.5%.

The internal circuit of pulse echo overlap system is designed with fully solid state version, which allows immediate calculation of the ultrasonic wave velocity as given in the following equation.

$v = 2l / t$

where l is the liquid length and t is the time interval.

The long ultrasonic waves are passed through the binary mixture. They are reflected from the reflector face and received by the same transducer, which now acts as a receiver. The transmitted pulse and the received echoes are seen in the CRO screen. Once, the echo pattern is achieved on the screen of the CRO, the pattern is adjusted to a suitable height. The transmitted pulse height is measured in mv/cm and noted as 'a0' on the screen. The height of first echo is noted as 'a1' and second echo as 'ao' and so on. The path length is noted using the micrometer attached to the reflector and is noted as 2l.

∴ The attenuation coefficient (á) is calculated as

$$á = 1/2 \log_e (a0/an) \text{ nepers/unit length.}$$

where ao → amplitude of transmitted pulse.

an → amplitude of n^{th} echo.

The absorptivity is measured by dividing á by the square of the frequency (2MHZ) of the ultrasonic wave propagated into the liquid media, i.e Absorptivity, $A = á/f$

Where f is the frequency of the ultrasonic wave propagated.

The coefficient of absolute viscosity (ç) has been determined using a Cannon- Fenske Viscometer. The results of viscosities are accurate to ± 0.3%.

3. RESULTS AND DISCUSSION

Ultrasonic velocity decrease in Aniline-Methyl Acetate, Aniline-Ethyl Acetate, Aniline-Amyl Acetate. Ultrasonic velocity is larger in Aniline-Amyl Acetate the reason being that Amyl Acetate is more alcoholic. Aniline is a basic component and possesses less number of H which causes for freer movement of Ultrasonic waves through the medium. Therefore Ultrasonic velocity increases with respect to the increase in Aniline concentration .These are in tune with [4]. The density values decrease with respect to the increase in Ester concentration in all the systems. The density values are lesser in Aniline-Amyl Acetate system and larger in Aniline-Methyl Acetate system. The order of densities is Amyl Acetate < Ethyl Acetate <Methyl Acetate. The attenuation coefficient is a quantity that characterizes how easily a material or medium can be penetrated by a beam of light, sound, particles, or other energy or matter [10-14]. A large attenuation coefficient means that the beam is quickly "attenuated" (weakened) as it passes through the medium, and a small attenuation coefficient means that the medium is relatively transparent to the beam [15-16]. The ultrasonic waves are passed through the specimen under study. They are reflected from the opposite face and received by the same transducer, which now acts as a receiver. The Pulse Echo Wave train pattern is observed on the screen. Gate pulse was made to coincide with the bottom of the secondary echo pulse and amplitude is adjusted to 80% of its maximum value. The amplitude pulse noted as ao and the amplitude of the n^{th} echo pulse as an.
A perusal of attenuation coefficient (α) obtained for various binary mixtures of the Aniline with Esters reveals the following factors.

(i) Attenuation coefficients (α) of binary mixture of Aniline with Methyl acetate lower compared to binary mixture of Ethyl acetate and Amyl acetate with Aniline. This means the chain length of the Esters is deciding the nature of binary mixture.

(ii) Attenuation coefficients (α) for Amyl acetate is higher than Methyl acetate and Ethyl acetate. Generally it can be said that, higher the chain length of the Esters, the higher will be the attenuation coefficient (α). In case of Methyl acetate, Ethyl acetate and Amyl acetate with Aniline binary mixtures is observed as Aniline-Amyl acetate>Aniline-Ethyl acetate >Aniline-Methyl acetate.

Table 1. Ultrasonic velocity (v), density (ρ), viscosity (η), relaxation time (τ), attenuation coefficient (α), absorptivity (A) of binary mixture of aniline in Methyl acetate at 300.15 K

Volume component percentage		Ultrasonic velocity (V)m/s	Density (ρ) 10^{-3} Kgm^{-3}	Viscosity (η) poise	Relaxation time (τ) 10^{-8}sec	Attenuation aoefficient (α)	Absorpitivity (A) 10^{-13}
Aniline	Methyl accetate						
90	10	1502	1.0182	0.025	1.4511	0.5531	1.3827
80	20	1439	1.0068	0.0178	1.1383	0.6192	1.548
70	30	1407	1.0053	0.0151	1.011	0.6247	1.56175
60	40	1370	0.9962	0.0117	0.8343	0.6347	1.55675
50	50	1327	0.9820	0.0098	0.7556	0.6491	1.62275
40	60	1258	0.9784	0.0084	0.6932	0.6568	1.642
30	70	1240	0.9718	0.0072	0.7002	0.6642	1.6605
20	80	1200	0.9521	0.0066	0.6418	0.6715	1.67875
10	90	1150	0.945	0.0053	0.5654	0.6821	1.70525

Table 2. Ultrasonic velocity (v), density (ρ), viscosity (η), relaxation time (τ), attenuation coefficient (α), absorptivity (A) of binary mixture of aniline in Methyl acetate at 300.15 K

Volume component percentage		Ultrasonic velocity (V)m/s	Density (ρ) 10^{-3} Kgm^{-3}	Viscosity (η) poise	Relaxation time (τ) 10^{-8}sec	Attenuation coefficient (α)	Absorpitivity (A) 10^{-13}
Aniline	Methyl accetate						
90	10	1502	1.0095	0.0248	1.4519	0.5531	1.3827
80	20	1457	1.0017	0.0194	1.2164	0.6247	1.56175
70	30	1412	0.9905	0.0166	1.1207	0.6347	1.58675
60	40	1373	0.9079	0.0137	0.9808	0.6491	1.62275
50	50	1329	0.9853	0.0111	0.5804	0.6568	1.642
40	60	1288	0.9717	0.0095	0.7857	0.6642	1.6605
30	70	1244	0.9489	0.0081	0.7354	0.6715	1.67875
20	80	1203	0.9289	0.007	0.6942	0.6821	1.70525
10	90	1153	0.9243	0.0059	0.6402	0.6977	1.74425

Table 3. Ultrasonic velocity (v), density (ρ), viscosity (η), relaxation time (τ), attenuation coefficient (α), absorptivity (A) of binary mixture of aniline in Methyl acetate at 300.15 K

Volume Component Percentage		Ultrasonic Velocity (V)m/s	Density (ρ) 10^{-3} Kgm^{-3}	Viscosity (η) poise	Relaxation Time (τ) 10^{-8}sec	Attenuation Coefficient (α)	Absorpitivity (A) 10^{-13}
Aniline	Methyl Accetate						
90	10	1504	1.0142	0.0249	1.4471	0.5531	1.3827
80	20	1460	1.0097	0.0186	1.1522	0.6491	1.62275
70	30	1417	0.9781	0.0160	1.0862	0.6568	1.642
60	40	1390	0.9641	0.0106	0.7587	0.6642	1.6605
50	50	1348	0.9520	0.0089	0.6859	0.6821	1.70525
40	60	1301	0.9423	0.0080	0.6687	0.6821	1.70525
30	70	1278	0.9208	0.0072	0.6383	0.6977	1.74425
20	80	1240	0.9023	0.0064	0.6150	0.7083	1.77075
10	90	1203	0.8906	0.0052	0.5379	0.7153	1.78825

4. CONCLUSION

Absorption studies are carried out apart from ultrasonic studies on Methyl Acetate, Ethyl Acetate, and Amyl Acetate with Aniline over entire volume component percentage range. It is found that Ultrasonic velocity increases with increase in Ester concentration. The density values decrease with respect to the increase in Ester concentration in all the systems. The Attenuation Coefficient and Absorptivity decrease as the concentration of the Esters increase.

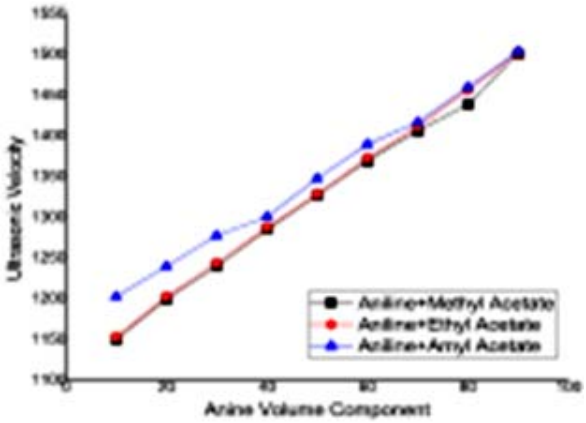

Fig. 1. Aniline Volume Component vs Ultrasonic Velocity

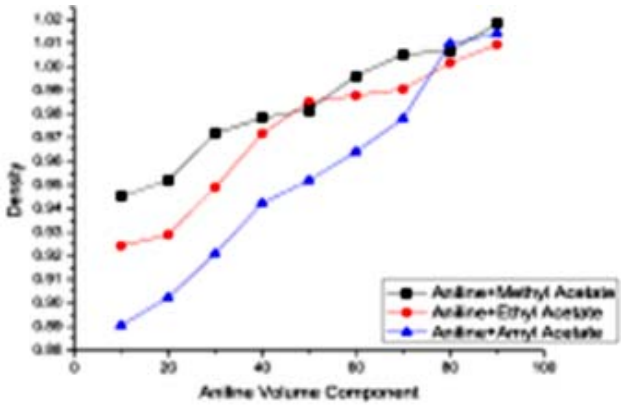

Fig. 2. Aniline Volume Component vs Density

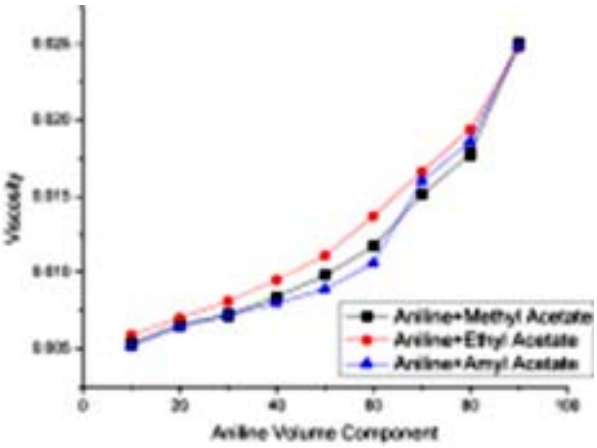

Fig. 3. Aniline Volume Component vs Velocity

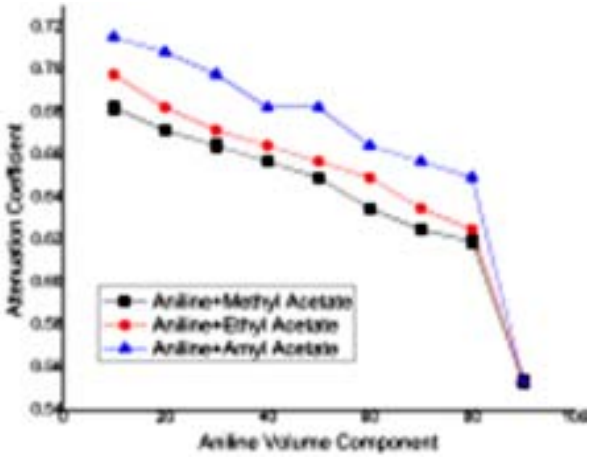

Fig. 4. Aniline Volume Component vs Relaxation time

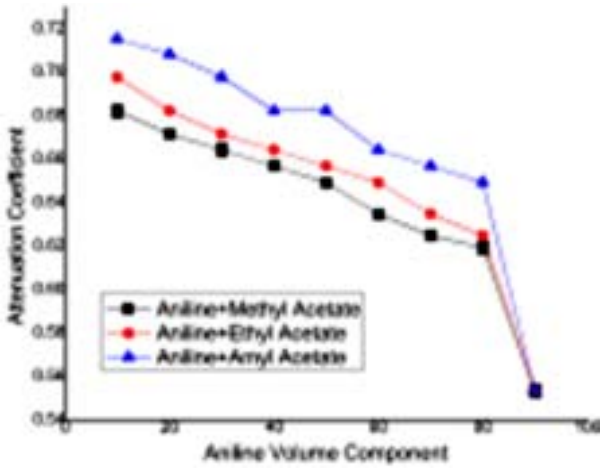

Fig. 5. Aniline Volume Component vs Attenuation Coefficient

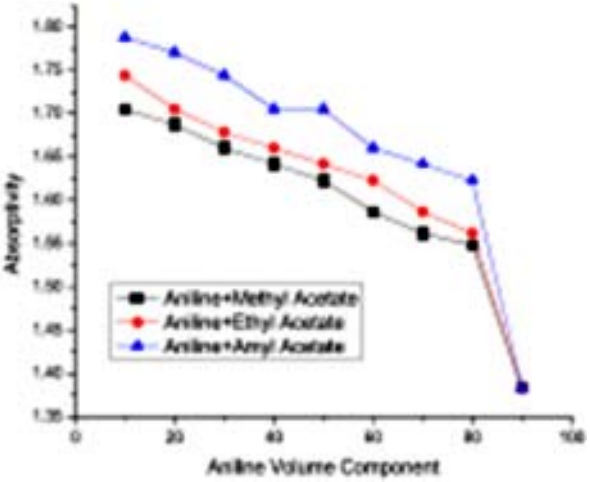

Fig. 6. Aniline Volume Component vs Absorptivity

5. REFERENCES

[1] H. EYRINGAND and J.O. HIRSCHFELDER, 1937 *J.Phy.chem*, **41**, 249.
[2] R.J. FORT and W.R. MOORE,1979 *Trans, Faraday Society* **61**, 687.
[3] K. SUBRAMANYAM REDDY and P.R. NAIDU, 1979 *Aust. J. Chem* **32**, 687.
[4] K. SATHI REDDY and D. LINGA REDDY, 2007 *Journal of Ultrasonics*.
[5] B. Ravinder Reddy and D. Linga Reddy, *Ind.J.Pure and Appl.Phy*.37, (1999)56.
[6] N. JAYA KUMAR, KARUNANIDHI and V. APPAN, 1999 *Ind.J.Pure and Appl. Phy*.**36**, 76
[7] S.V. Ranganayakulu, C. Sreenivas Reddy and D. Linga Reddy, 2003 *J. Acoustical Society of India* **31**, 295.
[8] H. EYRING and J.F. KINCAID, 1938 *J. Chem. Phy.* **6**, 67.
[9] V.K. SYAL, KUMARI, U. CHAUHAN, S. CHAUHAN, M.S. SUD and S.P. SINGH, 1992 *Indian J. Pure and Appl. Phy*.
[10] S. RAJAGOPALAN, 1988 *Acoustica*, **66**, 63.
[11] K.S. REDDY and P.R. NAIDU, 1985 *J. Chem. Liq*.**15**, 147.
[12] C. BACHEM and Z. PHYSIK 1936 **101**, 565.
[13] G.V. REDDY and R.P. SINGH, 1970 *Acustica* **23**, 31.
[14] S.C. BHATT, R.S. RAWAT and B.S. SEMWAL, 1999 *J. Acoust. Soc. India*, **27**, 297.
[15] J. PRAKASH and B. RAI, 1987 *Acoustica*, **64**, 226.
[16] O. NOMOTO 1953 *et al*, *J. Phy. Soc. Japan* **8 4**.

Journal of Acoustical Society of India : Vol. 40, No. 2, 2013 (pp.137-142)

Interaction Study of Pyridine and Acetone at 313.15 K

Prashant Dabrase[1]*, R.A. Patil[2] and B.M. Suryavanshi[3]
[1]Bhalerao Science College, Saoner-441 107
[2]S.S.S.K.R.Innani Mahavidyalaya, Karanja-444 105
[3]Dept. of Physics, Government Institute of Science, Nagpur-440 001 (M.S.)
**e-mail: prashantdabrase@gmail.com*

[Received: 18.01.2013; Revised: 22.03.2013; Accepted: 28.04.2013]

ABSTRACT

The Ultrasonic velocities (υ), density (ρ) and viscosity (η) measurements of pure & binary liquid mixtures of Pyridine and Acetone have been carried out at temperature 313.15 K to evaluate the other thermo dynamical parameters with their excess values such as adiabatic compressibility (β_α), free length (L_f), acoustical impedance (Z), free volume (V_f), internal pressure (π_i) and the excess values, υ^E, β_α^E, L_f^E, Z^E, V_f^E and π_i^E over the entire range of composition. The results thus obtained are discussed for molecular interaction. The non linearity observed in the plots of these ultrasonic parameters and their excess values with the composition range indicates presence of the intermolecular interaction between the components of the unlike molecules of the mixture. The nature of excess values of the compressibility β_α^E, free length L_f^E, acoustical impedance Z^E, free volume V_f^E and internal pressure π_i^E conforms about the existence of the molecular association between the components of the mixture.

1. INTRODUCTION

Ultrasonic studies have always played an important role in understanding the nature of intermolecular interaction in pure liquid and liquid mixtures. They find application in several industrial and technological processes. Because the Ultrasonic velocity is highly sensitive to molecular structures [1-4] and Ultrasonic investigations of liquid mixtures consisting of polar and non polar components are of highly importance in understanding the physical nature and strength of molecular interaction in the liquid mixtures [5]. For the better understanding of the physical and chemical properties and the inter-molecular interactions between the molecules of the mixture, ultrasonic velocity with density and the viscosity are measured at different concentration. The ultrasonic velocity of liquid is basically related to the bonding forces between the atoms and molecules, it helps to understand the nature of molecular interactions in pure and binary mixtures of the liquids [6-8]. Pyridine is an important liquid used currently in the extraction process for coal to analyze its compounds and in the manufacture of vitamin B6 and other drugs. These liquid mixtures are of interest to organic chemists to know about the type of bond and number of each molecule in the pyridine complex [9, 10].

In the present study the ultrasonic velocity, density and viscosity measurements have been carried out for pure acetone and pyridine and their binary mixtures for various concentrations at 313.15K. The variations of different ultrasonic parameters and their excess values with concentration of binary liquid mixtures are studied to understand molecular interaction between unlike molecules of the mixtures.

2. EXPERIMENTAL

The binary mixtures of various concentrations in mole fraction of the liquids Acetone and Pyridine were prepared at room temperature by obtaining the AR grade liquids with purity of 99.5% commercially and used

without further purification and were stored in special air tight glass bottles to avoid air contact. Ultrasonic velocities (υ) for different concentration of binary mixtures and pure liquids were measured using single crystal multi frequency Ultrasonic Interferometer at 1 MHz (Mittal enterprises- model M-81). The measurements of density of pure liquids and their binary mixtures were carried out by using specific gravity bottle on a sensitive mono-pan balance within ± 0.1mg accuracy. The viscosities were measured using suspended level viscometer which was calibrated with doubly distilled water at different temperatures. The experimentally measured density (ρ) in kg ms^{-1}, ultrasonic velocity (υ) in $ms^{-1}$and viscosity (η) in NS m^{-2} are used to evaluate various thermodynamic parameters like adiabatic compressibility (β_α), free length (L_f), acoustical impedance (Z), free volume (V_f), internal pressure(π_i) and their excess values as υ^E, η^E, β^E, L_f^E, Z^E, V_f^E and π_i^E by using standard relations as below.

Adiabatic Compressibility $$\beta_a = \frac{1}{\rho v^2} \quad (1)$$

Intermolecular free length (L_f) [8], $$f = K\beta_\alpha^{1/2} \quad (2)$$

Acoustic impedance (Z) $$Z = \upsilon\rho \quad (3)$$

free volume (V^f) $$V_f = \left[\frac{M_{eff}\, v}{\eta k}\right]^{3/2} \quad (4)$$

The internal pressure (π_i) $$\pi_i = bRT(k\eta/n)^{1/2}(\rho^{2/3}/M^{7/6}_{eff}) \quad (5)$$

and their excess values are determined by using the relation
by using $$A^E = A_{exp} - A_{id} \quad (6)$$

3. RESULTS AND DISCUSSION

From Table 1, it can be seen that the ultrasonic velocity (υ) and density (ρ) increases with the concentration of Pyridine in Acetone but the adiabatic compressibility (β_α) shows the negative trend than that of velocity at 313.15 K temperature. Free length (L_f) also shows similar relation with the concentration as that of compressibility but the viscosity (η) and acoustic impedance (Z) increases with the concentration of pyridine in the mixture. The intermolecular free length depends upon intermolecular attractive and repulsive force [11]. The free volume shows decreasing trend and internal pressure is seen as increasing with increasing concentration of pyridine in the mixture. The plots of these parameters with concentrations also conforms the non linear variation (Fig. 1), all the plots are non linear and the most variations can be seen at 0.6 of molar concentration of pyridine in the mixture. The values of adiabatic compressibility (β_α) and free length (L_f) decreases with increase in the mole fraction of Pyridine. The decrease in the values of free length with increasing concentration can be concluded as there is significant interaction between the two liquids [12]. It is also observed that as the concentration of pyridine increases, free volume decreases whereas the internal pressure increases. This suggests the close packing of the molecules, which may be concluded as the increasing magnitude of the interaction [13-15]. The non linear variation in the above parameters with the mole fraction of pyridine is an indication of existence of interaction between the components of the mixture [16, 17]. The viscosity values showing increasing trend is the indication of frictional resistive force that may be due to a change in effective molecular area of the cohesive or adhesive forces or relative random velocity between the components of the mixture. In this case this may be due to the tight packing and close structure of pyridine [10].

The existence of any inter molecular interaction can be supplemented with the help of excess values of the thermo dynamical parameters. The extent of deviation & sign of these functions depends on the strength of interaction between unlike molecules [18, 19]. Here Table 2, presents the data of excess values of the ultrasonic velocity (υ^E), excess viscosity (η^E), excess adiabatic compressibility (β_α^E), excess free length (L_f^E), excess impedance (Z^E), excess free volume (V_f^E) and excess internal pressure (π_i^E) corresponding to the molar concentration of pyridine in the mixture at temperature 313.15 K. The excess velocity here is seen to be positive.

Table 1. Values of density, ultrasonic velocity, viscosity, adiabatic compressibility (β_α) free length (L_f), acoustical impedance (Z), free volume (V_f) and internal pressure (π_i) for Acetone + Pyridine mixture at 313.15 K

Mole Fract of Pyridine	Density ρ kgm^{-3}	Velocity υ ms^{-1}	Viscosity η mPas	Compress β_α 10^{-10} m^2N^{-1}	Free length L_f	Impedance Z X $10^4 Kgm^{-2}s^{-1}$	Free volume V_f X 10^{-7} m^3	Internal pressure π_i X 10^8 Pa
0	767.3450	1098.955	240.174	10.7907	6.9394	0.84328	4.89277	3.69326
0.11582	791.9711	1134.233	264.342	9.8149	6.6182	0.89828	4.72475	3.71319
0.2341	819.1132	1173.568	296.5339	8.8642	6.2895	0.96129	4.44627	3.77244
0.35490	847.8668	1211.538	332.8187	8.0352	5.9882	1.02722	4.16186	3.84359
0.47833	874.1163	1249.795	377.9024	7.3244	5.717	1.09247	3.81971	3.93335
0.60446	897.7669	1282.649	427.3347	6.7705	5.4968	1.15152	3.49785	4.01926
0.73338	922.7287	1317.222	490.4197	6.2461	5.2796	1.21544	3.13258	4.14167
0.86520	944.7639	1348.500	559.3288	5.8207	5.0966	1.27401	2.81605	4.25322
1	962.8652	1377.257	690.5037	5.4753	4.9431	1.32611	2.23806	4.53858

Table 2. Excess values of ultrasonic velocity, excess viscosity (η^E), excess adiabatic compressibility ($\beta_\alpha{}^E$), excess free length ($L_f{}^E$), excess acoustical impedance (Z^E), excess free volume($V_f{}^E$) and excess internal pressure ($\pi_i{}^E$) for Acetone + Pyridine at 313.15 K temperature.

Mole Fract of Pyridine	υ^E ms^{-1}	$\beta_\alpha{}^E$ 10^{-10} m^2N^{-1}	η^E mPas	$L_f{}^E$ X 10^{-11} m	Z^E X $10^6 Kgm^{-2}s^{-1}$	$V_f{}^E$ X 10^{-7} m^3	$\pi_i{}^E$ X 10^8 Pa
0	0	0	0	0	0	0	0
0.115808	3.0459	-0.3602	-27.9878	-0.0899	-0.0009185	0.1394	-0.07797
0.234077	9.4653	-0.6822	-49.0578	-0.1826	0.0049804	0.1749	-0.1187
0.354882	13.8139	-0.8691	-67.1769	-0.2427	0.0125878	0.2112	-0.14967
0.478309	17.7206	-0.9239	-77.6765	-0.2674	0.0182353	0.1968	-0.16425
0.604441	15.4718	-0.8072	-85.0451	-0.2359	0.0163883	0.2097	-0.18496
0.733371	14.1645	-0.6464	-80.0193	-0.1957	0.018057	0.1867	-0.17154
0.865191	8.7584	-0.371	-70.4700	-0.1155	0.0129877	0.2201	-0.17141
1	0	0	0	0	0	0	0

The excess compressibility and free length shows negative values and the same trend can be observed in the excess viscosity but the values are more negative it means the strong attractive or repulsive forces are acting between the different components of the mixture. The close perusal of the excess values as shown in the Fig. 2, conforms the trend in excess free volume and excess internal pressure is opposite to each other. Excess free volume is positive and excess internal pressure is negative and in both the cases the nature of the cure is nearly

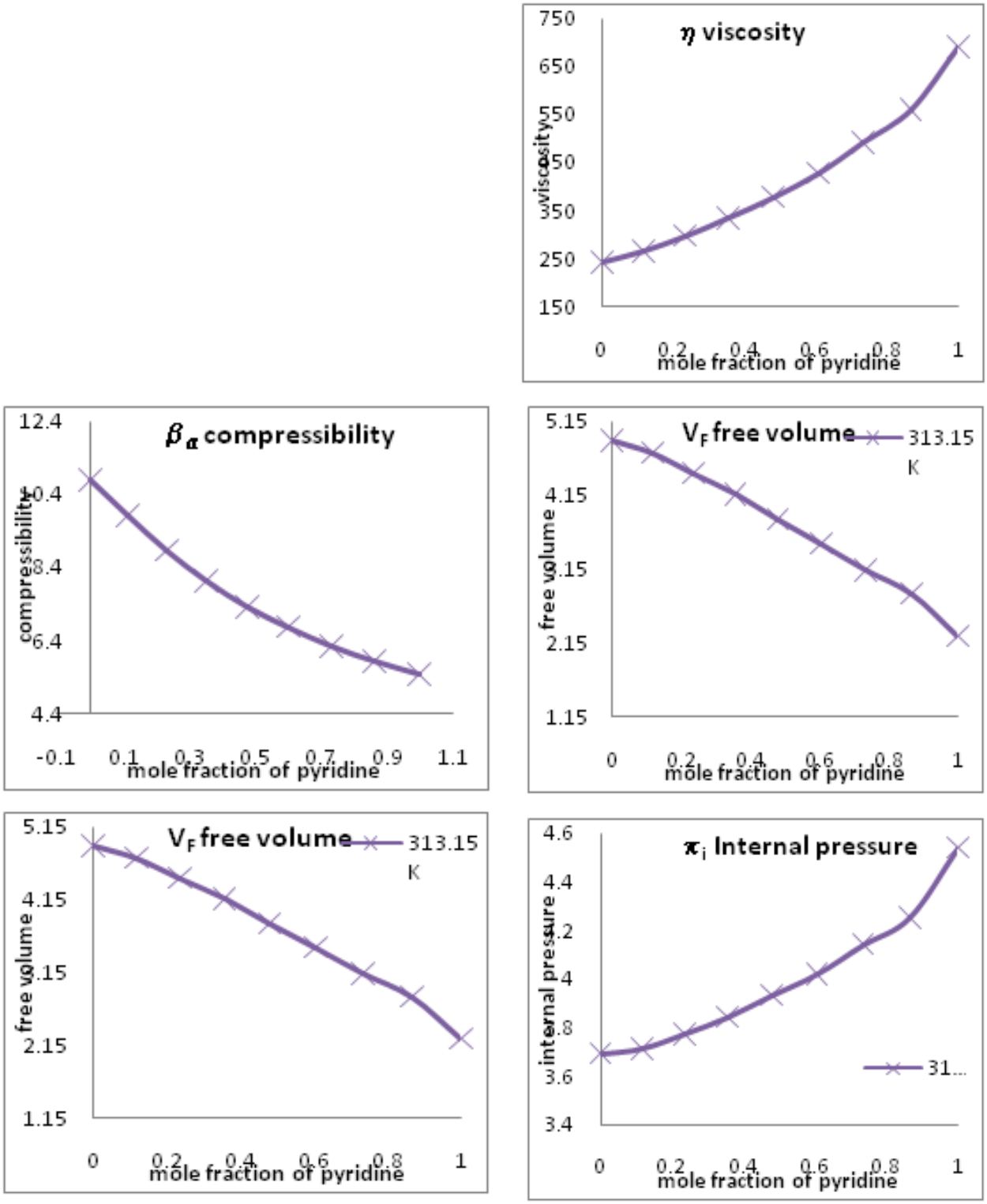

Fig. 1. Plots of ultrasonic velocity, viscosity, (βα) (L_f), (Z), (V_f) and ($_\pi$i) for Acetone + Pyridine mixture at 313.15 K

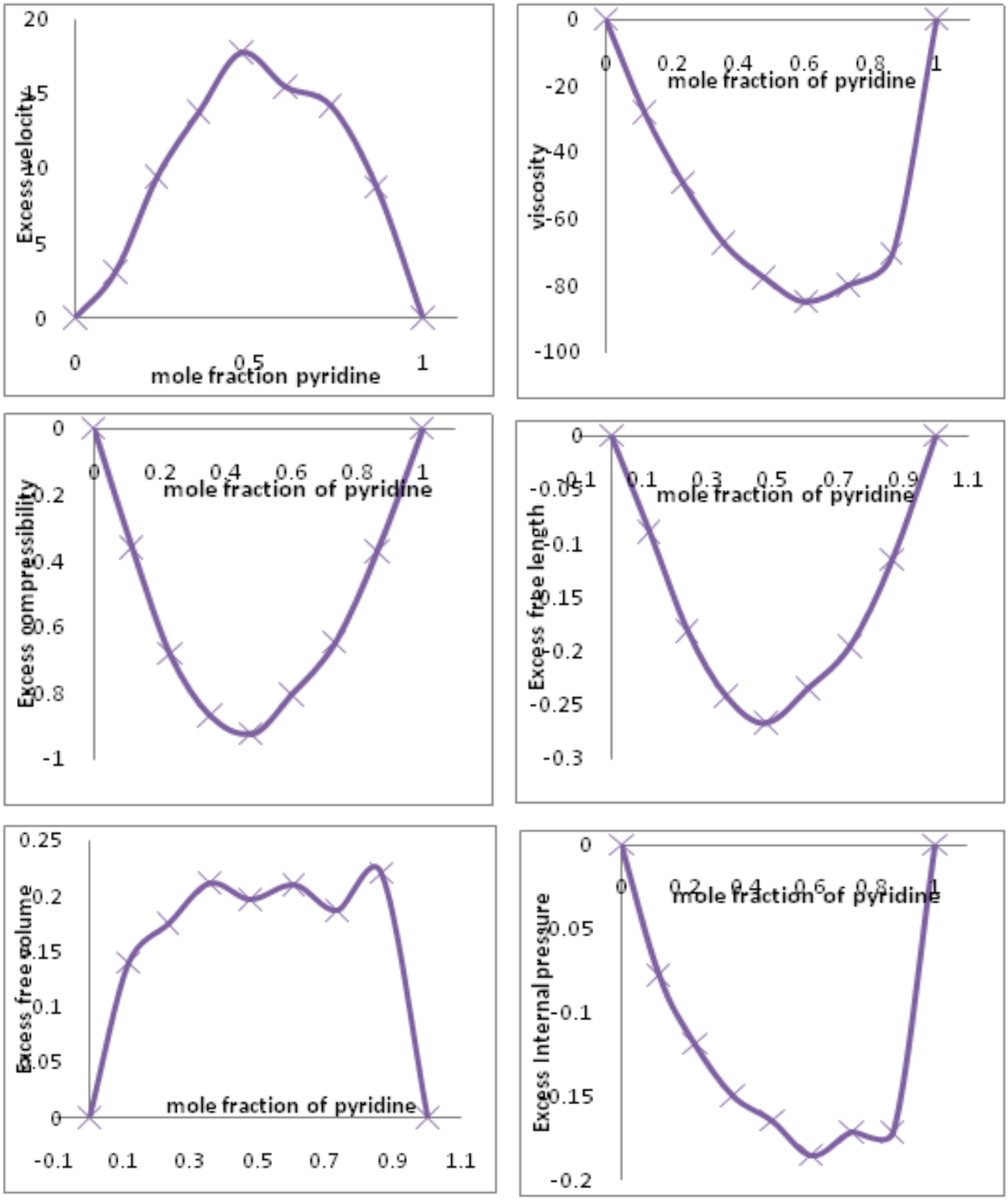

Fig. 2. Excess values of (υ^E), (η^E), (β_α^E), (L_f^E), (Z^E), (V_f^E) and (π_i^E) for Acetone + Pyridine at 313.15 K

flat showing the existence of interaction between the different components of the mixture for all the concentrations of the pyridine in the mixture.

The sign of excess free length plays a vital role in assessing compactness due to molecular interaction through dipole-dipole interaction [20, 21] leading to more compact structure making which enhances excess free length to have negative values. Graphs of excess adiabatic compressibility ($\beta_\alpha E$) and excess free length (L_f^E) are negative which indicates the strong molecular interaction between the components of the mixture. The deviation of excess impedance (Z^E) is found to be positive. The excess ultrasonic velocity (υ^E) for the binary mixture is positive. The positive deviation and non-linear dependence suggests the presence of strong interaction between the components of mixture [22, 23].

4. CONCLUSION

From the present study it can be concluded that the results are very basic in nature and indicates that the non linear variation of the all the parameters measured at 313.15 K for the mixture of Pyridine in the Acetone indicates existence of interaction between the different molecules of the compounds in the mixture. The non-linearity of the curve is common for all compositions. The negative values of excess compressibility (β_α^E), excess viscosity (η_E), excess free length (L_f^E) & excess internal pressure (π_i^E) and the positive values of excess ultrasonic velocity (υ^E), excess acoustic impedance (Z_E) and excess free volume (V_f^E) for the different combinations of the liquids in the mixture shows the presence of strong dispersive interaction between the components of molecule in the mixture. The excess values of thermodynamic parameters are sensitive to the molecular association present in the liquid mixture. The interaction is strong from 0.2 to 0.8 of concentration of the Pyridine in the mixture.

5. REFERENCES

[1] H. EYRING and J.F. KINCAID, 1938. *J. Chem. Phys*., **6**, 220-229.
[2] K.S. PITZER, 1995. *Thermodynamics*, 3rd edition (Mc.Graw-Hill book Co, NY.
[3] A.N. KANNAPAN, S. THIRUMAM and R. PALANI, 2009. *J. Phys. Science*, **20**(**2**), 97-108
[4] V.A. TABHANE, S. GHOSH and S. AGRAWAL, 1900. *J. Pure and Appl. Ultrasonic*, **21**, p. 122.
[5] R.J. FORT and W.R. MOORE, 1966. *Trans. Farady Society*, **62**, p. 1112.
[6] V. SRINIVASULU and P.R. NAIDU, 1995. *J. Pure and Appl. Ultrasonic*, **17**, 14-28.
[7] K. SWAIN and P. PRIYADARSHANI, 2010. *Indian J.Pure and Appl. Phys*., **48**, 539-542.
[8] B. JACOBSON, 1952. Ultras Velo. of liquids and liquid mixtures, *J. Chem. Phys*., **20**, 927-928.
[9] P.K. GUPTA and F.B. STUMP, 2010. *Indian J pure and Appl. Phys*., **48**, 326-333.
[10] G. ARUL and L PALANIAPPAN, 2005. *Indian J pure and Appl. Phys*., **43**, 755-758.
[11] H. EYRING and J.F. KINCAID, 1938. *J.Chem. Phys*., **6**, p. 620.
[12] K. RAJGOPAL and S. CHENTHILNATH, 1981. *Indian J. Pure and Appl. Phys*., **19**, p. 358.
[13] T.S. BANIPAL, A.F. TOOR and V.K. RATTAN, 2000. *Indian J. Chem*., **39A**, p. 809.
[14] P.S. NAIDU and K. RAVINDRA PRASAD, 2002. *Indian J.Pure and Appl. Phys*., **40**, p. 264.
[15] G. ARUL and L. PALANIAPPAN, 2001. *Indian J pure and Appl. Phys*., **39**, p. 561.
[16] A.N. KANNAPPAN and V. RAJENDRAN, 1999. *Indian J.Pure and Appl. Phys*., **73B**, p. 531.
[17] A. SADASIVA RAO and B VIJAYKUMAR NAIDU, 2000. *J Acoust Soc India*, **28**, p. 303.
[18] O. REDLICH and A.T. KISTER, 1948. *Ind. Eng. Chem*., **40**, p. 345.
[19] A. ALI and A.K. NAIN, 1999. Int. Conf. Exhi. on Ultrsonics (ICEU-99), New Delhi.
[20] D. ANBANANTHAN, 1979. *J. Acost. Soc. of India*, **7**, p. 123.
[21] NISHA SHARMA and B.P. SINGH, 2010. *Acta Ciencia India*, **XXXIV P**(**3**), p. 375.
[22] M.K. PRAHARAJ *ET AL*., 2012. *J. Chemical and Pharma. Research*, **4**(**4**), 1910-1920.
[23] A.N. KANNAPPAN and V. RAJENDRAN, 1991. *Indian J. Pure and Appl. Phys*., **29**, 465-468.
[24] P.B. DABRASE, R.A. PATIL and B.M. SURYAVANSHI, 2012. *Applied Ultras*, Shree Publi., New Delhi, 233-241.

Acoustical Society of India
(Regn. No. 65-1971)

Executive Council (2010 - 2014)

President	:	**Dr V Rajendran** [KSRCT, Tiruchengode; veerajendran@gmail.com; +91-99 94 13 03 03]
Vice President	:	**NS Naidu** [NSTL, Vizag; nsnaidu04@yahoo.com; +91-94 90 75 05 82]
General Secretary	:	**PVS Ganesh Kumar** [NSTL, Vizag; gkpakki@rediffmail.com; +91-98 66 40 08 94]
Jt. Secretary	:	**Dr K Trinadh** [NSTL, Vizag; hello_trinath@yahoo.co.in; +91-97 04 71 95 00]
Treasurer	:	**Prof AV Sharma** [AU, Vizag; sarmavakella@yahoo.co.in; +91-94 90 43 17 26]
Chief Editor	:	**Dr Mahavir Singh** [CSIR-NPL, New Delhi; mahavir@nplindia.org; +91-98 71 69 33 46]
Council Members	:	**Dr SV Ranga Nayakulu** [VITAE, Hyderabad; nayakulu@rediffmail.com; +91-98 66 53 26 13]
		Dr I Johnson [SJ College, Trichy; jnaadarsh@hotmail.com; +91-94 42 90 48 20]
		Dr Rajiv K Upadhayay [Govt PG College, Rishikesh; rku8@rediffmail.com; +91-94 12 97 28 90]
		Dr S Shekhar [Oxford College, Trichy; acousticssekar@yahoo.co.in; +91-99 94 92 00 30]
		Dr V Bhujanga Rao [Past President; NSTL, Vizag; vepcrew1@rediffmail.com; +91-98 66 44 10 74]
Co-opted Members	:	**Rajshekhar Uchil** [Josts, Bangalore; ruchil@josts.in; +91-98 80 17 08 95]
		Dr NK Narayanan [CIT, Kozhikode; csirc@rediffmail.com; +91-94 46 95 58 30]

INFORMATION FOR AUTHORS

ARTICLES

The Journal of Acoustical Society of India (JASI) is a refereed publication published quarterly by the Acoustical Society of India (ASI). JASI includes refereed articles, technical notes, letters-to-the-editor, book review and announcements of general interest to readers.

Articles may be theoretical or experimental in nature. But those which combine theoretical and experimental approaches to solve acoustics problems are particularly welcome. Technical notes, letters-to-the-editor and announcements may also be submitted. Articles must not have been published previously in other engineering or scientific journals. Articles in the following are particularly encouraged: applied acoustics, acoustical materials, active noise & vibration control, bioacoustics, communication acoustics including speech, computational acoustics, electro-acoustics and audio engineering, environmental acoustics, musical acoustics, non-linear acoustics, noise, physical acoustics, physiological and psychological acoustics, quieter technologies, room and building acoustics, structural acoustics and vibration, ultrasonics, underwater acoustics.

Authors whose articles are accepted for publication must transfer copyright of their articles to the ASI. This transfer involves publication only and does not in any way alter the author's traditional right regarding his/her articles.

PREPARATION OF MANUSCRIPTS

All manuscripts are refereed by at least two referees and are reviewed by the Publication Committee (all editors) before acceptance. Manuscripts of articles and technical notes should be submitted for review electronically to the Chief Editor by e-mail or by express mail on a disc. JASI maintains a high standard in the reviewing process and only accept papers of high quality. On acceptance, revised articles of all authors should be submitted to the Chief Editor by e-mail or by express mail.

Text of the manuscript should be double-spaced on A4 size paper, subdivided by main headings-typed in upper and lower case flush centre, with one line of space above and below and sub-headings within a section-typed in upper and lower case understood, flush left, followed by a period. Sub-sub headings should be italic. Articles should be written so that readers in different fields of acoustics can understand them easily. Manuscripts are only published if not normally exceeding twenty double-spaced text pages. If figures and illustrations are included then normally they should be restricted to no more than twelve-fifteen.

The first page of manuscripts should include on separate lines, the title of article, the names, of authors, affiliations and mailing addresses of authors in upper and lowers case. Do not include the author's title, position or degrees. Give an adequate post office address including pin or other postal code and the name of the city. An abstract of not more than 200 words should be included with each article. References should be numbered consecutively throughout the article with the number appearing as a superscript at the end of the sentence unless such placement causes ambiguity. The references should be grouped together, double spaced at the end of the article on a separate page. Footnotes are discouraged. Abbreviations and special terms must be defined if used.

EQUATIONS

Mathematical expressions should be typewritten as completely as possible. Equation should be numbered consecutively throughout the body of the article at the right hand margin in parentheses. Use letters and numbers for any equations in an appendix: Appendix A: (A1, (A2), etc. Equation numbers in the running text should be enclosed in parentheses, i.e., Eq. (1), Eqs. (1a) and (2a). Figures should be referred to as Fig. 1, Fig. 2, etc. Reference to table is in full: Table 1, Table 2, etc. Metric units should be used: the preferred from of metric unit is the System International (SI).

REFERENCES

The order and style of information differs slightly between periodical and book references and between published and unpublished references, depending on the available publication entries. A few examples are shown below.

Periodicals:

[1] S.R. Pride and M.W. Haartsen, 1996. Electroseismic wave properties, *J. Acoust. Soc. Am.*, **100** (3), 1301-1315.

[2] S.-H. Kim and I. Lee, 1996. Aeroelastic analysis of a flexible airfoil with free play non-linearity, *J. Sound Vib.*, **193** (4), 823-846.

Books:

[1] E.S. Skudzryk, 1968. *Simple and Comlex Vibratory Systems*, the Pennsylvania State University Press, London.

[2] E.H. Dowell, 1975. *Aeroelasticity of plates and shells*, Nordhoff, Leyden.

Others:

[1] J.N. Yang and A. Akbarpour, 1987. Technical Report NCEER-87-0007, Instantaneous Optimal Control Law For Tall Buildings Under Seismic Excitations.

SUMISSIONS

All materials from authors should be submitted in electronic form to the JASI Chief Editor: Dr Mahavir Singh, Acoustics, Ultrasonics & Vibration Section, CSIR-National Physical Laboratory, Dr. K. S. Krishnan Road, New Delhi-110 012 (email: mahavir@nplindia.org Tel: +91-11-4560.8317, Fax: +91-11-4560.9310). For the item to be published in a given issue of a journal, the manuscript must reach the Chief Editor at least twelve week before the publication date.

SUMISSION OF ACCEPTED MANUSCRIPT

On acceptance, revised articles should be submitted in electronic form to the JASI Chief Editor (mahavir@nplindia.org).

ISSN 0973-3302

JOURNAL OF ACOUSTICAL SOCIETY OF INDIA

Volume 40 Number 1 January 2013

A Quarterly Publication of the JASI
http://www.acousticsindia.org

JASI

Journal of Acoustical Society of India

The Refereed Journal of the Acoustical Society of India (JASI)

The Journal of Acoustical Society of India is a refereed journal of the Acoustical Society of India **(ASI)**. The **ASI** is a non-profit national society founded in 31st July, 1971. The primary objective of the society is to advance the science of acoustics by creating an organization that is responsive to the needs of scientists and engineers concerned with acoustics problems all around the world.

Manuscripts of articles, technical notes and letter to the editor should be submitted to the Chief Editor. Copies of articles on specific topics listed above should also be submitted to the respective Associate Scientific Editor. Manuscripts are refereed by at least two referees and are reviewed by Publication Committee (all editors) before acceptance. On acceptance, revised articles with the text and figures scanned as separate files on a diskette should be submitted to the Editor by express mail. Manuscripts of articles must be prepared in strict accordance with the author instructions.

All information concerning subscription, new books, journals, conferences, etc. should be submitted to Chief Editor:

Acoustics, Ultrasonics & Vibration Section, CSIR-National Physical Laboratory, Dr. KS Krishnan Road, New Delhi 110 012, Tel: +91.11.4560.8317, Fax: +91.11.4560.9310, e-mail: mahavir@nplindia.org

Annual subscription price including mail postage is Rs. 2000/= for institutions, companies and libraries and Rs. 2000/= for individuals who are not **ASI** members. The Journal of Acoustical Society of India will be sent to **ASI** members free of any extra charge. Requests for specimen copies and claims for missing issues as well as address changes should be sent to the Editorial Office:

Acoustics, Ultrasonics & Vibration Section, CSIR-National Physical Laboratory, Dr. KS Krishnan Road, New Delhi 110 012, Tel: +91.11.4560.8317, Fax: +91.11.4560.9310, e-mail: mahavir@nplindia.org

ISSN 0973-330

Printed at Alpha Printers, BG-2/38C, Paschim Vihar, New Delhi-110063 Tel.: 9811848335. JASI is sent to ASI members free of charge.

JASI

Journal of Acoustical Society of India (JASI)

A quarterly publication of the Acoustical Society of India

Volume 40, Number 3, July 2013

EDITORIAL

ARTICLES

INFORMATION

Physical Properties of Sound

The material gives a brief introduction to some of the terms used in building acoustics and the test methods used to characterize systems and materials. A very basic understanding of some fundamentals of acoustics and terms used in building acoustics, is all that is necessary to understand the material in this and the following chapters. To emphasize the simplicity of the approach, equations are kept to a minimum.

Sound is generated by creating a disturbance of the air, which sets up a series of pressure waves fluctuating above and below the air's normal atmospheric pressure, much as a stone that falls in water generates expanding ripples on the surface. Unlike the water waves, however, these pressure waves propagate in all directions from the source of the sound. Our ears sense these pressure fluctuations, convert them to electrical impulses, and send them to our brain, where they are interpreted as sound.

There are many sources of sound in buildings: voices, human activities, external noises such as traffic, entertainment devices and machinery. They all generate small rapid variations in pressure about the static atmospheric pressure; these propagate through the air as sound waves.

As well as travelling in air, sound can travel as vibrational waves in solids or liquids. The terms airborne and structure-borne sound are used depending on which medium the sound is travelling in at the time. For example, the noise from a radio set may begin as airborne sound, enter the structure of the building and travel for some distance as structure-borne sound, and then be radiated again as airborne sound in another place.

Air pressure is usually measured in units of Pascals (Pa). Atmospheric pressure is about 100 kPa. Sound pressure is a measure of the fluctuation of the air pressure above and below normal atmospheric pressure as the sound waves propagate past a listener.

The pressure variations in an individual sound wave are much less than the static atmospheric pressure, but the range of sound pressures encountered in acoustics is very large. The threshold of hearing is assumed to correspond to pressure fluctuations of 20 Micro Pascals; some individuals will have more acute hearing than this, some less. The threshold of pain in the ear corresponds to pressure fluctuations of about 200 Pa. This second value is ten million times the first. These unwieldy numbers are converted to more convenient ones using a logarithmic scale, the decibel scale. Sound pressure levels are expressed as a number followed by the symbol dB. Sound level meters convert electrical signals from a microphone to sound pressure levels in dB.

Decibels are more easily related to the response of the human ear, which also responds logarithmically to sound. The response of our ears, that is, our perception of loudness, does not increase linearly with a linear increase in sound pressure. For example, a 10 dB increase in sound pressure level would be perceived as a doubling of the loudness. In practical situations, level changes of about 3 dB are just noticeable.

It is very important to remember that decibels and similar acoustical quantities have properties different from more conventional units. Sound pressure levels, for example, cannot be added together as can kilograms. The combination of two noises with average levels of 60 dB does not give a sound pressure level of 120 dB, but 63 dB.

Mahavir Singh

Journal of Acoustical Society of India : Vol. 40, No. 3, 2013 (pp. 147-155)

Analysis of Breakout Noise from the Coupled Acoustic-structural HVAC Systems

B. Venkatesham
Department of Mechanical Engineering
Indian Institute of Technology Hyderabad-502 025 (Andhra Pradesh)
e-mail: venkatesham@iith.ac.in

[Received: 22.12.2012; Revised: 10.05.2013; Accepted: 15.05.2013]

ABSTRACT

Noise control in the heating, ventilation and air-conditioning (HVAC) systems is one of the critical design parameters in measuring the occupant comfort. The noise generated by air-handling units propagates through the ducts in the axial as well as transverse direction. Noise radiated in the transverse direction from the duct walls excited by the internal sound field is called the breakout noise. An analytical formulation has been discussed in order to predict the breakout noise from a cavity with one or four compliant walls (plenum) and a duct with all four compliant walls by incorporating three-dimensional effects along with the acoustical and structural wave coupling phenomena.

The first step in the breakout noise prediction is to calculate the interior acoustic response and flexural vibration displacement of the compliant walls. Dynamic interaction between the internal acoustic subsystem and flexible structural subsystem has been expressed in terms of the modal characteristics of the uncoupled response of the acoustic and structural sub-systems. Solutions of the inhomogeneous wave equation are rearranged in terms of impedance and mobility, and the equations describing the complete system are expressed in terms of matrices, which result in a compact matrix formulation.

The second step is to calculate the sound power radiated from complaint wall. The wall vibration velocity is a linear combination of the uncoupled flexural modes of the structural subsystem. It is substituted into the Rayleigh integral and Kirchhoff-Helmholtz (KH) integral formulation to predict the sound pressure radiated by the vibrating compliant wall. Sound power radiation from flexible walls of the plenum and duct walls has been calculated using an equivalent plate model. Analytical results are corroborated with numerical models.

1. INTRODUCTION

The air handling systems find application in the HVAC systems, aircraft industry, the appliances, gas turbine power generation, etc. A basic HVAC duct setup is depicted in Figure 1 with arrows indicating flow path and noise propagation. It consists of equipment like motor, fan or blower, and also components like plenum and duct system, to provide cool and conditioned air. Incidentally, they produce unwanted noise. Generally, sources for the unwanted noise in the air handling systems are: i) airflow velocity, ii) turbulence due to narrow and complex shaped ducts, iii) fan noise and motor noise, and iv) the motor and fan noise transmission through ducts.

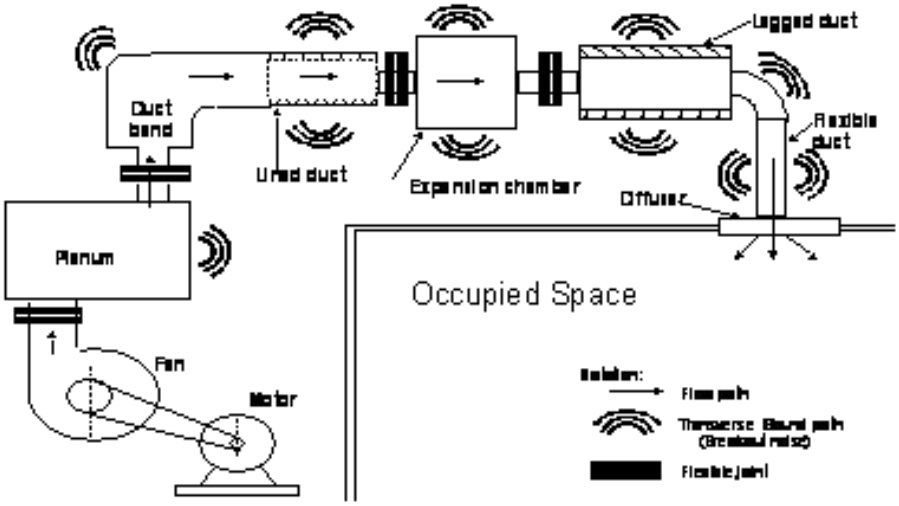

Fig. 1. Schematic of a simple HVAC setup

The HVAC systems consist of large air-handling units with thin flexible ducts, and plenums of different geometrical shapes and sizes connected in parallel and in series. The noise generated by air-handling units propagates through the ducts in the axial as well as transverse direction. Noise radiation in the transverse direction due to flexural vibration of the duct walls excited by the internal sound field is called the breakout noise. Generally, air-handling units generate most of the sound at low frequencies where the coupling phenomena are strong. The acoustic-structural coupling at low frequencies plays a critical role in understanding the breakout noise phenomena.So, any worthwhile analytical solution should be very accurate in the low frequency region [1].

Another source of thin rectangular duct wall excitation other than acoustic field is flow turbulence. The flow turbulence excitation is most likely to happen in the high-velocity ductwork and would dominate in the very low frequency range. The formulation proposed here will not consider this phenomenon, being below the frequency range of interest. Also, the flow speed is of magnitude less than 10 m/s.

The acoustic-structural coupling is the branch that investigates the interaction between the acoustic and the structural sub-systems. Dynamic interaction between acoustic space and flexible structure is an important problem in the field of acoustics for different practical applications like the HVAC duct breakout noise reduction, thin wall enclosures, aircraft skin panel vibration analysis, active noise control of panels, sound transmission measurement in building acoustics, etc. HVAC systems noise performance is characterized by the air-structural coupling. The response of the air-structural coupled system would not be essentially different from that of the uncoupled subsystems. The energy involved in the coupled interaction is much smaller than the energies in the subsystems. Mathematically, the coupled response can be expressed in terms of uncoupled responses of the constituent subsystems. Cummings [2]provided an excellent research overview of sound transmission through duct walls and discussed the basic phenomena of vibro-acoustic coupling and possible methods to solve this problem by using the common axial wave number approach and the finite element methods (FEM).A literature survey of the structural-acoustic coupling shows that a large amount of work has been done in calculating the free and forced response of different systems. Dowell [3] developed a comprehensive theoretical model for coupled responses in a structural-acoustic coupled system. Kim and Brennan [4]re-examined the formulation used by Dowell [3] and expressed the same in the impedance and mobility terms.

2. THEORETICAL FORMULATION

A cavity with one or four compliant walls (plenum) and a duct with all four compliant walls are considered to

study breakout noise phenomena. General formulation has been discussed briefly in this article and further details are provided in references [1,5-7].

2.1 Calculation of the Inside Pressure and Compliant Wall Vibration

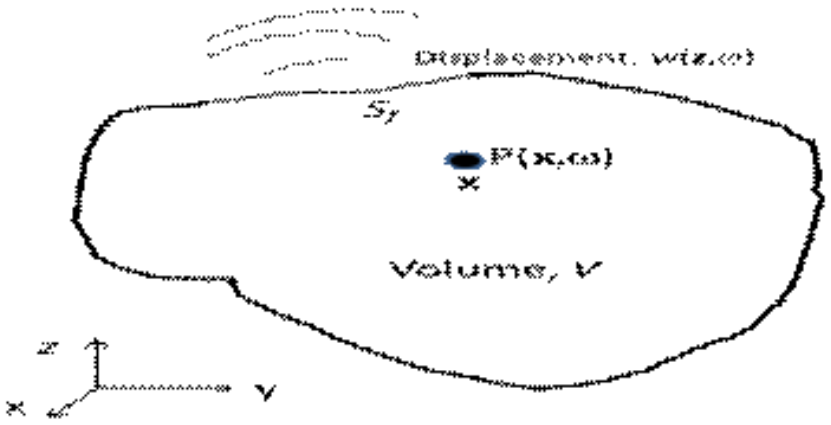

Fig. 2. Schematic diagram of acoustic-structure coupled system

Figure 2 shows the schematic diagram of a flexible structural system coupled with acoustical system. General equations of the inside system pressure *p* at location *x* and the compliant wall vibration velocity w at location z on the flexible wall for the uncoupled acoustic modes (N) and structural modes (M) are

$$p(\mathbf{x},\omega)=\sum_{n=1}^{N}\psi_n(\mathbf{x})\ a_n(\omega)=\boldsymbol{\psi}^T\mathbf{a} \tag{1}$$

$$w(\mathbf{z},\omega)=\sum_{m=1}^{M}\phi_m(\mathbf{z})\ b_m(\omega)=\boldsymbol{\varphi}^{\mathbf{T}}\mathbf{b} \tag{2}$$

where $\psi_n(\mathbf{x})$ is the uncoupled acoustic mode shape function, $a_n(\omega)$ is the complex amplitude of the nth acoustic pressure mode, $\phi_m(z)$ is the uncoupled vibration mode shape function, and $b_m(\omega)$ is the complex amplitude of the m^{th} vibration velocity mode [4].

Complex amplitude of the nth acoustic mode under structural and acoustic excitation is given by

$$a_n(\omega)=\frac{\rho_0 c_0^2}{V}A_n(\omega)\left(\int_V\psi_n(\mathbf{x})q_{vol}(\mathbf{x},\omega)dV+\int_{S_f}\psi_n(\mathbf{y})w(\mathbf{y},\omega)dS\right) \tag{3}$$

Similarly, the complex vibration velocity amplitude of the m^{th} mode can be expressed as

$$b_m(\omega)=\frac{1}{\rho_s h S_f}B_m(\omega)\left(\int_{S_f}\phi_m(\mathbf{z})f(\mathbf{z},\omega)dS-\int_{S_f}\phi_m(\mathbf{z})p(\mathbf{z},\omega)dS\right) \tag{4}$$

where, ρ_0 and c denote the density and speed of sound in air, respectively. Function $q_{vol}(x, \omega)$ denotes the acoustic source strength density function (volume velocity for unit volume) in the system volume *V* and $w(z, \omega)$ denotes normal velocity of the surrounding flexible structure of surface area S_f. The firstintegral within

brackets of eq. (3) represents the generalized acoustic source strength. Substitution of eq. (2) in second integral termof eq. (3) gives the coupling acoustic-structural mode shape coefficient $C_{n,m'}$. It provides a relationship between the mode matching of acoustic and structural uncoupled modes. ρ_s and h denote density of the plate material and thickness of the plate, respectively. $f(z, \omega)$ denotes the force distribution on the surface of the plate. $p(z, \omega)$ denotes the cavity acoustic pressure distribution on the surface of the plate. The first integral term in eq.(4) represents the generalized modal force, and substituting eq. (1) in the second integral term of eq. (4) $p(z, \omega)$ for gives the acoustic-structural coupling matrix coefficient.

Equations (3) and (4) can be expressed in the matrix form as:

$$a = Z_a(q+q_s),\ b = Y_s(g-g_a)\ \ g_a = C^T a \tag{5-7}$$

where, a isthe modal acoustic pressure vector, $Z_a = A\rho_0 c_0^2/V$ is an (N x N) diagonal matrix defined as the uncoupled acoustic modal impedance matrix: $q_s = Cb;q$ is the N-length modal source strength vector, and q is the modal source vector due to vibration of the structure. Matrix A is an (N x N) diagonal matrix. It contains acoustic mode resonance [3-4]. C is an (N x M) matrix defined as the coupling coefficient between the n^{th} acoustic mode and the m^{th} structural mode.

Combining eqs. (5) and (6) yields the acoustic and structural modal amplitude vectors a andb in terms of the modal excitation vectors q and g:

$$\mathbf{a} = \left(\mathbf{I} + \mathbf{Z_a C Y_s C^T}\right)^{-1} \mathbf{Z_a}\left(\mathbf{q} + \mathbf{C Y_s g}\right) \tag{8}$$

$$\mathbf{a} = \left(\mathbf{I} + \mathbf{Z_a C Y_s C^T}\right)^{-1} \mathbf{Z_a}\left(\mathbf{q} + \mathbf{C Y_s g}\right) \tag{9}$$

2.2 Sound Power Radiation Calculation

Sound power radiation from the flexible wall in terms of the radiation impedance and complex amplitude of the vibration velocity modes is [5-8].

$$W_{rad} = \frac{1}{2} b^H Re[Z] b \tag{10}$$

Radiation impedance, Z might be Z^{UBF} or Z^{BF}based on selected radiation model. The superscript H denotes the Hermitian of amatrix.

The radiation impedance of an unbaffled plate can be written as [6]

$$Z^{UBF} = j\omega S_t^T A^{-1} S_t \tag{11}$$

where S_t^T is transpose of the matrix, and

$$A = -\omega^2 M^A + K^A \tag{12}$$

$$S_{tm_1m_2m_1'm_2'} = \iint_{S_p} \phi_m(\vec{r})\phi_{m'}(\vec{r}')\,ds \tag{13}$$

$$M^A{}_{m1m2}{}'{}_{m2}{}' = 1/4\pi\rho_0 c_0{}^2 \int_{S_p} \int_{x} \int_{S_p} \int \phi_m(\bar{r})\, fm'(\bar{r}')e^{-jkR}/ds\, ds' \tag{14}$$

$$K^{A}_{m1m2m1'm2'} = 1/4\pi\rho_0 \int_{S_p}\int_{X}\int_{S_p} \int \{ \partial\phi_m(\bar{r})/\partial x ; \partial\phi_m(\bar{r}')/\partial x + \partial\phi_m(\bar{r}')/\partial\phi_m(r')/\partial x\} \, e^{jkR}/R \, ds \, ds' \tag{15}$$

Radiation impedance of a baffled plate can be written as [7]

$$Re\,[Z^{BF}] = \int_0^{L_2}\int_0^{L_1}\int_0^{L_2}\int_0^{L_1} \{ \phi_m(x,y)\,\phi_m(x',y')/\sin kR/R \, dx'dy'dx'dy' \tag{16}$$

2.3 Transverse Transmission Loss

Transverse Transmission Loss is defined as [5-8]

$$TL_{tp} = 10\log(W_{int}/W_{rad}) \tag{17}$$

The radiated power (W_{rad}) is calculated by using eq. (10). Incidence power (W_{int}) to the acoustic subsystem can be calculated based on wave equation.

3. FREE VIBRATION ANALYSIS

Expressions of the uncoupled acoustic modes of a cavity and duct can be found in references [4-8]. The structural uncoupled modes for a simple supported plate are available in literature. Expressions for uncoupled structural modes of a duct are obtained by representing it as unfolded plate [9].

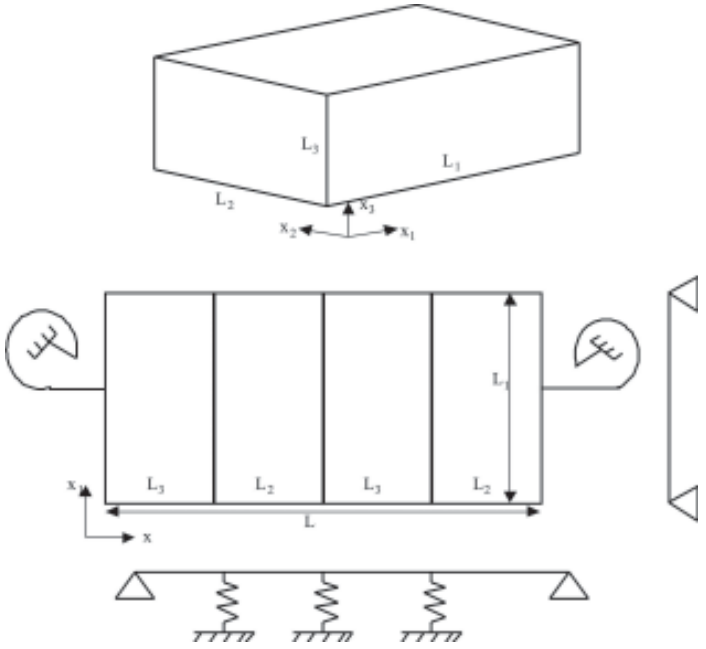

Fig. 3. Simply supported rectangular duct and its unfolded plate representation

Figure 3 shows an unfolded plate representation of the folded plate (duct) with four strips of the rectangular plate, made of the same isotropic material and of uniform thickness. The plate is considered to lie in the x-x1, plane, bounded by simple supported edges at x_1=0 and L^1. It is further assumed that thickness and flexural deflections of each plate are small compared with the wavelength of flexural vibrations, so that the thin plate theory is applicable.

4. NUMERICAL MODEL

The FEM-BEM based numerical model has been used here to validate the analytical method discussed in previous section in order to calculate the transverse transmission loss from different HVAC systems. The FEM-BEM analysis has been performed in the commercial package named SYSNOISE [10]. The procedure used inthe analysis of the coupled acoustic structural analysis by linking the 'FEM structure' and 'FEM fluid' models to simultaneously predict the inside pressure and compliant wall vibration displacement. The vibration displacement is then used as input for 'Indirect/Direct BEM' model to predict the radiated power from the flexible plate. Sound source input to the cavity is modeled by the equivalent constant velocity source in the SYSNOISE model. Weak coupling has been assumed in the calculation due to the presence of air medium inside & outside the cavity.

5. RESULTS AND DISCUSSION

Typical results based on the current approach have been discussed here. Consider a rectangular cavity and plenum of L_1= 0.3 m, L_2= 1.5 m, and L_3 = 0.4 m, and let the thickness of the flexible aluminum plate be 5 mm. Cavity with one wall flexible and four wall flexible (plenum), and duct with four wall flexible are considered to generate these results.

Free Vibration analysis of coupled system provides coupled natural frequency and decay time. The mechanical damping of the panel is represented in the modal decay times of the uncoupled panel modes. Figure 4 shows the variation of the decay time of the cavity-controlled mode with respect to panel decay time. There is an optimum condition for cavity controlled mode decay time. The physical explanation of this phenomenon is that increasing panel damping will dissipate energy until it reaches the minimum decay time of the cavity-controlled mode (1,0,0). Beyond this, the increased damping behaves like mass. It would restrict the panel motion, and effectively the acoustic energy would not transfer to the panel. Thus the modal characteristics would be similar to those of the uncoupled cavity subsystem. This physical understanding will be useful in designing the breakout noise control solutions.

Figures 5 show the effect of coupling on the inside cavity pressure. Equations (8) and(9) are modified for weak coupling by approximating $(I+Z_aCY_sC^T) \cong I$, and $(I+Y_sC^TZ_aC) \cong I$. Generally, the coupling is stronger for thin cavity walls compared to thick cavity walls.

Figure 6 shows the transverse transmission loss of a rectangular plenum with flexible walls. It is observed that analytical and computational results (FE-BE) are in good agreement. The "unbaffled equivalent unfolded

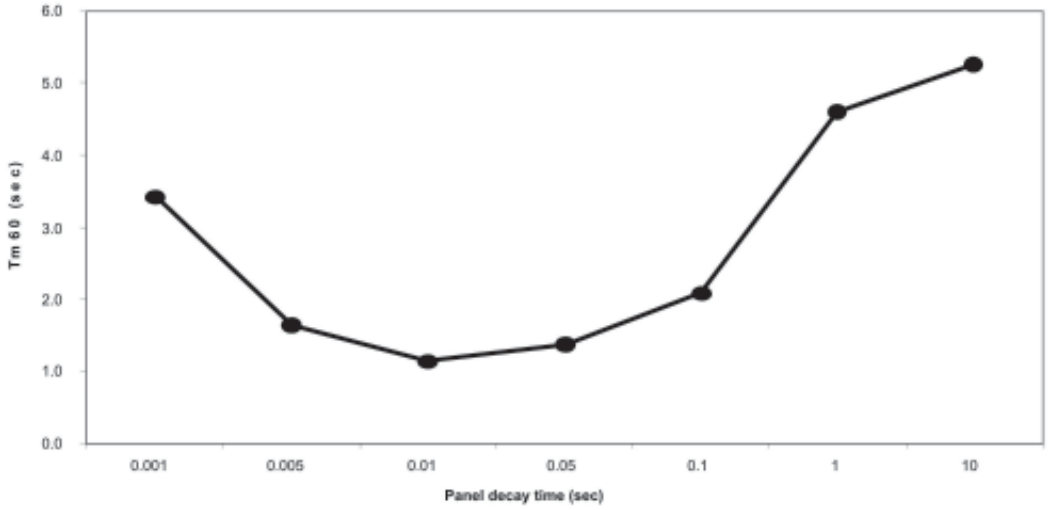

Fig. 4. Decay time of cavity controlled mode (1,0,0) as function of panel modal decay time (*h* = 5mm, cavity decay time of 5sec)

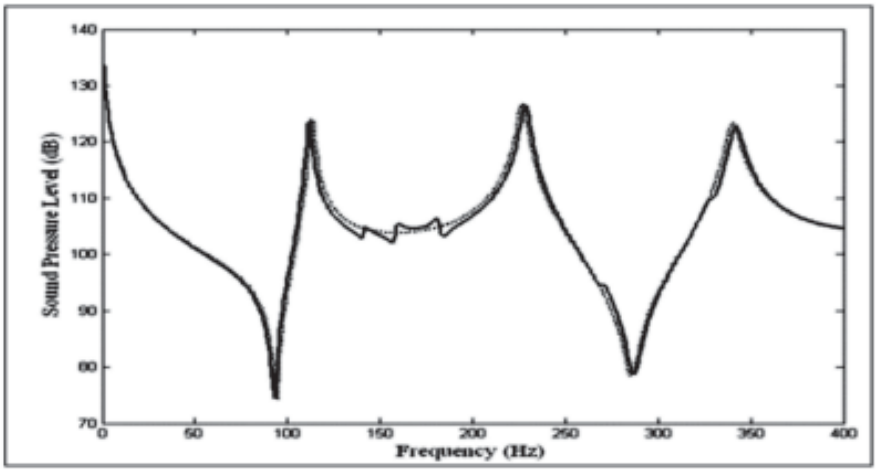

Fig. 5. Effect of coupling on the sound pressure level prediction inside a rectangular cavity of dimensions (0.3 m x 0.4 m x 1.5 m) with 5 mm aluminum flexible cavity wall, due to acoustic excitation of the structural-acoustic system. (- - -) uncoupled; (--) coupled.

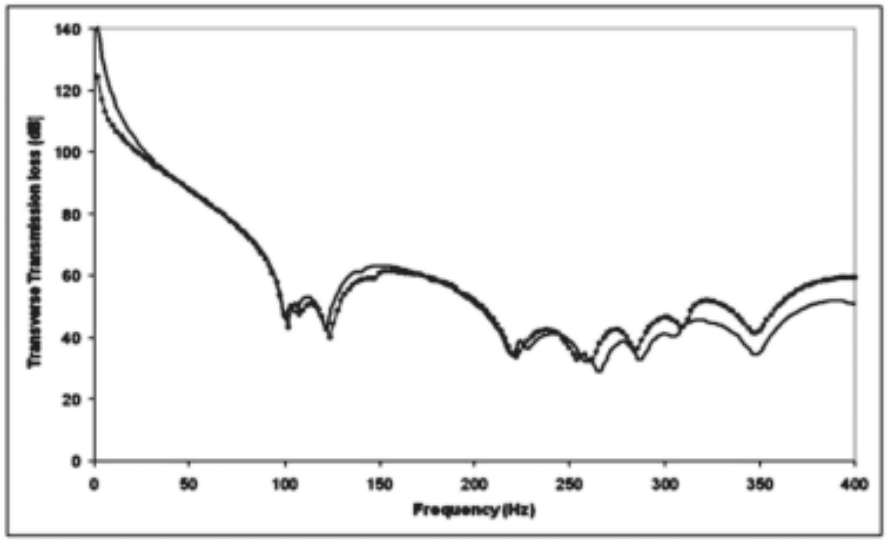

Fig. 6. Numerical corroboration of the analytical radiation model for a plenum (Sysnoise model; Analytical model).

plate" model is appropriate for analytical prediction of the breakout noise from a rectangular plenum with flexible walls. It is much faster than the numerical (FEM-BEM) model and needs little pre-computation effort.

Consider a rectangular duct of dimensions L_1= 1.5 m, L_2 = 0.3 m, and L_3 = 0.4 m, and the thickness of the flexible aluminum wall 5 mm. The acoustic and structural damping ratio loss factor = 0.01. Air properties are: sound speed = 340 m/sec and density = 1.2 kg/m^3. Three types of terminal impedances are investigated: (i) anechoic termination conditions ,(ii) rigid termination impedance condition , and (iii) open end termination.Figure 8 shows the effect of the acoustic termination of the duct on breakout noise for three types of terminations.

It may be noted that the anechoic termination condition over predicts the transverse transmission loss for the rigid and the open-end termination conditions at low to medium frequencies but this frequency range is important for the breakout noise problems. Acoustic boundary conditions will affect the inside standing wave

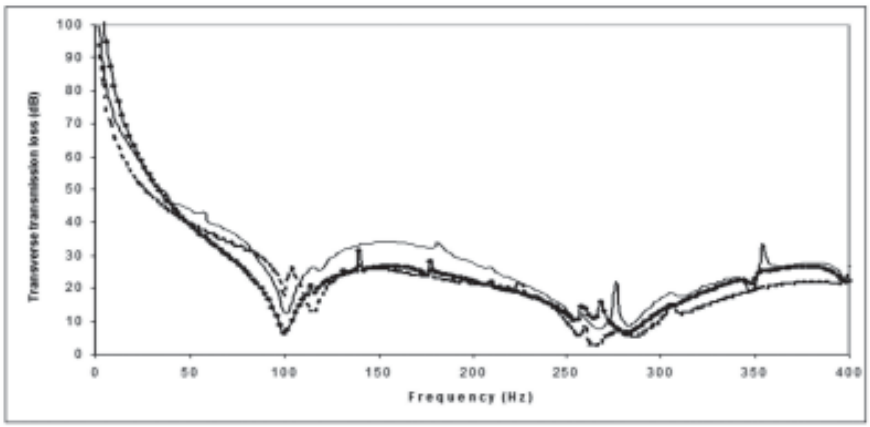

Fig. 7. Effect of the duct termination conditions on the transverse transmission loss.
(Open termination; anechoic termination; - - - - rigid termination

pressure pattern. It is important for the rigid termination condition that would create a strong standing wave pattern. It also increases the breakout noise from the HVAC ducts.

The effect of structural damping on transverse transmission loss is shown in Figure 8. The transverse transmission loss values are improved at the first transverse resonance (100 Hz) and also in the structural-acoustic coupling region at 250-280 Hz.

Acoustic-structural coupling is critical and limited to narrow frequency range. Most of the sound transmission occurs near the coupled natural frequencies, and dips in the transverse transmission loss relate to the transverse resonance frequencies and their magnitude controlled by damping. At very low frequencies, the transmission loss is controlled by stiffness of the structure.

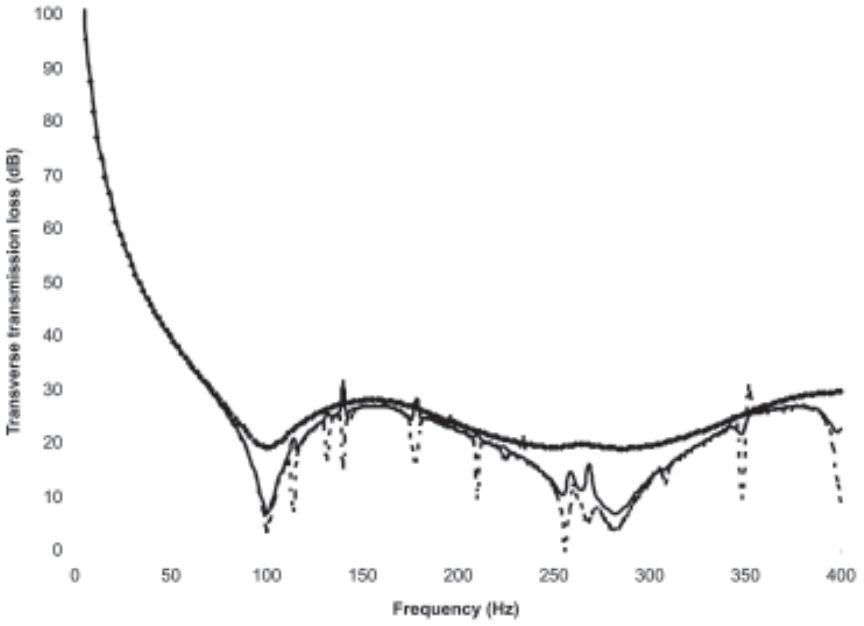

Fig. 8. Effect of damping on the transverse transmission loss in a rectangular duct with open terminal impedance.(η–0.1; η–0.01; - - - - η–0.001).

6. SUMMARY

A comprehensive theoretical model has been developed to calculate the breakout noise, based on the impedance and mobility approach. A computationally efficient method is suggested to predict the sound power models with application to a cavity with one or four compliant walls and a duct with all four compliant walls. A new intuitive way has been provided to model the folded plate as "Equivalent plate model" in free vibration analysis and sound power radiation calculation.

It is worthwhile to extend the current approach to predict breakout noise from an acoustically lined rectangular duct and plenum chamber with compliant walls. Further studies are required to develop analytical models in understanding the effect of stiffeners and damping (anti-drumming) on the duct breakout noise.

7. REFERENCES

[1] B. VENKATESHAM, 2008. Breakout Noise from the Coupled Acoustic-Structural HVAC Systems, PhD Thesis.

[2] A. CUMMINGS, 2001. Sound transmission through duct walls, *Journal of Sound and Vibration,* **239** (**4**), 731-765.

[3] E.H. DOWELL, G.F. GORMAN and D.A. SMITH, 1977. Acoustoelasticity: general theory, acoustic modes and forced response to sinusoidal excitation, including comparisons with experiment, *Journal of Sound and Vibration,* **52**, 519-542.

[4] S.M. KIM and M.J. BRENNAN, 1999. A compact matrix formulation using the impedance and mobility approach for the analysis of structural-acoustic systems, *Journal of Sound and Vibration*, **223** (**1**), 97-113.

[5] B. VENKATESHAM, MAYANK TIWARI and M. L. MUNJAL, 2008. Analytical prediction of the breakout noise from a rectangular cavity with one compliant wall, *Journal of the Acoustical Society of America*, **124**(**5**), 2952-2962.

[6] B. VENKATESHAM, MAYANK TIWARI and M.L. MUNJAl, 2010. Analytical prediction of the breakout noise from a reactive rectangular plenum with four flexible walls, *Journal of Acoustical Society of America*.

[7] B. VENKATESHAM, MAYANK TIWARI and M.L. MUNJAL, 2011. Prediction of Breakout Noise from a Rectangular Duct with Compliant Walls, *International Journal of Acoustics and Vibration*, **16** (**4**), 180-190.

[8] W.L. LI and H.J. GILBELING, 2000. Determination of the mutual radiation resistance of a rectangular plate and their impact on the radiated sound power, *Journal of Sound and Vibration*, **229**.

[9] H. P. LEE, 1993. Natural frequencies and modes of cylindrical polygonal ducts, *Journal of Sound and Vibration*, **164**(**1**), 182-187.

[10] Sysnoise Rev. 5.6, User's Manual, LMS International, 2003.

Journal of Acoustical Society of India : Vol. 40, No. 3, 2013 (pp.156-164)

Modeling and Recognition of Consonant-Vowel Units using Statistical Learning Algorithms

N.K. Narayanan* and T.M. Thasleema
Department of Information Technology
Kannur University, Kannur-670 567 (Kerala)
**e-mail: nknarayanan@gmail.com*

[Received: 16.04.2013; Revised: 29.05.2013; Accepted: 08.06.2013]

ABSTRACT

This paper investigates the use of statistical learning algorithms for the classification of Malayalam Consonant - Vowel (CV) utterances in speaker independent, noisy environments. The techniques we adopted here are k - Nearest Neighborhood (k - NN) and Support Vector Machine (SVMs) based Decision Directed Acyclic Graph Support Vector Machine (DDAGSVM) classifiers. Three different feature extraction algorithms viz., Mel Frequency Cepstral Coefficients (MFCC), Normalized Wavelet Hybrid Feature (NWHF) and State Space Point Distribution (SSPD) parameter, are extracted to evaluate the performance of the above two classifiers. From the experimental results it is found that the DDAGSVM classifier is performing well compared with k-NN in additive noisy condition.

1. INTRODUCTION

In the past few decades, significant progress has been made by researchers in the area of speech and language processing. In various traditional pattern recognition approaches, the statistical approach has been extensively studied and used in practice. More recently methods imported from statistical learning theory have been receiving increasing attention [1]. In the present work we are discussing two statistical pattern classifiers namely k - Nearest Neighborhood (k - NN) and Support Vector Machine (SVM) to classify Malayalam CV speech unit database.

The present research work is motivated by the knowledge that a little attempts were rendered for the automatic speech recognition of CV speech unit in Indian languages like Hindi, Tamil, Bengali, Marathi etc. But very less works have been found to be reported in the literature on Malayalam CV speech unit recognition, which is the principal language of South Indian state of Kerala. Very few research attempts were reported so far in the area of Malayalam vowel recognition. So more basic research works are essential in the area of Malayalam CV speech unit recognition.

Malayalam is one of the major languages from Dravidian language family. Other major languages include Kannada, Tamil, Telugu, Tulu and Konkani. Malayalam is the principal language of the South Indian state of Kerala and also of the Lakshadweep Islands off the west coast of India spoken by about 36 million people. Malayalam language now contains 51 V/CV units includes 15 long and short vowel sounds and the remaining 36 basic consonant sounds.

In the present work, all the experiments are carried out using 36 Malayalam CV speech unit database uttered by 96 different speakers. For the recognition experiments, database is divided into five different phonetic classes based on the manner of articulation of the consonants which are given in Table 1.

Phonetic Classes	Sounds
Unspirated	/ka/,/ga/,/cha/,/ja/,/ta/,/da/,/tha/,/dha/,/pa/,/ba/
Aspirated	/kha/,/gha/,/chcha/,/jha/,/tta/,/dda/,/ththa/,/dha/,/pha/,/bha/
Nasals	/nga/,/na/,/nna/,/na/,/ma/
Approximants	/ya/,/zha/,/va/,/lha/,/la/
Fricatives	/sha/,/shsha/,/sa/,/ha/,/ra/,/rha/

2. FEATURE EXTRACTION

Feature extraction is the one of the essential components of the study to develop an ASR system. In this paper three different approaches to phonemic feature extraction is discussed which are explained below.

2.1 Mel Frequency Cepstral Coefficient

The MFCC method uses the bank of filters scaled according to the mel scale to smooth the spectrum and to perform similar to that executed by the human ear. The filters with mel scale spaced linearly at low frequencies up to 1 kHz and logarithmically at higher frequencies are used to capture the phonetical characteristics of the CV speech signals. Thus MFCCs are used to represent human speech perception models. MFCCs are computed as follows.

After preemphasize the signal is divided into a sequences of frames with 256 samples in each frame that can be analyzed independently and represented by a single feature vector. In order to reduce the signal discontinuities at edges of each frame a hamming window is applied. Hamming window mathematically represented as

$$w_n = 0.54 - 0.46Cos\left(\frac{2\pi n}{N-1}\right), 0 \le n \le N-1 \quad (1)$$

Compute the Fast Fourier Transform (FFT) of each frame and obtain its magnitude. Twenty four triangular-shaped filter banks with logarithmic spacing (called Mel banks) are applied to each frame. A filter bank, in its simplest form, is a set of band pass filters with different frequencies covering the interesting part of the spectrum (the fundamental frequency and the formants). The output of the filters in each frame can be used as features. The center frequencies of the filters can be chosen in several ways. Usually they are set according to some perceptually motivated scale. It was created by modeling human auditory system and has been showed that this model empirically improves recognition accuracy. The following formula is used to compute the mels for a given frequency F in Hz.

$$F_{mel} = 2595\, log_{10}(1 + F_{Hz}/700) \quad (2)$$

For calculation of mel-frequency spectrum, a bank of filters with triangular bandpass frequency response is used. Such filters compute the spectrum around each center frequency with increasing bandwidth. The log energy at the output of each filter is computed afterwards. The Discrete Cosine Transform (DCT) is taken to give the cepstral coefficients. The first 12 coefficients, excluding the 0th coefficient are the features that are known as MFCCs . The advantage of computing MFCCs by using filter energies is that they are more robust to noise and spectral estimation errors.

2.2 Normalized Wavelet Hybrid Feature

Certain ideas of wavelet theory appeared quite a long time ago [2]. Over the last decades wavelet analysis has

turned to be a standard technique in the areas of geophysics, meteorology, audio signal processing and image compression [3][4][5]. Wavelet transform can be defined as the transformation of the signal under analysis into another representation which presents the signal in a more useful form [6].

The Discrete Wavelet Transform (DWT) has been treated as a Natural Wavelet Transform (NWT) for discrete time signals by different authors [7][8]. For computing the wavelet coefficients several discrete algorithms have been established [9]. Daubechies and some others had invented DWT peculiarly designed for analyzing finite set of observations over the set of scales using dyadic discretization [10][11]. As Daubechies mentioned in his work DWT can be interpreted as continuous wavelets with discrete scaling and translation factors. The WT is then evaluated at discrete scale and translation. More effective implementation of DWT is obtained using Multi Resolution Analysis (MRA) based subband coding technique. MRA is an effective tool for interpreting the information content of a signal. A MR representation produces a simple hierarchical model to develop the algorithms for the time-frequency analysis of the signal. At different resolution, the details of the speech signal generally characterize vocal characteristics of the speech signal. Each signal to be characterized is analyzed at a coarse resolution and then gradually increases the resolution. Thus MRA can be defined as a technique that permits us to analyze the signal in multiple frequency bands.

The main advantage of DWT over FT is the multi resolution analysis of signals with localization on both time and frequency. In the present work we utilize these characteristics of wavelet transform using two major wavelet decomposition techniques *viz.*, Classical Wavelet Decomposition (CWD) and Wavelet Packet Decomposition (WPD) for Malayalam CV speech unit recognition.

Normalized Wavelet Hybrid Feature (NWHF) vector for the present work is generated using CWD and WPD method. The process for extracting NWHF feature vector is described below.

In the first step for the CWD, the sound signal is made to undergo recursively to decompose into kth level of resolutions; therefore the approximation coefficient matrix at this level is a sufficiently small representative of the original speech signal and carries enough information content to describe s characteristics coarsely.

Let A_k represents this approximation matrix at decomposition level k, which can be written as

$$A_k = \begin{bmatrix} A_{1,1} & A_{1,2} & .... & A_{1,n} \\ A_{2,1} & A_{2,2} & .... & A_{2,n} \\ ... & ... & .... & .... \\ A_{k,1} & A_{k,2} & .... & A_{k,n} \end{bmatrix} \tag{3}$$

Then, the first component of NWHF feature vector v_1 is,

$$v_1 = \bigcup_{i=1}^{k} \bigcup_{j=1}^{n} \{A_{i,j}\} \tag{4}$$

In the second step, for Wavelet Packet Decomposition, decompose each speech segment using kth level of resolutions for the best level of wavelet packet decomposition tree. The first coefficient matrix at the best level tree contains enough information to represent the given input consonant CV speech unit without loss of much speech features. Let m represent mean of one row vector in the coefficient matrix then the WPD feature vector v_2 is given by

v_2, $m_i = 1,2,.....m$ (number of rows in the best level coefficient matrix). (5)

In the third step we combined v_1 and v_2 to fusion CWD and WPD coefficients.

$$V = \bigcup_{i=1}^{2} \{v_i\} \tag{6}$$

Then the final feature vector F after z-score normalization is given as

$$F = \frac{V - \mu(V)}{\sigma(V)} \tag{7}$$

Thus an NWHF vector is extracted using the proposed algorithm.

The feature vector of size 20 is estimated by concatenating CWD and WPD features for hybrid feature vectors. The NWHF vector for different speaker shows the identity of the same sound so that an efficient feature vector can be formed using NWHF vectors. The NWHF obtained for different sounds seems to be distinguishable, giving discriminate feature vector for speech unit recognition.

2.3 State Space Point Distribution Parameter

In dynamical system approach, by embedding a signal into adequately high dimensional space, a topologically equivalent to the original state space structure of the system generating the signal is formed [12, 13]. This embedding is known as Reconstructed State Space (RSS), is typically constructed by mapping time-lagged copies of the original signal onto axes of the new high dimensional space. The time evolution within the RSS traces out a trajectory pattern referred to as its attractor which is a representation of the dynamics of the underlying system [14]. Since the attractor of an RSS captures all the relevant information about the underlying system, it is an efficient choice for signal analysis, processing and classifications. The RSS approach proposed here has the advantage of extracting both linear and non-linear aspects of the entire system.

Takens' theorem states that under certain assumptions, state space of a dynamical system can be constructed through the use of time delayed versions of the original scalar measurements [15]. Thus a RSS can be considered as a powerful tool for signal processing domain in non-linear or even chaotic dynamical systems [16, 17]. According to Takens embedding theorem, a RSS for a dynamical system can be produced for a measured state variable S_n, n=1,2,3,…..N via method of delays by creating vectors given by

$$S_n = [S_n \;\; S_n+\tau \; S_n+2\tau \; \ldots\ldots\ldots \; S_n+(d\text{-}1)\tau] \tag{8}$$

where d is the embedding dimension and τ is the time delay value. The row vector S_n defines the position of a single point in the RSS. To completely define the dynamics of the system and to create a d dimensional RSS, corresponding trajectory matrix is given as

$$\text{Sd} = \begin{bmatrix} s_1 & s_{1+\tau} & \cdots & s_{1+(d-1)\tau} \\ s_2 & s_{2+\tau} & \cdots & s_{2+(d-1)\tau} \\ \cdots & \cdots & \cdots & \cdots \\ s_N & s_{N+\tau} & \cdots & s_{N+(d-1)\tau} \end{bmatrix} \tag{9}$$

A speech signal with amplitude values can be treated as a dynamical system with one dimensional time series data. Based on the above theory, this study investigates a method to model a RSS for speech signal through the use of time delayed versions of original scalar measurements. Thus a trajectory matrix S_2 with embedding dimension d=2 and τ=1 can be constructed by considering the speech amplitude values S_n as one dimensional time series data. Thus S_2 is given as

$$S_2 = [S_1 \;\; S_2 ; \;\; S_2 \;\; S_3 ; \ldots \;\; \ldots ; S_{N-1} \;\; S_N] \tag{10}$$

The State Space Map (SSM) for the Malayalam consonant CV unit is constructed as follows. The normalized N samples values for each CV unit is the scalar time series S_n where n =1,2,3……N. For every consonant speech signal a trajectory matrix is formed with embedding dimension d =2 and time delay τ =1. Now the scatter plot SSM is generated by plotting the row values of the above constructed trajectory matrix by plotting S_n versus S_n+1. Figure 1 shows the SSM for the first consonant sound /ka/.

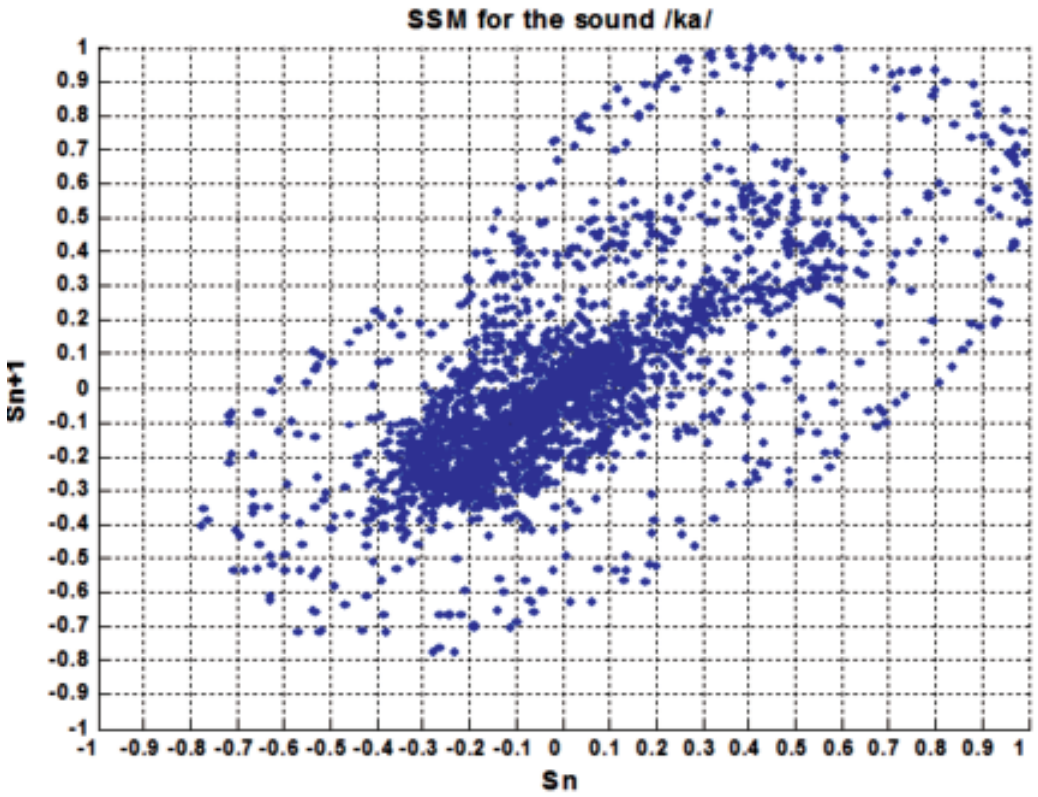

Fig. 1. Scatter plot for the sound /ka/ with d =2

In Automatic Speech Recognition (ASR), selection of distinctive features is certainly the most important factor for the high recognition performance. Present study uses non linear feature extraction technique called State Space Point Distribution (SSPD) from their SSM. For this purpose the SSM of the speech unit is divided into grids with 20 x 20 boxes. The box defined by co-ordinates (-1,0.9), (-0.9,1) is taken as box 1 and box just right side to it as taken as box 2 and so on in the x-direction with the last box being (0.9,0.9), (1,1) is taken as box 20. The process is repeated for all the rows and boxes are numbered consecutively for the 400 boxes. The SSPD for each pattern is calculated by estimating the number of points distributed in each of these 400 boxes. This can be mathematically represented as follows.

The reconstructed SSPD parameter for location 'i' in two dimensions can be defined as

$$(SSPD)i = \sum_{n-1}^{N} f([S_n, S_{n+1}]i) \tag{11}$$

where $f([S_n, S_{n+1}],i) = 1,$ if state space point defined by the row vector $[S_n, S_n+1]$ is in the location 'i'

$0,$ otherwise

Using this information the SSPD plot is plotted by taking the box number along x-axis and the number of points in each box along y-axis. The SSPD plot for the first Malayalam CV sound /ka/ is given in Fig. 2.

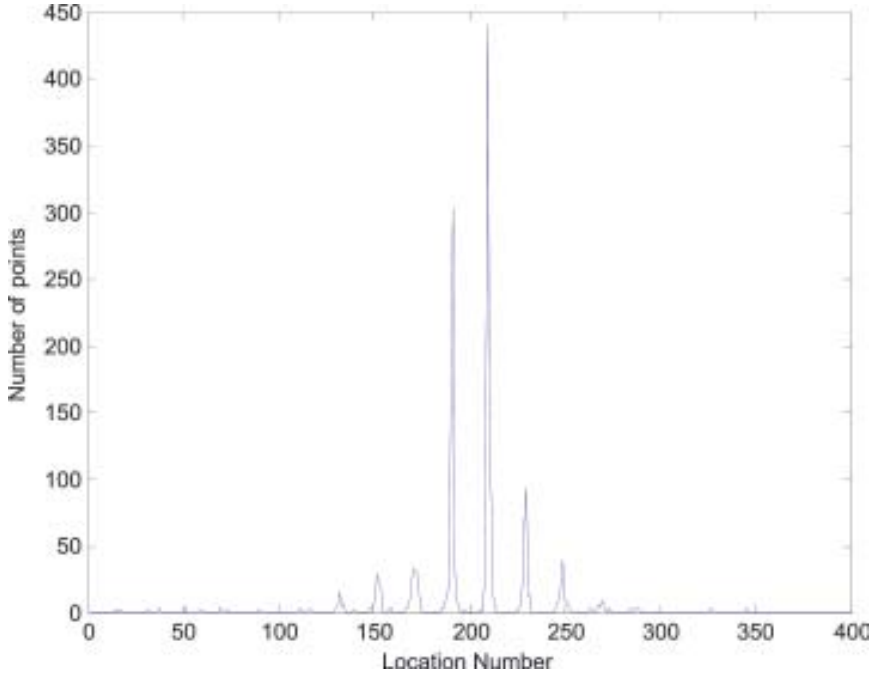

Fig. 2. SSPD plot for the sound /ka/

The SSM and the corresponding SSPD plot obtained for different speaker shows the identity of the sound so that an efficient feature vector can be formed using SSPD. The feature vector of size 20 is estimated by taking the average distribution of each row in the SSPD graph.

3. CLASSIFICATION

In the statistical learning approach, each pattern is represented in terms of a set of d features and can be viewed as a point in d dimensional feature space. The goal is to choose those features that allow pattern vectors belonging to different categories to occupy compact and disjoint regions in a d-dimensional feature space. The effectiveness of the representation space (feature set) is determined by how well patterns from different classes can be separated. Given a set of training patterns from each class, the objective is to establish decision boundaries in the feature space which separate patterns belonging to different classes. In the statistical decision theoretic approach, the decision boundaries are determined by the probability distributions of the patterns belonging to each class, which must either be specified or learned [18, 19].

3.1 k - Nearest Neighborhood

Pattern classification using distance function is an earliest concept in pattern recognition [20, 21]. Here the proximity of an unknown pattern to a class serves as a measure of its classifications. k - NN is a well known non - parametric classifier, where a posteriori probability is estimated from the frequency of the nearest neighbors of the unknown pattern [22]. For classifying each incoming pattern k - NN requires an appropriate value of k. A newly introduced pattern is then classified to the group where the majority of k nearest neighbor belongs [23]. Hand proposed an effective trial and error approach for identifying the value of k that incur highest recognition accuracy [24]. Various pattern recognition studies with highest performance accuracy are also reported based on these classification techniques [25] .

Consider the cases of m classes c_i, where $i = 1,2,\ldots\ldots m$, and a set of N samples pattern y_i, $i = 1,2,\ldots..N$ whose

classification is priory known. Let x denote an arbitrary incoming pattern. The nearest neighbor classification approach classifies 'x' in the pattern class of its nearest neighbor in the set y_i

i.e. If $||\ x\text{-}y_j||^2 = min||x\text{-}y^2||2\ \ 1 \le i \le N$ then x in c_j

This is 1 - NN rule since it employs only one nearest neighbor to x for classification. This can be extended by considering k - Nearest Neighbors to x and using a majority - rule type classifier.

3.2 Support Vector Machines

SVM is a linear algorithm with some specific properties. The basic principle of SVM in pattern recognition application is to build an optimal separating hyperplane in such a way to separate two classes of pattern with maximal margin [26]. SVM accomplish this desirable property based on the idea of Structural Risk Minimization (SRM) from statistical learning theory which shows that the error rate of a learning machine on test data (i.e generalization error report) is bounded by the sum of training error rate and the term that depending on the Vapnik - Chervonenkis (VC) dimension of the learning system [27, 28]. By minimizing this upper bound high generalization performance can be obtained. For separable patterns SVM produces a value of 0 for first term and minimizes the second term. Furthermore, SVMs are quite different from other machine learning techniques in generalization of errors which are not related to the input dimensionality of the problem, but to the margin with which it separates data. This is the reason why SVMs can have good performance even in large number of input problems [29] [30].

SVMs are mainly used for binary classifications. For combining the binary classification into multiclass classification a relatively new learning architecture namely Decision Directed Acyclic Graph (DDAG) is used. For N class problem, the DDAG contains, one for each pair of classes. DDAGSVM works in a kernel induced feature space and uses two class maximal margin hyperplane at each decision node of the DDAG. The DDAGSVM is considerably faster to train and evaluate comparable to other algorithms.

4. SIMULATION EXPERIMENTS AND RESULTS

All the simulation experiments are carried out using Malayalam CV speech unit database, uttered by 96 different speakers. We used 8 kHz sampled speech signal which is low pass filtered to band limit to 4 kHz. We divide the dataset into training and test set which contains CV speech unit database, uttered by first 48 speakers for training and next 48 for testing. Thus training and test set contains total of 1728 samples each. The main objective of this article is to design a robust CV speech unit recognizer in additive noisy condition. To perform this task each speech signal is corrupted by Additive White Gaussian Noise (AWGN) of different Signal to Noise Ratio (SNR) levels. The recognition accuracies obtained for Malayalam CV speech database for the five different phonetic classes at various SNR levels using MFCC, NWHF and SSPD parameters based on k-NN and DDAGSVM classifiers are tabulated in Tables 2-4, respectively.

Table 2. Recognition accuracies of 5 different phonetic classes using MFCC of different SNR values

Class	Recognition Accuracy											
	k-NN						DDAGSVM					
	0 dB	3 dB	10 dB	20 dB	30 dB	Clean	0 dB	3 dB	10 dB	20 dB	30 dB	Clean
Unaspirated	20.4	24.1	30.1	37.8	42.1	50.3	25.1	30.2	41.7	52.4	55.8	60.7
Aspirated	22.5	26.9	32.5	36.1	43.7	51.8	28.6	31.6	43.2	54.2	58.1	62.2
Nasals	26.9	30.2	37.3	39.2	45.9	54.8	30.7	33.8	45.9	57.1	61.5	64.9
Approximant	21.6	28.7	35.9	38.1	44.4	53.9	29.2	32.6	43.2	52.5	58.3	63.4
Fricatives	23.5	28.7	36.8	40.3	43.7	54.8	30.1	33.2	46.7	53.7	59.8	64.5

Table 3. Recognition accuracies of 5 different phonetic classes using NWHF of different SNR values

Class	Recognition Accuracy											
	k-NN						DDAGSVM					
	0 dB	3 dB	10 dB	20 dB	30 dB	Clean	0 dB	3 dB	10 dB	20 dB	30 dB	Clean
Unaspirated	25.7	28.9	45.5	56.2	62.4	62.6	45.8	52.2	61.2	72.7	75.2	76.8
Aspirated	29.1	36.4	47.9	59.6	63.9	63.3	48.3	55.3	63.7	74.6	78.8	79.9
Nasals	46.1	50.9	57.6	61.2	65.7	65.7	55.6	60.2	65.3	77.8	81.9	83.6
Approximant	41.7	48.3	55.2	60.6	64.8	64.9	50.3	55.7	63.8	72.8	78.5	81.9
Fricatives	43.3	49.1	56.5	60.9	63.1	63.5	53.6	59.4	66.9	78.6	82.1	84.2

Table 4. Recognition accuracies of 5 different phonetic classes using SSPD of different SNR values

Class	Recognition Accuracy											
	k-NN						DDAGSVM					
	0 dB	3 dB	10 dB	20 dB	30 dB	Clean	0 dB	3 dB	10 dB	20 dB	30 dB	Clean
Unaspirated	41.2	44.5	49.8	53.2	58.7	64.9	58.7	62.2	74.8	78.7	81.2	86.1
Aspirated	40.4	43.4	48.1	50.9	56.8	63.1	58.3	65.9	71.9	78.6	81.8	85.6
Nasals	48.1	51.2	53.1	59.3	63.6	70.2	65.4	70.8	75.3	81.4	88.5	94.2
Approximant	46.8	49.9	52.9	58.2	62.8	68.5	60.3	65.5	73.4	82.8	88.2	93.9
Fricatives	46.1	49.3	51.9	57.8	62.1	67.4	57.5	59.4	66.9	78.6	89.1	92.4

5. CONCLUSION

This paper describes two statistical learning approaches such as k - Nearest Neghborhod (k - NN) and Support Vector Machine (SVM) for the classification of Malayalam CV speech unit database in speaker independent environments. Three different modeling algorithms viz., MFCC, NWHF and SSPD parameters are discussed to evaluate the performance of these two classifiers. The recognition accuracies are calculated and compared using SVM and k - NN and it is observed that the time domain based SSPD parameters using DDAGSVM algorithms is performing well compared with NWHF and MFCC in speaker independent noisy environments. Classification of Malayalam consonants inherent with all the vowels are some of our future research direction.

6. REFERENCES

[1] ANIL K. JAIN, ROBERT P.W. DUIN and JIANCHANG MAO, 2000. Statistical Pattern Recognition : A Review, *IEEE Trans. on Pattern Analysis and Machine Intelligence*, **22**(**1**).

[2] A. GROSSMAN, J. MORLET and P. GAOUPILLAUD, 23. Cycle octave and related transforms in seismic signal Analysis, *Geoexploration*, **23**, 85-102.

[3] C. TORRENCE and G.P. COMPO, 1998. A practical guide to Wavelet Analysis, *Bull. Amer. Meteorological. Soc.*, **79**(**1**), 61-78.

[4] HONGYU LIAO, MRINAL KR and BRUCE F. COCKBURN, 2004. Efficient Architectures for 1 - D and 2 - D Lifting Based Wavelet Transform, *IEEE Trans. on Signal Processing*, **52**(**5**), 1315-1326.

[5] S. MALLAT, 2009.A wavelet Tour of Signal Processing, The Sparse Way", NewYork : Academic.

[6] K.P. SOMAN and K.I. RAMACHANDRAN, 2005. Insight into Wavelets, from Theory to Practice, Prentice Hall of India.

[7] M. VETTERLY and C. HERLEY, 1992. Wavelets and Filter banks : Theory and Design, *IEEE Trans. on Signal Processing*, Vol. 40(9), pp. 2207-2232, 1992.

[8] M.J. SHENSA, 1992. Affine Wavelets: Wedding the Atrous and mallat Algorithms, I*EEE Trans. on Signal Processing*, **40**, 2464-2482.
[9] S. MALLAT, 1989. Multi frequency Channel Decomposition of Images and Wavelet Models", IEEE. Trans on Acoustics, *Speech and Signal Processing*, **37**, 2091-2110.
[10] I. DAUBECHIES, 1992. Ten Lectures on Wavelets, Philadelphia, *PA: Soc. Appl. Math*.
[11] RONALD W. LINDSAY, DONALD B. PERCIVAL and D. ANDREW ROTHROCK, 1996. The Discrete Wavelet Transform and the scale analysis of the surface properties of Sea Ice, *IEEE Trans. on Geo Science and Remote Sensing*, **34**(**3**), 771-787.
[12] E. OTT, 1993. Chaos in Dynamical Systems, Cambridge University Press.
[23] G. L. BAKER and J. GOLLUB, 1996. Chaotic Dynamics : An Introduction, Cambridge University Press.
[14] MICHAEL T. JHONSON, RCHARD J. POVINALLi, ANDREW C. LINDGREN, JINJIN YE, XIAOLIN LIu and Kevin Indrebo, 2005. Time Domain Isolated Phoneme Classification using Reconstructed Phase Space", *IEEE Trans. On Speech and Audio Processing*, 13(4), 458-466.
[15] F. TAKENS, 1980. Detecting Strange Attractors in Turbulence, in Proc. Dynamical Systems and Turbulence, Warwick, U.K., pp. 366-381.
[16] H. KANTZ and T. SCHREIBER, 1997. Non Linear Time Series Analysis, Cambridge University Press.
[17] D. S. BROOMHEAD and G.P. KING, 1986. Extracting qualitative Dynamics from experimental data, *Physica D*, pp. 217-236.
[18] T.J. TOU and R.C. GONZALEZ, 1999. Pattern Recognition Principles, Addison - Wesley, London, 1974.
[19] Friedmen M and Kandel A, Introduction to Pattern Recognition: Statistical, Structural, Neural and Fuzzy Logic Approach, World Scientific.
[20] T.M. COVER and P.E. HART, 1967. Nearest Neighbor Pattern Classification", IEEE trans. on Information Theory, **13** (**1**), 21-27.
[21] MIN-CHUN YU, 2011. Multi - Criteria ABC analysis using artificial - intelligence based classification techniques, Elsevier - *Expert Systems With Applications*, **38**, 3416-3421.
[22] D.J. HAND, 1981. Discrimination and classification, NewYork, Wiley.
[23] A.K. RAY and B. CHATTERJEE, 1984. Design of a Nearest Neighbor Classifier System for Bengali Character Recognition, *Journal of Inst. Elec. Telecom. Eng.*, **30**, 226-229.
[24] B. ZHANG and S.N. SRIHARi , 2004. Fast k - Nearest Neighbor using Cluster Based Trees, *IEEE trans. on Pattern Analysis and Machine Intelligence*, **26**(**4**), 525 - 528 .
[25] F. PERNKOPF, 2005. Bayesian Network Classifiers versus selective k -NN Classifier, *Pattern Recognition*, 38, 1-10.
[26] YING TAN and JUN WANG, 2004. A Support Vector Machine with a Hybrid Kernel and Minimal Vapnik - Chervonenkins Dimension, *IEEE Trans. On Knowledge and Data Engineering*, 10(4) 385-395 .
[27] VLADIMIR N. VAPNIK, 1999, An Overview of Statistical Learning Theory", *IEEE Trans. On Neural Networks*, **10**(**5**), 988-999 .
[28] RAVI GUPTA, ANKUSH MITTAL and KULDIP SINGH, 2008. A time Series based Feature Extraction Approach for Prediction of Protein Structured Class, *EURASIP Journal on Bioinformatics and System* Biology.
[29] E. OSUNA, R. FREUND and F. GIROSI,1997. Training Support Vector Machines: An Application to Face Detection, Proc. *IEEE Conf.Computer Vision and Pattern Recognition*, pp. 17-19.
[30] M. PONTIL and A. VERRI,1998. Support Vector Machines for 3D Object ecognition," *IEEE Trans. Pattern Analysis and Machine Intelligence*, **20** (**6**) 637-646.

Journal of Acoustical Society of India : Vol. 40, No. 3, 2013 (pp. 165-169)

Measurement of Acoustics in ISRO Launch Vehicle Missions

A.R. Krishnan
Avionics Entity,VSSC, ISRO PO, Thiruvananthapuram-695 022 (Kerala)

[Received: 26.12.2012; Revised: 10.05.2013; Accepted: 15.05.2013]

ABSTRACT

1. INTRODUCTION

ISRO is in the process developing bigger launch vehicles to cater to future needs of heavier satellites in polar and GTO and re-entry missions. During the launch vehicle mission from lift off to satellite injection, the launch vehicle is subjected to acoustics and vibration fields. For a successful flight, it is important to ensure that the acoustic levels are within design limits of the various subsystems .The acoustic environment is severe during liftoff and atmospheric phase of the flight. At liftoff, the violent and turbulent mixing of the high temperature and high velocity exhaust of the jet with the surrounding air is the main cause of the acoustic noise. In the atmospheric flight the flight profile with the vehicle configuration determines the acoustic environment.. The acoustic excitation induces broadband vibration responses of the vehicle structure and the get transmitted to the interior of the vehicle where sensitive assemblies are kept. The acoustic levels (SPL) normally encountered are of 120 to 170 dB during these regions.

During the development phase of the launch vehicle, large no of acoustic measurements are made to characterize the vehicle structure, deduce test levels for various subsystems and generate database for improvements. A typical of 10-15 measurements are made during the development phase. A typical acoustic measurement chain consists of an acoustic sensor, charge amplifier and digital signal processing unit. Acoustic sensor converts sound pressure level to electric charge. The common types are condenser type and MEMS based transducers. The dynamic range of these sensors are in the range of 100-180 dB SPL and bandwidth more than 10 KHz. They are rugged and operate over a wide temperature range. The charge output from these sensors are converted to analog voltage using charge amplifiers and band limited to 8 KHz using higher order switched capacitor filters. The overall telemetry available in a Launch vehicle is 2-4 Mbps and each acoustic channel if transmitted as raw data would need 200 Kbps. Hence onboard signal processing is needed to reduced bit rate. The DSP based on board system is used to process these signal in real time and transmit the information at reduced bandwidth. The frequency analysis is done in the 1/3 rd octave band covering a frequency range of 31.5 Hz to 8 KHz. The details of the sensors, interface electronics and the DSP based processing system are explained below.

2. SENSORS

The condenser type and the MEMS type sensors are normally used in launch vehicles. Sensor 2510 from m/s Endevco was originally used in all measurements. Later it is replaced by indigenous MEMS acoustic sensor jointly developed by VSSC and CEERI ,Pilani. The endevco sensor uses Piezite as crystal material with a nominal capacitance of 5000 pF .It is rugged and hermitically sealed construction and operates over a wide temperature range (up to 250deg.C).. The MEMS sensor is a bulk micro machined device, etched out of silicon

bulk. A sense layer of silicon is deposited over the diaphragm. Appropriately patterned aluminum electrodes sandwich the ZnO layer. For strength the silicon chip is bonded to glass. The diaphragm converts the acoustic pressure into lateral stresses in silicon and Zinc oxide layers. ZnO layer converts lateral stresses in it into electric charge. A vent tunnel allows movement of air in and out of cavity under the diaphragm when any static ambient pressure changes(for low frequency acoustic pressure)while blocking the measurement band. The charge variation in the acoustic sensor is converted to voltage using a front end charge amplifier circuit and further amplified using a voltage amplifier. The picture, important specifications and the block diagram of acoustic measurement in launch vehicle are given below.

- Range 100 to 180dB (2Pa to 20KPa)
- Frequency Range 31.5Hz to 8KHz
- Sensitivity 150 to 200uV/Pa

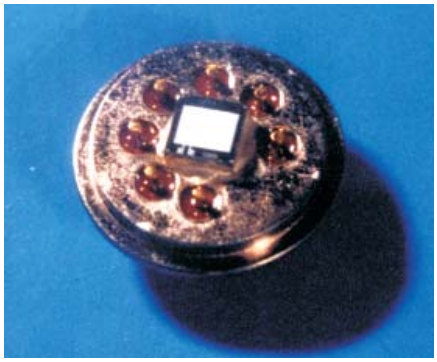

Structural design

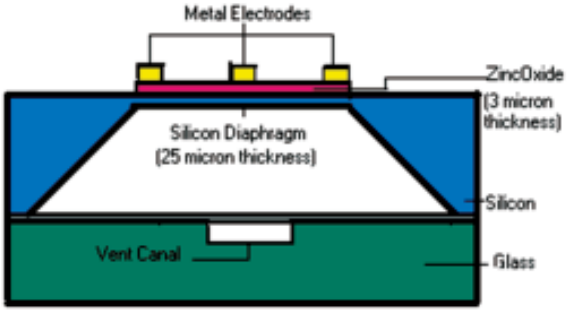

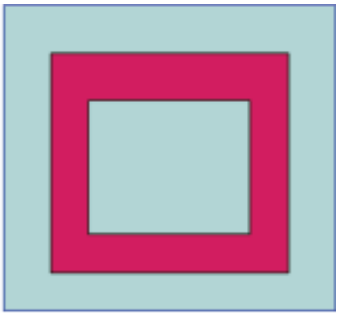

Metal electrodes sandwiching ZnO layer

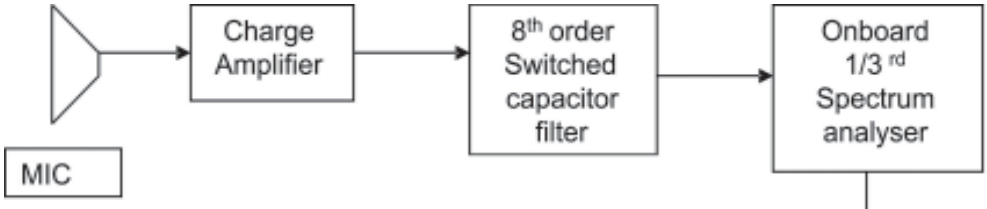

Schematic of acoustic measurement in Launch vehicle missions

The electrical function of the sensor can be illustrated by its Thevenin equivalent as shown in the fig below

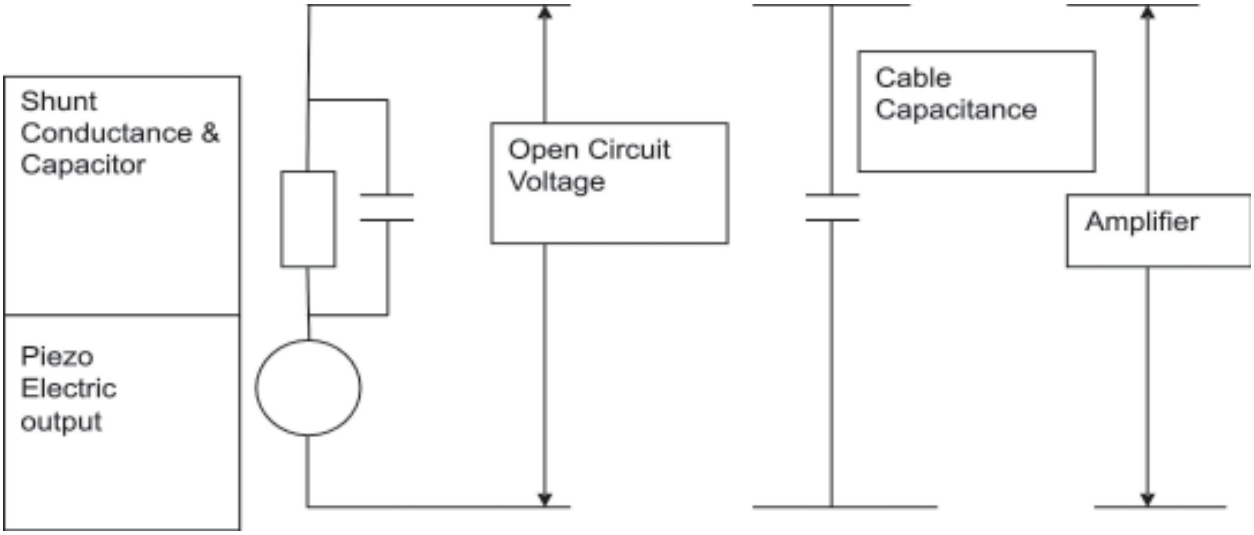

3. ONBOARD PROCESSING APPROACH

The general method for frequency analysis of any Signal is the bank of filter method. The measurement is done in the standard1/3rd octave bands depending on the application and required resolution. The two main types of frequency analysis used for signals are constant percentage bandwidth (filter bandwidth is constant percentage of centre frequency) and constant bandwidth(constant bandwidth independent of centre frequency of the filter). These techniques permit detailed analysis of the Spectrum Finally the rms value of each filter output is computed for finite period of time. For normal applications the rate is fixed as 250 milliseconds. For acoustics constant percentage bandwidth analysis is done.

The processing can be implemented both in analog or digital methods. In the analog approach, separate filters are employed for each frequency band. Even though each filter can be independently designed to have required bandwidth, this method has the disadvantage of requiring large number of analog tuning components. Since higher values of capacitances are required for low frequency analysis, the circuit becomes bulky. In the digital approach, the average energy in different frequency bands is calculated using DSP techniques. This gives accurate centre frequency and band width and there is no performance degradation due to temperature and ageing. The measurement parameters can be made programmable. Further there is repeatability of performance during production. This method is selected for processing of acoustics in launch vehicles.

The individual band filters are implemented using 6th order Elliptic Infinite Impulse Response (IIR) filters. This 6th order filter is obtained by cascading three bi-quad sections with appropriate coefficients. IIR implementation was preferred over FIR due to the lower computation requirements of the former in meeting the design specifications.

The acoustic signals are analyzed in nine 1/3 rd octave frequency bands The centre frequencies are logarithmically spaced and range from 25 Hz to 6.3 KHz. The filters corresponding to highest octave (6.3 KHz, 5 KHz and 4 KHz) are computed for all input samples. The next lower octave (3.15 KHz, 2.5 KHz and 2 KHz) is computed for alternate samples only. This means the input samples are decimated by a factor of 2. This is because the input was originally sampled for twice the maximum frequency of this filter band. Before doing computation for this octave, the input samples are low pass filtered so as to remove any higher frequencies corresponding to higher octave and then decimated by a factor of 2.This process is repeated for all lower octaves. This will reduce the computation requirement very much. The output of each filter bank is squared

and averaged for a time period of 250ms.Finally square root is taken before transmission and each byte represents the rms output in the corresponding frequency band. A typical output is shown below.

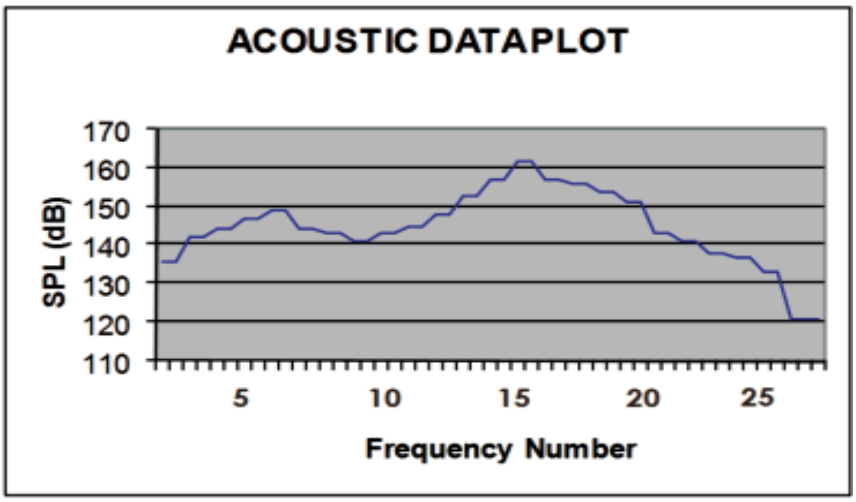

3. DESIGN CONSIDERATIONS

The following criteria were considered to meet the design objective:

1. Flexibility to choose different processing algorithm during development phase.
2. Programmability of important measurement parameters.
3. Sufficient dynamic range for measurement
4. Elimination of analog frequency trimming components
5. Hardware programmability of sampling clock generation

The task identified were highly computation intensive and had to be carried out in real time to maintain the design flexibility, programmability and to get sufficient dynamic range, a floating point DSP processor (ADSP 21060) was selected. The processor is fast and powerful to process multiple acoustic and also vibration channels simultaneously.

The hardware is based on a floating point DSP processor ADSP21060 as shown below.

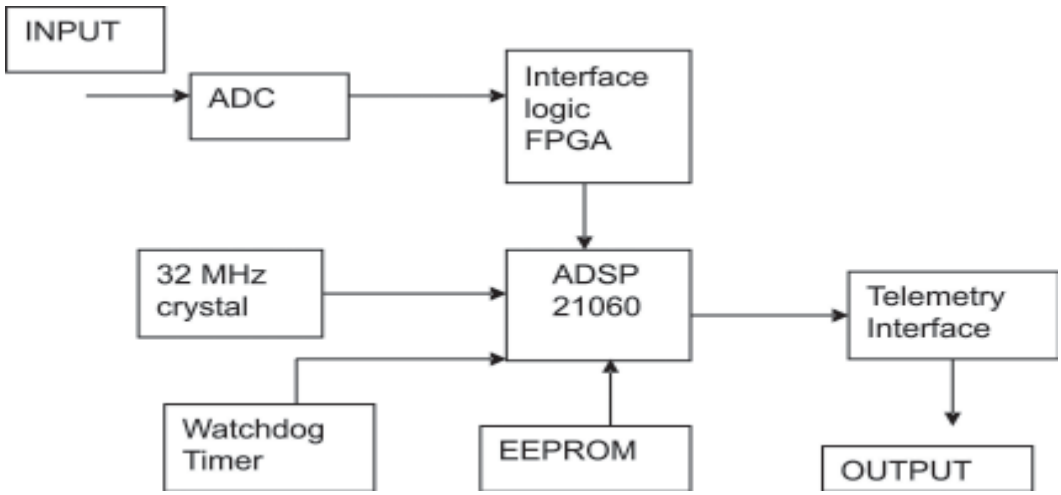

It can execute all instructions in single cycle and runs at 32MHz on target hardware. The input channels are taken through a multiplexer and given to ADC. The ADC outputs are written to a FIFO memory from where the processor can read it periodically. Glue logic and control signal generation circuitries are implemented using a field programmable logic array (FPGA). Anti aliasing filters are realized using 8 th order switched capacitor filter. To increases the system reliability, hardware watch dog .timer is incorporated.

In order to achieve the programmability of the system, the outputs of the filters are scaled by suitable factors which could be programmed from outside. In the case of acoustic channel, for a given overall sound pressure level (OASPL), the maximum SPL (Sound Pressure level) that can be measured in each band can be programmed . An EEPROM is provided for this purpose.

4. CONCLUSION

The presentation covered the details of acoustic measurements in launch vehicles including purpose, details of sensor and electronics and on-board processing using DSP techniques. With the high speed floating point architecture of ADSP21060, a dynamic range of 48db and a telemetry bit rate reduction of 250:1 was achieved. This enabled more number of such measurements to be made in each launch vehicle missions during development phase.

Journal of Acoustical Society of India : Vol. 40, No. 3, 2013 (pp. 170-175)

Vibration Analysis of Internal Combustion Engine - Modeling and Optimization

T. Ramachandran* and K.P. Padmanaban
PSNA College of Engineering & Technology, Dindigul-624 622
SBM College of Engineering & Technology, Dindigul-624 005
**e-mail : ramji_kkp@yahoo.com*

[Received: 26.12.2012; Revised: 10.05.2013; Accepted: 15.05.2013]

ABSTRACT

There is a discrepancy in the established number of lexical tones in Manipuri, a tonal language, as well as the terminology used to describe them. Hence, the present study attempts to describe the characteristics of lexical tones in Manipuri using acoustical analysis and it perception by native speakers. Monosyllable minimal pair words contrasting in tone were recorded from three native speakers of Manipuri language. Pitch values extracted for each word were used to identify different tone contours based on the configuration of the pitch contour, initial pitch and final pitch. Results revealed four pitch contours namely, level, falling, rising and falling-rising. In addition, individual differences were noticed in the configuration of pitch contours obtained for the same word across speakers. However, for each speaker, each minimal word pair contrasting in tones were always distinguishable using pitch contour, initial pitch and final pitch of the pitch contour. The meaning of all the words was identified correctly above chance level by four native speakers. It is possible that normalization of the lexical tones produced by different speakers was done by the listeners.

1. INTRODUCTION

Internal combustion (IC) engine produces intolerable vibrations during the operation, when the vibration forces transferred to the supporting structures the reliability and the driving comfortness are much reduced. It is necessary to reduce the vibrations from the engine to the engine mounts to satisfy customer requirements. The vibration from the engine is due to the inertial and unbalanced forces of the reciprocating and rotating components in the engine. In this work a mathematical model will be developed to determine the engine inertial and unbalanced forces and the model will be solved using a computer program to determine the displacements and velocity at the engine supports.

Engine vibrations are caused due to the reciprocating and rotating masses of the engine. The variations of inertial forces are due to the combustion and the compression differences of the piston cylinder arrangement during their operation The engine inertial forces leads to the unbalanced forces of the engine and they are quiet varying with respect to speed, fuel supply and combustion characteristics of the fuel. Though the supply and combustion of fuel is also the reasons of the vibration, they are not in the controllable sources for the vibration. Because, they are the parameters decide the performance of an engine. To predict the vibration output of an engine and to minimize the possible durability and consumer perceived quality problems associated with engine vibration, a robust and accurate design and simulation model is needed. Such model should execute quickly and requires relatively simple inputs.

The engine mounts should have characteristics of high stiffness and high damping in the low-frequency range and of low stiffness and low damping in the high-frequency range. Hydraulic mounts do not perfectly satisfy such requirements. Although hydraulic mounts greatly increase damping at low frequencies, they also degrade isolation performance at higher frequencies. Also hydraulic mounts are not cost effective, they had complexity in design and low reliability. Though various types of hydraulic mounts have been developed for the vehicle mount systems, it is still reported that the rubber mounts show significant importance in ride comfort and reduced noise levels. Rubber mounts can be designed for the necessary elastic stiffness rate characteristics in all directions for proper vibration isolation and they are compact, cost-effective, and maintenance free. Also the rubber mounts offer a trade-off between static deflection and vibration isolation. Rubber mounts have been successfully used for vehicle engine mounts for many years.

In this work, a 4-cylinder engine has been considered. The mass of balancing discs and their lead angles can control and reduce the engine vibrations and they are optimized using genetic algorithm. To demonstrate the genetic algorithm, the mass of balancing discs and their lead angles are considered as design variables. The objective function is the function of reaction forces at the engine mounts, inertial forces of the reciprocating parts, unbalanced forces from the crank shaft. The developed model is simulated at a particular speed for specific time and the design parameters of the engine are optimized such that objective function is minimized.

2. KINEMATIC MODELING OF THE ENGINE

Considering an internal combustion engine (shown in figure 3) mounted on its chassis through three rubber mounts, i.e., two at the front of the engine and the other at the rear end of the engine. The engine is idealized as a rigid body of mass 'M' attached to rigid chassis by means of elastic supports. The origin 'G' of the fixed global coordinate system 'Gxyz' is located at the centre of the mass 'C' of the engine when in static equilibrium. The z-axis is parallel to the crankshaft and the x-axis is in the vertical direction. Under the idling conditions, the centre of mass will of course not necessarily coincide with the origin. In certain applications, it is of paramount importance to go to extremes in order to eliminate acoustical radiation. In such cases, the counter weights or balancing masses are geared to rotate about the crankshaft at the same angular velocity as the crank may be justified.

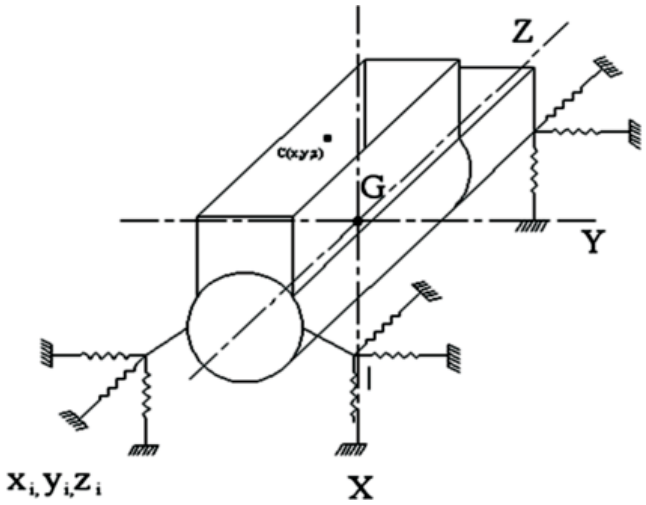

Fig. 1. Rigid body model of the engine

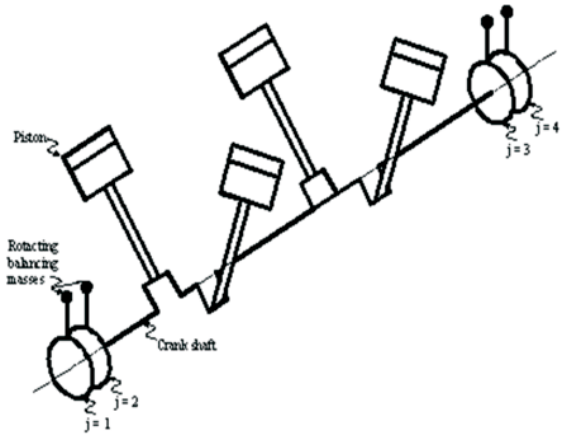

Fig. 2. Crank shaft with balancing masses

2.1 Kinematics and Dynamics of Piston and Connecting Rod

The engine vibration can be divided into two categories: vibration of engine parts relative to each other, called internal vibration, and the movement of the engine as a whole, called external vibration. Unbalanced forces and moments cause the external vibration. As for the vibration isolation, an engine is normally regarded

as a rigid-body having six degrees of freedom (DOF) about orthogonal axis through its center of gravity: linear vibrations along each axis and rotations about each axis . In the classical determination of diesel excitations, only three modes are usually of consideration:

- Vertical oscillations on the X axis due to unbalanced vertical forces,
- Rotation about the Z axis due to unbalanced vertical forces in different trans verse planes,
- Rotation about the Y axis due to cyclic variations in torque.

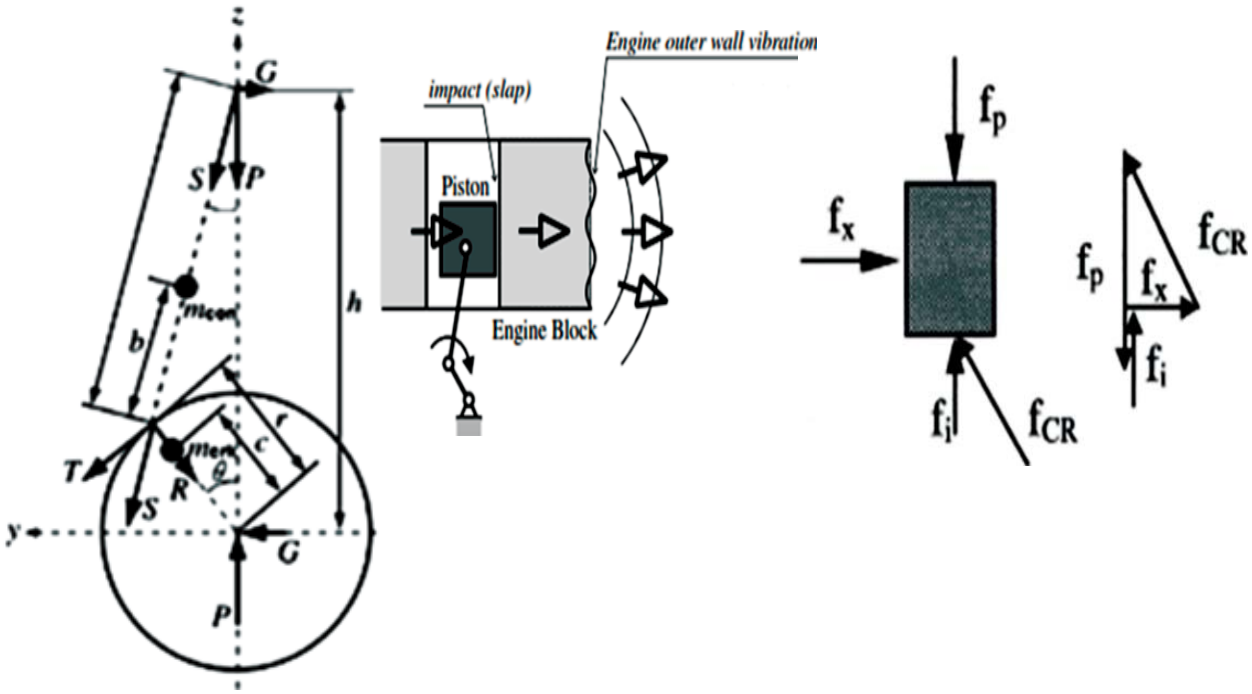

Fig. 3a. Kinematics of piston and connecting rod b. Typical slap mechanism c. Resolved forces in Cartesian coordinates

The variation of torque, which balances the torque from the shaft and must be absorbed by elements such as torsional elastic couplings outside the engine frame, will not be considered here. For in-line engines force couples about Z-axis due to unbalanced vertical forces in different transverse plane are fully balanced. In general the rotating masses are carefully balanced but periodic forces due to the reciprocating masses cannot be avoided. A crankshaft, connecting rod and piston assembly, see Fig.1, is subjected to a periodic force in the line of action of the piston given approximately by

$$f_i = m_p R\omega^2\left(\cos\theta + \frac{R}{L}\cos 2\theta\right) \quad f_x = (f_p - f_i)\tan\beta \quad \tan\beta = \frac{\sin\beta}{\sqrt{1-\sin^2\beta}} \cong \frac{R}{L}\tan\theta\left[1+\frac{1}{2}\left(\frac{R}{L}\right)^2\sin^2\theta\right]$$

for constant crankshaft rotational speed(ω) and where mp is the effective mass of the piston and includes that fraction of the mass of connecting rod. R and L are respectively the crank radius and connecting rod length. This inertia force associated with piston reciprocating motion is of most concern in classical analysis of engine vibration isolation. From the force diagram as shown in Fig. 2, the lateral piston- slap force can be written as:

$$f_x \cong \frac{R}{L}\sin\theta\left[\frac{\pi}{4}D^2 p - m_p R\omega^2\left(\cos\theta + \frac{R}{L}\cos 2\theta\right)\right]$$

Another one is called inertia-controlled impact which occurs in those parts of the cycle for which the pressure forces are negligible. Hence, the lateral piston-slap force Fig.1c for one cylinder is given by:

$$f_x \cong f_{xp} + f_{xi} \quad f_{xp} \cong \frac{\pi}{4} D^2 p \frac{R}{L} \sin\theta \quad f_{xi} \cong -m_p \omega^2 R \left(\cos\theta + \frac{R}{L} \cos 2\theta \right) \frac{R}{L} \sin\theta$$

The force exerted by the entire engine - the sum of all force of all cylinders and is given by

$$\sum f_i = m_p \omega^2 R \left(\sum \cos\theta_i + \frac{R}{L} \cos 2\theta_i \right) \quad \sum f_x = \left\{ \sum \left[\frac{\pi}{4} D^2 p_i - m_p \omega^2 R \left(\cos\theta_i + \frac{R}{L} \cos 2\theta_i \right) \right] \frac{R}{L} \sin\theta_i \right\}$$

Then the inertia based piston slap is given by $\sum f_{xi} = -m_p \omega^2 R \sum \left(\cos\theta_i + \frac{R}{L} \cos 2\theta_i \right) \frac{R}{L} \sin\theta_i = 0$

The unbalanced forces at the balancing discs is given by

$$f_{xbi} = m_j r_j \omega^2 \cos(\Delta_j - \theta) \quad f_{ybj} = m_j r_j \omega^2 \sin(\Delta_j - \theta)$$

Using the above procedure, the reciprocating mass exerted vertical inertia force and piston-slap imposed force on the mounts located at the chassis of a 4-stroke, 4-cylinder in- line diesel engine are calculated for a mass range of 0.2-04kg and for the lead angle range of 0-360o.

3. RESULTS AND DISCUSSION

In this model and optimization problem the engine balancing mass discs and their lead angles are considered as the parameter for the model and the displacements at the engine block. The model is programmed in the Matlab with optimization code. The model is simulated to a specified time of 0.04s and the force and displacement values are obtained for the different orientation of the piston connecting rod. In the optimization at the GA the initial population was generated as a set of binary strings of specified string length and the string is converted in to the real values to be used as input for the mathematical model. Based on the objective function obtained for the generated populations the reproduction was performed through the calculation of the fitness function and by the selection (roulette wheel) operators. In the binary strings obtained in the reproduction are reformed to form the new chromosomes in the crossover process.

After the single point cross over at the selected chromosomes the mutation at the selected points of the chromosomes were performed. The final sets of chromosomes are converted in to the real variables and fed in to the mathematical model to obtain the displacements for different sets of the new chromosomes. The genetic process was performed for the different combinations of cross over and mutation probabilities and minimum displacements at the block were obtained from different runs of the GA. The variables corresponding to the

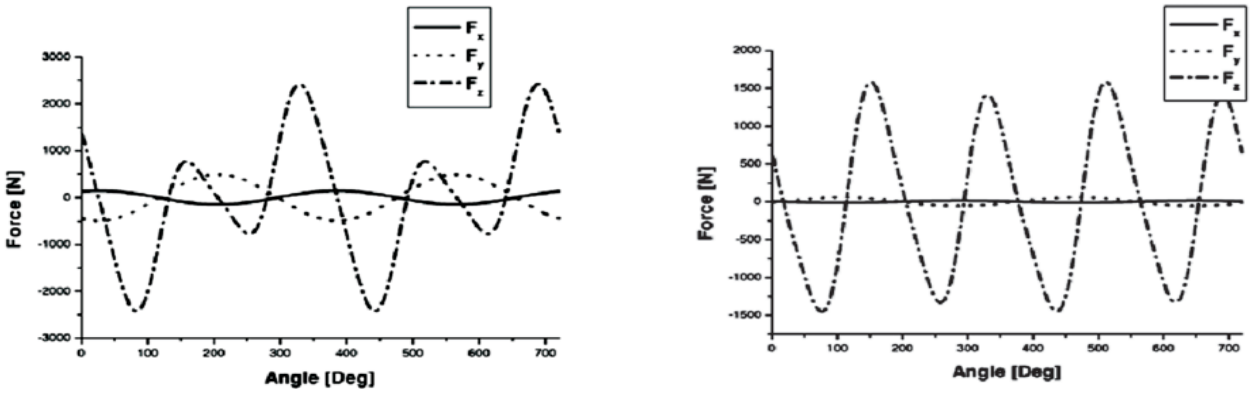

Fig. 4. Engine Forces: a) Before Optimization b) After Optimization

minimum displacement was used in the mathematical model and the inertial and slap forces at the engine cylinder wall at every angle are obtained (Table. 1). The slap forces at the cylinder wall were comparatively less and hence displacement Fig. 4 at block after the optimization was performed.

Table 1. Optimized GA results of displacement for different Crossovers and Mutations

GA Run	Least engine mount Resultant displacement (mm)	Mass of balancing discs (kg)				Lead angle (degrees)			
		m_1	m_2	m_3	m_4	Δ_1	Δ_2	Δ_3	Δ_4
1	0.0022	0.30	0.36	0.24	0.37	164	218	220	162
2	0.0022	0.36	0.39	0.30	0.39	198	194	130	142
3	0.0027	0.26	0.39	0.40	0.40	88	178	188	296
4	0.0020	0.30	0.40	0.38	0.37	166	194	162	206
5	0.0021	0.35	0.36	0.33	0.33	144	186	210	162

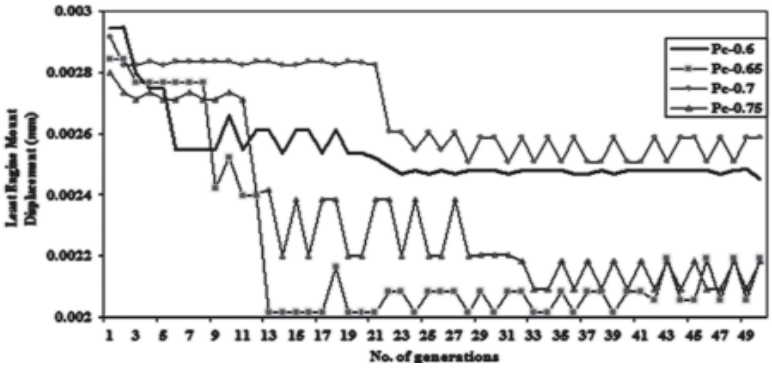

Fig. 3. GA Convergence for different runs

4. CONCLUSION

The dynamics analysis of diesel engine through investigation of the piston-slap force by considering the friction and connecting rod effects was conducted. Analytical calculations for kinematics and dynamics analysis were applied. Kinematics analysis was based on the vector analysis and dynamics analysis was based on the Cartesian coordinate principles. The design variables are optimized using GA to minimize the piston slap forces from the moving parts to the engine block. Although this analysis has led to predictions of the vibrations due to piston slap, the present work makes no attempt to assess the importance of piston-slap relative to that of other potential vibration sources.

One may reasonably expect piston slap to dominate the "mechanical noise" of reciprocating compressors with quiet accessories, where there is no "combustion noise". However, for reciprocating machines in general one requires experimental data in order to determine whether and under what conditions piston-slap noise predominates. A possible means for studying this dominance would consist of comparing experimentally observed dependences of noise and vibrations on various engine parameters with dependences implied by the development presented here.

However, it must be pointed out that the present analysis is not entirely complete, and that it may fail to consider some parameters conceivably of considerable importance. The most important likely discrepancy between the present analysis and reality is associated with the tacit assumptions that were made that all forces acting on the piston act through its center of gravity, and that the wrist-pin centerline passes through this center of gravity. Thus, rotation or cocking of the piston during its travel across the clearance space has been neglected, although such rotations may have possibly marked effects on the character as well as on the severity of the piston-slap impacts. Other shortcomings may be associated with the neglect of piston-ring friction, of oil film cushioning, of angular accelerations of the crankshaft, of clearances at the crankshaft bearings, and of clearances and friction torques at the wrist-pin and crank-pin. However, one may entertain the reasonable hope that these omissions are of minor importance.

5. REFERENCES

[1] ZHENG-DONG MA and NOEL C. PERKINS, 2003"An efficient multibody dynamics model for internal combustion engine systems", *Multibody System Dynamics* **10**, 363-391.

[2] S. RAJENDRAN and M.V. NARASIMHAN, 1997"Effect of inertia variation due to reciprocating parts and connecting rod on coupled free vibration of crank shaft". *ASME Journal of Engineering for Gas Turbine and power* vol **19**, 257-263.

[3] A.R. OHADI and G. MAGHSOODI, 2007"Simulation of engine vibration on non-linear hydraulic engine mounts", *ASME Journal of Vibrations and Acoustics* **129**, 417-42.

[4] CHUNG-HA SUH and CLIFFORD G. SMITH,"Dynamic simulation of engine mount system". *SAE Paper#971940.*

[5] TETSURO BUTSUEN and MASAAKI OOKUMA, Akio Nagamatsu,"Application of direct system identification method for engine rigid body mount system", *SAE Paper#860551.*

[6] SUDHIR KAUL, K. ANOOP DHINGRA and G. TIMOTHY HUNTER, 2007"Frame flexibility effects on engine mount optimization for vibration isolation in motor cycle", *ASME Journal of Vibrations and Acoustics* **129**, 590-600.

[7] P. CONTI and J. BRETL, 1989"Mount stiffness and inertia properties from modal test data", *ASME Journal of Vibrations and Acoustics-Stress and Reliability in Design* **111**, 134-141.

[8] J.A. SNYMAN, 1983"An improved version of the original leap frog dynamic method for unconstrained minimization : LFOPI ", *Appl. Math. Modelling* **7**, 216-218.

[9] NICCOLO BALDANZINI, DAVIDE CARPRIOLI and MARCO PIERINI, 2001"Designing the dynamic behaviour of an engine suspesion system through genetic algorithm", *ASME Journal of Vibrations and Acoustics* **123**,480-486.

[10] E. JAMES BERNARD and M. JOHN STARKEY , "Engine mount optimization", *SAE#830257.*

[11] Tsuneo Tanaka, Mitsuo Iwahara, Tetsuya Sakai, "The optimization of engine vibration reduction by simulation analysis", *SAE#962203.*

[12] H. ASHRAFIUON and C. NATRAJ, 1992"Dynamic Analysis of Engine-Mount Systems", *ASME J. Vibr. Acoust.* **114**, 79–83.

[13] H. ASHRAFIUON, 1993"Design Optimization of Aircraft Engine-Mount Systems", *ASME J. Vibr. Acoust.*, **115**, 463–467.

[14] G. KIM and R. SINGH, 1995"A Study of Passive and Adaptive Hydraulic Engine Mount Systems With Emphasis on Non Linear Characteristics", *J. Sound Vib.*, **179** (**3**), 427–453.

[15] JUN-HWA LEE and KWANG-JOON KIM, 2005"An Efficient Technique for Design of Hydraulic Engine Mount via Design Variable-Embedded Damping Modeling", *ASME Journal of Vibrations and Acoustics,* **127**, 93-99.

Journal of Acoustical Society of India : Vol. 40, No. 3, 2013 (pp.176-180)

Minimization of Downtime in Industries by Acoustical Vibration Control

D. Joslin Vijaya[1]* and S. Charles[2]
[1]*Department of Mechanical Engineering,Dhanalakshmi Srinivasan Engineering College, Perambalur-621 212*
[2]*Dhanalakshmi Srinivasan College of Engineering, Navakkarai Post, Coimbatore-641 105*
**e-mail: joslinvijayamech@rediff.com*

[Received: 10.04.2013; Revised: 26.05..2013; Accepted: 21.06.2013]

ABSTRACT

Several methods can be used to monitor the condition monitoring of a machine. They are Aural, Visual, Operational variables, Temperature, Wear debris and Vibration techniques In aural method a skilled technician, having an intimate knowledge of machines, can identify a failure simply by listening to the sound produced by a damaged machine. Sometimes a microphone or a stroboscope is used to hear the machine noise. The measured vibration levels can be extrapolated in order to predict whenthe vibration levels reach unacceptable values and when the machine must be serviced fully. Hence the periodic measurement of vibration characteristics of machinery and structures becomes very essential to ensure adequate safety margins. The occurrence of frequent resonant conditions during the operation of machinery is also avoided. By means of this the operating speeds of machinery and the productivity rate are tremendously increased which leads to the agility in manufacturing automation. The status of the product quality and of the machine is displayed in the simplest possible way, for example green / red light showing the status is good / bad and short messages in case of a bad process or machine situation.This requires fully automatic diagnostic algorithms and also a database to tore the records and perform a statistical long-term analysis. The time signal, FFT-spectra, cumulative FFT-spectra etc. allows the performance of standard signal processing and analysis.

1. OBJECTIVES

The days when engineers , operators and maintenance staff interact only with the process automation system are over. Plant staff will be required to interact with the production management systems and the process automation systems, virtually on a simultaneous basis. Production management automation allows optimization of production activities, ranging from the scheduling of job orders to the traceability of finished products. Computerized production management is also referred to as a "Manufacturing Execution System" (MES). One of the objectives of MES is zero breakdown. In recent years, the digital analyzers have become quit popular for real-time signal analysis. Real-time analyzers are especially useful for machinery health monitoring since a change in the noise can be observed at the same time the change in the machine occurs. Thus the calculation process must not take more time than the time taken to collect the signal data.

Most of the prime movers have vibration problems due to the inherent unbalance. The unbalance may be due to faulty design or poor manufacture. When the machine component is subjected to vibration it may fail

because of material fatigue resulting from the cyclic variation of the induced stress. The vibration causes more rapid wear of machine parts such as bearings.

and gears and also creates excessive noise. In machines, vibration causes fasteners such as nuts to become loose. In metal cutting processes, vibration can cause chatter, which leads to a poor surface finish. Whenever the natural frequency of a machine or a structure coincides with the external excitation, there occurs resonance, which leads to excessive deflections and failure. Because of the devastating effects that vibrations can have on all machines and structures, vibration testing has become a standard procedure in the design and development of most engineering systems. Many basic problems of vibrations are nonlinear. In nonlinear systems, phenomena may occur that are theoretically impossible to solve in linear systems. Then the mathematical theory of non linear vibrations were developed. The advent of high speed digital computers made it possible to treat even complex systems.

2. METHODOLOGY ADOPTED

Sound which can be either low, soft or loud is created by vibration. When an object moves rapidly back and forth, the air molecules around it are disturbed. The disturbance moves away from the object in waves, which is what is interpreted as sound. Often sensors like nono-power tilt, shock and vibration sensors, calibrated OEM board sensor, internal sensor systems for harsh environment. These sound waves are also measured by means of acoustical instruments such as sound level meters, noise dosimeter, sound calibrators, measurement microphones, octave band, third-octave band analyzers and signal analyzers. Spectrum or frequency analyzers can be used for signal analysis. This is a device that analyses a signal in the frequency domain by separating the energy of the signal into various frequency bands. The separation of signal energy into frequency bands is accomplished through a set of filters. The analyzers are usually classified according to the type of filter employed. For example, if an octave band filter band is used, the spectrum analyzer is called an octave band analyzer. The basic component of a spectrum analyzer is the band pass filter. A band pass filter is a circuit built by using resistors, inductors and capacitors that permits the passage of frequency components of a signal over a frequency and rejects all other frequency components of the signal. For a good band pass filter, the ripples within the band will be minimum and the slopes of the filter skirts will be steep to maintain the actual band width. There are two types of band pass filters: the constant percent bandwidth filters and constant bandwidth filters. Since the output impedance of transducers is not suitable for direct input into the signal analysis equipment, signal conditioners, in the form of charge or voltage amplifiers, are used to match and amplify the signals before signal analysis. The response signal, after conditioning, is sent to an analyzer for signal processing. A commonly used analyzer is FFT analyzer. This receives analog voltage signals from an amplifier, filter and digitizer for computations. It computes the discrete frequency spectra and these signals are used to find the natural frequency, damping ratios and mode shapes either in numerical or graphical form.

Many instruments are available now a days to custom sound and vibration measurement and analysis systems. The instruments are used for audio testing, acoustic measurements, environmental noise testing, vibration analysis, noise vibration and harshness measurements, noise and vibration control, machine condition monitoring, rotating machine evaluation etc.

The MATLAB commands to detect threshold crossings are based upon the use *ofthejindand interpl* functions as shown below.

% create a new vector, time shifiedby one data point

Shifidata = [data(l);data([l:length(data)-l])J;

Yofindthe time points which cross the threshold with

positive going slope.

Z=find(data>threshold&shifidata<threshold);

% interpolate on each zero crossingtofindan accurate

estimate of actual

% crossing time

n=length(z);

Jork=l:n

% construct the short 3ptx andy vectors for interpolation

at each revolution

y=[data(z(k)-l,data(z(k)),data(z(k)+l)];

x=[(z(k)-l)*dt,z(k)*dt.(k)+1)*dt];

s(k)=interp l ty.x.threshold.spline'):

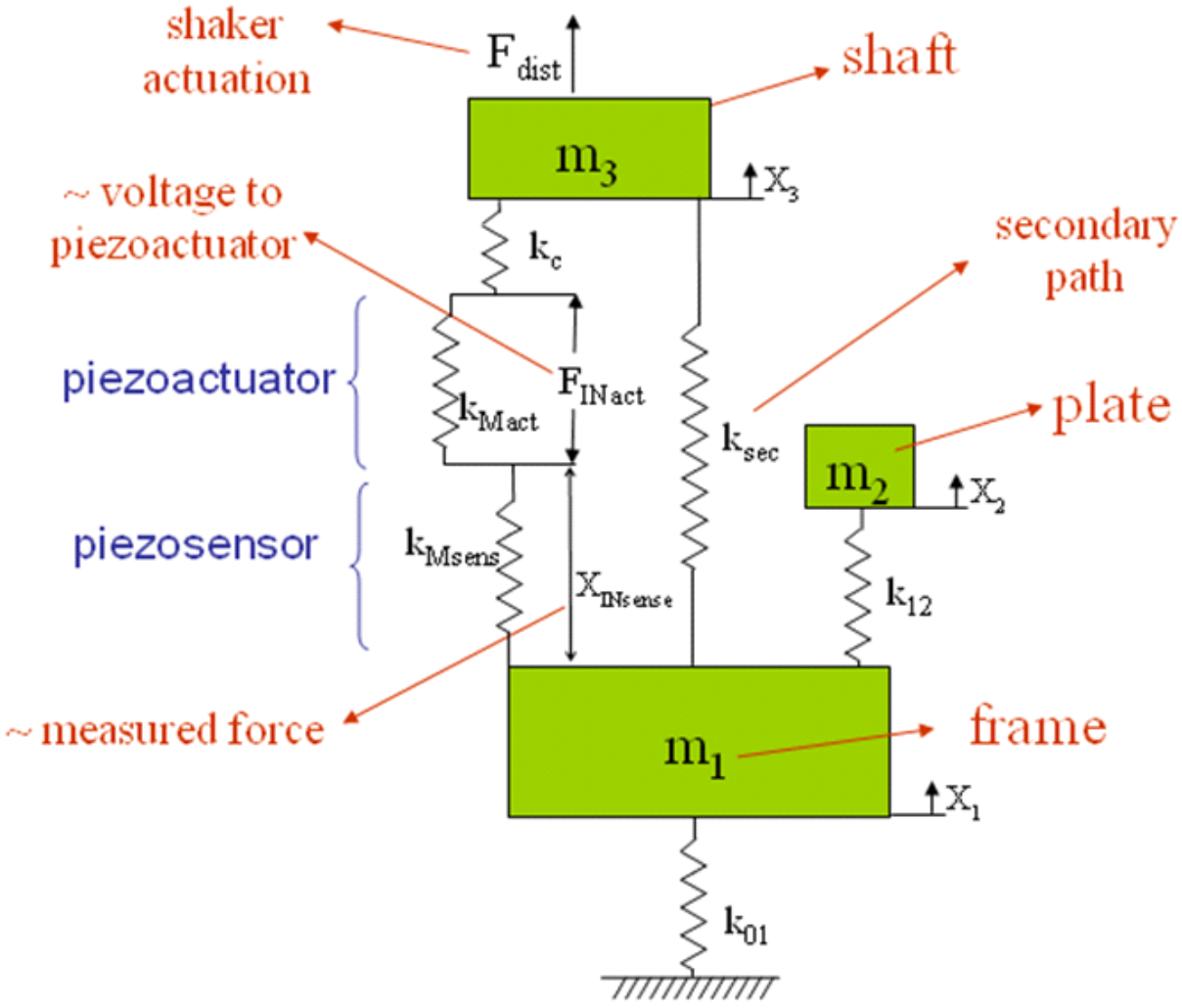

Fig. 1. Simplified lumped parameter model of the experimental test bed

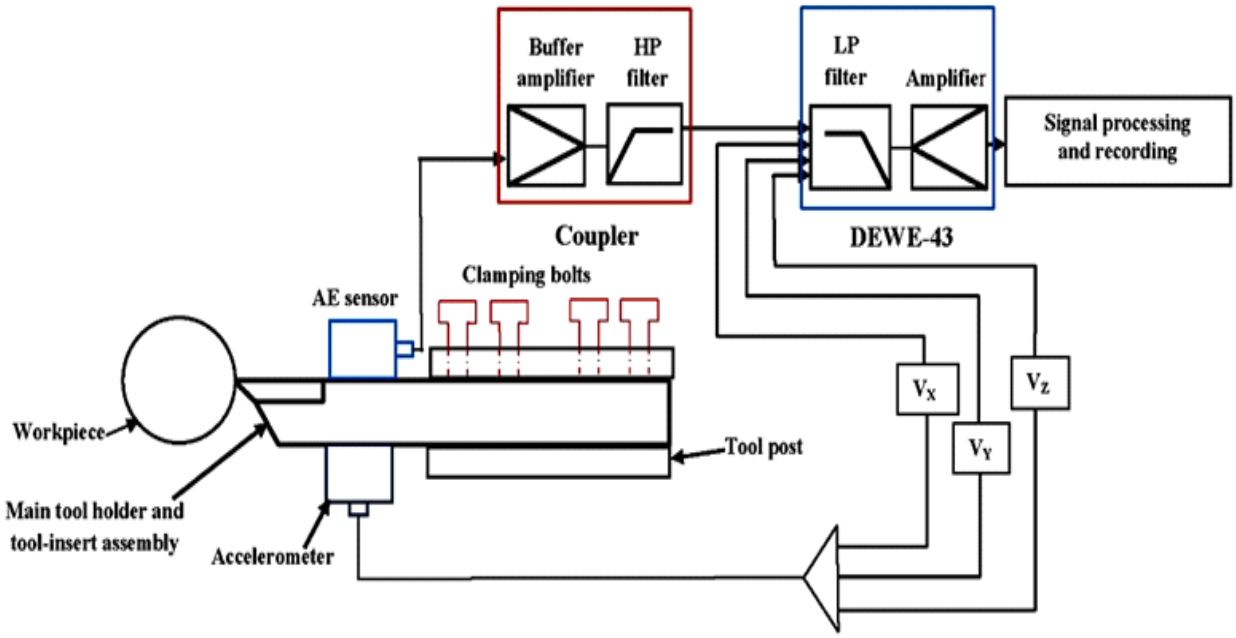

Fig. 2. Experimental setup to capture the acoustic emission and vibration signal from the cutting tool in turning

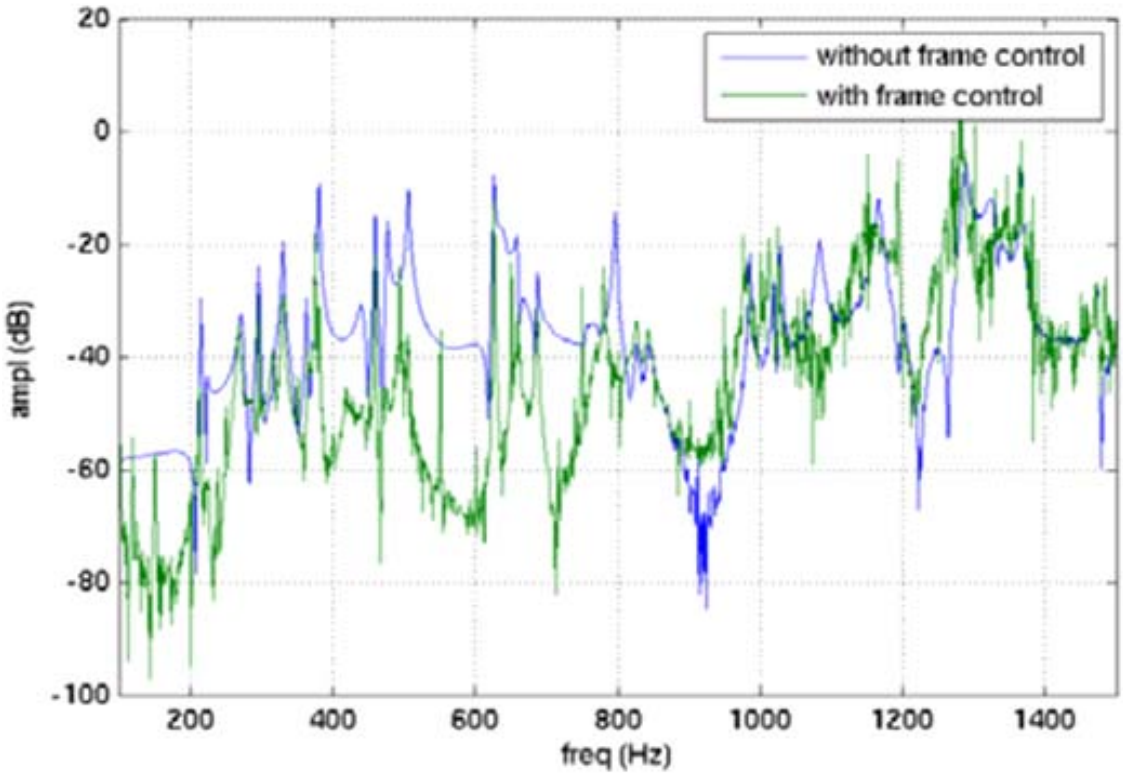

Fig. 3. Theoretical reduction of the plate acceleration when the frame acceleration would be ideally controlled to zero

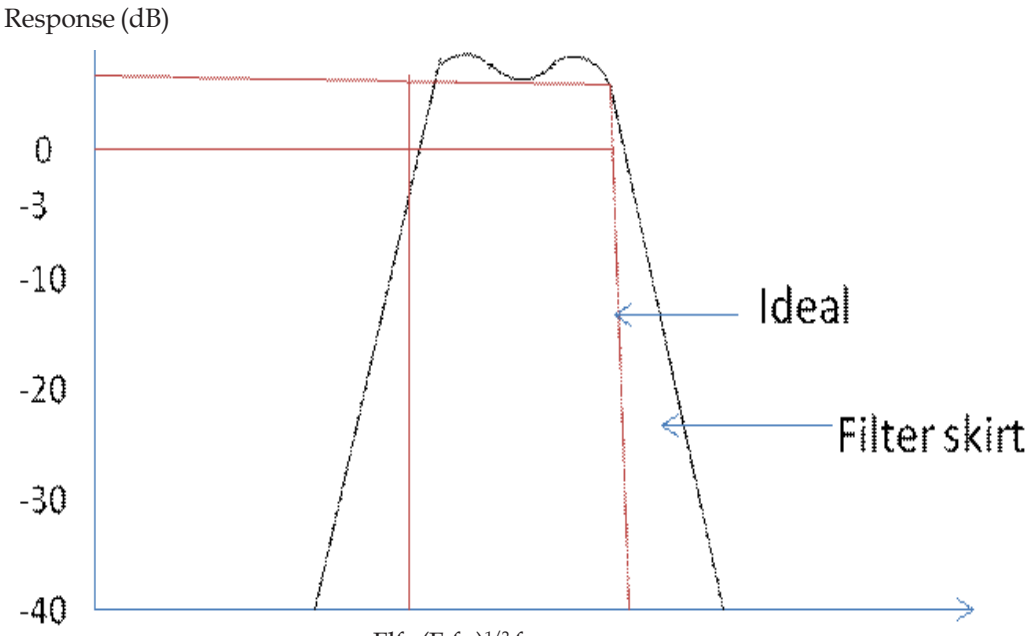

Response of a filter

end

3. CONCLUSION

The partticular feature of acoustic emission (AE) is its ability to directly detect the processes associated with wear and degradation (including friction, impacts, crushing, cracking, turbulance etc.). Another convenient feature of AE signals is that they generally have a high signal to noise ratio (SNR) which means that the signals related to machine condition can be clearly seen and are not buried in other consequential signals. This is a direct consequence of the high frequency and resonant nature of an AE sensor response. AE sensors, signals and positive consequences in practical terms. In the frequency domain a modified peak ratio was proposed and was proven to a better indicator than the original peak ratio references. Likewise many more properties could be enumerated.

4. REFERENCES

[1] Journal of Sound and Vibration.
[2] Asme Journal of Vibration and Acoustics
[3] Journal of the Acousticval Society of America
[4] Noise and Vibration Worldwide
[5] SINGARASU S. RAO, Mechanical Vibrations.
[6] SHIGLEY, Thoery of Machines.
[7] THOMAS BEVAN, Thoery of Machines.

Journal of Acoustical Society of India : Vol. 40, No. 3, 2013 (pp. 181-185)

A Study on the Effect of Sea Surface on Different Underwater Signals

R.P. Raju and P. Balasubramanian
Naval Physical and Oceanographic Laboratory, Kochi-682 021 (Kerala)

[Received: 05.04.2013; Revised: 28.05.2013; Accepted: 19.06.2013]

ABSTRACT

Active SONARs employ different signals like Continuous wave (CW) and Linear Frequency Modulated wave [LFM] for detection, range-bearing estimation and classification of targets.During propagation, these signals interact with sea-surface and sea-bottom. In an earlier paper1 [Acoustic waves (Proceedings of NSA-2011), Chapter 41, pp 392-40], the effect of the sea bottom on the shape and spectrum of the signals was brought out. In this paper, the effect of sea-surface on the shape and spectrum of the propagating signals is analyzed. A Pierson-Moskovitz sea-surface spectrum is employed to generate different surface realizations corresponding to different wind speeds. A Parabolic Equation Model based on Split-step Pade approximation is used to simulate the channel impulse response and received time series for different signals. This study will be highly useful for SONAR engineers in designing the SONARs.

1. INTRODUCTION

Active SONARs use different kinds of acoustic waveforms to detect the targets. The propagation of these signals is modeled to predict the range of SONAR corresponding to the prevailing ocean conditions. The modeling of acoustic wave propagation in ocean involves modeling of interaction of the acoustic wave with the medium and the ocean boundaries. Sea surface and bottom constitute the boundaries of ocean. In most of the cases the root mean square wave height of the sea surface is considered to calculate the reflection coefficient of the sea surface using empirical formulae. In this paper the undulations of the sea surface corresponding to different wind speeds are being generated using Pierson-Moskovitz (P-M) spectrum. A study on the effect of undulated sea surface on acoustic wave propagation is done using a parabolic equation (PE) model based on split-step Pade approximation.

2. METHODOLOGY

The PE model is a wave-theory based approach to formulate and solve problems of acoustic propagation in a medium. PE approach involves reducing the elliptic Helmholtz wave equation to parabolic differential equation by paraxial approximation[2]. The parabolic equation can be solved by various methods.

A broadband PE model based on split-step Pade approximation[2] which can include coordinates of the undulated sea surface as an input has been implemented. The sea surface scattering is included in this PE model by using conformal mapping technique[2]. Also, the sea surface has been generated from P-M wave number spectrum by using methodology outlined by Thorsos, I E, et al[3] (1988). This PE model is used to generate channel impulse response and received time series.

3. CASE STUDY AND RESULTS

The effect of sea surface on acoustic signals like LFM and CW pulse in two different ocean environments is studied. The summer and winter ocean environment parameters (Table 1) are fixed and sea surface is varied for three wind speeds. The received time series is generated for a range of 5000 m. The received time series is subjected to replica correlation. Replica correlation is a good tool to evaluate the change in shape and spectrum of a transmitted signal after propagation. In this case study the effect of sea surface will be evaluated using replica correlation, as only sea surface is varied for two different ocean environments. The received time series and replica correlator outputs for LFM signal are presented in Table 2. The received time series and replica correlator output for CW pulse is presented in Table 3.

Table 1. Ocean Environment

Environment	Depth of water column, m	Depth, m	Sound speed in water, ms^{-1}	Sound speed in sediment, ms^{-1}	Density of sediment, Kg m^{-3}	Attenuation in sediment, dB λ^{-1}
Summer[4]	100	0 20 50 100	1494.0 1494.3 1490.6 1491.3	1560	1800	1.00
Winter[4]	100	0 100	1490.0 1492.0	1560	1800	1.00

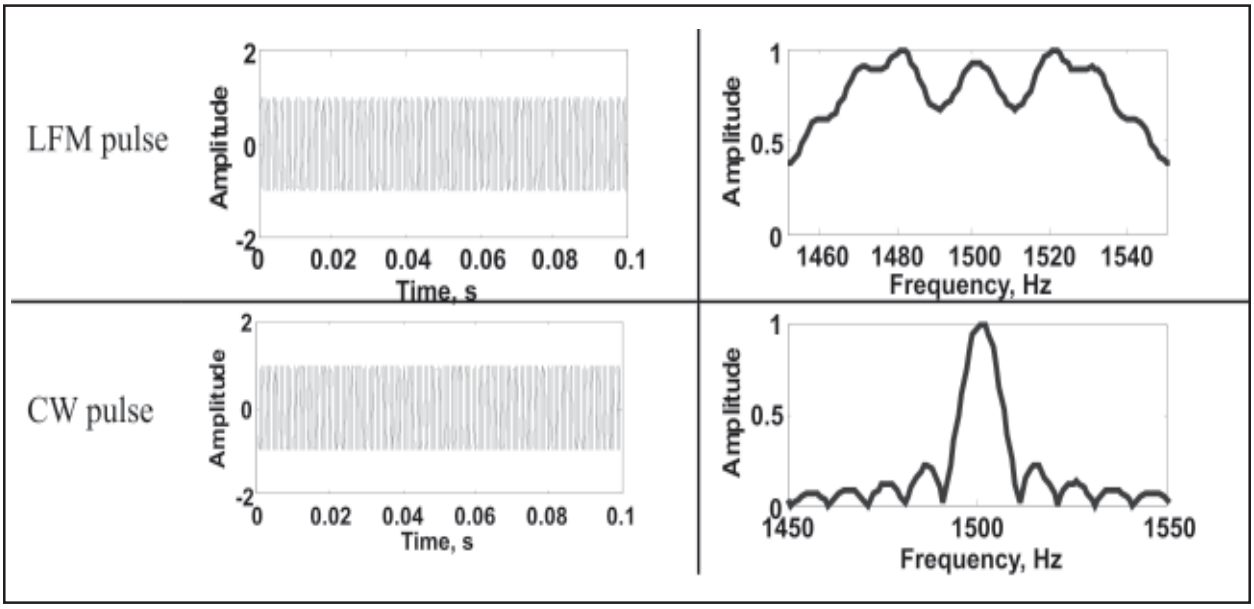

Fig. 1. Transmitted signal (Time series and frequency spectrum)

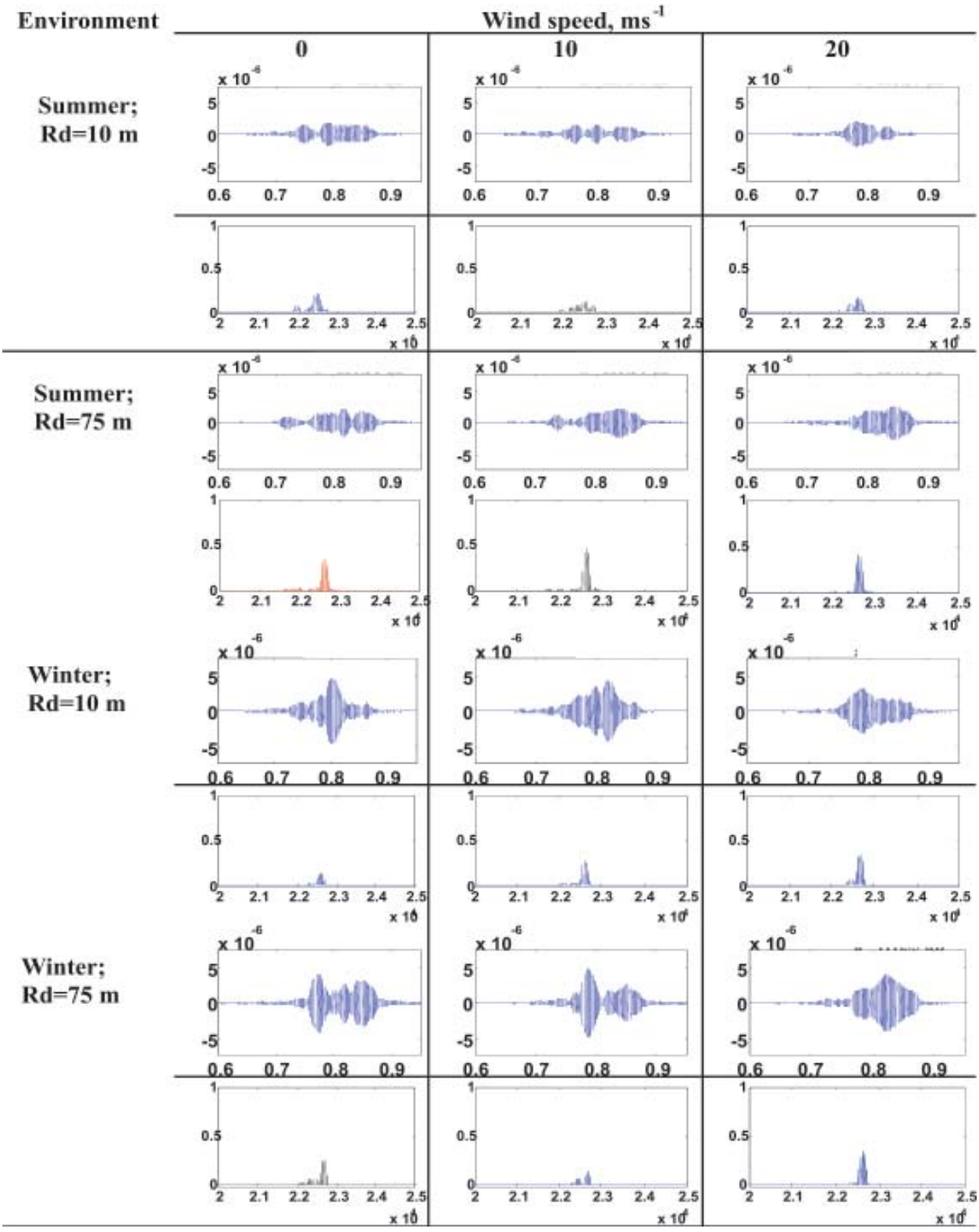

Table 2. Received time series and Replica correlator outputs for LFM signal

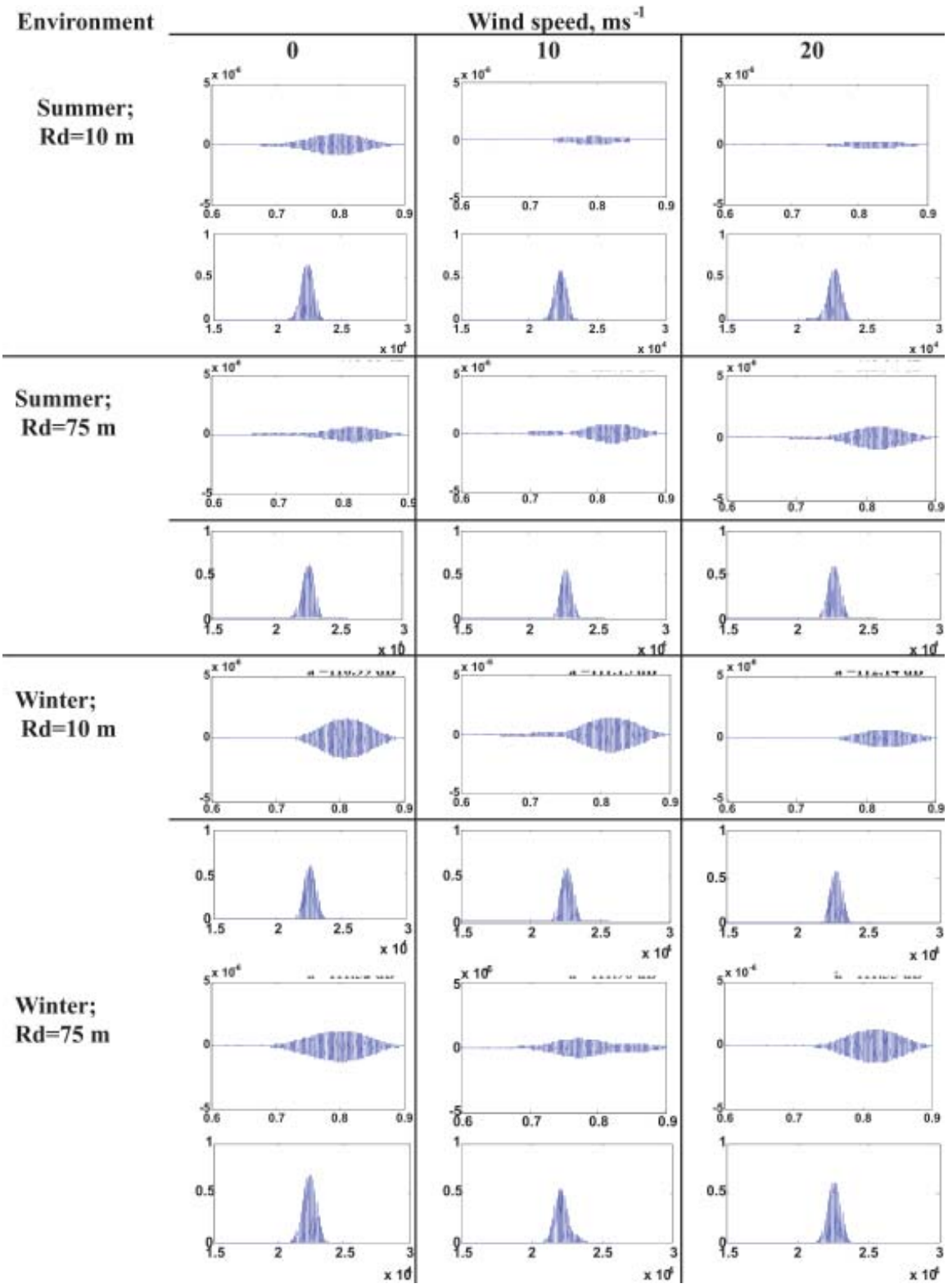

Table 3. Received time series and Replica correlator outputs for CW pulse

Propagation Model used: Broadband PE Model (Split-step Pade approximation)
Sea surface realization: P-M spectrum for wind speeds of 0, 10, 20 ms-1
Source depth: 50 m
Receiver Depth, Rd: 10 m and 75 m, Range: 5000 m
Waveform: 0.1 s LFM signal with a bandwidth of 100 Hz centered at 1500 Hz. (Fig.1)
0.1 s CW pulse of frequency 1500 Hz. (Fig. 1)

The plots in table 2 and 3 clearly indicate the distortion of the transmitted signal. The LFM and CW signals are stretched to approximately 0.2 s. The replica correlator outputs in Table 2 indicate that the received signals at a depth of 75 m are more correlated to the transmitted LFM signal than the ones received at 10 m. Also, in winter environment at 10 m depth the maximum correlation value increases as the wind speed increases from 0 to 20 ms-1. The maximum correlation at 10 m receiver is very low and the pulse may not be detected in a noise-limited environment after replica correlation. The rough sea surface leads to higher propagation losses4 and lower pulse distortion in the given environments. In case of flat sea surface, the trade-off is between low propagation losses and higher correlation in signals at 75 m depth. And in case of Rd at 10 m the trade-off is between high propagation losses and lower correlation in received signals.

In case of CW pulses it is observed from table 3 that there is not much change in the maximum correlation value (0.5-0.6) between received and transmitted signal due to change in the sea surface. But, the shape of the signal changes after propagation.

4. CONCLUSION

A broadband PE model based on split-step Pade approximation has been implemented. The effect of sea surface on acoustic pulse is clearly shown for the cases considered. The distortion in the pulse due to one-way propagation is characterized by low correlation values. The distortion in transmitted signal has to be considered during the implementation of detection techniques like Replica correlation, as it fails to be effective in realistic ocean conditions.

REFERENCES

[1] P. BALASUBRAMANIAN *et al*., 2011. *Acoustic waves*, **41,** 392-401.
[2] M.D. COLLINS, 1993. A split-step Pade solution for the Parabolic Equation Method", *JASA,* **93**, 1736-1742.
[3] E.I. THORSOS, 1990. Acoustic scattering from a "Pierson-Moskovitz" sea surface", *JASA*, **88**(**1**), 335-349.
[4] D.A. MILES, *et al*., 2003. Forward scattering of pulses from a rough sea surface by Fourier synthesis of parabolic equation solutions, *JASA*, **114**(**3**), 1266-1280.

Journal of Acoustical Society of India : Vol. 40, No. 3, 2013 (pp.186-190)

Effect of Harmonium Usage in Hindustani Music Performances: A Signal Processing Approach

Kaushik Banerjee, Anirban Patranabis, Ranjan Sengupta and Dipak Ghosh
Sir C V Raman Centre for Physics and Music, Jadavpur University, Kolkata-700 032 (WB)

[Received: 11.12.2012; Revised: 19.06.2013; Accepted: 09.05.2013]

ABSTRACT

In this paper we attempted to find out the influence of harmonium usage (ET scale) on the raga renderings in Hindustani music. The pitch period was extracted from 17 renderings of 12 eminent vocalists of Hindustani music, for two different ragas. Only the steady pitch periods were used for analysis. The approach was to study the duration distribution of steady pitch states against the ratio of each note in an octave. Prominent peaks indicate preferred ratios. Attempt was made to see whether these ratios obey ET scale or Indian 22 sruti intervals. The result shows that most of the vocalists follow a mixture of both systems with a preference of any one depending on the raga.

1. INTRODUCTION

Hindustani music (HM) has had some uniqueness and so it has been highly esteemed by the rest of the world. In HM, swara (note) is conceived not merely as a sound of fixed pitch position, but as the entire tonal range between itself and its previous swara. Though this interval can be theoretically divided into infinitesimal parts, the ancient musicologists believed that only a limited number, not exceeding four, sounds could be distinctly cognized by the ear in a swara-interval. These cognizable sounds are known as Srutis and the interval, which separated one swara from the next, was measured in terms of Srutis. Sruti was thought of both as the least audible interval between two sounds, as well as the sounds themselves, which were separated, by such an interval. The total number of Srutis was fixed unambiguously at 22 in ancient, musical treatises [1]. The tradition of teaching HM is an oral one. It is taught directly by the guru to the disciple, without the use of textual material. The basics starting from voice culture to the understanding of notes and Srutis are taught through direct oral communication accompanying with only tanpura. It was showed that the use of Srutis varies with gharanas as well as with the ragas and has also a student- teacher relationship [2]. It is likely that each gharana may have its own sense of aesthetic satisfaction of a raga and the use of Sruti may reflect these. It is also known that musicians feel that a particular note sounds better when placed relatively low for a particular raga while it may have to be raised much higher for some other raga. For example some say that komal re needs to be placed high in Todi but low in Bhairav. In the later part of the British rule in India, western musical instrument Harmonium (using ET scale) was introduced in HM in about middle of 19th century. The instrument was much nourished and developed in the eastern part of Indian, especially in Kolkata [3].

This paper presents the Sruti position as revealed from the performances of contemporary and older generation singers. Regarding the use of Srutis by the singers, substantive and distinctive preferences to different Srutis in two different ragas (Bhairav and Todi) are studied particularly in the context of the usage of Harmonium (ET scale).

2. EXPERIMENTAL DETAILS

17 renderings on two ragas namely Bhairav and Todi, sung by 12 singers from different gharanas of Hindustani music, collected from different archives, were taken for the study. For our analysis only slow tempo parts (mostly Vilambit Vistar) of each sample was selected from each raga. The digitization of the signal is done at the rate of 44100 samples/sec (16 bits/sample) in mono channel. Signal files, stored as 'wav files', are thus selected for analysis, which constitute the database. Pitch was extracted at 10 milliseconds interval using open source software Wavesurfer of KTH, Stockholm. Extraction of notes from the pitch profile needs the knowledge of the tonic used by the player. A skilled musician was requested to listen to the signal files one after another to detect the position of tonic Sa in the signal file. Cool edit software of Syntrellium corporation was used for further signal processing. The finding of the ratio-intervals is done by first dividing the smoothed pitch values for each song by the pitch value of the 'Sa', tonic of that raga rendering. This gives the frequency ratios for each pitch data. From the ratio data, steady state sequences are created with all consecutive pitch in a sequence, which is terminated when $| x_{i+1} - M | > M/30$ where $M = (1/i) \Sigma x_i$. If the duration of any sequence were less than that of a certain minimum value (60 milliseconds for this experiment) then the sequence is rejected. Elements of these sequences are considered as suitable candidate data for this analysis [4]. Whenever the ratio is less than 1 it is multiplied by a factor of 2 and when it is greater than 2 it is divided by 2. This effectively folds all pitch data into the middle octave. These are now distributed in 1200 bins of one-cent width each. The peaks of these distributions for each song are purported to be indicative of the Sruti positions for that raga rendering.

3. RESULTS AND DISCUSSION

Aim of this study is to examine closely the calculated Sruti intervals [5] for individual performers, which reveals discreet well-defined finer structures of their Sruti position. It also reveals that the sounds having two different pitches in the same Sruti-interval have the same note value and are identical in this perceptual sense. However in terms of consonance with another sound, these two may behave quite differently. One may be in consonance while the other may not. In this sense they are perceptually differentiable. This differentiability demands cognizance at least in modal music [6].

A Euclidean distance measurement technique (eqn. 1) is used to find the nearest neighbour of 22 Sruti intervals from that of ET scale.

$$d(p,q) = \sqrt{(p_1-q_1)^2+(p_2-q_2)^2+...+(p_i-q_i)^2+...+(p_n-q_n)^2} \quad (1)$$

As per the calculated minimum distance i.e. the nearest neighbour, values closer to 22 Srutis are marked in italics in TableS 1 and 2 while values closer to ET scale are in normal font.

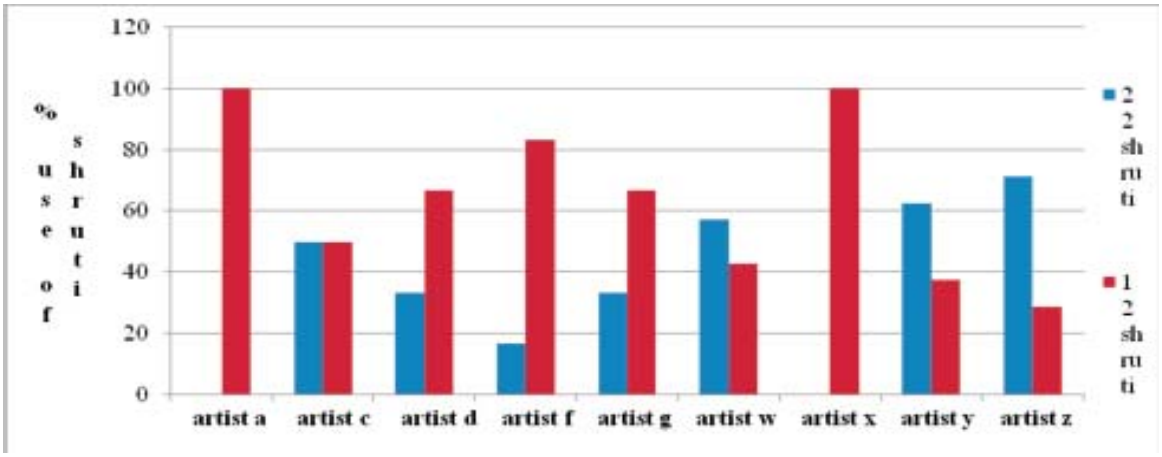

Fig. 1. Usage of Sruti by nine artists in raga Todi

Table 1. Sruti positions obtained from raga Todi for nine artists

Ratio (22)	Artist a	Artist c	Artist d	Artist f	Artist g	Artist w	Artist x	Artist	Artist z
sa	1.000	1.000	1.000	1.000	1.000	1.000	1.000	1.000	1.000
r1			*1.051*					*1.050*	
r2	1.059	1.061		1.050	1.059	1.060	1.061		1.061
r3									
r4			*1.158*			1.123		*1.136*	
g1	1.186			1.185	1.189		1.185		*1.179*
g2		*1.200*							
g3									
g4						*1.262*		*1.256*	
m1									
m2								1.333	1.338
m3		*1.413*	1.417			*1.412*	1.420	1.416	*1.401*
m4	1.428			1.427	1.431				
pa	1.497	1.498	1.501	*1.508*	*1.514*	*1.509*	1.488	*1.506*	*1.507*
d1					1.575				
d2	1.582	*1.597*	1.591	1.583			1.586		*1.597*
d3									
d4						1.681			
n1									
n2									
n3								*1.819*	
n4	1.910	1.903	1.893	1.903	*1.926*	*1.920*	1.890	1.888	*1.920*

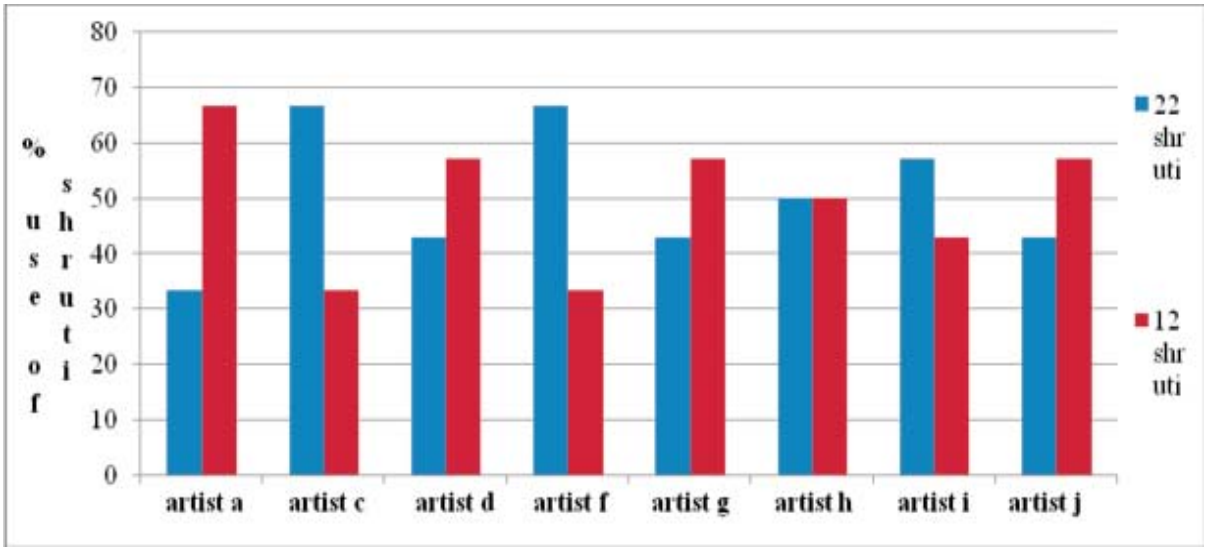

Fig. 2. Usage of sruti by eight artists in raga Bhairav

Table 2. Sruti positions obtained from raga Bhairav for eight artists

Ratio (22)	artist a	artist c	artist d	artist f	artist g	artist h	artist i	artist j
sa	1.000	1.000	1.000	1.000	1.000	1.000	1.000	1.000
r1		*1.043*			*1.047*	*1.053*	*1.043*	*1.049*
r2	1.061		1.058	1.059			*1.078*	
r3								
r4								
g1								
g2		*1.209*						
g3								
g4	*1.265*		*1.263*	*1.263*	*1.266*	*1.258*	1.263	*1.261*
m1		*1.313*					*1.327*	
m2	1.334		1.336	1.335	1.333	1.330		1.332
m3						*1.411*		
m4								
pa	*1.506*	1.498	*1.512*	*1.517*	*1.510*		1.494	1.497
d1		*1.562*				1.583		1.571
d2	1.593		1.596	*1.601*	1.586		1.588	
d3								
d4								
n1								*1.709*
n2					1.764			
n3			*1.795*					
n4	1.906	1.869	1.906	*1.914*	1.875	1.896	1.896	1.886

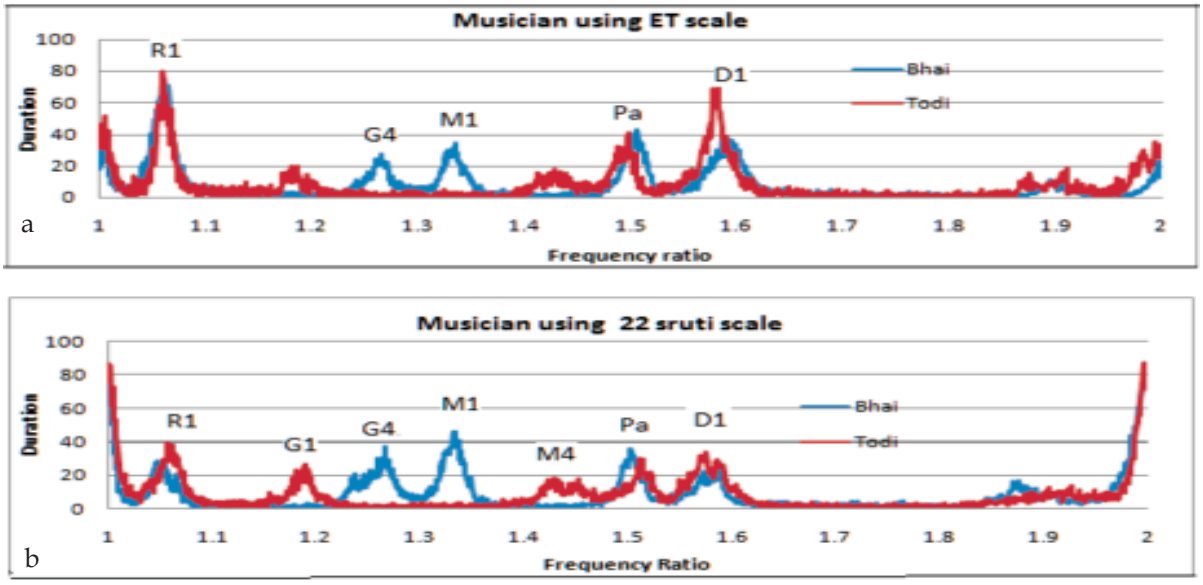

Fig. 3. (a and b). Frequency distribution of two renderings of raga Bhairav and Todi spread over 1200 bins of 1-cent interval. The peaks can be easily identified with the ratios, which correspond to different Sruti positions utilized by the artist in the rendering.

Usage of 22 Srutis (microtonal intervals) are perceptually distinguishable than that use of ET scale. And according to some people 22 Srutis are more pleasant to listen. Possibly the frequent use of harmonium as an accompaniment for some artists make their ratios mostly matched with the ET scale.

It is being observed from the tables and Figs. 1 and 2 that some musicians are using ET scale ratios and some musicians are using mixed ratios both 22 srutis and ET scale.

Figure 3 (a and b) shows the frequency of occurrence of the duration of ratio of the steady pitch periods and Sa (tonic) folded to middle octave and distributed over 100bins of one cent interval. Thus each peak corresponds to a note utilized by the artist in the raga. The height of the peak gives the number of times the note is sung in the processed signal. It is being observed from the distributions that the singer (a) uses ET scale mostly and the singer (b) uses the Indian Sruti system.

4 CONCLUSION

Influence of harmonium have enabled the vocalists of HM to deviate from the older 22 Sruti interval system and at present most of the musicians either follow a mixed system of ET and 22 Sruti intervals or purely ET scale. There is also a preference of the system on the raga

5. REFERENCES

[1] R.K. SHRINGLY and PREM LATA SHARMA, 1989. Sangitaratnakara of Saraingadeva (vol - II) : Text & English translation. Published by - Munshiram Manoharlal Publishers Pvt. Ltd. Delhi.

[2] ASOKE KUMAR DATTA, RANJAN SENGUPTA,NITYANANDA DEY and DIPALI NAG, 2006. "Experimental Analysis of Srutis from performances in Hindustani music", Monograph published by Scientific Research Department, ITC Sangeet Research Academy, ISBN 81-903818-0-6.

[3] http://en.wikipedia.org/wiki/Harmonium#India

[4] A.K. DATTA, 2006. "A methodology of note extraction from the song signals", Proc. Frontiers of Research on Speech and Music.

[5] A.K. DATTA and R. SENGUPTA *et al.*, 2004. "Sruti usage by old and contemporary singers in Khyal: An objective approach", Proc. Frontiers of Research on Speech and Music (FRSM-2004), Annamalai University, Tamilnadu, India

[6] A.K. DATTA and R. SENGUPTA *et al.*, 2011. "Objective analysis of srutis from the vocal performances of Hindustani Music using Clustering Algorithm", Published in EUNOMIOS - An open online journal for Theory, Analysis and Semiotics of Music, http://www.eunomios.org/.

[7] JOAN SERR`A, GOPALA K. KODURI, MARIUS MIRON and XAVIER SERRA, 2011."Assessing the tuning of sung Indian classical music", Int. Soc. for Music Information Retrieval Conf. (ISMIR), Miami, USA.

Journal of Acoustical Society of India : Vol. 40, No. 3, 2013 (pp. 191-195)

Numerical Investigation of Non-Cavitating Underwater Propeller Noise using FW-H Method

V. Rama Krishna[1], P.V.S. Ganesh Kumar[1], P. BangaruBabu[2] and S. Rama Krishna[3]

[1]*Naval Science and Technological Laboratory, Visakhapatnam, (AP)*
[2]*National Institute of Technology (NIT), Warangal, (AP)*
[3]*G V P College of Engineering, Madhurawada, Visakhapatnam, (AP)*

[Received: 15.12.2012; Revised: 22.06.2013; Accepted: 15.05.2013]

ABSTRACT

The Propeller is a vital component which is subtle for the safe operation of a ship at sea. The purpose of the propeller is to produce a thrust causing to move the ship in forward direction. But it is identified as major noise source. The noise produced by a propeller is very much importance to warship designers and military strategists for many years. A ship /Submarine noise signature of a few tens of watts could be sufficient to give enemy valuable information at a considerable range. Using noise signature analysis at remote locations, it is possible not only to determine which class of vessel has been located, but also if character of signature is sufficiently known to identify the particular ship. Clearly the ultimate goal of a warship designer must be to make the ship's signature vanish into the background noise of the sea which comprises contributions from the weather, marine life and also other shipping from a wide geographical area. This paper presents a numerical study on the non-cavitating noises of the underwater propeller using Computational Fluid Dynamics (CFD) Fluent software.Propeller behavior is investigated for its hydrodynamic parameters and then Computational Acoustic Analysis (CAA) is carried out using viscous model of large eddy simulation of Ffowcs Williams-Hawkings formulation(FW-H). Here solver is chosen as pressure based, unsteady formulation of second order implicit. Noise is predicted using time-domain acoustic analogy and finite volume method. Sound pressure levels are predicted at different receiver positions.

1. INTRODUCTION

Sound generated by a propeller is critical in underwater detection, and is often related to the survivability of the vessels especially for military purposes. Marine propeller noise can be classified into cavitating and non-cavitating noise. Cavitation of the marine propeller is the most prevalent source of underwater sound in oceans and is often the dominant noise source of a single marine vehicle.However, submarines and torpedoes are usually operated deep enough under the sea to avoid cavitation. Salvatore et al. [1] presented propeller-induced noise emission is studied through a general hydro acoustics formulation based on the Ffowcs Williams-Hawkings (FW-H) equation that allows describing the acoustic pressure field generated by lifting bodies in arbitrary motion through a fluid. Chang [2] applied a finite volume CFD method in conjuction with the standard k-? turbulence model to calculate the flow pattern and performance parameters of a DTNSRDC P4119 marine propeller in a uniform flow.

The essential step taken by Lighthill [3] was to incorporate the non-linear features of aerodynamic sound generation into a linear acoustic model. There are various ways to evaluate Ffowcs Williams and Hawkings [4] equation and the three types of noise source terms (monopole, dipole, and quadrupole) were proposed. Farrasat and Myers [5] proposed a time-domain formulation that can predict noise from an arbitrarily shaped object in motion without the numerical differentiation of the observer time. Through these studies, the dominant noise source of marine propellers is analyzed, which will provide basis for proper noise control strategies under non-cavitating conditions. Jin-minget al. [6] analyzed the blade frequency noise of non-cavitation propeller in a uniform flow in time domain. The unsteady loading (dipole source) on the blade surface is calculated by a potential-based surface panel method. Then the time-dependent pressure data is used as the input for FW-H formulation to predict the acoustic pressure.Yang et al. [7] presented a new method to measure the propeller noise level in the ship engineering by coupling with Large Eddy Simulation and boundary element numerical acoustics methods in the frequency domain to predict the underwater non cavitation noise of ship.

Compared with the extensive amount of literature concerning cavitation noise of propellers, works concerning the non-cavitation noise of propellers are hard to find and also many authors used Reynolds-averaged Navier- Stokes (RANS) for turbulence modelling. However RANS have limitation of capturing details of such transient events like unsteady force and pressure fluctuation of the blade with an acceptable accuracy. In that regard, Large Eddy Simulation (LES) has been considered having merits to resolve the least large scale turbulent structures, which is further justifiable for the unsteady flow around propellers operated at the stern of ships.

So in this paper an attempt is made to predict non-cavitation noise of propeller using FW-H equation coupled with LES computer code based on cell-centered finite volume method (FVM) on unstructured meshes for viscous flow field around propeller.

2. FFOWCS WILLIAMS-HAWKINGS EQUATION

The theory of hydrodynamic sound was developed by Lighthill [3], who rewrote the Navier-Stokes equations into an exact, inhomogeneous wave equation whose source terms are important only within the turbulent region. Lighthill acoustic analogy equation is given below

$$\left(\frac{1}{c^2}\frac{\partial^2}{\partial t^2}\nabla^2\right)\left[c^2\left(\rho-\rho_0\right)\right]=\frac{\partial^2 T_{ij}}{\partial_{xi}\partial_{xj}} \tag{1}$$

F fowcs Williams and Hawkings [4] extended the acoustic analogy developed by Lighthill [3], by taking into account the displacement of a rigid surface placed in the flow. The essential step taken by Lighthill was to incorporate the non-linear features of aerodynamic sound generation into a linear acoustic model. The acoustic analogy generalized by Ffowcs Williams and Hawkings is often applied in the prediction of the noise emission generated by the rotors of helicopters, axial fans, propellers etc. Ffowcs Williams & Hawkings equation is written in the following form:

$$\frac{1\partial^2 p}{c^2\partial t^2}-\Delta^2 p=\frac{\partial q}{\partial t}-\frac{\partial F_i}{\partial x_i}+\frac{\partial^2 T_{IJ}}{\partial x_i \partial x_j} \tag{2}$$

and shows three types of sources on the right hand side:

1) Monopolar, which results from introducing a mass (per unit volume) into the considered area.

2) Dipolar, that takes into account the hydrodynamic forces (Fi).

3) Quadrupolar, due to the turbulence and represented by the Lighthill's tensor.

The noise due to the hydrodynamic forces applied to the surface of the blades is dominant compared to the other sources of noise in the case of subsonic flow fans. The Ffowcs Williams - Hawkings equation is an exact rearrangement of the continuity and the momentum into the form of an inhomogeneous wave equation. This equation has two surface source terms, known as thickness and loading sources, and a volume source term, known as the quadruple source derived from the original Lighthill theory.

3. PROBLEM DESCRIPTION AND METHODOLOGY

In the present paper, propeller consisting of seven blades was considered for study. The diameter of propeller is 3.1m and hub to propeller diameter ratio is 0.2. In the present simulations for prediction of non-cavitation noise of propeller at rotating speed of propeller is taken as 242 rpm and the speed of ship is 9.26m/sec.

Modeling of the propeller is done using CATIA V5R16. In order to model the blade, it is necessary to have sections of the propeller at various radii. These sections are drawn and rotated through their respective pitch angles. Then all rotated sections are projected onto right circular cylinders of respective radii as shown in Fig. 1. Now by using multi section surface option, the blade is modelled. After enclosing the entire surfaces solid is created as shown in Fig. 2.

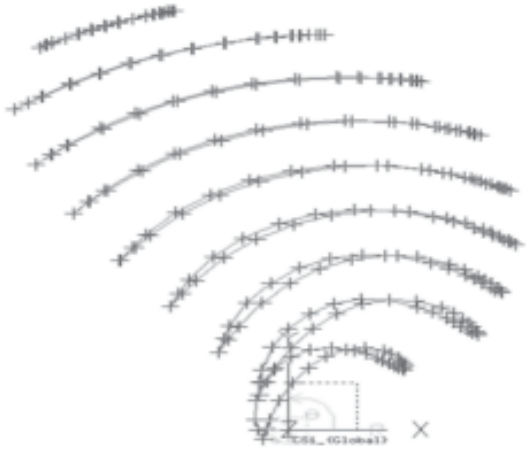

Fig. 1. Points on surface of the blade

Fig. 2. Solid model of Propeller

The objective of the present CFD and CAA analyses is to find overall SPL of a propeller at receiver positions. Three dimensional structural tetrahedral grids are generated to descretize the domain. In order to obtain better results tetrahedral element has been used by taking advantage of mesh consistency. The domain is discretized by minimum 10 linear elements per source wavelength to increase the accuracy of the acoustic propagation. Commercially available grid generation code GAMBIT is used to mesh the entire domain of propeller. Convergence is checked with various element sizes and it is observed that close results are observed with element size 10 and beyond. Hence finally element size 10 is used for mesh generation. After convergence there are 436445 and 680134 tetrahedral elements in the inner volume (propeller volume) and outer volume (far field volume) respectively. Figure 3. shows the meshed model of propeller in inner volume.

The numerical simulations have been carried out with a finite volume code method using FLUENT. The turbulent nature of the flow is incorporated through the LES. LES is chosen as viscous model because, it needs time dependent solution for hydrodynamic solution and it is not highly dependent on geometrical conditions. For steady-state simulations, the Multiple Reference Frames (MRF) model is used, and for unsteady simulations, the sliding mesh model is adopted. Surfaces that rotate relatively are defined as "moving wall". Moreover, as

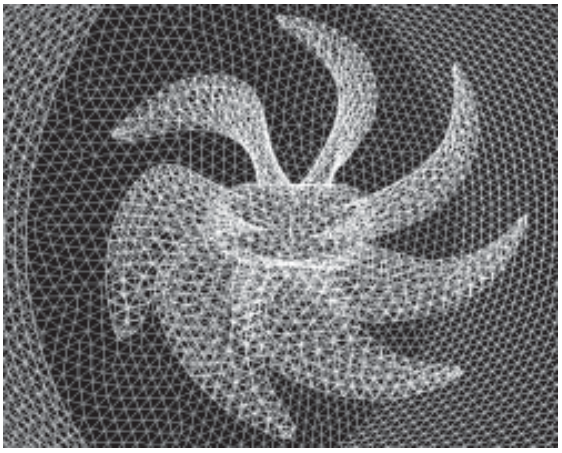

Fig. 3. Meshed model of propeller

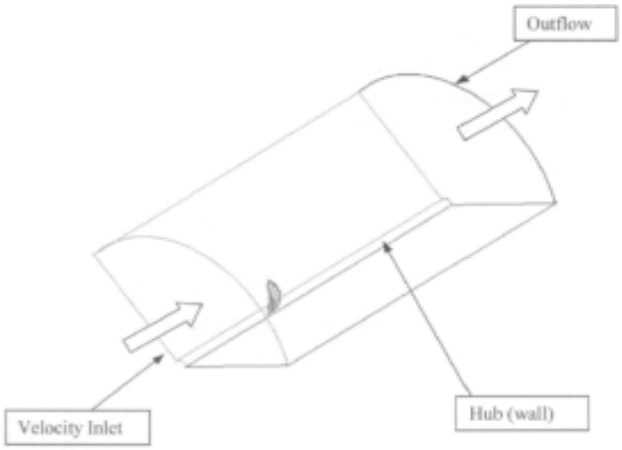

Fig. 4. Boundary conditions on propeller domain

they are dependent on the fluid around them and as they rotate, they are defined as "relative to adjacent cell zone" and "rotational motion". Cylinder walls are defined as "stationary wall" and the inlet and outlet are defined as "velocity inlet (9.26m/sec)" and "outflow". Fluid zone in the inner volume is defined as "moving mesh" and 242 rpm in x-direction. However, fluid in the outer volume is defined as "velocity inlet (9.26m/sec)". Fig. 4. shows the boundary conditions on entire domain of propeller. In order to give sliding mesh property, the same surfaces in the inner and outer volume families are defined as "interface", and then merged equations resolved iteratively at time increment of 6.88×10-4s for angular speed of 242rpm. Solution is stopped when changes in solution variables from one iteration to the next is negligible.

4. RESULTS AND DISCUSSION

Basic flow fields of propeller are obtained using a LES solver around the 7-bladed propeller in uniform flow and noise prediction results are presented for non-cavitating propeller at different receiver positions. The density and speed of sound in the sea water are considered as 1026 kg/m3 and 1500 m/s, respectively for the present simulations. The receiver positions considered are 10m and 15m in radial direction to the propeller. Fig 5 and 6 show the noise prediction graphs at 10m and 15m corrected to 1m from propeller. Fig. 5 and 6 clearly show that peak SPL values are observed at shaft rotational frequency. The basic noise source in propeller is dipolar noise source as generated due to hydrodynamic pressure fluctuation.

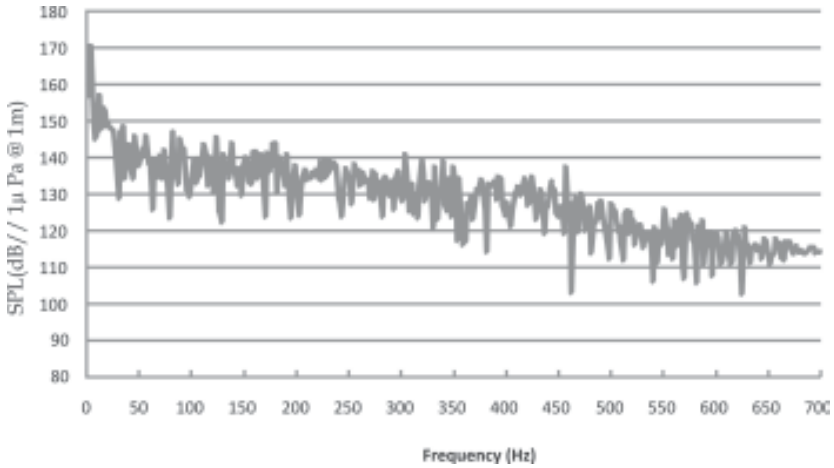

Fig. 5. Noise prediction graph for receiver at 10m corrected to 1m distance from propeller

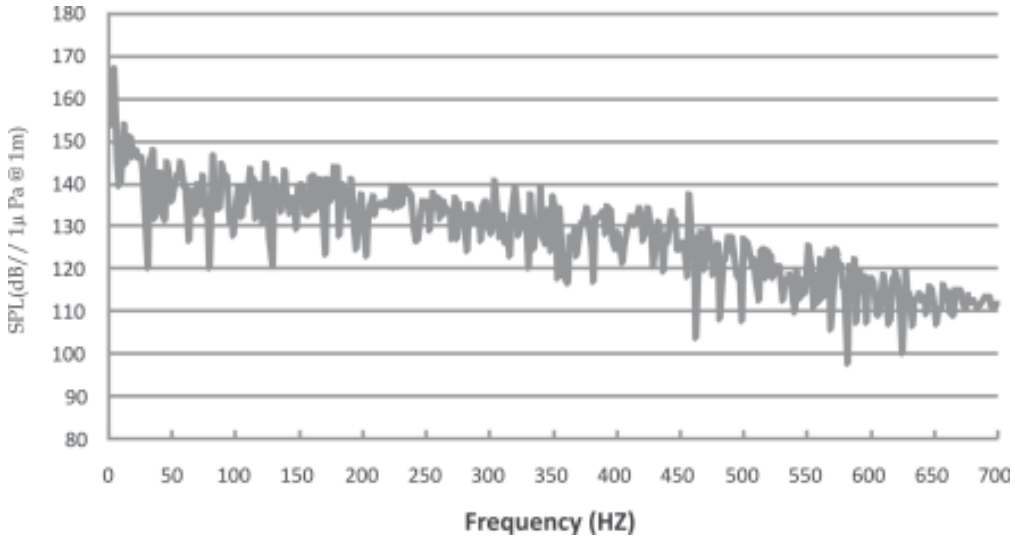

Fig. 6. Noise prediction graph for receiver at 15m corrected to 1m distance from propeller

5. CONCLUSION

Non-cavitation noise generated by underwater propeller has been analysed numericallyin this study using FW-H equation.Sound pressure levels are predicted and plotted at different receiver positions. From this study, noise prediction methodology has been developed with LES and FW-H equation.

6. ACKNOWLEDGMENT

Authors expresses their sincere thanks to Sri S.V.Rangarajan, Sc'H', Director NSTL, Visakhapatnam for his continuous support for publishing this paper.

7. REFERENCES

[1] F. SALVATORE, C. TESTA, S. IANNIELLO, and F. PEREIRA, 2006, Theoretical and modelling of unsteady cavitation and induced noise, INSEAN, Italian Ship Model Basin, Rome, Italy. Sixth International Symposium on Cavitation, CAV2006, Wageningen, The Netherlands.

[2] B. CHANG, 1998, Application of CFD to P4119 Propeller, 22nd ITTC Propeller RANS/Panel Method Workshop, France.

[3] M. J. LIGHTHILL, 1952, On sound generated aerodynamically: I. General theory, Proc. Royal Society (London), A 211, pp. 564-587, 1952.

[4] J.E. FFOWCS WILLIAMS and D.L. HAWKINGS, 1969, Sound generated by turbulence and surfaces in arbitrary motion, Philosophical transactions of Royal Society Series, A 264, No. 1151, pp. 321-342.

[5] F. FARASSAT and M.K. MYERS, 1988, Extensions of Kirchhoffs formula to radiation from moving surfaces, Journal of Sound and vibration, **123**(**3**), p. 451.

[6] JIN-MING YE, YING XIONG, CHANG-RUN XIAO and YI BI, 2012, Prediction of non-cavitation propeller noise in time domain, China Ocean Engineering, **25**(**3**), p. 531.

[7] Q. YANG, Y. WANG and M. ZHANG, 2011, Calculation of propeller's load noise using LES and BEM numerical acoustics coupling methods, Transactions of the Wessex Institute, Paper DOI: 10.2495/BE110081.

Journal of Acoustical Society of India : Vol. 40, No. 3, 2013 (pp.196-202)

Acoustical Behavior of NN Dimethyl-acetamide and Acetone at 313.15 K

R.A. Patil[1]*, Prashant Dabrase[2] and B.M. Suryavanshi[3]
[1]*S.S.S.K.R.Innani Mahavidyalaya, Karanja-444 105*
[2]*Bhalerao Science College, Saoner-441 107*
[3]*Department of Physics, Government Institute of Science, Nagpur-440 001 (MS)*
**e-mail: vgs.mpl@gmail.com*

[Received: 18.12.2012; Revised: 24.06.2013; Accepted: 18.05.2013]

ABSTRACT

The measurements of Ultrasonic velocities (υ), density (ρ) and viscosity (η) of pure & binary liquid mixtures of Acetone and N-N dimethyl acetamide have been carried out over the entire range of composition at temperature 313.15K to evaluate the other thermo dynamical parameters with their excess values such as adiabatic compressibility (β_α), free length (L_f), free volume (V_f), internal pressure (π_i) and their excess values, υ^E, $\beta_\alpha{}^E$, $L_f{}^E$, $V_f{}^E$ and $\pi_i{}^E$. The results thus obtained are discussed for molecular interaction with varying composition of binary system. The non linearity found in all the plots of these ultrasonic parameters and their excess values with the composition range indicates presence of the intermolecular interaction between the components of the unlike molecules of the mixture. The nature of excess values of the β_α, L_f, V_f and π_i conforms about the existence of the molecular association between the components of the mixture.

1. INTRODUCTION

There are many physical methods which play an important role in determining molecular structure & molecular properties of different materials. In recent years the advances in the ultrasonic technique has become a powerful tool in evaluating information about the physical and chemical behavior of molecules of the liquids [1-4]. The ultrasonic studies of the liquids are most preferred in many fields such as pharmaceutical industry, biomedical research, automobile industry, chemical industry, water research & scattering spectroscopy, etc.[5]. The information of density (ρ), ultrasonic velocity (υ) and viscosity (η) of the pure liquids and their mixtures plays very important role in different applications that include surface facilities, pipeline systems & mass transfer operations.

Here in the present study the ultrasonic velocity, density and viscosity measurements have been carried out for determination of ultrasonic parameters such as compressibility (β_α), molecular free length (L_f), free volume (V_f) and internal pressure (π_i) and their excess values (υ^E, $\beta_\alpha{}^E$, $L_f{}^E$, $V_f{}^E$ and $\pi_i{}^E$.) for the different composition range of NN-Dimethyl acetamide in acetone at the temperature 313.15K. The variations of these parameters with concentration of binary liquid mixtures are studied to understand molecular interaction between unlike molecules of the mixtures.

2. EXPERIMENTAL

The binary mixtures of the chemicals Acetone and NN- dimethyl acetamide for different range of composition were prepared at room temperature and kept in a special airtight glass bottles to avoid air contact. The chemicals

used here are of analytical reagent (AR) and used without further purification. The mixtures prepared are used within 24 hours of its preparation. The densities of the binary mixtures & pure liquids were measured using 25ml specific gravity bottle and a sensitive mono pan balance (K-Roy, K-12 classic) within ±0.1mg accuracy. The ultrasonic interferometer (Mittal enterprises, New Delhi, India) is a single and direct device to determine ultrasonic velocity in liquids with a high degree of accuracy [6]. Here the measurements of ultrasonic velocities were carried out on single crystal multi frequency ultrasonic interferometer operating at 1MHz (M-81). The constant temperature of the liquid inside the interferometer cell was maintained by circulating water through the outer jacket by electronically controlled thermostat. Accuracy of measurement of ultrasonic velocity was within ± 0.01m/s and the temperature of the test liquids during measurement were maintained within an accuracy of ± 0.1°C. The viscosity of the liquids and their mixtures are measured using the suspended level viscometer.

The experimentally measured ultrasonic velocity (υ) measured in ms^{-1}, density (ρ) in kgm^{-3} and viscosity (η) in Nsm^{-2} are used to evaluate various thermo dynamical parameters like---

Adiabatic compressibility (β_α),

$$\beta_\alpha = 1/\upsilon^2\rho \tag{1}$$

Intermolecular free length (L_f)

$$L_f = K\beta_\alpha^{1/2} \tag{2}$$

where, K is temperature dependant constant 211.25×10^{-8} at 313.15 K and T - absolute temperature [7],

$$V_f = \left[\frac{M_{eff}}{k_\eta}\nu\right]^{3/2} \tag{3}$$

where M_{eff} is the effective molecular weight ($M_{eff} = \Sigma m_i X_i$ in which mi and X_i are the molecular weight and mole fraction of the individual constituents respectively), k is temperature independent constant which is equal to 4.28×10^9 for all liquids.

$$= brt\ (k\eta/\nu)^{1/2}\ (\rho^{2/3}/M^{7/6}_{eff}) \tag{4}$$

where k is a constant, T is the absolute temperature; b is a constant equal to 2 for the liquid and the excess values are determined by using the relation

$$A^E = A_{exp} - A_{id} \tag{5}$$

A^E - excess parameters of all acoustic parameters, $Aid = \sum_{i-1}^{n} A_i X_i$, A_i is any acoustical parameter and X_i - the mole fraction of liquid component.

3. RESULTS AND DISCUSSION

The measured values of densities (ρ) and ultrasonic velocities (υ) of the pure liquids and their binary mixtures along with viscosity (η) were used to obtain the adiabatic compressibility (β_α), free length (L_f), free volume (V_f) and internal pressure (π_i) at different concentration and temperatures 313.15K and reported in (table 01). It is observed that Ultrasonic velocity (υ), density (ρ) and viscosity (η) increases with increase in the mole fraction of NN-dimethyl acetamide, in the binary mixture. The table observes the trends of all given acoustical parameters with variation in concentration at temperature 313.15K. The Ultrasonic velocity (υ) increases with concentration of mixture and the corresponding density also increases. As observed from the table 01. the values of viscosity increases with the increasing concentration and the same trend is observed for the internal pressure. The compressibility values shows decreasing trend with the increasing concentration of NN-Dymethyl-acetamide

(NN DMA) in the mixture. The same nature as that of compressibility is also observed in the free length and in the free volume values. The increase in ultrasonic velocity may be attributed to the cohesion. The values of adiabatic compressibility (β_α) and free length (L_f) decreases with increase in the mole fraction of N-N dymethyl acetamide and increases with temperature this suggests making and breaking of hydrogen bonding. The greater the attractive force among the molecules, the smaller will be the compressibility thus indicates formation of a complex [8]. The intermolecular free length depends upon intermolecular attractive and repulsive force. Eyring & Kincard have proposed that free length is a predominating factor in determining the variation of ultrasonic velocity of solutions [9, 10]. The decrease in adiabatic compressibility suggests that there is significant interaction between unlike molecules. The internal pressure first decreases and then increases due to various degree of dispersive interactions and coloumbic interactions existing between the component molecules [11].The free length and free volume values shows decreasing trends with increase in the concentration of NN DMA hence it can be concluded that there is significant interaction between the two liquids due to which the structural arrangement is also affected [12].

In order to highlight the presence of intermolecular interaction between molecules it is essential to study the excess parameters. The deviation of the physical properties of the liquid mixtures from the ideal behavior is a measure of interaction between the molecules which may be due to the either adhesive or cohesive force. Table 2 presents the values of excess velocity (υ^E), excess adiabatic compressibility (β_α^E), excess free length (L_f^E), excess free volume (V_f^E) and excess internal pressure (π_i^E).

The values of excess free length (L_f^E) are supported by the variation of excess compressibility exhibits interaction in the system. The excess compressibility and excess free length are negative which indicates the strong molecular interaction between the components. Negative excess free length indicates the ultrasonic wave's needs to cover larger distance because of dominant nature of interaction between unlike molecules [13]. The excess ultrasonic velocity (υ^E) for the binary mixture is observed to be positive. The positive deviation and non-linear dependence suggests the presence of strong interaction between the components of mixture [14]. According to Fort & Moore, a negative volume is an indication of strong hetero-molecular interaction in the liquid mixtures and is attributed to charge- transfer, dipole-dipole, dipole -induced dipole interactions & hydrogen bonding between the unlike compounds, while a positive sign indicates a weak interaction & is attributed to dispersive force, which are likely to be operative [15,16]. The excess free volume (V_f^E) and excess internal pressure (π_i^E) are also negative which convey that the chances of induced dipole-dipole interactions are overruled & strong dipolar interactions alone are conformed [17].

Table 1. Density, ultrasonic velocity, viscosity, and other thermodynamic parameters such as (β_α, L_f, V_f, and π_i for Acetone + NN- Dimethyl acetamide mixtures at temperature 313.15 -K

Mole fraction NNDMA	Density ρ kgm^{-3}	Velocity υ ms^{-1}	Compre-ssibility β_α $10^{-10}m^2N^{-1}$	Viscosity η μ Pas	Free L_f $\times10^{-8}$	Free V_f $\times10^{-16}$ m $\times10^8$ mole	Internal Pressure π_i m^3/ Pa
0.0000	771.610	1108.372	10.549	241.509	6.861	4.915	3.701
0.1024	791.959	1143.366	9.658	270.059	6.565	4.694	3.699
0.2103	813.891	1184.769	8.753	304.876	6.249	4.449	3.709
0.3240	832.431	1221.158	8.055	344.315	5.995	4.182	3.717
0.4441	853.262	1261.263	7.367	390.075	5.733	3.927	3.732
0.5711	871.849	1302.111	6.764	452.007	5.494	3.563	3.780
0.7056	891.621	1331.429	6.326	514.49	5.313	3.274	3.815
0.8483	908.249	1367.657	5.886	593.028	5.125	2.976	3.853
1.0000	924.980	1400.059	5.515	685.660	4.961	2.680	3.901

Table 2. Excess values of Ultrasonic Velocity and other thermodynamic parameters β_α^E, L_f^E, V_f^E and π_i for Acetone + NN-Dimethyl acetamide mixtures at temperature 313.15 K

Mole fraction NNDMA	Excess velocity υ^E ms^{-1}	Compressibility β_α^E $\times 10^{-10}$ m_2N^{-1}	Free length L_f^E $\times 10^{-8}m$	Free volume V_f^E $\times 10^{-17}$ m^3/mole	Internal pressure π_i^E $\times 10^8$ Pa
0.0000	0	0	0	0	0
0.1024	5.1049	-0.3747	-0.1013	0.0845	-0.0231
0.2103	15.0393	-0.7373	-0.2117	0.0482	-0.0346
0.3240	18.250	-0.8621	-0.2497	-0.0802	-0.0491
0.4441	23.3267	-0.9461	-0.2834	0.0475	-0.0587
0.5711	27.1344	-0.9092	-0.2815	-0.7515	-0.0354
0.7056	17.2221	-0.6703	-0.2069	-0.6307	-0.0276
0.8483	11.8318	-0.3925	-0.1241	-0.4275	-0.0183
1.0000	0	0	0	0	0

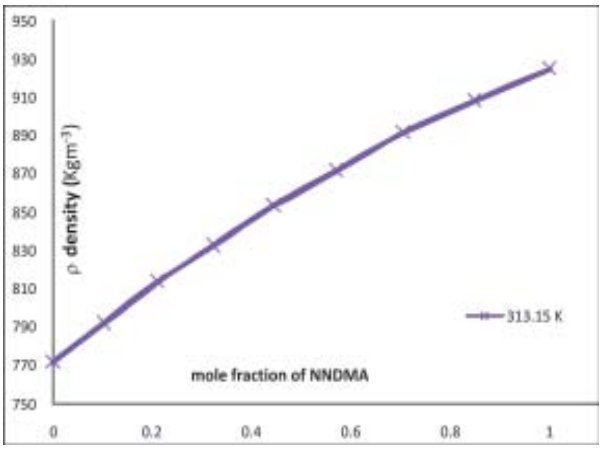

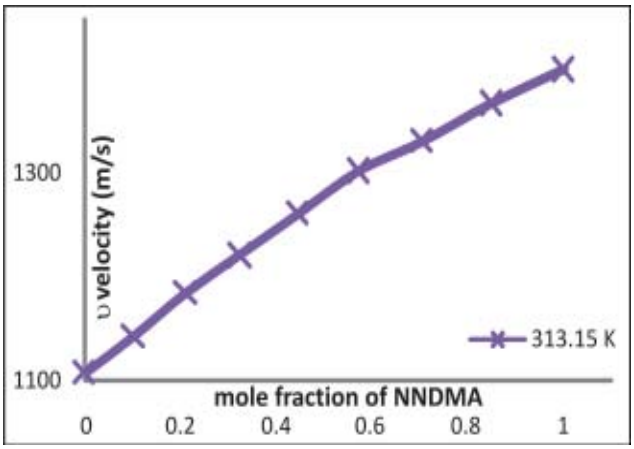

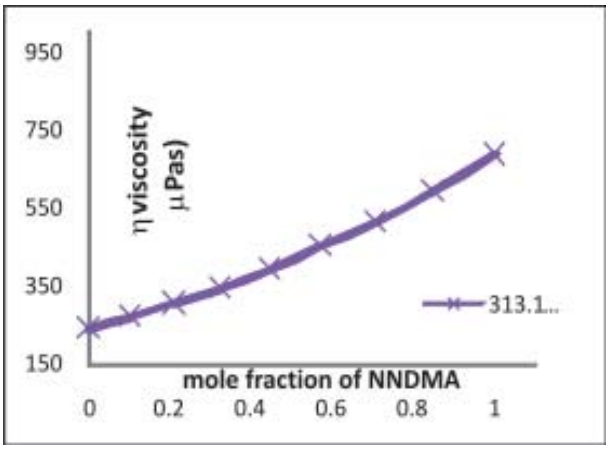

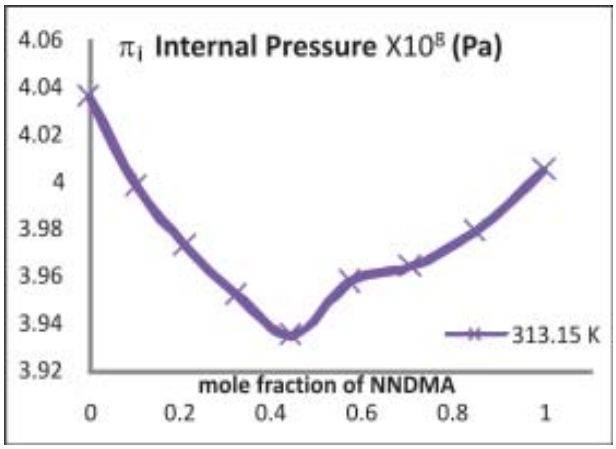

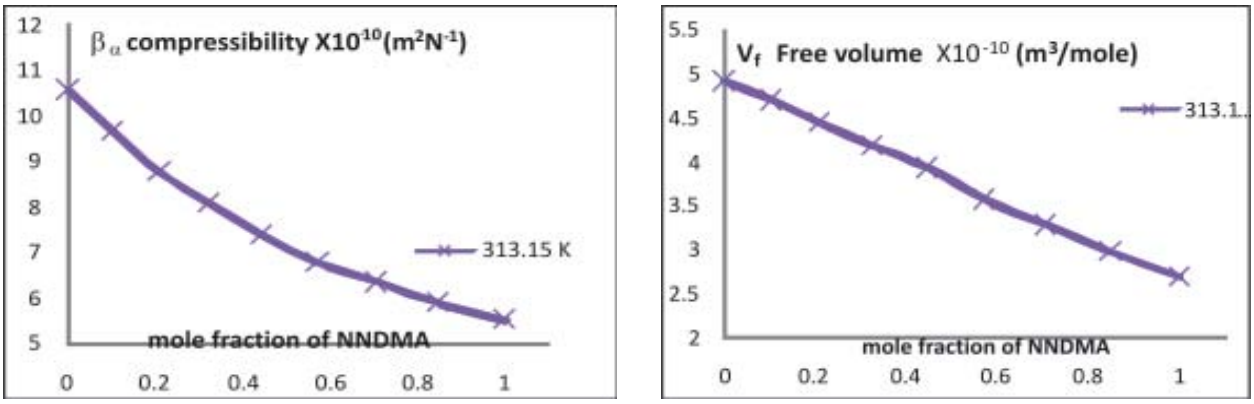

Fig. 1. Density, ultrasonic velocity, viscosity, β_{α}, L_f, V_f, & π_i for Acetone + NN- Dimethyl acetamide mixtures at temperature 313.15K.

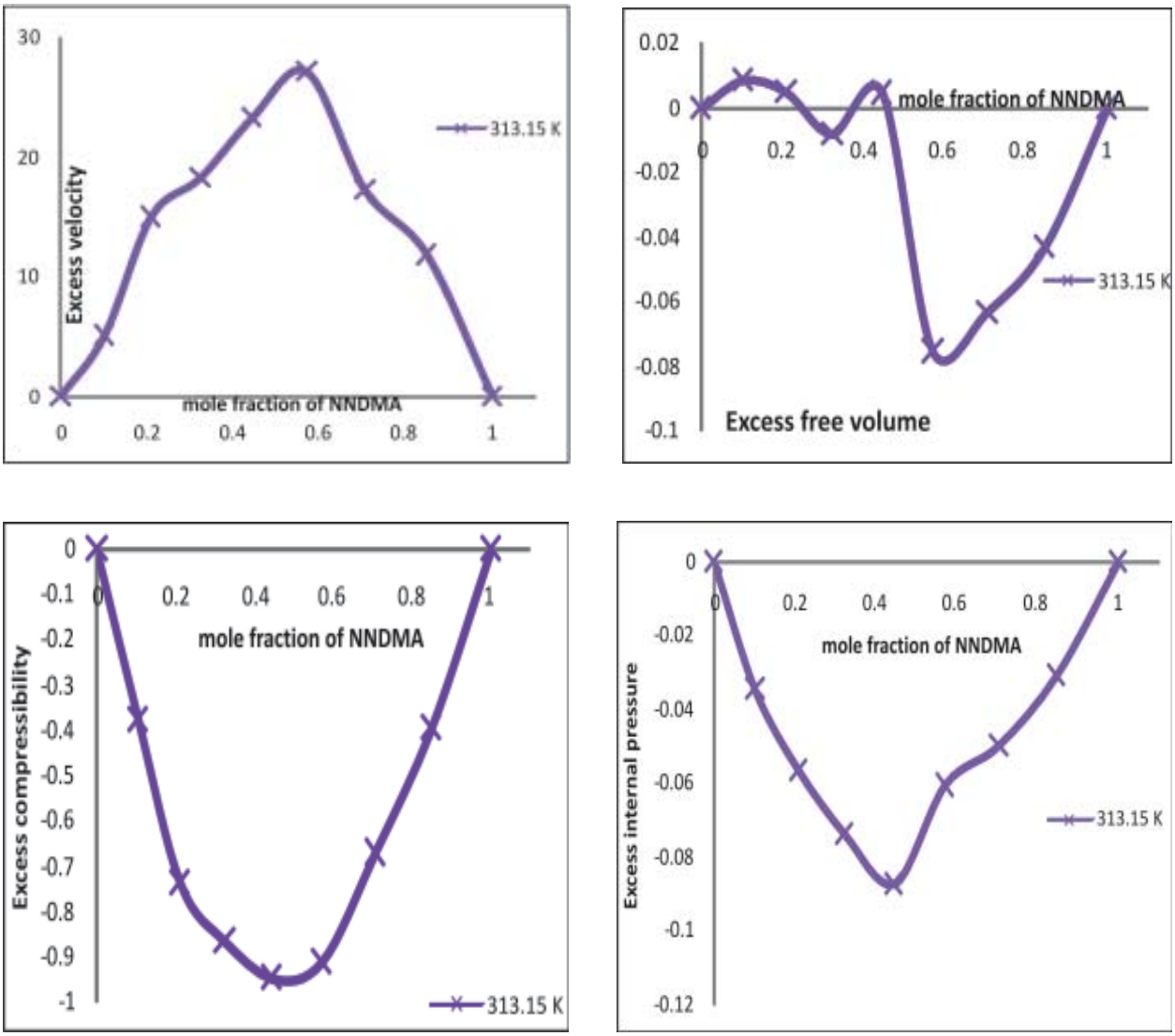

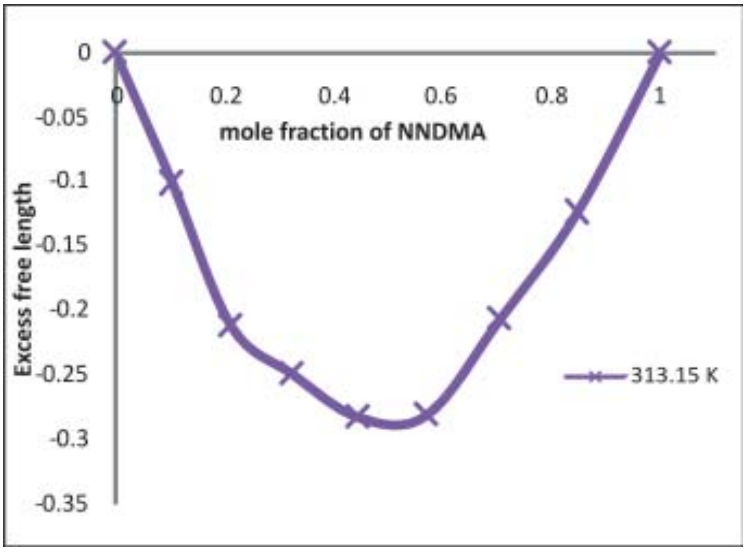

Fig. 2. Excess values of ultrasonic velocity β_α^E, L_f^E, V_f^E and π_i^E for Acetone + NN-Dimethyl acetamide mixtures at temperature 313.15K

Thus it is clear from the above evaluated parameters that there is a strong association between the acetone and NN -dimethyl acetamide molecules exists after 0.4 mole fraction of the NNDMA in the mixture.

4. CONCLUSION

The ultrasonic velocity, density and viscosity measurements have been carried out for determination of ultrasonic parameters such as compressibility (β_α), molecular free length (L_f), free volume (V_f) and internal pressure (π_i) and their excess values (υ^E, β_α^E, L_f^E, V_f^E and π_i^E) for the different composition range of NN-Dimethyl acetamide in acetone at the temperature 313.15 K.

The present investigations lead us to conclude that the excess values of thermodynamic parameters are sensitive to the molecular association present in the liquid mixture. The negative values of excess compressibility (β_α^E), excess free length (L_f^E) & excess internal pressure (π_i^E) and the positive values of excess ultrasonic velocity (E) in the mixture shows the presence of strong dispersive dipole-dipole interaction between the components of molecule in the mixture. The non-linearity of the curve also supports the interaction exists. The interaction is strong after 0.4 mole fraction of N-N dimethyl acetamide in the mixture of acetone and NNDMA.

5. REFERENCES

[1] H. EYRING and J.F. KINCAID, 1938. *J. Chem. Phys*., **6**, 220-229.
[2] K.S. PITZER, 1995. *Thermodynamics*, 3rd edition (Mc.Graw-Hill book co, NY).
[3] A.N. KANNAPAN, S. THIRUMAM and R. PALANI, 2009. *J. Phys. Science*, **20** (**2**), 97-108
[4] V.A. TABHANE, S. GHOSH and S. AGRAWAL, 1999. *J. Pure and Appl. Ultrasonic*, **21**, p. 122.
[5] V. SRINIVASULU and P.R. NAIDU, 1995. *J. Pure and Appl. Ultrasonic*, **17**, 14-28
[6] K. SWAIN and P. PRIYADARSHANI, 2010. *Indian J.Pure and Appl. Phys*., **48**, 539-542.
[7] B. JACOBSON, 1952. Ultras Velo. of liquids and liquid mixtures, *J.Chem.Phys*., **20**, p. 927.
[8] R.P. VARMA and SURENDRA KUMAR, 2000. *Indian J. Pure and Appl. Phys*., **38**, p. 96.
[9] K. RAJGOPAL and S. CHENTHILNATH, *Indian J.Pure and Appl. Phys.*
[10] A.N. KANNAPPAN and V. RAJENDRAN, 1991. *Indian J.Pure and Appl. Phys*., **29**, 465-468.
[11] M.K. PRAHARAJ and A. SATAPATHY *ET AL*., 2012. *J. Chem & Pharm. Research*, **4**(**4**), 1910-1920.
[12] H. EYRING and J.F. KINCAID, 1938. *J. Chem.Phys.*, **6**, 620-629.
[13] SHRIVASTAVA and DUBEY, 1985. *Indian J. Pure and Appl. Phys*.,
[14] P.B. DABRASE, R.A. PATIL and B.M. SURYAVANSHI, 2012. *App. Ultra.*, (Shree Publi, N Delhi, 233-241).

[15] R.T. FORT and W.R. MOORE, 1966. **Trans. Farad. Soc**., **62**, p. 1112.
[16] MOH. A. WAHAB *ET AL*., 2002. *Bull. Korean Chem. Soc*., **23** (**7**), 953-956.
[17] S. SOUNDHARAM, 2010. *Acta Ciencia India*, **XXXII** (**2**), p. 285.
[18] ALKA TADLKAR, PRAVINA PAWAR and GBICHILE, 2011. *J. Chem. Pharm. Research*, **3**(**3**), 165-168.

Journal of Acoustical Society of India : Vol. 40, No. 3, 2013 (pp.203-206)

Automatic Gear Teeth Defect Localization using Acoustic and Vibration Signal in Time Domain

Dibya Prakash Jena and S.N. Panigrahi*
School of Mechanical Science, Indian Institute of Technology Bhubaneswar
**e-mail: psatyan@iitbbs.ac.in*

[Received: 20.12.2012; Revised: 28.06.2013; Accepted: 22.05.2013]

ABSTRACT

In present work a customized gear mesh test setup is prepared. The acoustic and vibration signals are captured by introducing seeded defects in gear teeth. The bursts have been observed in time domain signals with presence of defects and are focused in analysis. A signal processing scheme is proposed for automatic defect identification and localization of the fault in time domain. Towards this, the proposed scheme initially denoises the signals to improve the sharpness of the burst. The Discrete Wavelet Transform (DWT) has been shown suitable in enhancing the peak of the signal burst. The time frequency information of denoised signals are computed by implementing Complex Morlet Wavelet Transform (CMWT). Furthermore, the instantaneous power spectrum is computed by integrating coefficients in time domain. A multi scale based wavelet peak detection technique is used to extract the peaks of the spectrum in time domain. The proposed technique has been evaluated and validated with captured acoustic and vibration signals. Experimental investigations reveal that the proposed technique can be implemented in real-time condition monitoring and fault diagnosis of gear systems.

1. INTRODUCTION

Gear system is a prime component of rotating machines, power transmissions, automobiles etc. Fault diagnosis and condition monitoring of such system is highly desired for predictive maintenance purpose. The feature of the amplitude modulated-frequency modulated gearbox fault signal usually cannot be directly extracted. Li and Liang have implemented the time-frequency analysis to diagnose gear box fault [1]. In recent years, Li *et al*. investigated mechanical fault diagnosis based on redundant second generation wavelet packet transform, neighborhood rough set and support vector machine. Wang et al. have investigated rotary system fault using dual-tree complex wavelet transform [3]. Moreover, one can find many literatures on implementation of DWT, CWT and DCT in non-stationary signal processing [4]. Rafiee *et al.* reported the importance on mother wavelet in wavelet transform in fault diagnosis [5].

From literature, one can find many reports on implementation of various techniques of signal processing but there is no single robust method to localize the signal burst (acoustic and vibration) in time domain to corroborate the defect in gear or bearing. In present work, a signal processing method is proposed based upon Continuous Morlet Wavelet Transform (CMWT) of the denoised signal followed by peak detection of the instantaneous power spectrum generated from scalogram.

2. PROPOSED TECHNIQUE

It is quite natural, that some time defect signature is carried by wider signal burst depends upon type of signal

and system. In such cases, the signals $x(t)$ is decomposed using discrete wavelet transform (DWT). In order to achieve a finer time frequency resolution, the decomposed detail component $D_n(t)$ processed through a continuous wavelet transform (CWT) to produce the two dimensional map of the CWT coefficients. The generated two dimensional maps of the CWT coefficients, $W\psi D_n(a,b)$, as defined below, correspond to maximum energy zone which helps in identifying the signal bursts due to defects in the piston-bore. Mathematically, the continuous wavelet transform of $x(t)$ is defined as its integral transform with a family of wavelet functions, $\psi_{ab}(t)$, described as [6,7]:

$$W_\psi D_n(a,b) = CWT(a,b) = \frac{1}{\sqrt{a}}\int_{-\infty}^{+\infty} D_n(t)\dot{\psi}\left(\frac{t-b}{a}\right)dt \text{ where } a>0, b\in\Re \quad (1)$$

where, ψ is the complex conjugate of the mother wavelet ψ. In present case, the complex Morlet wavelet is used as mother wavelet, i.e., $\psi(t) = (1/\sqrt{f_b\pi})\,e^{-t^2/f_b}\,e^{2\pi f_c t}$. The main advantage of CWT is its ability to provide information simultaneously in time and scale with adaptive windows. Next, the instantaneous power spectrum of the CWT coefficient spectrums is generated. A wavelet based multi-level peak detection technique is investigated to locate the signal burst in time domain. Finally, a simulated signal is generated having sharp peaks at the derived burst location and overlapped with signal $x(t)$ to provide sufficient information in time domain.

3. EXPERIMENT

Experiments are performed on gear mesh test setup, with driver gear having seeded defect in one tooth as shown in Figs. 1(a) and 1(b), respectively. One Behringer® ECM-8000 condenser microphone is mounted near the setup and a PCB® make internal excitation based piezoelectric (ICP) accelerometer with sensitivity of 50mV/g is mounted on bearing bracket to measure the generated acoustic emission and vibration. The acoustic and vibration signals are captured with the help of a NI SCXI-1530® DAQ system through a customized LabVIEW® based application. Experiments are conducted on a gear mesh test setup (the pinion, having 15 teeth, is meshed with driven gear of 30 teeth, and the driver shaft connected to a single phase 50Hz AC motor Crompton® make of power rating of 0.5 HP through a belt drive). The driver shaft operating frequency is maintained at 457 RPM. The faulty driven gear (gear defect type-1) is mounted on the driver shaft and the corresponding acoustic and vibration signals are captured and the signal sample of one second duration are shown in Figs. 2(c) and 3(c), respectively.

4. RESULTS AND DISCUSSION

At first the acquired acoustic signal is investigated with proposed algorithm. It is worth noticing that the

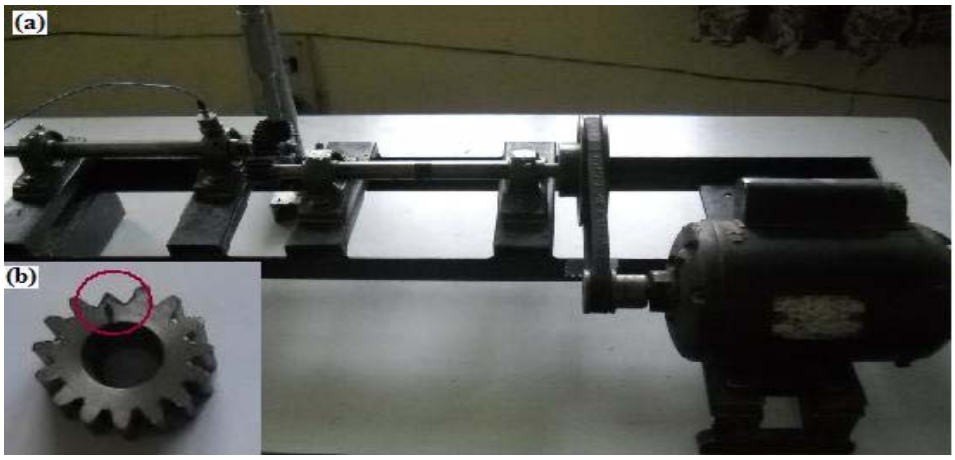

Fig. 1. Experiment; (a) Gear defect simulation test setup; (b) gear defect type-1

signal burst is having prominent width which needs to be enhanced. In order to achieve narrower peak, the acoustic signal *x(t)* (see Fig. 2(c)) is decomposed up to level 3 using discrete wavelet transform (DWT). Experimental investigation reveals that the coefficient (01), i.e., detail from the first level of decomposition $D_1(t)$ is suitable for further diagnosis. It is important to observe that the decomposition should not lose the desired signal attributes due to its down sampling properties. Next, the denoised signal $D_1(t)$ is investigated with Complex Morlet Wavelet Transform (CMWT). The generated scalogram is shown in Fig. 2(a). Then, the instantaneous power spectrum is generated from scalogram using a time marginal integration and is shown in Fig. 2(b). It is worth noticing that the instantaneous power spectrum is having sharper peak which corroborates well with signal burst due to defect in time domain. Next, a multi-scale wavelet peak detection algorithm is implemented to extract the peak location, as shown in Fig. 2(b). A synthetic signal is generated with sharper peak on time domain using extracted peak location and is overlapped with raw acoustic signal. Now, the defect localization is prominently visible without any ambiguity.

Subsequently, the acquired vibration signal is investigated with proposed algorithm. It is worth noticing that the signal bursts are sharper compared to acoustic signal, as shown in Fig. 3(c). In such cases un-necessary

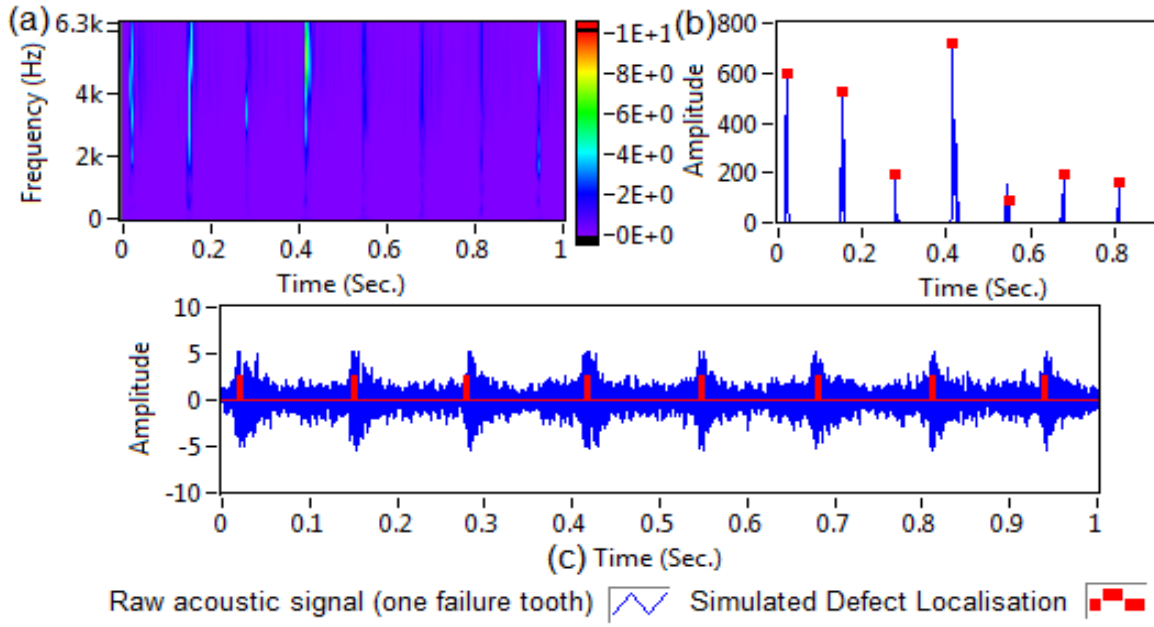

Fig. 2. Defect localization on acoustic signal using proposed technique; (a) scalogram from CMWT,(b) instantaneous power spectrum from scalogram, and (c) simulation of detected peak overlapped with raw signal.

signal processing is not encouraged and can be investigated as it is. In line with proposed method, the vibration signal *x(t)* is investigated with Complex Morlet Wavelet Transform (CMWT). The generated scalogram is shown in Fig. 3(a). Then, the instantaneous power spectrum is generated from scalogram using a time marginal integration and is shown in Fig. 3(b). It is worth noticing that the instantaneous power spectrum is having sharper peak which corroborates well with signal burst due to defect in time domain. Next, a multi-scale wavelet peak detection algorithm is implemented to extract the peak location, as shown in Fig. 3(b). A synthetic signal is generated with sharper peak on time domain using extracted peak location and is overlapped with raw acoustic signal. Now, the defect localization is prominently visible without any ambiguity. The precise signal burst localization corresponding to defect in time domain is achieved which is not reported by other investigators so far.

The x-axis (time domain) has been modified with a scale factor of 2742, i.e., (RPM/60× 360°) to convert the time axis into degrees of angular displacement of driver gear. It is worth noticing that the signal bursts are periodic in nature and having 360° periodicity. From experimental investigation, it is observed that acoustic

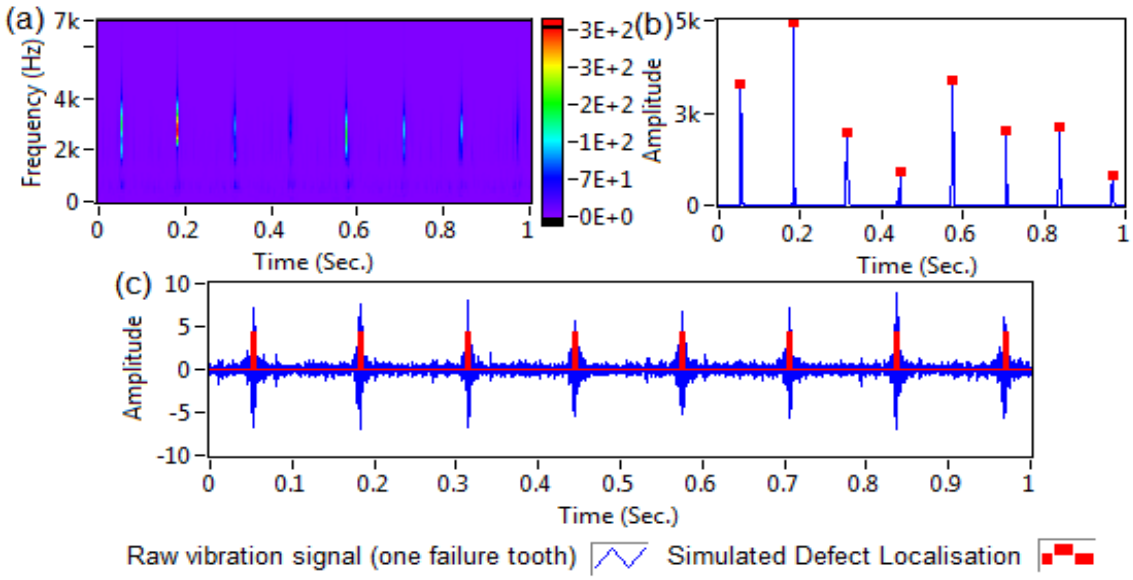

Fig. 3. Defect localization on vibration signal using proposed technique; (a) scalogram from CMWT, (b) instantaneous power spectrum from scalogram, and (c) simulation of detected peak overlapped with raw signal

signal inherent with more noise comparative to vibration signal. However, this proposed algorithm highly hinges on the signal and signal burst quality. On the demand of the situation, necessary denoising mechanism needs to be integrated to opt for the proposed method.

5. CONCLUSION

The experimental analysis presented here established a robust signal processing technique to localize the gear fault from acoustic and vibration signal together. The Continuous Morlet Wavelet Transform (CMWT) provides sufficient time-frequency resolution to analyze non-stationary acoustic and vibration signals. The instantaneous power spectrum generated from scalogram also corroborates well with signal burst, moreover, the peak detection technique localize the signal burst corresponding to defect precisely. Summarizing, the proposed method is suitable and reliable in localizing gear teeth fault in time domain using acoustic or vibration signals.

6. REFERENCES

[1] C. LI and M. LIANG, 2012. Time-frequency signal analysis for gearbox fault diagnosis using a generalized synchrosqueezing transform. *Mech. Syst. Signal Pr.*, **26**, 205-17.

[2] N. LI, R. ZHOU, Q. HU and X. LIU, 2012. Mechanical fault diagnosis based on redundant second generation wavelet packet transform, neighborhood rough set and support vector machine. *Mech. Syst. Signal Pr.*, **28**, 608-21.

[3] Y. WANG, Z., HE and Y. ZI, 2010. Enhancement of signal denoising and multiple fault signatures detecting in rotating machinery using dual-tree complex wavelet transform. *Mech. Syst. Signal Pr.*, **24**, 119-37.

[4] H. KHORRAMI and M. MOAVENIAN, 2010. A comparative study of DWT, CWT and DCT transformations in ECG arrhythmias classification. *Expert Syst. Appl.*, **37**, 5751-57.

[5] J. RAFIEE , M.A. RAFIEE and P.W. TSE, (2010. Application of mother wavelet functions for automatic gear and bearing fault diagnosis. *Expert Syst. Appl.*, **37**, 4568-79.

[6] R.B. RANDALL and J. ANTONI, 2011. Rolling element bearing diagnostics-A tutorial. *Mech. Syst. Signal Pr.*, **25**, 485-520.

[7] S. MALLAT, 2009. A wavelet tour of signal processing, 1st ed., Academic Press.

Acoustical Society of India
(Regn. No. 65-1971)

Executive Council (2010 - 2014)

President	:	**Dr V Rajendran** [KSRCT, Tiruchengode; veerajendran@gmail.com; +91-99 94 13 03 03]
Vice President	:	**NS Naidu** [NSTL, Vizag; nsnaidu04@yahoo.com; +91-94 90 75 05 82]
General Secretary	:	**PVS Ganesh Kumar** [NSTL, Vizag; gkpakki@rediffmail.com; +91-98 66 40 08 94]
Jt. Secretary	:	**Dr K Trinadh** [NSTL, Vizag; hello_trinath@yahoo.co.in; +91-97 04 71 95 00]
Treasurer	:	**Prof AV Sharma** [AU, Vizag; sarmavakella@yahoo.co.in; +91-94 90 43 17 26]
Chief Editor	:	**Dr Mahavir Singh** [CSIR-NPL, New Delhi; mahavir@nplindia.org; +91-98 71 69 33 46]
Council Members	:	**Dr SV Ranga Nayakulu** [VITAE, Hyderabad; nayakulu@rediffmail.com; +91-98 66 53 26 13]
		Dr I Johnson [SJ College, Trichy; jnaadarsh@hotmail.com; +91-94 42 90 48 20]
		Dr Rajiv K Upadhayay [Govt PG College, Rishikesh; rku8@rediffmail.com; +91-94 12 97 28 90]
		Dr S Shekhar [Oxford College, Trichy; acousticssekar@yahoo.co.in; +91-99 94 92 00 30]
		Dr V Bhujanga Rao [Past President; NSTL, Vizag; vepcrew1@rediffmail.com; +91-98 66 44 10 74]
Co-opted Members	:	**Rajshekhar Uchil** [Josts, Bangalore; ruchil@josts.in; +91-98 80 17 08 95]
		Dr NK Narayanan [CIT, Kozhikode; csirc@rediffmail.com; +91-94 46 95 58 30]

INFORMATION FOR AUTHORS

ARTICLES

The Journal of Acoustical Society of India (JASI) is a refereed publication published quarterly by the Acoustical Society of India (ASI). JASI includes refereed articles, technical notes, letters-to-the-editor, book review and announcements of general interest to readers.

Articles may be theoretical or experimental in nature. But those which combine theoretical and experimental approaches to solve acoustics problems are particularly welcome. Technical notes, letters-to-the-editor and announcements may also be submitted. Articles must not have been published previously in other engineering or scientific journals. Articles in the following are particularly encouraged: applied acoustics, acoustical materials, active noise & vibration control, bioacoustics, communication acoustics including speech, computational acoustics, electro-acoustics and audio engineering, environmental acoustics, musical acoustics, non-linear acoustics, noise, physical acoustics, physiological and psychological acoustics, quieter technologies, room and building acoustics, structural acoustics and vibration, ultrasonics, underwater acoustics.

Authors whose articles are accepted for publication must transfer copyright of their articles to the ASI. This transfer involves publication only and does not in any way alter the author's traditional right regarding his/her articles.

PREPARATION OF MANUSCRIPTS

All manuscripts are refereed by at least two referees and are reviewed by the Publication Committee (all editors) before acceptance. Manuscripts of articles and technical notes should be submitted for review electronically to the Chief Editor by e-mail or by express mail on a disc. JASI maintains a high standard in the reviewing process and only accept papers of high quality. On acceptance, revised articles of all authors should be submitted to the Chief Editor by e-mail or by express mail.

Text of the manuscript should be double-spaced on A4 size paper, subdivided by main headings-typed in upper and lower case flush centre, with one line of space above and below and sub-headings within a section-typed in upper and lower case understood, flush left, followed by a period. Sub-sub headings should be italic. Articles should be written so that readers in different fields of acoustics can understand them easily. Manuscripts are only published if not normally exceeding twenty double-spaced text pages. If figures and illustrations are included then normally they should be restricted to no more than twelve-fifteen.

The first page of manuscripts should include on separate lines, the title of article, the names, of authors, affiliations and mailing addresses of authors in upper and lowers case. Do not include the author's title, position or degrees. Give an adequate post office address including pin or other postal code and the name of the city. An abstract of not more than 200 words should be included with each article. References should be numbered consecutively throughout the article with the number appearing as a superscript at the end of the sentence unless such placement causes ambiguity. The references should be grouped together, double spaced at the end of the article on a separate page. Footnotes are discouraged. Abbreviations and special terms must be defined if used.

EQUATIONS

Mathematical expressions should be typewritten as completely as possible. Equation should be numbered consecutively throughout the body of the article at the right hand margin in parentheses. Use letters and numbers for any equations in an appendix: Appendix A: (A1, (A2), etc. Equation numbers in the running text should be enclosed in parentheses, i.e., Eq. (1), Eqs. (1a) and (2a). Figures should be referred to as Fig. 1, Fig. 2, etc. Reference to table is in full: Table 1, Table 2, etc. Metric units should be used: the preferred from of metric unit is the System International (SI).

REFERENCES

The order and style of information differs slightly between periodical and book references and between published and unpublished references, depending on the available publication entries. A few examples are shown below.

Periodicals:

[1] S.R. Pride and M.W. Haartsen, 1996. Electroseismic wave properties, *J. Acoust. Soc. Am.*, **100** (3), 1301-1315.

[2] S.-H. Kim and I. Lee, 1996. Aeroelastic analysis of a flexible airfoil with free play non-linearity, *J. Sound Vib.*, **193** (4), 823-846.

Books:

[1] E.S. Skudzryk, 1968. *Simple and Comlex Vibratory Systems*, the Pennsylvania State University Press, London.

[2] E.H. Dowell, 1975. *Aeroelasticity of plates and shells*, Nordhoff, Leyden.

Others:

[1] J.N. Yang and A. Akbarpour, 1987. Technical Report NCEER-87-0007, Instantaneous Optimal Control Law For Tall Buildings Under Seismic Excitations.

SUMISSIONS

All materials from authors should be submitted in electronic form to the JASI Chief Editor: Dr Mahavir Singh, Acoustics, Ultrasonics & Vibration Section, CSIR-National Physical Laboratory, Dr. K. S. Krishnan Road, New Delhi-110 012 (email: mahavir@nplindia.org Tel: +91-11-4560.8317, Fax: +91-11-4560.9310). For the item to be published in a given issue of a journal, the manuscript must reach the Chief Editor at least twelve week before the publication date.

SUMISSION OF ACCEPTED MANUSCRIPT

On acceptance, revised articles should be submitted in electronic form to the JASI Chief Editor (mahavir@nplindia.org).

ISSN 0973-3302

JOURNAL OF ACOUSTICAL SOCIETY OF INDIA

Volume 40 Number 1 January 2013

A Quarterly Publication of the JASI
http://www.acousticsindia.org

JASI

Journal of Acoustical Society of India

The Refereed Journal of the Acoustical Society of India (JASI)

The Journal of Acoustical Society of India is a refereed journal of the Acoustical Society of India **(ASI)**. The **ASI** is a non-profit national society founded in 31st July, 1971. The primary objective of the society is to advance the science of acoustics by creating an organization that is responsive to the needs of scientists and engineers concerned with acoustics problems all around the world.

Manuscripts of articles, technical notes and letter to the editor should be submitted to the Chief Editor. Copies of articles on specific topics listed above should also be submitted to the respective Associate Scientific Editor. Manuscripts are refereed by at least two referees and are reviewed by Publication Committee (all editors) before acceptance. On acceptance, revised articles with the text and figures scanned as separate files on a diskette should be submitted to the Editor by express mail. Manuscripts of articles must be prepared in strict accordance with the author instructions.

All information concerning subscription, new books, journals, conferences, etc. should be submitted to Chief Editor:

Acoustics, Ultrasonics & Vibration Section, CSIR-National Physical Laboratory, Dr. KS Krishnan Road, New Delhi 110 012, Tel: +91.11.4560.8317, Fax: +91.11.4560.9310, e-mail: mahavir@nplindia.org

Annual subscription price including mail postage is Rs. 2000/= for institutions, companies and libraries and Rs. 2000/= for individuals who are not **ASI** members. The Journal of Acoustical Society of India will be sent to **ASI** members free of any extra charge. Requests for specimen copies and claims for missing issues as well as address changes should be sent to the Editorial Office:

Acoustics, Ultrasonics & Vibration Section, CSIR-National Physical Laboratory, Dr. KS Krishnan Road, New Delhi 110 012, Tel: +91.11.4560.8317, Fax: +91.11.4560.9310, e-mail: mahavir@nplindia.org

ISSN 0973-330

Printed at Alpha Printers, BG-2/38C, Paschim Vihar, New Delhi-110063 Tel.: 9811848335. JASI is sent to ASI members free of charge.

JASI

Journal of Acoustical Society of India (JASI)

A quarterly publication of the Acoustical Society of India

Volume 40, Number 4, October 2013

EDITORIAL

ARTICLES

INFORMATION

Fundamental Noise Control Techniques

One method for controlling the sound level within a room is through dissipation of the sound energy in absorptive materials. Sound is absorbed when a portion of the sound energy striking a surface is not reflected, but passes into the material and is converted into heat energy. Generally, higher frequencies are more easily absorbed than low frequencies. Materials that are good absorbers permit sound to pass through them relatively easily; this is why sound absorbers are generally not good sound barriers. They reduce the level of noise inside an enclosure, because while the sound waves are being reflected from the surfaces in the room, they interact with the sound-absorbing materials and lose some energy each time.

However, it requires large thicknesses or many passes for the sound energy to be significantly reduced. It is important to understand the difference between sound-absorption and sound transmission loss. Materials that prevent the passage of sound are usually solid, fairly heavy and non-porous. A good sound absorber is 15 mm of glass fiber; a good sound barrier is 150 mm of poured concrete.

Sound-absorptive materials are used to reduce the level of steady sound in a room, from a machine for example, and to reduce the reverberance. The reverberance or liveness of a room is usually characterized by its reverberation time, the time it would take the energy of an abruptly stopped sound source to decay through a range of 60 dB. Just as sound-absorption varies with frequency, so too does reverberation time. No single figure rating is used to summarize reverberation time information, but the value at 500 Hz is often used for this purpose.

Most machines generate vibration, which can be transferred to the structure of a building through the machine supports. The vibration level can be reduced by balancing the machines to reduce the forces at the source. Transmission into the building structure can be reduced by using resilient, anti-vibration mountings between the machine and the supporting structure. Common materials used as vibration isolators are rubber, cork, various types of steel springs, and glass fiber pads. The transmission of vibrational energy depends on the resonance frequency of the machine on the resilient supports and on the energy damping in the system. The design or selection of resilient mounts is a complicated subject, best left to a competent acoustical consultant, but it is important to know in principle where such devices should be used.

Three important measures are used in almost all noise control work. Noise shows a source placed on a resilient support inside an enclosure with high sound transmission losses and lined with sound-absorbing material. If the resilient supports were omitted, the vibrational energy from the machine would pass into the building structure with very little attenuation, to radiate as sound elsewhere. If the solid enclosure were not there, the sound would pass through the sound-absorbing material with very little attenuation. If the sound-absorbing material were omitted, the reverberant sound inside the enclosure would build up and the energy loss through the enclosure would be much less than expected. All three elements should be present.

Mahavir Singh

Journal of Acoustical Society of India : Vol. 40, No. 4, 2013 (pp. 211-218)

Aeroacoustics of Space Vehicles Prediction, Experimental Determination and Suppression

P. Jeyajothiraj
VSSC, ISRO, Trivandrum (Kerala)
e-mail: p_jeyajothiraj@vssc.gov.in

[Received: 09.12.2012; Revised: 29.06.2013; Accepted: 27.10.2013]

ABSTRACT

Aeroacoustic loading is one of important parameter in the design of space vehicle. Prediction methods for the estimation of aeroacoustic loading are described. Comparisons of predicted acoustic levels with flight measurements of a typical space vehicle are given. Need for accurate determination is brought out. Methods of accurate determination of acoustic levels are presented. Ways of suppressing/ reducing the aeroacoustic loading are mentioned.

1. INTRODUCTION

Aeroacoustics is the youngest of classical mechanics branch. It can be defined as the study of "science of sound generated aerodynamically". Turbulence is the main source of aerodynamics sound generation. Physical understanding of the origin of sound produced by turbulence was first brought out by Micheal James Lighthill [1]. Success of supersonic and hypersonic commercial transport aircraft depends on meeting stringent acceptable sound level specification specified by civil aviation authorities. Besides, a reduction of 5 dB in sound levels on hypersonic aircraft increases its fatigue life by an order of magnitude. In space transportations, specification of low sound levels in the payload bay of launch vehicles is one of the finest features for offering commercial launch services.

Space vehicles experience very high intensity aeroacoustic levels. Shock wave oscillation can generate levels as high as 172 dB. Separated flow regime in boat-tail region of payload fairing induces levels of magnitude 160 dB. For space vehicle components, acoustic levels higher than 150 dB are dangerous. They can lead to (i) fatigue failure of light weight structural components, electronic circuit boards and electrical connections, (ii) wear and deformation of bearings and (iii) malfunction of electronic components. Hence, it is essential to characterize the aeroacoustic loading at preliminary stage of the space vehicle design.

Even with the exponential growth in the computational capability and advancement in numerical schemes, it is not possible to characterize the aeroacoustic loading of space vehicle from first principle. Hence, one needs to resort to semi-analytical or empirical method to determine the aeroacoustic loadings and use them for the initial design. After finalization of the space vehicle configuration, accurate aeroacoustic levels are determined through subscale model tests. Based on the severity of the aeroacoustic levels, proper suppression/ reduction schemes are planned. These aspects are described in this paper.

2. METHODS OF ESTIMATING SPACE VEHICLE AEROACOUSTIC LOADING

2.1 Prediction of Lift-off Aeroacoustics (Jet Noise)

Lift-off aeroacoustic levels can be predicted by two methods; (i) *Apparent Source Allocation Method* and (ii) *Spectrum Source Distribution Method* [2]. In first method, discrete sources of single frequencies are distributed along jet axis. Apparent source locations and their acoustic power are obtained from experiments with rocket motors. Acoustic efficiency, which is defined as ratio of acoustic power generated to mechanical power of jet, is assumed as 1% (maximum value observed in experiments). Local directivity of sound along with inverse square law detemine the aeroacoustic loading at the required location on the space vehicle. Predicted aeroacoustic loading compares well with measurements on payload fairing location Fig. 1. Near nozzle locations, predicted values are not accurate. Beside, acoustic shielding, if any, cannot be considered by this method.

To predict near nozzle acoustic levels and to take into account of acoustic shielding, second method, *Spectrum Source Distribution Method* was developed. In this methodology, jet is divided into number of slices. Sources of all frequency are present in each slice. Sound power and sound power spectrum for each slice are obtained from the experimentally determined non-dimensional curve. By utilizing these curves, along with inverse square law and local directivity, acoustic level at the required location from each slice of the jet can be estimated. Addition of contribution all slices gives the acoustic loading at the required location.

Eldred formula for potential core length is $x_t/de = 3.45*(1+0.38\,Me)**2$ where x_t is potential core length, de is nozzle exit diameter and M_e is nozzle exit Mach number. This formula is derived from vast majority of experiments conducted with cold jets. For hot jets, based on experiments with rocket jets, the above formula

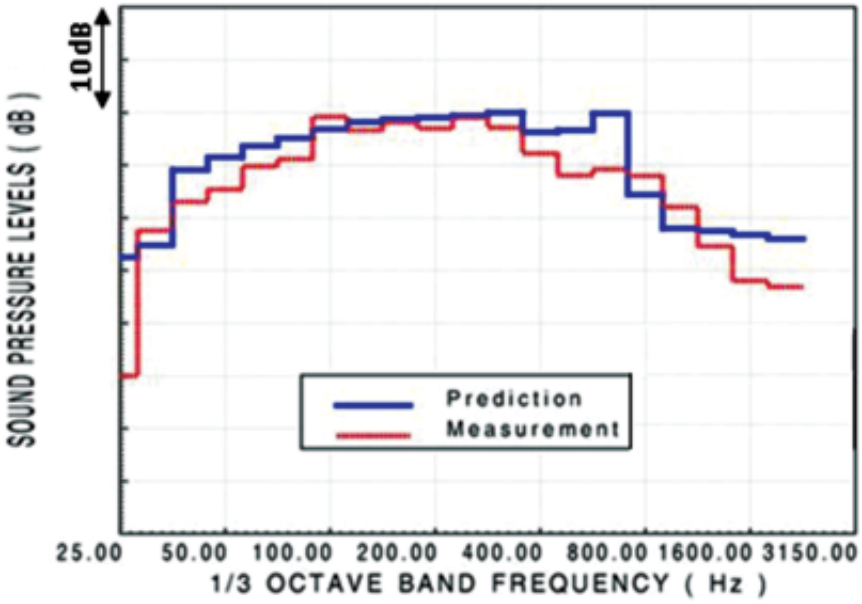

Fig. 1. Comparison of prediction jet noise levels with that of flight measurement (DSA method)

was modified as $x_t/de = 1.75*(1+0.38\,Me)**2$ Predictions carried out with modified core length compare well with flight measurements at all locations of space vehicle and a typical comparison is shown in Fig. 2.

2.2 Predictions of In-flight Aeroacoustics

Coe [3] conducted a series of experiments in the transonic and supersonic regime (upto Mach number of 3.5) and developed a Power Spectral Density (PSD) curves for shock, attached boundary layer and separated boundary noise. The prediction carried out for space vehicle, by these PSD curves, compares well with flight measurements for the shock induced intense aeroacoustic loading (Fig. 3), but does not compare well for the turbulent separated flow noise.

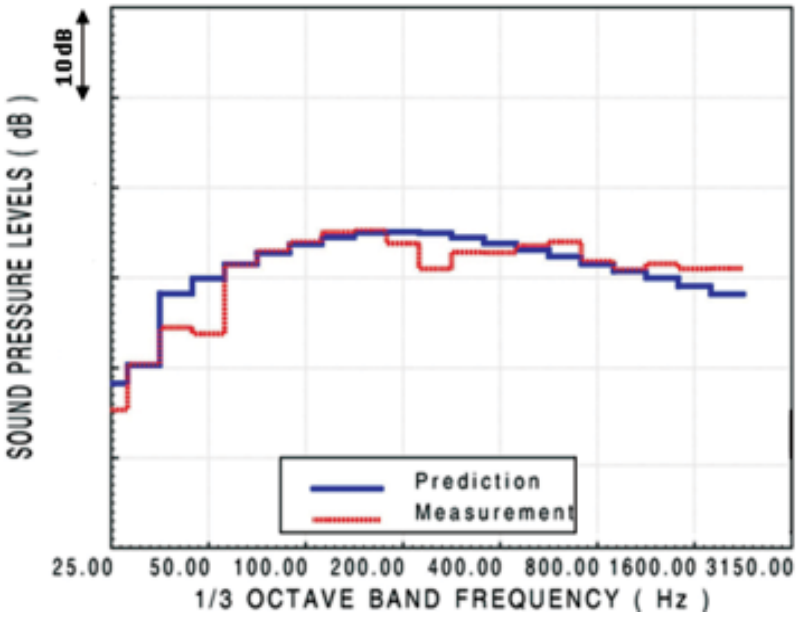

Fig. 2. Comparison of predicted jet noise levels with that of flight measurement (SSD method)

To develop a new prediction methodlogy which will characterize the in-flight aeroacoustic environment, specially the aeroacoustic loading due to turbulent separated flow, unsteady pressure measurements are carried on a typical space vehicle configuration. Measurements are carried out, at selected locations on the vehicle, in subsonic, transonic and supersonic flow regime. Power Spectral Density (PSD) is obtained for each measurement location. Dynamic pressure is used for non-dimensionalization of PSD. Strouhal number is a similarity criterion, or parameter, used in analyzing unsteady fluid flow dynamics problems. Boundary layer parameters, obtained from in-house code, are used to obtain the Strouhal number.

To classify type of flow and associated acoustic phenomena, numerical simulations are carried out to obtain flow field at wind tunnel conditions using a finite volume code. The simulations indicate shock location, flow separation location and flow reattachment location for each Mach number. Based on detailed analysis of the Non-dimensional Power Spectral Density (NPSD) curves and their trends, the flow regimes are divided into (i) Supersonic ($M > 1.2$), (ii) High Transonic ($1.0 < M \leq 1.2$), (iii) Low Transonic ($0.8 \leq M \leq 1.0$) and (iv) Subsonic ($M < 0.8$). Further, each flow regimes are classified into Attached Flow Zone, Separated Flow Zone, Reattachment Flow Zone, Shock Zone etc and unified NPSDs are generated for each zone.

Derived NPSD for supersonic flow is shown in Fig. 4. In the figure, x-axis is Strouhal number based on boundary layer parameters, y-axis is Non-dimensional Power Spectral Density, ä* is displacement thickness, u_e is velocity at edge of boundary layer, q_e is dynamic pressure at edge of boundary layer and G is Power Spectral Density. Similar curves are derived for other flow regimes also. A typical comparison of predicted value on a space vehicle with flight measurement is shown in Fig. 5. This code is christened as *"AEROACOUST"*.

3. DETERMINATION OF AEROACOUSTIC LOADING

3.1 Lift-off or Jet Noise Level Determination

3.1.1Need for Subscale Model Testing

Prediction methods have an accuracy of ± 5 dB. Experimentally determined noise levels are estimated to have an accuracy of ± 1 to 1.5 dB. Hence, when one goes for bigger thrusters, experimental estimation is essential. While prediction methods could be used for the preliminary design of vehicle, launch facilities etc.., once the

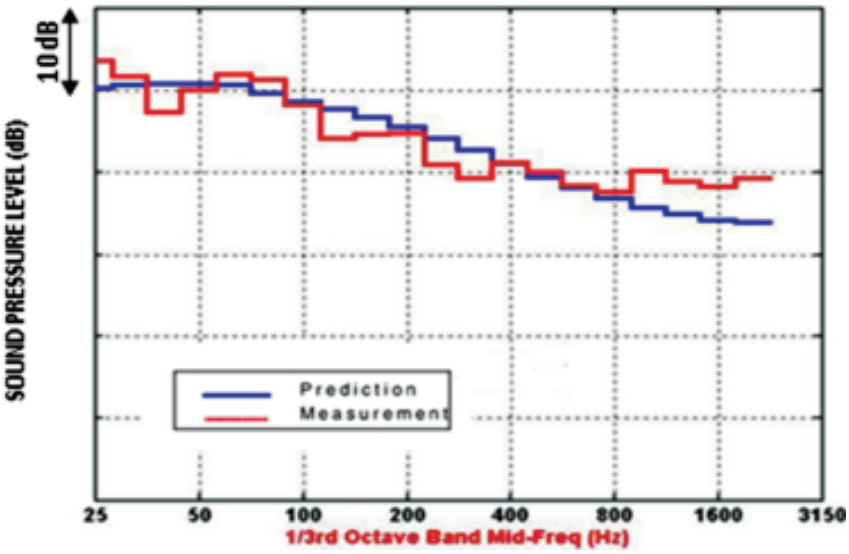

Fig. 3. Comparison of predicted In-flight noise level at shock location by Coe's method with that of flight measurement

configuration and specifications for thrusters and launch facilities are finalized, experimental technique should be used for estimating the acoustic loading on the vehicle having bigger thrusters.

3.1.2 Mode of Subscale Test

To determine jet noise level accurately, exact lift-off scenario has to be simulated. i.e (i) subscale motors have to be fired vertically and (ii) launch vehicle, jet deflector, umbilical tower and launch pedestal have to be scaled down exactly.

3.1.3 Scaling Law

For geometrically similar models exhibiting thermodynamically and fluid dynamically similar characteristics, noise spectra for actual launch vehicle can easily be obtained. No adjustment for sound pressure levels are required and only frequencies need to be adjusted by the non-dimensional acoustic parameter known as Strouhal Number, which is defined as $S= (f * D_{e)} / U_e$, where f is frequency, D_e is effective nozzle exit diameter and U_e is effective nozzle exit velocity

3.1.4 Selection of Model Size

Higher model size will cost more for testing but smaller model size may not give the accurate spectral values in the required range. In other words, model size selection should be such that measuring instruments available presently should provide the spectral content in the required frequency range without any error.

3.1.5 Simulation Parameters

Thermo-physical properties of all nozzle exit like pressure, temperature, density, Mach Number etc. of the subscale models have to be the same as that of full scale. The geometrical parameters like vehicle diameter, nozzle exit diameter, dimensions of jet deflector, umbilical tower, launch pedestal etc. are scaled down by the model size. For Ariane 4, $1/20^{th}$ and $1/10^{th}$ scale model tests were carried out Fig. 6. For space shuttle, more than 200 acoustic tests were carried out on 6.4% model.

3.2 In-flight Noise Level Determination

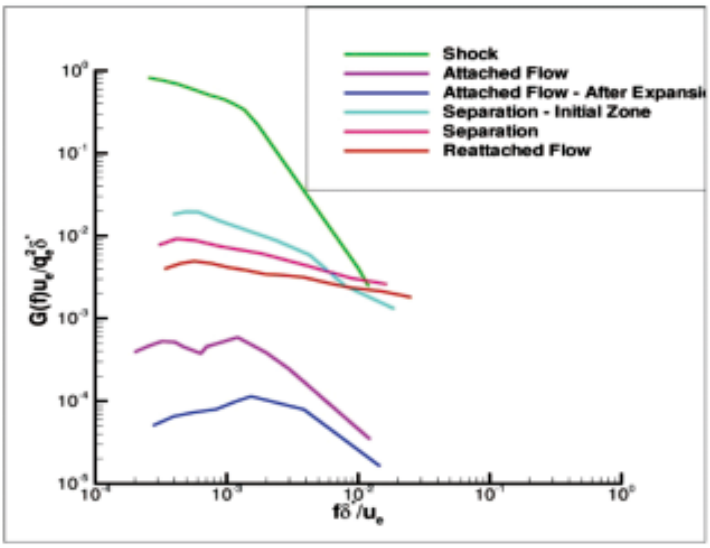

Fig. 4. Power Spectral density curve for supersonic flow

Unsteady measurements are carried-out on subscale model of the space vehicle in transonic and supersonic Mach numbers in a wind tunnel. Low background noise wind tunnel has to be chosen for the testing to obtain higher accurate acoustic values.

4. SUPPRESSION OF AEROACOUSTIC LOADING

4.1 Lift-off Noise Suppression

Lift-off acoustic environment is higher by 10 to 20 dB compared that of free flight rocket exhaust noise levels. This increased noise levels during lift-off can be reduced by (i) by covering jet deflector exit duct and (ii) by massive injection of water into the deflected jet. Process of covering the jet deflector duct brings down the acoustic levels considerable. Even then, resultant acoustic loading on space vehicle can be higher than that of free jet. Massive water injection about 2 to 4 time the mass flow rate of jet exhaust into jet to suppress the acoustic levels by 5 to 10 dB. Effect of water injection in hot jet test of Ariane 5 subscale model [4] is shown in Fig. 7.

During Space Shuttle lift-off [5], about 2 times the mass flow rate was injected into Solid Rocket Booster (SRB) exhausts and about 3.5 times mass flow rate was injected into Main Engine exhausts (Fig. 8). For Ariane 5 also, similar mass flow rate of water was used.

4.2 In-flight Noise Reduction

By proper aerodynamic shaping of the space vehicle configuration, the in-flight aeroacoustic levels can be reduced. Ogive payload fairing eliminates the transonic terminal shock formation. This brings down aeroacoustic levels by 10 to 15 dB on payload fairing. Any local protuberances produce shock/separated flow and induce high acoustic levels. Hence, minimizing the number of protuberances and shaping them reduces the in-flight noise levels. Reducing the dynamic pressure of the space vehicle (by proper selection rocket motors and trajectory optimization), in-flight aeroacoustic loading can be brought down.

5. CONCLUSION

Lift-off aeroacoustic level prediction methods Apparent Source Allocation Method and Spectrum Source Distribution Methods are described and their prediction capabilities are briefly stated. In-flight noise prediction based on Coe's PSD curves and in-house developed code for different flow regimes and types are presented. These methods can be used for the preliminary design of space vehicles. To obtain aeroacoustic loading

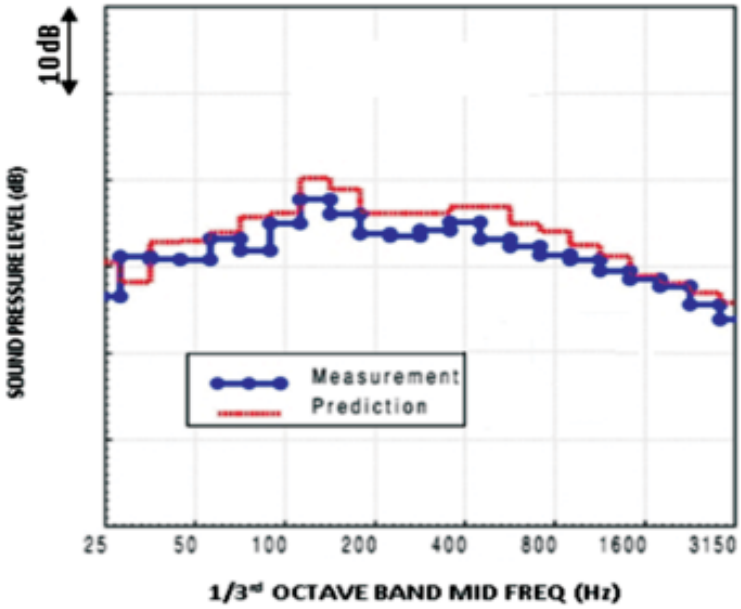

Fig. 5. Comparison of in-flight noise levels on core based shroud by "AEROACOUST" software with that of measurement

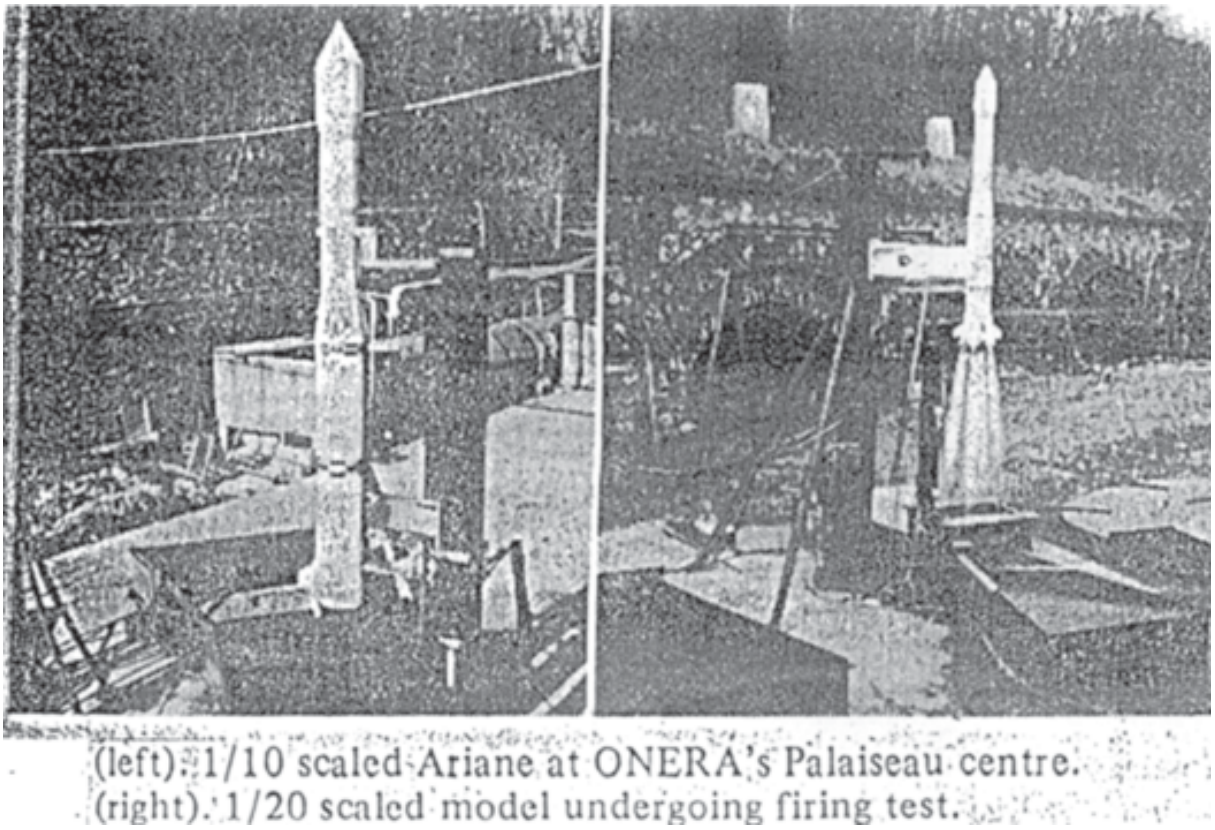

Fig. 6. Photograph of subscale model tests of Ariane

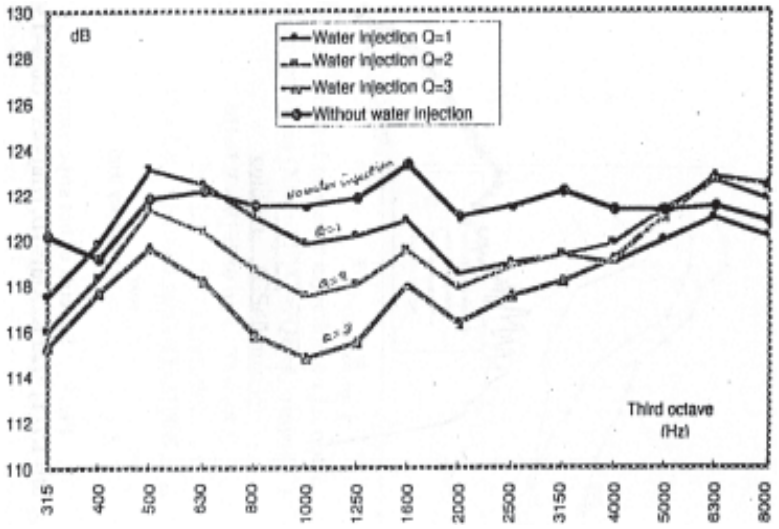

Water mass flow rate influence-Flue device

Fig. 7. Water injection effects on jet noise levels reduction

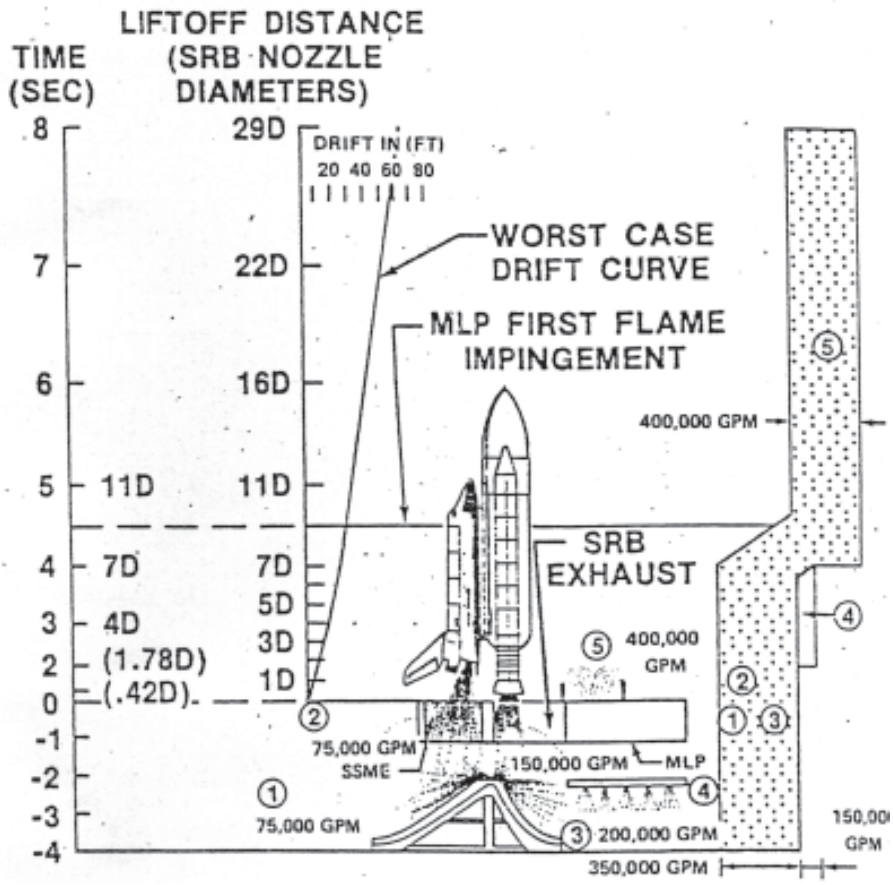

Fig. 8. Water injection system of space shuttle

accurately, subscale model tests have to be carried out. Simulation parameters for subscale and scaling methods are presented. Lift-off aeroacoustic levels can be reduced by covering jet deflector exit duct and by massive water injection into deflected jets. In-flight aeroacoustic levels can be reduced by minimizing number of protubrances and by reducing dynamic pressure encountered by space vehicle.

6. REFERENCES

[1] M.J. LIGHTHILL, 1952. Proceedings of the Royal Society of London, *On Sound Generated Aerodynamically, I. General Theory,* **211A**(**1107**), 564-587.

[2] K.M. ELDRED, 1971. *Acoustic Loads Generated by the Propulsion System,* NASA SP-8072, Langley Research Center, Virginia, United States.

[3] C.F. COE, W.J. CHYU and J.B. DODS JR, 1973. *Pressure Fluctuations Underlying Attached and Separated Supersonic Turbulent Boundary Layers and Shock Waves*", AIAA No 73-996, Aeroacoustics Conference, Seattle, Washington.

[4] D. GELY, G. ELIAS, C. BRESSON, H. FOULTUNAND and S. RADULOVIc, 2000. *Reduction of Supersonic Jet Noise. Application to the Ariane 5 Launch Vehicle*, AIAA 2000-2026, 6th AIAA/CEAS Aeroacoustic Conference, Lahaina, Hawaii.

[5] M. C. COODY, H. K. PRAtt and D. E. NEWBROUGH, 1982. *The Development and Verification of Shuttle Orbiter Random Vibration Test Requirements*, Shock and Vibration Bulletin, **52** (**2**), 71–80.

Journal of Acoustical Society of India : Vol. 40, No. 4, 2013 (pp.219-227)

Advancements in Acoustics - Indian Scenario

B.V.A. Rao
FNAE.,Advisor (International Relations),
K L University, Vijayawada (Andhra Pradesh)

[Received: 13.02.2013; Revised: 26.05.2013; Accepted: 27.09.2013]

1. INTRODUCTION

The science of acoustics, one of the oldest branches of physics, embraces the design of indoor environment to achieve acceptable levels of communication, comfort and privacy for the occupants. Acoustical issues include room shaping, reverberation control, speech clarity and Noise control. Virtually every space demands acoustic attention in order to function for its specified purpose like homes, offices, classrooms, factories, auditoriums, theaters and conference rooms.

Acoustical designing, problem solving needs technical expertise and experience in this field. It also has to be carried out with close association with other designing agencies and giving required flexibility to aesthetics.

Acoustics is an increasingly active subject in India. The awareness for sound control is growing by the day. With the industry growing at a rapid pace combined with innovative architectural designs, challenges in the acoustical design are increasing. In India, acoustics is a serous business today with plenty of acoustical research happening industrial as well as in architectural acoustics. NVIT is the criteria for modern automobiles. In addition, quieter technologies is the buzz word for all our industrial machinery.

2. INDUSTRIAL ACOUSTICS

Industrial acoustics primarily deals with noise control. With the pollution control board of India issuing gazette notification of sound levels to be emitted from machines, the design for quieter technologies is the need of the hour. Every major machine manufacturer is working towards manufacturing quieter machines. In this process, there are a lot of acoustical test cells and anechoic chambers are being constructed. NVH unit has become a compulsory department in big industries.

Major automotive companies in India like Tata Motor Ltd. Mahindra and Mahindra, Hero Honda, TVS Motor, Toyota Kirloskar Motors, Bajaj Auto, all have their own NVH test centres. The NVH test centres include engine test cells, dynamometer test cells and an anechoic chamber for noise labeling. Every machinery or appliance that have to be exported must carry a label declaring the sound power levels emitted by the product. Appliances majors like the BPL, Videocon, etc also claim their own acoustical testing centres. GE BEL, GE ITC, Tatas have all invested in test cells for acoustical testing.

Many public sector companies have been involved in NVH testing. Institutions like National Aerospace Laboratories, Gas Turbine Research Establishment, Fluid Control Research Institute, Automotive Research Authority of India, etc have invested in huge Test Cells and Anechoic Chambers. We have the National Physical Laboratory in Delhi that has an anechoic chamber used for testing and certifying acoustical materials. IISc, the premier research institute of India has its own acoustical department with valuable research happening in vibro-acoustics, mufflers, aero and ocean acoustics. IIT Madras contributed significantly to machine dynamic problems and noise studies.

3. ARCHITECTURAL ACOUSTICS

The need for good acoustic within buildings has become a criterion. More and more people rely on acoustical consultants for designing acoustically good spaces, be it in modern day office spaces, conference rooms, auditoriums or home theaters.

The modern day office spaces are being designed and constructed keeping acoustics as an important criterion. With people spending more and more time in the offices, it is important to provide them with better work places to improve efficiencies. There are also international guidelines for the decibel level, noise criterion within office spaces, which are followed by many of the MNC's setting up offices in India. Hence office acoustical design has become a must in India. Also, with respect to Call-Centres, the design of acoustical barriers between seats has become important.

Most of the offices have video conferencing facilities installed in their conference rooms and training centres. Good acoustics with least distortions are a must and should be in these kinds of facilities.

Coming to auditorium designs. Any new auditorium being constructed has an acoustical consultant in its design team. The acoustical consultant is being involved from the concept stage of the auditorium construction. Older are being completely refurbished to accommodate for good acoustics. All the universities are inclined to improve the acoustics of their auditoriums, which have exited for a while now. Though majority of the auditoriums being constructed are for multi-purpose usage, there are a few auditoriums coming in places like Bangalore and Mysore that are being specially constructed for either drama, concerts or for speech purposes. The syndicate of Mysore University have decided to refurbish their syndicate hall to comply with the modern day standards by acoustically isolating the hall as well as providing good acoustics within the hall including electro acoustical facilities.

There are number of studios that have come up in India. With ever increasing television channels and radio stations, studio designing has become very important. Unlike yesteryears, companies opening up studios are very particular about acoustical consultants being involved with their studio design. Satellite radio station World Space recently set up 6 RJ studios in Bangalore and one in Hyderabad. The A R Rehman studio in Chennai can be considered as one of the best sound recording studios in India.

With the number of multiplexes growing in numbers rapidly in India, single screen theatres could be history soon. With four to twelve auditoriums constructed adjacent to each other with common walls in between, the acoustical design becomes very critical and important. This apart, the multiplexes are generally situated inside shopping malls make noise control measures inside the auditoriums even more significant. The new companies issue these certificates, only when the theatres comply with the acoustical parameters issued by these companies.

Home Theatres have become a life style statement. More and more houses insist in having a room dedicated for music and movies. Acoustical deign for such spaces have become popular and competitive.

Medical institutions and hospitals too are seeking acoustical consultants expertise in construction of their Audiometric Rooms. All India Institute of Speech and Hearing in Mysore have half a dozen audiometric rooms constructed. There are independent hearing clinics with audiometric rooms that have come up in large cities.

Acoustical design is widely used in HVAC installations too. Be it for offices, theatres or auditoriums, the chiller machines noise should not be carried through the ducts. This apart, apartments and buildings situated close to noisy points like a busy road near an airport are seeking the services of acoustical experts for solution from noise

4. ACOUSTICAL MATERIALS

One finds a wide range of companies that are manufacturing acoustical materials like tiles and barriers. There

are many materials like gypsum-based products, fibreglass wool based, rockwool based, mineral wool based, wood wool based, foam based and latest, polyster fibre base products. Various companies manufacture these products in India who would also provide acoustical design and to name few:

- Noise and Heart Control System - Bangalore
- Acoustics India Limited - Tiruchirappalli, Tamil Nadu
- Sound Wizard - Pondicherry
- Anutone Acoustics - Bangalore
- Rockwell India Limited - Mumbai
- Jal Mistry Consultants - Mumbai
- Sanjay Suri Consultants - New Delhi
- Mikasha International - New Delhi
- Air Control - Chennai
- Parimal Mehtha Consultants - Mumbai

Considerable researching is done in these fields at Building Research Institute (Roorkee), NPL (Delhi) and many other private industries like Beardsell, Anutone., etc.,

Classical examples of acoustic materials can be seen in the following illustrations

4.1 Acoustical Analysis Shows Temple Transforms Echoes into Sound of Nature

Mayan tombs have been analyzed and researchers have found that they were designed to produce incredibly weird sound effects. If you stand in front of the staircase of the E1 Castillo pyramid and clap your hands, you'll hear an echo that sounds like the chirp of a bird. If you walk up the stones steps, it produces a flurry of echoes that sounds like rain falling into a bucket. Declercq's team has shown that the height and spacing of the pyramid's steps creates like an acoustic filter that emphasizes some sound frequencies, while suppressing others. But more detailed calculations of the acoustics shows that the echo is also influenced by other, and more complex factors, such as the mix of frequencies of the sound source.

Rani Gumpha is the current local name given to the largest structure in a group of excavated caves near Khandagiri, very close to Orissa's state capital, Bhubaneswar. The structure dates to about 2 to 3 century BC, the period just after Ashoka.

In Indian archaeological terms, it is a very early site, and represents an important transitional period in the country's history.Could this have been a theatre? Or at least, some kind of a performance space? The suggestion has been put forward before, notably by the art historian Percy Brown and Dhiren Dash, a theatre activist from the region. But the general explanation (offered by the archaeological Survey India and others) has been these were just another set of caves set apart for meditation.

4.1.1 Physical, Underwater & Atmospheric Acoustics (includes Ultrasound & Sonars)

60 to 70% of the publications at NSA conferences belong to this category, essentially application of ultrasonic to Sensors, Sonars and Chemical activity. IIT, Delhi; NOI, Goa; NPOL, Cochin; NSTL, Vizag are some other leading institutions.

4.1.2 Medical, Psycho & Bio Acoustics

Considerable work is going on in the field of Audiology, Cochlear implants and similar studies involving human health and consequent physiological and psychological effects for both low frequency and high frequency sounds. Good work is done at MMC, Chennai, AIIMH, New Delhi etc., They have also contributed

to the Mitigation of Noise Pollution and awareness of biological effects. There is a large population, who cannot understand the implications or consequences of this. After all noise is an invisible pollution, and what the eyes cannot see, the mind does not register it. In most of our industries, one can witness workers operating without using ear muffs and getting exposed to more than 100 to 120 dBA. Most of our carpenters are easily prone to duffness, so also drill operators.

4.2 Establishment of Bio-acoustic Analysis Facility at Wildlife Institute of India: Acoustical Studies on Pycnonotus bubuls

Bioacoustics is the study of animal acoustic signals, their production and perception mechanisms. It attempts to understand relationships between the structure of sounds and the nature of environment in which they are used. Proper documentation and recording of acoustics signals provide important base-line date for research in the field of systematic, behaviour, and play-back tools for survey and census. Establishment of bio-acoustic laboratories and animal sound archives are the fundamental needs to initiate such studies. Acoustic signals of Red-vented bulbul and Himalayan bulbul were recorded in their natural habitats during March 2002 to June 2003. Both species used their own vocal repertories.

4.3 Acoustic technology by Japanese Team to Study Dolphins in Chilka

A seven-member Japanese team, led by Prof. Tamaki Ura University of Tokyo, has introduced an acoustic technology to observe the behavoiur and eco-system of rare endangered Irrawady Dolphins in Chilka Lake.

The team in association with the Chilka Development Authority, and experts from IIT, Delhi, and WWF India, conducted a pilot application of the study. Dr Ura mentioned that such acoustic study using the sound pulses of a specified signal has been carried out with the support of the Japanese Ministry of Education, Culture, Sports, Science and Technology. The Chilka system, he said, would be a major step for introducing and testing a day and night automated acoustic survey system for different species of endangered marine mammals. He hinted that a more ambitious survey of the Ganges River Dolphin would be soon carried out with the participating agencies using the new technology. Prof Ura said the pilot study carried out by the team revealed the presence of the Irrawady Dolphins at selected five pockets of the Chilka Lagoon. He said the team received many preliminary data on the concentration of the Dolphins at four points, which would be further analyzed at Tokyo to find out the underwater behaviour of the marine mammal.

The team claimed that the pilot study revealed that the Irrawady Dolphin moves at two meter per second.

4.3.1 Engineering & Machinery Acoustics (including transportation)

This is one of the largest contributors to our noise pollution in various forms including traffic covering both surface and air. India failed to meet global challenges in term of noise standards. Our machines produce more sound and vibration than their counterparts manufactures elsewhere. For the designers, this is the last priority. With more global inputs, things are getting better due to usage of suitable materials as well as manufacturing and assembling skills. Lot of attention is being paid to this aspect now to meet the challenges by going to quieter technologies. We have noise standards, but rarely these are strictly followed. Our industry appreciates both vibrations and noise diagnostics as a strategy for CBM, but very few organizations are serious about this implementation. For the past three decades considerable awareness has gone in this direction, yet we have to go a long way. IIT Madras, IIT Delhi, IIPE, many of our power plants and cement plants have contributed significantly to this novel technique. Academic Research involved considered such aspects as efficiency of sensors and instrumentation, inspection systems, and lastly economic benefits through cost model developments. This is one of the area in which I have personally taken interest in last three decades including introduction of courses like Diagnostic Maintenance in Condition Monitoring programmes. These were also highlighted in number of seminars and conferences. There are both passive and active techniques that are being researched in this quieter effort. IITs, IISc, Space and Defence Organizations have played a major role.

4.3.2 Music, Speech and Signal Processing (Electro Acoustics)

Next to Physical Acoustics, comes this field in our country with considerable contributions. This is essentially contributed by our electronic specialists from TIFR, Mumbai, IISc., Bangalore, CEERI (Pilani & Delhi), AIISH (Mysore) and many other centres throughout the country. There is a small group working on Musical Acoustics in Pune. The work involves speech analysis, speech processing & speech therapy. Most of our medical units dealing with ENT have good audiology sections and significant contributions.

4.4 IBM India Research Lab - Speech Technologies

The design and implementation of computer systems that can cover whole range of human-like interaction by using faces and voices is one of the challenging objectives of the Speech Group at the India Research Lab (IRL). The group aims to build state-of-the-art speech recognition/ synthesis system for Indian languages and improve the existing techniques in general. IRL is currently pursuing activities in the areas of:

- Indian Language Desktop Speech Recognition
- Indian language Telephony Speech Recognition
- Indian-English Text-to-speech synthesis I

4.4.1 Environmental & Community Noise (Noise pollution)

This is one of the major problems in the country due to lack of knowledge and education. This is a country that pays considerable weightage for religious, cultural and political ceremonies, where noise dominates. Noise legislations are there, framed by both CPCB and State PCB's. But hardly people pay attention. The industry, traffic and the community all contribute together to produce the Noise Pollution. I was one of the expert members to draft noise standards for the Ministry of Environment. It pains me to say the whole effort has gone waste, as no serious attention is paid at any level. Honking is anybody's business in this country, and when no honking is heard, the person thinks nothing is coming behind him or her. Movies have been made on this for screening in theatres, and many other steps were taken. During 1982-84, I served as Chairman for construction noise in Singapore introducing 5 mn standard for Leq. There was an opposition, but it was Singapore! Discipline is lacking in our country.

4.4.2 Random and Non-linear Acoustics, Jet Noise, Aero Acoustics & Chaos

These are highly specialized areas involving modern jet noises and their control (more due to aerodynamic effect). Some work was done at IIT Madras for producing 160-180 dB noise levels to impinge on rocket models to study their acoustic transmissibilities. These facilities have now been created at NAL Bangalore. Significant practical work was carried out both at IISc., Bangalore & NAL. Considerable work is being done on random noise, non linear acoustics and chaos theory relating to stabilities. I was involved in establishing NEF contours for the Meenambakkam airport in Chennai and extrapolate it to Pondicherry. This was done some 15 years ago and still Pondicherry airport has not yet been commissioned, though the airfield was put up at an enormous cost.

> Fluent announced coupling with LMS SYSNOISE for Acoustics Modeling on August 8, 2003. Lebanon, NH, USA and Leuven, Belgium Fluent Inc. and LMS International announced later the release of the world leading Vibro-Acoustics software LMS SYSNOISE Rev 5.6, which supports import of transient data from FLUENT 6.1, the leading computational fluid dynamic (CFD) software from Fluent. This allows results from FLUENT to be used for comprehensive computational aero-acoustics simulations within SYSNOISE Rev5.6, complementing FLUENT 6.1's native aero-acoustics modeling capabilities.
>
> Computational aero-acoustics is a critical technology for engineers in virtual prototyping environments, who want to predict and compare the aero-acoustics performance of proposed designs. By using computational tools to identify and rank sources of flow-induced noise, engineers are able to design for noise reduction early in their design cycle, enabling them to produce better products, while reducing the need for expensive physical testing, and shortening the overall time to market.

4.4.3 Application of Holography in Jet Acoustics Studies

Source strength distribution on a jet boundary was obtained from measurements using the principle of acoustic holography. Measurements were conducted in an open field. Measurement of acoustics pressure on a cylindrical two dimensional contour located close to the vibrating jet boundary was used to obtain the acoustic source strength distribution of the sound field on to a cylindrical surface. A jet emanating from 5mm convergent nozzle was used for the holography experiments, assuming symmetry. Experimental results were compared with results obtained from holography.

4.4.4 Low Frequency Sound And Physiological Effects

- In 1665, people in London heard the gun fire from English and Dutch men in the battle in North Sea.
- In 1883, volcanic eruption in Krakotoa from infrasonic waves traveled 5 times around the world.
- In 1933 Greenwood's famous novel 'Love on the Dole' mentions that 'the thump of the presses makes the workers feel sick'.
- In 1973 the 1st International conference on Informative was held in Paris.
- In 1980 the 1st International Conference on low frequency noise. Regrettably even there is widespread ignorance as to its quantitative and subjective effects, no convenient measurement unit to describe it and no definitive guidelines as to extent to which it should be controlled. Unfortunately people exhibit offering levels of individual sensitivity to low frequencies.

Tests conducted in Berlin on the effects of infrasound showed marked physiological disturbances such as elevated BP, ECG disorder and change in adrenaline. Females show earlier sensitivity than male.

Its effect on auditory systems such as NIHL and Tinnitus are well known. It has also a profound effect on non-auditory systems such as blood pressure, perspiration, heart rate, contraction of muscles, ischemic heart diseases, hypotension, hormonal secretions, physiological stresses, neurological disorders and epileptic seizures. Its effect on animals, sleep, foetus, visual acuity, loss of balance and whole body vibration are all well known.

Loudness sensation can be measured up to 1 Hz, and that produced by gasturbines in the range of 3.5 Hz has annoying characteristics. But usually the high frequency noises acting at the same time (like pop music) from a translator radius mask, the low frequency noises and sensitivity changes.
Examples of Low Frequency Noise:

- Silencing of a gas turbine test bed
- Telex rooms (around 17 Hz)
- Ventilating fan noise(20 Hz)
- Reciprocating type air compressors(20-31.5 Hz)
- Diesel powered transport - with its low firing and of immense power is a source for low frequency noise. Ship noise spectrum contain both infrasonic and low frequency bands. Active control techniques help here.
- Low frequency noise and wind throb in cars (especially when windows are opened) act like a Helmholtz Resonator induces great SPL's.

- Buildings in the wind - telephone cables exposed to wind produces distinctive humming sound. The frequency calculated from strohaul's equation on windy days, it is difficult to manage children in schools. Some of the depression symptoms exhibited by dwellers in high buildings are noise induced.
- Distant guns - dull thud gun fire.
- Bristol hum - from gas turbines producing low frequency noise.

For Control of low frequency noise, 'A' network is not suitable as it is only in the audio range. They now recommend 'P' weighting. It falls at 12dB/octave. This has a disadvantage. Hence another weighted network 'N' is used, which falls at 6dB/octave. ISO is standardizing all these and coming out with reasonable standards.

Low frequency sound due to its low extenuation, its decay rate approximates to the simple inverse square law, as the long wavelengths involved causes the sound to spread in a spherical manner and covers a wide area.

5. CONCLUSION

Mayan tombs haveAcoustics in India - yes, we create enough sound, as we like to be loudly heard. But we don't bother and we do not know even how to control it, when it is needed or parts damaged as in machinery. In Architecture, we overdesign than needed costing significantly. In countries like Australia (Queensland) and New Zealand, they have Ministries for Noise Abatement. In Germany, noise legislations are stringent. Noise maps are displayed in their town halls, curtailing the sound depending on the importance of those areas, and one cannot put up any noise unit that exceeds those values. Noise maps are prepared earlier for turn key projects, so that industrial noise affecting communities can be controlled.

In India, we have to go a long way to reach any of those norms or standards. Public awareness is still in its infancy here and the hazards involved limitless. We have each year NSA conferences, and how much of it, stresses on these aspects and the country gets thereby benefited has not been assessed. It is a cry in the wilderness. But we are sure one day our cries will be heard by future generations and a better sense dawns in the country.

6. ACKNOWLEDGEMENT

Many citations here have been drawn from sources earlier published in newspapers or magazines and other literature, which cannot be recollected. Special thanks and gratitude to all those authors. Considerable work also has been carried out by me and my colleagues, while I worked at IIT Madras. All of them are being acknowledged here. Appendix A gives some standards adopted. Appendix B gives the list of my involvement as consultancy projects, which will be briefly highlighted while presentation.

APPENDIX B

Industrial Consultancies in Acoustics

(By the author)

IS:2526-1963	Code of practice for acoustical design of auditoriums and conference halls.
1S:9736-1981	Glossary of terms applicable to acoustics in buildings.
IS:9000(PART 21)-1985	Basic environmental testing procedure for electronic and electrical items. Acoustic Noise Test.
IS:2264-1963	Preferred frequencies for acoustical measurements.
IS:9876-1981	Guide to the measurement of airborne acoustical noise and evaluation of its effects on man.

IS:4954-1968	Recommendations for noise abatement in town planning.
IS:7194-1973	Specification for assessment of noise-exposure during work for hearing conservation purposes.
IS:4242-1967	Method of measurement of acoustical noise emitted by ballasts for gaseous discharge lamps.
IS:6964-1973	Specification for octave, half-octave and third-octave band filters for analysis of sound and vibrations.
IS:10775-1984	Specification for body level hearing aids.
IS:1885(PART III/Sec 1)-1965	Electro technical vocabulary Acoustics
IS: 1885(PART III/Sec 2)-1966	Electro technical vocabulary Acoustical Electro-Acoustical System
IS: 1885(PART III/Sec 4)-1966	Electro technical vocabulary Sonics, Ultrasonic and Underwater acoustics
IS: 1885(PART III/Sec 5)-1966	Electro technical vocabulary Speech and Hearing
IS: 1885(PART III/Sec 6)-1967	Electro technical vocabulary Acoustical Instruments
IS: 1885(PART III/Sec 7)-1978	Electro technical vocabulary music
IS: 1885(PART III/Sec 8)-1974	Electro technical vocabulary Architectural Acoustics

APPENDIX B

Industrial Consultancies in Acoustics

(By the author)

1. Impact noise studies through strain measurement on reactor domes ('76)
2. Dynamic characteristics of indigenous machine tools ('76)
3. Effect of machinery and noise vibration on neighbourhood for large Hotel complex ('76)
4. Acoustic tests on SLV 3 model - VSSC, ('77)
5. Dynamic and acoustic transmissibility test on rocket models, solar panels and antenna dishes ('77)
6. Acoustic tests on Solar panels and Antenna Dish for ASLV & SROSS - ISAC, Bangalore {'84}
7. Noise analysis and measurement of 1.3 MW induction motor - Jyoti Ltd., Baroda, 1985
8. Diesel Generator vibration and noise and foundation studies - India Cements, Sankar nagar & tube investments, Avadi (1986)
9. Airport noise survey - Ministry of Tourism, Govt. of Pondicherry
10. Development of NEF contours for the Madras Airport and its extrapolation to the proposed Pondicherry Airport for aircraft noise at critical locations
11. Acoustic design and treatment of community hall for CCI at Yerraguntla and Kallakurchi
12. Acoustical enclosure design for the gas turbines for BHEL, through SOL Engineers, Hyderabad and many other industries through Viprah Engineers, Coimbatore
13. Evaluation of the NEF contours for the proposed airport at Pondicherry, Ministry of Tourism (1987)
14. Acoustical treatment and reverberation of studies for a community hall, CCI, Yerranguntla (1987)
15. Noise measurement and analysis of a 1.3 MW Induction motor for Jyoti Ltd., Baroda (1987)
16. Vibration and Noise Studies on DG sets for India Cements, Sankarnagar and Tube Investments, Madras (1987)

17. Design of an acoustical enclosure for a pump-motor set for Beacon Weir, Madras (1987)
18. Environmental noise studies from exhaust fans for Kerala Laxmi Mills, Trichur (1988)
19. Refrigerator compressor noise studies for Godrej and Boyce, Bombay (1988)
20. Environmental noise studies from DG sets for Hydraulics India, Madras (1988)
21. Acoustic treatment for the Turf Club, Beard Sell ltd., Bangalore
22. Acoustic enclosure for gas turbine for BHEL, SOL Engineers, Hyderabad
23. Noise analysis of inlet silencer for coincidence effect, Anutone, Bangalore
24. Noise from A/C plant for Hotel Sangam, Tanjore
25. Noise from Diesel - Generator sets for number of industries and residential complexes and enclosure designs (Indo-American Hybrid, Ramco Systems, Raheja Complexes, etc.
26. Consultation on choice of pneumatic isolators for a anechoic tank for sonar studies -NPOL, Cochin
27. Study on a non-linear vibration / noise of an aircraft gas turbine - Kaveri Engine, GTRE, Bangalore
28. Design of a pneumatic isolated foundation bed for an accuracy of 0.03 - IBM, Bangalore

Journal of Acoustical Society of India : Vol. 40, No. 4, 2013 (pp. 228-232)

Aerodynamic and Aeroacoustic Analysis of Centrifugal Blower for Noise Reduction

S. Rama Krishna[1], Vommi Krishna[2], A. Rama Krishna[3] and K. Ramji[3]
[1]Department of Mechanical Engineering, G.V.P. College of Engineering(A), Visakhapatnam-530 041 (A.P.)
[2]Department of Mechanical Engineering, ANITS, Visakhapatnam (A.P.)
[3,4]Department of Mechanical Engineering, A.U.C.E(A), Visakhapatnam (A.P.)
e-mail:shinagamsai@gmail.com

[Received: 13.04.2013; Revised: 22.06.2013; Accepted: 24.08.2013]

ABSTRACT

Centrifugal blowers, which are designed for high rotating frequencies, generate high levels of noise. Thus noise reduction is a key parameter in the design of centrifugal blowers. The objective the present study is to estimate the aerodynamic and aeroacoustic parameters like pressure, velocity and noise of centrifugal blower with three different types of impellers namely forward, backward and radial by both experimental and numerical analysis. Reverse engineering method is used to get the dimensions of centrifugal blower. The modelling of the blower is performed by using Solid modelling software 2010 and blower is meshed with a three dimensional tetra mesh by using HYPERMESH 9.0. Numerical analysis is performed using CFD-Fluent software package for the three types of impellers. These numerical results are compared with experimental results for validation. From the study it is observed that backward impeller generates less noise and more discharge than forward and radial impellers.

1. INTRODUCTION

A centrifugal blower is a roto-dynamic blower that uses a rotating impeller to increase the pressure of a fluid. With the growing importance of blowers in industries, several researches have focused their work on subject. Different problems associated with the blower like noise and vibration reduction have been received due to concern. Son et al. [1] presented the effects of bell mouth geometries on the flow rate of centrifugal blowers were numerically simulated using a commercial Computational Fluid Dynamics (CFD) code, Fluent. Ramesh kumar *et al.* [2] observed that mechanical malfunctions such as, rotor unbalance and shaft misalignment are the most common causes of vibration in rotating machineries. Chen-kang and Hsieh [3] explained the performance analysis and optimized design of backward-curved airfoil centrifugal blower. CFD package FLUENT is used to simulate four backward curved air foil centrifugal blowers. Kolla et al. [4] proposed to carry out a study to evaluate the effectiveness of composites in reducing noise levels of the casing. Jianfeng et al. [5] conducted experimental study to reduce the noise of the centrifugal fan, whose impeller has equidistant forward-swept blades. Two new impellers with different blade spacing were designed for noise reduction. Moreland et al. [6] explained the housing effect of centrifugal blower. The sound power spectrum for a centrifugal blower operating at free delivery is characterized by enhancement at various frequencies owing to acoustical resonances in the blower housing.

Noise, generated by a centrifugal blower, can be divided according to its origin, into aerodynamically induced noise and vibration-induced noise. The contribution of the individual noise source to the total emitted noise is hard to determine, but it is crucial for the design of noise reduction measures. In order to reduce the noise of the centrifugal blower in a broad range of operating conditions, an identification of noise sources needs to be performed. The present blower is of 5 HP capacity with 12 blades is rotating at constant speed of 2660 rpm. The present work is aimed to determine the aerodynamic and aero acoustic analysis of centrifugal blower experimentally and comparing with numerical analysis by using FW-H equation coupled with LES computer code based on cell-centered finite volume method (FVM) on unstructured meshes for viscous flow field around blower.

2. METHODOLOGY

2.1 Experimental Setup

The experimental set up consists of centrifugal blower driven by motor and it is mounted on an adjustable bed. An orifice meter is fixed in the outlet pipe line to measure the actual discharge. A set of pitot tube and thermometer is provided at the outlet to measure the velocity and temperature. The pitot tube can also be used to measure the velocity profile at the blower inlet. U-tube Manometers are provided to measure the pressure difference across the orifice meter in the pitot tube and the delivery pressure. Three types of interchangeable impellers with radial vanes, backward curved vanes and forward curved vanes are provided with test rig to study the different effects of vanes types. Fig. 1 shows the experimental set up for aerodynamic measurements.

Fig. 1 Experimental set up for aerodynamic measurements

Fig. 2 Experimental Setup for aeroacoustic Measurements

The noise of centrifugal blower is measured by Bluer Kjaer Sound Level Meter (SLM)-2260 for backward, forward and radial impeller. The B&K 2260 investigator is a precision hand-held SLM with real-time displays of 1/3-octave and octave band spectra and statistical distributions. Also included is a PC compatible filing system and large memory. The 2260 conforms to the BS EN 61672 Class 1 standard. Fig. 2 shows the experimental set up for aeroacoustic measurements

2.2 Modelling and Meshing of Centrifugal Blower

Reverse engineering method is used to obtain the dimensions of the centrifugal blower with forward, radial, and backward curved impeller blades and modelled using Solid works 2010. In order to model the centrifugal blower it is necessary to model the parts of the blower which are spiral casing, impellers, pulley, shaft, hub, suction arrangement, supporting structure then it was assembled to forward, radial, and backward curved impeller blades positioned in housing between two housing faces that are spaced apart along the impeller

axis. A bell mouth shaped inlet is attached to the one of the facing and the housing is substantially closed with exception of the inlet and outlet. The impeller is attached to the hub which is keyed to the shaft.The solid model is imported as surface set to HYPERMESH 9.0 in ANSYS environment. The solid model is repaired by toggle section option the gaps are stitched. After repairing, the closed surface set was converted into solid. Each component was loaded in the separate component collector. The model was tetra meshed in volume tetra mesh by considering various values like element size, featured angles of the elements and by selecting gradual mesh. After convergence total 439506, 441314 and 435689 elements are for entire blower with backward radial and forward impellers respectively. Fig. 1 and Fig. 2 shows the solid model and meshed model of backward impeller.

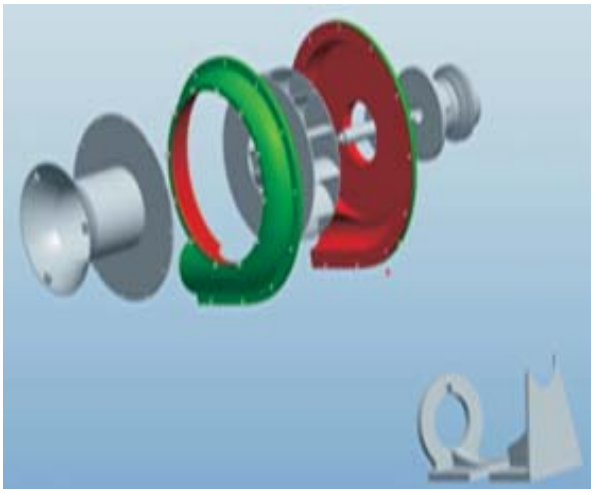

Fig. 1. Solid model of blower

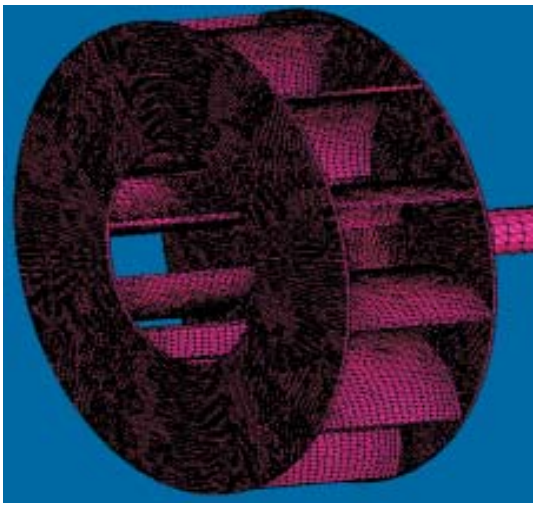

Fig. 2. Meshed model of backward impeller

2. 3 Numerical Simulations

The numerical simulations have been carried out with a finite volume code method using Fluent. The turbulent nature of the flow is incorporated through the LES. LES is chosen as viscous model as it is used because, it needs time dependent solution for aeroacoustic solution and it is not highly dependent to geometrical conditions. For unsteady-state simulations, the Multiple Reference Frames (MRF) model is used. Surfaces that rotate relatively are defined as "moving wall". Moreover, as they are dependent on the fluid around them and as they rotate, they are defined as "relative to adjacent cell zone" and "rotational motion". Cylinder walls are defined as "stationary wall" and the inlet and outlet are defined as "pressure inlet" and "pressure outlet". Fluid zone in the inner volume is defined as "MRF" and rotates with 2660rpm in x-direction.

3. RESULTS AND DISCUSSION

The aerodynamic and aeroacoustic properties of blower with radial, forward and backward impellers are predicted with numerical simulations (CFD-Fluent software) and same is compared with the measurements. Table 1 shows the aerodynamic results comparison. From this table it is observed that blower with backward impeller develop maximum discharge (0.399m3/sec) and pressure (2079.5Pa) compared with other forward and back and impellers. For all noise measurements carried out at 1m from the inlet of blower. The measurement position is aligned to the impeller axis. Fig. 3 shows the noise prediction graph at inlet of blower with backward impeller from measurements. It is clearly shows that maximum peak is observed at fundamental blade passing frequency (532Hz) and some of other peaks are observed due to interaction between casing and impeller noise.Table 2 shows the aeroacoustic results comparison. The results shows that blower with backward impeller was generating less noise (92.2dB) compared with other forward and radial impellers. Fig. 4 shows the noise prediction graph at inlet of blower from numerical simulations with Fluent software.

Table 1. Aerodynamic results comparison

Vane type	Experimental Results			Numerical Results			Error in
	Pressure (N/m^2)	Velocity (m/sec)	Discharge (m^3/sec)	Pressure (N/m^2)	Velocity (m/sec)	Discharge (m^3/sec)	
Backward	2079.5	29.6	0.399	103.8	99.4	0.453	13.53
Forward	1471.38	28.95	0.346	92.2	90.1	0.386	11.56
Radial	1481.19	25.66	0.378	101.5	98.6	0.414	9.53

Table 2. Aeroacoustic results comparison

Vane type	Experimental Results (dB)		Numerical Results (dB)		Error (%)	
	Inlet	Outlet	Inlet	Outlet	Inlet	Outlet
Backward	83.3	81.2	92.2	90.1	10.68	10.96
Forward	89.2	86.8	101.8	99.4	14.13	14.51
Radial	85.4	83.6	98.1	96.1	14.87	14.95

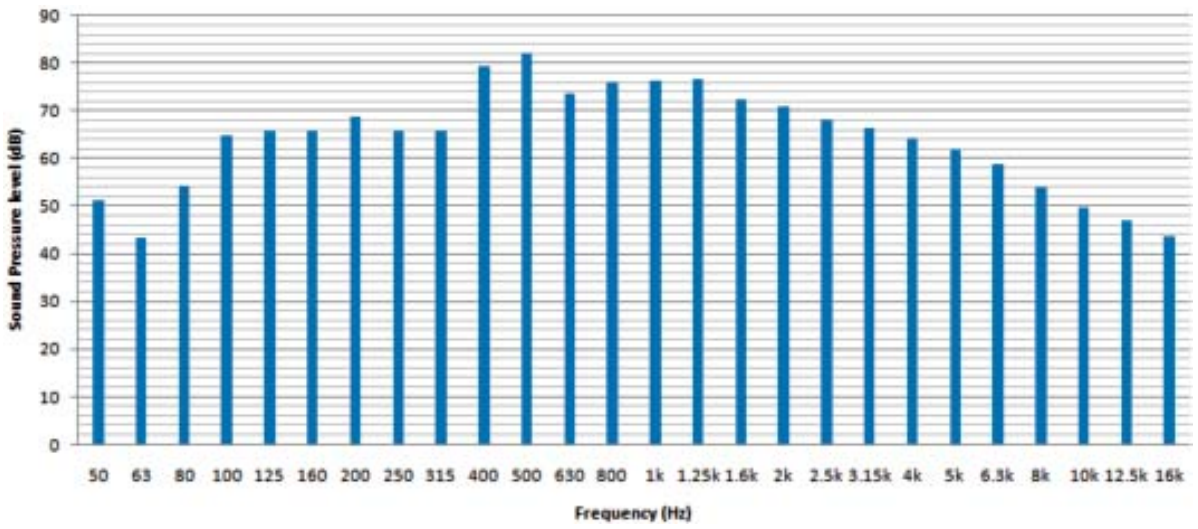

Fig. 3. Noise prediction graph at inlet of blower with backward impeller from measurements

4. CONCLUSION

The aerodynamic and aeroacoustic parameters of centrifugal blower with forward, backward and radial impellers with are measured and these results are compared with CFD-Fluent software. Errors between measured and predicted results are less than 15%. So CFD analysis results are close to the experimental results. From the analysis it is concluded that backward impeller generates less noise and high pressure when compared to other forward and radial impellers.

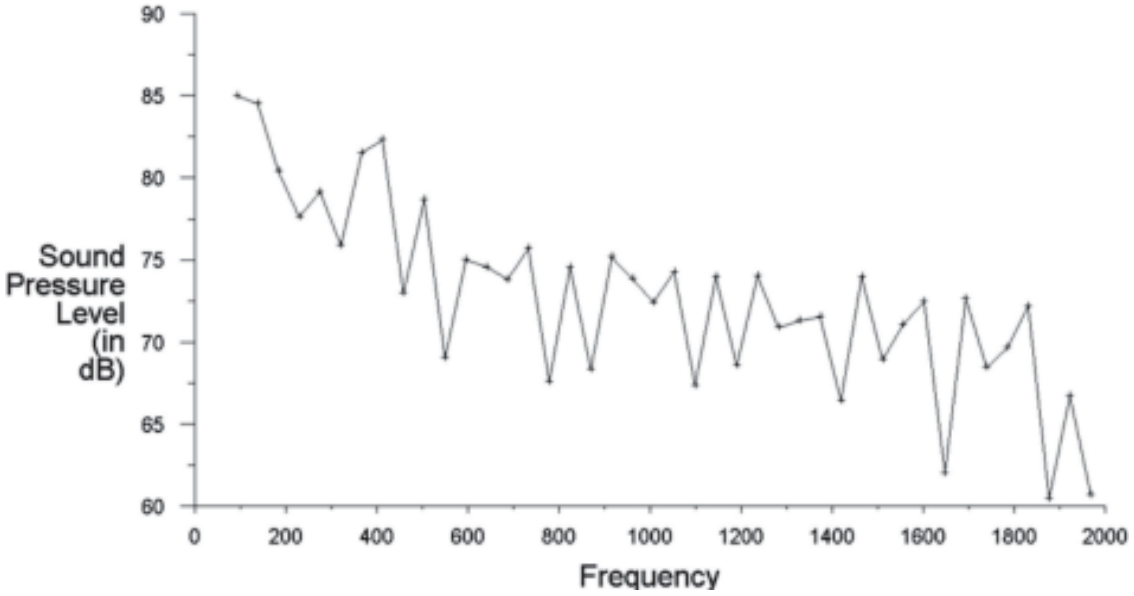

Fig. 4. Noise prediction graph at inlet of blower from numerical simulations with Fluent software

5. REFERENCES

[1] PHAM NGOC SON, JAEWON KIM and E.Y. AHN, 2011, Effect of bell mouth geometries on the flow rate of centrifugal blower, J. of Mech. Sci. and Tech., **25** (**9**), p. 2267-2276.

[2] G.R. RAMESHKUMAR, B.V.A. RAO and K.P. RAMACHANDRAN, 2010, Condition monitoring of forward curved centrifugal blower using coast down time analysis, Hindawi Publishing Corporation, International Journal of Rotating Machinery, Article ID 962804, 12 pages, doi:10.1155/2010/962804

[3] HUANG CHEN-KANG and HSIEH MU-EN, 2009, Performance analysis and optimized design of backward curved airfoil centrifugal blowers, American society of heating, refrigeration and air condition engineers.

[4] S. KOLLA, Y. ANIL KUMAR and S. RAJESH, 2009, Noise reduction of air blower casing using composites, Vibration Problems ICOVP-2007, Springer Proceedings in Physics, **126**, p. 215-222, DOI: 10.1007/978-1-4020-9100-1_22.

[5] M.A. Jianfeng, Q.I. Datong, M.A.O. Yijun, 2008. Noise reduction for centrifugal fan with non-isometric forward swept blade impeller, Front. Energy power engg. China, **2**(**4**), p. 433-437 doi 10.1007/s11708-008-0082-6.

[6] J.B. MORELAND, 1974, Housing effect on centrifugal blower noise, *J. Sound and Vibration*, **36**(**2**), p. 191-205.

Journal of Acoustical Society of India : Vol. 40, No. 4, 2013 (pp. 233-238)

Optimization of Secondary Sources for Active Noise Control in a Car Like Rigid Cavity

T. Ramachandran, M.C. Lenin Babu* and S. Muruga Poopathy
Department of Mechanical Engineering,
PSNA College of Engineering and Technology, Dindigul-624 622
**e-mail: lenin_babu@yahoo.com*

[Received: 18.12.2012; Revised: 27.07.2013; Accepted: 21.09.2013]

ABSTRACT

In this paper genetic algorithm has been used for optimal placement of secondary sources in a three-dimensional rectangular rigid cavity for active noise control system. In this genetic algorithm a multivariable binary coding scheme along with a random initial population are used. Numerical examples are presented to illustrate the effect of location on sound pressure level. Result shows that the locations obtained by genetic algorithm are very effective than arbitrary locations.

1. INTRODUCTION

The internal sound field in the enclosed cavity is significantly affected by the acoustic modal characteristics of the cavity, Porous material absorption efficiency is mostly apparent at high frequencies. Passive control has the disadvantage of minimal low frequency absorption; it can be bulky and heavy when used for low frequencies. To attenuate this low frequency noise, active noise control (ANC) system can be used in enclosed spaces without passive techniques. It has the specific advantage of reduction in size, volume and cost when compared with passive control. Nelson *et al*. (1987) examined the active noise control methods in harmonic enclosed sound fields. Further, the theory was verified by both numerical simulation (Bullmore *et al*. (1987)) and experimentally (Elliott et al. (1987)). They considered a rectangular enclosure with rigid walls and shown that minimizing the sum of the squared pressures at several points could lead to significant reduction in acoustic potential energy and sound pressure levels (SPL). Parkins *et al*. (2000) investigated active control system of three-dimensional enclosures based on acoustic energy density method. In their study, minimization of energy have been carried out by sensing both the potential and kinetic energy densities, while the most popular control systems of the past have relied on the potential energy density alone. Energy density control method shown to be more effectively than pressure based measurements especially for off-resonance control. Akl and Baz (2006) investigated the effectiveness of structural acoustics of the cavity/plate system, which is lined with smart foam.

In this work optimal location of secondary sources have been examined to enhance the reduction of the sound pressure level in a three dimensional rigid cavity as shown in Fig. 1.

2. FORMULATION

The Helmholtz equation, for a cavity of volume V, enclosed by a rigid surface for harmonic variation in acoustic pressure p is given by (eq. 1);

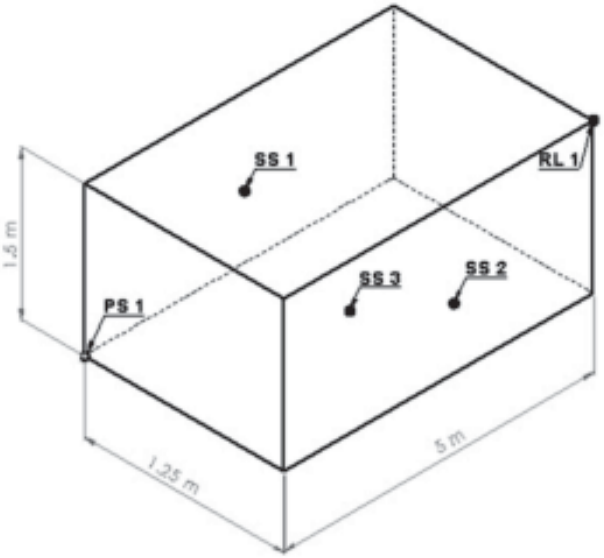

Fig. 1. Geometry of the car like rigid cavity

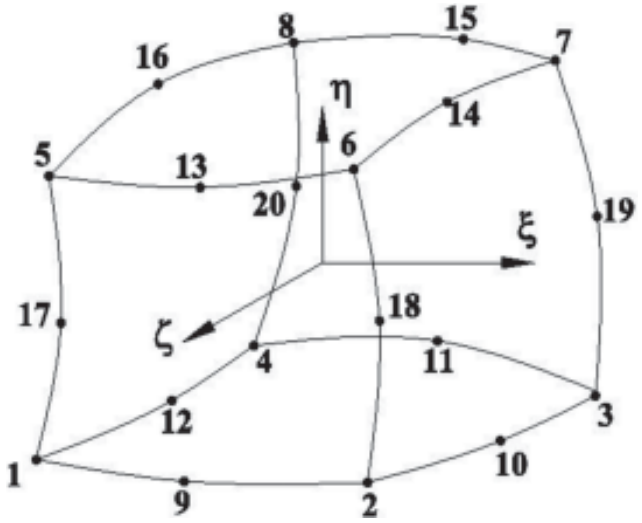

Fig. 1. 20-noded quadratic volume element

$$\nabla^2 p + \left(\frac{\omega}{c}\right)^2 p = 0 \tag{1}$$

where ω is the circular frequency and 'c' the speed of sound. The weak integral form of the cavity equation can be found in Sgard *et al.* (2005) and is given as

$$\int_{\Omega_a} \left[\frac{1}{\rho_a} \nabla p_a . \nabla \delta p_a - \frac{\omega^2}{p_a c^2} p_a \delta p_a \right] d\Omega - \frac{1}{\rho_a} \int_{\Gamma_a} \frac{\partial p_a}{\partial n} \delta p_a d\Gamma = 0, \quad \forall \delta p. \tag{2}$$

In this equation p_a and ρ_a representing pressure and density of the acoustic domain. In order to discretize the acoustic domain a 20-noded quadratic finite element is used which has only pressure as a degree-of-freedom (DOF) at each node. Figure 2 shows the reference 20-noded element and node numbering. The weak form of eq. 2 discretized with this 20-noded quadratic finite element subject to boundary conditions can be in matrix form as:

$$\left([H]_a - \omega^2 [Q]_a \right) \{ p_a \} = \{ F_a \}; \tag{3}$$

where $[H]_a$ and $[Q]_a$ represent the kinetic and compression energy matrices for the cavity, $[P]_a$ represents the global nodal acoustic pressures for cavity, while $[F]_a$ denotes the acoustic loading vector for the cavity. Above can be written in the form of:

$$[A]\{Z\} = F; \quad [A]\{Z\} = F; \quad [A] = [H] - \omega^2 [Q]_a; \tag{4}$$

The amplitude produced by primary primary $\{Z_{ps}\}$/ secondary $\{B_{55}\}$ source distributions inside the cavity is given by:

$$\{Z_{ps}\} = [A]^{-1} \{F_{ps}\}; \quad \{B_{ss}\} = [A]^{-1} \{F_{ss}\}; \quad \{q_s\} = -\left[\{B_{ss}\}^H \{B_{ss}\} \right]^{-1} \{Z_{ps}\}; \tag{5}$$

where $\{F_{ps}\}$ and $\{F_{55}\}$ denote the loading vectors due to primary sources alone and secondary sources alone. The secondary source strengths for the ANC system are computed using quadratic minimization of acoustic potential energy as shown in eq. 5, suggested by Nelson *et al*. (1987). The optimized source strength due to primary and M secondary sources can be calculated for each exciting frequency as:

$$Z_n = Z_{ps} + \sum_{m=1}^{M} B_{ssm} q_{ssm} \tag{6}$$

3. VALIDATION

The SPL of a cavity excited by a primary monopole source controlled by various secondary source controlled by various secondary sources were analysed by Raghu (2005) has considered for ANC validation. In this study ANC is applied to a rectangular cavity having dimensions of 4 m × 5 m × 3 m and the SPLs are calculated with two secondary sources (SS). It is assumed that a monopole primary source is located with coordinates (3.33 m, 0.833 m and 0 m) and a frequency range of excitation for primary source is 30-90 Hz and the source strength of the primary source is taken as 0.1 m_3/s. Two secondary sources are placed arbitrarily within the enclosure with coordinates (1.33 m, 1.67 m and 3 m) and (1.33 m, 0 m and 1 m) respectively. Fig. 3 shows the sound SPL at coordinates (0 m, 3.33 m and 1 m). From Fig. 3, it is clear that with ANC the SPLs are considerably reduced at resonant frequencies. The agreement is good for the entire frequency range where the analysis performed.

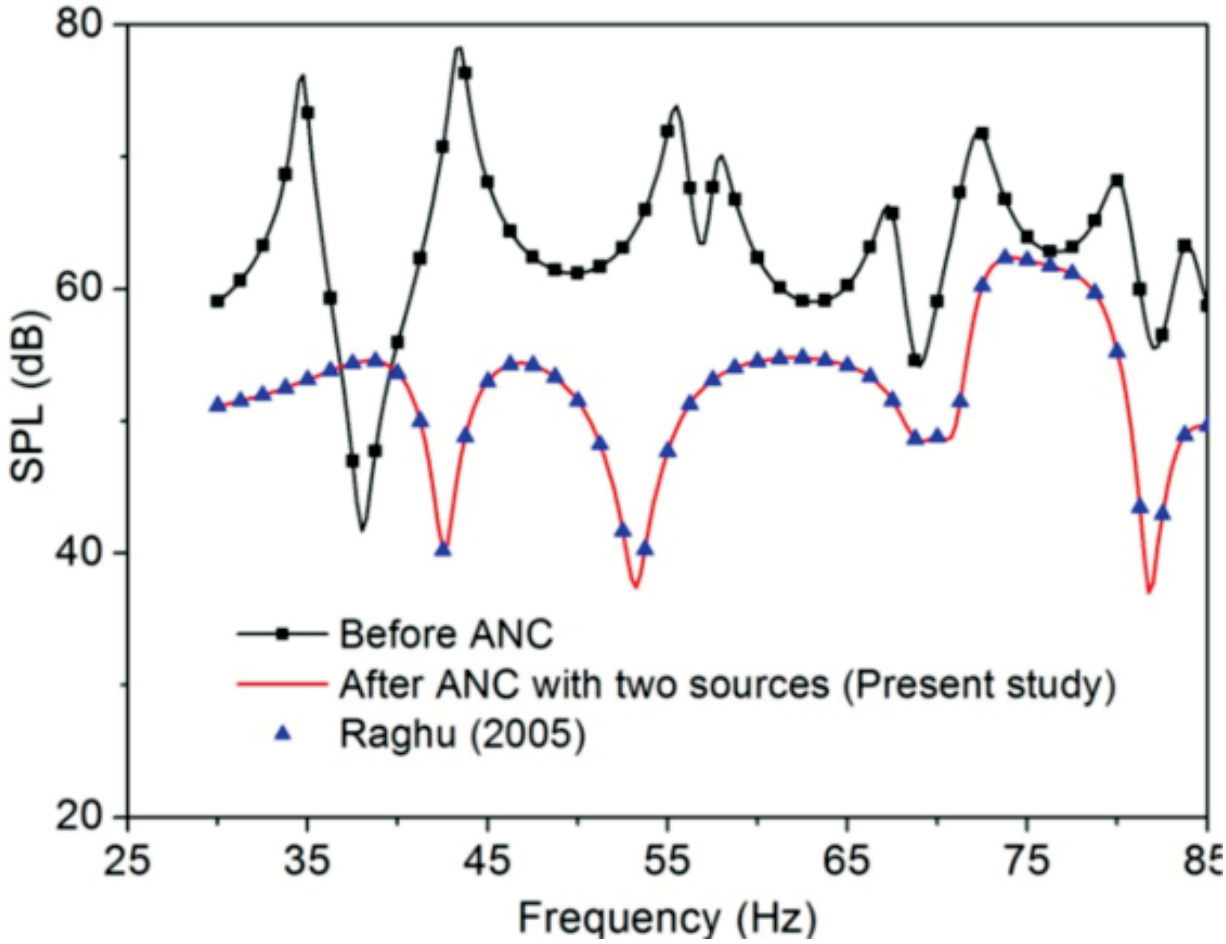

Fig. 3. Sound pressure level comparison

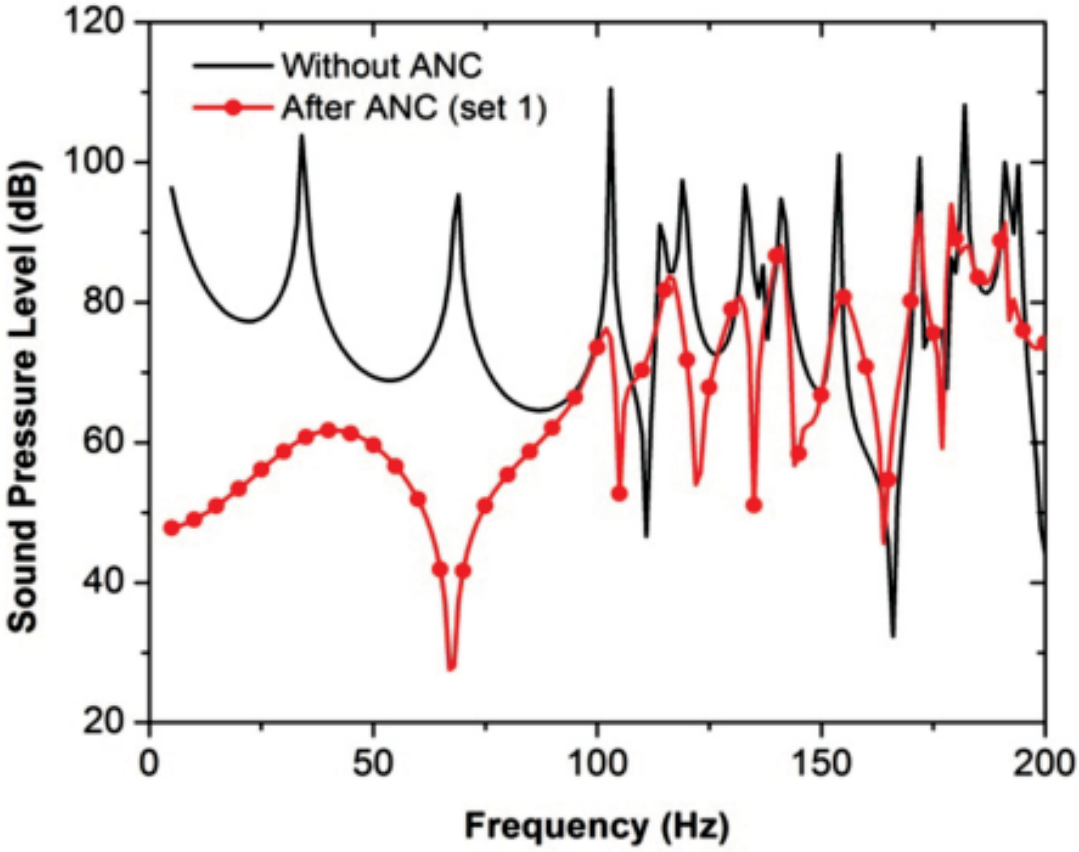

Fig. 4. Influence of ANC on SPL based on set 1 locations

4. CAR LIKE CAVITY

The structure under investigation is a three dimensional rectangular car like rigid cavity as shown in Fig. 1. The acoustic cavity is modeled using FEM with pressure as a field variable. Cavity is modelled with 20-noded brick finite element model with pressure as field variable as shown in Fig. 2. This finite element model is implemented using MATLAB. The programs implement the equations derived by Nelson *et al.* (1987) in section 2. In order to find the converged mesh size calculated eigenvalues from the finite element model are compared with the natural frequencies of the cavity obtained by analytical method. It is assumed that the cavity is excited by a monopole primary source, and the frequency range of excitation for primary source is 5-200 Hz and the source strength of the primary source is taken as 0.1 m^3/s. Three secondary sources are placed inside the cavity and its source strengths are predicted using eq. 5. Three secondary sources are placed arbitrarily for various different positions within the enclosure as shown in Table 1. Figures 4 and 5 show the SPL at coordinates (1.25 m $\times$ 1 m $\times$ 5 m) for set 1 and set 4 locations of secondary sources. From Figures 4 and 5, one can see that ANC is very effective below 100 Hz. In order to find the optimized secondary sources locations genetic algorithm has been used. The number of genes in each chromosome is assumed to be three to represent the magnitude of location of three secondary sources and their orientations with the Primary source. Here, the length of chromosome is 8 in which first four genes indicate the magnitude of location of secondary sources and the initial population size is assumed as 20. The main objective is minimization of the sound pressure level at receivers location by optimal location of secondary sources. The fitness function is established by mapping the objective function through mapping, scaling and normalization. Figure 6 shows the SPL at receivers location due to optimized secondary sources locations. It is clear that optimized secondary sources locations leads to 20-25 dB reduction in SPL from 100-200 HZ at receivers location.

Table 1. Sources and its locations

Secondary sources		Location	Coordinate (m)		
			X	Y	Z
Arbitrary Set 1	SS1	1285	0	0.75	2.5
	SS2	1292	1.25	0.75	2.5
	SS3	2524	0.72	1.5	4
Arbitrary Set 2	SS1	1153	0	0.65	3.25
	SS2	1160	1.25	0.65	3.25
	SS3	1979	0.72	1.18	4
Arbitrary Set 3	SS1	347	1.2	0.22	0
	SS2	486	1.25	0.22	3
	SS3	2543	0.36	1.5	4.5
Arbitrary Set 4	SS1	330	0.72	0.11	5
	SS2	425	1.25	0.22	1.75
	SS3	2521	0.45	1.5	4
Optimized	SS1	1971	0.72	1.18	3.5
	SS2	246	0.1	0.11	0.3
	SS3	806	0.1	1.5	5

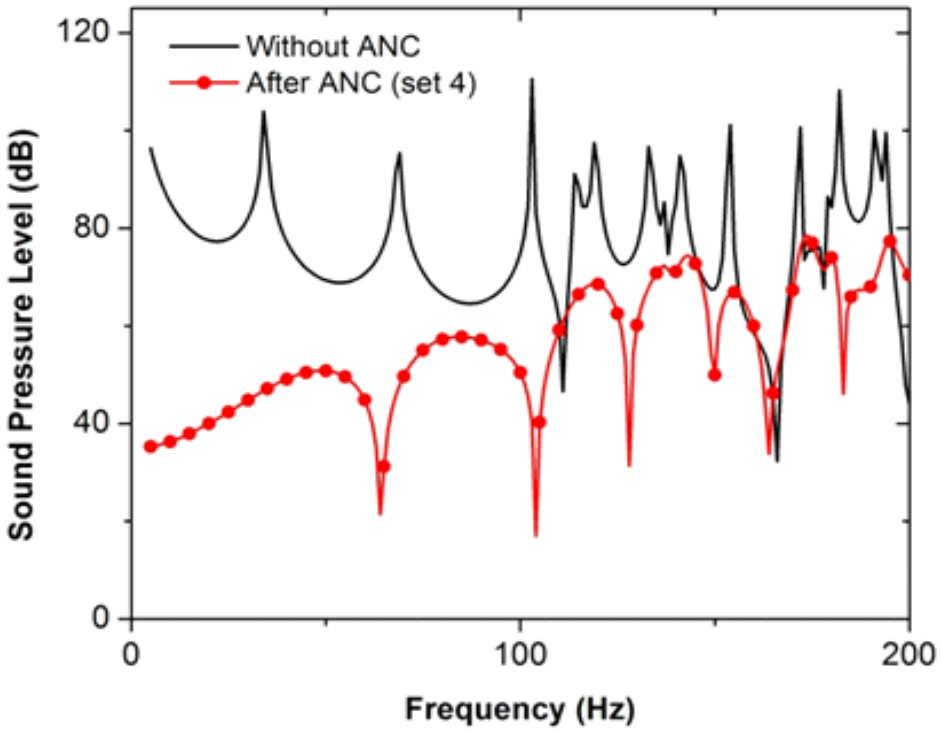

Fig. 5. Influence of ANC on SPL based on set 4 locations

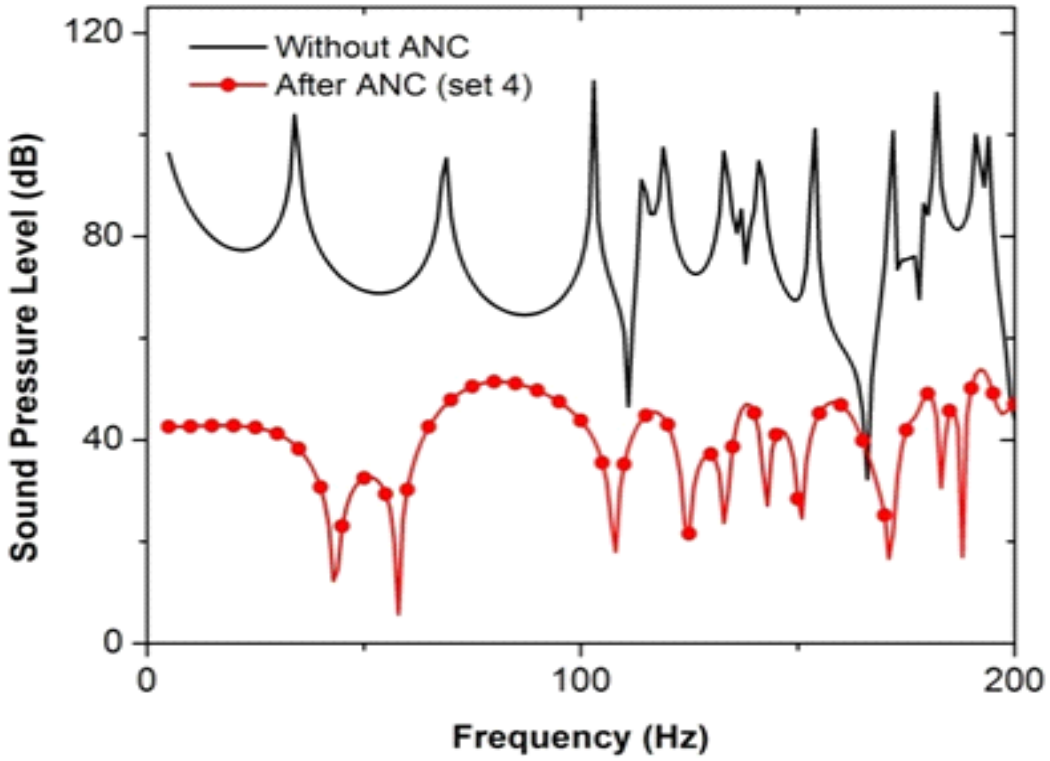

Fig. 6. Influence of ANC on SPL based on optimized locations

5. CONCLUSION

In this work optimization of secondary sources for active noise control in a car like rigid cavity has been investigated. Sound pressure level at receives location has been obtained due to a point source excitation. Genetic algorithm has been used to obtain the optimum secondary sources locations in order to minimize the sound pressure level inside the cavity at receivers location. Results obtained from the model shows the reduction of mean sound pressure level up to 20-25 dB in 100 - 200 Hz band by changing the secondary sources positions from arbitrary to optimized locations.

6. REFERENCES

[1] P.A. NELSON, A.R.D. CURTIS, S.J. ELLIOTT and A.J. BULLMORE, 1987. The active minimization of harmonic enclosed sound fields, Part I: Theory, *Journal of Sound and Vibration*, **117**, 1-13.

[2] A.J. BULLMORE, P.A. NELSON, A.R.D. CURTIS and S.J. ELLIOTT, 1987. The active minimization of harmonic enclosed sound fields. Part II: A computer simulation, *Journal of Sound and Vibration*, **117**, 15-33.

[3] S.J. ELLIOTT, A.R.D. CURTIS, A.J. BULLMORE and P.A. NELSON, 1987. The active minimization of harmonic enclosed sound fields. Part III: Experimental verification, *Journal of Sound and Vibration*, **117**, 35-58.

[4] W. PARKINS, S.D. SOMMERFELD and J. TICHY, 2000. Narrowband and broadband active control in an enclosure using the acoustic energy density, *The Journal of the Acoustical Society of America*, **108**, 192-203.

[5] W. AKL and A. BAZ, 2000. Active vibration and noise control using smart foam, *Journal of Vibration and Control*, **12**, 1173-1203.

[6] F.C. SGARD, X. OLNY, N. ATALLA and F. CASTEL, 2005. On the use of perforations to improve the sound absorption of porous material, *Applied Acoustics*, **66**, 625-651.

[7] V. RAGHU, 2005. Optimization of secondary sources for active noise control, M.S.Thesis, Indian Institute of Technology Madras, Chennai, pp.10-55.

Journal of Acoustical Society of India : Vol. 40, No. 4, 2013 (pp. 239-244)

Performance Analysis of Speckle Noise Filters for Medical Ultrasound Images

P. Thirumoorthy[1]* and K.M. Prabusankarlal[2]
[1]Department of Electronics& Communication,
Government Arts& Science College, Paramakkudi
[2]Department of Electronics & Communication,
K.S.R. College of Arts and Science, Tiruchengode
**e-mail:tmoo@rediffmail.com*

[Received: 19.02.2013; Revised: 18.07.2013; Accepted: 22.10.2013]

ABSTRACT

Ultrasound is a relatively inexpensive, noninvasive, and portable technique for imaging the internal anatomy for medical diagnosis. The Speckle noise, an inherent nature of ultrasound often contaminates the image, significantly degrades the quality by discriminating fine details which may contain vital information and complicates the diagnostic decisions. The Speckle noise removal is the general pre-processing step for feature extraction, analysis, and recognition of ultrasound imaging. This paper analyzes the performance of different techniques proposed for the suppression of this multiplicative noise which is very difficult to be removed. Statistical quantity measures such as Mean Square Error (MSE), Root Mean Square Error (RMSE) and Peak Signal-to-Noise Ratio (PSNR) are used to measure and compare the quality of the enhanced images.

1. INTRODUCTION

Ultrasonic plays an important role in medical diagnosis by revealing the internal anatomy of organs to medical practitioners for accurate prediction of abnomabilities which may be treated if detected at the earliest [1]. The main problem faced by them is the noise introduced due to the consequence of the coherent nature of the wave transmitted during the ultrasonic process. These noises tend to corrupt the quality of the image and an inferior quality image may lead to incorrect diagnosis [2]. Speckle noise affects the ultrasound images which are a complex phenomenon, which degrades image quality with a backscattered wave appearance which originates from many microscopic diffused reflections that passing through internal organs and makes it more difficult for the observer to discriminate fine detail of the images in diagnostic examinations [3]. Suppressing this speckle noise from an ultrasonic image by retaining the thin and small image features is the primary step in processing medical ultrasonic images [4].For the early detection of cancers, such as breast cancer ,prostate cancer, lung Cancer and cervical cancer, Ultrasound imaging method is suitable to diagnose and progenies. The accurate detection of region of interest in ultrasound image is crucial.

In this paper, different methods proposed for suppressing and removing speckle noise are analyzed. Using statistical measures such as Signal-to-Noise Ratio (SNR), Peak Signal-to-Noise Ratio (PSNR), and Root Mean Square Error (RMSE) the performance of the speckle filters are compared and evaluated with different medical images. This paper is organized as follows: Section 2 describes problems associated with noise generated during ultrasound process. Section 3 describes various spatial filtering techniques for denoising the speckle noise in the ultrasound medical image. Section 4 discusses about our experimental analysis and discussion. Section 5 concludes this paper and provides direction for further research.

2. PROBLEM DESCRIPTION

A digital image is defined as a two dimensional functionf(x,y), where x and y are spatial coordinates and the amplitude of f at any pair of coordinates (x,y) is called the intensity or grey level of the image [5]. The noise contaminates the data sets collected by image sensor and the region of interest in the image is degraded, which makes the original image not suitable for applying image processing techniques and analysis for medical diagnosis. As a preprocessing step, an image enhancement technique is mandatory before image is processed and analyzed. The noise removal in the image is still a challenging problem and so an efficient filtering method is necessary for removing noise in the images which introduces artifacts and causes blurring of the image. The speckle noise [6] is observed in ultrasound images where images are corrupted by a random granular pattern that delays the interpretation of the image content and reduces the chances of detection of features of interest. Noise is generally grouped into two categories viz., image data independent noise [7] and image data dependent [8] noise.

2.1 Speckle Noise

Speckle noise is a kind of data dependent noice found in the ultrasonic image is caused by errors in data transmission [10]. The corrupted pixels by speckle noise are either set to the maximum or minimum value which appears as something like a snow in image or have single bits flipped over. Speckle noise has the characteristic of multiplicative noise [11] and it follows a gamma distribution and is given as

$$F(g)=\left[\frac{g^{\propto-1}}{(\propto-1)!\alpha^{\propto}}e^{\frac{g}{a}}\right]\cdot$$ Where, variance is α^2 and g is the gray level.

3. SPECKLE FILTERING TECHNIQUES

The primary goal of an image enhancement technique is to adjust the digital image so that the resultant image is more suitable than the original image for further processing and analysis [12]. The image processing function in a spatial domain can be expressed as g(x,y) = T(*f*(*x,y*)). Where, T is the transformation function, *f*(*x,y*) is the pixel value of input image, and g(x,y) is the pixel value of the processed image. Different filtering techniques such as Median Filter [13], FIR Filter [14], DCT Filter [15] and FFT filter are used for denoising the different medical images and four other filters are also proposed.

3.1 Entropy Filter

The proposed entropy filter filters image by replacing every value by the information entropy of the values in its range r neighborhood [17]. The entropy H(L) of the belief over L is defined as H(L)= - $\sum_{\tau}$ Bel(L=l) log Bel(L=*l*). The s denote the measurement, the change of the entropy of Bel(L) given s is defined as $\Delta H(L \mid s) :=$ H(L | s) -H(L). The term H(L | s) is the entropy of the belief Bel(L) after incorporating the measurements.

3.2 Range Filter

This filter uses the local-intensity subrange of pixel intensity values within a window [18]. It uses the morphological functions to determine the maximum and minimum values in the specified neighborhood and uses the padding behavior of these morphological functions, $h(x) = k_r^{-1}(x) \int_{-\infty}^{\infty}\int_{-\infty}^{\infty} f(\xi)sf(\xi)\, f(x)d\xi$. The *sf*(*ξ*), *f*(*x*))measures the photometric similarity between the pixel at the neighborhood center x and that of a nearby point.

3.3 Standard Deviation Filter

The standard deviation filter [12] calculates the standard deviation for each group of pixels in the subimage, and assigns this value to the center pixel in the output image. The objective function of standard deviation filter is given by

$$S_w = \sqrt{\frac{1}{n^2 \sum_{r=1}^{n} \sum_{c=1}^{n} (x_{rc} - \bar{x})^2}}$$

where, nxn is the total number of pixels in a subimage, w denotes the indices of the subimage, x_rc is the value of the pixel at row r and column c in the subimage and x is the mean of pixel values in the window.

3.4 Tophat Filter

The Tophat filter is proposed for speckle noise removal which performs morphological top-hat filtering on grayscale or binary input image [19]. This algorithm computes the morphological opening of the image and then subtracts the result from the original image. In Fourier space, a top hat filter selects a band of signal of desired frequency by the specification of lower and upper bounding frequencies. Let $f:E \rightarrow R$ be a grayscale image, mapping points from a Euclidean space or discrete grid E (such as R^2 or Z^2) into the real line. Letb(x) be a grayscale structuring element. The white top-hat transform of f is given by: $T_w(f) = f - f \circ b$, Where, the o denotes the opening operation.

5. EXPERIMENTAL ANALYSIS AND DISCUSSION

The proposed algorithms have been implemented using MATLAB 7.8. The performance of various spatial enhancement approaches are analyzed and discussed. The images are categorized into three groups; Breast, Prostate and cervix. More than 240 images are taken as samples and these images are fed into appropriate functions of all the eight filters. The parameters related with the image are commonly set in the filter functions for all images. Over 240 ultrasonic medical images in three categories are fed to all the eight filter algorithms and to evaluate the performance of filters three standard measures are taken;the Mean Square Error (MSE), Root Mean Square Error (RMSE), and Peak Signal-to-Noise Ratio (PSNR). The PSNR computes the peak signal-to-noise ratio, in decibels, between the input ultrasound image and output enhanced image which illustrates quality measurement between the original and enhanced image. The higher the PSNR, the better the quality of the enhanced image. To compute the PSNR, the MSE is calculated first using the following equation $MSE = \frac{\sum_{M,N} (I_1(m,n) - I_2(m,n)^2)}{M * N}$

where, M and N are the number of rows and columns in the images. The RMSE is given by RMSE = √MSE The following equation computes the PSNR. $PSNR = 10 \log_{10} \left[\frac{R^2}{MSE} \right]$

Table 1. Filter performance for Ultrasound Breast , Prostate and Cervix images

Filter	Breast image			Prostate image			Cervix image		
	MSE	RMSE	PSNR	MSE	RMSE	PSNR	MSE	RMSE	PSNR
Median Filter	8196	90.53	8.99	7536	86.81	9.36	5892	76.75	10.42
FIR Filter	14512	120.46	6.51	12635	111.19	7.11	23765	154.16	4.37
DCT Filter	9453	97.22	8.37	6755	82.18	9.83	5763	75.9	10.52
FFT Filter	5432	73.7021	10.78	4537	67.35	11.56	5547	74.47	10.69
Entropy Filter	8237	90.75	8.97	9459	97.25	8.37	7845	88.57	9.18
Range Filter	5841	76.42	10.46	5661	75.23	10.60	6687	81.77	9.87
SD Filter	7829	88.48	9.19	8228	90.7	8.97	8438	91.85	8.86
Tophat Filter	4627	68.02	11.47	3959	62.92	12.15	5287	72.71	10.89

where, R is the maximum fluctuation in the input image data type. Since we defined them as an 8-bit unsigned integer data type, R is 255.The Table 1 shows the calculated values using core i3 based PC with MATLAB 7.8. The kernel size of images is kept at 3x3.

ULTRASOUND BREAST IMAGES

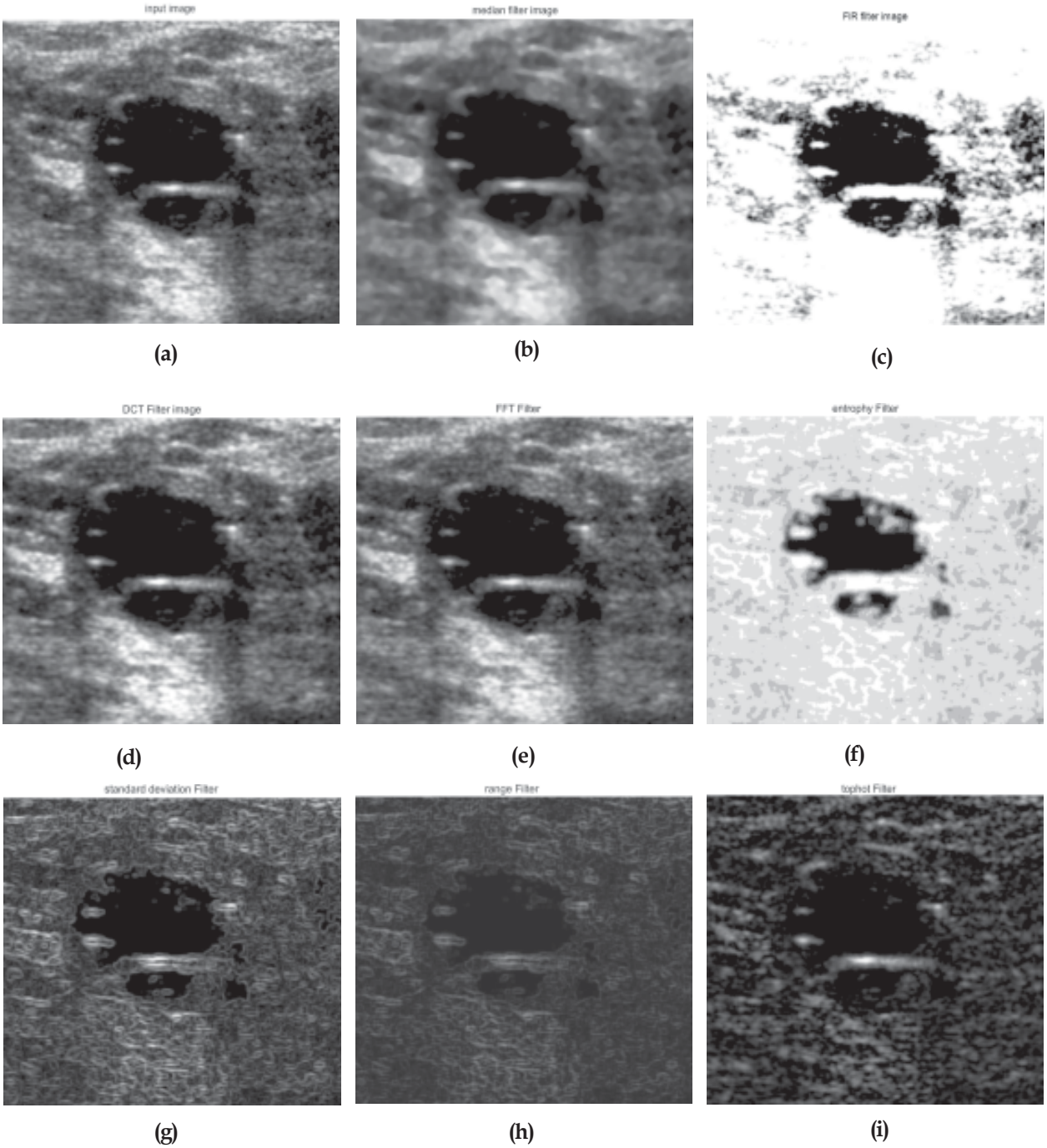

Fig 1. Ultrasound Breast image (a)Input image (b) Median Filter (c) FIR Filter(d) DCT Filter(e) FFT Filter (f) Entropy Filter (g) Range Filter (h) Standard Deviation Filter (i) Tophat Filter

The original ultrasound image and filtered images obtained by various filtering techniques are shown in figure 1. Medical ultrasonic images of the breast, prostate (not shown) and cervix (not shown) are filtered and their performance parameters are analyzed. If the value of MSE is low and the value PSNR are larger and the enhancement approach is better. The Table 1 shows the performance analysis of the different filtering techniques we have used. It is observed from the tables in terms of high PSNR and visual observation of the enhanced image, the proposed tophat filter removes the speckle noise better than other existing and proposed approaches.

6. CONCLUSION

The performance of noise filters are compared analyzed and evaluated using quantitative measures such as MSE, RMSE and PSNR and also in term of visual quality of the images. Some methods removed speckle noise better but the quality of the image too degraded. Since the finest details of the images are crucial for further processing such as edge detection and segmentation process, they have to be preserved. Very few algorithms removed speckle noise as well as preserved the details of the breast, prostate and cervix medical images during the evaluation process, among them the tophat filter performed better than others.

7. REFERENCE

[1] YANONG ZHU, STUART WILLIAMS and REYER ZWIGGELAAR, 2006 Computer Technology in Detection and Staging of Prostate Carcinoma: A review, *Medical image Analysis* **10**, p 178-199.

[2] S. SUDHA, G.R. SURESH and R. SUKANESH 2009 Speckle Noise Reduction in Ultrasound Images by Wavelet Thresholding based on Weighted Variance, *International Journal of Computer Theory and Engineering*, 1, No. **1**, 1793-8201

[3] HOSSEIN RABBANI, MANSUR VAFADUST and PURANG ABOLMAESUMI, 2008 Speckle Noise Reduction of Medical Ultrasound Images in Complex Wavelet Domain Using Mixture Priors, *IEEE transactions on biomedical engineering*, **55**, no. 9.

[4] ARPIT SINGHAL and MANDEEP SINGH, 2011 Speckle Noise Removal and Edge Detection Using Mathematical Morphology, *International Journal of Soft Computing and Engineering* (IJSCE) ISSN: 2231-2307, **1**, 5.

[5] R.C. GONZALEZ and R. WOODS 1992 'Digital Image Processing', Addison-Wesley Publishing company.

[6] Image Processing Fundamentals - Statistics, "Signal to Noise Ratio", 2001.

[7] YUNYI YAN and BAOLONG GUO. 2006 Application of Wavelet Neural Network (WNN) and Gradient Descent Method (GDM) in Natural Image Denoising. *Journal of Computational Information Systems*, **2**(**2**):625-631.

[8] D. ROBERT NOWAK, 1999"Wavelet based Rician noise Removal", *IEEE Transaction on image processing*, 8, no. **10**, PP 1480.

[9] A.K. JAIN, 1989 fundamental of digital image processing. Englewood cliffs, NJ Prentice-Hall.

[10] MATIAS BARBER, FRANCISCO GRINGS, PABLO PERNA, MARCELA PISCITELLI, MARTIN MAAS,CINTIA BRUSCANTINI, JULIO JACOBO-BERLLES, and HAYDEE KARSZENBAUM. 2012 Speckle Noise and Soil Heterogeneities as Error Sources in a Bayesian Soil Moisture Retrieval Scheme for SAR Data. *IEEE journal of selected topics in applied earth observations and remote sensing*, **5**, 3.

[11] K. BALA PRAKASH, R. VENU BABU and B. VENU GOPAL. 2011 Image Independent Filter for Removal of Speckle Noise. *IJCSI International Journal of Computer Science Issues*, **8**, Issue 5, 3.

[12] K. THANGAVEL and R. MANAVALAN, 2009 Laurence Aroquiaraj. I ,Removal of Speckle Noise from Ultrasound Medical Image based on Special Filters: Comparative Study, ICGST-GVIP Journal, ISSN 1687-398X, (**9**), Issue (III).

[13] LIM and S. JAE , 1990 Two-Dimensional Signal and Image Processing, Englewood Cliffs, NJ, Prentice Hall.

[14] N.J. FLIEGE, 1994 Multirate Digital Signal Processing: Multirate Systems, Filter Banks, Wavelets. West Sussex, England: John Wiley & Sons.

[15] HAITHAM HASSANIEH, 2012 Piotr Indyk, Dina Katabi, and Eric Price, "Simple and Practical Algorithm for Sparse Fourier Transform," ACM-SIAM Symposium on Discrete Algorithms (SODA), Kyoto, January
[16] R. SIVARANJANI, 2011 Performance Analysis of Transform based Image Compression Algorithms. CiiT International Journal of Digital Image Processing, December.
[17] R.C. GONZALEZ, R.E. WOODS and S.L. EDDINS, 2003 Digital Image Processing Using MATLAB, New Jersey, Prentice Hall, Chapter 11.
[18] C. TOMASI and R. MANDUCHI, 1998 Bilateral Filtering for Gray and Color Images. Proceedings of the IEEE International Conference on Computer Vision, Bombay, India.
[19] MING ZENG, JIANXUN LI and ZHANG PENG , 2006 The design of Top-Hat morphological filter and application to infrared target detection, Infrared Physics & Technology, **48**, 1, 67-76.

Journal of Acoustical Society of India : Vol. 40, No. 4, 2013 (pp. 245-249)

Ultrasonic Study of Chemical Mixture Used for Preparation of Fiber from Date Palm Leaves

G. Nath[1]*, A. Sarangi[1] and R. Paikaraay[2]
[1]*Dept. of Physics, VSS University of Technology, Burla, Sambalpur (Odisha)*
[2]*Dept. of Physics, Ravenshaw University, Cuttack (Odisha)*
**e-mail:ganeswar.nath@gmail.com*

[Received: 29.04.2013; Revised: 25.06.2013; Accepted: 25.10.2013]

ABSTRACT

Propagation of ultrasonic waves in chemical mixture have greater importance in study of different acoustic parameter which are provides information about the strength of different composite materials prepared from different agricultural wastes.Measurement of ultrasonic velocity and density at different concentration of solvent mixture has been carried out at different temperature using multi frequency ultrasonic interferometer. The data obtained are used to evaluate various acoustic parameters in view of identification of the presence of different interaction under prevailing conditions. The variation of ultrasonic velocity, density and other acoustic parameters with concentration under different physical conditions provides information about the mechanical strength of the fiber.

1. INTRODUCTION

High intensity ultrasonic waves are generally employed in the areas of cleaning, plastic welding, machining etc.In addition to these applications, it is observed that if a liquid mixture is subjected to irradiation of high intensity ultrasonic waves, alternate compression and expansion modes takes place which leads to change in some thermodynamic properties of the liquid mixture. As a result of which the variation in speed of ultrasonic waves takes place which affects some of the mechanical properties of the natural fiber. Ultrasonic methods are directly sensitive to these changes and can be used to assess the integrity of the composite structure. The absorption of ultrasound in polymer composite systems is governed by local modes of motion and cooperative because of the existence of strong intermolecular interaction within the liquid mixture. The manner in which the propagation of the ultrasonic wave is affected by structure of the liquid results in parameters that can lead to the binding between the natural fibers. Variation in thermal and acoustic properties with composition provides added information regarding the intermolecular interactions present in a system. The sign and magnitude of the nonlinear deviations from ideality as a function of composition and frequency may be ascribed to the presence of weak or strong type of interaction between unlike molecules. The excess acoustic parameters of binary mixtures have been satisfactorily used in explaining the extent of interactions between mixing components [1-3].The present investigation deals with two important liquids namely acetone and methanol. Both the liquids under investigation are very useful chemicals and of industrial significance. The mixture of these liquids is used in the preparation of date palm leaf fiber.This treatment removes a certain amount of lignin, wax and oils covering the external surface of the fiber cell wall, depolymerizes cellulose and exposes the short length crystallites. This treatment has two effects on the fiber i.e. it increases surface roughness resulting in better mechanical interlocking, and it increases the amount of cellulose exposed on the fiber surface, thus increasing the number of possible reaction sites. Date palm leaves as agricultural waste generated

from regular pruning of older leaves have low economic utilization values. Normally, farmers leave this waste outdoors which could provide good environment for certain pests like rodents and insects. Therefore, from both environmental and economic points of view, simultaneous utilization of plastic and date palm leaves wastes for producing a plastic-palm leaves fiber composite wood with good physical, mechanical and chemical properties can be as alternative to natural wood.

2. EXPERIMENTAL DETAILS

In the present study the chemicals used are of analytical grade purified by standard procedure [4-6] and redistilled before use. Density was determined with a Pyknometer of 25cm3 capacity, calibrated with de-ionized double distilled water. Ultrasonic speed was measured by a single crystal variable path ultrasonic interferometer model MX-3, Mittal Enterprises New Delhi, India operating at different frequencies of 1MHz, 3MHz and 5MHz. The temperature stability is maintained within 0.1K by circulating thermo stated water around the interferometer cell that contains the liquid, with circulating pump. Binary mixtures of acetone were prepared with methanol and kept in an enclosed container properly.

3. THEORY

The experimental measured values of ultrasonic speed and computed values of density are used to compute acoustic parameters such as intermolecular free length (L_f), isentropic compressibility (β), acoustic impedance (Z) and bulk modulus (K) and their excess values. The above acoustic parameters are determined with the help of the following relationship [7].

Isentropic compressibility, $\beta = (\rho C^2)^{-1}$ …….. (1)

Intermolecular free length, $L_f = K\beta^{1/2}$ …….. (2)

Acoustic impedance, $Z = \rho C$ …….. (3)

Bulk modulus, $K = \rho C^2$ …….. (4)

and their excess values are calculated as

$\beta^E = \beta_{mix} - (X_A\beta_A + X_B\beta_B)$ …….. (5)

$L_f{}^E = L_{fmix} - (X_A L_{fA} + X_B L_{fB})$ …….. (6)

$Z^E = Z_{mix} - (X_A Z_A + X_B Z_B)$ …….. (7)

$K^E = K_{mix} - (X_A K_A + X_B K_B)$ …….. (8)

where X_A, X_B, β_A, β_B, β_{mix}, L_{fA}, L_{fB}, L_{fmix} Z_A, Z_B, Z_{mix} B_A, B_B and B_{mix} are mole fraction, isentropic compressibility, inter molecular free length, acoustic impedance bulk modulus of methanol, acetone and mixture respectively. The constant K is temperature dependent which is given as $[93.875 + (0.375T)] \times 10^{-8}$ [8].

4. RESULTS AND DISCUSSION

The ultrasonic speed in methanol increases smoothly with mole fractions of acetone as shown in Fig.1. Acetone contains carbonyl functional group, which is polar and hence it can interact with methanol like polar molecules through dipole- dipole interaction. In pure acetone there is dipole-dipole as well as the dispersive interactions.

As the concentration of acetone gradually increases the different type of interaction comes into existence due to tautomerisim. In acetone molecules the hydrogen bonding comes into existence between the like molecules of aldol at –OH end. In addition with hydrogen bonding, keto and enol form of tautomerisim comes

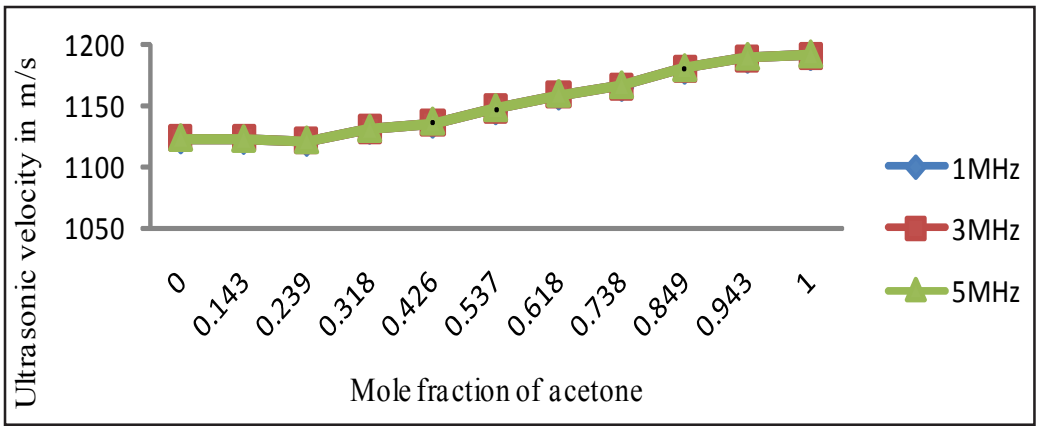

Fig. 1. Variaton of ultrasonic velocity in methanol with acetone

into exisistence with maximum percentage of keto form for which the dipole - dipole interaction takes vital role for increasing the ultrasonic speed in high concentration of acetone .As seen from the profile, the frequency has no significant contribution in variation of ultrasonic speed in the binary mixture though the frequency varies from1MHz-5MHz. Figures 2 and 3 demonstrates the variation of $\hat{a}^E$ and L_f^E for binary mixture of acetone and methanol which are found to be negative over the entire composition range.

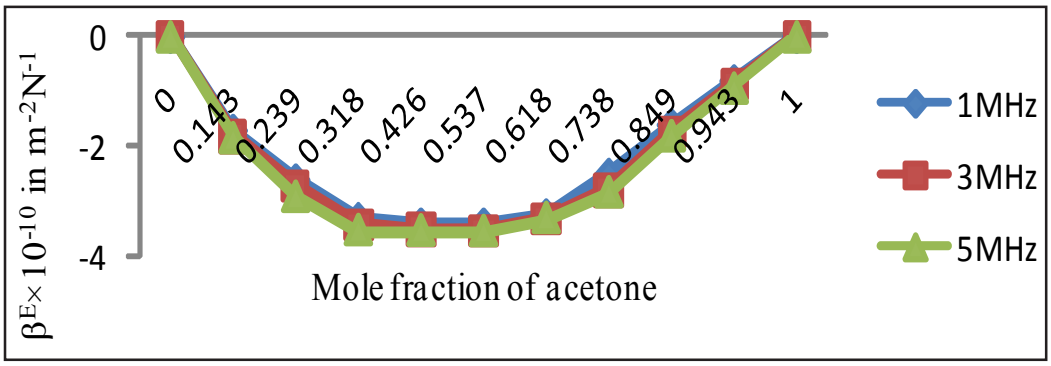

Fig. 2. Variaton of excess isentropic compressibility in methanol with acetone

The negative values of excess isentropic compressibility indicates that the liquid mixture is less compressible than the pure liquids forming the solution and molecules in the mixture are more tightly bound than in pure liquids. Thus negative values of excess isentropic compressibility indicate strong specific interactions between component molecules and interstitial accommodation of smaller molecules in the void created by bigger molecules. The negative excess isentropic compressibility results reduction of volume of mixture favoring the fitting of component molecules in to each other. Greater the negative value of ?E stronger is the attractive interaction between the component molecules such as hydrogen bonding; dipole-dipole interaction and other specific interactions between unlike molecules are operative in the system [9]. This indicates that the interaction is stronger in acetone-methanol mixture .This supports the facts that acetone - methanol mixture is more compatible in bleaching of the surface date palm leaves due to interaction between the composition of date palm leaves and chemical mixture. Again, the variation of frequency is also not given any significant result in excess values of isentropic compressibility except in equimolar region due to strong interaction there is slight separation in profiles. The variation of excess free length is presented in Fig. 3.

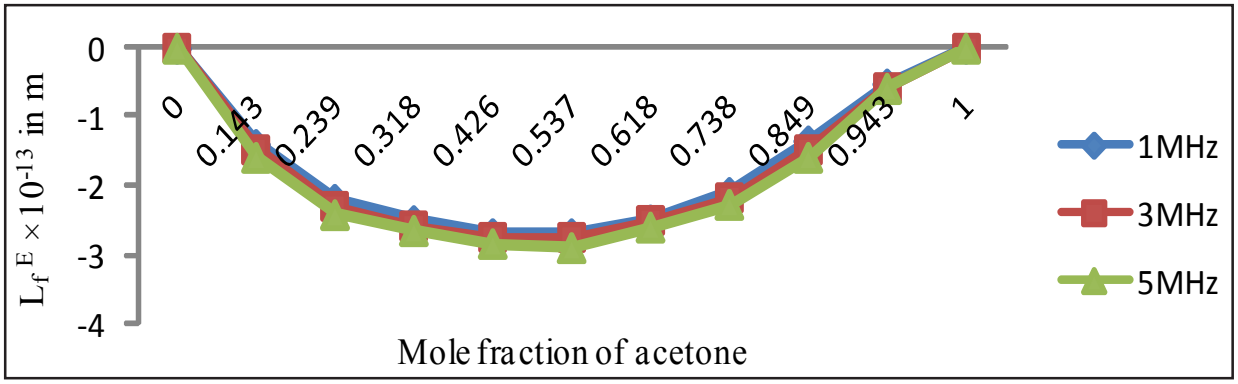

Fig. 3. Variaton of excess intermolecular free length in methanol with acetone

The excess free length is negative over the entire range of composition investigated exhibiting a broad minimum around equimolar region of acetone and methanol. Considering the effect of frequency, it was observed that no significant results also obtained in this case like the above situations. The variation of excess free length further supports the variation of other excess parameters like excess acoustic impedance and excess bulk modulus of the mixtures.

The excess acoustic impedance in the mixtures was found to be negative for the entire composition range of acetone. From the Fig. 4 it is instructive that the variation of acoustic impedance is very smooth in acetone-

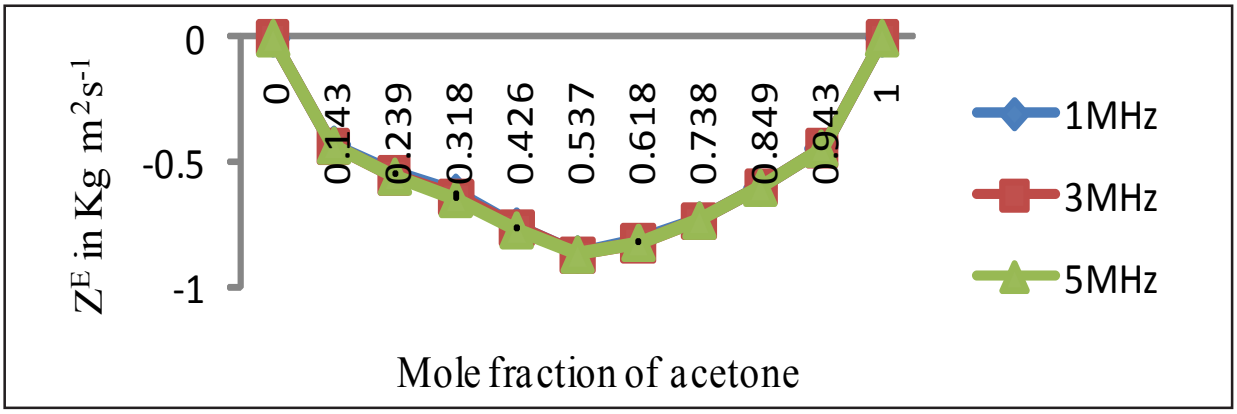

Fig. 4. Variaton of excess acoustic impedance in methanol with acetone

methanol mixture. This due to fact that the occurrences of different intermolecular interactions like dipole-dipole interactions, dipole-induced dipole interactions, Vander Waals interactions in the liquid mixtures. The liquid mixture acetone-methanol has a clear minima in indicating the fact that more structural changes takes place in this mole fraction of chemical mixture which may favors the interaction of the liquid mixture with the chemical composition of the date palm leaves. As the bulk modulus is the reciprocal of compressibility so its variation is supported by variation of excess compressibility.

From the profiles for excess bulk modulus as shown in Fig. 5 it is informative that with decrease of volume of the mixture pressure increases. As a result of which the intermolecular interaction between the liquid molecules increases and the components of the mixture are tightly bound with each other and also with the chemical composition of the date palm leaves. This results in increase of surface roughness and interlocking in edges of the date palm leaves.

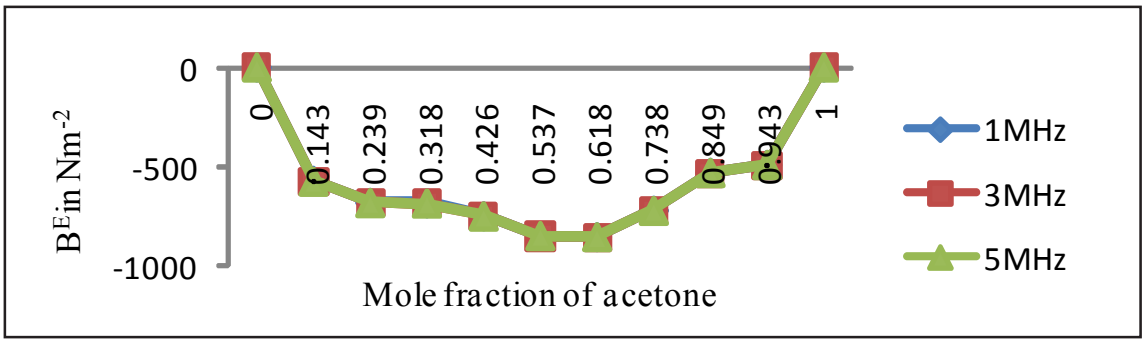

Fig. 5. Variaton of excess bulk modulus in methanol with acetone

5. CONCLUSION

The behavior of different acoustic parameter clearly indicates that there is compatibility between the selected solvent mixtures. The compatibility is strongly dependent on different concentration of binary mixture rather than factor frequency of ultrasonic waves. This compatibility leads to presence of different intermolecular interactions like dispersions, H-bonding, dipole-dipole interaction and dipole - induced dipole interaction etc. Due to presence of such fundamental interactions, the treatment of this mixture increases the surface roughness removing certain amount of lignin wax and oils covering the external surface of the date palm leaf cell wall. As a result it is found that better mechanical interlocking takes place and increases the no. of possible reaction sites which improves the fiber matrix adhesion, increases the strength of the composites, decreases its water absorption and improves its thermal stability.

6. REFERENCES

[1] A. ALI and A.K. NAIN, 1997 *Indian J. Pure and Appl*. physics, Vol-**19**, 41.
[2] J.D. PANDEY, P. JAIN and V.VYAS, 1994 Praman, *J. Physics*, **43**, 361.
[3] G. NATH, S.ACHARAYA and R. PAIKARAY, 2007 *Journal of acoustic society of India*, **34** No-4, pp 135.
[4] A.I. Vogel, Text Book of Practical Organic Chemistry, Third Edition (Longmans, London). 1937
[5] J.A. RIDDICK and W.B. BUNGER, 1970 Organic Solvents (Wiley - Inter-Science, New York).
[6] A. WEISBERGER, Techniques of organic chemistry, (Interscience, New York), Vol-III, (1955)
[7] K.P. THAKUR and N K GUPTA, 1983 Acustica, **53**, 59.
[8] B. JACOBSON and J.CHEM. 1952 Phys. **20**, 927.
[9] R.J. FORT and W.R. Moore, 1963 Trans Faradays, Soc., **61**, 2102, 18.

Journal of Acoustical Society of India : Vol. 40, No. 4, 2013 (pp. 267-272)

Prcessing for Emotions Induced by Hindustani Instrumental Music

Ranjan Sengupta[1], Anirban patranabis[1], Kaushik Banerjee[1], Tarit Guhathakurta[1], Samabrata Sarkar[1], Gautam Ganguli[2], Atanu Biswas[2], P.K. Saha[2] and Dipak Ghosh[1]

[1]Sir C V Raman Centre for Physics and Music, Jadavpur University, Kolkata
[2]Bangur Institute of Neuroscience, Kolkata

[Received: 25.04.2013; Revised: 28.07.2013; Accepted: 28.09.2013]

ABSTRACT

Music has an intriguing ability to evoke powerful emotions without having such an intrinsic link. However, establishing exactly how music communicates emotion is a topic of much debate. The present study concentrates on the signal analysis of two ragas (Chayanat and Darbari Kannada) played by an eminent sitar player as well as performing listening tests and EEG analysis on naïve listeners. An attempt was made to correlate the changes of EEG signal characteristics due to emotion with the note sequence of the ragas.

INTRODUCTION

Western classical music which is based on harmonic relation between notes versus the melodic mode (raga) structures in the Hindustani music system (HM) within the rhythmic cycle music may demand qualitatively different cognitive engagement. Each raga in the HM is conventionally assigned to a corresponding rasa/ emotion is known to consistently evoke certain emotions [1]. The artist exploits ones creativity and elaborates the raga well within the melodic framework to bring out the rasa or the emotion. The human brain, which is one of the most complex organic systems, involves billions of interacting physiological and chemical processes that give rise to experimentally observed neuro-electrical activity, which is called an electroencephalogram (EEG). The use of EEG signals as a vector of communication between men and machines represents one of the current challenges in signal theory research. The present study concentrates on the signal analysis of the aalap part of two ragas (eliciting contrast emotions, ie, joy/romantic and sorrow/pathos) played by an eminent sitar player and subsequently conducting listening tests with the raga clips along with the EEG analysis to study the emotion as processed in the brain.

1. EXPERIMENTAL DETAILS

Two ragas chosen are for our analysis are Chayanat (romantic/joy) and Darbari Kannada (pathos/sorrow). Each of these sound signals was digitized with sample rate of 44.1 kHz, 16 bit resolution and in a mono channel. From the complete playing of the ragas, segments of about 3mins and 40 seconds were taken out for analysis for each raga. Detection of pitch was done by using the open source software package WAVESURFER of KTH, Stockholm. The tonic (Sa) was extracted from the signal by the help of a musician and then the note sequence was found out. Signals processing was performed to find out the tempo, pitch sift and note distribution of the emotion revealing part. From the sequences the phrases which contain the emotion as identified by a

musician was played and subjected to listening tests by 30 listeners. The listeners' opinions were collected in the score sheet as in [1]. The listeners were asked to assign each raga clip to only one emotional category, if possible. Statistical elaboration of results in work was performed taking into account the choices of each listener. The data from the responses found in the score sheet was accumulated in a matrix where columns represented the number of the sound clips and the rows represented the listeners. Each value in the matrix gives the number indicating the emotion using the following code values:

1 anger, 2 joy, 3 sorrow, 4 heroic, 5 romantic, 6 serenity, 7 devotion, 8 anxiety, 9 nil emotion

EEG was done subsequently to record the brain-electrical response of two such listeners. Each listener was prepared with an EEG recording cap with 19 electrodes (Ag/AgCl sintered ring electrodes) placed in the

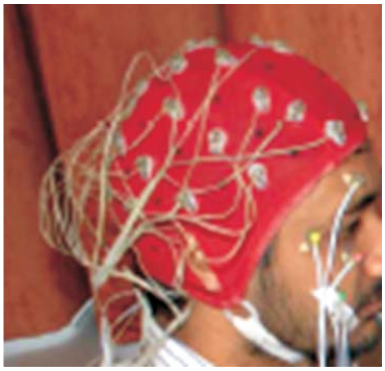

international 10/20 system. Impedances were checked below 5 kOhms. The EEG recording system (Recoders and Medicare Systems) was operated at 256 samples/s recording on customized software of RMS. The data was bandpass-filtered between 0.5 and 35Hz to remove DC drifts and suppress the 50Hz power line interference. Each listener was asked to be seated comfortably on a chair in a shielded measurement cabin. He was also asked to close his eyes. A sound system (Logitech R _ Z-4 speakers) with very low S/N ratio was set up in the measurement room that received input from outside the cabin. After initialization, a 16mins 20secs recording period was started, devoting 3minutes each at the start, 3minutes at the end and 3minutes in between the signals because of the relaxation from the preceding signal period. Each signal length was 3mins. 40 secs. Markers were set at start, signal onset/offset, and at the end of the recording.

2. RESULT AND DISCUSSION

After extracting note duration and transition time for the whole signal, it was observed a negligible difference between the two signals. Then with the help of expert musicians we have sorted out the portions of each raga signal where the emotion of that signal reveals. The notation of that part of the signals for each raga is shown below:

The phrase containg emotion as identified from the raga Chayanat sound clip by a musician. The time span of this phrase is 2.56.646 - 03.23.229 secs in the complete signal.

The phrase containg emotion as identified from the raga Darbari Kannada sound clip by a musician. The time span of this phrase is 03:17.496 - 03:39.550 secs in the complete signal. Extraction of the note duration of the above portions the distribution is shown in Fig. 1. In Darbari most dominating note is Re while in Chayanat it is MA and Pa.

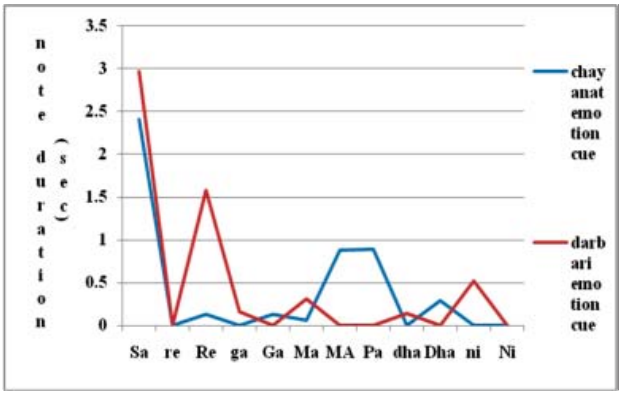

Fig. 1. Note distribution of emotion

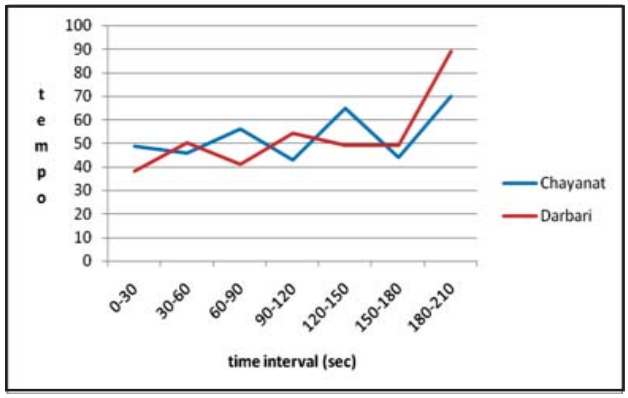

Fig. 2. Tempo at 30 sec interval revealing part

Tempo is the speed or pace of a musical piece. Studies indicate an association between fast tempo and happiness or excitement [2]. Slow tempo may be associated with sadness or serenity Measurement is done for the entire signal and then over the small sections of time interval 30 seconds each and is shown in Fig. 2. Comparing Fig. 2. with the emotion revealing phrases in the signal, as labeled by a musician, it may be inferred that the emotion revealing part of Chayanat have higher tempo than Darbari. But considering the whole signal at a time, we find very little difference. Analysis was also done with pitch pattern behavior/harmonic behavior of each signal, in which we have made a distribution of pitch/ harmonic shift of each peaks of LTAS from the spectral centroid. In both the distributions, the best fit polynomial curve is of order six and the R2 value is shown in the Fig 3. The figure reveals the fact that the partials are more harmonically distributed around the spectral centroid. The figure also shows that pitch shift decreases linearly with the harmonic number for the ragas Darbari Kannada which may be an spectral attribute of negative valence emotion. The raga Chayanat showed a complex nature of the variation of pitch shift with harmonic number showing an indication of positive valence emotion in the signal.

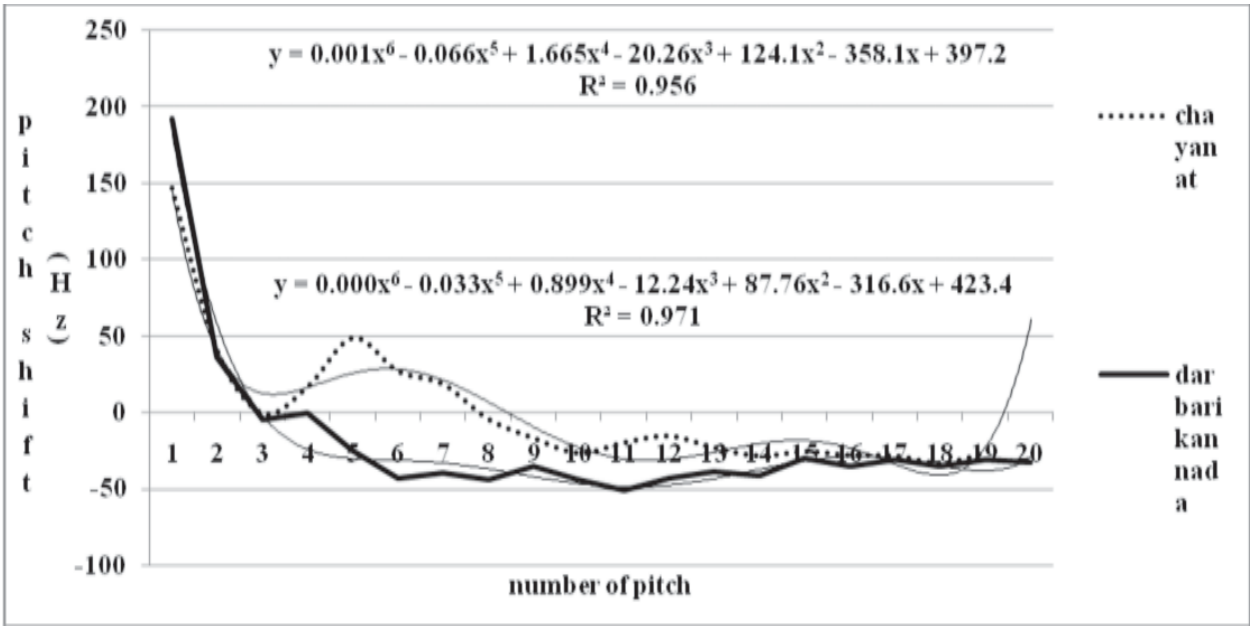

Fig. 3. Distributions of pitch shift are shown with best fit trend line and R^2 value

Table 1. Listener's emotional response in percentage for the ragas Chayanat and Darbari Kannada

Raga	Anger	Heroic	Joy	romantic	serenity	devotion	Sorrow	Anxiety
Chayanat	3.571	3.571	32.14	32.143	7.1429	3.57143	10.71	7.1429
Darbari	3.448		6.897		20.69	13.7931	44.83	10.345

It is observed from Table 1 that 45% of the listeners' pointed out sorrow for raga Darbari and 32% each pointed joy or romantic for raga Chayanat, which is quite interesting. 71.4% listeners indicated positive valence emotion for raga Chayanat and the rest indicated negative valence emotion. It is said in the music treatises that there is an element of pathos in the romantism of raga Chayanat. 28.6% of negative valence emotion might reflect this. In raga Darbari 90% listeners correctly indicated negative valence emotion. Thus it can be said that timbre effects very little in the recognition of emotion in Hindustani music. Fig. 4 below presents the distribution of emotional responses in circular graphical form.

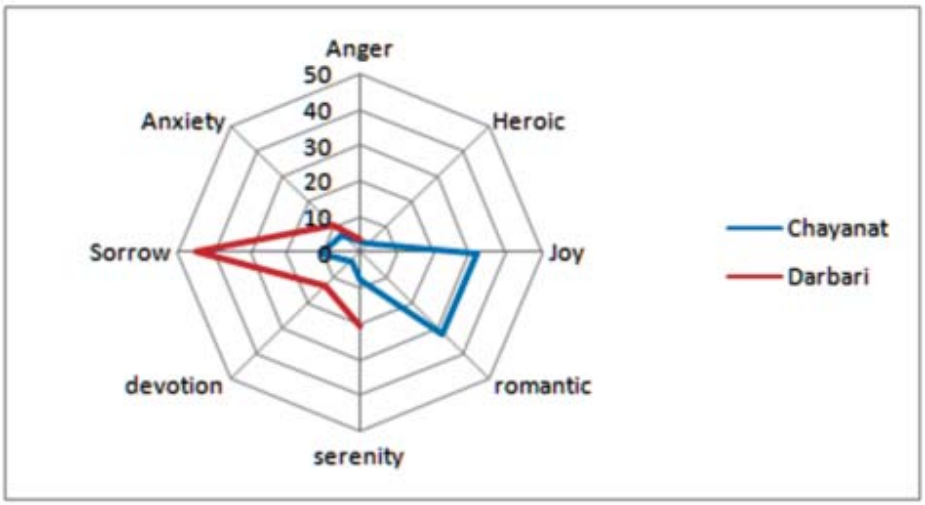

Fig. 4. Emotional responses of the two raga sound clips

Two listeners were subjected to EEG while listening to music. They were asked to sit in a relaxed manner in a shielded measurement cabin and the electrode cap was properly fitted on their head. The ground electrode was they properly fitted and adjusted. After settings were adjusted then recording of EEG was started without music. After 3 minutes the raga Chayanat was played in the speaker. Then raga Darbari Kannada was played and EEG was continued. After that EEG was continued for 3mins. The output from each electrode was observed and it was seen that there is a marked variation of electric potential with the change of the ragas. The frequency content of the EEG signal is a fundamental thing for appraising the EEG. Most of the valuable information is hidden within the frequency of 10 Hz. In general, EEG rhythms are classified into four basic types: (i) delta (1/2 - 4 cycles per second), (ii) theta (4-7 cycles per second), (iii) alpha (8-13 cycles per second) and (iv) beta (13- 40 cycles per second). Variation in frequency bands clearly shows the changes of functional and emotional states of listener. This type of arousal effect was also observed in the tanpura sound induced EEG [3].

Fig. 5. shows the frequency analysis for 2 seconds interval FP2-F4 electrodes. The distribution shows an increase in alpha activity while the music listening to music. It is observed from the figure that in no music condition the theta activity increases. After removal of the first music clip (raga Chayanat) we see that the theta activity is on the rise. When the second music clip (raga Darbari Kannada) was removed then again theta predominates alpha. It is said that alpha pattern appears when in wakefulness where there is a relaxed and effortless alertness.

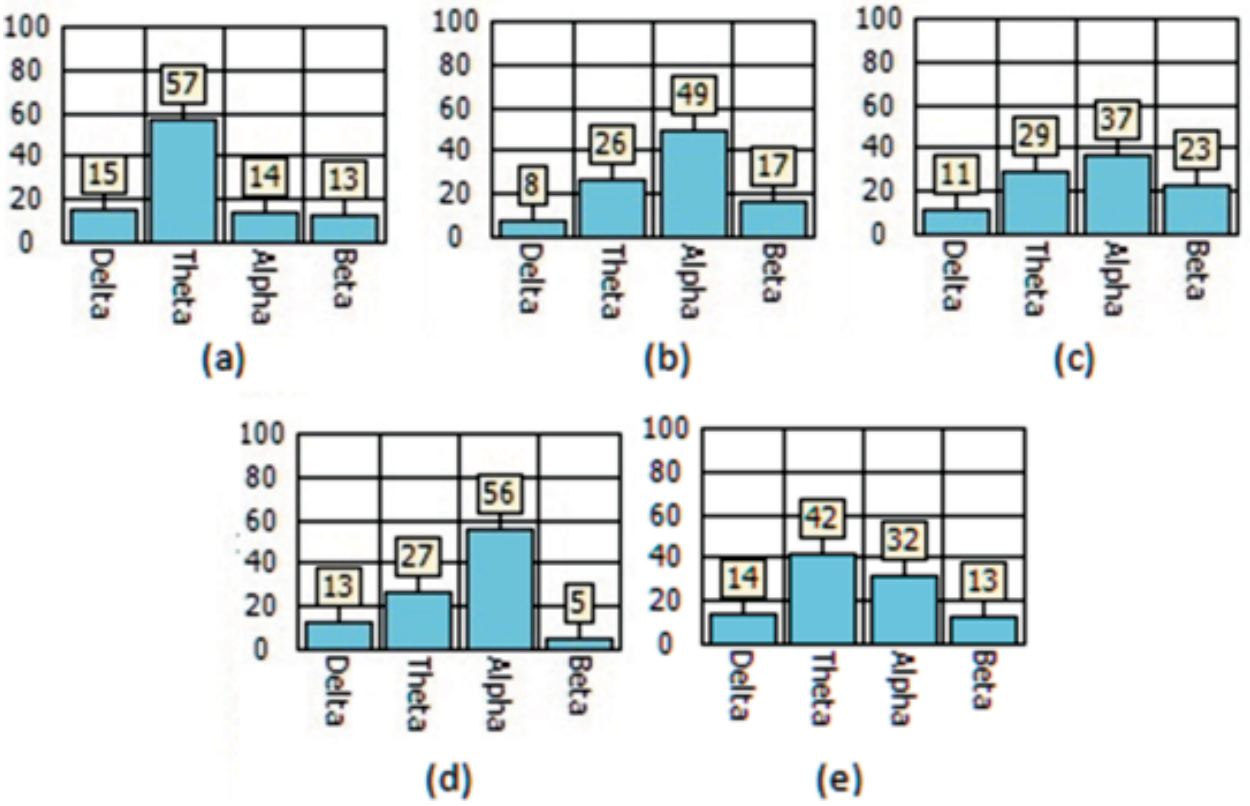

Fig. 5. (a) Relaxed mode -before music started (b) Raga Chayanat was established (c) After raga Chayanat was stopped (d) Raga Darbari Kannada was established (e) After raga Darbari Kannada was stopped

It was interesting to observe that the alpha activity was very high during 2.6 - 2.8 secs for the music clip (raga Chayanat) and nearly maximum during 3.2 secs- 3.4 secs for the clip (raga Darbari Kannada). This is well within the note sequences as containing emotion of that raga mentioned above. It is being observed that almost no discrimination regarding the contrasting emotions is being observed from the frequency analysis of the EEG potential structure. Both the signals produce arousal in the brain mapping of both the listeners though the variations are different between the listeners. Fig. 6 shows the frequency mapping of 2 secs interval for a particular listener when he was listening to raga Chayanat. The alpha predominance is very well observed.

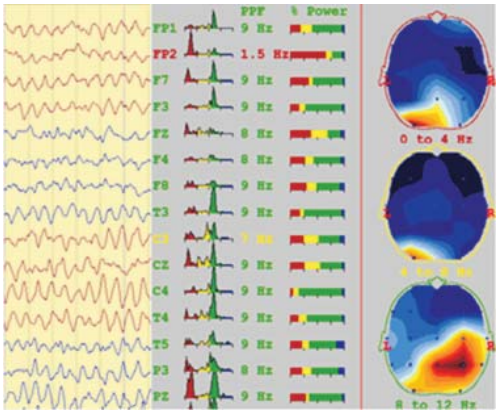

Fig. 6. Frequency map of 2 secs. while the second listener was enjoying raga Chayanat

3. CONCLUSION

Emotion in music clip (raga rendering) is embedded in some specific note sequences of the clip. Arousal occurs to a listener while listening to the music clip particularly when that sequence in being played. Our present EEG analysis is unable to distinguish between contrasting emotions. As evidenced by the listening test, emotion in the Hindustani raga music is timbre independent and mainly concentrated on the particular note sequences, note to note transitions (meends) and other ornaments. Listening test result shows that naïve listeners can distinguish between contrast emotions. More rigorous analysis of EEG data with different types of music needs to be done to frame a robust algorithm to have a thorough knowledge of music processing in the brain. This is our future work.

4. REFERENCES

[1] A. ALICJA WIECZORKOWSKA, ASHOKE KUMAR DATTA, RANJAN SENGUPTA, NITYANANDA DEY, and BHASWATI MUKHERJEE, 2010 "On Search for Emotion in Hindusthani Vocal Music", *Adv. in Music Inform. Retrieval, SCI 274*, p. 285 Springer-Verlag Berlin Heidelberg.

[2] S.O. ALI and Z F PEYNIRCIOGLU, 2010 "Intensity of emotions conveyed and elicited by familiar and unfamiliar music" *Music Perception: An Interdisciplinary Journal* **27**: 177.

[3] MATTHIAS BRAEUNIG, RANJAN SENGUPTA and ANIRBAN PATRANABIS, 2012 "*On Tanpura Drone and Brain Electrical Correlates*", LNCS 7172, p. 53. Springer-Verlag Berlin Heidelberg.

Journal of Acoustical Society of India : Vol. 40, No. 4, 2013 (pp. 255-260)

Performance Analysis of DCT and DFT Based Speech Coding

Shijo M. Josep* and P. Babu Anto
School of Information Science & Technology
Kannur University (Kerala)
**e-mail: shijomjose71@gmail.com*

[Received: 19.04.2013; Revised: 20.07.2013; Accepted: 24.09.2013]

ABSTRACT

Speech compression system focuses on reducing the amount of redundant data while preserving the integrity of the signals. Speech compression algorithms are generally classified in to three categories. They are parametric coders, hybrid coders and transform's coders. This paper analyzes the effectiveness of different transform technique on Indian regional language. Speech data base used for this experiment is created in Malayalam, one of the South Indian languages. To remove insignificant coefficient from the feature vector we apply hard thersholding technique on Discrete Cosine transformed coefficient. Lossless run length encoding algorithms is used to encode the remaining coefficients. Performance of this experiment is evaluated in terms of NRMSE, SNR, PSNR, MOS and percentage of compression occurred. It has been found that Discrete Cosine Transforms (DCT) is superior to Discrete Fourier Transforms (DFT).

1. INTRODUCTION

In information theory, data compression or source coding is the process of encoding information using fever bits than the original one. Data compression is useful because it helps to reduce consumption of expensive resources such as memory, HDD and transmission bandwidth etc[1]. On the down side of encoding and decoding process demands some amount of computation. The design of data compression schemes therefore involves trade off among various factors including the degree of computation the amount of distortion and computational resource required to compress and uncompress the data [2].

Compression algorithms are classified in to lossless compression and lossy compression. Lossless algorithms are usually exploiting statistical redundancy in the input data. Perfect reconstruction is possible in lossless compression without any loss of fidelity. But in the case of lossy compression there are many trade off where by some degradation in the quality of data will occur as part of compression [3]. There is mechanism to measure the efficiency of compression without which an effectives rating of compression techniques may not be possible. There are many parameter used to evaluate the effectiveness of data compression [4]. The main area of data compression is speech, image and multimedia processing.

Speech is a very unique signal by the nature due to many reasons. The most prominent factor is that the speech is a non stationary signal. This makes the speech signal hard to analyze and model. Second factor is that speech signal contains not only the information part but also many information like emotion, health condition, age and gender of speaker etc [5]. This make analyses and synthesis of speech signal more complex. There are many type of algorithms are available to process speech signal. Each one has its own merit and demerits. So far no algorithms have 100% perfection in analyses and synthesis of speech signal. Therefore demand for perfect algorithm is still exist in the area of compression.

Speech coding or speech compression is a process of obtaining a compact representation for the speech signals, for the purpose of efficient transmission over band limited wired or wireless channels and also for efficient storage. In the modern digital world speech coding is an essential part of telecommunication and multimedia application. Speech coding algorithms enable to carry out more calls per channel which leads to reduce the cost of communication [6]. The main areas of speech coding are telecommunication, satellite communication, video conferring, and storage media.

This paper deals with a well known DFT and DCT transforms (lossy) along with run length encoding (lossless) and evaluate its effectiveness in continuous Malayalam speech coding. Different quantitative (SNR, PSNR, NRMSE) and qualitative parameters are used to evaluate the performance of the system and compared with others. The system developed proved to be very efficient in terms of compressing speech files. This paper is organized as follows: A brief introduction of speech compression is presented in section 1. Section 2 gives overview about Discrete Fourier Transforms (DFT) and Discrete Cosine Transforms (DCT). Section 3 furnishes the details of data base created for this experiment. Section 4 discusses the methodology used in this experiment. Finally Section 5 presents the simulation and result and concludes this paper with remarks in section 6.

2. DIFFERENT TRANSFORM TECHNIQUES

2.1 Discrete Fourier Transforms (DFT)

The fast Fourier transform (FFT) is a discrete Fourier transform (DFT) algorithm which reduces the number of computations needed for N points from $2N^2$ to 2N logN, where log is the base 2 algorithm. A DFT is used in Fourier analysis of signal. It transforms the signal in to frequency domain. DFT decompose a set of values in to components of different frequency values[7]. The way it does this is defined by the following eq. [1].

$$X(f) = \int_{-\infty}^{\infty} x(t) \bullet e^{-2j\pi ft} dt \tag{1}$$

and inverse FFT can be describe in eq. 2.

$$x(t) = \int_{-\infty}^{\infty} X(f) \bullet e^{2j\pi ft} df \tag{2}$$

In this equation 't' stands for time 'f' for frequency and 'x' denotes the signal at hand 'X' denotes the signal in the frequency domain.

2.2 Discrete Cosine Transforms (DCT)

The Discrete is in a class of mathematical operations that includes the well known fast Fourier transforms (FFT) and many others. The basic operation performed by these transforms is to take a signal and transform it from one type of representation to another. DCT transformation identifies pieces of information in the signal that can be effectively "thrown away" without seriously compromising the quality of speech signal or image. The formula for one-dimensional DCT is shown in equation 1 with its partner the IDCT shown immediately below eq. 4.

Discrete Cosine transform (DCT) of 1-D sequence b[n] of length N is

$$\mathrm{B[m]}=\left(\frac{2}{\mathrm{N}}\right)^{\frac{1}{2}} C_m \sum_{m=0}^{N-1} b[n] \cos\left[\frac{(2n+1)m\pi}{2N}\right] \tag{3}$$

where m=0,1,……N-1

Similarly the inverse transformation IDCT is defined as

$$b[n]=\left(\frac{2}{N}\right)^{\frac{1}{2}} C_m \sum_{m=0}^{N-1} B[m]\cos\left[\frac{(2n+1)m\pi}{2n}\right] \quad (4)$$

In eqs. (3) & (4), cm is defined as:

$C_m = \left(\frac{1}{2}\right)^{\frac{1}{2}}$ for m = 0 or $C_m = 1$ for $m \neq 0$

In DCT the coefficient B[0] which is directly related to the average value of the time-domain block, is termed as the DC coefficient, and the remaining coefficients are called AC coefficients [8].

3. SPEECH DATA BASE CREATION

Aim of this section is to give details of the speech data base created for this experiment. For this part of the experiment continuous speech samples were collected from six hundred individuals of different age and gender. First and second sentence of the Indian National pledge is selected for the creation of database. This sentence is uttered in Malayalam (one of the regional languages). The first sentence consists of three words and has average duration of 1.5seconds and second utterance contains five words and has average duration of 2.4 seconds. Each word contains vowels, consonants, fricatives and diphthongs. The Malayalam sentences and its corresponding International Phonetic Alphabet (IPA) are given in Table 1. Speech samples were recorded using unidirectional USB microphone with following specifications: frequency response 100-10,000 Hz and sensitivity: 62dBV/µBar -42 dBV/Pa +/-d 3dB. 'Goldwave' the software at a sampling rate of 8 KHz (4 KHz)

Table 1. Speech sentence and its IPA format

Malayalam	1. §Lc/®æa/øÞ¼cÎÞÃí.
	2. ®ÜïÞ/§LcAÞøá¢/®æa/ØçÙÞÆøß/ØçÙÞÆøÎÞøÞÃí.
English	1. India/ ente/ rajamanu.
	2. Ella/ indiyakarum/ enete/ sahothari/ sahotharamranu.

band limited was used for capturing and processing the speech signal. The speakers were native speakers of Malayalam and free from speech disabilities. The recorded speech samples are trimmed by removing prefix and suffix silence from the utterances and it is labelled and stored in the data base for further processing.

4. SPEECH COMPRESSION

The experimental module consists of three phases they are, transforming the signal, thersholding the coefficients and encoding the remaining coefficients. We utilize Discrete Cosine transforms and Discrete Fourier transform to transform signal in to its corresponding domain. The transformed signal reveals relevant information. This process extracts information from the signal that is the essential for signal compression. In this experiment DCT and DFT decompose the signal only. These coefficients are used to create feature vector.

Feature vector is undergoing a dimensionality reduction process known as thersholding. Thersholding is a procedure which takes place after decomposing the signal. This algorithm is a lossy algorithm since the signal cannot be reconstructed exactly [9]. Coefficients below this threshold level are zeroed. There are two types of thersholding techniques are used, soft thresholding and hard thresholding. Mathematically these two thersholdings are represented by the following equations. Equation 6 represent the hard thersholding and eq. 7

represent the soft thresholding. In this experiment we use hard thersholding.

$$D_H^{\lambda}(w) = \begin{Bmatrix} \text{W} \quad \text{for all } |\text{w}|>\lambda \\ 0 \text{ otherwise} \end{Bmatrix} \tag{6}$$

$$D_s^{\lambda}(w) = \text{sgn}(w)\max(0;|\,w\,|-\lambda \tag{7}$$

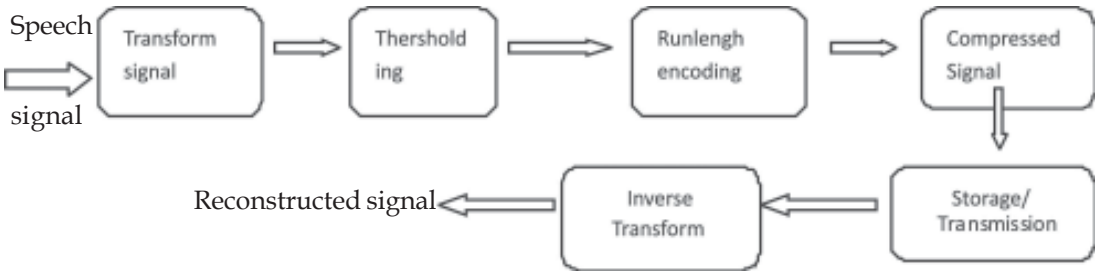

Fig. 1. Speech coding using transforms technique

The third phase of this experiment is encoding threshold signal by lossless Run length Encoding (RLE) algorithm. In this implementation consecutive zero valued coefficient are encoded with two bytes. One byte is used to specify a staring string of zero and the second bytes keeps track of the number of successive zeros. Figure 1 illustrating the compression process involved in compression of speech signal. Inverse process is applied to reconstruct the speech signal. Performance of the encoding and decoding process are evaluated in a number of quantitative and qualitative analyses.

4.1 Performance Evaluation

In this section we talk about the performance of the synthesized signal in terms of five parameters [9]. The following are the parameters we compared in addition to mean opinion score (MOS).

Compression Percentage (CR)

Signal to Noise Ratio (SNR)

Peak Signal to Noise Ratio (PSNR)

Normalized Root Mean Square Error (NRMSE)

The results obtained for the above quantities are calculated using the following formulas:

4.1.1 Compression -Percentage

This is the simplest way to measure the performance of compression algorithm. Compression-percentage can be calculated by the following formula:

CR=(1-(Compressed-size/raw-size))*100 (8)

4.1.2 Signal to Noise Ratio (SNR)

This value gives the quality of reconstructed signal, higher the value the better and it is calculated by

$$\text{SNR}=10\log_{10}\left(\frac{\sigma_x^2}{\sigma_e^2}\right) \tag{9}$$

σ^2_x is the mean square of the speech signal and σ^2_e is the mean square difference between the original and reconstructed signals.

4.1.3 Peak Signal to Noise Ratio (PSNR)

This value indicates the ratio between the peak signal and noise within the reconstructed signals. Higher value is better. PSNR is calculated by the following formula.

$$PSNR = 10\log_{10}\frac{NX^2}{\| x-r \|^2} \tag{10}$$

In this equation N is the length of the reconstructed signal, X is the maximum absolute square value of the signal x and | |x-r| |2is the energy of the difference between the original and reconstructed signals.

4.1.4 Normalized Root Mean Square Error (NRMSE)

$$NRMSE = \sqrt{\frac{x\left(x(n)-r(n)\right)^2}{\left(x(n)-\mu_X(n)\right)^2}} \tag{11}$$

x(n) is the speech signal, *r(n)* is the reconstructed signal, and $\mu_x(2)$ is the mean of the speech signal.

4.1.5 Mean Opinion Score (MOS)

Subjective evaluation by listeners is still a method commonly used in measuring quality of reconstructed speech. MOS provides a numerical indication of the perceived quality of received media after compression and / or transmission. The MOS is expressed as a single number in the range 1 to 5. Where 1 is the highest perceived quality and 5 is the lowest perceived quality. When taking subjective test, listeners focus on the difference between the original and reconstructed signal and rate it. The MOS is generalized by averaging the result of a set of standards, subjective tests, where a number of listeners rate reconstructed speech signals. In our experiment the MOS rate was excellent in DCT experiment and it was good in DFT based experiment.

Table 2

Sentence 1	DFT	DCT	Sentence 2	DFT	DCT
CP%	58.4662	80.4025	CP%	60.312	72.87
SNR	1.1148	2.17112	SNR	1.00657	1.01972
PSNR	4.6556	4.7269	PSNR	2.5001	3.5161
NRMSE	0.16503	0.16058	NRMSE	0.0187	0.0178

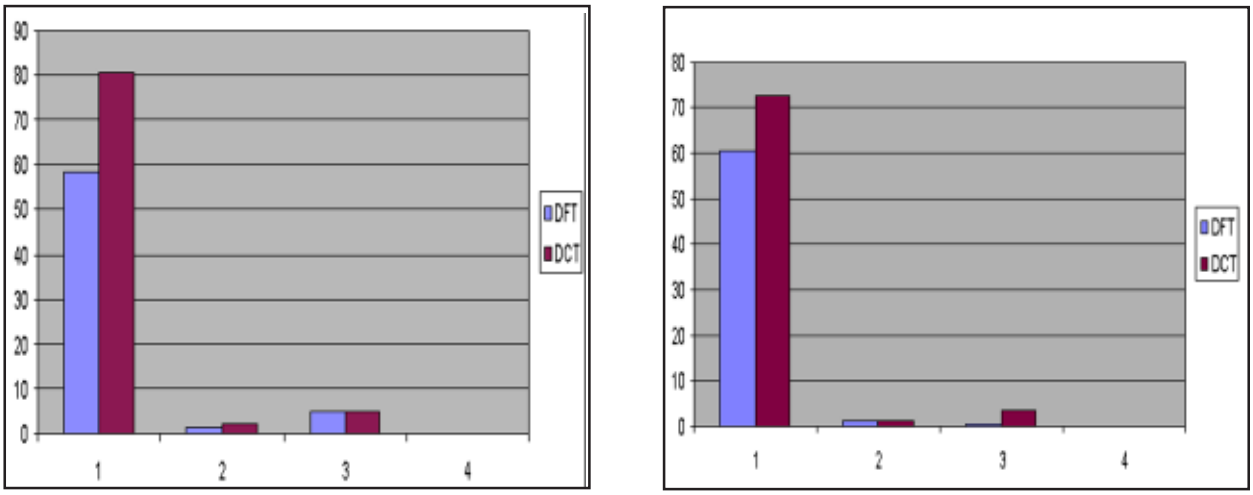

Fig. 2. DFT vs. DCT Performance comparison based on first & second sentence

5. RESULTS

Continuous Malayalam speech compression is implemented by different transform techniques along with thersholding and run length encoding. In these experiments the qualitative and qualitative performances are measured in terms of NRMSE, SNR, PSNR, Compression Percentage and MOS.

The results obtained in these experiments are tabulated in Table 2 and corresponding measures are graphically illustrated in Fig. 2. Average measures of DFT experiments of first and second sentence are SNR is 1.0606, PSNR is 3.57788, NRMSE is 0.0918 and compression percentage is 59.3891. Similarly in DCT experiments the obtained average values are SNR is 1.59542, PSNR is 4.1215, NRMSE is 0.08918 and compression percentage is 76.6366.

6. CONCLUSION

The main aim of speech coding is to represent speech signal with minimum number of bits for storage or transmission. This paper discusses the efficiency of well known transform based speech coding on Indian regional language. From the stated results it is proved that, Discrete Cosine Transform (DCT) perform better than the DFT in Indian regional languages.

7. REFERENCES

[1] MARK NELSON and JEAN LOUP GAILLY, 2003. The Data Compression Book, 2nd Edition, BPB publications.

[2]. KHALID SAYOOD, 2005. Introduction to Data Compression, Morgan Kaufmann Publishers 2nd edition.

[3]. DAVID SALOMON, 2011. Data Compression, the Complete Reference, Springer International Edition, 4th edition.

[4]. LAWRENCE RABINER and BIING HWANG JUANG, 2009. Fundamentals of Speech Recognition", Pearson Education.

[5]. THOMAS F. QUATIERI, 2012. Discrete-Time Speech Signal Processing Principle and Practice', Pearson Publication 8th edition.

[6]. K.P. SOMAN and K.I. RAMACHANDRAN, 2008. Insight in to wavelets from theory to practice", Prentice-Hall of India Private limited, 2nd edition.

[7]. G. RAJESH, A. KUMAR and K. RANJEET, 2011. Speech compression using different transform techniques", Second IEEE International Conf. on Computer, and Communication Technology, pp. 146-151.

Journal of Acoustical Society of India : Vol. 40, No. 4, 2013 (pp. 261-266)

Study of Molecular Interactions in Binary Mixtures through Ultrasonic Measurements

S. Ponnancy and Beulah J.M. Rajkumar
PG & Research Department of Physics, Lady Doak College, Madurai 625 002, India
e-mail: physics.dept@gmail.com

[Received: 22.04.2013; Revised: 23.07.2013; Accepted: 26.09.2013]

ABSTRACT

The density (ρ), viscosity (η) and ultrasonic velocity (U) have been measured for the binary mixtures of Dimethylformamide (DMF) with Isopropanol, DMF with Carbon tetrachloride and Carbon tetrachloride with Isopropanol over the entire range of composition (0:20 to 20:0 in steps of 2ml). The measured data are used to compute thermodynamic acoustical parameters such as acoustic impedance (z), adiabatic compressibility (β), free length (L_f), free volume(V_f).Excess values of the above said parameters were plotted and interpreted in terms of intermolecular interactions.

1. INTRODUCTION

Interaction between solute - solvent molecules brings out tremendous change in nature. Physicochemical properties of two different liquids change when they mix together. These changes lead to various applications in industry, medicine and in chemical engineering processes [1]. The interaction between liquid mixtures may be weak or strong depending on the whether the liquid is polar, non-polar, protic or aprotic. Ultrasonic investigation is a powerful tool to probe these interactions [2]. Many research works have been carried out in analyzing the structural changes of binary mixtures with ultrasonic and thermo acoustical parameters. This paper focuses on the analysis of structural changes of like and unlike molecules through ultrasonic parameters.

2. METHODOLOGY

Binary mixtures of ten different proportions from 0:20 to 20:0 were prepared for DMF+ 1-ol, DMF + CCl4 and CCl4 + 1-ol. The density of the mixture has been found by the relative measurement method. Viscosity of the liquid mixture was measured by Oswald viscometer and the ultrasonic velocity was measured by using the ultrasonic interferometer B1 Microsoft model -83 with high degree of accuracy operating at 3 kHz.

The thermo acoustical parameters can be calculated from the measured data.

Acoustical impedance (z) $z = U\rho$

Adiabatic compressibility (β) $$\beta = \frac{1}{U^2 \rho}$$

Free length (L_f) $$L_f = K\sqrt{\beta}$$

Free volume (V_f) $$V_f = \left(\frac{M_W U}{k \eta_t} \right)^{3/2}$$

where, U - Ultrasonic velocity of binary mixture (ms^{-1})

ρ - Density of binary mixture (Kg m^{-3})

K - Temperature dependent Jacob constant (93.875+ 0.3757)10^{-8} [3]

M_W - Molecular weight (Kg)

k - Temperature independent constant ($4.28x10^9$)

η_l - Viscosity of binary mixture (Ns m^{-2})

The excess values of above said parameters can be found by the expression $\sum_{i=0}^{i=1} m_i X_i$

where, P is the experimental value of the binary mixture, mi is the theoretical value of each component and Xi is the mole fraction.

The degree of molecular interaction can be found from the expression $\alpha = \frac{U_{\exp}^2}{U_{IMR}^2} - 1$

where, U_{IMR} is ideal mixture relation[4] of ultrasonic velocity and is given as

$$\frac{1}{(X_1M_1 + X_2M_2)U_{IMR}^2} = \frac{X_1}{M_1U_1^2} + \frac{X_2}{M_2U_2^2}$$

3. RESULT AND DISCUSSION

3.1 DMF + Isopropanol

Fig. 1 gives the variation of the different excess values with increasing DMF concentration. Fig 2 represents the degree of molecular interaction (α) as calculated from theoretical considerations using the ideal mixture relation. The density of the mixture increases linearly with mole fraction of DMF. As DMF is the denser component, the resultant increase in density causes sound energy to be quickly transferred in the medium which increases ultrasonic velocity. The increase in ultrasonic velocity also indicates a large association among the molecules of the mixture. The random non-linear variation in viscosity with increasing molar concentration of DMF indicates the presence of intermolecular interaction [5]. The decrease in adiabatic compressibility indicates the formation of a large number of tightly bonded systems leading to a decrease of inter molecular free length was observed in Table 1.

Table 1. Thermo acoustic parameters of DMF + Isopropanol

Mole fraction of DMF	Density ρ **10^3 Kgm^{-3}**	Viscosity η **10^{-3} Nsm^{-2}**	Ultrasonic velocity **U ms^{-1}**	Acoustic Impedance **Z** 10^3 **Kgm^{-2}s^{-1}**	Adiabatic Compress-ability	Free length **L_f**	Free volume **V_f**
0.0000	0.7646	1.4360	1118.067	0854.8155	10.4631	6.7362	0.3616
0.0912	0.7683	1.2531	1149.273	0883.0340	09.8537	6.5371	0.4760
0.2399	0.8428	1.2314	1187.437	1000.7480	08.4152	6.0411	0.5376
0.2835	0.7756	1.0243	1213.090	0940.8742	08.7614	6.1641	0.7416
0.3996	0.8186	1.0383	1251.963	1024.7898	07.7942	5.8140	0.7890
0.4863	0.8004	1.0313	1279.876	1024.3535	07.6275	5.7514	0.8452
0.5998	0.8540	1.0312	1309.593	1118.3921	06.8276	5.4415	0.9042
0.7073	0.8686	1.0120	1346.230	1169.2951	06.3527	5.2488	0.9994
0.8116	0.8825	0.9881	1378.559	1216.6277	05.9623	5.0850	1.1051
0.9103	0.9139	1.0300	1405.655	1284.6256	05.5379	4.9007	1.0983
1.0000	0.9581	1.0575	1441.508	1381.1492	05.0228	4.6672	1.1232

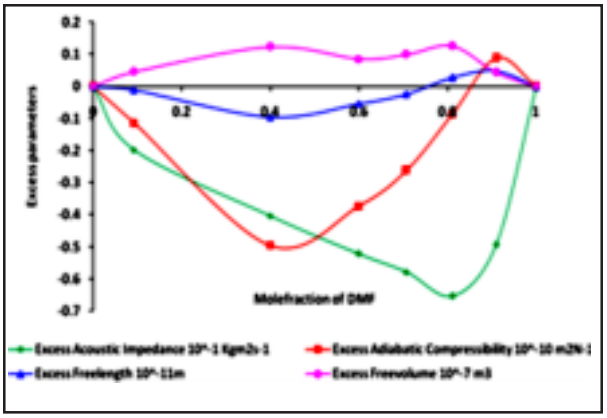

Fig. 1. Excess parameters of DMF + IPA

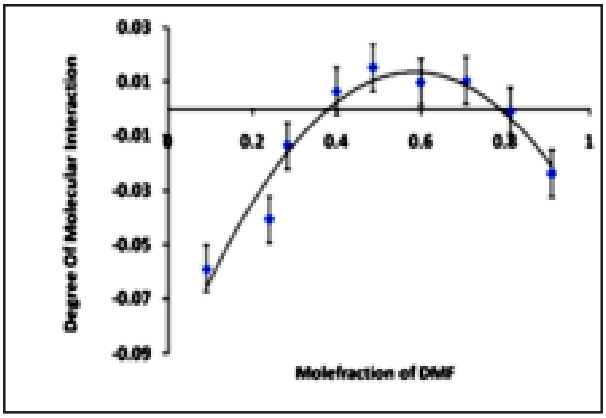

Fig. 2. Molecular interaction of DMF + IPA

The positive excess volume reaches its maximum when the concentration of both species in the binary mixture is almost the same, indicating that the interaction of both species is responsible for the increase in free volume. Dipolar interaction between the two molecules can mutually form dipoles and this dipolar interaction supports the existence of more space between the components. Because of this structure formation, the actual acoustic impedance is smaller than the expected value leading to a negative excess value.

The negative deviation in excess adiabatic compressibility may be attributed to the presence of dipole - dipole interaction between the compound molecules [1]. Negative excess adiabatic impedance suggest that the rupture of the hydrogen bond chain of isopropanol dominates over the hydrogen bond formed between the unlike molecules.

Table 2. Thermo acoustic parameters of DMF + CCl_4

Mole fraction of DMF	Density ρ 10^3 **Kgm^{-3}**	Viscosity η 10^{-3} **Nsm^{-2}**	Ultrasonic velocity **U ms^{-1}**	Acoustic Impedance **Z** 10^3 **Kgm^{2}s^{-1}**	Adiabatic Compress-ibility β 10^{-10} **m^{2}N^{-1}**	Free length L_f 10^{-11} **m**	Free volume V_f 10^{-7} **m^3**
0.0000	1.5610	1.4907	894.3550	1396.0852	8.0090	5.8935	1.0012
0.1115	1.4841	1.4363	938.1960	1392.4142	7.6549	5.7617	1.0390
0.2899	1.4387	1.4884	990.1569	1424.5247	7.0897	5.5450	0.9126
0.3299	1.3288	1.4046	1037.0050	1377.9921	6.9980	5.5090	1.0276
0.4561	1.2849	1.4255	1092.3020	1403.5062	6.5229	5.3187	0.9587
0.5391	1.1990	1.3733	1149.2730	1377.9221	6.3147	5.2331	1.0015
0.6468	1.1852	1.3679	1230.4250	1458.2897	5.5732	4.9163	0.9868
0.7524	1.0969	1.2137	1285.9850	1410.6534	5.5124	4.8894	1.1061
0.8400	1.0380	1.1518	1327.3850	1377.8827	5.4675	4.8695	1.1145
0.9277	0.9841	1.1198	1398.8960	1376.6178	5.1928	4.7455	1.1057
1.0000	0.9581	1.1186	1441.5080	1381.1492	5.0228	4.6672	1.0323

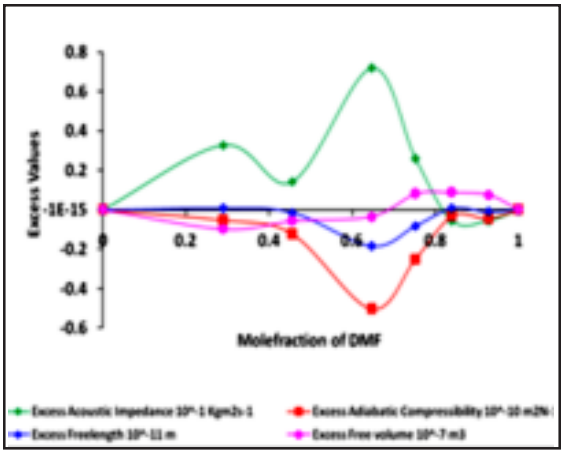

Fig. 3. Excess parameters of DMF+$CC1_4$

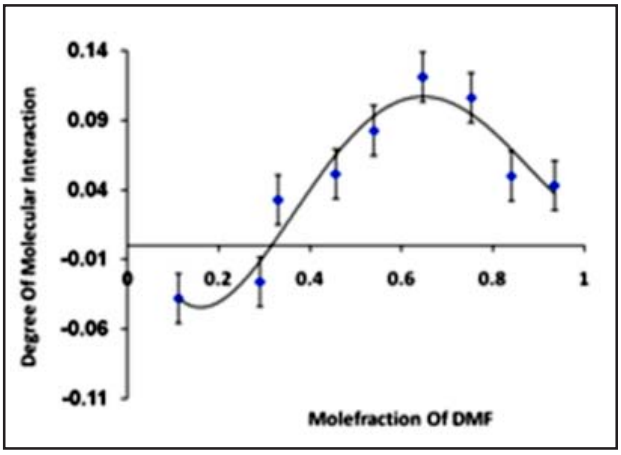

Fig. 4. Molecular interaction of DMF+$CC1_4$

At lower concentrations of DMF there is a high molecular association between the IPA molecules due to hydrogen bonding. This leads to a low degree of molecular interaction between the two compounds. As the concentration of DMF is increased, these bonds break and DMF may occupy the interstitial position of IPA. With a further increase of DMF, the degree of molecular interaction decreases due to repulsive force between the DMF molecules.

3.2 DMF + CCl_4

Figues 3 and 4 give the variation of the different excess values and the calculated degree of molecular interaction respectively with increase in the DMF concentration The binary mixture of DMF and CCl4 involves a zero dipole moment liquid CCl4. Like in the case of DMF+IPA, the viscosity decreases in a non-linear fashion indicating interaction between the molecules. The acoustic impedance changes randomly with increasing mole fraction of DMF although the velocity increases uniformly. This further justifies the possibility of molecular interactions between the solute and the solvent molecules. Since DMF is a polar solvent, it induces a dipole in CCl4 which orients itself such that there is repulsion between molecules thereby increasing the free volume. Therefore weak dipole - induced dipole interactions exist between them.

The negative deviation in excess adiabatic compressibility and a small negative deviation in excess free length were observed between 0.6 and 0.8. This indicates weak interaction involving dispersion forces. Decrease in free length between the component molecules indicates that the system is more resistant to the sound propagation, which is supported by the positive values of excess acoustic impedance. The random positive excess acoustic impedance observed indicates structural changes due to hydrogen bonding between the solute molecules. Fig 2.2 indicates that the formation of complex structure due to dipole -induced dipole interaction.

3.3 CCl_4 + Isopropanol

Figures 5 and 6 depict excess value variations and a negative degree of molecular interaction with increasing CCl4 concentration. The ultrasonic velocity of the mixture correspondingly decreases while the viscosity and density increases. The behavior of viscosity and velocity shows that the interaction between the CCl4 and IPA is very weak[6]. Table 3 shows a random decrease in the free length. This is because the addition of non-polar molecules in the mixture causes the molecular structure to be loosely packed contributing to a decrease in velocity. This is further supported by the increasing values of acoustic impedance and decreasing values of adiabatic compressibility. It is also clear that the value of free volume increases with increasing mole fraction of CCl4.

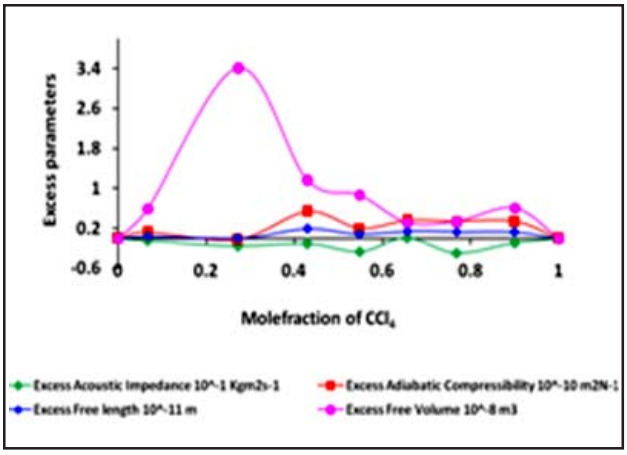

Fig. 5. Excess parameters of $CC1_4$ + IPA

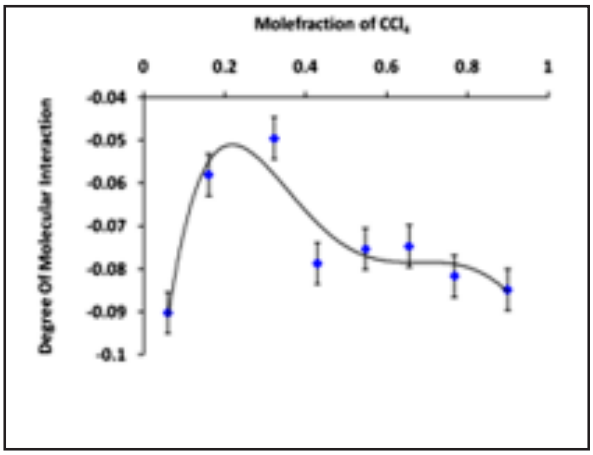

Fig. 4. Molecular interaction of $CC1_4$ +IPA

The positive trend in excess adiabatic compressibility and excess free volume is due to rupture of hydrogen bonded chains of IPA which predominate over the attractive force between unlike molecules [7]. This is also confirmed by negative deviation in acoustic impedance. The positive contribution of intermolecular free length arises from the breaking of hydrogen bonds of the self associated structure of alcohols. Degree of molecular interaction is negative which indicates that there is no significant interaction between the components.

Table 3. Thermo acoustic parameters of CCl4 + Isopropanol

ole fraction of CCl_4	Density ρ $\mathbf{10^3\ Kgm^{-3}}$	Viscosity η $\mathbf{10^{-3}\ Nsm^{-2}}$	Ultrasonic velocity **U** $\mathbf{ms^{-1}}$	Acoustic Impedance **Z** 10^3 $\mathbf{Kgm^2s^{-1}}$	Adiabatic Compressibility $\mathbf{10^{-10}\ m^2N^{-1}}$	Free length $\mathbf{L_f}$ $\mathbf{10^{-11}\ m}$	Free volume $\mathbf{V_f}$ $\mathbf{10^{-8}\ m^3}$
0.0000	0.7645	1.4569	1118.067	854.8155	10.4631	6.7362	3.5385
0.0674	0.8177	1.3583	1079.860	883.0287	10.4872	6.7439	4.3342
0.1605	0.9174	1.3620	1048.206	961.6186	9.9209	6.5593	4.9672
0.2721	0.8580	1.1726	1081.355	927.8027	9.9672	6.5747	7.9216
0.3224	1.0999	1.3700	993.7779	1093.038	9.2061	6.3186	5.9889
0.4293	1.1128	1.3259	950.669	1057.918	9.9430	6.5667	6.8920
0.5482	1.2430	1.3988	929.215	1155.018	9.3174	6.3567	7.1975
0.6561	1.2991	1.5018	914.210	1187.672	9.2100	6.3200	7.1919
0.7681	1.3843	1.5246	899.884	1245.731	8.9205	6.2198	7.7744
0.9001	1.4654	1.5290	891.420	1306.299	8.5877	6.1027	8.7294
1.0000	1.5610	1.6462	894.355	1396.085	8.0090	5.8935	8.6280

4. CONCLUSION

From the thermo acoustical studies, it can be concluded that molecular association between DMF and Isopropanol arise from the hydrogen bonding between the solute and solvent molecules, structure breaking tendency because of repulsive force between the dipole and induced dipole and solute-solute interaction occurs between the polar and non-polar mixtures, DMF and CCl4 and there is no significant interaction between CCl4 and Isopropanol.

5. REFERENCES

[1] A. MCHAWEH, A. ALSAYGH, AND M.A. MOSHFEGHIAN, 2004 *Fluid Phase Equilibria,* **224,** 157 – 167.
[2] V. TIWARI AND J.D. PANDEY, 1980 *Indian J. Pure Appl. Phys*., **18**, 51.
[3] S. PRABAKAR AND K. RAJAGOPAL, 2005 *J. Pure Appl. Ultrason*., **27** , 41–48.
[4] J.D. PANDEY, GYAN PRAKASH DUBEY, B.P. SHUKLA and S.N. DUBEY, 1991 *Pramana J. Phys*., **37**(**6**), 497-503.
[5] P. VASANTHARANI, V. PANDIYAN and A.N. KANNAPPAN, 2009 *Asian J. Appl. Sci*., **2**(**2**), 169-176.
[6] MADHU RASTOGI, AASHEES AWASTHI, MANISHA GUPTHA and J.P. SHUKLA, 2002 *Ind. J. Pure Appl. Phys*., **40**, 256-263.
[7] R. VADAMALAR , P. MANI , R. BALAKRISHNAN AND V. ARUMUGAM, 2008 *Invertis J. Sci. Tec.* , **2**(**4**), 252-260.

Journal of Acoustical Society of India : Vol. 40, No. 4, 2013 (pp. 250-254)

Vowel Duration in the Geminate Contexts: Observations from Oriya Speaking Children and Adults

Venkat Raman Prusty[1] and Lakshmi Venkatesh[2]
[1]*MediCiti Institute of Medical Sciences, Ghanpur (Andhra Pradesh)*
[2]*S.R. Chandrasekhar Institute of Speech & Hearing, Bangalore (Karnataka)*

[Received: 17.04.2013; Revised: 18.07.2013; Accepted: 21.09.2013]

ABSTRACT

Temporal characteristics of vowels in geminate contexts (phonological long vowels) were observed through acoustic analyses of vowels occurring in word pairs of Oriya language. Productions of Oriya speaking typical developing children in the age range of 3-14 years and young adults (25-35 years) in response to recorded model were subjected to acoustic analyses to measure the duration of vowels. Results revealed a developmental trend such that the duration of all geminate vowels differed across the different age groups with no difference was observed between male and female participants in each age group. Findings are discussed in terms of the age at which children's productions reached adult like durations and comparison with duration of singleton production of vowels reported in an earlier study.

1. INTRODUCTION

Phonemes are converted into phonetic units during the process of speech production through the realization of different rules. Durational properties observed at the level of phonetic output are the result of both segmental and suprasegmental factors. Variations due to intrinsic (segment specific) and extrinsic (contextual) specifications may arise from maturation, predisposition and cognitive learning. An analysis of developmental changes helps understanding aspects of normal maturation. Quantifying effects of language dependent factors are helpful in identification of abnormal forms of productions in development.

Vowel length is contrastive in many languages with varied language-specific realizations of the length contrast. Several languages (e.g., Sanskrit, Kannada, Japanese, Hungarian etc) from around the world make a phonemic distinction between long and short vowels. Long vowels are distinct phonemes from short vowels leading to doubling the number of vowel phonemes in a particular language. Long vowels in Japanese for example are analyzed as two same vowels or a vowel + the pseudo-phoneme /h/ (e.g., short /i/ and long /ii/ or /ih/). Languages such as Japanese or Finish are referred to as "Geminate vowel" languages which allow a long vowel (a phoneme) to be analyzed as sequences of short vowels [1]. In Finnish, both consonant length and vowel length contrasts are phonemic and are independent of each other. For example, words such as *taka* /*taka*/ "back", *takka* /*tak:a*/ "fireplace", *taakka* /*ta:k:a*/ "burden", and so forth are different, unrelated words. Ladefoged defines geminates as "long consonants (or vowels) that can be analyzed as double consonants (or vowels)" [2]. In several languages, gemination is not productive in the creation of phonemes and only occurs only in allophonic variation.

Gemination is contrastive in Japanese or Finnish as seen from examples above, whereas it is not contrastive

at the phonemic level and only occurs at lexical boundaries in English. The "Geminate Vowel" languages are in contrast to several "Tense-Lax" languages such as English, in which the "length" contrast is realized by quality as well as duration [3].

Oriya is an Indo-Aryan language spoken by about 31 million people in state of Orissa and some areas of neighboring states. The features of this language which makes it marked include the vowel [ɔ] without a front vowel counterpart and the vowel /a/ considered as secondary cardinal vowel. Table 1 shows the classification of vowel sounds in Oriya in terms of tongue height, tongue root advancements and mouth opening [4].

Investigations of acoustic characteristics of vowels in geminate contexts have been limited to languages having geminate vowels (arising out of suffixation or compounding) or a long vowel. Oriya is a language which has neither genuine geminate vowels nor long vowels. Several languages such as Oriya which have

Table 1. Classification of vowel sounds in Oriya

Feature	Front	Central	Back
Close (High)	i		u
Half Close (High Mid)	e		o
Half Open (Low Mid)			ɔ
Open (Low)		a	

large number of words ending in a vowel have phonological long vowels or vowels which occur in geminate context in running speech. Investigations of the developmental changes in production of such vowel contexts may help in understanding the complex process of phonemic- phonetic- perceptual- cognitive interaction during production.

An earlier study [5] reported preliminary data on the temporal characteristics of six vowels (/ɔ /,/a/, /i/,/u/,/e/ and /o/) in Oriya. Developmental changes occurred in duration of vowels; duration of vowels decreased with increase in age for all vowels in Oriya in the context of voiced and voiceless post-vocalic stop consonant for both male and female speakers. Duration of vowels in the post-vocalic voiceless stop context was lower than in the voiced stop consonant context. Such context based differences were present from the age of three years and developed with age. The current study was aimed at investigating developmental changes in duration of Oriya vowels in geminate contexts (phonologically long vowels). Effects of age, gender and vowel type on vowel duration were also targeted for analysis.

2. METHOD

Native Oriya speaking children (40 males and 40 females) of 3 years to 14 years and young adults (10 males and 10 females) were included based on following criteria as reported by parents in case of children and self in case of the adult group: 1) Oriya as their primary language, 2) typical development of speech and language, 3) no prior enrollment in speech or language intervention 4) normal hearing status and 5) absence of a history of neurological and/or psychological disorder. Exposure to English and Hindi was limited. The structure and function of oral articulators were assessed to be within normal limits. The first five age groups of children were separated by an interval of one year and next three groups by an interval of two years for precise analysis of developmental changes in the very young children.

Frequently used bi-syllabic words were paired to form utterances of the form- CVCV1 - V1CV, where V1 was the target vowel to be analyzed resulting in the production of the target vowel in a geminate form or

phonologically long vowel CVCVlongCV. Stimuli comprised of six word pairs judged to be familiar or most familiar by a group of 10 Oriya speakers. Word pairs judged as unfamiliar by any of the listeners were not included. The six word pairs included /kad;T-Td;a/, /iˆa-at**T/, /pTˆi-iˆa/, /babu-upi/, /goˆe-eka/ and /Tˆo-od;a/ representing the six vowels /T:/, /a:/, /i:/, /u:/, /e:/ and /o:/ respectively.

Productions of these words pairs by a native female speaker of Oriya were recorded and presented in random order as model for imitation by the participants. Both children and adult participants produced three attempts of each word pair in response to the recorded model presented via a computer. Feedback regarding accuracy of production was not provided. Production of the word pairs of all participants was recorded and analyzed with PRAAT (version 5.0.33). Vowels were identified based upon the regularity of the vertical striations in the time domain waveform and simultaneous display of formants on the spectrograph. The onset of vowel was marked as the cycle after the burst portion of the consonant and offset was marked as the last cycle of periodicity on the acoustic waveform. The duration of the vowel segment as defined by the onset and offset of the vowel was measured for each production after confirmation by highlighting and playback by the experimenter.

3. RESULTS AND DISCUSSION

Two-way repeated measures ANOVA was performed on the duration of geminate vowels with age groups and gender as between subject factors and vowels (six vowels) as within subject factors. There was a main effect for age groups ($F(8, 69) = 73.582$, $p<0.01$) indicating that the duration of vowels produced by children differed among the different age groups. The main effect for gender was not significant. A main effect was also found for geminate vowel type ($F(1, 69) = 95.049$, $p<0.01$) indicating that there was a statistically significant difference in the duration of the six geminate vowels. No interaction effect existed for geminate vowel types across groups, indicating that the differences observed across vowel types were similar in all age groups. As evidenced from Fig. 1. the duration of geminate vowels were longest in age group I (3-3;11) and shortest in the adult group.

Developmental effects in germination: Post hoc analyses between durations produced by participants in the different age groups showed that there was no difference among children for the production of geminate vowel /a:/, /i:/ and /o:/ in the age groups of 3-to-4, 4-to-5 and 5-to-6 years. Duration of vowels /u:/ and /e:/ showed no difference in the 3-to-4 and 4-to-5 years of age. Duration of vowel / ɔ :/, was not different in

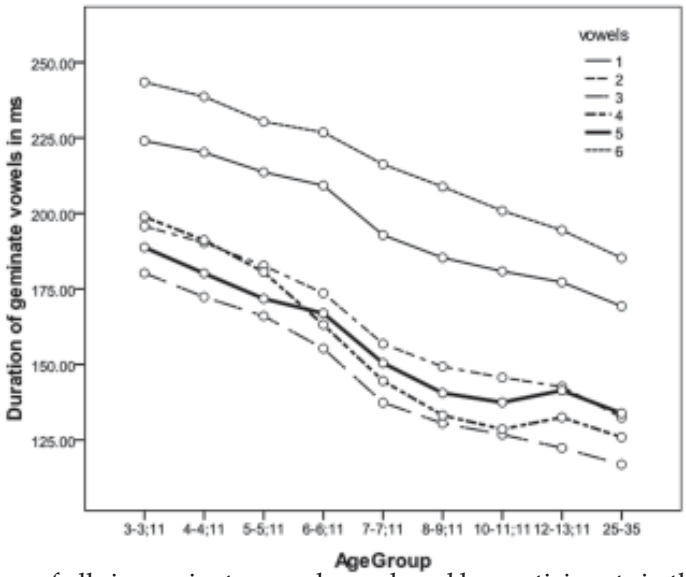

Fig. 1. Mean duration of all six geminate vowels produced by participants in the nine age groups

children in the age range of 3-to-4, 4-to-5, 5-to-6, and also 6-to-7 years of age. The duration produced by children in the age group of 7-to-8 years was significantly different from those of the children of younger age groups, but did not show any difference from children of 8-to-10 years and 10-to-12 years. For production of vowels /i:/, /u:/ and /e:/, there was no difference in the durations of vowels produced by children in the age groups of 8-to-10, 10-to-12, 12-to-14 years and those produced by the adult group indicating children reached adult like productions by 8-to-10 years of age. For vowels /ɔ:/ and /a:/, the adult group did not vary significantly from children of 10-to-12 years; for vowel /o:/, the adult group did not vary significantly from children in the age groups of 12-to-14 years. The age at which children's productions reached adult like durations differed by vowel type. It could be inferred that the early acquisition of specific characteristics of vowels involves an interaction between factors specific to languages, and related to articulatory mechanism.

Geminate contexts versus. singleton context: Mean duration of each of the six vowels in geminate vowel as produced by speakers of the adult group are shown in Table 2 in comparison to the mean vowel duration in singleton post-vocalic voiced consonant context (SVD) and post-vocalic voiceless consonant context (SVL) as reported in an earlier study [5]. Vowels in singleton production and geminate context were not compared statistically as the structure of words taken differed in both syllable size and syllable structure and this might affect the durations of vowels [6,7]. Although statistical analyses were not performed, it can be seen that the duration of geminate vowel was longer than singleton vowels.

Similar findings have been reported in study on gemmination in Lebanese Arabic [8], where geminate vowels were longer than singleton vowels and vowels were longest when they were phonologically long

Table 2. Vowel duration in geminate context and singleton contexts

Vowel	Singleton context: post vocalic voiced consonant	Singleton context: post vocalic unvoiced consonant	Geminate
/?/	110.7	77.3	169.3
/a/	122.2	81.2	132.4
/i/	93.3	62.1	117
/u/	98.1	67.2	125.9
/e/	99.1	70.5	133.8
/o/	102.3	73.4	185.2

vowels. A study of durational characteristics of Hindi vowels and consonants in continuous speech found that the duration of geminate vowel /e/ was 87% longer than the singleton vowel production [9].

The current study provided preliminary data on the temporal characteristics of vowels in Oriya. The data added to the much needed corpus of acoustic characterization of vowels and consonants in Indian languages. Such data may serve useful in analysis of speech of children with speech sound disorders as well as adults with neurological disorders. The values of vowel duration may inform models for speech recognition and synthesis for Oriya language. It was evident that the early acquisition of vowel specifications involves an interaction between language specific features and articulatory predispositions associated with phonetic context.

REFERENCES

[1] M. SHIBATANI 1990. The Languages of Japan. Cambridge: Cambridge University Press.
[2] P. LADEFOGED 2006. A course in Phonetics. Boston: Thomson Wadsworth.
[3] J. DURAND 2005. Tense/lax, the vowel system of English and phonological theory. In Headhood, Elements, Specification and Contrastivity, 77-97.

[4] N. RAMASWAMI 1994. Common linguistic features in Indian languages: Phonetics. Central Institute of Indian Languages, Mysore.
[5] V.R. PRUSTY AND L. VENKATESH (in submission). Duration of vowels in Oriya: A developmental perspective.
[6] R.K. NAGAMMA 1988. The influence of plosive consonant voicing and aspiration on duration of vowels in Telugu and Hindi. Journal of Institution of Electronics and Telecommunication Engineers, Special Issue of JIETE on Speech Processing, New Delhi, **34**, No.1.
[7] R.K. NAGAMMA 1985. Phonetic conditioning of Duration of vowels and consonants in Telugu. Osmania Papers in Linguistics, **11**, 54-83.
[8] G. KHATTAB 2007. A phonetic study of gemination in Lebanese Arabic. Proc. 16th ICPhS, Saarbrücken, 153-158.
[9] K. SAMUDRAVIJAYA 2003. Durational characteristics of Hindi phonemes in continuous speech. Technical Report, TIFR.

Acoustical Society of India
(Regn. No. 65-1971)

Executive Council (2010 - 2014)

President	:	**Dr V Rajendran** [KSRCT, Tiruchengode; veerajendran@gmail.com; +91-99 94 13 03 03]
Vice President	:	**NS Naidu** [NSTL, Vizag; nsnaidu04@yahoo.com; +91-94 90 75 05 82]
General Secretary	:	**PVS Ganesh Kumar** [NSTL, Vizag; gkpakki@rediffmail.com; +91-98 66 40 08 94]
Jt. Secretary	:	**Dr K Trinadh** [NSTL, Vizag; hello_trinath@yahoo.co.in; +91-97 04 71 95 00]
Treasurer	:	**Prof AV Sharma** [AU, Vizag; sarmavakella@yahoo.co.in; +91-94 90 43 17 26]
Chief Editor	:	**Dr Mahavir Singh** [CSIR-NPL, New Delhi; mahavir@nplindia.org; +91-98 71 69 33 46]
Council Members	:	**Dr SV Ranga Nayakulu** [VITAE, Hyderabad; nayakulu@rediffmail.com; +91-98 66 53 26 13]
		Dr I Johnson [SJ College, Trichy; jnaadarsh@hotmail.com; +91-94 42 90 48 20]
		Dr Rajiv K Upadhayay [Govt PG College, Rishikesh; rku8@rediffmail.com; +91-94 12 97 28 90]
		Dr S Shekhar [Oxford College, Trichy; acousticssekar@yahoo.co.in; +91-99 94 92 00 30]
		Dr V Bhujanga Rao [Past President; NSTL, Vizag; vepcrew1@rediffmail.com; +91-98 66 44 10 74]
Co-opted Members	:	**Rajshekhar Uchil** [Josts, Bangalore; ruchil@josts.in; +91-98 80 17 08 95]
		Dr NK Narayanan [CIT, Kozhikode; csirc@rediffmail.com; +91-94 46 95 58 30]

INFORMATION FOR AUTHORS

ARTICLES

The Journal of Acoustical Society of India (JASI) is a refereed publication published quarterly by the Acoustical Society of India (ASI). JASI includes refereed articles, technical notes, letters-to-the-editor, book review and announcements of general interest to readers.

Articles may be theoretical or experimental in nature. But those which combine theoretical and experimental approaches to solve acoustics problems are particularly welcome. Technical notes, letters-to-the-editor and announcements may also be submitted. Articles must not have been published previously in other engineering or scientific journals. Articles in the following are particularly encouraged: applied acoustics, acoustical materials, active noise & vibration control, bioacoustics, communication acoustics including speech, computational acoustics, electro-acoustics and audio engineering, environmental acoustics, musical acoustics, non-linear acoustics, noise, physical acoustics, physiological and psychological acoustics, quieter technologies, room and building acoustics, structural acoustics and vibration, ultrasonics, underwater acoustics.

Authors whose articles are accepted for publication must transfer copyright of their articles to the ASI. This transfer involves publication only and does not in any way alter the author's traditional right regarding his/her articles.

PREPARATION OF MANUSCRIPTS

All manuscripts are refereed by at least two referees and are reviewed by the Publication Committee (all editors) before acceptance. Manuscripts of articles and technical notes should be submitted for review electronically to the Chief Editor by e-mail or by express mail on a disc. JASI maintains a high standard in the reviewing process and only accept papers of high quality. On acceptance, revised articles of all authors should be submitted to the Chief Editor by e-mail or by express mail.

Text of the manuscript should be double-spaced on A4 size paper, subdivided by main headings-typed in upper and lower case flush centre, with one line of space above and below and sub-headings within a section-typed in upper and lower case understood, flush left, followed by a period. Sub-sub headings should be italic. Articles should be written so that readers in different fields of acoustics can understand them easily. Manuscripts are only published if not normally exceeding twenty double-spaced text pages. If figures and illustrations are included then normally they should be restricted to no more than twelve-fifteen.

The first page of manuscripts should include on separate lines, the title of article, the names, of authors, affiliations and mailing addresses of authors in upper and lowers case. Do not include the author's title, position or degrees. Give an adequate post office address including pin or other postal code and the name of the city. An abstract of not more than 200 words should be included with each article. References should be numbered consecutively throughout the article with the number appearing as a superscript at the end of the sentence unless such placement causes ambiguity. The references should be grouped together, double spaced at the end of the article on a separate page. Footnotes are discouraged. Abbreviations and special terms must be defined if used.

EQUATIONS

Mathematical expressions should be typewritten as completely as possible. Equation should be numbered consecutively throughout the body of the article at the right hand margin in parentheses. Use letters and numbers for any equations in an appendix: Appendix A: (A1, (A2), etc. Equation numbers in the running text should be enclosed in parentheses, i.e., Eq. (1), Eqs. (1a) and (2a). Figures should be referred to as Fig. 1, Fig. 2, etc. Reference to table is in full: Table 1, Table 2, etc. Metric units should be used: the preferred from of metric unit is the System International (SI).

REFERENCES

The order and style of information differs slightly between periodical and book references and between published and unpublished references, depending on the available publication entries. A few examples are shown below.

Periodicals:

[1] S.R. Pride and M.W. Haartsen, 1996. Electroseismic wave properties, *J. Acoust. Soc. Am.*, **100** (3), 1301-1315.

[2] S.-H. Kim and I. Lee, 1996. Aeroelastic analysis of a flexible airfoil with free play non-linearity, *J. Sound Vib.*, **193** (4), 823-846.

Books:

[1] E.S. Skudzryk, 1968. *Simple and Comlex Vibratory Systems*, the Pennsylvania State University Press, London.

[2] E.H. Dowell, 1975. *Aeroelasticity of plates and shells*, Nordhoff, Leyden.

Others:

[1] J.N. Yang and A. Akbarpour, 1987. Technical Report NCEER-87-0007, Instantaneous Optimal Control Law For Tall Buildings Under Seismic Excitations.

SUMISSIONS

All materials from authors should be submitted in electronic form to the JASI Chief Editor: Dr Mahavir Singh, Acoustics, Ultrasonics & Vibration Section, CSIR-National Physical Laboratory, Dr. K. S. Krishnan Road, New Delhi-110 012 (email: mahavir@nplindia.org Tel: +91-11-4560.8317, Fax: +91-11-4560.9310). For the item to be published in a given issue of a journal, the manuscript must reach the Chief Editor at least twelve week before the publication date.

SUMISSION OF ACCEPTED MANUSCRIPT

On acceptance, revised articles should be submitted in electronic form to the JASI Chief Editor (mahavir@nplindia.org).